Journal of Applied Mechanics

(Contributions of the ASME Applied Mechanics Division)

Topics in Gyroscopic Motion . . . . . *H. Poritsky* 1
Stability Criteria for Forced Vibrations in Nonlinear Systems . . . . *K. Klotter and E. Pinney* 9
Rails on Elastic Foundations . . . . . *H. E. Criner and G. D. McCann* 13
Stability of Thin Elastic Plates . . . . . *G. A. Zizicas* 23
Effect of Surface Condition on Creep . . . . . *E. D. Sweetland and E. R. Parker* 30
The New Approach to Shell Theory . . . . . *E. H. Kennard* 33
Forced Oscillations of the Centrifugal Pendulum . . . . . *F. R. E. Crossley* 41
A Nondestructive Test for Thin Shells . . . . . *J. C. New* 48
Analysis of Forced Vibration of Beams . . . . . *N. O. Myklestad* 53
On Asymmetric Flow in Axial-Flow Compressor Stage . . . . . *W. R. Sears* 57
Turbulent Mixing of Two Parallel Streams . . *T. P. Torda, W. O. Ackermann, and H. R. Burnett* 63
Some Problems of Orthotropic Plane Stress . . . . . *H. D. Conway* 72
The Bending of a Wedge-Shaped Plate . . . . . *S. Woinowsky-Krieger* 77
Stress Distribution Under Concentrated Loads . . . . . *H. D. Conway* 82
The End Problem of Rectangular Strips . . . . . *G. Horvay* 87
Nonlinear Distribution of Bending Stresses . . . . . *H. H. Bleich* 95
Necking and Rupture of Rods Under Tensile Loads . . . . . *N. J. Hoff* 105
On Turbulent Flow Between Parallel Plates . . . . . *S. I. Pai* 109
Analogue to High-Velocity Combustion . . . . . *A. K. Oppenheim* 115
Elastic Waves Created During Tensile Fracture . . . . . *Julius Miklowitz* 122
Influence Coefficients of Tapered Cantilever Beams Computed on SEAC . . . . *Samuel Levy* 131
Design Data and Methods
On the Maximum Numerical Value of the Tangential Stress in Thick-Walled Cylinders . . . . . *T. Ranov and F. R. Park* 134
Stresses in Curved Beams—A Tabular Method of Solution Based on Winkler's Theory . . . . . *W. Wright* 138
Brief Notes
Movies of Stress Waves in Photoelastic Rubber . . . . . *H. C. Perkins* 140
Bending of Clamped Wedge Plates . . . . . *Herbert Reismann* 141
Discussion on previously published papers by *F. R. E. Crossley; W. J. Carter and J. B. Oliphint; M. Feigen; J. Gallagher and E. Volterra; L. Green, Jr.; R. Holm; J. Kaye, J. H. Keenan, K. K. Klingensmith, G. M. Ketchum, and T. Y. Toong; T.-C. Lee; C. M. Tyler, Jr., and J. G. Christiano; E. H. Lee and P. S. Symonds; and E. H. Lee.*
Book Reviews 154

MARCH, 1953

VOL. 20, NO. 1

Transactions of The American Society of Mechanical Engineers

Journal of Applied Mechanics

Papers Contributed to the Transactions by the ASME Applied Mechanics Division

EXECUTIVE COMMITTEE OF THE APPLIED MECHANICS DIVISION

DANA YOUNG, *Chairman* N. M. NEWMARK, *Secretary*

JOHN M. LESSELLS, *Technical Editor*

Published Quarterly by

The American Society of Mechanical Engineers

Publication Office, 20th and Northampton Streets, Easton, Pa.
Editorial Department at the Headquarters of the Society, 29 West Thirty-Ninth Street, New York 18, N. Y.

OFFICERS OF THE SOCIETY

FREDERICK S. BLACKALL, JR., *President*

JOSEPH L. KOBY, *Treasurer* C. E. DAVIES, *Secretary*
E. J. KATES, *Assistant Treasurer*

PUBLICATIONS COMMITTEE

GEORGE R. REICH, *Chairman* GEORGE A. STETSON, *Editor*
K. W. CLEDENNING, *Mgr. Editor*

By-Law: The Society shall not be responsible for statements or opinions advanced in papers or . . . printed in its publications (B13, Par. 4).

Published quarterly by The American Society of Mechanical Engineers. Publication office at 20th and Northampton Streets, Easton, Pa. The editorial department is located at the headquarters of the Society, 29 West Thirty-Ninth Street, New York 18, N. Y. Cable address, "Dynamic," New York. Price $1.25 a copy, $5.00 a year; to members $2.50 a year; single copy price to members, $1.00. Changes of address must be received at Society headquarters four weeks before they are to be effective on the mailing list. Please send old as well as new address. . . . By-Law: The Society shall not be responsible for statements or opinions advanced in papers or . . . printed in its publications (B13, Par. 4). . . . Entered as second-class matter March 14, 1933, at the Post Office at Easton, Pa., under the act of August 24, 1912. . . . Copyrighted, 1955, by The American Society of Mechanical Engineers. Reprints from this publication may be made on condition that full credit be given the JOURNAL OF APPLIED MECHANICS and the author, and that date of publication be stated.

Topics in Gyroscopic Motion

By H. PORITSKY,[1] SCHENECTADY, N. Y.

After a brief review of the fundamental kinetic equations of gyroscope motion, the following topics are considered: (*a*) The erection of an electrically driven gyroscope when an electrical torque is applied. (*b*) The effect of inequality of the principal moments of inertia normal to the spin axis, on gyroscope motion. (*c*) The effect of inertia of the gimbals on motion of the gyroscope.

1 Introduction

REVIEWING briefly the kinematic and dynamical concepts which are fundamental for the study of motion of a gyroscope (and of rigid bodies generally), a gyroscope with perfect alignment and balance will be considered. Fig. 1 shows schematically a gyroscope rotor R_1 and the inner and outer gimbals R_2, R_3 by means of which R_1 is suspended in a fixed reference system R_4. Here A_1 is the spin axis of R_1, α_1 the angle of rotation about A_1 of R_1 relative to R_2; A_2 is the axis of rotation of R_2 relative to R_3 and α_2 is the angle of rotation of R_2 about A_2; A_3 is the axis of rotation of R_3 relative to the fixed reference frame R_4, and α_3 the angle of rotation of R_3 about this axis.

The assumption of perfect alignment implies that the axes A_1, A_2, A_3 intersect at a common point O, and that the axis A_2 is perpendicular both to A_1 and A_3. In Fig. 1 these axes are shown in what might be called "the initial position" for which each angle α_i vanishes, A_1, A_2, A_3 are mutually perpendicular and coincide, respectively, with fixed rectangular co-ordinate axes x, y, z. In Fig. 2 are shown on a unit sphere S with center at O the intersection with S of these axes as well as A_i after proper rotations through angles α_i have been carried out. For ease of visualization, R_1, R_2, R_3 are indicated in Fig. 2 by means of heavy line quadrants of great circles.

In addition to the fixed (x, y, z)-axes, it is convenient to introduce several other co-ordinate systems, namely, systems fixed relative to R_3, R_2, R_1, with subscripts 3, 2, 1, respectively, and initially coincident with the (x, y, z)-system; also unit vectors along these axes, $\mathbf{i}, \mathbf{j}, \mathbf{k}$; $\mathbf{i}_1, \mathbf{j}_1, \ldots$, are introduced. Some of these unit vectors are shown on the unit sphere with center at O in Fig. 2. The relations between the co-ordinates or the unit vectors for each system and those of other systems are deduced readily by inspection of Fig. 2. Thus, since the vectors $\mathbf{i}_3$, $\mathbf{j}_3$ are obtained by rotating the vectors $\mathbf{i}, \mathbf{j}$ about the A_3 axis through an angle α_3, there follows from Fig. 2

$$\mathbf{i}_3 = \mathbf{i} \cos \alpha_3 + \mathbf{j} \sin \alpha_3, \quad \mathbf{j}_3 = -\mathbf{i} \sin \alpha_3 + \mathbf{j} \cos \alpha_3, \quad \mathbf{k}_3 = \mathbf{k}. \quad [1]$$

Similarly, the relations between any two sets of unit vectors can be written down by inspection from Fig. 2 and by manipulating the resulting equations. The relations between the corresponding co-ordinates are of the same form, with the respective co-ordinates replacing the unit vectors.

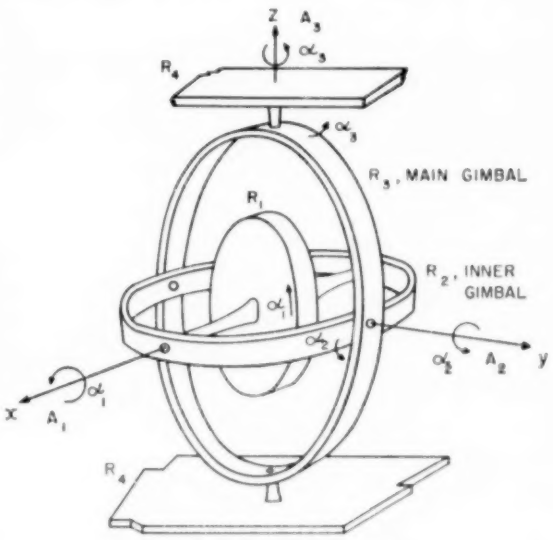

Fig. 1 Gyroscope and Gimbal Rings

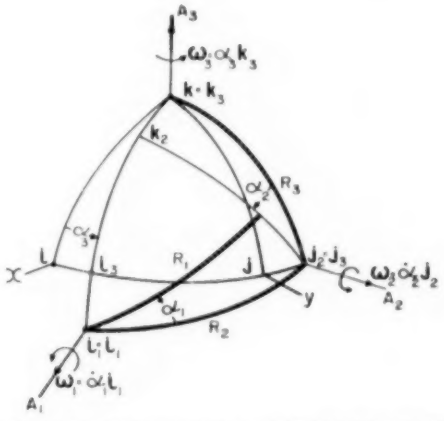

Fig. 2 Schematic Representation of Gyroscope and Gimbals on a Unit Sphere

Since R_1 is a rigid body, its (true) velocities (that is, the velocities relative to a fixed Newtonian system—the $[x, y, z]$-system or the R_4 system) can be specified at any instant by means of a rotation vector $\boldsymbol{\omega}$. By applying the law of relative velocities, this vector $\boldsymbol{\omega}$ may be represented as a sum of three rotation vectors $\boldsymbol{\omega}_1 = \dot{\alpha}_3 \mathbf{k}_3, \boldsymbol{\omega}_2 = \dot{\alpha}_2 \mathbf{j}_2, \boldsymbol{\omega}_3 = \dot{\alpha}_1 \mathbf{i}_1$ representing, respectively, the rotations of R_3 relative to R_2, of R_2 relative to R_3, of R_3 relative to R_4. The traces of these vectors on S are also indicated in Fig. 2. By resolving $\mathbf{k}_2$ along $\mathbf{i}_2, \mathbf{k}_2$ one obtains

$$\left.\begin{aligned} \boldsymbol{\omega} &= \boldsymbol{\omega}_1 + \boldsymbol{\omega}_2 + \boldsymbol{\omega}_3 \\ &= \dot{\alpha}_3 \mathbf{i}_3 + \dot{\alpha}_2 \mathbf{j}_2 + \dot{\alpha}_1 \mathbf{k}_1 \\ &= (\dot{\alpha}_1 - \dot{\alpha}_3 \sin \alpha_2) \mathbf{i}_2 + \dot{\alpha}_2 \mathbf{j}_2 + \dot{\alpha}_3 \cos \alpha_2 \mathbf{k}_2 \\ &= \omega_{x2} \mathbf{i}_2 + \omega_{y2} \mathbf{j}_2 + \omega_{z2} \mathbf{k}_2 \end{aligned}\right\} \quad \ldots [2]$$

[1] General Engineering Laboratory, General Electric Company. Mem. ASME.

Presented at the National Conference of the Applied Mechanics Division, State College, Pa., June 19–21, 1952, of The American Society of Mechanical Engineers.

Discussion of this paper should be addressed to the Secretary, ASME, 29 West 39th Street, New York, N. Y., and will be accepted until July 10, 1953, for publication at a later date. Discussion received after the closing date will be returned.

Note: Statements and opinions advanced in papers are to be understood as individual expressions of their authors and not those of the Society. Manuscript received by ASME Applied Mechanics Division, August 13, 1951.

the subscripts x_2, y_2, z_2 denoting components relative to the R_2-system of axes. The motion of the R_2, R_3 systems is similarly represented by the rotation vectors $\boldsymbol{\omega}_2 + \boldsymbol{\omega}_3, \boldsymbol{\omega}_3$.

To pass from the fixed system R_4 to the gyro rotor R_1 starting from the initial position where $\alpha_i = 0$, one carries out the rotations in the order $\alpha_3, \alpha_2, \alpha_1$.[2]

The angles α_1, α_2, α_3, though introduced in the foregoing by means of gimbal rings and their relative rotations, may, of course, be used in absence of gimbals as convenient variables to describe the (rotational) motion of a general rigid body with a fixed point O. These angles are different from but closely related to the commonly used Euler angles ψ, θ, φ.

Turning to dynamical considerations, it will be assumed that the rotor R_1 is balanced. This implies now not only that its center of mass (gravity) is on the axis of spin A_1 (this is also the x_1-axis), but also that it lies at O. Hence A_1 is one of the principal axes of inertia of R_1 through O. The moment of inertia of R_1 about A_1 is denoted by I. It is further assumed at first that J, K, the other two principal moments of inertia of R_1 about the two principal axes of inertia through O normal to A_1, are equal to each other. These axes can then be chosen as any two mutually perpendicular axes, normal to the x_1-axis, such as the y_1, z_1-axes, fixed in R_1 or as the y_2, z_2-axes fixed in R_2. If $J \neq K$, then only a fixed set of axes in R_1 can be used as principal axes, and these will be chosen as the y_1, z_1-axes.

If the inertia of the gimbals is negligible, then the motion of the gyro can be derived from the vector equation

$$\frac{d\mathbf{M}}{dt} = \mathbf{Q} \qquad [3]$$

where $\mathbf{M}$ is the moment of momentum vector of R_1 about O, and $\mathbf{Q}$ is the net vector torque representing the sum of the vector moments about O of the external forces acting on R_1.[3] Here $\mathbf{M}$ may be expressed in either of the forms

$$\mathbf{M} = I\,\omega_{x1}\,\mathbf{i}_1 + K(\omega_{y1}\,\mathbf{j}_1 + \omega_{z1}\,\mathbf{k}_1) \qquad [4]$$

$$\mathbf{M} = I\,\omega_{x2}\,\mathbf{i}_2 + K(\omega_{y2}\,\mathbf{j}_2 + \omega_{z2}\,\mathbf{k}_2) \qquad [5]$$

where ω_{x1}, ω_{y1}, ω_{z1} are the components of $\boldsymbol{\omega}$ along the axes of R_1 and ω_{x2}, ω_{y2}, ω_{z2}, as in Equation [2], its components along the axes of R_2. Since R_1, R_2 (and R_3) rotate, the several vectors $\mathbf{i}_1, \mathbf{j}_1, \ldots$, $\mathbf{k}_2$ (also $\mathbf{i}_3, \mathbf{j}_3, \mathbf{k}_3 \ldots$) vary with time, and this fact of course must be taken into account in carrying out the time differentiations. The (vector) velocity of each of these unit vectors may be found by inspection from Fig. 2 or from the vector product of the proper rotation vector by the unit vector in question. Using the R_1-components one obtains from Equation [3] the Euler differential equations

$$\left.\begin{aligned} I\,\dot{\omega}_{x1} &= Q_{x1} \\ K\,\dot{\omega}_{y1} + (I - K)\omega_{x1}\,\omega_{z1} &= Q_{y1} \\ K\,\dot{\omega}_{z1} - (I - K)\omega_{x1}\,\omega_{y1} &= Q_{z1} \end{aligned}\right\} \qquad [6]$$

where the right-hand members are the components of torque along (about) the axes of R_1. Similarly, using R_2-components, there results

$$\left.\begin{aligned} I\,\dot{\omega}_{x2} &= Q_{x2} \\ K(\dot{\omega}_{y2} + \dot{\alpha}_1\omega_{z2}) + (I - K)\omega_{x2}\,\omega_{x2} &= Q_{y2} \\ K(\dot{\omega}_{z2} - \dot{\alpha}_1\omega_{y2}) - (I - K)\omega_{y2}\,\omega_{x2} &= Q_{z2} \end{aligned}\right\} \qquad [7]$$

The appearance of the $\dot{\alpha}_1$-terms is due to the fact that while $\boldsymbol{\omega}$ is the rotation vector of R_1, the R_2-system has a different rotation vector, namely $\boldsymbol{\omega} - \alpha_1\mathbf{i}_2$.

Expressing ω_{x2}, ω_{y2}, ω_{z2} in terms of α_1, α_2, α_3 one obtains from Equation [7]

$$I\,\frac{d}{dt}\,(\dot{\alpha}_1 - \dot{\alpha}_3 \sin\alpha_2) = Q_{x2}$$

$$K\left(\frac{d\dot{\alpha}_2}{dt} + \dot{\alpha}_1\dot{\alpha}_3\cos\alpha_2\right) + (I - K)\,(\dot{\alpha}_1 - \dot{\alpha}_3\sin\alpha_2)\,\dot{\alpha}_3\cos\alpha_2 = Q_{y2} \qquad [8]$$

$$K\left[\frac{d}{dt}\,(\dot{\alpha}_3\cos\alpha_2) - \dot{\alpha}_1\dot{\alpha}_2\right] - (I - K)\,(\dot{\alpha}_1 - \dot{\alpha}_3\sin\alpha_2)\dot{\alpha}_2 = Q_{z2}$$

Alternatively, the equations of motion may be derived by starting with the kinetic energy of R_1, say, in the form

$$T = \frac{1}{2}\,[I\omega_{x1}^2 + K(\omega_{y1}^2 + \omega_{z1}^2)] \qquad [9]$$

expressing $\omega_{x1}, \ldots$ in terms of α_i, and applying Lagrange's equations. Utilizing Equation [2], there results

$$\left.\begin{aligned} I\,\frac{d}{dt}\,(\dot{\alpha}_1 - \dot{\alpha}_3\sin\dot{\alpha}_2) &= Q_{\alpha 1} \\ K\frac{d\dot{\alpha}_2}{dt} + I\dot{\alpha}_1\dot{\alpha}_3\cos\alpha_2 - (I - K)\dot{\alpha}_3^2\sin\alpha_2\cos\alpha_2 &= Q_{\alpha 2} \\ \frac{d}{dt}\,[K\dot{\alpha}_3 + (I - K)\dot{\alpha}_3\sin^2\alpha_2 - I\dot{\alpha}_1\sin\alpha_2] &= Q_{\alpha 3} \end{aligned}\right\} \qquad [10]$$

where $Q_{\alpha i}$ are the torques about the axes A_i so that

$$dW = Q_{\alpha 1}\,d\alpha_1 + Q_{\alpha 2}\,d\alpha_2 + Q_{\alpha 3}\,d\alpha_3 \qquad [11]$$

is the work done by the external forces during a displacement which increases $\alpha_1, \alpha_2, \alpha_3$ by the amounts $d\alpha_1, d\alpha_2, d\alpha_3$.

The foregoing equations suffice for Section 2. In Section 3 where it is no longer assumed that $J = K$, Equation [4] is modified as in Equation [26]. If, as in section 4, the inertias of the gimbals, R_2, R_3 must be taken into account, then, to formulate the dynamical equations, one must include the moments of momentum $\mathbf{M}_2$, $\mathbf{M}_3$ of R_2, R_3 or their kinetic energies T_2, T_3. One either resorts to separate moment of momentum relations for R_1, R_2, R_3, similar to Equation [3] and including the interaction torques in the external torques, or one may add these equations vectorially, eliminating the equal and opposite interaction torques. In the Lagrange equations the total kinetic energy is the (scalar) sum of the energies of R_1, R_2, and R_3.

The motion of R_1 under no torques, consisting of its rotation with constant spin velocity s about A_1 held fixed, is too trivial to illustrate the dynamical equations. A less trivial illustration is offered by precession where under the action of a torque $\mathbf{Q}$ about an axis normal to A_1, the direction of A_1 changes so that the end point of $\mathbf{i}_1$ rotates at a rate p given by

$$Q = Isp, \quad p = Q/Is \qquad [12]$$

The usefulness of a gyro lies in the fact that with high spin s, the changes of the direction of the axis, represented by the precession rate p, is small.

The simple motion of rotation about a fixed (spin) axis is not the only possible motion under the action of zero torque. A more complicated motion, known as "nutation," is possible, and will result if the rotor R_1, while spinning about its axis A_1, is also given an initial component of rotation about an axis normal to the A_1-

[2] The reason for this retrograde notation is due to the fact that in some problems the reference system R_4 is itself not fixed, but moves relative to a fixed system. This happens, for instance, when R_4 is an airplane executing a loop or a turn, or when R_4 "stands still," that is, partakes of the rotation of the earth. It is then necessary to add further co-ordinate systems, and one resorts to $i_4, \ldots, x_4, \ldots$, while reserving x, y, z for the truly fixed Newtonian system co-ordinates.

[3] The contribution to $\mathbf{M}$ of a force $\mathbf{F}$ acting at P is the vector product $\mathbf{F} \times \overrightarrow{OP}$.

axis. In this motion the spin axis A_1 and the instantaneous vector $\boldsymbol{\omega}$ describe a circular cone (herpolhode) C in space and a circular cone (polhode) C_1 relative to R_1. This motion is discussed by J. L. Synge and B. A. Griffith.[4]

For inertialess R_2, R_3 the motion of these gimbals during nutation of the rotor R_1 is shown in Fig. 3 and may be described on the unit sphere as the motion of a spherical three-bar linkage, with A_3 fixed, A_1 describing a circle or cone C_s with uniform velocity, where the pole of C_s is along the constant $\mathbf{M}$ direction.

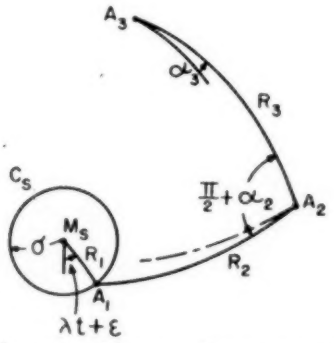

Fig. 3 Nutational Motion of Gyroscope and Gimbals

The explicit expressions of α_1, α_2, α_3 during nutation as functions of time are quite complicated. However, for small displacements of A_1 from a fixed position and small deviations of $\dot{\alpha}_1$ from a constant spin s things simplify. For small values of $\dot{\alpha}_1 - s$, $\dot{\alpha}_3$, $\dot{\alpha}_2$ one may neglect their products in Equations [10] and one obtains

$$\left.\begin{aligned} &\ddot{\alpha}_1 - \ddot{\alpha}_3 \sin \alpha_2 = 0 \\ &K\,\ddot{\alpha}_2 + I\,s\,\dot{\alpha}_3 \cos \alpha_2 = 0 \\ &K\,\ddot{\alpha}_3 + (I - K)\ddot{\alpha}_3 \sin^2 \alpha_2 - Is \cos \alpha_2 \dot{\alpha}_2 \\ &\qquad\qquad - I\ddot{\alpha}_1 \sin \alpha_2 = 0 \end{aligned}\right\} \quad \ldots [13]$$

Neglecting variations in s, $\sin \alpha_2$, $\cos \alpha_2$, one solves Equations [13] by putting

$$\dot{\alpha}_1 - s = B_1 e^{pt}, \quad \alpha_2 = B_2 e^{pt}, \quad \alpha_3 = B_3 e^{pt} \quad \ldots [14]$$

where p, B_1, B_2, B_3 are constants. Substituting in Equations [13], eliminating B_1, B_2, B_3, and neglecting the solution $p = 0$, there results

$$p^2 = -I^2 s^2 / K^2 = -\lambda^2, \quad \lambda = Is/K \quad \ldots [15]$$

This leads to small sinusoidal variations in α_i of (angular) frequency $\lambda = sI/K$ which is constant and independent of α_3, α_3.

2 Effect of Variable Rotor Speed and Reaction on Gimbal Rings

The condition of constant spin velocity at zero torque is, of course, an ideal one. Any gyro rotor must experience torques due to friction in its bearings and air drag. For an electrically driven gyro the rotor R_1 and the gimbal R_2 form the rotor and stator of a synchronous electrical motor, and constant rotor spin is obtained, say, by making it run in synchronism with the stator field. The rotor is driven by the electromagnetic torque which at synchronism adjusts itself so that it just overcomes friction in the bearings and air drag.

When the power is suddenly turned on or off, the torque balance existing at steady spin is disturbed, and the rotor experiences a large torque $Q_{\alpha 1}$ which tends to accelerate or decelerate it. Similarly, if the applied field varies in frequency or amplitude, the electric torque varies too, and there is a tendency for the rotor speed to change. It will now be shown that if $\alpha_2 \neq 0$, an accelerating (electrical) torque $Q_{\alpha 1}$ will also cause the spin axis A_1 to precess about A_2 so that α_2 approaches zero.

Let $\mathbf{Q}_1$ be the net torque which the stator R_2 exerts on the rotor R_1. The component of $\mathbf{Q}_1$ along A_1, $Q_{\alpha 1}$, is the electrical torque (less the friction torque in the bearing), but $\mathbf{Q}_1$ may also have components normal to A_1 which are transmitted through the bearings as a force at one bearing and an equal and opposite force at the other one. Clearly R_2 must experience the reaction torque $-\mathbf{Q}_1$ which is exerted by the rotor R_1 on it. Suppose R_2, R_3 are of negligible inertia. Then R_2 can only transmit the torque $-\mathbf{Q}_1$ to R_3, and the latter, in turn, must transmit this reaction $-\mathbf{Q}_1$ through its bearings on the axis A_2 to the outer supporting frame R_4.

While there is some friction in the bearings along each axis A_1, A_2, A_3, this friction is generally small. This means that only a limited torque component can be transmitted by R_2 to R_3 along the A_2-axis, and by R_3 to R_4 along the A_3-axis. Neglecting friction along the A_2, A_3 bearings altogether, it follows that $\mathbf{Q}_1$ must be normal both to A_2 and to A_3, or referring to Fig. 2, $\mathbf{Q}_1$ must point along the vector $\mathbf{i}_3$

$$\mathbf{Q}_1 = Q_1 \mathbf{i}_3 \quad \ldots [16]$$

Thus while an electrical torque

$$Q_e \mathbf{i}_1 \quad \ldots [17]$$

is exerted by the stator R_2 upon the rotor R_1 about the spin axis A_1, the reaction of such a torque cannot be supported by the supports of the stator.

This difficulty can be overcome by supposing that the stator R_2 also exerts on R_1 a further torque component such that when added to $Q_e \mathbf{i}_1$ it leads to a net torque along $\mathbf{i}_3$. As will be seen from Figs. 2, 4, the vectors $\mathbf{i}_1$, $\mathbf{i}_3$, $\mathbf{k}_2$, $\mathbf{k}$ all lie in plane normal to A_2.

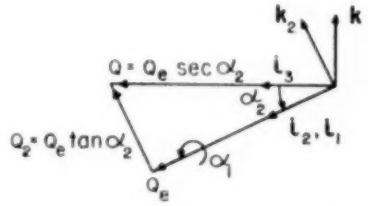

Fig. 4 Vector Representation of Applied and Reaction Torques

Hence the added torque must be directed along (about) $\mathbf{k}_2$; it is given by

$$Q_e \tan \alpha_2 \mathbf{k}_2 \quad \ldots [18]$$

Indeed, addition of the Torques [17], [18] yields

$$\left.\begin{aligned} &Q_e(\mathbf{i}_1 + \tan \alpha_2 \mathbf{k}_2) \\ &= Q_e \sec \alpha_2 [\mathbf{i}_2 \cos \alpha_2 + \mathbf{k}_2 \sin \alpha_2] \\ &= Q_e \sec \alpha_2 \mathbf{i}_3 = \mathbf{Q}_1 \end{aligned}\right\} \quad \ldots [19]$$

The torque component given by Equation [18], being normal to A_1, will produce a precession p, of magnitude

$$p = -\frac{d\alpha_2}{dt} = -\frac{Q_e \tan \alpha_2}{Is} \quad \ldots [20]$$

causing the spin axis A_1 to move toward $\mathbf{k}_2$. This precession is just of the type discussed in Section 1. For positive Q_e it leads

[4] "Principles of Mechanics," by J. L. Synge and B. A. Griffith, second edition. McGraw-Hill Book Company, Inc., New York, N. Y., 1949.

to a decrease in the angle α_2 toward 0, thus displacing the axis A_1 in Fig. 2 into perpendicularity to the axis A_3.

We proceed to study the motions in greater detail. Under the Torque [18] Equation [8] yields, upon neglecting the terms in $\ddot{\alpha}_2$, $\ddot{\alpha}_3$, $\dot{\alpha}_2^2$, $\dot{\alpha}_2\dot{\alpha}_3$

$$\left.\begin{aligned} &I\frac{d}{dt}(\dot{\alpha}_1 - \dot{\alpha}_3\sin\alpha_2) = Q_s \\ &I\,\dot{\alpha}_1\dot{\alpha}_3\cos\alpha_2 = 0 \\ &I\,\dot{\alpha}_1\dot{\alpha}_2 = -Q_s\tan\alpha_2 \end{aligned}\right\} \quad \ldots\ldots\ldots [21]$$

The second Equation [21] leads to $\dot{\alpha}_3 = 0$ showing that R_3 is stationary, and that the precession consists of a rotation about the fixed $\mathbf{j}_3$-axis. The first and third Equations [21] now yield

$$\frac{Q_s dt}{I\dot{\alpha}_1} = \frac{d\dot{\alpha}_1}{\dot{\alpha}_1} = -\frac{d\,\alpha_2}{\tan\alpha_2} = -\frac{d(\sin\alpha_2)}{\sin\alpha_2} \quad \ldots\ldots [22]$$

Thus if Q_s is positive and $\dot{\alpha}_1 = s$ is positive, the spin velocity will be increasing; $d\alpha_2$ and α_2 will be of opposite sign so that α_2 approaches the value zero. An accelerating torque (positive Q_s) will therefore "rectify" the gyro, that is, will cause α_2 to approach zero, bringing the spin axis into perpendicularity to A_3. On the other hand, a decelerating torque will cause α_2, if the latter is initially different from zero, to depart further from it, and will thus "upset" the gyro, swinging the spin axis A_1 toward A_3.

Integration of Equations [22] yields

$$\dot{\alpha}_1\sin\alpha_2 = \text{const} \quad \ldots\ldots [23]$$

$$\dot{\alpha}_1 = \int Q_s dt/I \quad \ldots\ldots [24]$$

In particular, if a constant torque Q_s is "turned on" at the time $t = 0$ when $\dot{\alpha}_1 = \dot{\alpha}_{10}$, $\alpha_2 = \alpha_{20}$, there results

$$\sin\alpha_2 = \sin\alpha_{20}/(\dot{\alpha}_{10} + Q_s t/I) \quad \ldots\ldots [25]$$

Owing to the neglected terms the solution obtained is not exact. This may be explained by means of the vector $\mathbf{M}$ in Fig. 5. The

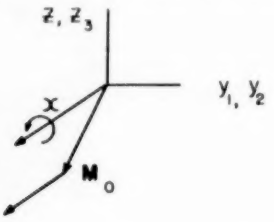

FIG. 5 MOMENT OF MOMENTUM VARIATION IN GYROSCOPE ERECTION

initial $\mathbf{M}$-vector points along the spin axis $\mathbf{i}_2$. The torque given by Equation [18], acting about the fixed x-axis, causes the end point of $\mathbf{M}$ to move along a line parallel to the x-axis and thus makes the spin axis rotate into parallelism with the x-axis. Such a rotation, however, implies a small rotation component about the y-axis and involves small torque components about this axis.

Actually the bearings *do* possess slight friction. So long as the torque Q_s exceeds the bearing friction in magnitude, the foregoing results essentially apply, since only a limited torque component can be transmitted normally to A_3. However, when the torque Q_s gets to be of the same order of magnitude as the friction torques, then the argument just used no longer applies, since the bearings can then transmit that torque. For small $|\alpha_2|$ the tendency to exact perpendicularity between A_3 and A_1-axes is resisted by friction. Friction about the A_2-gimbals may be relied on to supply the small torques about the A_2-axis whose need was indicated previously.

The swinging of the spin axis A_1 into perpendicularity to the axis A_3 is one of the most noticeable effects produced when the power is turned on in starting a gyro. "Upsetting" the gyro axis is sometimes induced by reversing the applied voltage.

3 ROTOR WITH UNEQUAL MOMENTS OF INERTIA

We shall now consider the effect of dropping the assumption $J = K$ which was made in section 1. This is of interest, of course, for rotating of bodies which are not solids of rotation (for instance, airplane propellers), but also for gyros, since, even under perfect balance, the assumption $J = K$ is generally not quite satisfied.

In place of Equation [4] we now start with

$$\mathbf{M} = I\omega_{x_1}\mathbf{i}_1 + J\omega_{y_1}\mathbf{j}_1 + K\omega_{z_1}\mathbf{k}_1 \quad \ldots\ldots [26]$$

for the moment of momentum.

We consider first uniform precessions, and the torques required to produce them. As in section 1, assume a uniform spin $\dot{\alpha}_1 = s$, and suppose that the spin axis A_1 rotates with a uniform velocity p about the $\mathbf{j}_2$-axis, assumed fixed. Expressing the rotation vector (see Equation [2])

$$\boldsymbol{\omega} = \dot{\alpha}_1\mathbf{i}_2 + \dot{\alpha}_2\mathbf{j}_2 = s\mathbf{i}_2 + p\mathbf{j}_2 \quad \ldots\ldots [27]$$

in the R_1-system

$$\boldsymbol{\omega} = s\mathbf{i}_1 + p(\mathbf{j}_1\cos\alpha_1 - \mathbf{k}_1\sin\alpha_1) \quad \ldots\ldots [28]$$

we obtain from Equation [26]

$$\mathbf{M} = Is\mathbf{i}_1 + Jp\cos\alpha_1\mathbf{j}_1 - Kp\sin\alpha_1\mathbf{k}_1 \quad \ldots\ldots [29]$$

and, introducing once more R_2-vectors

$$\mathbf{M} = Is\mathbf{i}_2 + \mathbf{j}_2 p\left[\frac{(J+K)}{2} + \frac{J-K}{2}\cos 2\alpha_1\right] + \mathbf{k}_2\, p\,\frac{J-K}{2}\sin 2\alpha_1 \quad \ldots\ldots [30]$$

Hence, differentiating

$$\frac{d\mathbf{M}}{dt} = Is\frac{d\mathbf{i}_2}{dt} - \mathbf{j}_2 p\dot{\alpha}_1(J-K)\sin 2\alpha_1 + \mathbf{k}_2 p\dot{\alpha}_1(J-K)\cos 2\alpha_1 + p\,\frac{d\mathbf{k}_2}{dt}\,\frac{J-K}{2}\sin 2\alpha_1 \quad \ldots\ldots [31]$$

Replacing α_1 by s, and noting from Fig. 2 that

$$\frac{d(\mathbf{i}_2, \mathbf{j}_2, \mathbf{k}_2)}{dt} = (-p\mathbf{k}_2, 0, p\mathbf{i}_2) \quad \ldots\ldots [32]$$

one obtains

$$\frac{d\mathbf{M}}{dt} = (ps\mathbf{j}_2 + p^2\mathbf{i}_2)(J-K)\sin 2\alpha_1 + ps\,\mathbf{k}_2\,[-I + (J-K)\cos 2\alpha_1] \quad \ldots\ldots [33]$$

This is the torque $\mathbf{Q}$ required to produce the assumed precessional motion.

From Equation [33] it will be noticed that, in addition to the steady precessional torque $-Isp\,\mathbf{k}_2$, there are pulsating torque components along all three directions $\mathbf{i}_2$, $\mathbf{j}_2$, $\mathbf{k}_2$ of frequency $2s$, i.e., double the spin frequency. Usually, for large s, the magnitude of p is small compared to s, the p^2-term may be neglected in comparison with the other terms, and the variable component of $d\mathbf{M}/dt$ (and torque $\mathbf{Q}$) is of magnitude $(J-K)ps$ and rotates about the $\mathbf{i}_2$-axis in direction opposite to the gyro spin.

The (reaction of this) pulsating torque is exerted on the engine

and its mountings by two-bladed propellers during banking and looping maneuvers of a plane.

The motion of a solid with three unequal moments of inertia under the action of zero torques, is a classical problem whose solution may be found in any advanced book on dynamics such as references.[4,5,6] We shall review this solution briefly.

Differentiation of Equation [26] and substitution in Equation [3] leads for $Q = 0$ to the general Euler equations

$$\left.\begin{aligned} I\dot{\omega}_{x1} + (K - J)\omega_{y1}\omega_{z1} &= 0 \\ J\dot{\omega}_{y1} + (I - K)\omega_{z1}\omega_{x1} &= 0 \\ K\dot{\omega}_{z1} + (J - I)\omega_{x1}\omega_{y1} &= 0 \end{aligned}\right\} \quad \ldots\ldots\ldots\ldots [34]$$

Multiplying Equations [34], respectively, by ω_{x1}, ω_{y1}, ω_{z1}, adding, and integrating, there results the energy integral

$$\frac{1}{2}(I\omega_{x1}^2 + J\omega_{y1}^2 + K\omega_{z1}^2) = T = \text{const} \ldots\ldots [35]$$

where T is a constant. Next, since $\mathbf{M}$ is a constant vector $\mathbf{M}_0$, the equation

$$I^2\omega_{x1}^2 + J^2\omega_{y1}^2 + K^2\omega_{z1}^2 = \mathbf{M}^2 = \mathbf{M}_0^2 \ldots\ldots [36]$$

yields another integral.

Replace the components of $\boldsymbol{\omega}$ by x_1, y_1, z_1 in Equations [35], [36]. The former equation yields an ellipsoid

$$\frac{1}{2}(Ix_1^2 + Jy_1^2 + Kz_1^2) = T \ldots\ldots\ldots\ldots [37]$$

which for $T = 1$ will be recognized as the ellipsoid of inertia for the gyro rotor. Similarly, Equation [36] leads (for unequal I, J, K) to an ellipsoid which is different from the ellipsoid of Equation [35]. The intersection of the two ellipsoids for various M_0^2/T gives the possible paths C_E of $\boldsymbol{\omega}$ in the R_1-space. The family of curves C_E is shown on Fig. 6.[6,7]

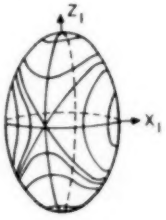

FIG. 6 POSSIBLE LOCI OF ROTATION VECTORS IN SPACE R_1

Consider next the dot product of $\boldsymbol{\omega}$ by $\mathbf{M}_0$ (with the same substitution of $x_1, \ldots$ in place of $\omega_{x1}, \ldots$)

$$\boldsymbol{\omega} \cdot \mathbf{M} = Ix_1^2 + Jy_1^2 + Kz_1^2 = 2T \ldots\ldots\ldots [38]$$

From the constancy of the right-hand member of Equation [38] it follows that in the fixed space (R_4) the end point of the vector $\boldsymbol{\omega}$ lies on a fixed plane B-B which is normal to the invariant vector $\mathbf{M}_0$. Let Q, Fig. 7, be the point of intersection of $\mathbf{M}_0$ with this plane; then from Equation [38] it follows that

$$OQ = d = 2T/M_0 \ldots\ldots\ldots\ldots [39]$$

From Equations [25], [35] it will be noted that in R_1, with x_1, y_1, z_1 unrestricted, $\mathbf{M}$ is the gradient of the function $T(x_1, y_1, z_1)$

$$\mathbf{M} = \text{grad } T = \nabla T \ldots\ldots\ldots\ldots [40]$$

Hence $\mathbf{M} = Ix_1\mathbf{i}_1 + Jy_1\mathbf{j}_1 + Kz_1\mathbf{k}_1$ is normal to the ellipsoid, Equation [37], at x_1, y_1, z_1, the end point of $\boldsymbol{\omega}$. Therefore the ellipsoid, Equation [37], touches the fixed plane B-B at the end point of the rotation vector $\boldsymbol{\omega}$. Since the points of $\boldsymbol{\omega}$ are instantaneously at rest, no slipping can occur between the ellipsoid and the plane B-B at their contact point P. Hence the motion of R_1 may be described by saying that the ellipsoid which is fixed in R_1, has its center fixed at O, and rolls without slipping on the fixed plane B-B. The body cone C_1 is the cone joining O to the proper curve C_E in Fig. 7.

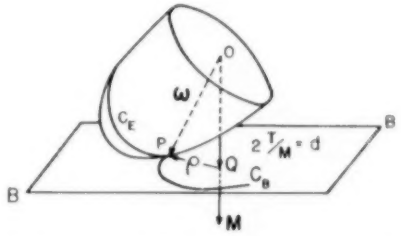

FIG. 7 ROLLING OF INERTIA ELLIPSOID ON FIXED PLANE

At the ellipsoid rolls without slipping on the fixed plane B-B, the contact point P (the end point of $\boldsymbol{\omega}$) describes on B-B a plane curve C_B from which the space cone C is obtained by joining its points to O; the curve C_B is shown as a plane curve in Fig. 7. Since no slipping occurs between C_E, C_B, at corresponding points which are at the same distance from O

$$ds_E^2 = ds_B^2 = \rho^2\,d\theta^2 + d\rho^2, \quad \rho^2 = r^2 - d^2, \quad d = 2T/M_0 \ldots [41]$$

where ds_E, ds_B are the elements of length along C_E, C_B, and ρ, θ polar co-ordinates in B-B with the pole $\rho = 0$ at Q. The curve C_B, in general, is not a closed curve. Let C_B be expressed in the polar form

$$\rho = f(\theta) \ldots\ldots\ldots\ldots [42]$$

with $\theta = 0$ corresponding to one of the four points of symmetry of C_E; the function $f(\theta)$ is periodic in θ, of period Π generally different from π, and $f(\theta)$ is symmetric in θ about $\theta = 0$, $\theta = \Pi/2$. A complete description of C_E corresponds to an increase 2Π in θ. The general shape of C_B is shown in Fig. 8.

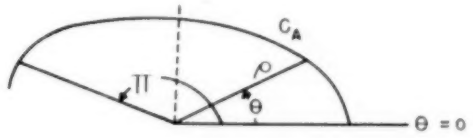

FIG. 8 PATH OF ROTATION VECTOR END POINT ON FIXED PLANE

To describe the motion in time we recall the analytical solution of the Equations [34]. Their integration is carried out by converting one of them into the form (here k is a proper constant)

$$\left(\frac{d\xi}{d\tau}\right)^2 = (1 - \xi^2)(1 - k^2\xi^2) \ldots\ldots\ldots [43]$$

obtained through elimination of two of the components ω_{x1}, ω_{y1}, ω_{z1} by means of Equations [35], [36], and introducing τ, ξ as proper multiples of t and the remaining ω-component.

[6] "Dynamics of Particles and of Rigid, Elastic and Fluid Bodies," by A. G. Webster, sections 82–88.

[5] "Introduction to Theoretical Physics," by L. Page, second edition, D. Van Nostrand Company, Inc., New York, N. Y., 1935, section 42.

[7] Based on a figure from reference 6, p. 135.

The solution of Equation [43] leads to the elliptic integral of the first kind

$$\tau = \int d\tau = \int \frac{d\xi}{[(1-\xi^2)(1-k^2\xi^2)]^{1/2}} = sn^{-1}\,\xi \quad [44]$$

yielding for ξ the sn-function

$$\xi = sn\tau \quad [45]$$

The other two ω-components likewise may be expressed in terms of the elliptic functions cn, dn defined by

$$\left.\begin{aligned} cn\tau &= \sqrt{1-sn^2\tau} \\ dn\tau &= \sqrt{1-k^2\,sn^2\tau} \end{aligned}\right\} \quad [46]$$

More explicitly, assuming that

$$I > J > K \quad [47]$$

one obtains the following results:[8]

Case (a): If

$$M^2 > 2JT \quad [48]$$

then the solution of Equations [34] is given by

$$\omega_{x1} = P\,dn\tau, \quad \omega_{y1} = -Q\,sn\tau, \quad \omega_{z1} = R\,cn\tau \quad [49]$$

where, with positive radicals

$$\left.\begin{aligned} \tau &= p(t-t_0) \\ P^2 &= \frac{M^2-2KT}{I(I-K)},\quad Q^2 = \frac{2TI-M^2}{J(I-J)},\quad R^2 = \frac{2IT-M^2}{K(I-K)} \\ p^2 &= \frac{(M^2-2KT)(I-J)}{IJK}, \\ k^2 &= \frac{(J-K)(2IT-M^2)}{(I-J)(M^2-2KT)} \end{aligned}\right\} \quad [50]$$

Case (b): If

$$M^2 < 2JT \quad [51]$$

then the solution of Equations [34] is given by

$$\omega_{x1} = P\,cn\tau, \quad \omega_{y1} = -Q\,sn\tau, \quad \omega_{z1} = R\,dn\tau \quad [52]$$

where P, R, τ are as in Equation [50] and

$$\left.\begin{aligned} Q^2 &= \frac{M^2-2TK}{J(J-K)} \\ p^2 &= \frac{(2IT-M^2)(J-K)}{IJK} \\ k^2 &= \frac{(I-J)(M^2-2KT)}{(J-K)(2IT-M^2)} \end{aligned}\right\} \quad [53]$$

These two cases correspond to the two sets of closed curves in Fig. 6 which are separated by the plane curves passing through the y_1-axis. Case (a) corresponds to polhode curves C_E enclosing the x_1-axis; case (b) to the curves C_E enclosing the z_1-axis.

For a gyro rotor rotating about the x_1-axis the convention of labeling axes to satisfy Equation [47] may contradict the choice of x_1-axis as the spin axis, and a proper permutation of the coordinates x_1, y_1, z_1 in Equations [47] to [70] may be required.

To complete the determination of the motion choose the z-axis in Figs. 1, 2 along the vector $\mathbf{M}_0$

$$\mathbf{M} = \mathbf{M}_0 = M_0\,\mathbf{k} \quad [54]$$

[8] Reference 4, p. 409.

Introducing R_2-components in Equations [26] there results

$$\mathbf{M} = I\omega_{x1}\mathbf{i}_2 + (J\omega_{y1}\cos\alpha_1 - K\omega_{z1}\sin\alpha_1)\mathbf{j}_2 + (J\omega_{y1}\sin\alpha_1 + K\omega_{z1}\cos\alpha_1)\mathbf{k}_2 \quad [55]$$

while from Equation [54] there results

$$\mathbf{M} = M_0(-\sin\alpha_2\mathbf{i}_2 + \cos\alpha_2\mathbf{k}_2) \quad [56]$$

Upon equating $\mathbf{i}_2$-, $\mathbf{j}_2$-components, there follows

$$\sin\alpha_2 = -I\omega_{x1}/M_0 \quad [57]$$

$$\tan\alpha_1 = J\omega_{y1}/K\omega_{z1} \quad [58]$$

and recalling Equation [2]

$$\omega_{x2} = \omega_{x1} = \dot\alpha_1 - \dot\alpha_2\sin\alpha_2 \quad [59]$$

One obtains upon utilizing Equation [57]

$$\dot\alpha_3 = \frac{M}{I} + \frac{\dot\alpha_1}{\sin\alpha_2} = \frac{M}{I}\left(1 - \frac{\dot\alpha_1}{\omega_{x1}}\right) \quad [60]$$

Solving for $\dot\alpha_1$ from Equations [59], [34] there results

$$\dot\alpha_1 = \omega_{x1}\left[1 - \frac{I(J\omega_{y1}^2 + K\omega_{z1}^2)}{J^2\omega_{y1}^2 + K^2\omega_{z1}^2}\right] \quad [61]$$

and upon substituting in Equation [59] and integrating

$$\alpha_3\Big]_0^t = M\int_0^t \frac{J\omega_{y1}^2 + K\omega_{z1}^2}{J^2\omega_{y1}^2 + K^2\omega_{z1}^2}\,dt \quad [62]$$

After expressing t, ω_{z1} in terms of ω_{y1} by means of Equations [49] to [53] one obtains an integral which may be expressed in terms of elliptic integrals of the first and third kinds. Corresponding to a complete description of C_E and an increase of[9] $4K^*$ in τ in Equation [49], [53], α_3 increases by a period $2\,\Pi$.

The path of the end point of $\mathbf{i}_1 = \mathbf{i}_2$ is determined by α_3 and α_2. This path is generally not a closed curve, and resembles the curve C_H in Fig. 8 (except for its being spherical, rather than plane).

With $\mathbf{i}_1$ determined as in the foregoing, Equation [58] determines α_1, and this completes the description of the motion of R_1.

The description of the motion of R_1 just given is based upon the choice of the axis A_3 along the invariant direction of $\mathbf{M}$. However, once the motion has been so obtained, it can be described in terms of the angles α_i in Fig. 2 for an arbitrary position of A_3 unrelated to $\mathbf{M}$. Fig. 9 shows schematically the curve C_{i1}, the

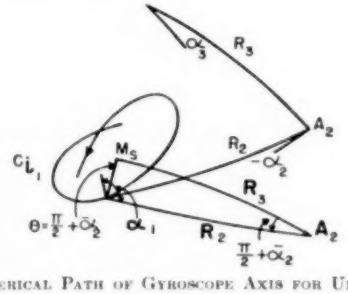

Fig. 9 Spherical Path of Gyroscope Axis for Unequal Moments of Inertia

path of $\mathbf{i}_1$, and the gimbals R_3, R_2 and angles α_2, α_3 both for the special choice of axes and for a general choice. This figure should be compared with Fig. 3.

[9] K^* is used in place of the usual K to avoid confusion with the moment of inertia about the z_1-axis.

Of interest also are the loci in R_1 described by the vector $\mathbf{M}_0$. From Equations [49] one obtains for the curve C_M described by the end point of $\mathbf{M}_0$

$$C_M: M_{x1} = IP\,dn\tau, \quad M_{y1} = -JQ\,sn\tau, \quad M_{z1} = KR\,dn\tau. \quad [63]$$

The curves C_M for various motions may be plotted in R_1 in a manner similar to the curves C_E, and are shown schematically in Fig. 10. They lie on a sphere of radius M_0, and may be obtained from C_E by stretching the ellipsoid in Fig. 6 in the ratios $I:1, J:1, K:1$.

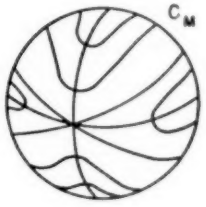

FIG. 10 (*left*) POSSIBLE LOCI OF FIXED MOMENTUM VECTOR RELATIVE TO THE SPACE R_1

As the motion proceeds the vector given by Equation [63] indicates the point of C_M which coincides with the fixed vector $\mathbf{M}_0$. To complete the determination of the displacement of R_1, a rotation about $\mathbf{M}_0$ is now effected such that the end point P of the corresponding $\boldsymbol{\omega}$-vector given by Equation [49] is brought into the invariant plane B-B in Fig. 7.

For a gyro rotor with high spin, say, about the x_1-axis, k^2 in Equation [50] is small, and, neglecting powers of k higher than k^2, Equations [49] reduce to

$$\omega_{x1} = P(1 - k^2 \sin^2 \tau/2), \quad \omega_{y1} = -Q \sin \tau, \quad \omega_{z1} = R \cos \tau \quad \ldots\ldots [64]$$

where τ, P, Q, R, p are given by Equations [50], and where Q, R are now small compared to P. The same result follows from Equations [34] when one neglects ω_{y1}, ω_{z1} in comparison with ω_{x1}. The curves C_E thus reduce to ellipses, described with a period $2\pi/p$ and average angular velocity $-p$.

Neglecting k^2-terms one obtains from the foregoing equations the following values and relations

$$\omega_{x1} = P, \quad 2T = IP^2, \quad M = IP,$$

$$p^2 = P^2(I - K)(I - J)/JK \quad \ldots\ldots [65]$$

$$\sin \alpha_2 \doteq -1, \quad \alpha_2 \doteq -\pi/2 \quad \ldots\ldots [66]$$

$$\tan \alpha_1 = -\frac{JQ}{KR} \tan \tau = -\sqrt{\frac{J(I-K)}{K(I-J)}} \tan \tau \quad \ldots [67]$$

$$\dot{\alpha}_2 = -\dot{\alpha}_1 + P \quad \ldots\ldots [68]$$

From Equations [67], [68] it will be seen that

$$\dot{\alpha}_1 = -p \quad \ldots\ldots [69]$$

$$\bar{\dot{\alpha}}_3 = p + P = P\left[1 + \sqrt{\frac{(I-K)(I-J)}{JK}}\right] = q \quad \ldots [70]$$

where bars denote average or mean values. The last relation agrees with Equation [15] for $J = K$.

A similar treatment is possible for nutations near the K-axis of inertia. On the other hand, rotations initially near the J-axis are unstable, and their curves C_E, C_A depart widely from the neighborhood of the J-axis as the motion proceeds.

4 INERTIA OF THE GIMBAL RINGS

We shall now include the effect of inertia of the gimbals, returning, however, to the assumption $J = K$. Furthermore, it is assumed that R_2, R_3 (as well as R_1) are perfectly balanced, so that O is the center of gravity of all the R_i, and A_1, A_2 are principal axes of inertia of R_2, hence that $\mathbf{i}_2$, $\mathbf{j}_2$, $\mathbf{k}_2$ are its three principal axes of inertia, with I_2, J_2, K_2 the principal moments of inertia about the axes, and A_3 a principal axis of inertia of R_3 with K_3 as its moment of inertia.

As pointed out in section 1, the motions of R_3, R_2, R_1 are specified by the rotation vectors

$$\left.\begin{aligned} \boldsymbol{\omega}_3 &= \dot{\alpha}_3\mathbf{k}_3 \\ \boldsymbol{\omega}_2 + \boldsymbol{\omega}_3 &= \dot{\alpha}_2\mathbf{k}_3 + \dot{\alpha}_2\mathbf{j}_2 \\ \boldsymbol{\omega} = \boldsymbol{\omega}_1 + \boldsymbol{\omega}_2 + \boldsymbol{\omega}_3 &= \dot{\alpha}_1\mathbf{k}_3 + \dot{\alpha}_2\mathbf{j}_2 + \dot{\alpha}_3\mathbf{i}_1 \end{aligned}\right\} \quad \ldots\ldots [71]$$

respectively. Introducing the R_2-components, adding the separate $\mathbf{M}$ and T, there results

$$\mathbf{M} = [I\dot{\alpha}_1 - (I + I_2 + K_3)\dot{\alpha}_3 \sin \alpha_2]\mathbf{i}_2 + (K + J_2)\dot{\alpha}_2\mathbf{j}_2 + (K + K_2 + K_3)\dot{\alpha}_3 \cos \alpha_2 \mathbf{k}_2 \quad \ldots\ldots [72]$$

$$2T = I(\dot{\alpha}_1 - \dot{\alpha}_3 \sin \alpha_2)^2 + (K + J_2)\dot{\alpha}_2^2 + [K_3 + K + K_2 \cos^2 \alpha_2 + I_2 \sin^2 \alpha_2]\dot{\alpha}_3^2 \quad \ldots\ldots [73]$$

One is led to the Lagrange equations

$$\left.\begin{aligned} I\frac{d}{dt}(\dot{\alpha}_1 - \dot{\alpha}_3 \sin \alpha_2) &= Q_{\alpha 1} \\ (K + J_2)\frac{d\dot{\alpha}_2}{dt} + I\dot{\alpha}_1\dot{\alpha}_3 \cos \alpha_2 & \\ -(I - K + I_2 - K_2)\dot{\alpha}_3^2 \sin \alpha_2 \cos \alpha_2 &= Q_{\alpha 2} \\ \frac{d}{dt}[(K + K_2 + K_3)\dot{\alpha}_3 + (I - K + I_2 - K_2)\dot{\alpha}_3 \sin^2 \alpha_2 & \\ - I\dot{\alpha}_1 \sin \alpha_2] &= Q_{\alpha 3} \end{aligned}\right\} \quad \ldots [74]$$

Comparing these with Equations [10] it will be noted that the first equation has not been changed, while the second and third equations retain their general form except for certain changes in the values of the constant coefficients, namely, the values of inertia terms. However, no unique change of inertias enables one to pass from Equations [10] to Equations [74].

Again, comparing with the case studied in the preceding section of negligible R_2, R_3 inertias and three unequal R_1-inertias, it will be found that the two cases cannot be reduced one to the other by replacing one set of the inertia constants by another one.

We consider the case of zero applied torques and zero friction torques in the gimbals, $Q_{\alpha i} = 0$. Then $\mathbf{M}$ is a constant vector in space, and T also may be shown to be constant. Unlike the case $J \neq K$ and negligible R_2, R_3 inertias, the integrals

$$\mathbf{M} = \mathbf{M}_0, \quad \mathbf{M}^2 = \text{const} \quad \ldots\ldots [75]$$

$$T = \text{const} \quad \ldots\ldots [76]$$

do not lead to simple equations for the polhode curves (paths of $\boldsymbol{\omega}$) in the R_1-system, due to the fact that R_3 is always tied down to the fixed axis A_3 and R_2 is partially tied down to A_3 (namely, by having A_2 normal to A_3). The shape of the solutions of Equations [75], [76] (the polhode curves) in R_1 is therefore not independent of α_2, α_3.

For $Q_{\alpha 1} = 0$ the first Equation [74] integrates into

$$\dot{\alpha}_1 - \dot{\alpha}_3 \sin \alpha_2 = A \quad \ldots\ldots [77]$$

where A is a constant; this shows that ω_{x1} is constant. This relation may be used to eliminate $\dot{\alpha}_1$ from the second Lagrange Equation [74] which takes on the form (for $Q_{\alpha 2} = 0$)

$$(K + J_2)\frac{d\dot{\alpha}_2}{dt} + IA\,\dot{\alpha}_3 \cos \alpha_2 + (K - I_2 - K_2)\dot{\alpha}_3 \sin \alpha_2 \cos \alpha_2 = 0 \quad \ldots\ldots [78]$$

and from the third one which integrates (for $Q_{\alpha_3} = 0$) into

$$\dot{\alpha}_3 [(K + K_2 + K_3) + (I_2 - K - K_2) \sin^2 \alpha_2] = C + AI \sin \alpha_2 \quad [79]$$

where C is a proper constant. Elimination of $\dot{\alpha}_3$ leads to the second-order differential equation for α_2

$$(K + J_2)\ddot{\alpha}_2 + \frac{[IA \cos \alpha_2 + (K - I_2 - K_2) \sin \alpha_2 \cos \alpha_2] [C + AI \sin \alpha_2]}{(K + K_2 + K_3) + (I_2 - K - K_2) \sin^2 \alpha_2} = 0 \quad [80]$$

A first integral of this is furnished by

$$(K + J_2)\dot{u}^2 + 2(1 - u^2)F(u) = 0 \quad [81]$$

where $u = \sin \alpha_2$ and F is a proper integral of the second term in Equation [80]

$$u = \sin \alpha_2, \; F(u) = \int \frac{[IA + (K - I_2 - K_2)u][C + AIu]}{(K + K_2 + K_3) + (I_2 - K - K_2)u^2} \, du \quad [82]$$

This integration is expressible in the form

$$F(u) = \text{const } u + \text{const} \ln (u - r) + \text{const} \ln (u + r)$$

where

$$r = \sqrt{\frac{K + K_2 + K_3}{K + K_2 - I_2}} \quad [83]$$

but the next integration leading to u as a function of time

$$\int dt = \sqrt{K + J_2} \int \frac{du}{\sqrt{2(1 - u^2)F(u)}} \quad [84]$$

cannot be carried out in terms of elementary functions.*

A somewhat different set of differential equations is obtained by equating the components of the constant vector $\mathbf{M}$ in the R_2-system, given by Equation [72], to the right-hand members of the first Equation [75]. No loss of generality results from a choice of the fixed axes so that $M_y = 0$, whereupon there follows upon recalling Equation [77]

$$\begin{aligned} (I_2 + K_3)\dot{\alpha}_3 \sin \alpha_2 &= IA - M_x \cos \alpha_3 \cos \alpha_2 + M_z \sin \alpha_2 \\ (K + J_2)\dot{\alpha}_2 &= -M_x \sin \alpha_3 \\ (K + K_2 + K_3)\dot{\alpha}_3 \cos \alpha_2 &= M_x \cos \alpha_3 \sin \alpha_2 + M_z \cos \alpha_2 \end{aligned} \quad [85]$$

Multiplying the first equation by $\sin \alpha_2$, the third one by $\cos \alpha_2$, and adding, there results

$$\dot{\alpha}_3 [(I_2 + K_3) \sin^2 \alpha_2 + (K + K_2 + K_3) \cos^2 \alpha_2] = IA \sin \alpha_2 + M_z \quad [86]$$

and this can be identified with Equation [79], showing that $C = M_z$. From Equation [86] and the second Equation [85] follows

$$-\frac{M_x \sin \alpha_3 \, d\alpha_3}{(K + J_2) \, d\alpha_2} = \frac{IA \sin \alpha_2 + M}{(K + K_2 + K_3) + (I_2 - K - K_2) \sin^2 \alpha_2} \quad [87]$$

This integrates into

$$\left.\begin{aligned} &\frac{M_x \cos \alpha_3}{(K + J_2)} = G(\alpha_2)] \\ &\text{where} \\ &G(\alpha_2) = \int \frac{[IA \sin \alpha_2 + M_z] \, d\alpha_2}{(K + K_2 + K_3) + (I_2 - K - K_2) \sin^2 \alpha_2} \end{aligned}\right\} \quad [88]$$

As in Equation [82], the integral can be expressed in terms of elementary functions.

Equation [88] yields α_2 as a function of α_2 and enables one to calculate the path described by the A_1-axis. However, to determine the manner in which this path is described in time requires a further integration for t derived from Equation [86] or [85].

Steady rotation of R_1 about a fixed axis A_1 with stationary R_2, R_3, is of course, a possible motion even when R_2, R_3 possess inertia. It is represented by

$$\dot{\alpha}_1 = s = \text{const} = A, \quad \dot{\alpha}_2 = \dot{\alpha}_3 = 0 \quad [89]$$

Equation [72] now yields

$$\mathbf{M} = I\dot{\alpha}_1 \mathbf{i}_2 \quad [90]$$

and, expressing $\mathbf{i}_2$ in terms of $\mathbf{i}$, $\mathbf{j}$, $\mathbf{k}$ from Fig. 2

$$\mathbf{M} = I\dot{\alpha}_1 [\mathbf{i} \cos \alpha_3 \cos \alpha_2 + \mathbf{j} \sin \alpha_3 \cos \alpha_2 - \mathbf{k} \sin \alpha_2] \quad [91]$$

Under the assumption $M_y = 0$ used above Equation [89] yields

$$\alpha_3 = 0 \quad [92]$$

$$M_x = IA \cos \alpha_2, \quad M_z = -IA \sin \alpha_2 \quad [93]$$

and these relations are verified from Equations [85], [86] when $\dot{\alpha}_2$, $\dot{\alpha}_3$ are equated to zero.

We consider next small nutations near the steady rotation just considered. For small displacements from $\alpha_2 = \alpha_{20}$, $\alpha_3 = 0$ Equations [85], [86], [93] yield the linearized differential equations

$$\left.\begin{aligned} (K + J_2)\ddot{\alpha}_2 &= -M_x \alpha_3 \\ [(K + K_2 + K_3) + (I_2 - K - K_3) \sin^2 \alpha_{20}] \, \dot{\alpha}_3 &= IA \cos \alpha_{20} (\alpha_2 - \alpha_{20}) \end{aligned}\right\} \quad [94]$$

Expressing M_x, A in terms of s from Equations [90], [93] there results for $\alpha_2 - \alpha_{20}$, α_3 exponential solutions $e^{\lambda t}$ leading to (approximately) elliptic curves C_{λ} for the $\mathbf{i}_1$-vector, described with (angular) frequency λ, where

$$\lambda^2 = \frac{s^2 I^2 \cos^2 \alpha_2}{(K + J_2)[(K + K_2 + K_3) + (I_2 - K - K_2) \sin^2 \alpha_2]} \quad [95]$$

This frequency depends upon the gimbal and gyro inertias, as well as upon the angle α_2. Equation [95] agrees with Equation [15] for vanishing gimbal inertias.

A Comprehensive Stability Criterion for Forced Vibrations in Nonlinear Systems

By K. KLOTTER[1] and E. PINNEY[2]

This paper deals with the forced vibrations described by the differential equation

$$a\ddot{q} + cq + c\Phi(q, \dot{q}) = P \cos \Omega t$$

wherein Φ denotes a nonlinear function of q and/or $\dot{q}$. It presents a criterion for determining their stability. It is shown that under very weak restrictions, which equivalently means, for a large variety of cases (including all of practical importance) the stability depends on the sign of $\partial q^*/\partial P$ (q^* denoting the maximum value of $q(t)$ within a period). The motion is stable if this derivative is positive; it is unstable if it is negative.

Formulation of Problem

THE investigations in this paper pertain to the forced vibrations in a so-called quasilinear system, as described by the differential equation

$$a\ddot{q} + cq + c\Phi(q, \dot{q}) = P \cos \Omega t \quad \ldots\ldots\ldots\ldots [1]$$

where Φ denotes a nonlinear function of q and/or $\dot{q}$ of not too large numerical value, so that the deviation from linearity is within certain limits. Vibrations of this kind have already been given considerable attention.

In many cases one is not so much interested in the steady-state periodic solution $q(t)$ itself, but rather in the maximum value $\max(q) = q^*$ of that function within a period, and in how this maximum value q^* depends on the frequency Ω of the driving term $P \cos \Omega t$. The plot of q^* versus Ω or Ω^2 is known as a response curve, and the function describing the relation as a response function.

Even for rather simple expressions $\Phi(q, \dot{q})$, as, e.g., $\Phi = \mu^2 q^2$ (μ^2 being a constant), Equation [1] has no known exact solution. One, therefore, must resort to methods of integration which provide approximate results. A considerable number of such methods have been suggested and are in use.[3] The more prominent among them are perturbation and iteration methods of various types and the averaging methods, for which the so-called Ritz or Galerkin method may be quoted as an example.[4] Every one of these methods may lead to curves for which Fig. 1 gives two qualitative examples. Once these response curves are established, the next concern is to decide whether the motion corresponding to any one point on these curves is a stable one or not. By this expression we mean, whether a slight disturbance to the motion tends to fade away or tends to build up. The intermediate case, where a disturbance continues to have the original magnitude, may be reckoned among either the stable or the unstable cases, as some particular viewpoint may suggest.

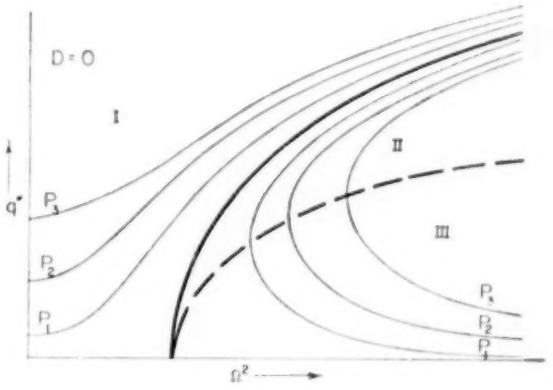

Fig. 1(*a*)

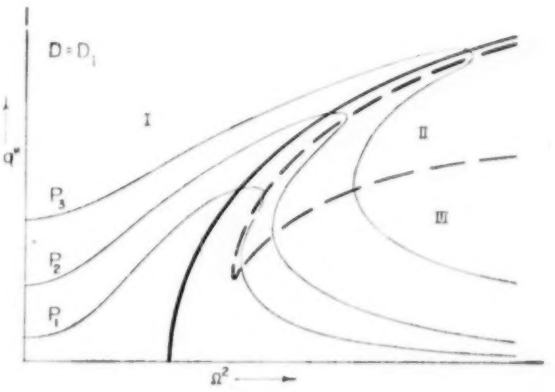

Fig. 1(*b*)

---

[1] Professor of Engineering Mechanics, Stanford University, Stanford, Calif.

[2] Associate Professor of Mathematics, University of California, Berkeley, Calif.

[3] "Non-Linear Vibrations," by J. J. Stoker, Interscience Publishers, Inc., New York, N. Y., 1950.

[4] "Nonlinear Vibration Problems Treated by the Averaging Method of W. Ritz," by K. Klotter, Contract N6-onr-251-2, Technical Report 17, Part I, Part II, Stanford University, or Proceedings of First National Congress for Applied Mechanics, Chicago, Ill., 1951, Paper 140.

Presented at the West Coast Meeting of the Applied Mechanics Division, Los Angeles, Calif., June 26–28, 1952, of The American Society of Mechanical Engineers.

Discussion of this paper should be addressed to the Secretary, ASME, 29 West 39th Street, New York, N. Y., and will be accepted until April 10, 1953, for publication at a later date. Discussion received after the closing date will be returned.

Note: Statements and opinions advanced in papers are to be understood as individual expressions of their authors and not those of the Society. Manuscript received by ASME Applied Mechanics Division, January 25, 1952.

One way toward the answer to this question is to set up a differential equation for a variational quantity δ, in the dependent variable q, of small amount, thus allowing linearization, and to inspect the long-range behavior of the solution of this linear differential equation. Investigations along this line have been carried out for particular cases, especially for the "Duffing equation,"[5] when $\Phi = \mu^2 q^3$. The differential equation for the variational quantity δ, in this case, is a Mathieu equation, and the behavior of its solution as to stability is well known; it is fully described by the so-called Ince-Strutt chart.

This method, which up to the present time has been applied to special cases only, allows considerable generalizations. Even the generalizations of this method, however, are confined to certain classes of nonlinearities $\Phi(q, \dot{q})$. So far no general rule or criterion has been offered which would allow one to determine the stability of the motion from a comprehensive point of view. It is the purpose of the present paper to tender a criterion which has a wide range of applicability.[6]

The Criterion

In the response diagrams of many special cases, for which Fig. 1 shows the prototype, we can distinguish three regions, denoted by I, II, and III, respectively. In regions I and III the sequence of the individual curves in the family of curves is such that, for a fixed value of Ω, q^* increases as the parameter P increases, whereas in region II, q^* decreases as P increases. In other words, Regions I and III are characterized by $\partial q^*/\partial P > 0$, region II by $\partial q^*/\partial P < 0$. In all special cases, which have been investigated, regions I and III contain the representative points of a stable motion, whereas region II contains the points representing an unstable motion.

From these special cases one may derive the conjecture that

$$\frac{\partial q^*}{\partial P} \gtrless 0 \qquad [2]$$

will be a very general stability criterion.

In the next two sections we will prove that the conjecture holds true under very weak restrictions and we will establish and discuss the conditions of its validity.

Derivation of "Significant Equation"

We rewrite Equation [1] by dividing it by the factor a of $\ddot{q}$

$$E \equiv \ddot{q} + \kappa^2 q + \kappa^2 \Phi(q, \dot{q}) - p \cos \Omega t = 0 \qquad [3]$$

making use of the abbreviations

$$\kappa^2 = \frac{c}{a} \quad \text{and} \quad p = \frac{P}{a} \qquad [4]$$

Under the assumption that the driving frequency Ω does not differ too much from κ (the natural frequency of the linearized system), we may adopt the procedure known in the literature on nonlinear systems as the method of Kryloff-Bogoliuboff.[7]

The procedure starts out with giving the function $q(t)$ the form

$$q = Q(t) \cos [\kappa t + \varphi(t)] \qquad [5]$$

or, denoting

$$\kappa t + \varphi(t) = x(t) \qquad [5a]$$

equivalently

$$q = Q(t) \cos x(t) \qquad [5b]$$

Assuming

$$\dot{Q} \cos x - Q\dot{\varphi} \sin x = 0 \qquad [6]$$

the first and second derivatives of q become

$$\dot{q} = -\kappa Q \sin x \qquad [7]$$

and

$$\ddot{q} = -\kappa \dot{Q} \sin x - \kappa^2 Q \cos x - \dot{\varphi} \kappa Q \cos x \qquad [8]$$

respectively. Inserting $\ddot{q}$ into Equation [3] and dividing by κ we obtain the first equation of the following set, the second being identical with Equation [6]

$$\left.\begin{aligned} -\dot{Q} \sin x - \dot{\varphi}\, Q \cos x + \kappa \Phi(q, \dot{q}) &= \frac{p}{\kappa} \cos \Omega t \\ \dot{Q} \cos x - \dot{\varphi} Q \sin x &= 0 \end{aligned}\right\} \qquad [9]$$

Multiplying these equations first by $-\sin x$ and $\cos x$, respectively, second by $\cos x$ and $\sin x$, and adding, we obtain in turn

$$\left.\begin{aligned} \dot{Q} &= \kappa \Phi(q, \dot{q}) \sin x - \frac{p}{\kappa} \cos \Omega t \sin x \\ Q\dot{\varphi} &= \kappa \Phi(q, \dot{q}) \cos x - \frac{p}{\kappa} \cos \Omega t \cos x \end{aligned}\right\} \qquad [10]$$

In view of the assumptions made (Φ and p sufficiently small) $\dot{Q}$ and $\dot{\varphi}$ are small, meaning that $Q(t)$ and $\varphi(t)$ are slowly varying functions of time.

Now we introduce a new argument into the trigonometric functions by putting

$$\vartheta(t) = \varphi(t) + (\kappa - \Omega)t \qquad [11a]$$

then

$$\Omega t = \varphi(t) + \kappa t - \vartheta(t) = x(t) - \vartheta(t) \qquad [11b]$$

After denoting

$$\left(1 - \frac{\Omega}{\kappa}\right) = \Delta \qquad [11c]$$

Equations [10] become

$$\left.\begin{aligned} \kappa \dot{Q} &= \kappa^2 \Phi \sin x - p \sin x (\cos x \cos \vartheta + \sin x \sin \vartheta) \\ \kappa \dot{\vartheta} Q &= \kappa^2 \Phi \cos x - p \cos x (\cos x \cos \vartheta + \sin x \sin \vartheta) \\ &\qquad + \kappa^2 Q \Delta \end{aligned}\right\} \qquad [12]$$

It was noted previously that both Q and φ are slowly varying functions of time; the same remark applies to ϑ, if $\Delta \ll 1$.

According to the general procedure of the adopted method, we now derive the average value of both $\dot{Q}$ and $\dot{\vartheta}$, denoted by $\bar{\dot{Q}}$ and $\bar{\dot{\vartheta}}$, by integrating over a period of $\sin x$ and $\cos x$ and dividing by the length of the period. Thus we obtain

$$\left.\begin{aligned} \kappa \bar{\dot{Q}} &= \frac{\kappa^2}{2\pi} \int_0^{2\pi} \Phi(q, \dot{q}) \sin x \, dx - \frac{p}{2} \sin \vartheta \\ \kappa \bar{\dot{\vartheta}} Q &= \frac{\kappa^2}{2\pi} \int_0^{2\pi} \Phi(q, \dot{q}) \cos x \, dx - \frac{p}{2} \cos \vartheta + \kappa^2 Q \Delta \end{aligned}\right\} \qquad [13]$$

[5] See footnote 3, p. 213, et seq.

[6] For more specific systems, investigations leading to similar results are included in the following: "On Simple Harmonic Vibrations of a System With Non-Linear Characteristics," by F. John, Studies in Nonlinear Vibration Theory, Institute for Mathematics and Mechanics, New York University, New York, N. Y., 1946.

[7] "Introduction to Non-Linear Mechanics," by N. Kryloff and N. Bogoliuboff. Translated by S. Lefschetz, Princeton University Press, Princeton, N. J., 1949.

Introducing the abbreviations

$$s = \frac{p}{\kappa^2} = \frac{P}{c} \quad \ldots\ldots [14a]$$

and

$$\left.\begin{aligned} S(Q) &= \frac{1}{2\pi}\int_0^{2\pi} \Phi(q, \dot{q}) \sin x \, dx \\ C(Q) &= \frac{1}{2\pi}\int_0^{2\pi} \Phi(q, \dot{q}) \cos x \, dx \end{aligned}\right\} \quad \ldots\ldots [14b]$$

Equations [13] may be written

$$\left.\begin{aligned} \frac{1}{\kappa}\dot{Q} &= S(Q) - \frac{s}{2}\sin\vartheta \\ \frac{1}{\kappa}\dot{\vartheta}\,Q &= C(Q) - \frac{s}{2}\cos\vartheta + Q\Delta \end{aligned}\right\} \quad \ldots\ldots [15]$$

These equations, the result of applying the Kryloff-Bogoliuboff procedure, are the starting point for a new line of reasoning. In the steady state

$$\dot{Q} = 0, \quad \dot{\vartheta} = 0 \quad \ldots\ldots [16a]$$

the constant values of Q and ϑ being denoted by

$$Q = Q_0, \quad \vartheta = \vartheta_0 \quad \ldots\ldots [16b]$$

Therefore the quantities with subscript zero satisfy the pair of relations

$$\left.\begin{aligned} S(Q_0) &= \frac{s}{2}\sin\vartheta_0 \\ Q_0\Delta + C(Q_0) &= \frac{s}{2}\cos\vartheta_0 \end{aligned}\right\} \quad \ldots\ldots [17]$$

from which follows

$$\left.\begin{aligned} \left(\frac{s}{2}\right)^2 &= S^2(Q_0) + [C(Q_0) + Q_0\Delta]^2 \\ \tan\vartheta_0 &= \frac{S(Q_0)}{C(Q_0) + Q_0\Delta} \end{aligned}\right\} \quad \ldots\ldots [18]$$

The quantities Q and ϑ themselves may now be expressed by their mean values Q_0 and ϑ_0 and the deviations ξ and η

$$Q = Q_0 + \xi, \quad \vartheta = \vartheta_0 + \eta \quad \ldots\ldots [19]$$

By Equations [15] ξ and η satisfy the differential equations

$$\left.\begin{aligned} \dot{\xi}/\kappa &= \xi\, S'(Q_0) - \frac{s}{2}\,\eta\cos\vartheta_0 \\ Q_0\dot{\eta}/\kappa &= \xi[C'(Q_0) + \Delta] + \frac{s}{2}\,\eta\sin\vartheta_0 \end{aligned}\right\} \quad \ldots\ldots [20]$$

These are two simultaneous linear differential equations of first order with constant coefficients. They can be integrated by adopting the familiar procedure assuming

$$\xi = Ae^{\lambda t}, \quad \eta = Be^{\lambda t} \quad \ldots\ldots [21]$$

A and B, then, have to satisfy the pair of homogeneous algebraic equations

$$\left.\begin{aligned} A\left[\frac{h}{\kappa} - S'(Q_0)\right] + B\,\frac{s}{2}\cos\vartheta_0 &= 0 \\ -A\,[C'(Q_0) + \Delta] + B\left[Q_0\frac{h}{\kappa} - \frac{s}{2}\sin\vartheta_0\right] &= 0 \end{aligned}\right\} \quad \ldots\ldots [22]$$

which are compatible only if the determinant of their coefficients vanishes. This condition, by making use of the first of Equations [17], leads to the quadratic equation for h/κ

$$\left(\frac{h}{\kappa}\right)^2 Q_0 - \left(\frac{h}{\kappa}\right)\left[S(Q_0) + Q_0 S'(Q_0)\right] + S(Q_0)S'(Q_0) + [C'(Q_0) + \Delta]\,[Q_0\Delta + C(Q_0)] = 0 \quad \ldots [23]$$

By differentiating the first Equation [18] we obtain

$$\frac{s}{2}\,\frac{d\left(\frac{s}{2}\right)}{dQ_0} = SS' + (C + Q_0\Delta)(C' + \Delta)$$

and therefore Equation [23] may be written as follows

$$\left(\frac{h}{\kappa}\right)^2 Q_0 - \left(\frac{h}{\kappa}\right)[S(Q_0) + Q_0 S'(Q_0)] + \frac{s}{2}\,\frac{d\left(\frac{s}{2}\right)}{dQ_0} = 0 \quad \ldots [24]$$

Solving the quadratic equation we finally arrive at

$$\left(\frac{h}{\kappa}\right) = \frac{1}{2Q_0}\left\{[S(Q_0) + Q_0 S'(Q_0)] \pm \sqrt{[S + Q_0 S']^2 - Q_0 s\,\frac{ds}{dQ_0}}\right\} \quad \ldots\ldots [25]$$

an equation which we are going to call the "significant equation" because it contains the information regarding the stability, as will become clear from the discussion in the next section.

Discussion of Significant Equation

The motion $q(t)$ is stable, if the deviations ξ and η, described by Equations [19] and satisfying the set of differential Equations [20], do not tend to grow as time goes on; it is unstable, if they do. This means that the motion is stable if $\mathrm{Re}\,(h/\kappa) \leq 0$ and it is unstable if $\mathrm{Re}\,(h/\kappa) > 0$. (We include the stationary oscillatory behavior of ξ and η in the stable range.) From Equation [25] one concludes, therefore, that

$$[S(Q_0) + Q_0 S'(Q_0)] \leq 0 \text{ together with } (ds)/(dQ_0) > 0 \quad \ldots [26a]$$

insures stability

$$[S(Q_0) + Q_0 S'(Q_0)] \leq 0 \text{ together with } (ds)/(dQ_0) < 0 \quad [26b]$$

insures instability, whereas

$$[S(Q_0) + Q_0 S'(Q_0)] > 0 \quad \ldots\ldots [26c]$$

insures instability irrespective of the sign of $(ds)/(dQ_0)$. s being proportional to P (Equation [14a]), and Q_0 being the maximum value q^* of $q(t)$ in the notation of the first two sections, the sign of $(ds)/(dQ_0)$ is the same as that of $\partial q^*/\partial P$ in the former notation.

The result means that the criterion, as formulated in the second section, holds true provided that

$$B \equiv [S(Q_0) + Q_0 S'(Q_0)] \leq 0 \quad \ldots\ldots [27]$$

Then, the sign of $(ds)/(dQ_0)$ or equivalently $\partial q^*/\partial P$ decides on the stability. In case $B \equiv [S(Q_0) + Q_0 S'(Q_0)] > 0$ the criterion is not valid; the vibration, then, is unstable whatever the sign of $\partial q^*/\partial P$ may be.

It remains, now, to be shown that in all cases which we had in mind when speaking of the response curves in the first two sections, the expression B in Equation [27] is not positive, so that in those cases, the criterion is valid.

We assume that the nonlinear term $\Phi(q, \dot{q})$ in Equation [1] or [3] is composed of two constituents, each depending on q or $\dot{q}$ alone

$$\kappa^2\Phi(q, \dot{q}) = 2D\kappa g(\dot{q}) + \kappa^3 f(q) \quad [28]$$

where $g(\dot{q})$ (having the dimension of $\dot{q}$) and $f(q)$ (having the dimension of q) denote any (linear or nonlinear) single-valued functions of their respective arguments. This applies to systems where the restoring force depends merely on the displacement, the damping force merely on the velocity.

Considering Equations [5b] and [7] we find from the first equation of [14b]

$$2\pi S(Q_0) = \int_0^{2\pi} \left[\frac{2D}{\kappa} g(-\kappa Q_0 \sin x) + f(Q_0 \cos x) \right] \sin x \, dx \quad [29]$$

The second part of the integral vanishes identically, because

$$\int_0^{2\pi} f(Q_0 \cos x) \sin x \, dx = -\int_0^{2\pi} f(Q_0 \cos x) \, d(\cos x) = 0 \quad [29a]$$

for any single-valued function f. As to the function $g(\dot{q})$ we are going to specify that g be either zero or an odd function of $\dot{q}$, such that

$$g(\dot{q}) > 0 \text{ for } \dot{q} > 0$$

$$g(\dot{q}) < 0 \text{ for } \dot{q} < 0$$

(as e.g., for an actual damping force) and be either continuous throughout or discontinuous at $\dot{q} = 0$. In case g is continuous $g(0)$ is zero, of course.

With these specifications the expression for $S(Q_0)$ becomes

$$S(Q_0) = -\frac{2D}{\pi\kappa} \int_0^{\pi} g(\kappa Q_0 \sin x) \sin x \, dx \quad [30]$$

and, therefore

$$S'(Q_0) = -\frac{2D}{\pi} \int_0^{\pi} g'(\kappa Q_0 \sin x)(1 - \cos^2 x) \, dx \quad [31]$$

After splitting the second integral into two terms, applying integration by parts to the second term and inserting the results into the expression for B (Equation [27]), we end with

$$B = -\frac{2D}{\kappa} \left[\int_0^{\pi} g'(\kappa Q_0 \sin x) \, dx + \frac{2}{\kappa Q_0} g(+0) \right] \quad [32]$$

As B has to be either zero or negative, if the criterion is to be valid, one realizes that all depends on the sign of the derivative $g'(\dot{q})$. In case this derivative is either zero or positive throughout (as e.g., for $g = \text{const}$ with $g' = 0$ or $g = \dot{q} + \nu^2\dot{q}^3$ with $g' = 1 + 3\nu^2\dot{q}^2$, etc.) the expression B will not be positive, and the criterion is valid. In case g' is negative in parts of the interval of integration, there will be a limit for Q_0 beyond which the criterion ceases to be valid. This limit is determined by

$$-\int_0^{\pi} g'(\kappa Q_0 \sin x) \, dx = \frac{2}{\kappa Q_0} g(+0) \quad [33]$$

Take, the example

$$g(\dot{q}) = \dot{q} - \nu^2\dot{q}^3 \text{ with } g'(\dot{q}) = 1 - 3\nu^2\dot{q}^2 \quad [34a]$$

From Equation [33] the limit for Q_0 is determined by

$$\nu\kappa Q_0 = \sqrt{\frac{2}{3}} \quad [34b]$$

We do not intend to elaborate on other systems than those described by Equation [28]. Whenever other nonlinearities arise a discussion of Equation [27] will give the necessary information.

Acknowledgment

The results presented in this paper were obtained in the course of research conducted at Stanford University under a contract sponsored jointly by the Office of Naval Research and the Air Research and Development Command.

Rails on Elastic Foundations Under the Influence of High-Speed Traveling Loads

By H. E. CRINER[1] and G. D. McCANN,[2] PASADENA, CALIF.

This paper presents an electric-analog-computer technique for the analysis of beams on elastic foundations that are subjected to traveling loads. This method is applicable to the study of such conditions as nonuniform beams, load magnitude and velocity variations, and such nonlinear conditions as the beam leaving contact with the foundation for upward deflections. A general set of dimensionless solutions is presented for the specific case of a point load of constant magnitude and velocity traveling over an infinite uniform linear track beam. These show high values of deflection and moment for a rather narrow range of velocity above and below the critical velocities producing peak disturbances. It was found that quite high accelerations are required to produce significantly less disturbance than in the constant velocity case. A range of nonlinear track-bouncing conditions was studied in connection with a specific design problem. For none of these cases could more severe conditions be produced than indicated by the linear solutions.

Introduction

IN project SNORT the Naval Ordnance Test Station, Inyokern, is planning a high-speed test track capable of carrying relatively high carriage loads at very high speeds.

For the design of such tracks, dynamic loading considerations are of considerable importance. Therefore the problem was undertaken of calculating the motion and stresses for various designs of track beams imbedded in the earth and under the action of vertical loads traveling at various velocities. The results obtained are considered to be sufficiently comprehensive to be of general interest and have been prepared in dimensionless form suitable for general applications.

If calculations are restricted to the steady-state solution for a track of uniform characteristics under the action of a constant loading traveling at a fixed speed, the problem may be reduced to the solution of an ordinary differential equation by choice of a space co-ordinate system moving with the load. A few such solutions were obtained by numerical methods for the completely linear case. However, the time required for a sufficient number of even the simpler cases was estimated to be so long that this method was considered impracticable. Furthermore, it was desired to consider the effect of carriage acceleration and certain types of discontinuities in the track. Thus the problem had to be solved as a distributed constants system represented by a partial differential equation. Also, certain nonlinear cases were to be analyzed all of which made the direct electrical-mechanical analogy methods, used on the California Institute of Technology electric analog computer, seem most attractive.

Upon first consideration, however, there appeared to be one important difficulty in the application of such a computing technique. It seemed that if a direct electric-circuit analogy were to be set up for the finite-difference form of the track equation the number of finite-difference cells required for a steady-state constant velocity solution of the motion and stresses, on a long track, would be prohibitively large. To obtain an accurate solution for appreciable times after the starting of the carriage and at large distances from the ends of the track, long sections of track must be simulated. The maximum length that can be represented by a single finite-difference cell is limited by the wave length of the highest important frequency in the solutions.

From the initial numerical solutions which were obtained it was determined that the maximum permissible cell length had to be in the range of 2 to 10 ft (the value varying with the parameters of the problem). Only 50 cells could be set up conveniently on the computer so that only 100 to 500 ft of track could be simulated. However, the initial solutions indicated that for the practical range of damping provided by the earth, the total length covered by the solution (both in front of and behind the point load) would fall within this range for most cases of interest. It thus appeared that the very long track could be simulated on the computer by connecting the two ends of the electric circuit together and thereby obtaining an endless circular track. It was this interesting technique which permitted solutions for a difficult problem to be obtained quite rapidly. Of course as each solution was obtained it had to be examined to insure that sufficient track length had been simulated and that the individual cell lengths were not too great.

Electrical Analogies

A detailed general treatment of the basic electromechanical analogies for distributed elastic media has been given elsewhere.[3,4] However, since the rail with distributed linear and nonlinear restraints, such as imposed by earth imbedding, and the methods of simulating traveling loads have not been treated, their analogies will be developed.

Rail With Linear Earth Foundation. A continuous rail in simple bending without shear or rotary inertia but with linear earth constraints, consisting of spring coupling and damping, is described by the following partial differential equation

$$\frac{\partial^2}{\partial y^2}\left(EI\frac{\partial^2 h}{\partial y^2}\right) + m\frac{\partial^2 h}{\partial t^2} + K_f h + G\frac{\partial h}{\partial t} = F(y,t) \quad \ldots [1]$$

All quantities can be defined with reference to Fig. 1 which also presents the finite-difference elastic model of the track and the corresponding electrical analogy. All terms of Equation [1] are forces which also may be written as follows

[1] William Miller Corporation. Jun. ASME.

[2] Professor of Electrical Engineering, Electrical Engineering Department, California Institute of Technology. Mem. ASME.

Presented at the West Coast Meeting of the Applied Mechanics Division, Los Angeles, Calif., June 26–28, 1952, of THE AMERICAN SOCIETY OF MECHANICAL ENGINEERS.

Discussion of this paper should be addressed to the Secretary, ASME, 29 West 39th Street, New York, N. Y., and will be accepted until April 10, 1953, for publication at a later date. Discussion received after the closing date will be returned.

NOTE: Statements and opinions advanced in papers are to be understood as individual expressions of their authors and not those of the Society. Manuscript received by ASME Applied Mechanics Division, West Coast Group, April 23, 1952.

[3] "Beam-Vibration Analysis With the Electric-Analog Computer," by G. D. McCann and R. H. MacNeal, JOURNAL OF APPLIED MECHANICS, Trans. ASME, vol. 72, 1950, p. 13.

[4] "The Solution of Elastic Plate Problems by Electrical Analogies," by R. H. MacNeal, Trans. ASME, vol. 73, 1951, p. 59.

TABLE 1 DEVELOPMENT OF FINITE-DIFFERENCE ANALOGY FOR TRACK BEAM

QUANTITY	MECHANICAL SYSTEM			ELECTRICAL ANALOGY CIRCUIT EQUATIONS (4)
	DIFF. EQNS. (1)	FINITE DIFFERENCE EQUATIONS		
		DISPLACEMENTS AS COORDINATES (2)	VEL. AS COORDINATES LOADS LUMPED FOR EA. CELL (3)	
DEFLECTION	h	h	$\frac{dh}{dt} = ph$	$E_h = ph$
SLOPE	$\theta = \frac{\partial h}{\partial y}$	$\theta_{n+\frac{1}{2}} = \frac{h_{n+1} - h_n}{\Delta y}$	$(p\theta)_{n+\frac{1}{2}} = \frac{(ph)_{n+1} - (ph)_n}{\Delta y}$	$(E_\theta)_{n+\frac{1}{2}} = \frac{(E_h)_{n+1} - (E_h)_n}{T}$
MOMENT	$M = -EI\frac{\partial \theta}{\partial y}$	$M_n = -\frac{EI}{\Delta y}(\theta_{n+\frac{1}{2}} - \theta_{n-\frac{1}{2}})$	$M_n = -\frac{EI}{\Delta y p}[(p\theta)_{n+\frac{1}{2}} - (p\theta)_{n-\frac{1}{2}}]$	$(i_\theta)_n = -\frac{1}{L_\theta p}[(E_\theta)_{n+\frac{1}{2}} - (E_\theta)_{n-\frac{1}{2}}]$
SHEAR	$Q = \frac{\partial M}{\partial y}$	$Q_{n+\frac{1}{2}} = \frac{M_{n+1} - M_n}{\Delta y}$	$Q_{n+\frac{1}{2}} = \frac{M_{n+1} - M_n}{\Delta y}$	$(i_h)_{n+\frac{1}{2}} = \frac{(i_\theta)_{n+1} - (i_\theta)_n}{T}$
LOAD	$q = -\frac{\partial Q}{\partial y}$	$q_n = -\frac{Q_{n+\frac{1}{2}} - Q_{n-\frac{1}{2}}}{\Delta y}$	$\Delta y \cdot q_n = -\left[Q_{n+\frac{1}{2}} - Q_{n-\frac{1}{2}}\right]$	$(i_q)_n = -\left[(i_h)_{n+\frac{1}{2}} - (i_h)_{n-\frac{1}{2}}\right]$
INERTIA LOAD	$q_i = m\frac{\partial^2 h}{\partial t^2}$	$q_i = m\frac{\partial^2 h}{\partial t^2}$	$\Delta y \cdot q_i = \Delta y \cdot m\frac{\partial (ph)}{\partial t}$	$(i_i)_n = C\frac{\partial (E_h)_n}{\partial t}$
ELASTIC FOUNDATION LOAD	$q_e = K_f h$	$q_e = K_f h$	$\Delta y \cdot q_e = \frac{\Delta y \cdot K_f}{p}(ph)$	$(i_e)_n = \frac{1}{L_f p}(E_h)_n$
FOUNDATION DAMPING LOAD	$q_d = G\frac{\partial h}{\partial t}$	$q_d = G\frac{\partial h}{\partial t}$	$\Delta y \cdot q_d = \Delta y \cdot G(ph)$	$(i_d)_n = \frac{1}{R}(E_h)_n$

$$q + q_i + q_e + q_d = F(y, t) \quad [2]$$

where the respective forces are the elastic, inertia, earth spring, and earth damping on the left side and the traveling load on the right side of the equation. In the electrical analogy each of the loading terms will be represented in finite-difference form as currents flowing into each of the nodal points n. Thus in the circuit analogy the independent variable time will be represented continuously as such while the space variable y will be represented at discrete values by the nodal points n.

The complete derivation of the finite-difference form for the elastic model and its analogous electrical circuit are contained in Fig. 1 and Table 1. Referring to Table 1, it is seen that column 2 contains the finite-difference form for all terms in Equations [1] and [2]. Since the most convenient electrical analogy to use has currents analogous to forces or torques and voltages analogous to velocities, it is desirable to rewrite all equations of column 2 in terms of the derivative of the bending deflections h and slopes θ, or in terms of the bending and the slope velocities. This form is given in column 3. The finite-difference form of Equation [1] becomes for the nth interval

$$\Delta y_n(q)_n + \Delta y_n(q_i)_n + \Delta y_n(q_e)_n + \Delta y_n(q_d)n = \Delta y_n[F(t)]_n \quad [3]$$

which is represented by the elastic model in Fig. 1(b).

The electrical equations for the circuit in Fig. 1(c) are given in column 4 of Table 1. Here it is seen that the voltages to ground E_h, at the nodal points n, are analogous to the bending velocities ph, and the voltages to ground E_θ, at points $(n + 1/2)$ are analogous to the slope velocities $p\theta$. The second equation of column 4, Table 1, relates the voltages across the lower side of each transformer to that across the upper side which is the voltage $(E_\theta)\, n + 1/2$. These, of course, differ by the transformer turns ratio T. The third equation gives the current flowing in each inductor I_θ, which is proportional to the voltage difference across the inductor divided by its operational impedance and is analogous to the moment M. The fourth equation of column 4 relates the currents on the two sides of each transformer, the shear currents i_h, being equal to the difference between the moment currents i_θ, at each slope nodal point divided by the transformer turns ratio T. The fifth equation gives the elastic load currents $(i_q)_n$. The other equations give the currents analogous to the inertia, spring, and damping loadings in terms of the nodal voltages $(E_h)_n$ divided by the appropriate operational impedances.

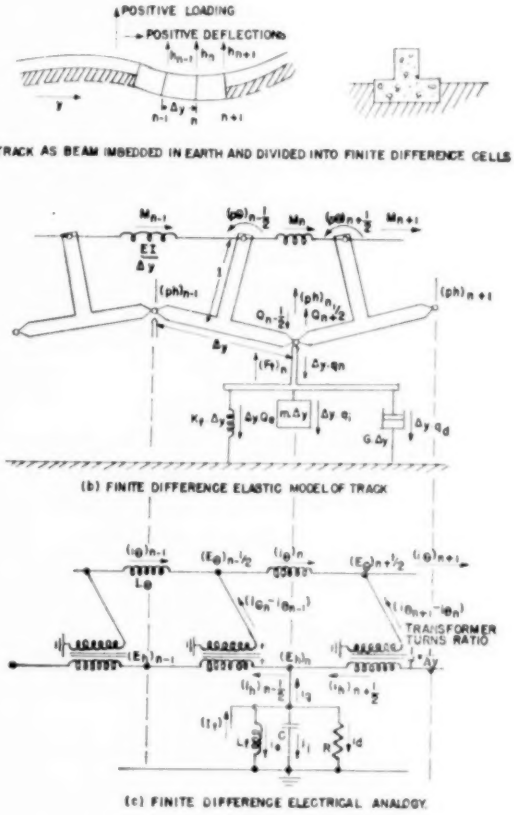
POSITIVE LOADING
POSITIVE DEFLECTIONS
(a) TRACK AS BEAM IMBEDDED IN EARTH AND DIVIDED INTO FINITE DIFFERENCE CELLS
(b) FINITE DIFFERENCE ELASTIC MODEL OF TRACK
TRANSFORMER TURNS RATIO
(c) FINITE DIFFERENCE ELECTRICAL ANALOGY

FIG. 1 REPRESENTATION OF TRACK FOR ANALYSIS

Thus the complete correspondence between the electrical and mechanical quantities can be summarized as in Table 2 for a one-to-one relationship between the respective sets of physical units.

Representation of Traveling Load. In terms of the finite-difference model of the elastic system a traveling load moving with a

TABLE 2. ELECTRICAL-MECHANICAL ANALOGIES FOR ONE-TO-ONE CORRESPONDENCE BETWEEN RESPECTIVE UNITS

$E_h = ph$	$i_d = \Delta y\, qd$
$E_\theta = p\theta$	$I(t)_n = \Delta y\, [F(t)]_n$
$i_\theta = M$	$I_{\theta p} = \dfrac{\Delta y}{EI}\, p$
$i_h = Q$	$C = m\, \Delta y$
$i_c = \Delta y\, q$	$L_f = \dfrac{p}{\Delta y\, K_f}$
$i_i = \Delta y\, qi$	
$i_e = \Delta y\, qe$	$R = \dfrac{1}{\Delta y\, G}$
$p = \dfrac{\partial}{\partial t}$	Turns ratio $T = \Delta y$

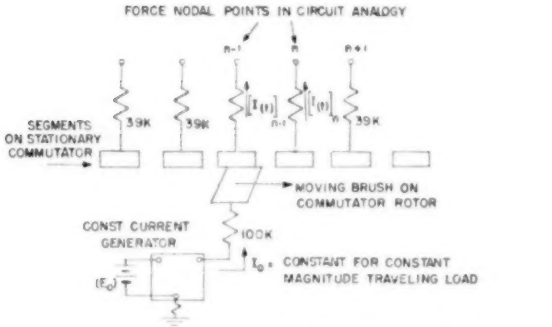

(a) ELECTRICAL CIRCUIT FOR CURRENT ANALOGOUS TO TRAVELING LOAD

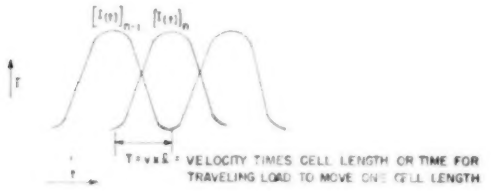

(b) CHARACTER OF TRAVELING LOAD CURRENT AS APPLIED TO EACH CELL

FIG. 2 METHOD OF APPLYING TRAVELING LOAD TO ELECTRIC CIRCUIT ANALOGY

continuous velocity is represented as a force pulse applied sequentially at each finite-difference cell. Its force-time function should rise smoothly to a crest value and decay smoothly back to zero. The quantity of particular importance is the impulse value or the integral of the force-time curve for each cell. For a constant-magnitude constant-velocity load the impulses on each cell should be identical and they should be separated in time by the product of each cell length and the velocity of the load. The corresponding analogous loading current for the electrical analogy was generated by means of the segmental commutator circuit shown schematically in Fig. 2(*a*). The corresponding current pulses are shown in Fig. 2(*b*). To simulate variations in velocity the rotating brush need only be accelerated or decelerated by the appropriate amount. To represent variations in load with time, the voltage E_o, controlling the output of the current generator is varied. Measurement of the direct current i_o, flowing out of the current generator gives the true value of the analogous loading current.

Analogy for Nonlinear Earth Constraints. For certain types of carriage loadings high upward track forces are anticipated. Also, for very high downward track loads, appreciable upward track deflections may occur both ahead of and behind the point of application of the load. If the track rises above the normal unloaded position of the earth its elastic properties are assumed to change abruptly from a stiff spring to a very weak one. For purposes of the analogy it can be assumed that at this position the track abruptly leaves contact with the earth and that both the elastic and damping constraints are suddenly removed and not reapplied until the beam returns to the normal unloaded position. This characteristic is to be considered separately for each finite-difference cell.

To represent this condition in the analogous electric circuit it is necessary to disconnect the L_f and R elements of each cell, Fig. 1(*c*), at the proper voltage conditions and keep them disconnected until this voltage condition again has been reached and forces can again be transmitted between the beam and the earth.

Unfortunately, this type of physical discontinuity has no direct passive circuit analogy that may be added to Fig. 1(*c*). However, the electric analog computer has sufficient electronic elements to simulate properly the desired nonlinearity by the circuit technique illustrated in Fig. 3. The removal and reapplication of forces between the beam and the earth (currents in the analogy) is controlled at each cell by the two diodes connected back to back as shown and the current i_o, fed into their mid-point. Assuming them to be effectively perfect diodes, only a positive bias current i_o can be forced through each of them by the current generator. When such a bias current is flowing, the earth-force currents ($i_e + i_d$) can flow up to the magnitude of the bias current. This bias current therefore must be high enough for all desired solutions. Thus the condition of the beam being separated from the earth is obtained by having the current generator output current i_o zero. This is accomplished by having the generator try to put out negative current.

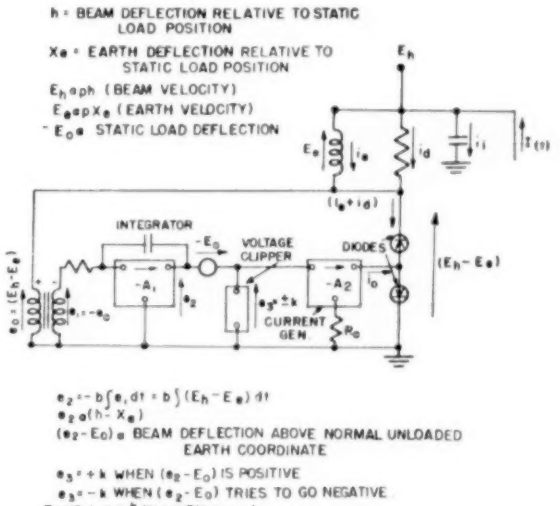
h = BEAM DEFLECTION RELATIVE TO STATIC LOAD POSITION
X_e = EARTH DEFLECTION RELATIVE TO STATIC LOAD POSITION
$E_h = ph$ (BEAM VELOCITY)
$E_e = pX_e$ (EARTH VELOCITY)
$-E_o$ = STATIC LOAD DEFLECTION
E_h
E_e
i_e
i_d
i_i
$I(t)$
$(i_e + i_d)$
INTEGRATOR
$-E_o$
VOLTAGE CLIPPER
DIODES
$(E_h - E_e)$
$e_o = (E_h - E_e)$
$-A_1$
e_2
$e_3 = \pm k$
$-A_2$
i_o
CURRENT GEN
R_o
$e_1 = -e_o$
$e_2 = -b\int e_1\, dt = b\int (E_h - E_e)\, dt$
$e_2 = (h - X_e)$
$(e_2 - E_o)$ = BEAM DEFLECTION ABOVE NORMAL UNLOADED EARTH COORDINATE
$e_3 = +k$ WHEN $(e_2 - E_o)$ IS POSITIVE
$e_3 = -k$ WHEN $(e_2 - E_o)$ TRIES TO GO NEGATIVE
THUS $i_o = +k/R$ WHEN $e_3 = -k$
$i_o = 0$ WHEN $e_3 = +k$

FIG. 3 CIRCUIT ANALOGY USED TO REPRESENT NONLINEAR EARTH CONSTRAINTS AT EACH FINITE DIFFERENCE

In the analogy of Fig. 3 the voltages E_h and E_e are analogous to the beam and earth velocities, respectively. They must be integrated to obtain the analogous deflections. For controlling the discontinuity the difference voltage $(E_h - E_e)$ is used in Fig. 3. This is integrated by the electronic integrating circuit shown. However, since the integration necessarily produces a sign change,

the additional sign-changing transformer of very high magnetizing impedance is used. The voltage e_2 in Fig. 3 is analogous to the relative displacement of the beam and earth. This is in terms of the static equilibrium deflection due to the static weight of the beam. To this voltage e_2 must be added a voltage $-E_o$ to represent the static load deflection. Thus whenever the voltage $(e_2 - E_o)$ is positive the beam has left contact with the earth. If this voltage were negative the beam would be represented as going below the earth co-ordinate. However, the instant it becomes slightly negative the current generator starts to put out a large positive current i_o, and the diodes conduct. In this manner the voltage $(E_h - E_e)$ is held effectively at zero and the integral or $(e_2 - E_o)$ does not further increase negatively.

To insure that the slightly negative value for $(e_2 - E_o)$ be negligible, the gain in the integrator is made very high and the voltage $(e_2 - E_o)$ is clipped to $(e_3 = \pm k)$ which constant voltage controls the current generator. The manner in which the nonlinear earth constraint operates will become more apparent when actual solutions are considered.

Dimensional Relationships

Conversion Between Electrical and Mechanical Parameters. The use of a one-to-one correspondence (as assumed previously) between the electrical and mechanical systems is, of course, not practical in many cases. As shown by Equation [1], four arbitrary conversion constants can be used since there are the four variations t, y, h, and F. The standard beam-conversion-formula notation that has been adopted for use on the computer defines the four arbitrary conversion constants n, B, a, and P as follows

$$t = nt', \qquad p = \frac{\partial}{\partial t} = \frac{p'}{n} \qquad [4]$$

where t is the time base in the mechanical system and t' is the computer time base.

$$(\text{Forces})\ F = \frac{B}{a}\,(i)\ (\text{currents}) \qquad [5]$$

$$\frac{\partial h}{\partial t} = ph = \frac{Ba}{n} E_a \qquad [6]$$

$$P = \frac{y}{y'} = \frac{\Delta y}{T} \qquad [7]$$

where T is transformer turns ratio, Fig. 1(*c*).

The use of these conversion constants produces the relationships summarized in Table 3.

TABLE 3 ELECTRICAL-MECHANICAL ANALOGIES FOR DIMENSION CONVERSION CONSTANTS USED ON COMPUTER

$t = nt',\ p = \frac{p'}{n}$	$P = \frac{\Delta y}{T}$
$F = \frac{B}{a}\,(i_f)$	$M = \frac{BP}{a}\,m$
$ph = \frac{Ba}{n} E_h$	$p\theta = \frac{Ba}{nP} E_\theta$
$h = \frac{Ba}{p'}$	$\theta = \frac{Ba}{P_{p'}} E_\theta$
$C = \Delta y\,\frac{ma^2}{n}$	$\frac{1}{L_\theta} = \frac{EI}{\Delta y}\,\frac{a^2}{p^2}$
$\frac{1}{R} = \Delta y\,\frac{Ga^2}{n}$	
$\frac{1}{L_f} = \Delta y\, L_f a^2$	

Dimensionless Form for Track Equation. The foregoing conversion technique is used to prepare an actual mechanical system for the computer. To present the solutions to the track problem in general form, the following co-ordinate changes will be used in order to secure the minimum number of dimensionless coefficients.

Let

$$y = \sqrt[4]{\frac{EI}{K_f}}\,\xi; \quad \frac{\partial^4}{\partial y^4} = \frac{K_f}{EI}\,\frac{\partial^4}{\partial \xi^4} \qquad [8]$$

$$h = \frac{F_o}{K_f}\,\eta \qquad [9]$$

$$t = \sqrt{\frac{m}{K_f}}\,\tau; \quad \frac{\partial}{\partial t} = \sqrt{\frac{K_f}{m}}\,\frac{\partial}{\partial \tau}; \quad \frac{\partial^2}{\partial t^2} = \frac{K_f}{m}\,\frac{\partial^2}{\partial \tau^2} \qquad [10]$$

Thus Equation [1] becomes

$$\frac{\partial^4 \eta}{\partial \xi^4} + \frac{\partial^2 \eta}{\partial \tau^2} + \frac{G}{\sqrt{mK_f}}\,\frac{\partial \eta}{\partial \tau} + \eta = \frac{F}{F_o}\left(\sqrt[4]{\frac{EI}{K_f}}\,\xi;\ \sqrt{\frac{m}{K_f}}\,\tau\right) \qquad [11]$$

For the constant-velocity traveling load, the loading function is the following

$$F(y, t) = F(y - vt) = F\left[\sqrt[4]{\frac{EI}{K_f}}\,(\xi - V\tau)\right] \qquad [12]$$

where the dimensionless velocity is

$$V = v\sqrt[4]{\frac{m^2}{EI\,K_f}} \qquad [13]$$

The dimensionless acceleration is given by the equation

$$A = \frac{\partial^2 \xi}{\partial \tau^2} = \frac{m}{K_f}\sqrt[4]{\frac{K_f}{EI}}\,\frac{\partial^2 y}{\partial t^2} \qquad [14]$$

Since the loading function is expanded by the factor

$$\left(\sqrt[4]{\frac{EI}{K_f}}\right)$$

F_o must be modified as follows

$$F_o' = F_o\sqrt[4]{\frac{EI}{K_f}}$$

It is therefore convenient to plot bending deflections in the dimensionless form

$$\eta' = \sqrt[4]{\frac{EI}{K_f}}\,K_f\,\frac{h}{F_o} = \frac{h}{F_o}\,\sqrt[4]{EI\,K_f^3} \qquad [15]$$

In this new co-ordinate system the important parameter in addition to the dimensionless velocity V of Equation [13] is the dimensionless damping parameter

$$D = \frac{G}{\sqrt{mK_f}} \qquad [16]$$

The bending moments can be treated in a similar manner. Since

$$M = -EI\,\frac{\partial^2 h}{\partial y^2} \text{ and } \frac{\partial^2}{\partial y^2} = \sqrt{\frac{K_f}{EI}}\,\frac{\partial^2 \eta}{\partial \xi^2}$$

its form in terms of the dimensionless co-ordinate system becomes

$$M = -\sqrt[2]{\frac{EI}{K_f}}\, F_o \frac{\partial^2 \eta}{\partial \xi^2}$$

$$M = -\sqrt[4]{\frac{EI}{K_f}}\, F_o' \frac{\partial^2 \eta}{\partial \xi^2}$$

giving for the dimensionless moment

$$\frac{M}{F_o'} = \sqrt[4]{\frac{EI}{K_f}} \frac{\partial^2 \eta}{\partial \xi^2} = \sqrt[4]{\frac{K_f}{EI}} \frac{M}{F_o} \quad \ldots\ldots\ldots\ldots [17]$$

It is thus apparent that this system of units requires only two parameters to describe any given track, the dimensionless damping D, and the dimensionless velocity V. Bending deflection and moment solutions plotted in the foregoing per unit forms of Equations [14] and [16], respectively, can be converted readily for any given track.

Generalized Solutions for Linear Track

Although the analysis made pertained to the particular problems of the SNORT project it was found that sufficient solutions were obtained which, when presented in dimensionless form, covered the principal range of interest for general traveling load track studies.

Linear Track. Figs. 4 through 7 present solutions to the linear track under constant-velocity point loading in the dimensionless form described. Fig. 4 gives bending deflection curves as a function of either ξ or τ, and for the important range of dimensionless velocity V that gives large deflections and stresses. The range of the dimensionless damping factor shown in the figures corresponds to the principal range of actual damping provided by earth imbedding. Fig. 5 shows similar bending-moment curves and in Figs. 6 and 7 are plotted the crest deflections and moments as a function of velocity and damping. These solutions were plotted from oscillograms similar to those presented in Fig. 8 and spot numerical check calculations. Referring to the circuit analogy in Fig. 1(*c*), it is seen that deflection measurements are obtained by recording the current i_e, which is proportional to the integral of the voltage E_A. Hence this gives the actual deflections instead of the bending velocities. The moments are recorded directly as the currents i_θ.

The general character of the deflection curves in Fig. 4 is of some interest. It will be noted that as the traveling load speed is increased from zero velocity, the point of load application rides further and further forward on the deflection-space wave. This effect is more noticeable as the damping increases. For each value of damping there exists a critical velocity producing maximum deflections which approach the undamped critical velocity as the damping is decreased. The undamped critical velocity is

$$v = \sqrt{2}\sqrt[4]{\frac{EI\,K_f}{m^2}}$$

In the dimensionless form used here it is given by $V = \sqrt{2}$. Of further interest is the fact that the roots of the solution produce a forward wave ahead of the load whose frequency increases with increasing velocity and a wave behind the load whose frequency decreases with increasing velocity. Thus referring to the moment curves in Fig. 5, it might be expected that the crest moment would be at the point of application of the load for lower velocities and then transfer to the leading peak at higher velocities. This effect is shown in Fig. 7. However, the leading peak moment exceeds the load point peak only for velocities appreciably above the critical velocities and where the magnitudes have dropped off considerably. It is of interest to note that (as seen in Fig. 4), the damping of these terms decreases rapidly for speeds above the critical velocity.

Effect of Accelerating Loads. Rapid accelerations through the critical speed have, of course, the effect of reducing the magnitude of the deflection and moment. However, it was found that for dimensionless accelerations A, up to about 1.8×10^{-3} deflections and moments are essentially as great as obtained for any given constant velocity. In any particular case this is a rather high rate of acceleration as will be shown later.

Nonlinear Track. The oscillograms in Fig. 8 present typical solutions to the nonlinear track configuration for three values of upward loading. In the first case the loading is not sufficient to cause the track beam to rise above the unloaded rest position of the earth. This is a linear solution. In the second case sufficient loading was applied that the static deflection of the track owing to its own mass loading is only 64 per cent of the peak dynamic track deflection. Thus, as shown, the track leaves the earth for a short period of its travel. In Fig. 8(*c*) the loading is further increased, resulting in a track leaving the earth by a greater amount. In the electric circuit analogy in Fig. 3 the track deflection was obtained by integrating the voltage, E_A. The earth-deflection solution was obtained by recording directly the current i_e. The moment is still recorded as the current i_θ in Fig. 1(*c*).

In Fig. 9 and Table 4 are presented all of the nonlinear cases studied that were of interest. These were obtained for the lower limit of damping considered in the linear case since the most severe effects of track bouncing occurred in the lower range of damping. The ratio F_o/F_s is used to indicate the degree of nonlinearity for each solution. F_s represents the limiting traveling-load magnitude for a linear solution. F_o is the actual magnitude of the traveling load.

Examination of the data presented in Fig. 9 and Table 4 shows that even for this low value of damping severe conditions are not introduced by bouncing of the track. In no case is the deflection or moment appreciably worse than would be obtained for the same loading in the linear solutions. In some instances they were found to be less severe than in the linear case.

Application of Solutions

Damping. The range of the damping constant G considered in this study was determined from actual dynamic tests made by the Naval Ordnance Test Station for track cross sections typical of the ones being considered and for several soil conditions corresponding to a range of sand and clay soils. The tests were conducted with the percentage of the beam that was buried, ranging from zero to one half the beam height. These tests provided values of G ranging from about 4000 to 9000 lb/ft/ft/sec and values of K_f from one to three million lb/ft/ft. The linear data presented here cover a range about twice this great for the same beam configurations actually tested. Sufficient data are not available to predict what the damping should be for soils radically different than those tested. However, referring to Equation [16] for the damping parameter D, it will be noted that it is virtually independent of the geometry of the beam. This assumes that (for a given case) m, K_f, and G are all proportional to the beam width. Furthermore, D varies only as the square root of m or K_f. It is thus believed that the principal range of interest has been covered by the data presented in the foregoing with D ranging down to 0.23.

It is of course realized that these solutions are applicable to cases other than that of earth imbedding. One such example is a pontoon bridge.

Velocity of the Traveling Load. It will be noted from Figs. 6 and 7 that the important range of variation in the velocity corresponds to values of V lying between 1.0 and 1.7. The actual critical velocity for maximum disturbance varies from about 1.2 for high damping of 1.41 (or $\sqrt{2}$) for zero damping. This also

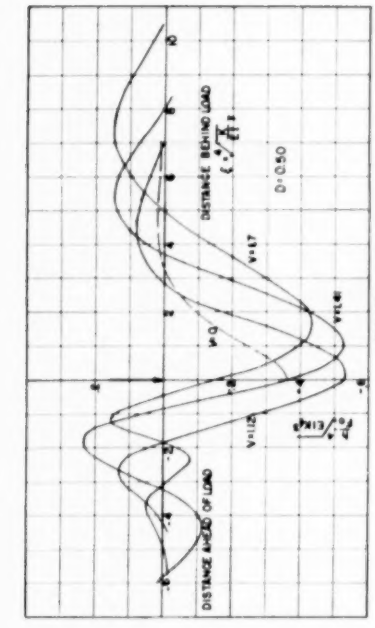

FIG. 4b

(*b*) $D = 0.50$

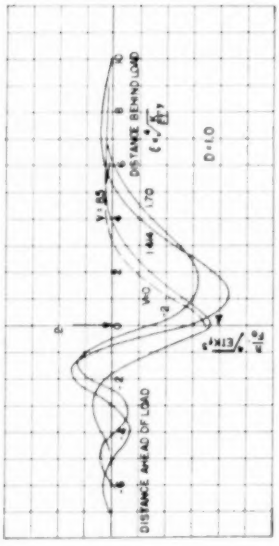

FIG 4d

(*d*) $D = 1.0$

FIG. 4 DEFLECTION CURVES FOR CONSTANT-VELOCITY POINT LOADING OF LINEAR TRACK. TO OBTAIN SOLUTION AS A FUNCTION OF TIME DIVIDE THE ξ-CO-ORDINATE BY $\sqrt[4]{\frac{m^2}{EI\,K}}$

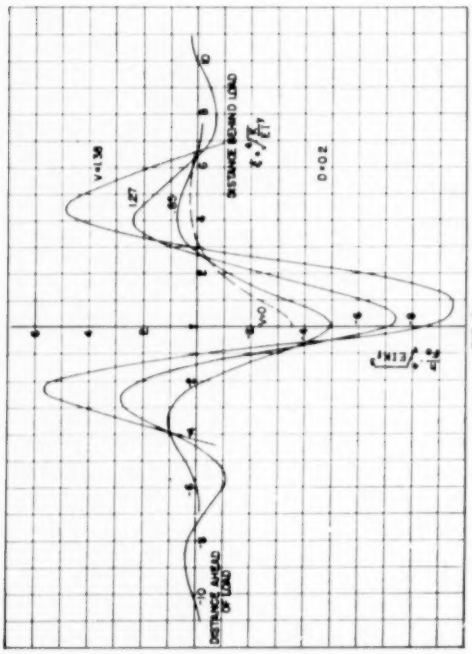

FIG 4a

(*a*) $D = 0.20$

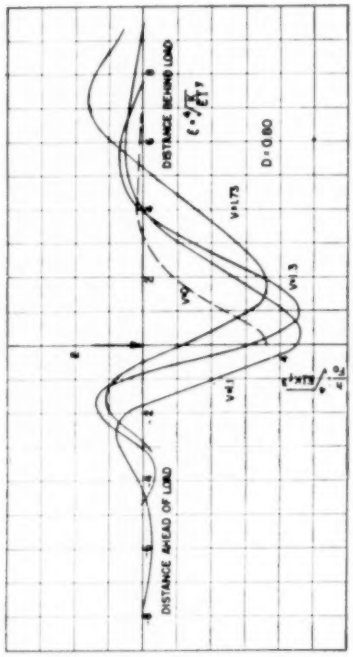

FIG. 4c

(*c*) $D = 0.80$

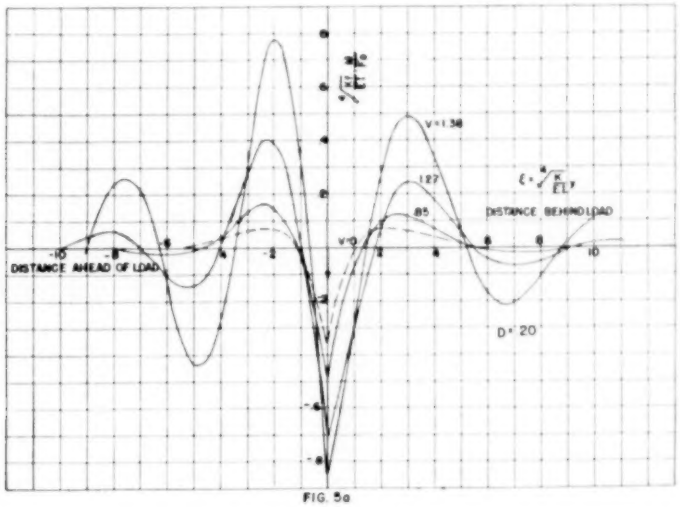

FIG. 5a

(*a*) $D = 0.20$

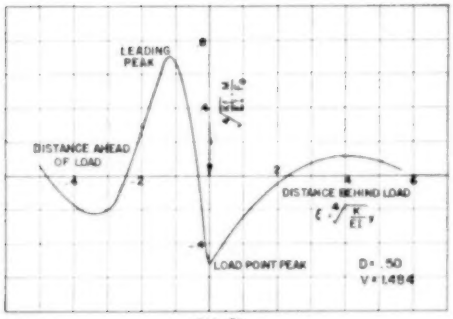

FIG. 5b

(*b*) $D = 0.50$

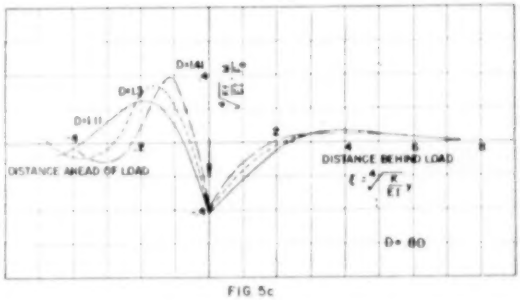

FIG. 5c

(*c*) $D = 0.80$

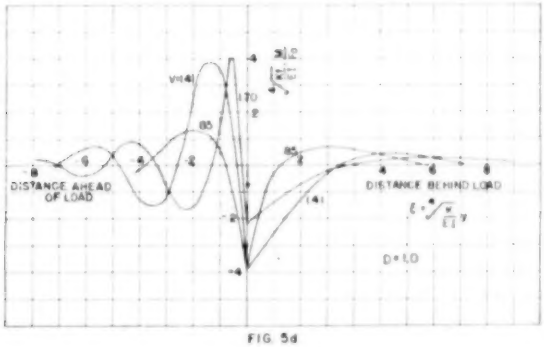

FIG. 5d

(*d*) $D = 1.0$

FIG. 5 MOMENT CURVES FOR CONSTANT-VELOCITY POINT LOADING OF LINEAR TRACK

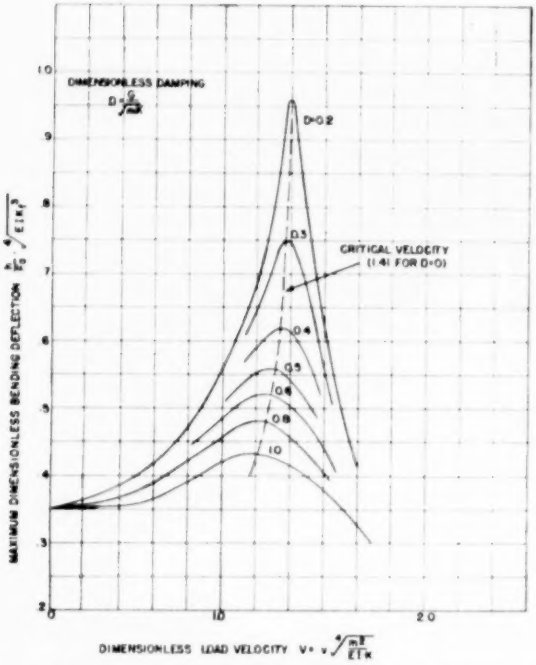

FIG. 6 CREST DEFLECTIONS AS A FUNCTION OF VELOCITY AND DAMPING FOR CONSTANT-VELOCITY POINT LOADING OF LINEAR TRACK

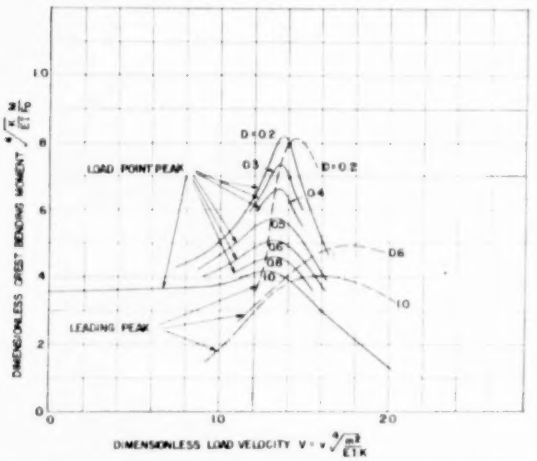

FIG. 7 CREST MOMENTS AS A FUNCTION OF VELOCITY AND DAMPING FOR CONSTANT-VELOCITY POINT LOADING OF LINEAR TRACK
(See Fig. 5 for definition of peaks.)

represents a rather narrow range of actual velocities as can be seen from the definition of V as given by Equation [13]. This shows that the ratio between the dimensionless and actual velocity is the factor

$$\sqrt[4]{\frac{m^2}{EI\,K_f}}$$

For practical tracks the moment should vary over a range of only about 3 or 4.

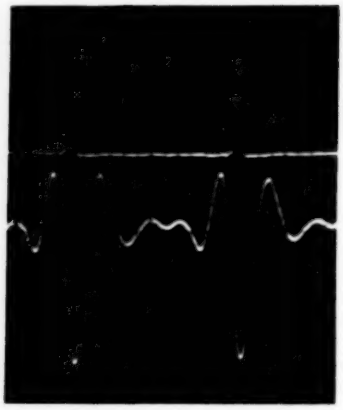

FIG. 8(*a*) TYPICAL OSCILLOGRAPHIC COMPUTER DEFLECTION SOLUTION FOR CONSTANT-VELOCITY POINT LOADING OF LINEAR TRACK

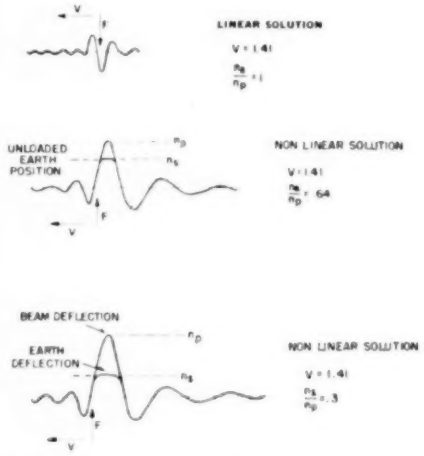

FIG. 8(*b*) TYPICAL NONLINEAR DEFLECTION SOLUTIONS

The beam density might vary as much as a factor of 10 and K_f might vary as much as 10 to 1. The maximum range of variations of

$$\frac{m^2}{EI\,K_f}$$

might then be as much as 300 or 400. However, the term

$$\sqrt[4]{\frac{m^2}{EI\,K_f}}$$

would then only vary over a range of about 4. The minimum important velocity thought to require detailed dynamic analysis is thus not less than 400 to 500 fps or about 300 to 400 mph. This means that such dynamic track studies are only important for truly high-speed tracks. With the actual beams considered, the critical velocities were 1400 to 1600 fps.

Distributed Loads. In the case of the linear solutions it is, of course, a relatively simple matter to superimpose the solutions for a series of point loadings and this was done for several carriage designs in connection with the SNORT project. However, this

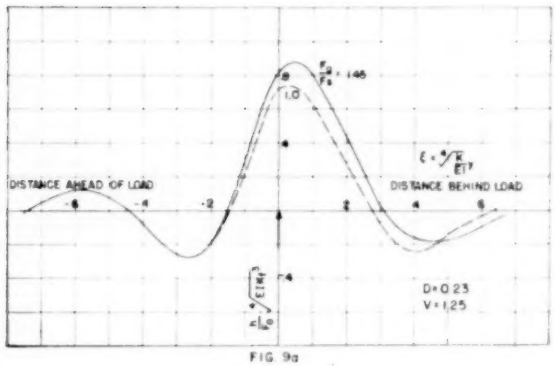

FIG. 9a

(*a*) Upward loading: $D = 0.23$, $V = 1.25$

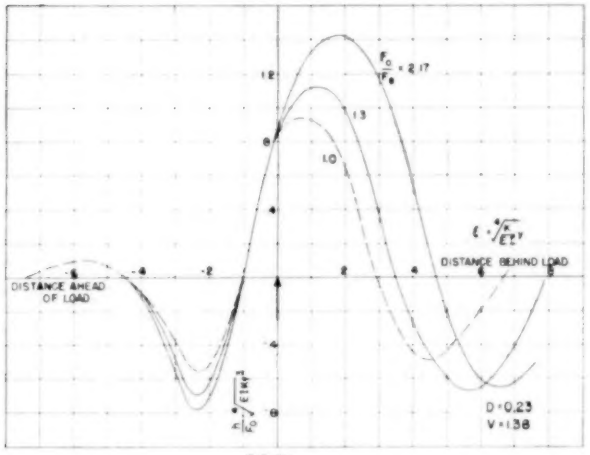

FIG. 9b

(*b*) Upward loading: $D = 0.23$, $V = 1.38$

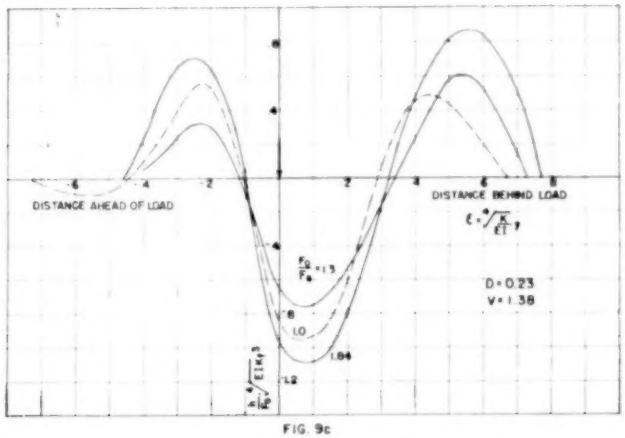

FIG. 9c

(*c*) Downward loading: $D = 0.23$, $V = 1.38$

TABLE 4 DIMENSIONLESS CREST MOMENTS FOR NONLINEAR CASES IN FIG. 9. ($D = 0.23$)

V	$\frac{F_0}{F_s}$	$\frac{M}{F_s'}$
	For Uploads	
1.25	1.0	0.68
	1.45	1.04
1.41	1.0	0.82
	1.30	1.13
	2.17	1.24
1.52	1.0	0.77
	1.74	1.01
	For Downloads	
1.41	1.0	0.82
	1.3	1.15
	1.84	1.46
1.52	1.0	0.77
	1.76	0.90

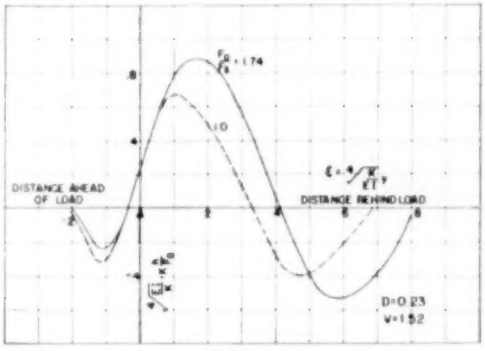

FIG. 9d

(*d*) Upward loading: $D = 0.23$, $V = 1.52$

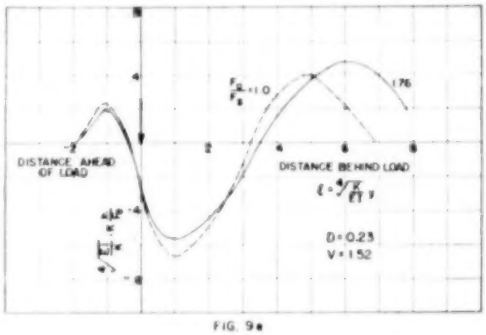

FIG. 9e

(*e*) Downward loading: $D = 0.23$, $V = 1.52$

FIG. 9. DIMENSIONLESS NONLINEAR DEFLECTION SOLUTIONS. F_s IS DYNAMIC LOAD JUST SUFFICIENT FOR TRACK TO REACH NORMAL UNLOADED EARTH POSITION

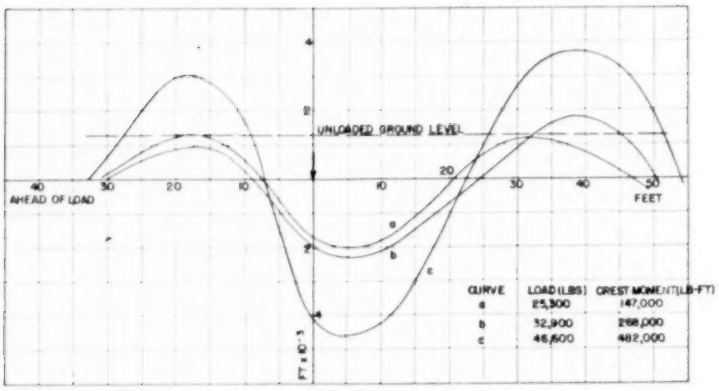

FIG. 10a

(*a*) For upward loading

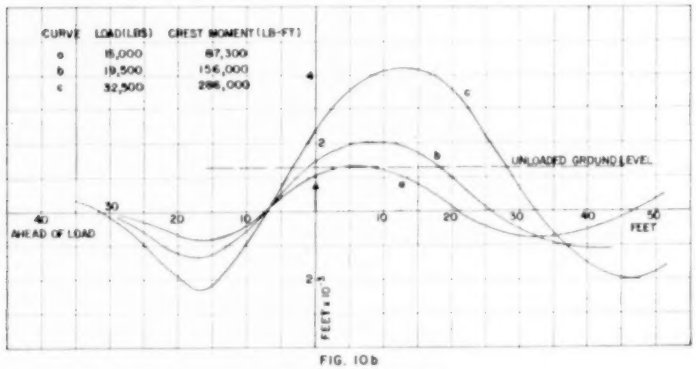

FIG. 10b

(*b*) For downward loading

FIG. 10 APPLICATION OF GENERAL SOLUTIONS TO A SPECIFIC TRACK CONFIGURATION

Track Constants:

$I = 9$ ft⁴
$EI = 3.89 \times 10^9$
$G = 2300$ lb/ft/ft/sec
$K_f = 1.56 \times 10^6$ lb/ft/ft
$m = 62$ slugs/ft
Static deflection $k_s = 1.28 \times 10^{-2}$ ft
$v = 1550$ fps

Conversion Formula:

From Equation [13] $V = v \sqrt[4]{\dfrac{m^2}{EI\,K_f}} = 1550 \times 8.9 \times 10^{-4} = 1.38$

Equation [16]

$$D = \frac{G}{\sqrt{mK_f}} = \frac{2300}{9840} = 0.233$$

Equation [15]

$$\eta' = \frac{h}{F_o} \sqrt[4]{EI\,K_f^3} = 1.104 \times 10^7 \frac{h}{F_o}$$

Equation [17]

$$\frac{M}{F_o'} = \sqrt[4]{\frac{K_f}{EI}} \frac{M}{F_o} = 0.141 \frac{M}{F_o}$$

Equation [14]

$$A = a \frac{m}{K_f} \sqrt[4]{\frac{K_f}{EI}} = 3.97 \times 10^{-5} \times 0.141\, a = 5.60 \times 10^{-6} a$$

cannot be done with the now linear solutions. Such cases would have to be studied individually.

Numerical Example. As an example of the application of the general solutions to a specific case, consider a beam having the constants given in Fig. 10. The necessary formula for conversion of the dimensionless solutions is also given in Fig. 10. From this it is seen that the dimensionless velocity V is 1.38 and the per unit damping D is 0.233. The deflection curves are thus plotted from Fig. 4(*a*), for the linear case and Figs. 9(*b*) and (*d*) for the nonlinear solutions. Only the crest moments are computed and listed in Fig. 10. They were determined directly from Table 4. It will be noted from the actual deflections and moments given in Fig. 10 for the various loadings, that any practical design consideration could just as well be based on the purely linear solutions.

It was noted previously that essentially full magnitude deflections and moments were obtained for dimensionless accelerations A, up to 1.8×10^{-3}. In this example the actual acceleration is about 320 ft per sec² or $10G$. Thus no reduction in stresses from those given by the constant-velocity solution can be expected for accelerating loads below $10G$.

REFERENCE

"The Solution of Aeroplastic Problems by Means of Electrical Analogies," by R. H. MacNeal, G. D. McCann, and C. H. Wilts, *Journal of Aeronautical Sciences*, vol. 18, 1951, p. 777.

Stability of Thin Elastic Plates Covering an Arbitrary Simply Connected Region and Subject to any Admissible Boundary Conditions[1]

By G. A. ZIZICAS,[2] LOS ANGELES, CALIF.

The Bergman method of solving boundary-value problems by means of particular solutions of the differential equation, which are constructed without reference to the boundary conditions, is applied to the problem of stability of thin elastic plates of an arbitrary simply connected shape and subject to any admissible boundary conditions. A direct method is presented for the construction of particular solutions that is applicable to both anisotropic and isotropic plates. Previous results of M. Z. Krzywoblocki for isotropic plates are obtained in a simple manner.

Nomenclature

The following nomenclature is used in the paper:

a_{ij} = coefficients of the system of Equations [18] $(i, j = 1, 2, 3, \ldots n)$

$A = |a_{ij}|$ = determinant of the coefficients a_{ij} of Equations [18]

b_{ij} = coefficients entering Equation [2] $(i, j = 1, 2, 6)$

A, B, C, E, F = coefficients of Equation [22] defined by Equations [23]–[25]

A, B = complex conjugates of A and B correspondingly

C = boundary line of the middle plane of the plate

c_i, c_j = constant coefficients entering Equations [9], [10], and [35] $(i, j = 1, 2, 3, \ldots)$

$f(x, y)$ or $f(\xi, \eta)$ = function of variables x, y, or ξ, η satisfying equation of equilibrium

F = function of coefficients $c_1, c_2, \ldots c_n$ entering Equation [17]

$g(x, y)$ or $g(\xi, \eta)$ = function of x and y or ξ and η prescribed along boundary line C of middle plane of plate and entering boundary conditions, Equations [11]

G = a differential operator depending on type of boundary conditions, Equations [11]

$i = \sqrt{-1}$, the imaginary unit

i, j, k = integers $(1, 2, 3, 4 \ldots)$

k = undetermined scale factor entering Equations [5] and related to λ by Equation [7]

$L(w)$ = a differential operator of fourth order entering Equation [1] and defined by Equations [2]–[4]

K, L, M = coefficients of Equation [22] defined by Equations [23]

N = force in middle plane, per unit length, lb-in^{-1}

m, n = integers $(1, 2, 3, 4, \ldots)$

$m!$ = $1.2.3. \ldots m$

$n!$ = $1.2.3. \ldots n$

$P(\bar{z}), P_1(\bar{z})$ = analytic functions of complex variable $\bar{z}$

$Q(z), Q_1(z)$ = analytic functions of complex variable z

$U(z, \bar{z})$ = a function of the complex variables z and $\bar{z}$ defined by Equation [26], analytic in both

$U_1(z, \bar{z}), U'_1(z, \bar{z})$ = functions of complex variables z and $\bar{z}$ defined by Equations [33] and [34] correspondingly, analytic in both z and $\bar{z}$

$w(x, y)$ or $w(\xi, \eta)$ = transverse displacement of middle plane of plate at point (x, y) or (ξ, η), in.

$w_{,x}, w_{,xy}$ etc. = $\dfrac{\partial w}{\partial x}, \dfrac{\partial^2 w}{\partial x \partial y}$ etc. (see footnote 5)

x, y = rectangular co-ordinates within middle plane of plate

$z = \xi + i\eta$

$\bar{z} = \xi - i\eta$

η = rectangular co-ordinate related to y by Equation [5]

κ = parameter entering equilibrium equation of orthotropic plates, Equation [3]

λ = undetermined parameter in equation of equilibrium, Equation [1]

ξ = rectangular co-ordinate related to x by Equation [5]

$\nabla\nabla^2 = \dfrac{\partial^4}{\partial x^4} + 2\dfrac{\partial^4}{\partial x^2 \partial y^2} + \dfrac{\partial^4}{\partial y^4}$ or $\dfrac{\partial^4}{\partial \xi^4} + 2\dfrac{\partial^4}{\partial \xi^2 \partial \eta^2} + \dfrac{\partial^4}{\partial \eta^4}$

Subscripts and superscripts:

i, j, m, n = $1, 2, 3, \ldots\ldots$

x or y = in direction x or y

$,x$ or $,xy$, etc. = partial derivative with respect to x or xy, etc. (footnote 5)

xy = applied to an element normal to x-direction and directed in y-direction

---

[1] The results presented in this paper are based on a dissertation submitted in partial fulfillment of the requirements for the degree of Doctor of Philosophy in Engineering at the University of California, Los Angeles, Calif., June, 1952. The investigation was carried in part when the author was research assistant under a grant, administered by Prof. I. S. Sokolnikoff, from Research Corporation, New York, to the Regents of the University of California.

[2] Assistant Engineer, Department of Engineering, University of California.

Presented at the West Coast Meeting of the Applied Mechanics Division, Los Angeles, Calif., June 26–28, 1952, of The American Society of Mechanical Engineers.

Discussion of this paper should be addressed to the Secretary, ASME, 29 West 39th Street, New York, N. Y., and will be accepted until April 10, 1953, for publication at a later date. Discussion received after the closing date will be returned.

Note: Statements and opinions advanced in papers are to be understood as individual expressions of their authors and not those of the Society. Manuscript received by ASME Applied Mechanics Division, West Coast Group, May 8, 1952.

ξ or η = in direction ξ or η
$\xi\eta$ = applied to an element normal to the ξ-direction and directed in the η-direction
$,\xi$ or $,\xi\eta$, etc. = partial derivative with respect to ξ or $\xi\eta$, etc. (footnote 5)

Introduction

The simplest problems of elastic stability of plates and the only ones for which an exact solution has been attained, appear when the variables of the differential equation of equilibrium are completely separable in an appropriate co-ordinate system. Then either the energy method as first applied by G. H. Bryan (2)[3] or the differential-equation approach followed by S. Timoshenko (1, 3, 5) and H. Reissner (4) can be used for the computation of the critical loads. For nonseparable variables the Rayleigh-Ritz approximate method (6, 7, 8), originally used in buckling problems of plates by S. Timoshenko (9), gives an estimate higher than the actual critical value. The easiest way of applying the method consists in using a very simple expression satisfying the boundary conditions. The approximation can be brought to any prescribed degree of accuracy however (10) by using a sufficiently large number of terms from a "complete" set of functions satisfying the boundary conditions; i.e., a set of functions such that any function with continuous fourth-order derivatives satisfying the boundary conditions can be expanded in an absolutely and uniformly convergent series in terms of these functions and the same is possible for its partial derivatives up to the fourth order included.[4] One method of obtaining such a set is by associating the boundary conditions with a fourth-order equation with separable variables. This is one way of looking into the method used by W. Ritz for characteristic value problems of free rectangular plates (8), by S. Timoshenko for simply supported rectangular plates under moment or shear loading (9, 11), and by J. M. Klitchieff (12) for triangular plates. For rectangular plates with various combinations of simply supported and clamped edges complete sets were also given by S. Iguchi (13, 14). The original approach of W. Ritz (8) which is based on a combination of the normal modes of vibration of beams has been applied to rectangular and skew plates with various boundary conditions by D. Young (15) and M. V. Barton (16). Several other equivalent variational methods, the most prominent ones due to B. G. Galerkin and L. V. Kantorovich, have also been developed. References and short expositions in English are given by I. S. Sokolnikoff (17).

In certain cases complete sets can be obtained by means of the differential equations and part of the boundary conditions. Such a case is that of a rectangular clamped plate which has been considered by G. I. Taylor (18), O. H. Faxén (19), and K. Sezawa and W. Watanabe (20). The complete set is combined so as to satisfy the remaining conditions as closely as possible. Essentially the procedure consists of obtaining approximate solutions by relaxing the boundary conditions, and because of this relaxation according to Courant's principle (21), the minimum of the energy expression cannot increase. Thus the obtained estimates of the critical load are lower than the exact value. A systematic treatment of this approach based on the mentioned principle was given by A. Weinstein (22, 24) and E. Trefftz (23). The same method has been reconsidered recently by B. Budiansky, P. Hu, and R. W. Conner (25, 26). They based their discussion on the concept of Lagrangian multipliers and in particular adjusted the technique so as to give both an upper and lower bound for the critical values.

Of wider range of applicability is the method of finite differences. It was applied to buckling problems of plates by J. J. Stoker (27), M. V. Barton (28), and M. G. Salvadori (29). An electric analog method based on finite differences is due to R. H. MacNeal (30). D. G. Christopherson, L. Fox, J. R. Green, and R. V. Southwell (31) used the versatile relaxation method for solving plate-buckling problems.

In the method of finite differences the deflected surface in the buckled state is approximated by an increasing number of discrete points to obtain the desired degree of accuracy. An alternative approach consists in expressing the shape of the plate in terms of a sufficiently general set of functions satisfying the differential equation irrespective of boundary conditions. This is done in the previously mentioned cases of completely separable variables, where however the obtained functions can be adjusted to the imposed boundary conditions. If the variables are not separable because of either the type of equation or the kind of boundary conditions, particular solutions satisfying the differential equation of equilibrium can be obtained by recalling that the equation is of the elliptic type and hence at least for coefficients which are polynomials in x and y possesses analytic solutions. This suggests the use of two complex conjugate variables instead of the real ones. Such an approach was originated by S. Bergman with his doctoral dissertation (32) and applied subsequently to various problems. It was recently extended to the equation of equilibrium of isotropic plates including forces within the middle plane (33). For second-order equations he also developed a systematic technique for carrying out the rather involved numerical computations by means of punch-card machines (34). His results were brought to a more explicit form and applied to thin elastic plates by M. Z. Krzywoblocki (35).

In the present paper a method of constructing particular solutions is presented which is valid for both isotropic and anisotropic cases. Krzywoblocki's results for isotropic plates become a special case and are reached directly in a simple way. For a more detailed exposition of certain phases of the paper and additional bibliography the reader is referred to the author's doctoral dissertation (36). The method is presented here in principle. Further details and specific examples will be reported separately.

Principle of Bergman Method

One mathematical formulation of the problem of stability of thin elastic plates consists in finding the smallest value of a positive parameter λ for which a homogeneous partial differential equation of the type[5]

$$L(w) - \lambda (N_x w_{,xx} + 2 N_{xy} w_{,xy} + N_y w_{,yy}) = 0 \quad \ldots [1]$$

subject to appropriate homogeneous boundary conditions, has a solution different from the trivial one $w = 0$. Here N_x, N_{xy}, N_y are certain reference values of the loading in the middle plane and $L(w)$ is a differential operator of the fourth order the form of which depends on the elastic properties of the plate.

For homogeneous anisotropic plates with elastic properties symmetric with respect to the middle plane

$$L(w) = b_{11} w_{,xxxx} + 4b_{16} w_{,xxxy} + 2(b_{12} + 2b_{66}) w_{,xxyy} + 4b_{26} w_{,xyyy} + b_{22} w_{,yyyy} \quad [2]$$

The coefficients b_{ij} ($i, j = 1, 2, 6$) are related to the elastic constants of the material in a well-known manner (36, 37). In the

[3] Numbers in parentheses refer to the Bibliography at the end of the paper.

[4] Certain convergence requirements for the sequences involved in an approximation by means of such a set of functions are assumed to be satisfied.

[5] Subscripts following a comma stand for differentiation; e.g.

$$w_{,x} = \frac{\partial w}{\partial x}, \quad w_{,xyy} = \frac{\partial^3 w}{\partial x \partial y^2}, \quad w_{,xxyy} = \frac{\partial^4 w}{\partial x^2 \partial y^2}, \text{ etc.}$$

presence of three mutually perpendicular planes of elastic symmetry the plate is called orthotropic. For such plates the coordinate planes are usually chosen as planes of elastic symmetry. Then the coefficients b_{16} and b_{26} vanish and a change of variables indicated by M. T. Huber (38) brings the operator $L(w)$ to the form

$$L(w) = w_{xxxx} + 2\kappa w_{xxyy} + w_{yyyy} \quad [3]$$

without changing the form of the remaining part of Equation [1]. The parameter κ obtains the value $\kappa = 1$ for isotropic plates so that the differential operator reduces to the well-known biharmonic expression

$$L(w) = \nabla^2\nabla^2 w = w_{xxxx} + 2w_{xxyy} + w_{yyyy} \quad [4]$$

Particular solutions of Equation [1] are functions of the parameter λ. When N_x, N_{xy}, N_y are constants, however, it is helpful to introduce another parameter k of the length scale related to λ in a way that makes the equation independent of any parameter. As suggested by M. Z. Krzywoblocki (35) the following change of variables is introduced

$$\xi = kx, \quad \eta = ky \quad [5]$$

and the differential equation of equilibrium, Equation [1], takes the form

$$L(w) - \frac{\lambda}{k^2}(N_x w_{\xi\xi} + 2N_{xy} w_{\xi\eta} + N_y w_{\eta\eta}) = 0 \quad [6]$$

There is no loss of generality if the parameter k is defined so that

$$\frac{\lambda}{k^2} = 1; \text{ i.e., } \lambda = k^2 \quad [7]$$

Then Equation [6] reduces to

$$L(w) - (N_x w_{\xi\xi} + 2N_{xy} w_{\xi\eta} + N_y w_{\eta\eta}) = 0 \quad [8]$$

and this equation is independent of any parameter. Once solutions of it are found, the ones of Equation [1] corresponding to a given value of the positive parameter λ are obtained by a simple change of variables given by Equation [5] with the value of k computed in terms of λ from Equation [7].

Assume now that a set of functions $f_i(\xi, \eta)$ $(i = 1, 2, 3, \ldots)$ is known satisfying Equation [8] without reference to any prescribed boundary conditions and suppose that every function $w(\xi, \eta)$ with continuous fourth-order partial derivatives can be represented in the form of an absolutely and uniformly convergent series

$$w(\xi, \eta) = \sum_{i=1}^{\infty} c_i f_i(\xi, \eta) \quad [9]$$

where c_i are constant coefficients and the same is possible for its partial derivatives up to the fourth order included.[4] As an approximation a finite number of terms can be considered

$$w_n(\xi, \eta) = \sum_{i=1}^{n} c_i f_i(\xi, \eta) \quad [10]$$

An expression of the type of Equation [9] or [10] in general does not satisfy the prescribed boundary conditions. The coefficients c_i $(i = 1, 2, 3, \ldots)$ can be chosen, however, in a way that insures at least an approximate fulfillment of these conditions.

The Boundary Conditions

The mathematical form of the boundary conditions depends on the way the edge of the plate is supported and expresses the fact that the transverse displacement, slope, moment, shearing force, and so on, are either zero or equal to prescribed values. As established by G. Kirchhoff two conditions of the general form

$$G_i[w(\xi, \eta)] = g_i(\xi, \eta) \qquad (i = 1, 2) \quad [11]$$

result. Here G_i $(i = 1, 2)$ is a differential operator depending on the particular case and $g_i(\xi, \eta)$ a function of ξ and η prescribed along the boundary line C of the middle plane of the plate. In case of a clamped plate, for example, the two conditions denoted by Equations [11] are explicitly

$$w = 0, \; w_n = \frac{\partial w}{\partial n} = 0 \quad [12]$$

where n denotes length measured within the middle plane of the plate in the direction of the normal to the boundary line C.

For $g_i(\xi, \eta)$ and $G_i[w(\xi, \eta)]$ sectionally continuous functions of ξ and η an equivalent formulation of the conditions of Equations [11] is

$$\int_c \{G_i[w(\xi, \eta)] - g_i(\xi, \eta)\}^2 ds = 0 \quad (i = 1, 2) \quad [13]$$

where the integration extends along the entire length s of the boundary line C of the middle plane of the plate. Since the integrand in each of the two Equations [13] is always positive it must be zero all along the boundary C except for isolated points; i.e., Equations [11] hold true at least in the absence of concentrated loads. The converse is obvious.

Instead of Equations [13] a single equation

$$\int_c \{G_1[w(\xi, \eta)] - g_1(\xi, \eta)\}^2 ds + \Lambda \int_c \{G_2[w(\xi, \eta)] - g_2(\xi, \eta)\}^2 ds = 0 \quad [14]$$

where Λ is any positive real number, can be used. Indeed if the sum of two positive numbers is zero each number must be equal to zero and Equations [13] follow. Then Equations [11] are true. The converse is again obvious.

If the infinite series of Equation [9] in terms of a sufficiently general set of functions $f_i(\xi, \eta)$ is used as an expression for $w(\xi, \eta)$, it should be possible to choose the coefficients c_i $(i = 1, 2, 3, \ldots)$ so that the conditions of Equations [13] or [14] are satisfied to any desired degree of approximation without the c_i themselves being vanishingly small. For a finite number of terms as given by Equation [10] the best that can be achieved is to make the positive expression on the left-hand side of Equation [14] as close to zero as possible; i.e., choose the coefficients c_i so that

$$\int_c \{G_1[w(\xi, \eta)] - g_1(\xi, \eta)\}^2 ds + \Lambda \int_c \{G_2[w(\xi, \eta)] - g_2(\xi, \eta)\}^2 ds = \text{minimum} \quad [15]$$

This formulation amounts to an approximation of the boundary conditions by the method of least squares.

A remark about the values of Λ is necessary here. In the exact formulation of Equation [14] the numerical value of Λ, as long as it remains positive, is immaterial. This is not true in the approximate form of Equation [15] where one can consider Λ as an additional parameter in the minimizing process. In general the value of Λ indicates the weight attributed in the satisfaction of each boundary condition. A reasonable assumption is to try to satisfy equally well both boundary conditions. This implies $\Lambda = 1$.

The approximate satisfaction of the boundary conditions in the sense described here was suggested by S. Bergman (39). As he pointed out, the practical value of an approximate formulation of the boundary conditions in the form of Equation [15] is enhanced

by the fact that a mathematically exact satisfaction of these conditions does not occur in actuality anyway.

For plate-stability problems the boundary conditions are homogeneous; i.e., $g_1(\xi, \eta) = g_2(\xi, \eta) = 0$ and the condition of Equation [15] specializes to

$$\int_c \{G_1[w(\xi, \eta)]\}^2 ds + \Lambda \int_c \{G_2[w(\xi, \eta)]\}^2 ds = \text{minimum} \quad [16]$$

Computation of Critical Values

With $w(\xi, \eta)$ expressed in terms of the particular solutions $f_s(\xi, \eta)$ by Equation [10] and after the indicated integration has been performed, the left-hand side of Equation [16] becomes a function $F(c_1, c_2, c_3, \ldots c_n)$ of the unknown coefficients $c_1, c_2, c_3, \ldots c_n$. For a fixed value of Λ a necessary condition for the minimum is

$$F_{,c_i} = \frac{\partial F}{\partial c_i} = 0 \qquad (i = 1, 2, 3, \ldots n) \quad [17]$$

There results a system of n linear homogeneous equations with n unknowns $c_1, c_2 \ldots c_n$

$$\sum_{j=1}^{n} a_{ij} c_j = 0 \qquad (i, j = 1, 2, 3, \ldots n) \quad [18]$$

where the a_{ij} are found after substitution from Equation [10] to Equation [16] and performance of the indicated integrations along the boundary.

In general the value of the determinant

$$A = |a_{ij}| \quad [19]$$

of the coefficients a_{ij} in the system of Equations [18] is different from zero and the only solution is $c_j = 0$ $(j = 1, 2, 3, \ldots n)$. Then Equation [10] shows that the only solution for the displacement is the trivial one $w = 0$. The values of the a_{ij} however depend on the parameter k and for certain values $k = k_i$ $(i = 1, 2, 3, \ldots)$ the determinant A may vanish. The system of Equations [18] has then an infinite number of solutions generally all proportional to one of them by an arbitrary factor. If the k with the smallest positive value is introduced in Equation [7] an estimate of the critical λ is obtained. The corresponding form of the buckled surface is given within a constant factor by Equation [10] with the values c_i obtained by solving the system of Equations [18] with vanishing determinant A of the coefficients a_{ij}. An expression in terms of the original co-ordinates x and y is found by a change of variables indicated by Equation [5].

Construction of Particular Solutions

All that is now necessary in principle is a sufficiently general set of particular solutions of the differential equation of equilibrium. This equation is of the elliptic type and, at least when the coefficients are polynomials in x and y, it has analytic solutions in the finite xy-plane. This suggests the use of the two complex conjugate variables

$$z = \xi + i\eta \qquad \bar{z} = \xi - i\eta \quad [20]$$

i.e.,

$$\xi = \frac{z + \bar{z}}{2} \qquad \eta = \frac{z - \bar{z}}{2i} \quad [20a]$$

Through them the displacement function $w(\xi, \eta)$ is transformed into a function $U(z, \bar{z})$ of the variables z and $\bar{z}$.

The differential equation satisfied by $U(z, \bar{z})$ is obtained from Equation [8] by means of the equations of transformation

$$\left.\begin{aligned}
w_{,\xi} &= U_{,z} + U_{,\bar{z}} \qquad w_{,\eta} = i(U_{,z} - U_{,\bar{z}}) \\
w_{,\xi\xi} &= U_{,zz} + 2U_{,z\bar{z}} + U_{,\bar{z}\bar{z}} \\
w_{,\xi\eta} &= i(U_{,zz} - U_{,\bar{z}\bar{z}}) \\
w_{,\eta\eta} &= -U_{,zz} + 2U_{,z\bar{z}} - U_{,\bar{z}\bar{z}} \\
w_{,\xi\xi\xi\xi} &= U_{,zzzz} + 4U_{,zzz\bar{z}} + 6U_{,zz\bar{z}\bar{z}} + 4U_{,z\bar{z}\bar{z}\bar{z}} + U_{,\bar{z}\bar{z}\bar{z}\bar{z}} \\
w_{,\xi\xi\xi\eta} &= i(U_{,zzzz} + 2U_{,zzz\bar{z}} - 2U_{,z\bar{z}\bar{z}\bar{z}} - U_{,\bar{z}\bar{z}\bar{z}\bar{z}}) \\
w_{,\xi\xi\eta\eta} &= -U_{,zzzz} + 2U_{,zz\bar{z}\bar{z}} - U_{,\bar{z}\bar{z}\bar{z}\bar{z}} \\
w_{,\xi\eta\eta\eta} &= -i(U_{,zzzz} - 2U_{,zzz\bar{z}} + 2U_{,z\bar{z}\bar{z}\bar{z}} - U_{,\bar{z}\bar{z}\bar{z}\bar{z}}) \\
w_{,\eta\eta\eta\eta} &= U_{,zzzz} - 4U_{,zzz\bar{z}} + 6U_{,zz\bar{z}\bar{z}} - 4U_{,z\bar{z}\bar{z}\bar{z}} + U_{,\bar{z}\bar{z}\bar{z}\bar{z}}
\end{aligned}\right\} \quad [21]$$

By substituting these values into Equation [8], an equation of the type

$$A\,U_{,zzzz} + B\,U_{,zzz\bar{z}} + C\,U_{,zz\bar{z}\bar{z}} + E\,U_{,z\bar{z}\bar{z}\bar{z}} + F\,U_{,\bar{z}\bar{z}\bar{z}\bar{z}} + K\,U_{,zz} + L\,U_{,z\bar{z}} + M\,U_{,\bar{z}\bar{z}} = 0 \quad [22]$$

is obtained.

For anisotropic plates the operator $L(w)$ present in Equation [8] is given by Equation [2] and the coefficients of Equation [22] are

$$\left.\begin{aligned}
A &= b_{11} + b_{22} - 2(b_{12} + 2b_{66}) + 4i(b_{16} - b_{26}) \\
B &= 4(b_{11} - b_{22}) + 8i(b_{16} + b_{26}) \\
C &= 6(b_{11} + b_{22}) + 4(b_{12} + 2b_{66}) \\
E &= 4(b_{11} - b_{22}) - 8i(b_{16} + b_{26}) = \bar{B} \\
F &= b_{11} + b_{12} - 2(b_{12} + 2b_{66}) - 4i(b_{16} - b_{26}) = \bar{A} \\
K &= -N_x + N_y - 2iN_{xy} \\
L &= -2(Nx + Ny) \\
M &= -N_x + N_y + 2iN_{xy} = \bar{K}
\end{aligned}\right\} \quad [23]$$

For orthotropic plates these coefficients become

$$A = F = 2(1 - \kappa), \quad B = E = 0, \quad C = 4(\kappa + 3) \quad [24]$$

and for isotropic plates they reduce further to

$$A = B = E = F = 0, \quad C = 16 \quad [25]$$

The values of K, L, M are independent of the elastic properties of the material and are given for all cases by Equations [23].

Since the solutions are analytic in both z and $\bar{z}$ they possess a power series expansion about the origin $z = \bar{z} = 0$ with respect to each of the independent variables z and $\bar{z}$. Therefore it can be written

$$U(z, \bar{z}) = \sum_{n=0}^{\infty} P^{(n)}(\bar{z}) \frac{z^n}{n!} = \sum_{n=0}^{\infty} Q^{(n)}(z) \frac{\bar{z}^n}{n!} \qquad (n = 0, 1, 2, 3, \ldots) \quad [26]$$

A particular solution of Equation [22] can now be obtained by substituting either one of the foregoing expressions in place of $U(z, \bar{z})$. Since the obtained result is a power series expression and equal to zero for all values of the independent variable, the coefficient of each power must be equal to zero. $P^{(n)}(\bar{z})$ and $Q^{(n)}(z)$ may be evaluated from the resulting equations and the particular solutions are then given by Equations [26].

For homogeneous anisotropic plates subject to a homogeneous force field N_x N_{xy}, N_y, the coefficient of z^n which must be zero is

$$AP^{(n+4)} + BP_{,\bar{z}}^{(n+3)} + (CP_{,\bar{z}\bar{z}}^{(n+2)} + KP^{(n+2)}) + (EP_{,\bar{z}\bar{z}\bar{z}}^{(n+1)} + LP_{,\bar{z}}^{(n+1)}) + (FP_{,\bar{z}\bar{z}\bar{z}\bar{z}}^{(n)} + MP_{,\bar{z}\bar{z}}^{(n)}) = 0 \qquad (n = 0, 1, 2, 3, \ldots) \quad [27]$$

This gives a recursion formula for $P^{(n+4)}$ in terms of $P^{(n)}$, $P^{(n+1)}$, $P^{(n+2)}$, $P^{(n+3)}$. Four arbitrary analytic functions of $\bar{z}$ can be taken as $P^{(0)}$, $P^{(1)}$, $P^{(2)}$, $P^{(3)}$ and the remaining $P^{(n)}$ (where $n = 4, 5, 6, \ldots$) evaluated by means of Equations [27]. A particular solution is then obtained from the first of Equations [26].

The result is somewhat different for isotropic plates for which $A = B = E = F = 0$ and $C = 16$. The recursion formulas become the differential equations

$$16\,P_{,\bar{z}\bar{z}}^{(n+2)} + KP^{(n+2)} = -LP_{,\bar{z}}^{(n+1)} - MP_{,\bar{z}\bar{z}}^{(n)} \quad (n = 0, 1, 2, 3, \ldots) \ldots [28]$$

There are only two arbitrary functions $P^{(0)}$ and $P^{(1)}$ involved in Equations [28], but they have each two independent solutions. This is equivalent to the four arbitrary analytic functions for anisotropic plates. One means of defining the arbitrary functions is by adding to the system of Equations [28] the two equations

$$16\,P_{,\bar{z}\bar{z}}^{(0)} + KP^{(0)} = 0 \qquad 16\,P_{,\bar{z}\bar{z}}^{(1)} + KP^{(1)} = -LP_{,\bar{z}}^{(0)} \ldots [29]$$

The boundary conditions

$$P^{(n)}(0) = 1 \qquad P_{,\bar{z}}^{(n)}(0) = 0 \qquad (n = 0, 1) \ldots [30]$$

imposed on Equations [29] give two functions and the conditions

$$P^{(n)}(0) = 0 \qquad P_{,\bar{z}}^{(n)}(0) = 1 \qquad (n = 0, 1) \ldots [31]$$

another independent two. Then for the remaining Equations [28] the following boundary conditions can be imposed

$$P^{(n+2)}(0) = P_{,\bar{z}}^{(n+2)}(0) = 0 \qquad (n = 0, 1, 2, 3, \ldots) \ldots [32]$$

Additional particular solutions, also analytic in z and $\bar{z}$, are obtained by means of expansions of the type

$$U_j'(z, \bar{z}) = z^j \sum_{n=0}^{\infty} P_1^{(n)}(\bar{z}) \frac{z^n}{n!} = z^j \sum_{n=0}^{\infty} Q_1^{(n)}(z) \frac{\bar{z}^n}{n!} \ldots [33]$$

where j is an integer. Without loss of generality these expressions can be written

$$U_j(z, \bar{z}) = \sum_{n=0}^{\infty} P^{(n)}(\bar{z}) \frac{z^{j+n}}{(j+n)!} = \sum_{n=0}^{\infty} Q^{(n)}(z) \frac{\bar{z}^{j+n}}{(j+n)!} \ldots [34]$$

A substitution in the differential equation of equilibrium shows that the recursion relations for $P^{(n)}(\bar{z})$ remain the same as previously. Therefore, once $P^{(n)}(\bar{z})$ are found, particular solutions are obtained from Equations [34] by assuming $j = 0, 1, 2, 3, \ldots$. In particular $j = 0$ gives the expansion of Equation [26]. The expressions of Equation [34] correspond to power series with the coefficients of the first j-terms equal to zero.

No recursion formulas are given explicitly for the $Q^{(n)}(z)$ (where $n = 0, 1, 2, \ldots$). They are obtained from the recursion formulas for $P^{(n)}(\bar{z})$ by substituting correspondingly P, $\bar{z}$, A, B, E, F, K, M by Q, z, F, E, B, A, M, K.

If a transformation back to the real variables is performed by means of Equations [20], the original equation of equilibrium, Equation [8], results. A particular solution $U(z, \bar{z})$ is separated in its real and imaginary parts. Since Equation [8] has real coefficients each of these parts separately satisfies the equation of equilibrium. Thus the real and imaginary parts of each particular solution $U_j(z, \bar{z})$ are particular solutions of Equation [8].

Linear Independence and Combination of Particular Solutions

It already has been pointed out that any analytic function satisfying the equation of equilibrium possesses a power series expansion. If the term of the expansion independent of $\bar{z}$ is nonzero a particular solution of the type of Equation [26] results. If the first few coefficients are zero a particular solution is obtained in the form of Equations [34] with appropriate value of the integer j. In other words every solution of Equation [22] can be written in the form of Equations [34] and, in specific cases, of Equations [26].

A linear combination of the particular solutions given by Equations [34] for $j = 0, 1, 2, 3, \ldots m$ multiplied by constants c_j $(j = 0, 1, 2, 3, \ldots m)$ gives

$$\sum_{j=0}^{m} c_j U_j(z, \bar{z}) = \sum_{n=0}^{\infty} P^{(n)}(\bar{z})\, z^n \left[\sum_{j=0}^{m} \frac{c_j}{(j+n)!} z^j \right] \ldots [35]$$

This expression cannot be identically equal to zero unless all the c_j are zero. Therefore the particular solutions are linearly independent. They are also infinite in number, one being obtained for each value of the integer m. The particular solutions in terms of $Q^{(n)}(z)$ are also linearly independent and can be combined in the manner indicated by Equations [35] to give particular solutions of Equation [22].

Particular solutions of Equation [8] can now be easily obtained by taking a linear combination of real and imaginary parts of the expressions

$$U_j(z, \bar{z}) = \sum_{n=0}^{\infty} \left\{ P^{(n)}(\bar{z}) \frac{z^{j+n}}{(j+n)!} + Q^{(n)}(z) \frac{\bar{z}^{j+n}}{(j+n)!} \right\}$$

$$(j = 0, 1, 2, \ldots) \ldots [36]$$

One may expect that a linear combination of a sufficiently large number of such particular solutions would be general enough for approximating the buckled surface.

Fairly general expressions should be obtained also by using, as arbitrary analytic functions in the construction of particular solutions, such functions as

$$\left.\begin{matrix} \sin z, & \sin 2z, & \sin 3z \ldots \ldots \\ \cos z, & \cos 2z, & \cos 3z \ldots \ldots \end{matrix}\right\} \ldots [37]$$

possessing non-zero derivatives of all orders. Specifically any four of these functions can be taken as $P^{(0)}$, $P^{(1)}$, $P^{(2)}$, $P^{(3)}$ and introduced in the recursion formulas of Equations [27]. Two such functions would be sufficient for the differential equations of isotropic plates, Equations [28]. Further research may clarify if this alternative possesses any advantages against the choice of particular solutions indicated by Equation [35].

Nonuniform Loading in Middle Plane—Inhomogeneous Materials

For homogeneous materials the coefficients A, B, C, E, F are real or complex constants, but in general K, L, M, depend on both z and $\bar{z}$, as for example in the case of cantilever plates; for nonhomogeneous materials even the coefficients A, B, C, E, F are functions of z and $\bar{z}$. In such cases the change of variables indicated by Equations [5] is no longer useful. The general method however for constructing particular solutions is still applicable if the functions N_x, N_{xy}, N_y are polynomials in x and y or can be approximated with sufficient closeness by polynomials. A transformation to the complex conjugate variables z and $\bar{z}$ defined by Equations [20] can again be performed and the power series of Equations [26] and [34] assumed; but the form of the resulting recursion formulas or equations cannot be predicted without knowing the explicit form of the functions N_x, N_{xy}, N_y. Nevertheless, once they are found and if they can be solved the particular solutions are given again by Equations [26] or [34].

A certain modification is further necessary in the actual process of computing the critical value of λ. The particular solutions will be functions of λ. Then various values of λ should be assumed and the value of the determinant A of the coefficients a_{ij} of the system of Equations [18] be computed. The smallest positive value of λ for which this determinant vanishes is the critical value sought.

Evaluation of Vibrational Modes and Frequencies

In cases of transverse vibrations with separable time variable and always for free transverse vibrations the equation of motion after a separation of the time variable reduces to the general form

$$L(w) - (N_x w_{,xx} + 2N_{xy} w_{,xy} + N_y w_{,yy}) - \omega^2 w = 0 \quad \ldots\ldots [38]$$

and the procedure followed for Equation [1] can be repeated. No specific discussion however will be given in the present paper.

Comparison With Related Investigations

For isotropic plates M. Z. Krzywoblocki (35), on the basis of integral representations and recursion formulas of S. Bergman (33), arrived at equations that are essentially equivalent to Equations [28] and [29] of the $P^{(\nu)}(\bar{z})$ with the imposed boundary conditions, Equations [30]–[32], and gave explicitly solutions for the first three $P^{(\nu)}(\bar{z})$. For $K = M = 16$ and $L = 32$ which corresponds (within a constant factor that can be absorbed in λ) to uniform compression in one direction, he takes as approximations of particular solutions ($\nu = 1, 2, 3, \ldots$)

$$U(z, \bar{z}) = (\cos \bar{z})\, z^\nu + (\sin \bar{z} - \bar{z} \cos \bar{z}) \frac{z^{\nu+1}}{\nu + 1} + \frac{1}{2} \bar{z}^2 (\cos \bar{z}) \frac{z^{\nu+2}}{(\nu + 2)(\nu + 1)} \quad [39]$$

Utilizing Krzywoblocki's solutions,[6] the results for Equations [28] and [29] for this case can be obtained. They are

$$P^{(0)}(\bar{z}) = \cos(\bar{z}), \quad P^{(1)} = \sin \bar{z} - \bar{z} \cos \bar{z},$$

$$P^{(2)}(\bar{z}) = \frac{1}{2} \bar{z}^2 \cos \bar{z} + \frac{1}{2} \bar{z} \sin \bar{z} \quad [40]$$

and from Equation [34] the first few terms of a particular solution become

$$U(z, \bar{z}) = \frac{16}{n!} \left\{ \cos(\bar{z})\, z^n + (\sin \bar{z} - \bar{z} \cos \bar{z}) \frac{z^{n+1}}{n + 1} + \frac{1}{2} (\bar{z}^2 \cos \bar{z} + \bar{z} \sin \bar{z}) \frac{z^{n+2}}{n + 2} \right\} \quad [41]$$

which, except for the immaterial constant factor $16/n!$ and one term not included in Krzywoblocki's expression, is identical to his particular solution, Equation [39]. The four arbitrary analytic functions in Bergman's integral representations (33) are replaced in the present paper by the four arbitrary analytic functions of the recursion formulas.

Concluding Remarks

The approach presented here is an extension of the classical mathematical method of solving ordinary differential equations by power series. The use of conjugate complex variables rather than real variables becomes necessary because real variable expressions, as of the type $\sum_{m=1}^{\infty} \sum_{n=1}^{\infty} \sin mx \sin ny$, may vanish along continuous lines and thus present unacceptable restrictions. Indeed, the undetermined scale of length k indicated by Equations [5] shows that the zero displacement along a continuous line may fall within the undefined boundary. The zero displacement may be also unacceptable in the case of variable force field in the middle plane of the plate or of inhomogeneous materials, for which the technique of a linear change of variables in accordance with Equations [5] is not applicable.

The only example based on Bergman's method for the isotropic plate equation (33), was given by M. Z. Krzywoblocki (35) and refers to the buckling of a triangular plate. It is sufficient however to indicate the feasibility of the method. Further examples based on the present paper will be reported separately by the author. The use of an additional restraining condition by Krzywoblocki in the minimal formulation of the boundary conditions will also be discussed. The case of concentrated loads can be readily reduced to the procedure reported in the paper.

[6] See reference (35) pp. 37–40.

Acknowledgment

The author wishes to express his appreciation to his dissertation adviser Prof. I. S. Sokolnikoff for encouragement and helpful criticism during the investigation.

BIBLIOGRAPHY

1 "Theory of Elastic Stability," by S. Timoshenko, McGraw-Hill Book Company, Inc., New York, N. Y., and London, England, 1936, pp. 324–418.

2 "On the Stability of a Plane Plate Under Thrusts in Its Own Plane, With Applications to the Buckling of the Sides of a Ship," by G. H. Bryan, Proceedings of the London Mathematical Society, vol. 22, 1891, pp. 54–67.

3 "On the Stability of Rectangular Compressed Plates" (in Russian), by S. Timoshenko, Bulletin of the Polytechnic Institute of Kiev, 1907.

4 "Über die Knicksicherheit ebener Bleche," by H. Reissner, *Zentralblatt der Bauverwaltung*, vol. 14, 1909, pp. 93–96 and p. 151.

5 "Einige Stabilitätsprobleme der Elastizitätstheorie," by S. Timoshenko, *Zeitschrift für Mathematik und Physik*, vol. 58, 1910, pp. 343–360.

6 "The Theory of Sound," by Lord Rayleigh, first edition, 1877, London, England; first American edition, Dover Publications, New York, N. Y., 1945, vol. 1, pp. 113–118.

7 "Über eine neue Methode zur Lösung gewisser Variationsprobleme der mathematischen Physik," by W. Ritz, *Journal für die reine und angewandte Mathematik*, vol. 135, 1909, pp. 1–61.

8 "Theorie der Transversalschwingungen einen quadratischen Platte mit freien Rändern," by W. Ritz, *Annalen der Physik*, Vierte Folge, vol. 28, 1909, pp. 737–786.

9 "Sur la Stabilité des Systèmes Élastiques," by S. Timoshenko, *Annales des Ponts et Chaussées*, 1913; vol. 13, p. 496; vol. 14, p. 73; vol. 17, p. 372.

10 "Konvergenz und Fehlerabschätzung beim Ritzschen Verfahren," by E. Trefftz, *Mathematische Annalen*, vol. 100, 1928, pp. 503–521.

11 "Über die Stabilität versteifter Platten," by S. Timoshenko, *Der Eisenbau*, vol. 12, 1921, p. 147.

12 "Buckling of a Triangular Plate by Shearing Forces," by J. M. Klitchieff, *Quarterly Journal of Mechanics and Applied Mathematics*, vol. 4, September, 1951, pp. 257–259.

13 "Allgemeine Lösung der Knickungsaufgabe für Rechteckige Platten," by S. Iguchi, *Ingenieur Archiv*, vol. 7, 1936, pp. 207–215.

14 "Die Knickung der Vierseitig Eingespannten Rechteckigen Platte durch Schubkräfte," by S. Iguchi, Proceedings of the Royal Mathematical Society, Japan, vol. 20, 1938, p. 814.

15 "Vibration of Rectangular Plates, by the Ritz Method," by D. Young Journal of Applied Mechanics, Trans. ASME, vol. 72, 1950, pp. 448–453.

16 "Vibration of Rectangular and Skew Cantilever Plates," by M. V. Barton, Journal of Applied Mechanics, Trans. ASME, vol. 73, 1951, pp. 129–134.

17 "Theory of Elasticity," by I. S. Sokolnikoff, McGraw-Hill Book Co., New York, N. Y., London, England, 1946, pp. 304–334.

18 "The Buckling Load for a Rectangular Plate With Four Clamped Edges," by G. I. Taylor, *Zeitschrift für angewandte Mathematik und Mechanik*, vol. 13, 1933, pp. 147–152.

19 "Die Knickfestigkeit Rechteckiger Platten," by O. H. Faxén,

Zeitschrift für angewandte Mathematik, und Mechanik, vol. 15, 1935, pp. 268–277.

20 "Buckling of a Rectangular Plate With Four Clamped Edges Reexamined With an Improved Theory," by K. Sezawa and W. Watanabe, Reports of the Aeronautical Research Institute, Tokyo Imperial University, vol. 11, 1936, pp. 409–418.

21 "Methoden der Mathematischen Physik," by R. Courant and D. Hilbert, second edition, Julius Springer, Berlin, Germany, 1931; Photolithoprinted reproduction, Interscience Publishers, Inc., New York, N. Y., vol. 1, chapter 6, p. 353.

22 "On a Minimal Problem in the Theory of Elasticity," by A. Weinstein, *Journal of the London Mathematical Society*, vol. 10, 1935, pp. 184–192.

23 "Die Bestimmung der Knicklast gedrückter, rechteckiger Platten," by E. Trefftz, *Zeitschrift für angewandte Mathematik und Mechanik*, vol. 15, 1935, pp. 339–344.

24 "Étude des Équations aux Derivées Partielles de la Theorie des Plaques Élastiques," by A. Weinstein, Memorial des Sciences Mathematiques, vol. 88, 1937, pp. 1–62.

25 "The Lagrangian Multiplier Method of Finding Upper and Lower Limits to Critical Load of Clamped Plates," by B. Budiansky and P. C. Hu, National Advisory Committee for Aeronautics, Technical Note 1103, 1946, 32 pp.

26 "Note on the Lagrangian Multiplier Method in Elastic Stability Analysis," by B. Budiansky, P. C. Hu, and R. W. Conner, National Advisory Committee for Aeronautics, Technical Note 1558, May 1948, 46 pp.

27 "Bending and Buckling of Elastic Plates" (mimeographed), by J. J. Stoker, New York University, 1941, pp. 54–56.

28 "Finite Difference Equations for the Analysis of Thin Rectangular Plates With Combinations of Fixed and Free Edges," by M. V. Barton, Defense Research Laboratory, University of Texas, Austin, Texas, DRL-212, CF-1258, May 1949.

29 "Numerical Computation of Buckling Loads by Finite Differences," by M. G. Salvadori, Proceedings of the American Society of Civil Engineers, vol. 75, 1949, pp. 1441–1475.

30 "The Solution of Elastic Plate Problems by Electrical Analogies," by R. H. MacNeal, JOURNAL OF APPLIED MECHANICS, Trans. ASME, vol. 73, 1951, pp. 59–67.

31 "The Elastic Stability of Plane Frameworks and of Flat Plating," by D. G. Christopherson, L. Fox, J. R. Green, and R. V. Southwell, Philosophical Transactions of the Royal Society of London, series A, vol. 239, 1945, pp. 461–485.

32 "Über die Entwicklung der harmonischen Funktionen der Ebene und des Raumes nach Orthogonalfunktionen," (Doktordissertation) by S. Bergman, *Mathematische Annalen*, vol. 86, 1922, pp. 238–371.

33 "Solutions of Linear Partial Differential Equations of the Fourth Order," by S. Bergman, *Duke Mathematical Journal*, Duke University, Durham, N. C., vol. 11, 1944, pp. 617–649.

34 "Construction of a Complete Set of Solutions of a Linear Partial Differential Equation in Two Variables by Use of Punch-card-machines," by S. Bergman, *Quarterly of Applied Mathematics*, vol. 4, 1946, pp. 233–245.

35 "A General Approximation Method in the Theory of Plates of Small Deflection," by M. Z. Krzywoblocki, *Quarterly of Applied Mathematics*, vol. 6, 1948, pp. 31–52. See also vol. 7, 1949, p. 236.

36 "Stability of Thin Anisotropic Elastic Plates," by G. A. Zizicas, a dissertation for the degree of Doctor of Philosophy in Engineering, University of California, Los Angeles, Calif., June 1952, 154 pp.

37 "Mathematical Theory of Elasticity" (mimeographed), by I. S. Sokolnikoff, Brown University Notes, Providence, R. I., 1941, pp. 319–329.

38 "Die Theorie der kreuzweise bewehrrten Eisenbetonplatten nebst Anwendungen auf mehrere bautechnish wichtige Aufgaben über recteckige Platten," by M. T. Huber, Der Bauingenieur, vol. 4, 1923, pp. 354–360, 392–395.

39 "Über Schubknickung von isotropen und anisotropen Platten," by S. Bergman, Proceedings of the Third International Congress of Applied Mechanics, Stockholm, Sweden, 1930, pp. 83–87.

Effect of Surface Condition on Creep of Some Commercial Metals

By E. D. SWEETLAND[1] and E. R. PARKER[2]

The relative creep rate of specimens of 2S aluminum and commercial drawn copper were investigated with the oxide surface layers removed and then, under the same conditions, after the oxide was permitted to form. The oxide was removed mechanically by stripping the test specimens in an inert atmosphere furnace so equipped that an axial stress could be applied and the creep rate determined without disturbing the atmosphere. After the oxide-free specimen was observed to be creeping essentially linearly with time (i.e., the quasiviscous, secondary creep range was established), air was admitted to the furnace. The extension versus time plot was continued after admission of air and the temperature held constant. Since all of the known parameters affecting creep rate (temperature, grain size, degree of work hardening, stress, and so on) except the gaseous environment were the same before and after admitting air, the effect of this change could be isolated. A decrease in creep rate was observed after air had been admitted to the furnace. These experimental results indicate that the presence of an oxide surface layer on the commercial grades of pure copper and aluminum increases the creep strength of these metals. The manner in which this relatively thin surface layer contributes to the strength of the parent metal is not clear, but the phenomenon is consistent with the theory of dislocations as presented by G. I. Taylor if it is assumed that the oxide inhibits the generation and/or migration of dislocations.

Introduction

SOME recent investigations (1, 2)[3] have indicated that the surface condition of a metal plays an important role in determining its creep rate. These observations are consistent with the theory of dislocations first presented by G. I. Taylor (3) since the external surface, as well as phase and grain boundaries, present discontinuities wherein dislocations might form most readily. There is abundant evidence (4, 5) that oxidation affects the rupture life of many metals. The authors have encountered instances wherein the oxide surface film has tended to decrease the creep rate of commercially pure aluminum and copper specimens.

Experimental Apparatus

The setup for mounting and stripping the oxide from the specimen is shown in Fig. 1. A $\frac{1}{4}$-in-diam specimen, 4 in. long, was mounted in a yoke-and-gimbal assembly in an inert-atmosphere furnace as shown. The hardened-steel stripping die, which was 0.0005 in. smaller in diameter than the specimen, was drawn over the specimen in an inert atmosphere. Thus the outer layer of the specimen was removed, leaving a metal surface free from oxide. Weights were added, thereby applying a tensile load, and the extension was read on a dial indicating gage coupled to the lower shaft below the furnace. Provision was made so that the inert atmosphere (helium) could be shut off and air introduced when desired.

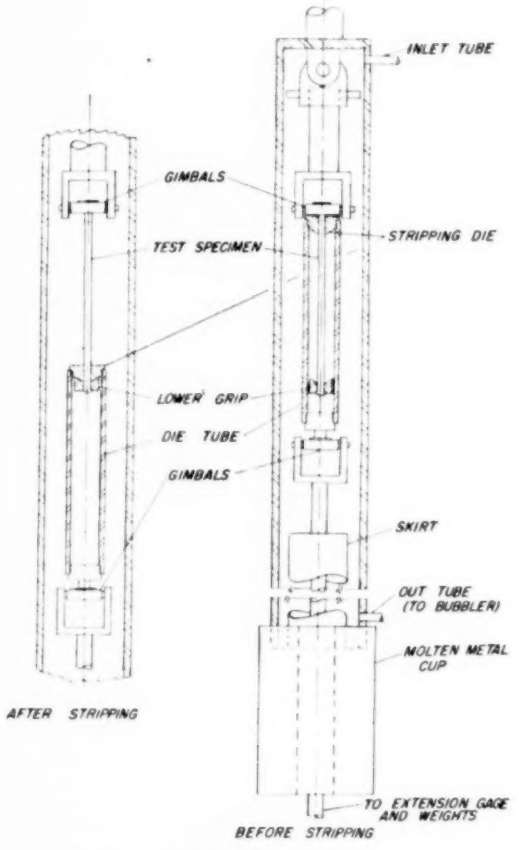

Fig. 1 Test Setup

Experimental Results

The effect of the introduction of air on the 2S aluminum specimens is shown in Fig. 2, while Fig. 3 shows the results for a drawn-copper specimen. The creep rates and the relative changes in rates after admission of air are shown in Table 1.

[1] Consulting Engineer, San Francisco, Calif. Jun. ASME.

[2] Professor of Metallurgy, University of California, Berkeley, Calif.

[3] Numbers in parentheses refer to the Bibliography at the end of the paper.

Presented at the West Coast Meeting of the Applied Mechanics Division, Los Angeles, Calif., June 26–28, 1952, of The American Society of Mechanical Engineers.

Discussion of this paper should be addressed to the Secretary, ASME, 29 West 39th Street, New York, N. Y., and will be accepted until April 10, 1953, for publication at a later date. Discussion received after the closing date will be returned.

Note: Statements and opinions advanced in papers are to be understood as individual expressions of their authors and not those of the Society. Manuscript received by ASME Applied Mechanics Division, West Coast Group, November 26, 1951.

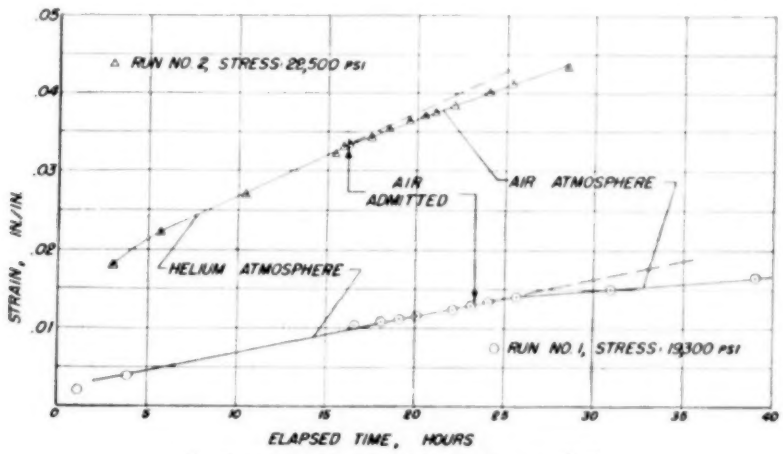

FIG. 2 CREEP CURVES OF 28 ALUMINUM AT 400 F

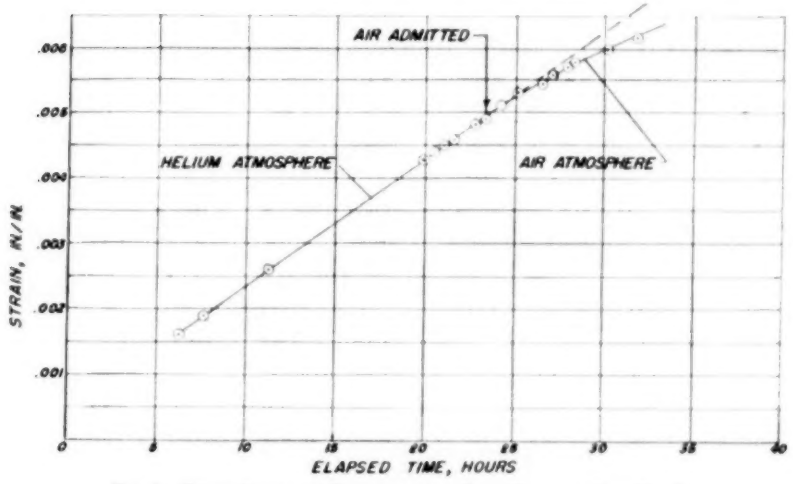

FIG. 3 CREEP CURVE OF COMMERCIALLY PURE COPPER; RUN NO. 3

TABLE 1 CREEP RATE OF SPECIMENS

Run no.	Metal	Tensile stress, psi	Temp, deg F	Creep rates, in/in/hr — After stripping	After admission of air	Decrease in creep rate, per cent
1	28 Al	19300	400	0 00048	0 00020	58 3
2	28 Al	22500	400	0 00107	0 00087	18 7
3	Cu	52000	400	0 00020	0 000125	37 5

POSSIBLE CAUSES FOR CHANGE IN CREEP RATE

The data recorded in Table 1 and shown in Figs. 2 and 3 clearly indicate a decrease in creep rate after the copper and aluminum specimens are permitted to form their oxides. There is too little known about the plastic flow of metals in general, and of creep in particular, to permit a rigorous theoretical analysis of the observed results—even if the data covered a much broader range of conditions than the foregoing. However, the several different ways in which an oxide film could affect creep rate will be considered and some deductions may be made as to the relative magnitudes of these effects:

1 The oxide film might contribute directly to an increase in strength by assuming a higher portion of the total tensile load than did the same metal before being oxidized. This effect would, at best, be relatively small and probably would tend to increase rather than decrease the strain rate for the following reasons: (*a*) The oxide film formed in dry air on both copper and aluminum is much less than 0.001 in. thick (6); thus, for a $^1/_8$-in-diam specimen as used, the cross section of oxide film is less than 3 per cent of the cross section of the unoxidized metal. (*b*) While the authors were unable to find any quantitative data on the tensile strength of the oxides formed in this manner, it seems doubtful that the relatively imperfect (6) film could take much, if any, tensile stress. (*c*) Since there is a volumetric increase accompanying both the aluminum-and-copper-oxide formation, the oxide film could not take any tensile stress until the specimen had elongated sufficiently to put the film in tension; however, as the specimen elongates, new oxide could continue to form and the film would remain under compression. Therefore this effect would tend to increase rather than decrease the creep rate. If the oxide did not form rapidly enough to keep this layer in compression, it still presumably could not take an appreciable tensile load due to its imperfections (6).

2 Residual stresses developed in the oxide-free core by the formation of the oxide might alter the creep rate. This effect is closely associated with that considered in the preceding paragraph, and it also would tend to increase rather than decrease the creep rate. In the case of copper there is more than a 10 per cent increase in volume when a given amount of copper becomes CuO, which would indicate that the parent metal below the oxide would be under a tensile rather than a compressive load. Also the very tightly packed oxide film of aluminum (partly responsible for the "self-stopping" nature of aluminum oxidation (6)), would tend to put the metal underneath the film in tension. Since, in both of these cases, these residual stresses are acting in the same direction as the applied tensile load, the creep rate would be expected to increase rather than decrease if this were the predominant effect.

3 The oxide film may form a protective layer which tends to inhibit the formation or growth of dislocations on the surface, thereby decreasing the creep rate. This theory seems compatible with the dislocation theory (3) and the results found by Pickus and Parker (2) with the electroplating and deplating of specimens under load. Since the theory of dislocations indicates that dislocations may be generated at grain boundaries, phase boundaries, and external surfaces, the effect of the surface oxide would be expected to be greater with larger grain sizes; and, indeed, a much more pronounced effect was noted in reference (2) where single crystals were used, than with the polycrystals used in the authors' experiments. Work by Sherby and Dorn (7) indicates that the larger grain sizes in 28 aluminum promote lower creep rates at elevated temperatures. This consideration suggests another experimental investigation which might prove illuminating; that is, to determine the relative change in creep rates before and after oxide formation with grain size as a parameter.

4 A final consideration as a possible cause of the change in creep rate is that the oxide film, aside from inhibiting the generation of dislocations, might also tend to restrain their migration by preventing their escape at the surface. If this were the case, the strength of the specimen should be increased in two ways, namely, by restraining dislocations at the outer layers, creep would be lessened directly, and the building up of dislocations in the outer surface would cause work-hardening which would increase the tensile strength of these regions. Thus, indirectly, the oxide formation might be the cause of beneficial residual stresses being built up in the specimen as creep progressed. A distinction is here being made between this effect and any direct effect the oxide film might have in producing residual stresses as the oxide forms, as considered in the foregoing.

Conclusions

1 The oxide surface film decreases the creep rate of 28 aluminum and commercial grade of tough pitch copper wire.

2 This decrease in creep rate is probably primarily attributable to the oxide inhibiting the generation and/or migration of dislocations.

3 Metals designed for use in high-temperature environments should be tested under conditions which produce the same type and degree of surface oxidation as the environment under which the metal is to operate.

Bibliography

1 "Creep as a Surface Dependent Phenomenon," by M. R. Pickus and E. R. Parker, ASTM Special Technical Publication No. 108, Symposium on Corrosion of Materials at Elevated Temperatures, 1951.

2 "Creep Behavior of Zinc Modified by Copper in the Surface Layer," by M. R. Pickus and E. R. Parker, *Journal of Metals*, vol. 191, September, 1951, pp. 792–796.

3 "The Mechanism of Plastic Deformation of Crystals," by G. I. Taylor, Proceedings of the Royal Society of London, series A, vol. 145, 1934, pp. 362–404.

4 "Intercrystalline Cohesion and the Stress-Rupture Test," by H. H. Bleakney, Proceedings of the ASTM, vol. 47, 1947, pp. 575–595.

5 "The Effect of Environment on the Stress-Rupture Properties of Metals at Elevated Temperatures," by O. C. Shepard and W. Schalliol, ASTM Special Technical Publication No. 108, Symposium on Corrosion of Materials at Elevated Temperatures, 1951.

6 "Corrosion Handbook," by H. H. Uhlig, John Wiley & Sons Inc., New York, N. Y., 1948.

7 "Effect of Annealing on the Creep Properties of 28-O Alloy," by O. D. Sherby and J. E. Dorn, Proceedings of the ASTM, vol. 51, 1951.

The New Approach to Shell Theory: Circular Cylinders

By E. H. KENNARD,[1] WASHINGTON, D. C.

Taking Epstein's[2] basic work on elastic vibrations in plates and shells, the author proceeds to construct expressions for the distributions of stress and displacements. From these, stress resultants are calculated. The principal effects of external load on the faces of the shell are included, and the validity of the approximation and practical applications of results are discussed.

THE theory of thin elastic shells has been developed mostly on the basis of physical analysis and with the help of certain simplifying assumptions. Usually it has been assumed that lines normal to the median surface of the shell remain normal to it, and effects of the Poisson contraction in the direction of the thickness are partly or wholly ignored.

In 1942, however, P. S. Epstein published a more thoroughgoing analysis.[2] Starting from the three-dimensional equations of elasticity, he, in effect, considers all variable quantities to be expanded in a series of powers of a co-ordinate perpendicular to the median surface and then introduces the restriction to a thin shell by satisfying the boundary conditions on the two faces of the shell only through the third power of this co-ordinate. In harmony with this restriction, only terms through the second power of the thickness are retained. Details are worked out only for cylindrical shells, for which the equations of motion were found to differ considerably from those used by other writers on shell theory.

Since Epstein's paper seems not to have attracted attention, one purpose of the present paper is to offer a paraphrase that proceeds along more concrete and more usual lines. Expressions for the distributions of stress and displacements are constructed and from these the stress resultants are calculated. These resultants are actually needed in some static problems. The treatment also will be generalized a little by including the principal effects of external load on the faces of the shell. Finally, the validity of the approximation and the practical application of the results will be discussed.

Fundamental Equations

Let h denote the thickness of the shell and R the radius of its undistorted median surface. Let x, s, r be cylindrical co-ordinates with x taken in the longitudinal direction and r denoting distance from the axis; $s = R\phi$ where ϕ is the azimuth angle about the axis, Fig. 1. For convenience, radial distance from the initial median surface will on occasion be denoted by z; thus $z = r - R$. The components of displacement of any point of the shell, assumed infinitesimal, in the x, s, and r-directions, respectively, will be denoted by u, v, w.

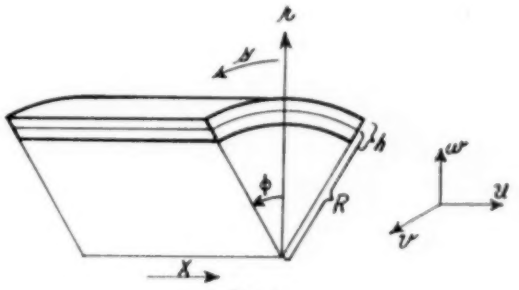

FIG. 1

It is readily seen that the six components of strain at any point, in an obvious modification of Timoshenko's notation, can be written

$$\epsilon_x = \frac{\partial u}{\partial x}, \quad \epsilon_s = \frac{R}{r}\frac{\partial v}{\partial s} + \frac{w}{r}, \quad \epsilon_r = \frac{\partial w}{\partial r}$$

$$\gamma_{xs} = \frac{R}{r}\frac{\partial u}{\partial s} + \frac{\partial v}{\partial x}, \quad \gamma_{xr} = \frac{\partial u}{\partial r} + \frac{\partial w}{\partial x}$$

$$\gamma_{sr} = \frac{\partial v}{\partial r} - \frac{v}{r} + \frac{R}{r}\frac{\partial w}{\partial s}$$

Here the factor R/r results from the fact that the element of length in the s-direction is rds/R.

To shorten the notation, subscripts will be written hereafter to denote $\partial/\partial x$ and $\partial/\partial s$ and (following Epstein) a prime for $\partial/\partial r$. To avoid confusion, it also will be well to write for the stresses, starting with Timoshenko's notation

$$\sigma_1 = \sigma_{xx}, \ \sigma_2 = \sigma_{ss}, \ \sigma_3 = \sigma_{rr}$$

$$\tau = \tau_{xs}, \ \tau_1 = \tau_{xr}, \ \tau_2 = \tau_{sr}$$

Then, from the usual equations for the stresses in terms of the strains, it is readily found that

$$\sigma_1 = E_z\left[u_x + \nu\left(R\frac{v_s}{r} + \frac{w}{r}\right)\right] + \theta\nu\sigma_3 \quad [1a]$$

$$\sigma_2 = E_z\left(\nu u_x + R\frac{v_s}{r} + \frac{w}{r}\right) + \theta\nu\sigma_3 \quad [1b]$$

$$\sigma_3 = E_1\left[(1-\nu)w' + \nu\left(u_x + R\frac{v_s}{r} + \frac{w}{r}\right)\right] \quad [2]$$

$$\tau_1 = \frac{1}{2}(1-\nu)E_z(u' + w_x) \quad [3a]$$

$$\tau_2 = \frac{1}{2}(1-\nu)E_z\left(v' - \frac{v}{r} + R\frac{w_s}{r}\right) \quad [3b]$$

---

[1] Physicist, David Taylor Model Basin.

[2] "On the Theory of Elastic Vibrations in Plates and Shells," by P. S. Epstein, *Journal of Mathematics and Physics*, vol. 21, 1942, p. 198; also W. Z. Chien, *Quarterly of Applied Mathematics*, vol. 1, 1943, p. 297; vol. 2, 1944, pp. 43, 120.

Contributed by the Applied Mechanics Division and presented at the Fall Meeting, Chicago, Ill., September 8–11, 1952, of THE AMERICAN SOCIETY OF MECHANICAL ENGINEERS.

Discussion of this paper should be addressed to the Secretary, ASME, 29 West 39th Street, New York, N. Y., and will be accepted until April 10, 1953, for publication at a later date. Discussion received after the closing date will be returned.

NOTE: Statements and opinions advanced in this paper are to be understood as individual expressions of the author and not those of the Navy Department or of the Society. Manuscript received by ASME Applied Mechanics Division, December 12, 1951. Paper No. 52—F-9.

$$\tau = \frac{1}{2}(1-\nu)E_s\left(R\frac{u_s}{r} + v_s\right) \qquad [4]$$

where

$$E_s = \frac{E}{1-\nu^2},\ \theta = \frac{1}{1-\nu},\ E_3 = \frac{E}{(1+\nu)(1-2\nu)} \qquad [5a, b, c]$$

E being Young's modulus and ν the Poisson ratio. Here w' has been eliminated from σ_1 and σ_2 by means of Equation [2], since for a thin-shell theory all reference to the co-ordinate r, or to σ_3, τ_1, and τ_2 must be eliminated.

The equations of motion at any point of the shell then are, ρ being the density of the material

$$\rho\ddot{u} = \sigma_{1s} + R\frac{\tau_s}{r} + \tau_1' + \frac{\tau_1}{r} \qquad [6a]$$

$$\rho\ddot{v} = R\frac{\sigma_{2s}}{r} + \tau_s + \tau_2' + 2\frac{\tau_2}{r} \qquad [6b]$$

$$\rho\ddot{w} = \sigma_3' + \frac{\sigma_3}{r} - \frac{\sigma_2}{r} + \tau_{1s} + R\frac{\tau_{2s}}{r} \qquad [6c]$$

These equations are obtained by considering a volume element with faces perpendicular to x, s, and r, whose respective areas are $dr(rd\,\phi)$ or $(r/R)dx\,ds$, $dx\,dr$, $rd\,\phi\,dx$ or $(r/R)\,ds\,dx$; the volume of the element is $rd\,\phi\,dx\,dr$ or $(r/R)dx\,ds\,dr$. Half of the term $2\,\tau_2/r$ arises from the difference in direction of the shearing forces on faces perpendicular to s.

In preparation for the final suppression of the r-derivatives, we solve Equations [6a, b, c], [2], and [3a, b] for these derivatives and then differentiate once more

$$\sigma_3' = -\frac{\sigma_3}{r} - \tau_{1s} - R\frac{\tau_{2s}}{r} + \frac{\sigma_2}{r} + \rho\ddot{w} \qquad [7a]$$

$$\tau_1' = -\frac{\tau_1}{r} - \sigma_{1s} - R\frac{\tau_s}{r} + \rho\ddot{u} \qquad [7b]$$

$$\tau_2' = -2\frac{\tau_2}{r} - R\frac{\sigma_{2s}}{r} - \tau_s + \rho\ddot{v} \qquad [7c]$$

$$u' = -w_s + 2\theta\frac{\tau_1}{E_s} \qquad [8a]$$

$$v' = -R\frac{w_s}{r} + \frac{v}{r} + 2\theta\frac{\tau_2}{E_s} \qquad [8b]$$

$$w' = -\theta\nu\left(u_s + R\frac{v_s}{r} + \frac{w}{r}\right) + \theta\frac{\sigma_3}{E_3} \qquad [8c]$$

$$\sigma_3'' = -\frac{\sigma_3'}{r} + \frac{\sigma_3}{r^2} - \tau_{1s}' - R\frac{\tau_{2s}'}{r} + R\frac{\tau_{2s}}{r^2} + \frac{\sigma_2'}{r} - \frac{\sigma_2}{r^2} + \rho\ddot{w}' \qquad [9a]$$

$$\tau_1'' = -\frac{\tau_1'}{r} + \frac{\tau_1}{r^2} - \sigma_{1s}' - R\frac{\tau_s'}{r} + R\frac{\tau_s}{r^2} + \rho\ddot{u}' \qquad [9b]$$

$$\tau_2'' = -2\frac{\tau_2'}{r} + 2\frac{\tau_2}{r^2} - R\frac{\sigma_{2s}'}{r} + R\frac{\sigma_{2s}}{r^2} - \tau_s' + \rho\ddot{v}' \qquad [9c]$$

$$u'' = -w_s' + 2\theta\frac{\tau_1'}{E_s} \qquad [10a]$$

$$v'' = -R\frac{w_s'}{r} + R\frac{w_s}{r^2} + \frac{v'}{r} - \frac{v}{r^2} + 2\theta\frac{\tau_2'}{E_s} \qquad [10b]$$

$$w'' = -\theta\nu\left(u_s' + R\frac{v_s'}{r} - R\frac{v_s}{r^2} + \frac{w'}{r} - \frac{w}{r^2}\right) + \theta\frac{\sigma_3'}{E_3} \qquad [10c]$$

All equations so far written are general. Our ultimate interest lies, however, in equations pertaining to the median surface. Hence it will be convenient hereafter to enclose in parentheses all symbols denoting stress or displacements at a general point of the shell and to understand that all quantities not so enclosed refer to points on the median surface ($r = R$, $z = 0$).

The boundary conditions on the faces of the shell will now be that σ_3, τ_1, and τ_2 take on prescribed values, which will be denoted by σ_3^+, τ_1^+, τ_2^+, on the face $z = h/2$ and σ_3^-, τ_1^-, τ_2^-, on the face $z = -h/2$. These quantities vanish if there is no external load. Then, expanding in powers of z and using the new notation just described

$$(\sigma_3) = \sigma_3 + z(\sigma_3)_0' + \frac{1}{2}z^2(\sigma_3)_0'' + \frac{1}{6}z^3(\sigma_3)_0''' + \cdots\cdots$$

$$\sigma_3^+ = \sigma_3 + \left(\frac{h}{2}\right)(\sigma_3)_0' + \left(\frac{h^2}{8}\right)(\sigma_3)_0'' + \left(\frac{h^3}{48}\right)(\sigma_3)_0''' + \cdots\cdots$$

$$\sigma_3^- = \sigma_3 - \left(\frac{h}{2}\right)(\sigma_3)_0' + \left(\frac{h^2}{8}\right)(\sigma_3)_0'' - \left(\frac{h^3}{48}\right)(\sigma_3)_0''' + \cdots\cdots$$

with similar equations for τ_1 and τ_2. Here $(\sigma_3)_0'$, $(\sigma_3)_0''$, $(\sigma_3)_0'''$ denote $\partial(\sigma_3)/\partial z$, $\partial^2(\sigma_3)/\partial z^2$, $\partial^3(\sigma_3)/\partial z^3$ taken at $z = 0$.

It will be more convenient, however, to express the final results in terms of the following notation

$$Z_1 = \frac{\tau_1^+ - \tau_1^-}{h},\quad Z_2 = \frac{\tau_2^+ - \tau_2^-}{h},\quad Z_3 = \frac{\sigma_3^+ - \sigma_3^-}{h}$$

$$S_1 = \frac{1}{2}(\tau_1^+ + \tau_1^-),\quad S_2 = \frac{1}{2}(\tau_2^+ + \tau_2^-),\quad S_3 = \frac{1}{2}(\sigma_3^+ + \sigma_3^-)$$

Here Z_1, Z_2, Z_3 are connected with the net external load on the faces of the shell. The quantities S_1, S_2, S_3 represent in a crude sense external actions tending either to curl the shell by shearing its faces or to alter its thickness.

Addition and subtraction of the equations for σ_3^+ and σ_3^-, and of the similar ones for τ_1 and τ_2, then yield as the boundary conditions on the faces, in terms of stress components and their derivatives on the median surface

$$\sigma_3 = -\frac{1}{8}h^2(\sigma_3)_0'' + S_3,\quad (\sigma_3)_0' = -\frac{1}{24}h^2(\sigma_3)_0''' + Z_3 \qquad [11a, b]$$

$$\tau_1 = -\frac{1}{8}h^2(\tau_1)_0'' + S_1,\quad (\tau_1)_0' = -\frac{1}{24}h^2(\tau_1)_0''' + Z_1 \qquad [11c, d]$$

$$\tau_2 = -\frac{1}{8}h^2(\tau_2)_0'' + S_2,\quad (\tau_2)_0' = -\frac{1}{24}h^2(\tau_2)_0''' + Z_2 \qquad [11e, f]$$

By repeated substitutions in the equations of motion, Equations [6 a, b, c], specialized to refer to the median surface, all r derivatives can now be eliminated from those equations except $(\sigma_3)_0'''$, $(\tau_1)_0'''$, $(\tau_2)_0'''$, which remain unknown. Epstein obtains zero-order values for these latter derivatives by differentiating Equations [9 a, b, c] once more. In the alternative method to be followed here, only the equations already written are needed and the final equations of motion are obtained in a different way. It can be shown by a general argument that the two methods must necessarily yield the same final result.

Stress and Displacement Patterns

Equations of motion for the shell, expressed in terms of quan-

tities referring to the median surface and free from all z-derivatives, are to be obtained in the usual way by calculating the stress resultants and then substituting these in the usual equations of motion for an element of the shell. To obtain equations of motion correct through order h^2, stress resultants must be calculated through h^3, since the mass of the shell is itself of order h; this requires stresses accurate through z^2, zh, or h^2. The distribution of certain stresses over the thickness of the shell, represented by (τ_1), (τ_2), (σ_1), (σ_2), and (τ) must be known, and to find the latter three quantities, expressions for (u), (v), (w) also must be known. These quantities can all be found by substitution in appropriate Taylor series, for example

$$(u) = u + z(u)_0' + \frac{1}{2}z^2(u)_0'' + \cdots,$$

where $(u)_0'$, $(u)_0'''$, and so on, denote derivatives with respect to z taken at $z = 0$. Values of second derivatives such as $(u)_0''$, or $(\sigma_3)_0''$ need to be known only through zero order in h, and first derivatives such as $(u)_0'$ or $(\sigma_3)_0'$ only through h^1. Values of σ_3, τ_1, τ_2, $(\sigma_3)_0'$, $(\tau_1)_0'$, $(\tau_2)_0'$ are given by Equations [11*a* to *f*], in which the h^2-terms can be dropped except for substitution in the first terms of the Taylor series for (σ_3), (τ_1), (τ_2). Then $(u)_0'$, $(v)_0'$, $(w)_0'$ are given by Equations [8*a*, *b*, *c*] with $r = R$, and $(u)_0''$, $(v)_0''$, $(w)_0''$ similarly by Equations [10 *a*, *b*, *c*], in which $w_x' = \partial(w)_0'/\partial x$, and so forth. Zero-order values of $(\sigma_3)_0''$, $(\tau_1)_0''$, $(\tau_2)_0''$ are taken from Equations [9 *a*, *b*, *c*]. For substitution in these equations, zero-order values at $r = R$ of σ_3, τ, σ_1', σ_2', τ' are found from Equations [1*a*, *b*] and [4], or from the derivatives of these equations with respect to r. Since $u' = (d^2/dt^2)u'$, the zero-order value of $\rho u'$ for use in Equation [9*b*] is easily found by differentiating Equation [8*a*] twice with respect to t and then using Equation [6*c*]; and similarly for $\rho\ddot{v}'$, $\rho\ddot{w}'$, in Equations [9*a*, *c*].

The distributions of stress and displacement thus found are given in Equations [12*a* to *f*] which follow. The values of the various derivatives that were used in constructing these expressions can be recovered if desired by differentiating.

$$(u) = u + z\left(-w_x + 2\theta\frac{S_1}{E_1}\right) + \frac{1}{2}\theta z^2\left(\nu u_{xx} + \nu v_{xx} + \nu\frac{w_x}{R} + 2\frac{Z_1}{E_1} - \frac{S_{1x}}{E_1}\right) \quad [12a]$$

$$(v) = v + z\left(-w_x + \frac{v}{R} + 2\theta\frac{S_2}{E_2}\right) + \frac{1}{2}\theta z^2\left(\nu u_{xx} + \nu v_{xx} + \nu\frac{w_x}{R} + 2\frac{Z_2}{E_2} + 2S_{2z}/RE_2 - S_{2x}/E_1\right) \quad [12b]$$

$$(w) = w + z\left[-\theta\nu\left(u_x + v_x + \frac{w}{R}\right) + \theta\frac{S_3}{E_1}\right] + \frac{1}{2}\theta z^2\left[\nu(w_{xx} + w_{xx}) + \theta\nu\left(\nu\frac{u_x}{R} + \nu\frac{v_x}{R} + \frac{w}{R^2}\right) + Z_3/E_1 - \theta\nu\frac{S_3}{RE_1} - 2\theta\nu(S_{1x} + S_{2x})/E_2\right] \quad [12c]$$

$$(\sigma_3) = S_3 + zZ_3 + \frac{1}{2}\left(z^2 - \frac{h^2}{4}\right)\left\{\theta E_3\left[-\nu(u_{xxx} + u_{xxx} + v_{xxx} + v_{xxx}) - \nu\frac{w_{xx}}{R} - \frac{w_{xx}}{R} - 2\nu(1-\nu)\frac{u_x}{R^2} - (1-\nu)\frac{v_x}{R^2} - 2(1-\nu)\frac{w}{R^2}\right] - \theta\left[(1-\nu)\frac{Z_3}{R} - 2(1-2\nu)\frac{S_3}{R^2} + Z_{1x} + Z_{2x} - (3-1\nu)S_{3z}/R + \theta\nu^2(S_{1xx} + S_{2xx})\right] + \theta\rho\frac{\ddot{S}_3}{E_3}\right\} \quad [12d]$$

$$(\tau_1) = S_1 + zZ_1 + \frac{1}{2}\left(z^2 - \frac{h^2}{4}\right)\left\{\theta E_1\left[(1-\nu)(w_{xxx} + w_{xxx}) + \nu\frac{u_{xx}}{R} + (1-\nu)^2\frac{u_{xx}}{R} + (1-\nu+\nu^2)\frac{v_{xx}}{R} + \frac{w_x}{R^2}\right] - Z_1/R + S_1/R^2 - \theta Z_{1x} - \theta^2(1-2\nu)S_{1x}/R - \theta(3-\nu)S_{1xx} - S_{1xx} - 2\theta S_{2xx} + 2\theta\rho\ddot{S}_1/E_1\right\} \quad [12e]$$

$$(\tau_2) = S_2 + zZ_2 + \frac{1}{2}\left(z^2 - \frac{h^2}{4}\right)\left\{\theta E_2\left[(1-\nu)(w_{xxx} + w_{xxx}) + (1+2\nu-2\nu^2)\frac{u_{xx}}{R} + (3-2\nu)\frac{v_{xx}}{R} + (1-3\nu)\frac{w_x}{R^2}\right] - \frac{Z_2}{R} + 4\frac{S_2}{R^2} - \theta Z_{2x} - \theta^2(2-7\nu+4\nu^2)\frac{S_{2x}}{R} - S_{2xx} - \theta(3-\nu)S_{2xx} - 2\theta S_{1xx} + 2\theta\rho\frac{\ddot{S}_2}{E_2}\right\} \quad [12f]$$

The Stress Resultants

The ten stress resultants are now easily calculated from the usual formulas

$$N_x = \int_{-h/2}^{h/2}\left(1 + \frac{z}{R}\right)(\sigma_1)dz, \quad N_{xs} = \int_{-h/2}^{h/2}\left(1 + \frac{z}{R}\right)(\tau)dz$$

$$Q_x = \int_{-h/2}^{h/2}\left(1 + \frac{z}{R}\right)(\tau_1)dz,$$

$$N_s = \int_{-h/2}^{h/2}(\sigma_2)dz, \quad N_{sx} = \int_{-h/2}^{h/2}(\tau)dz, \quad Q_s = \int_{-h/2}^{h/2}(\tau_2)dz$$

$$M_x = \int_{-h/2}^{h/2} z\left(1 + \frac{z}{R}\right)(\sigma_1)dz,$$

$$M_{xs} = \int_{-h/2}^{h/2} z\left(1 + \frac{z}{R}\right)(\tau)dz$$

$$M_s = \int_{-h/2}^{h/2} z(\sigma_2)dz, \quad M_{sx} = \int_{-h/2}^{h/2} z(\tau)dz$$

Here, as illustrated in Fig. 2, N_x is the tension and N_{xs} and Q_x are the shearing forces transmitted negatively across a unit section perpendicular to x, Q_x being normal to the median surface, M_x is the bending moment and M_{xs} the twisting moment across the same section, taken positive when the outer surface of the shell is urged toward the positive axis for one of the co-ordinates, and the other five symbols refer similarly to a section perpendicular to s. The calculation is straightforward. In using Equations

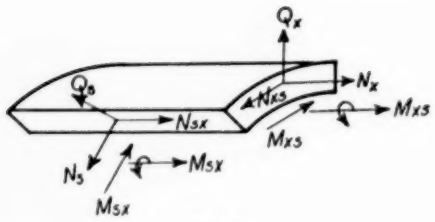

FIG. 2

[1*a*, *b*] and [4] for σ_1, σ_2, τ, general values are inserted, for example, $(u)_x$ for u_x, and $1/r$ is expanded thus

$$\frac{1}{r} = \frac{1}{R+z} = \frac{1}{R} - \frac{z}{R^2} + \frac{z_2}{R^3} \cdots\cdots$$

The external load on the faces of the shell gives rise to complicated h^3 terms which are probably useless and will be omitted here. As thus abbreviated, the expressions found are, in terms of quantities referring to the median surface

$$N_x = hE_s\left(u_x + \nu v_s + \nu\frac{w}{R}\right)$$
$$+ \left(\frac{\theta^2}{24}\right)h^3E_s\left[\nu(1+\nu)(u_{xxx}+v_{xxs}) + \nu^2(3-\nu)(u_{xss}+v_{sss})\right.$$
$$-(2-5\nu+\nu^3)\frac{w_{xx}}{R} + 2\nu(1+\nu-\nu^2)\frac{w_{ss}}{R}$$
$$\left.+\nu(4-3\nu)\left(\nu\frac{u_x}{R^2}+\frac{w}{R^3}\right)+\nu(2-2\nu+\nu^2)\frac{v_s}{R^2}\right] + \theta\nu hS_3 \quad \ldots[13a]$$

$$N_s = hE_s\left(v_s + \nu u_x + \frac{w}{R}\right)$$
$$+ \left(\frac{\theta^2}{24}\right)h^3E_s\left[\nu(1+\nu)(u_{xxs}+v_{sss}) + \nu^2(3-\nu)(u_{xxx}+v_{xxs})\right.$$
$$+\nu(1+2\nu-\nu^2)\frac{w_{xx}}{R} + 2\frac{w_{ss}}{R} + \nu(2+3\nu-4\nu^2)\frac{u_x}{R^2}$$
$$\left.+\nu(4-3\nu)\frac{v_s}{R^2} + (2+3\nu-4\nu^2)\frac{w}{R^3}\right] + \theta\nu h\,S_3 \ldots[13b]$$

$$N_{xs} = \frac{1}{2}(1-\nu)hE_s(u_s+v_x)$$
$$+\frac{1}{24}h^3E_s\left[\nu(u_{xxs}+v_{sss}) - (1-2\nu)\frac{w_{xs}}{R} + (1-\nu)\frac{v_x}{R^2}\right] \ldots[13c]$$

$$N_{sx} = \frac{1}{2}(1-\nu)hE_s(u_s+v_x)$$
$$+\frac{1}{24}h^3E_s\left[\nu(u_{xxs}+v_{sss}) + \frac{w_{xs}}{R} + (1-\nu)\frac{u_s}{R^2}\right] \ldots[13d]$$

$$Q_x = -\left(\frac{\theta}{12}\right)h^3E_s\left[(1-\nu)(w_{xxx}+w_{xss}) + \nu\frac{u_{xx}}{R}\right.$$
$$\left.+(1-\nu)^2\frac{u_{ss}}{R} + (1-\nu+\nu^2)\frac{v_{xs}}{R} + \frac{w_x}{R^2}\right] + hS_1 \ldots[13e]$$

$$Q_s = -\left(\frac{\theta}{12}\right)h^3E_s\left[(1-\nu)(w_{xxs}+w_{sss})\right.$$
$$\left.+(1+2\nu-2\nu^2)\frac{u_{xs}}{R} + (3-2\nu)\frac{v_{ss}}{R} + (4-3\nu)\frac{w_s}{R^2}\right] + hS_2 \ldots[13f]$$

$$M_x = -\left(\frac{\theta}{12}\right)h^3E_s\left[(1-\nu)(w_{xx}+\nu w_{ss})\right.$$
$$\left.-(1-\nu-\nu^2)\frac{u_x}{R} - \nu(1-2\nu)\frac{v_s}{R} + \nu^2\frac{w}{R^2}\right] \ldots[13g]$$

$$M_s = -\left(\frac{\theta}{12}\right)h^3E_s\left[(1-\nu)(\nu w_{xx}+w_{ss})\right.$$
$$\left.+\nu\frac{u_x}{R} + \nu\frac{v_s}{R} + \frac{w}{R^2}\right] \ldots[13h]$$

$$M_{xs} = -\frac{1}{12}h^3E_s(1-\nu)\left(w_{xs} - \frac{v_x}{R}\right) \ldots\ldots[13i]$$

$$M_{sx} = -\frac{1}{12}h^3E_s(1-\nu)\left(w_{xs} + \frac{1}{2}u_s/R - \frac{1}{2}v_x/R\right) \ldots[13j]$$

The nature of the omitted load terms will be illustrated by appending those which arise from Z_3 and S_3, the most important type of loading in practice. The terms to be added on the right in the equations representing the quantity shown below in parentheses are as follows

(N_x): $\left(\theta^2\frac{h^3}{24}\right)\left[\nu(5-6\nu)\frac{Z_3}{R} - \theta\nu(4-11\nu+6\nu^2)\frac{S_3}{R^2}\right.$
$-\theta(1-3\nu+2\nu^2-2\nu^3)S_{3xx} - \theta\nu(1-3\nu)S_{3ss}$
$\left.-2\theta\nu(1-2\nu)\rho\frac{\ddot{S}_3}{E_s}\right]$

(N_s): $\left(\theta^2\frac{h^3}{24}\right)\left[(1-2\nu^2)\frac{Z_3}{R} - \theta(2-\nu-10\nu^2+8\nu^3)\frac{S_3}{R^2}\right.$
$-\theta\nu(1-3\nu)S_{3xx} - \theta(1-3\nu+2\nu^2-2\nu^3)S_{3ss}$
$\left.-2\theta\nu(1-2\nu)\rho\frac{\ddot{S}_3}{E_s}\right]$

(N_{xs}) and (N_{sx}): $-\left(\frac{h^3}{24}\right)\theta(1-2\nu)\,S_{3xs}$

(Q_x): $\left(\theta\frac{h^3}{12}\right)\left[Z_{3x} + \theta(1-2\nu)\frac{S_{3x}}{R}\right]$

(Q_s): $\left(\theta\frac{h^3}{12}\right)\left[Z_{3s} + \theta(2-7\nu+4\nu^2)\frac{S_{3s}}{R}\right]$

(M_x): $\left(\theta\frac{h^3}{12}\right)\left[\nu Z_3 + \theta\nu(2-3\nu)\frac{S_3}{R}\right]$

(M_s): $\left(\theta\frac{h^3}{12}\right)\left[\nu Z_3 + \theta(1-2\nu)\frac{S_3}{R}\right]$

(M_{xs}) and (M_{sx}): nil

Equations of Motion for the Shell

From the stress resultants, equations of motion can now be formed by substitution in the following equations

$$\rho\frac{\partial^2}{\partial t^2}\int\frac{r}{R}(u)dz = \frac{\partial}{\partial x}N_x + \frac{\partial}{\partial s}N_{sx} + h\left(Z_1 + \frac{S_1}{R}\right)$$

$$\rho\frac{\partial^2}{\partial t^2}\int\frac{r}{R}(v)dz = \frac{\partial}{\partial s}N_s + \frac{\partial}{\partial x}N_{xs} + \frac{Q_s}{R} + h\left(Z_2 + \frac{S_2}{R}\right)$$

$$\rho \frac{\partial^2}{\partial t^2} \int \frac{r}{R} (w) dz = \frac{\partial}{\partial x} Q_x + \frac{\partial}{\partial s} Q_s - \frac{N_s}{R} + h \left(Z_3 + \frac{S_3}{R} \right)$$

The terms in Z and S represent the external forces on the faces of the shell, taken per unit area of the median surface. To obtain equations referring to the median surface, the integrals on the left are evaluated using Equations [12*a*, *b*, *c*], and resulting terms in h^3, after substituting in them zero-order values of $\rho\ddot{u}$, $\rho\ddot{v}$, $\rho\ddot{w}$ from Equations [6*a*, *b*, *c*], are combined with similar terms in the right-hand members. Corresponding treatment of the three moment equations shows that these equations are satisfied identically.

The equations of motion thus obtained for the shell, in terms of quantities referring to the median surface, with omission of the complicated and probably useless h^2 terms arising from external load on the faces, are as follows

$$\rho\ddot{u} = E_s \left[u_{xx} + \frac{1}{2}(1-\nu) u_{ss} + \frac{1}{2}(1+\nu) w_{xs} + \nu \frac{w_x}{R} \right] + \frac{1}{24} \theta^2 h^2 E_s \left[2\nu^2 (u_{xxxx} + u_{xxss} + v_{xxxs} + v_{xsss}) - (2 - 5\nu + \nu^2) \frac{w_{xxx}}{R} + (1 - \nu + 4\nu^2 - 2\nu^3) \frac{w_{xss}}{R} - \nu(2 - 9\nu + 6\nu^2) \frac{u_{xx}}{R^2} + (1-\nu)^3 \frac{u_{ss}}{R^2} - (2 - 7\nu + 5\nu^2 - \nu^3) \frac{v_{xs}}{R^2} - (2 - 9\nu + 6\nu^2) \frac{w_x}{R^3} \right] + Z_1 + \frac{S_1}{R} + \theta\nu S_{3x} \quad [14a]$$

$$\rho\ddot{v} = E_s \left[v_{ss} + \frac{1}{2}(1-\nu) w_{xx} + \frac{1}{2}(1+\nu) u_{xs} + \frac{w_s}{R} \right] + \frac{1}{24} \theta^2 h^2 E_s \left[2\nu^2 (v_{xxxs} + v_{xxss} + u_{xxxs} + u_{xsss}) + \nu(3-\nu) \frac{w_{xss}}{R} - (3 - 9\nu + 6\nu^2 - 2\nu^3) \frac{w_{xxx}}{R} - (3 + \nu - 17\nu^2 + 12\nu^3) \frac{u_{xs}}{R^2} - (10 - 23\nu + 12\nu^2) \frac{v_{xx}}{R^2} - (10 - 26\nu + 15\nu^2) \frac{w_s}{R^3} \right] + Z_2 + 2\frac{S_2}{R} + \theta\nu S_{3s} \quad [14b]$$

$$\rho\ddot{w} = -E_s \left(\nu \frac{u_x}{R} + \frac{v_s}{R} + \frac{w}{R^2} \right) - \frac{1}{24} \theta^2 h^2 E_s \left[2(1-\nu)^2 (w_{xxxx} + 2w_{xxss} + w_{ssss}) + 3\nu^2 \frac{u_{xxx}}{R} + (4 - 5\nu + \nu^2 + 3\nu^3) \frac{u_{xss}}{R} + (2 - 7\nu + 11\nu^2 - 3\nu^3) \frac{v_{sss}}{R} + 3(2 - 4\nu + 3\nu^2) \frac{v_{xxs}}{R} + (2 - 2\nu + \nu^2 + 2\nu^3) \frac{w_{xx}}{R^2} + (10 - 17\nu + 10\nu^2) \frac{w_{ss}}{R^2} + 2\nu(1 + 2\nu - 3\nu^2) \frac{u_x}{R^2} + 5\nu(1-\nu) \frac{v_s}{R^2} + 2(1 + 2\nu - 3\nu^2) \frac{w}{R^4} \right] + Z_3 + \theta(1-2\nu) \frac{S_3}{R} + S_{1x} + S_{2s} \quad [14c]$$

These equations of motion agree with Epstein's[2] provided two misprints in the latter are corrected.[3] They agree also, as Epstein remarks, with the known exact solutions for special cases. The terms to be added on the right if h^2-terms arising from Z_3 or S_3 are to be included are as follows

$$(\rho\ddot{u}): \left(\theta^2 \frac{h^2}{24} \right) \left[(2 - 3\nu^2) \frac{Z_{3x}}{R} + \theta(2 - 13\nu + 24\nu^2 - 12\nu^3) \frac{S_{3x}}{R^2} - \theta(1 - 3\nu + 3\nu^2 - 3\nu^3)(S_{3xxx} + S_{3xss}) + \theta(1 - 5\nu + 6\nu^2)\rho \frac{\ddot{S}_{3x}}{E_s} \right]$$

$$(\rho\ddot{v}): \left(\theta^2 \frac{h^2}{24} \right) \left[(5 - 9\nu + 3\nu^2) \frac{Z_{3s}}{R} + \theta(4 - 26\nu + 47\nu^2 - 24\nu^3) \frac{S_{3s}}{R^2} - \theta(1 - 3\nu + 3\nu^2 - 3\nu^3)(S_{3xxs} + S_{3sss}) + \theta(1 - 5\nu + 6\nu^2)\rho \frac{\ddot{S}_{3s}}{E_s} \right]$$

$$(\rho\ddot{w}): \left(\theta^2 \frac{h^2}{24} \right) \left[-(1-\nu) \frac{Z_3}{R^2} + 2\theta(1-\nu)(1 + \nu - 6\nu^2) \frac{S_3}{R^2} + (1-\nu)(2-\nu)(Z_{1x} + Z_{2s}) + \theta(2 - 6\nu + 6\nu^2 - 5\nu^3) \frac{S_{3xx}}{R} + \theta(5 - 22\nu + 29\nu^2 - 15\nu^3) \frac{S_{3ss}}{R} - (1 - 2\nu)\rho \frac{\ddot{Z}_3}{E_s} - \theta(2 - 9\nu + 10\nu^2)\rho \frac{S_3}{RE_s} \right]$$

Validity of the Approximation

The right-hand members of Equations [14*a*, *b*, *c*] may be regarded as the first terms in an expansion of the expressions for a thick shell in powers of h. In considering the corresponding equations of equilibrium, however, a difficulty was encountered (section "Axiradial Equilibrium With Axial Symmetry," near the end) whose solution led to an altered view of the basis on which the validity of the expansion should be assumed to rest. The new view is also of practical interest.[4] The two imaginable bases for the expansion are as follows:

The Analytic Assumption. According to the usual point of view in mathematical work, all quantities would be assumed to be analytic functions of the thickness h and to be expanded in positive integral powers of this parameter, with retention of terms only through order h^3. The first- or zero-order approximation to the solution of any problem is then obtained by dropping all terms containing h, so that the equations of motion reduce to the simple membrane equations; inclusion of terms through h^2 results in a better approximation; inclusion of h^4 terms would be still better; and so on.

In certain cases, however, the analytic assumption is impossible, so that to cover all cases of interest a broader principle of approximation must be found. The most satisfactory one ap-

[2] In the first paragraph of Epstein's equations [22], read $-3A(A-1)^2\gamma^2$ for $A(A-1)^2\gamma^2$ in the last line, and at the end of the first line of the third equation read $+2)m^2$ for $-2)m^2$.

[4] The ideas employed here are not new. Compare "Discussion of Thin Shell Theory," by L. H. Donnell, Proceedings of Fifth International Congress for Applied Mechanics, 1939, p. 66; "Equilibrium of Thin Elastic Shells," by A. E. Green and W. Zerna, *Quarterly Journal of Mechanics and Applied Mathematics*, vol. 3, 1950, p. 9.

pears to be furnished by a careful formulation of what is meant by a thin-shell theory of a thin shell.

The Thin-Shell Assumptions. (*a*) A cylindrical shell is thin if h/a is very small, and (*b*) a thin-shell approximate theory is one such that on all quantities pertaining to the median surface the operators $h\partial/\partial x$ and $h\partial/\partial s$ are in general strongly diminishing operators, that is, if q is any such quantity, then $h\partial q/\partial x$ and $h\partial q/\partial s$ are both in general much smaller numerically than q itself. In other words, q varies in general relatively little in a displacement of the order of h on the median surface. Near a zero value, of course, q will usually vary relatively rapidly.

A little reflection indicates that this principle suffices to validate the preceding deduction of the equations of motion. If the calculation were pushed to higher powers of h, each of the added terms would differ from one of the h^2 terms by multiples of the operators h^2/R^2, $h^2\partial^2/\partial x^2$ or $h^2\partial^2/\partial s^2$, and would thus be small relatively to the h^2 term. Singular cases are, of course, possible in which this criterion might fail and the dropping of certain terms in h^4 would not be justified. It seems doubtful, however, whether such cases will arise in practice.

The significance of these latter assumptions and the degree of accuracy of the final equations may be correlated with the behavior of the membrane equations ($h = 0$). If, under given boundary conditions, the membrane equations possess a unique solution, then that solution of Equations [14*a*, *b*, *c*] which satisfies the same boundary conditions and which passes continuously into the membrane solution as $h \to 0$ constitutes an approximate solution containing a first correction for shell thickness. In such cases, either principle of approximation may be assumed. If, on the other hand, the membrane solution is nonexistent, or perhaps merely not unique, only the thin-shell assumptions are applicable, and in such cases the essential character of the solution is fixed by the h^2 terms.

These features and others of special interest will be illustrated in a brief discussion of two special cases.

Flat Plate in Two-Dimensional Motion

With $R = \infty$, $v = 0$, and $\partial/\partial s = 0$, Equation [14*a*] becomes, for the plate unloaded on its faces

$$\rho u = E_s u_{xx} + \left(\frac{h^2}{12}\right) E_s \theta^2 \nu^2 u_{xxxx} \qquad [15]$$

The last term represents small corrections not included in the usual analysis.

The high order of the differential Equation [15], however, is spurious. For the harmonic case, $u = C \cos \omega t \sin kx$, two values of k occur for given ω of which the larger is k_2 where

$$k_2^2 = \frac{6}{h^2\theta^2\nu^2}\left[1 + \left(1 - h^2\theta^2\nu^2\rho\,\frac{\omega^2}{3E_s}\right)^{1/2}\right]$$

With this value of k, $h\,\partial u/\partial x$ is large, u varying enormously in a distance h. Furthermore, $\sin k_2 x$ is not expansible in positive powers of h. Thus for this type of solution the method of deducing the differential equation is not valid by either principle of approximation. Apparently such a form of u is a parasitic solution that has been brought in by the process of differentiating differential equations; it must be rejected, only the smaller value of k being used.

The general equations of motion Equations [14*a*, *b*, *c*] appear to admit an analogous class of parasitic solutions. Presumably, by rejecting these as physically irrelevant, the variety of the possible modes of vibration of given frequency always becomes reduced from 12, as suggested by the order of the equations, to 8, in correspondence with the number of boundary conditions that can be satisfied physically (for example, assigned values of u, v, w, w_x at each end of the cylinder).

In further confirmation of this view, it will be noted that the form, $u = C \cos \omega t \sin k_2 x$, suggests for the plate, as $\omega \to 0$, an equilibrium deformation, $u = C \sin (\sqrt{6}x/h\theta\nu)$, which is certainly impossible. Actually, the corresponding equation of equilibrium

$$u_{xx} = -\left(\frac{h^2}{12}\right)\theta^2\nu^2 u_{xxxx} \qquad [16]$$

can be replaced by an equally plausible simpler one by the following argument. If Equation [16] is differentiated twice, and if the expression thus found for u_{xxxx} is substituted back into Equation [16], there results

$$u_{xx} = \left(\frac{h^4}{144}\right)\theta^4\nu^4 u_{xxxxxx}$$

Terms in h^4, however, have been systematically dropped. The only consistent course, therefore, is to drop the h^4 term here also and to take as the equation of equilibrium the usual one

$$u_{xx} = 0 \qquad [17]$$

This reduction automatically eliminates also the spurious solution. It may be remarked that the only solutions of Equation [16] which are analytic in h are the solutions of Equation [17].

Axiradial Equilibrium With Axial Symmetry

The equations of equilibrium of a cylindrical shell unloaded on its faces with $v = 0$ and $\partial/\partial s = 0$, as obtained from Equations [14*a*, *c*], are

$$u_{xx} + \nu\frac{w_x}{R} + \left(\theta^2\frac{h^2}{24}\right)\left[2\nu^2 u_{xxxx} - (2 - 5\nu + \nu^2)\frac{w_{xxx}}{R} - (2 - 9\nu + 6\nu^2)\left(\nu\frac{u_{xx}}{R^2} + \frac{w_x}{R^3}\right)\right] = 0 \qquad [18a]$$

$$\nu\frac{u_x}{R} + \frac{w}{R^2} + (\theta^2h^2/24)\left[2(1-\nu)^2 w_{xxxx} + 3\nu^2\frac{u_{xxx}}{R} + (2 - 2\nu + \nu^2 + 2\nu^3)\frac{w_{xx}}{R^2} + 2(1 + 2\nu - 3\nu^2)\left(\nu\frac{u_x}{R^3} + \frac{w}{R^4}\right)\right] = 0 \qquad [18b]$$

To simplify these equations, we may note first that each is of the form $P + h^2Q = 0$ where P and Q are expressions free of h. If Q is replaced by $Q + b\,(\partial^n P/\partial x^n)/R^m$ where n and m are positive integers or zero and b is any constant, the terms thus added to Q can be written $-bh^2(\partial^n Q/\partial x^n)/R^m$, since $P = -h^2Q$. These terms are thus of the same order, according to the thin-shell assumptions, as similar terms that were dropped during the deduction of the equation and can, therefore, do no harm; they are as likely to decrease the error caused originally by dropping other h^4 terms as to increase it. Inclusion of these new terms will only change the solution by terms of order h^4.

By using this device twice with proper choices of b, n, and m, all derivatives of u can be eliminated from the h^2 terms in Equations [18 *a*, *b*]. The resulting equations are

$$u_{xx} + \nu\frac{w_x}{R} - \left(\theta\frac{h^2}{24}\right)\left[(2 - 3\nu - 2\nu^2)\frac{w_{xxx}}{R} + (1 + \nu)(2 - 9\nu + 6\nu^2)\frac{w_x}{R^3}\right] = 0 \qquad [19a]$$

$$\nu u_x + \frac{w}{R} + \left(\theta \frac{h^2}{24}\right)\left[2(1-\nu)Rw_{xxxx} + (2-3\nu-2\nu^2)\frac{w_{xx}}{R}\right] = 0 \quad [19b]$$

whence also, by differentiation of the second

$$\nu u_{xx} + \frac{w_x}{R} + \left(\theta \frac{h^2}{24}\right)\left[2(1-\nu)Rw_{xxxxx} + (2-3\nu-2\nu^2)\frac{w_{xxx}}{R}\right] = 0 \quad [19c]$$

Now, treating the h^2 expressions as known quantities, let Equations [19*a*] and [19*c*] be solved for u_{xx} and w_x/R. In the expression thus obtained for u_{xx} and also in Equation [19*b*], substitute, in the h^2 terms only, for w_x/R the expression just found and for w_{xx}/R and w_{xxx}/R expressions obtained therefrom by differentiation. All h^4 terms thus created are negligible, by the thin-shell assumptions, each relatively to an h^2 term containing w_{xxxx} or w_{xxxxx}. Dropping these negligible terms, simplified equations of equilibrium are found in the form

$$(1-\nu^2)u_{xx} = \left(\nu R \frac{h^2}{12}\right) w_{xxxxx} \quad [20a]$$

$$\nu u_x + \frac{w}{R} = -\frac{1}{12} Rh^2 w_{xxxx} . \quad [20b]$$

Or, integrating the first of these equations twice and then substituting the value of u_x thus found in the second, the equations also can be put into the form, A and B being arbitrary constants (in agreement with Timoshenko's equations for $N_x = 0$)

$$(1-\nu^2)u = \left(\nu R \frac{h^2}{12}\right) w_{xxx} + A\frac{x}{R} + B \quad [21a]$$

$$(1-\nu^2)w = -\left(R^2 \frac{h^2}{12}\right) w_{xxxx} - \nu A \quad [21b]$$

It is impossible to say whether Equations [19*a*, *b*] or the simpler [20*a*, *b*] will furnish the more accurate solution. It is worth noting that if the value of w_x/R found originally, and values of w_{xxx}/R and of w_{xxxx}/R found from this by differentiation, are substituted back into the expression for w_x/R itself, it is found that w_x is equal to a quantity containing h^4 as a factor. It would seem that this quantity should be dropped, in the name of consistency, with the result that $w_x = 0$. Such a conclusion, however, is unacceptable, for the cylinder can certainly be loaded at its ends so as to bend the generators. It appears that dropping the term in w_{xxxxx} from the expression for w_x/R is not justified because it contains the operator $R^2\,\partial^2/\partial x^2$, whose magnitude is not known a priori. Actually, since the basic solutions of Equation [21*b*] are of the form, $w = Ce^{kx} + \text{const}$, where $k = [-12(1-\nu^2)]^{1/4}/\sqrt{Rh}$, the quantity $R^2\partial^2 w/\partial x^2$ is of order R/h relatively to w and hence is relatively large. It also may be noted that since such an expression for w cannot be expanded in positive powers of h, the analytic assumption is inapplicable here.

Analogous modifications of the equilibrium conditions can be made in general and of course in many different ways. Thus there appears to exist an indeterminateness in the expressions representing the approximate conditions of equilibrium.

Practical Simplification of The Equations

The h^2 terms in the equations of motion represent in part small corrections for shell thickness that are usually unimportant. For many engineering purposes a simpler approximation is needed.

When the membrane equations possess a solution, it may be sufficiently accurate to drop all h^2 terms and employ simply the membrane equations themselves. In other cases, however, at least some of the h^2 terms must be retained. The following method of selection seems to be plausible:

All of the h^2 terms are small, in the sense of the thin-shell assumptions, each relatively to a membrane term in the same equation, except the three fourth-order terms in the w-equation. These terms contain, as compared with w/R^2, in addition to $h^2\,\partial^2/\partial x^2$ or $h^2\,\partial^2/\partial s^2$, the operator $R^2\,\partial^2/\partial x^2$ or $R^2\,\partial^2/\partial s^2$, concerning whose magnitude no general statement can be made. A further complication arises from the fact that the binomial, $v_{xx} + w_x/R$, in the v-equation is the derivative of the binomial, $v_x + w/R$, in the w-equation. As a consequence, if $h = 0$, a continuous set of inextensional equilibrium deformations is possible, for which these binomials vanish. These deformations can be regarded as membrane vibrations at frequency zero, and the shell vibrations that pass into some of them as $h \to 0$ are essentially controlled by certain terms of order h^2.

These latter vibrations should not be seriously falsified, however, if we subtract from the h^2 terms expressions of the form h^2bP/R^2 or $h^2b\partial^2P/\partial x^2$ or $h^2b\partial^2P/\partial s^2$ where P is the binomial just mentioned in the same equation and b is an arbitrary constant. In this way the h^2w_{xxx}/R term can be eliminated from Equation [14*b*], with a change in the coefficient of h^2v_{xxx}. All other derivatives of v in the h^2 terms of Equations [14*b*, *c*] can be eliminated similarly in favor of derivatives of w. Terms in h^2 and v_{xxx} or a derivative of u in these equations and all h^2 terms in the u-equation can then be dropped as being small, by the thin-shell assumptions, relatively to appropriate membrane terms in the same equation. It seems reasonable to drop h^2w_{xx}/R^2 as well, in comparison with w/R^2.

The approximate equations of motion thus obtained are

$$\rho\ddot{u} = E_s\left[u_{xx} + \frac{1}{2}(1-\nu)u_{ss} + \frac{1}{2}(1+\nu)w_{xs} + \nu\frac{w_x}{R}\right] + Z_1 + \frac{S_1}{R} + \theta\nu S_{1x} \quad [22a]$$

$$\rho\ddot{v} = E_s\left[v_{ss} + \frac{1}{2}(1-\nu)w_{xx} + \frac{1}{2}(1+\nu)u_{xs} + \frac{w_s}{R}\right] + \frac{1}{8}h^2E_s\theta\nu\left(\frac{w_{sss}}{R} + \frac{w_s}{R^3}\right) + Z_2 + 2\frac{S_2}{R} + \theta\nu S_{2x} \quad [22b]$$

$$\rho\ddot{w} = -E_s\left(\nu\frac{u_x}{R} + \frac{v_s}{R} + \frac{w}{R^2}\right) - \left(\frac{h^2}{24}\right)E_s\theta\left[2(1-\nu)(w_{xxxx} + 2w_{xxss} + w_{ssss}) + (4-\nu)\frac{w_{ss}}{R^2} + (2+\nu)\frac{w}{R^4}\right] + Z_3 + \theta(1-2\nu)\frac{S_3}{R} + S_{1x} + S_{2s} \quad [22c]$$

The following set of approximate stress resultants leads to Equations [22*a*, *b*, *c*] upon substitution in the usual equations of motion (with allowance for external load on the faces), and they also satisfy the moment equations (except for possible h^3 terms due directly to external load).

$$N_x = hE_s\left[u_x + \nu\left(v_s + \frac{w}{R}\right)\right] - \frac{1}{12}h^3E_s(2-\nu)\frac{w_{xx}}{R} + h\theta\nu S_3$$

$$N_s = hE_s\left(\nu u_x + v_\theta + \frac{w}{R}\right) + \frac{1}{24}h^3E_s\theta(2+\nu)\left(\frac{w_{\theta\theta}}{R} + \frac{w}{R^3}\right) + h\theta\nu S_3$$

$$N_{x\theta} = \frac{1}{2}(1-\nu)hE_s(u_\theta + v_x) + \frac{1}{12}h^3E_s\frac{w_{x\theta}}{R}$$

$$N_{\theta x} = \frac{1}{2}(1-\nu)hE_s(u_\theta + v_x) + \frac{1}{12}h^3E_s(2-\nu)\frac{w_{x\theta}}{R}$$

$$Q_x = -\frac{1}{12}h^3E_s(w_{xxx} + w_{x\theta\theta}) + hS_1$$

$$Q_\theta = -\frac{1}{12}h^3E_s\left(w_{xx\theta} + w_{\theta\theta\theta} + \frac{w_\theta}{R^2}\right) + hS_2$$

$$M_x = -\frac{1}{12}h^3E_s(w_{xx} + \nu w_{\theta\theta})$$

$$M_\theta = -\frac{1}{12}h^3E_s\left(\nu w_{xx} + w_{\theta\theta} + \frac{w}{R^2}\right)$$

$$M_{x\theta} = M_{\theta x} = -\frac{1}{12}h^3E_s(1-\nu)w_{x\theta}$$

The h^3 terms in N_x, $N_{x\theta}$, and $N_{\theta x}$ are fictitious and often may be dropped as negligible.

It is thought that Equations [22*a*, *b*, *c*] may give fair approximate results in all cases. The approximation may be somewhat uneven, however; for example, in some cases the dropped term in w_{xx}/R^2 may be comparable with the term in w_{xxxx}, but in such cases the latter itself will be relatively small and might as well be dropped. The terms in w_θ, $w_{x\theta}$, and $w_{\theta\theta\theta}$ are such as to ensure that Equations [22*a*, *b*, *c*] agree with the complete Equations [14 *a*, *b*, *c*], not only in permitting rigid displacements, but also in giving for the frequency of purely lobar vibration of the shell ($u = 0$, $\partial/\partial x = 0$), through order h^2 the simple formula obtained long ago by Rayleigh,[5] as was noted by Epstein.

[5] "Theory of Sound," by Baron John W. Rayleigh, second edition, The Macmillan Company, New York, N. Y., vol. 1, 1894, p. 417.

The Forced Oscillation of the Centrifugal Pendulum With Wide Angles[1]

By F. R. E. CROSSLEY,[2] NEW HAVEN, CONN.

The simple pendulum mounted to a rotor suffering torsional oscillation is used as an effective dynamic damper which may be tuned to any one harmonic order of vibration. The nonlinear equations of motion are here developed to investigate whether wider angles of swing, or whether larger or smaller sizes of pendulum relative to its carrier, are more effective. Resonance-type curves are drawn by assuming a single harmonic excitation and hyperelliptic pendulum motion without damping; it is shown that theoretically oscillations up to 90 deg may be used which are predictable, and that in all cases the tuning must be higher than that indicated by small-angle theory.

Nomenclature

The following nomenclature is used in the paper; of the symbols used, many were introduced in the analysis of the free oscillations (2):[3]

A = amplitude of carrier from applied torque M, with locked pendulum, radians, Equation [34]
$a_c = \sqrt{R/L}$, order of small-angle natural circular frequency; $\omega_0 = a\Omega$
c = constant of momentum (after $\div 2mL^2$) } when $\varphi = \varphi_0$
d = constant of energy (after $\div mL^2$) } when $\dot{\theta} = \dot{\theta}_0$
$e^2 = mR^2/(mR^2 + I_c)$, moment of inertia ratio
E = second elliptic integral, E' complete integral
f, F, g = functions
I_c = mass moment of inertia of carrier about its axis
k = $\sin \varphi_0/2$, modulus of hyperelliptic functions
L = length of simple pendulum from pivot to mass
L' = complete hyperelliptic integral function
m = mass of simple pendulum
M = forcing torque acting on carrier, Equation [4]
n = order of harmonic of forcing torque referred to carrier rotational speed
p, q = Fourier coefficients, Equations [17], [21], constants
Q = torque from pendulum on carrier
R = radius of attachment pivot of pendulum from axis of carrier
t = time
T = kinetic energy of system in Lagrange's equations
y = function of φ; see Equation [13] and Fig. 2
α = oscillatory angle of carrier about steady rotation
α_0 = maximum value of α
$\beta = (I_c + mR^2 + mL^2) \div 2mRL$, moment of inertia ratio
η = angle (just mathematical) defined by Equation [28]
$\theta = \Omega t + \alpha$, instantaneous angular position of carrier
$\dot{\theta}_0$ = angular velocity of carrier at instant $\varphi = \varphi_0$ and $\dot{\varphi} = 0$
φ = angle of pendulum relative to radial line on carrier through pivot point
φ_0 = maximum value of φ
ψ'' = angular acceleration which would be caused by M applied to inertia mR^2, Equation [5]
ψ_0 = amplitude of ψ''; maximum of torque $M \div mR^2$, Equation [23]
ω, ω_n = circular frequencies
Ω = constant mean speed of carrier

Introduction

If a simple pendulum is mounted on a rotating disk, (which will be called the carrier) and is free to oscillate about an axis at considerable radius from the center of rotation of the carrier, it has been found to act very effectively as a dynamic damper of torsional vibrations in the carrier shaft.

The system to be analyzed is shown diagrammatically in Fig. 1. The carrier need not be a disk, and in actual designs the pendulum needs a very short length L, so that there are two principal types: the bifilar suspension form of Sarazin and Chilton, and the rolling-puck type of Salomon. But all designs can be reduced easily to their equivalent simple pendulum, provided geometrical relationships are known, so that here only the simple pendulum is dealt with.

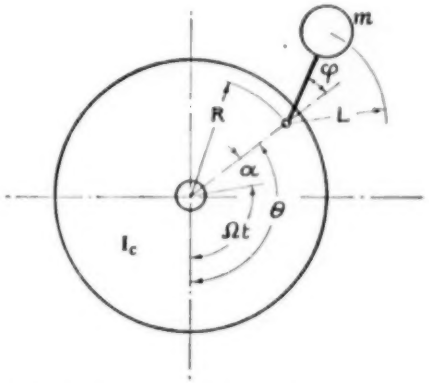

Fig. 1 Diagram of Pendulum and Carrier

The case of small-angle motion is a linear one and it is presented in most vibration textbooks. However, any wide-angle motion of the pendulum is nonlinear. Two previous analyses (1, 3) have been developed, but assumptions are made from the start which have obscured certain vital relationships; for in-

[1] This paper was part of a dissertation presented to the faculty of the Yale University School of Engineering in partial fulfillment of the requirements for the degree of doctor of engineering, which was awarded in 1949.

[2] Assistant Professor of Mechanical Engineering, Yale University. Mem. ASME.

[3] Numbers in parentheses refer to the Bibliography at the end of the paper.

Contributed by the Applied Mechanics Division and presented at the Fall Meeting, Chicago, Ill., September 8–11, 1952, of The American Society of Mechanical Engineers.

Discussion of this paper should be addressed to the Secretary, ASME, 29 West 39th Street, New York, N. Y., and will be accepted until April 10, 1953, for publication at a later date. Discussion received after the closing date will be returned.

Note: Statements and opinions advanced in papers are to be understood as individual expressions of their authors and not those of the Society. Manuscript received by ASME Applied Mechanics Division, February 4, 1952. Paper No. 52—F-11.

stance, the assumption that the carrier can be reduced to a state of steady rotation without vibration shows a motion of the pendulum expressible in elliptic functions, which are independent of the ratio of the moments of inertia of pendulum and carrier. The latter was shown to be a great influence in the author's analysis (2) of the free oscillation and is also affirmed by Timoshenko and Young (4).

The analysis presented here makes use of the hyperelliptic functions used in the free-motion analysis after developing the equations without any assumptions.

Equations of Motion

The angular displacement of the carrier θ, and of the pendulum φ, may be found by the Lagrangian method to be governed by the two equations

$$mR^2\,[2a^2(\beta + \cos\varphi)\ddot{\theta} + (1 + a^2\cos\varphi)\ddot{\varphi} - a^2\sin\varphi\,(2\dot{\varphi}\dot{\theta} + \dot{\varphi}^2)] = a^4M \quad [1]$$

$$\ddot{\varphi} + (1 + a^2\cos\varphi)\,\ddot{\theta} + a^2\dot{\theta}^2\sin\varphi = 0 \quad [2]$$

Also, from the consideration of kinetic energy it follows that

$$T = a^2(\beta + \cos\varphi)\dot{\theta}^2 + (1 + a^2\cos\varphi)\dot{\theta}\dot{\varphi} + \frac{1}{2}\dot{\varphi}^2 = \frac{a^4}{mR^2}\int M\,\dot{\theta}\,dt + d \quad [3]$$

Only two of these three equations are mutually independent of course.

The term M refers to the forcing torque which, in general, may be

$$M = \sum M_n \sin(n\Omega t + \gamma_n) \quad [4]$$

Because M appears as it does, we introduce an abbreviation

$$M/mR^2 = \psi'' \quad [5]$$

Now θ may be eliminated between the equations as follows: Integrate Equation [1] for the angular momentum of the system

$$2a^2(\beta + \cos\varphi)\dot{\theta} + (1 + a^2\cos\varphi)\dot{\varphi} = a^4\dot{\psi} + 2c \quad [6]$$

where c is a constant. Then using this value for $\dot{\theta}$ in Equation [3]

$$(1/e^2 - \cos^2\varphi)\dot{\varphi}^2 + (a^2\dot{\psi} + 2c/a^2)^2 = 4(\beta + \cos\varphi)\times\left\{\frac{d}{a^2} + \int\psi''\left[\frac{a^4\dot{\psi} + 2c - (1 + a^2\cos\varphi)\dot{\varphi}}{2(\beta + \cos\varphi)}\right]dt\right\} \quad [7]$$

At this point it may be noted that if $\psi'' = \dot{\psi} = 0$ we have the same free-motion equation in φ as before (2).

The integral in Equation [7] is not pretty, so differentiate

$$\ddot{\varphi} + \left[\frac{1}{2(\beta + \cos\varphi)} + \frac{\cos\varphi}{(1/e^2 - \cos^2\varphi)}\right]\sin\varphi\,\dot{\varphi}^2 + \frac{(1 + a^2\cos\varphi)\psi'' + (a^4\dot{\psi} + 2c)^2}{1/e^2 - \cos^2\varphi}\,\frac{\sin\varphi}{2a^4(\beta + \cos\varphi)} = 0 \quad [8]$$

Approximate Linearization of Equation

Now, no damping has been included in this analysis, so the middle term in Equation [8] must have occurred from differentiating a function of φ twice. For instance, even a simple harmonic function can appear nonlinear with both $\ddot{\varphi}$ and $\dot{\varphi}^2$ terms in its defining equation, like this

$$x = a\sin\varphi$$

$$\dot{x} = a\cos\varphi\,\dot{\varphi}$$

$$\ddot{x} = a\cos\varphi\,\ddot{\varphi} - a\sin\varphi\,\dot{\varphi}^2$$

Then

$$\ddot{x} + \omega^2 x = 0$$

appears as

$$\ddot{\varphi} - \tan\varphi\,\dot{\varphi}^2 + \omega^2\tan\varphi = 0$$

If this be so, there is some substitution $y = f(\varphi)$ which will eliminate the $\dot{\varphi}^2$ term from Equation [8]. Suppose then that

$$y = f(\varphi)$$

$$\dot{y} = f'\,\dot{\varphi}$$

$$\ddot{y} = f'\,\ddot{\varphi} + f''\,\dot{\varphi}^2$$

where

$$f' = \frac{d}{d\varphi}f(\varphi) \text{ and } \dot{\varphi} = \frac{d\varphi}{dt}$$

$$\ddot{\varphi} + \frac{f''}{f'}\,\dot{\varphi}^2 = \frac{1}{f'}\,\ddot{y}$$

which may better be written

$$\ddot{\varphi} + \frac{F'}{F}\,\dot{\varphi}^2 = \frac{1}{F}\,\ddot{y} \quad [9]$$

where $F = f' = df/d\varphi$; or $y = \int F\,d\varphi$.

Comparing Equations [8] and [9], set

$$\frac{F'}{F} = \frac{1}{F}\frac{dF}{d\varphi} = \left[\frac{1}{2(\beta + \cos\varphi)} + \frac{\cos\varphi}{(1/e^2 - \cos^2\varphi)}\right]\sin\varphi$$

$$2\log F = -\log(\beta + \cos\varphi) + \log(1/e^2 - \cos^2\varphi) + \log\epsilon$$

where ϵ is an arbitrary constant

$$F^2 = \frac{\epsilon\,(1 - e^2\cos^2\varphi)}{e^2\,(\beta + \cos\varphi)} \quad [10]$$

$$y = \sqrt{\frac{\epsilon}{e^2}}\int\sqrt{\frac{1 - e^2\cos^2\varphi}{\beta + \cos\varphi}}\,d\varphi \quad [11]$$

This substitution will therefore, by Equation [9], reduce the first two terms of Equation [8] to the simpler form $(1/F)\ddot{y}$.

Any value of ϵ satisfies both Equation [9] and Equation [10] so let us set $\epsilon = e^2$ and we are left with the two equations

$$\ddot{y} + e^2\left\{\frac{(1 + a^2\cos\varphi)\psi'' + \dfrac{(a^2\dot{\psi} + 2c/a^2)^2\sin\varphi}{2(\beta + \cos\varphi)}}{\sqrt{(1 - e^2\cos^2\varphi)\,(\beta + \cos\varphi)}}\right\} = 0 \quad [12]$$

$$y = \int_0^{\varphi}\sqrt{\frac{1 - e^2\cos^2\varphi}{\beta + \cos\varphi}}\,d\varphi \quad [13]$$

It is to be noted that we set the lower limit of the integral in Equation [13] as zero, for we desire the relation of y to φ to be a curve passing through the origin. The relation is obviously hyperelliptic, of a type very similar to those encountered in the free-oscillation analysis (2), except that in that case there was a constant h less than unity, while now β is generally large. The integral is discussed by the author in a paper (5) where it is shown to be not unlike an elliptic amplitude curve, for with large β it may be written closely

$$y = \frac{1}{\sqrt{\beta}} \int_0^{\varphi} \sqrt{1 - e^2 \cos^2 \varphi}\, d\varphi \qquad \beta >> 1$$

and this, by a substitution such as $\xi = \varphi + \pi/2$, gives a second elliptic integral or

$$\sqrt{\beta}\, y = E(e, \varphi + \pi/2) - E' \quad \ldots\ldots\ldots\ldots [14]$$

That the curve is usually nearly straight may be seen from the case shown in Fig. 2.

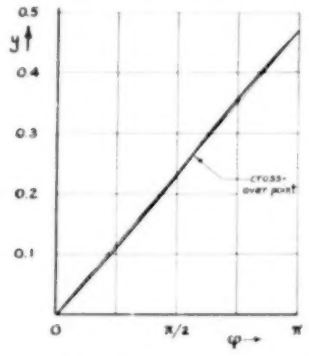

FIG. 2 HYPERELLIPTIC FUNCTION USED IN REDUCTION
(With a fine straight line for comparison.)

Now, separating the terms without ψ in Equation [12], it appears as

$$y + 2(ec/a^2)^2 \sin\varphi(1 - e^2\cos^2\varphi)^{-1/2}(\beta + \cos\varphi)^{-3/2} = g_1(\psi, \varphi) \quad \ldots\ldots [15]$$

Then, substituting y for φ and expanding the trigonometric functions into series, it is plain that this can be written in Poincaré's form (6, 7)

$$y + \omega_n^2\, y = \epsilon^2\, g_2(\psi, y). \quad \ldots\ldots [16]$$

where ω_n would be a first harmonic frequency.

Proceeding along this line, the first step is to write the hyperelliptic relation of y to φ in series form, and then to invert the relation. The integrand in Equation [13] becomes, by binomial expansion

$$\sqrt{\frac{1 - e^2\cos^2\varphi}{\beta + \cos\varphi}} = \beta^{-1/2}[p_0 + p_1\cos\varphi + 2p_2\cos 2\varphi + 3p_3\cos 3\varphi + \ldots] \quad \ldots\ldots [17]$$

where

$$p_0 = 1 + \frac{3}{16}\frac{1}{\beta^2} - \frac{1}{4}e^2 - \frac{3}{64}e^4 - \frac{9}{128}\frac{e^2}{\beta^2} + \ldots.$$

$$p_1 = -\left(\frac{1}{2}\frac{1}{\beta} + \frac{15}{32}\frac{1}{\beta^3} - \frac{3}{16}\frac{e^2}{\beta} - \frac{5}{128}\frac{e^4}{\beta} - \frac{25}{128}\frac{e^2}{\beta^2} + \ldots\ldots\right)$$

$$2p_2 = -\left(\frac{1}{4}e^2 - \frac{3}{16}\frac{1}{\beta^2} + \frac{1}{16}e^4 + \frac{3}{32}\frac{e^2}{\beta^2} + \ldots\ldots\right)$$

$$3p_3 = \frac{1}{16}\frac{e^2}{\beta} - \frac{5}{32}\frac{1}{\beta^3} + \frac{25}{256}\frac{e^2}{\beta^3} + \ldots\ldots$$

$$4p_4 = -\left(\frac{1}{64}e^4 + \frac{3}{128}\frac{e^2}{\beta^2} + \ldots\ldots\right) \text{ etc.}$$

Now integrating term by term

$$y = \beta^{-1/2}(p_0\varphi + p_1\sin\varphi + p_2\sin 2\varphi + p_3\sin 3\varphi + \ldots) \quad \ldots\ldots [18]$$

To determine the number of significant terms, we take cognizance of the maximum likely range of values. If we allow, for any design, the wide range

$$\left.\begin{aligned} 40 > \frac{I_s}{mR^2} > 0.2 \\ 2 \leqq a \leqq 12 \end{aligned}\right\} \quad \ldots\ldots [19]$$

where $a = \sqrt{R/L} = n$ the order of resonance in small-angle design, then

$$\left.\begin{aligned} 0.025 < e^2 < 0.833 \\ 2.5 < \beta < 3000 \\ 0.0003 < 1/\beta < 0.40 \end{aligned}\right\} \quad \ldots\ldots [20]$$

Now, if the largest values are used, the values of p are

$$p_0 = 0.783;\ p_1 = -0.178;\ p_2 = -0.125;\ p_3 = +0.004;\ p_4 = -0.002$$

so it is apparent that the first three terms are enough in any case. In the event of a large β, which is the case of Equation [14], the term in p_1 may even be suppressed.

If the curve of y and φ is drawn, and the axes interchanged, as, for example, in Fig. 2,[4] it appears that the inverse function can be written approximately from consideration of the quarter-points of the cycle

$$\varphi = q_0 y + q_1 \sin q_0 y + q_2 \sin 2q_0 y \quad \ldots\ldots [21]$$

where

$$q_0 = \frac{\sqrt{\beta}}{p_0};\ q_1 = \frac{p_1/p_0}{\cos\, p_1/p_0}$$

$$q_2 = \frac{0.707\ p_1/p_0 + p_2/p_0 + q_1 \sin(\pi/4 + 0.707\ p_1/p_0 + p_2/p_0)}{\cos\left(\sqrt{2}\ p_1/p_0 + 2p_2/p_0\right)}$$

If this Relation [21] is substituted in Equation [15], Equation [16] in y alone results and may be solved by successive approximation. However, this will be the complete forced motion; that is, it will include the free motion and possible transients. Our interest is principally in a steady-state forced motion, as will now be developed.

RESONANCE CURVES FOR A GIVEN PENDULUM

It is desired to find the amplitudes of swing of both the pendulum and the carrier in the steady state when a torque of known frequency is imposed on the system. A simple method of approximating these is suggested by several authors (8, 9, 10). It consists of substitution of a harmonic assumption for each variable in the general equation. But because of the lengthening of the period with the swing, the method exhibits shortcomings in this

[4] So the reader may judge the variation of the y-curve from straight, the following values are given from which Fig. 2 was plotted. The second set of values is merely for comparison, and are those from the approximation of Equation [14]:

φ	$\pi/8$	$\pi/4$	$3\pi/8$	$\pi/2$
y	0.05495	0.11184	0.17156	0.23337
Approx (y)	0.05586	0.11347	0.17364	0.23532
φ	$5\pi/8$	$3\pi/4$	$7\pi/8$	π
y	0.29546	0.35596	0.41405	0.4704
Approx (y)	0.29701	0.35718	0.41479	0.47065

case; considerable disagreement appears between the amplitudes caused by a negligibly small forcing torque and those calculated in the free motion. An adaptation is therefore better.

Equation [8] must hold true for the maximum swing φ_0 as well as all other values of φ for a given case. Since there is no damping, the phase of the pendulum relative to the torque can only be 0 or π. Let it therefore be assumed that for a single harmonic "torque" applied, ($\psi'' = \psi_0 \sin n\Omega t$), the motion of the pendulum is hyperelliptic after the manner of the free motion

$$\sin \varphi/2 = k \operatorname{sham} \omega t \quad \ldots\ldots\ldots\ldots\ldots\ldots [22]$$

where φ_0 may be either positive or negative with respect to ψ_0. Now, there can be no error in substituting in Equation [8] the following (as they occur simultaneously)

$$\left.\begin{matrix} \psi'' = \psi_0 \\ \varphi = \varphi_0 \end{matrix}\right\} \quad \left\{\begin{matrix} \dot{\psi} = 0 \\ \dot{\varphi} = 0 \end{matrix}\right\} \quad \ldots\ldots\ldots\ldots\ldots\ldots [23]$$

Then if Equation [22] is approximately as true for large forced motions as it is for small, the value of $\ddot{\varphi}$, found in general by differentiation of Equation [22] or

$$\ddot{\varphi} = \frac{-e^2 \sin \varphi}{1 - e^2 \cos^2 \varphi} (\cos \varphi \, \dot{\varphi}^2 + 2d/a^3)$$

will give for the instant $\varphi = \varphi_0$

$$\ddot{\varphi} = \frac{-\omega^2 \sin \varphi_0}{1 - e^2 \cos^2 \varphi_0} \quad \ldots\ldots\ldots\ldots\ldots\ldots [24]$$

Now, furthermore, for the steady-state condition the periods of the two variables must synchronize. The period of the hyperelliptic motion, Equation [22], is given in the free-motion analysis (2) and the calculations of these functions (5) as

$$\tau = 4L'/\omega$$

where L' is the complete hyperelliptic function

$$L' = \int_0^{\pi/2} \sqrt{\frac{1 - e^2(1 - 2k^2 \sin^2 \zeta)^2}{1 - e^2 \sin^2 \zeta}} \, d\zeta$$

For synchronization

$$2\pi/n\Omega = 4L'/\omega$$

$$\omega = \left(\frac{L'}{\pi/2}\right) n\Omega \quad \ldots\ldots\ldots\ldots\ldots\ldots [25]$$

These then can be substituted in Equation [8], together with the substitution for the momentum constant c, which is taken as

$$c = a^2\Omega \, (\beta + \cos \varphi_0)$$

for this involves only the neglect of higher and smaller harmonics of $\dot{\alpha}$. The relationship of φ_0 to ψ_0 appears as

$$n^2 = \left(\frac{\pi/2}{L'}\right)^2 \left\{ 2e^2(\beta + \cos \varphi_0) + \left(\frac{1 + a^2 \cos \varphi_0}{\sin \varphi_0}\right) \frac{\psi_0}{\Omega^2} \right\} \quad [26]$$

For any chosen pendulum (data a, e^2 and thus β) the response to a range of applied torque frequencies n and torque intensities [ψ_0/Ω^2] may then be found. The graph in Fig. 3 shows one such family of curves; it is seen that they exhibit the expected backward slope of the "soft-spring" nonlinear resonance curve. Greater intensities of torque produce greater pendulum amplitudes—the parameter used is explained through Equation [5] as

$$\psi_0/\Omega^2 = M_0/mR^2\Omega^2$$

Note that though the small-angle theory for the case shown in Fig. 3 indicates resonance from ninth-order harmonics for $a = \sqrt{R/L} = 9$, yet here small angle swing is excited at twice that order harmonic.

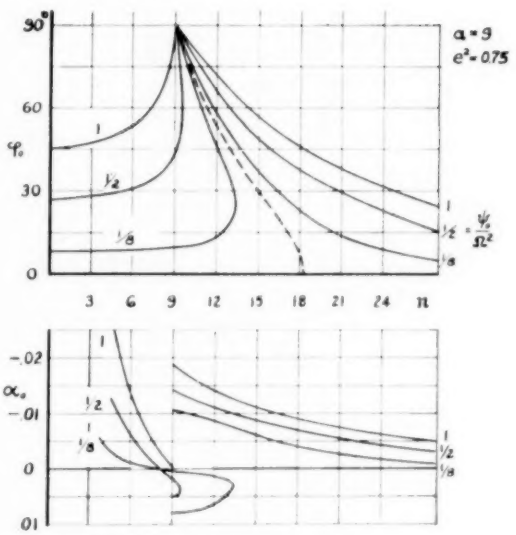

FIG. 3 FORCED AMPLITUDES OF PENDULUM AND CARRIER IN RESPONSE TO VARIOUS FREQUENCIES OF EXCITATION

FORCED MOTION OF CARRIER

In analyzing the free motion of the carrier, it was found advantageous to introduce an angle variable η, given by

$$2a^2(\beta + \cos \varphi)\dot{\eta} + (1 + a^2 \cos \varphi)\dot{\varphi} = 0 \quad \ldots\ldots [27]$$

In this the variables may be separated, and integration yields

$$\tan \frac{\sqrt{\beta^2 - 1}}{\beta - 1/a^2} (\eta + \varphi/2) = \sqrt{\frac{\beta - 1}{\beta + 1}} \tan \varphi/2 \quad \ldots [28]$$

Equation [27] may be subtracted from Equation [6] for

$$2a^2(\beta + \cos \varphi)(\dot{\theta} - \dot{\eta}) = a^4 \dot{\psi} + 2c \quad \ldots\ldots [29]$$

Now, also from Equation [6], if ψ'' (and torque M) are assumed to be a single harmonic of the same period as φ

$$c = a^2(\beta + \cos \varphi_0)\, \dot{\theta}_0$$

Equation [29] thus reduces, by setting $\dot{\theta} = \Omega + \dot{\alpha}$

$$\dot{\alpha} = \dot{\eta} + \frac{a^2 \dot{\psi}}{2(\beta + \cos \varphi)} + \left[\frac{(\beta + \cos \varphi_0)\, \dot{\theta}_0 - (\beta + \cos \varphi)\Omega}{\beta + \cos \varphi} \right]$$

The last term will be negligible; also, usually $\beta >> 1$ so that by integrating

$$\alpha = \eta - \frac{a^2 \psi}{2\beta} \approx \eta - e^2 \psi \quad \ldots\ldots\ldots\ldots [30]$$

For the steady-state amplitude α_0, the assumption is made along with those in Equation [23] that

$$\alpha = \alpha_0 \sin n\Omega t$$

which gives

$$\alpha_0 = \eta_0 - \frac{a^2 \psi_0}{2\beta n^2 \Omega^2} \approx \eta_0 - \frac{e^2 \psi_0}{n^2 \Omega^2} \quad \ldots\ldots\ldots [31]$$

η is the influence on the carrier by the pendulum and is found by

Equation [28] or in most cases by the much simpler expression

$$\eta = -\frac{\sin \varphi}{\lambda} \approx -\frac{\sin \varphi}{2\beta} \quad \ldots\ldots [32]$$

where $\lambda = \beta + \sqrt{\beta^2 - 1}$ as used in the free motion.

A curve from Equation [31] is shown for the same parameters in Fig. 3 under each φ_0-curve.

Designer's Approach

The designer is anxious not so much to know how a given pendulum responds to various exciting frequencies but rather how to choose the best pendulum for a known frequency excitation. The best pendulum should greatly reduce or eliminate the swing α of the carrier. This will occur when the right-hand side of Equation [31] vanishes.

It is thus obvious that smaller pendulums (small e^2) can only counteract torques proportional to their relative moment of inertia, and that amplitudes will diminish with the square of the frequency in the usual manner.

Let us then write Equation [31] as

$$\alpha_0 = A + \eta_0 \quad \ldots\ldots [33]$$

The symbol A then may be called the angular amplitude suffered by the carrier under torque M if the pendulum were locked as appears from

$$A = -\frac{a^2 \psi_0}{2\beta\, n^2\, \Omega^2} \quad \ldots\ldots [34]$$

$$= -\frac{M_0}{n^2 \Omega^2 \,[I_c + m(R^2 + L^2)]}$$

and η is the influence of the swinging pendulum.

With this term A, Equation [26] is now transposed to enable a solution in a to be obtained from a known n. It entails the approximation already used that $2e^2\beta \approx a^2$

$$a^2 = \frac{\left(\frac{L'}{\pi/2}\right)^2 n^2 - 2e^2 \cos \varphi_0 + \frac{An^2}{e^2} \operatorname{cosec} \varphi_0}{1 - \frac{An^2}{e^2} \cot \varphi_0} \quad \ldots\ldots [35]$$

Four examples of the relations given in Equations [33] and [35] are shown in Figs. 4 to 7, inclusive. It should be borne in mind that if the pendulum were locked, all the α-curves would reduce to horizontal lines with ordinate A_1, A_2 or A_3.

A Linear Simile

The precise meaning of the principal symbols is elucidated through a linear simile. Suppose a simple Frahm absorber is suggested to suppress the response of a body to an external harmonic excitation. We take the torsional case—where a torque $M = M_0 \sin \omega t$ is first applied to a single body with moment of inertia $(I + i)$. The proposition is to divide the body into two, respectively I and i, connected by a short shaft of stiffness k, in order to find the best proportion $\epsilon^2 = i/(I + i)$ to reduce the angular amplitude α_0 of the principal body I. The response φ of the secondary body i relative to the principal body is of no concern.

Originally the body is united so that the response to the torque imposed is given by

$$M = M_0 \sin \omega t = (I + i)\, \ddot{\alpha}$$

$$\alpha = -\frac{M_0}{(I + i)\, \omega^2} \sin \omega t$$

The forced amplitude is thus of magnitude

$$A = -\frac{M_0}{(I + i)\, \omega^2} \quad \ldots\ldots [36]$$

Now, with the mass split in two, it is to be shown that the amplitude of oscillation may be expressed as

$$\alpha_0 = A + \eta_0 \quad \ldots\ldots [37]$$

where η_0 is negative in some cases and may even reduce α to zero.

The equations of forced motion for the two bodies I and i, are

$$\left.\begin{aligned} I\,\ddot{\alpha} &= k\,\varphi + M \\ i(\ddot{\alpha} + \ddot{\varphi}) &= -k\varphi \end{aligned}\right\} \quad \ldots\ldots [38]$$

where the senses of the terms are shown in Fig. 8. Since these show simple harmonic relations, the amplitudes may be found by substitution of

$M = M_0 \sin \omega t$, $\alpha = \alpha_0 \sin \omega t$, and $\varphi = \varphi_0 \sin \omega t$, giving

$$\left.\begin{aligned} \alpha_0 &= \left(\frac{k}{i\omega^2} - 1\right) \varphi_0 \\ \varphi_0 &= \frac{M_0/I}{\omega^2 - \omega_n^2} \end{aligned}\right\} \quad \ldots\ldots [39]$$

where ω_n refers to the free vibration of the two bodies against each other or

$$\omega_n^2 = \frac{k(I + i)}{Ii} \quad \ldots\ldots [40]$$

Now, in terms of A from Equation [36]

$$(1 - e^2)\, \varphi_0 = A \Big/ \left(\frac{\omega_n^2}{\omega^2} - 1\right)$$

$$\eta_0 = -e^2 \varphi_0 \quad \ldots\ldots [41]$$

The amplitude α_0 will be found less than A, by Equation [37], if

$$(1 - e^2)\,(\omega_n/\omega)^2 - 1 < (1 - e^2)\,[(\omega_n/\omega)^2 - 1]$$

or for

$$1 - e^2 < 1$$

which is always true, showing that the split into I and i is always helpful.

The motion α may be eliminated if

$$(1 - e^2)\,(\omega_n/\omega)^2 = 1$$

Conclusions

In the graphs shown in Figs. 4 to 7 inclusive, the values of the parameter A were chosen carefully. It was thought perhaps that the pendulum might be induced to swing just sufficiently to counter any torque that was within its maximum ability. Now, since in Equations [33] the influence of the pendulum on the carrier is η (which is expressed by Equation [32]), and also approximately $2\beta = a^2/e^2$, then a pendulum whose maximum swing is φ_0 might be expected to counteract a torque given by

$$A = \frac{e^2 \sin \varphi_0}{a^2}$$

that is, proportional to the moment of inertia in the pendulum and inversely as the square of the frequency.

Two values of φ_0 were therefore chosen, for the value of A_1, $\varphi_0 = 30$ deg, and for A_2, $\varphi_0 = 60$ deg. For a, n was used since

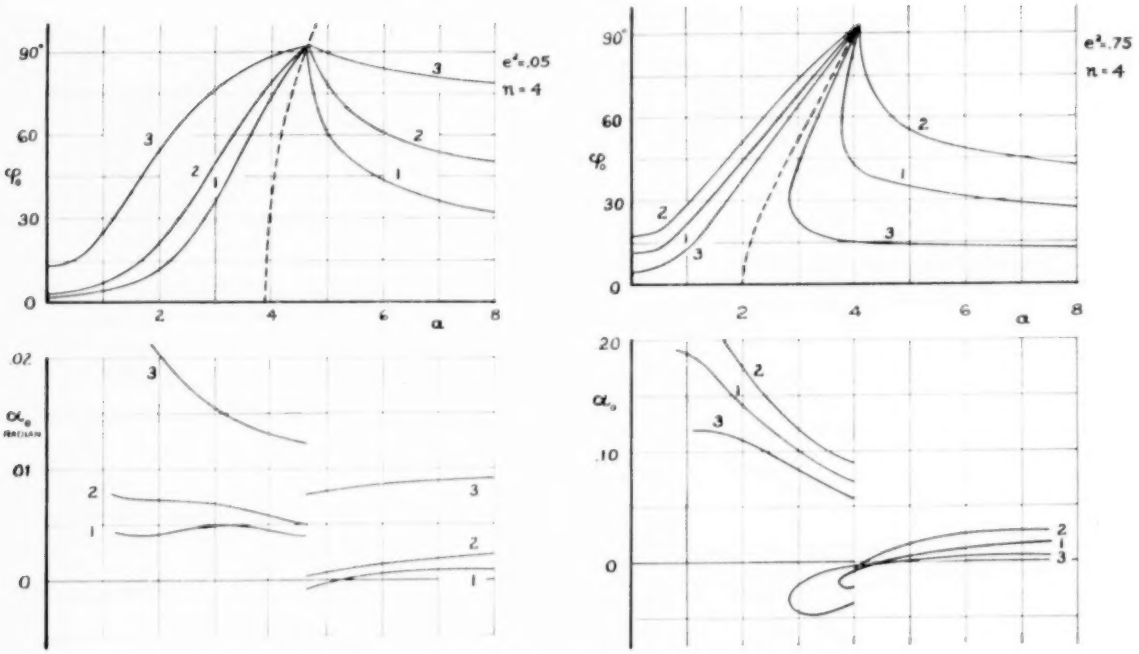

FIGS. 4 AND 5 RESPONSE OF PENDULUM OF VARYING LENGTH TO FOURTH-ORDER EXCITATION

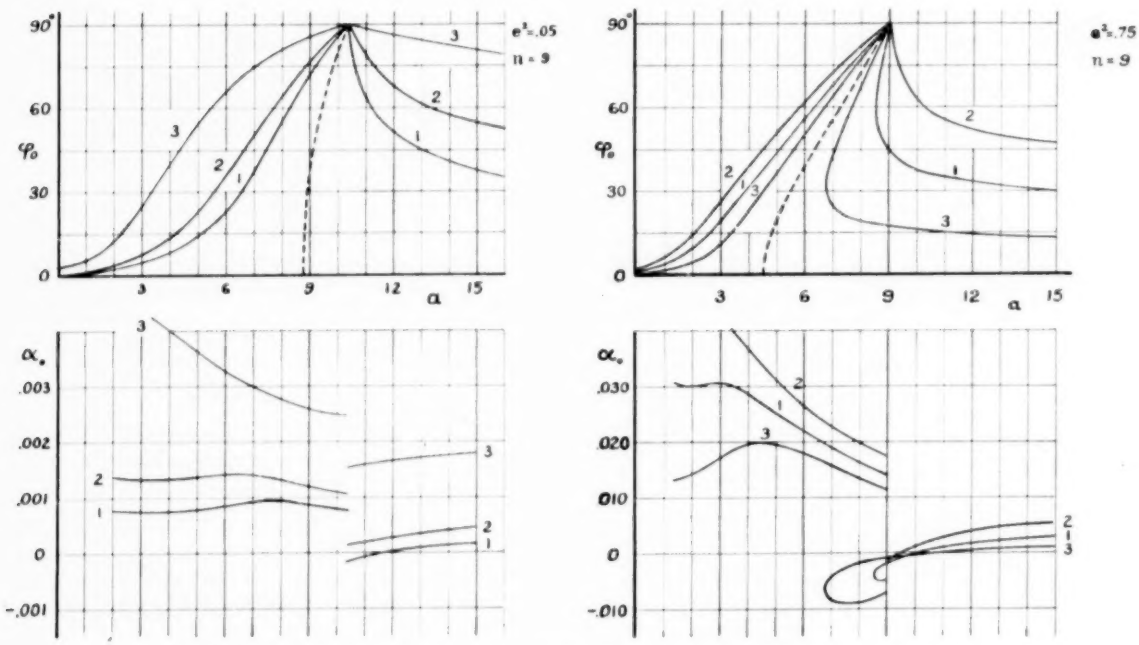

FIGS. 6 AND 7 RESPONSE OF PENDULUM OF VARYING LENGTH TO NINTH-ORDER EXCITATION

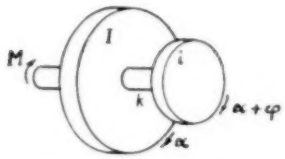

FIG. 8 FRAHM ABSORBER

the value of a when φ_0 was to be 30 deg or 60 deg could not be determined in advance.

A third value of A was also taken, which reckoned with a change with n^2 but took no account of changing e^2, to see if under a given torque a small pendulum could be just as useful in eliminating vibration by swinging more widely. The three values of A are given in radian measure in Table 1.

TABLE 1

Fig.	n	e^2	A_1	A_2	A_3
4	4	0.05	0.00156	0.00271	0.010
5	4	0.75	0.02344	0.04060	0.010
6	9	0.05	0.00031	0.00053	0.002
7	9	0.75	0.00463	0.00802	0.002

Thus some correspondence between all curves marked 1 and between those marked 2 (meaning A_1, A_2) should appear.

It is remarkable that the curves in Figs. 4 and 6, and in Figs. 5 and 7, are almost identical, except for the change in a proportional to n in the abscissa, and the change in α_0 inversely proportional to n^2 as expected.

In Figs. 5 and 7 the pendulum does appear to exert itself according to the demand: on the A_2 and A_1-curves swings of approximately 73 deg and 37 deg by the pendulum are able to reduce α to zero. These are greater than the assumed values of 60 deg and 30 deg because a is rather more than the assumed values of 4 and 9, which results in greater values for β and less effectiveness of the pendulum torque.

In Figs. 4 and 6 the point of zero α is moved to a value of a some 30 per cent higher than those assumed, with the result that the A_1-curve shows need of φ_0 climbing to 55 deg instead of 30 deg, and the A_2 excitation sends φ_0 up to 90 deg and even so succeeds in reducing α by only about 75 per cent.

In general, therefore, in all cases pendulums should have a length L shorter than that given by the small-angle theory. In heavier pendulums a value of a in the order of 10 per cent over n is indicated and with smaller pendulums 30 per cent or more is needed.

A pendulum should never have too long a length, for on the left-hand side of all Figs. 4 to 7, inclusive, the pendulum is seen to aggravate the condition. Where several different harmonics occur in a given system, only the lowest frequency can thus be counteracted by a pendulum damper; multiple pendulum units, tuned differently, will rarely be useful, for the pendulums tuned to the higher will augment the lower-order trouble very considerably.

The optimum tuning appears as a dependent on the torque intensity. If the intensity of a given order excitation varies, as it will, for example, with speed in an internal-combustion engine, then the pendulum can be designed only to reduce and not to eliminate the trouble.

It therefore may be concluded that occasions often arise where wide angle swing of a pendulum can be incorporated. There is a limit to the useful angle of a bifilar design due to jumping off one of the supports, which occurs near the amplitude position and depends on the moment of inertia about its own centroid. In the puck type, with small e, detuning occurring with the sliding of the puck is known to occur and must be reckoned with. Space does not permit dealing with either of these adjustments here.

In general, the small-angle theory of tuning for a resonance where $R/L = n^2$ is not adequate.

BIBLIOGRAPHY

1 "Tuned Pendulums as Torsional Vibration Eliminators," by J. P. Den Hartog in S. Timoshenko 60th Anniversary Volume, The Macmillan Company, New York, N. Y., 1938, pp. 23–26.

2 "The Free Oscillation of the Centrifugal Pendulum With Wide Angles," by F. R. E. Crossley, JOURNAL OF APPLIED MECHANICS, Trans. ASME, vol. 74, 1952, pp. 315–319.

3 "The Centrifugal Pendulum Dynamic Damper," by F. P. Porter, in "Evaluation of Effects of Torsional Vibration," SAE War Engineering Board, New York, N. Y., 1945, p. 269 seq.

4 "Advanced Dynamics," by S. Timoshenko and D. H. Young, McGraw-Hill Book Company, Inc., New York, N. Y., 1948, pp. 313–314.

5 "A Hyperelliptic Function as a Non-Linear Oscillation," by F. R. E. Crossley, *Journal of Mathematics and Physics*, vol. 30, January, 1952, pp. 214–225.

6 "Introduction to Non-Linear Mechanics," by N. Minorsky, J. W. Edwards Bros., Ann Arbor, Mich., 1947, chapters 15, 16, and 17.

7 "Theory of Oscillations," by A. Andranow and S. Chaikin, Princeton University Press, Princeton, N. J., 1949.

8 "Mechanical Vibrations," by J. P. Den Hartog, McGraw-Hill Book Company, Inc., New York, N. Y., third edition, 1948, p. 431.

9 "Vibration Problems in Engineering," by S. Timoshenko, D. Van Nostrand Company, Inc., New York, N. Y., second edition, 1937, p. 137.

10 "Applied Mathematics for Engineers and Physicists," by L. A. Pipes, McGraw-Hill Book Company, Inc., New York, N. Y., first edition, 1946, p. 601.

A Nondestructive Differential-Pressure Test for Thin Shells

By J. C. NEW,[1] SILVER SPRING, MD.

The differential-pressure test is an original, nondestructive, experimental technique for determining incipient buckling pressures of thin shells subjected to external pressure. Extensions of the basic test permit study of many buckling parameters as well as other mechanical factors in thin-shell design and evaluation. The salient feature of the technique is the filling of the internal volume of the shell with a compressible fluid, such as water, to control the magnitude and rate of shell deformation. The incipient buckling pressure is detected by noting the point at which the difference in internal and external pressure becomes constant. Experimental verification of the technique and its nondestructive aspect is presented. Applications and limitations of the test are discussed.

Nomenclature

The symbols used in this paper are defined as follows:

P = pressure acting on thin shell
P_c = collapsing pressure for thin shell subjected to external pressure
P_e = external pressure acting on thin shell
P_i = internal pressure acting on thin shell
P_d = $P_e - P_i$, differential pressure acting on thin shell
D = mean diameter of thin cylindrical shell
t = wall thickness of thin shell
E = modulus of elasticity in compression
K = bulk modulus
μ = Poisson's ratio
C = a function of elastic constants defined as $E/K(5/4 - \mu)$
V = original internal volume of thin cylindrical shell before application of pressure

Units: All linear dimensions are in inches
All pressures, stresses, and elastic moduli are in psi
All volumes are in cu in.
All constants and ratios are dimensionless

Introduction

Thin shells occupy a significant and often critical place in many modern engineering structures. Examples of such shells are pressure vessels, submarine hulls, penstocks, boiler tubes, submerged gas lines, airplane fuselages, vacuum tanks, and underwater ordnance such as mines and torpedoes.

These structures are, in general, loaded by an external pressure. Their failure is most often characterized by a sudden and dramatic collapse. Thus intelligent and precise design must be executed for a safe and efficient structure. Mathematical theory and past experience must be supplemented in new and unusual design by experimental results.

It is the object of this paper to present an experimental technique for studying and evaluating thin shells in a novel and nondestructive manner through the use of a differential-pressure test. The experimental results presented will illustrate the detail and versatility of this technique but are not given in support of any theory on the buckling of thin shells. Applications and limitations are presented to suggest areas in which this test may be useful.

Differential-Pressure Test

The buckling or collapse of a thin shell is a manifestation of the lack of equilibrium between the external applied pressure and the stress developed in the shell wall. If such a stress is substantially below the elastic limit, we characterize such a failure as being due to elastic instability. If the stress at the time of buckling is in the inelastic range of the material, then, in popular terms, a failure by yielding is noted. In either case, a state of unstable equilibrium exists causing an uncontrolled reaction to take place, namely, an almost explosive collapse of the shell.

Since the shell rigidity is inadequate to maintain equilibrium, then some additional force must be introduced, if a sudden collapse is to be prevented or if it is desired to control the rate of collapse. If this force is related to the external force through the mechanism of the shell rigidity, then at the point of incipient buckling a null balance must exist such that for each incremental increase in external load an equal and opposite increase is developed by the restoring force, thus maintaining equilibrium.

From this reasoning we may postulate the following thesis which is the basis for the differential-pressure test:

If a closed shell subjected to external pressure is filled with a compressible fluid, such as water, the point of incipient buckling of the shell may be detected by observing the point at which the difference between the external and internal pressures becomes constant. Furthermore, the extent of shell deformation after buckling is started may be controlled by regulating the external pressure acting on the shell until a state of yield exists.

For an ideal thin cylindrical shell, it has been shown[2] that the volume change in the shell, the material properties, and the external loads are related as follows

$$\frac{\Delta V}{V} = \frac{P_d D}{Et}(5/4 - \mu) \quad \ldots\ldots [1]$$

By definition the bulk modulus of a liquid such as water is

$$K = \frac{\Delta P}{\Delta V / V} \quad \ldots\ldots [2]$$

For the present case

$$\Delta P = P_e = K \frac{\Delta V}{V} \quad \ldots\ldots [3]$$

and by combining Equations [1] and [3] we obtain

---

[1] Mechanical Engineer, Naval Ordnance Laboratory.

Contributed by the Applied Mechanics Division and presented at the Fall Meeting, Chicago, Ill., September 8–11, 1952, of The American Society of Mechanical Engineers.

Discussion of this paper should be addressed to the Secretary, ASME, 29 West 39th Street, New York, N. Y., and will be accepted until April 10, 1953, for publication at a later date. Discussion received after the closing date will be returned

Note: Statements and opinions advanced in papers are to be understood as individual expressions of their authors and not those of the Society. Manuscript received by ASME Applied Mechanics Division, March 7, 1952. Paper No. 52—F-10.

[2] "A Nondestructive Method for Detecting the Incipient Buckling Pressures of Thin-Walled Shells," by J. C. New, Naval Ordnance Laboratory Report No. 1154, May 28, 1951, pp. 15–17.

$$\frac{P_d}{P_e} = \frac{Et}{KD(5/4 - \mu)} \quad [4]$$

For simplicity, we now define C in terms of the elastic constants as

$$C = \frac{E}{K(5/4 - \mu)} \quad [5]$$

then

$$\frac{P_d}{P_e} = Ct/D \quad [6]$$

Since by definition

$$P_d = P_e - P_i \quad [7]$$

we may combine Equations [6] and [7] and obtain finally

$$\frac{P_d}{P_e} = \frac{C}{C + D/t} \quad [8]$$

Equations [6] and [8] define the relationship between the differential pressure and the internal or external pressures, respectively. If a Cartesian plot is made of P_d against either P_i or P_e, the resulting curve is a straight line having a slope defined by the right-hand member of the equation used.

Fig. 1 illustrates the theoretical pressure curve which the test method yields and relates the various portions of this curve to the stress-strain curve of the material. In the region O to A the specimen undergoes a uniform contraction. At point A the specimen starts to buckle because of elastic instability. As the external pressure is increased, the shell deforms until the internal pressure is increased just sufficiently to regain equilibrium with the external pressure. Thus, if the external pressure is increased 10 psi, the internal pressure increases 10 psi. Consequently, the difference between the external and internal pressures P_d, becomes constant and the curve between points A and C is horizontal. Although between A and B the differential pressure is

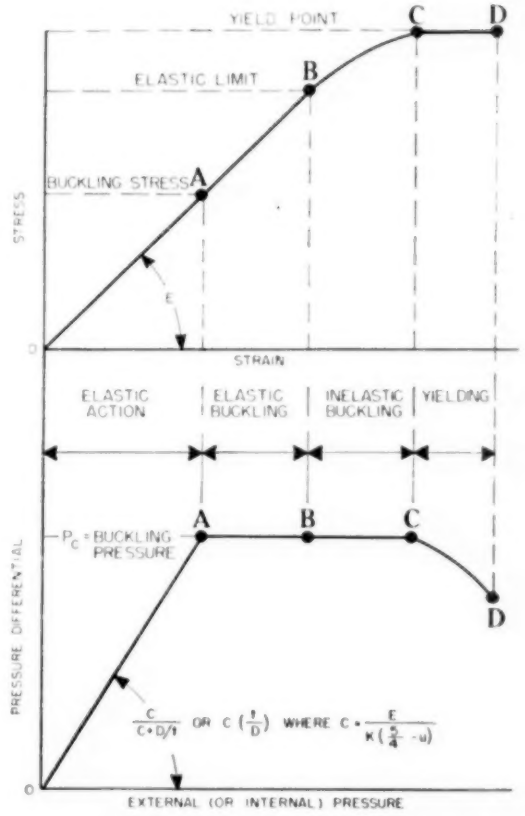

FIG. 1 THEORETICAL PRESSURE AND STRESS-STRAIN CURVES

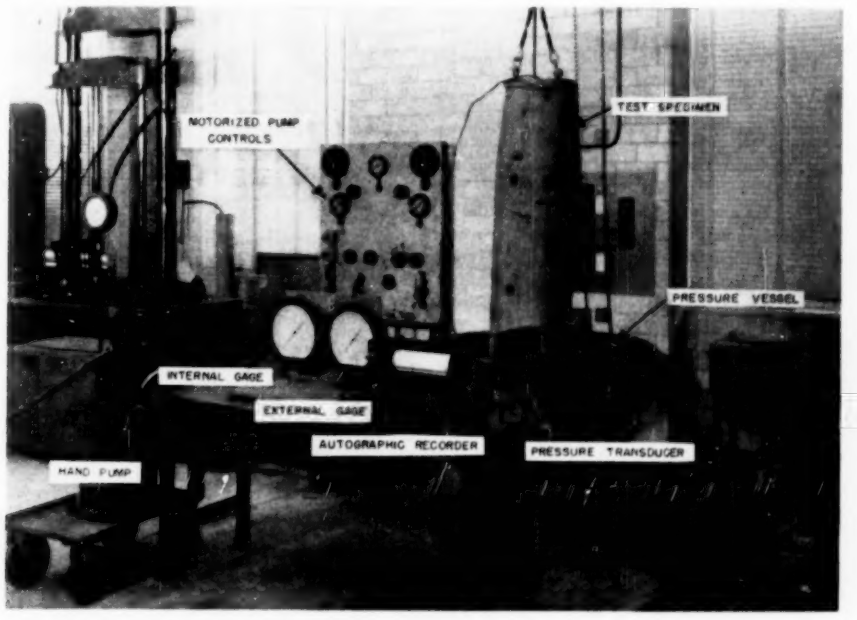

FIG. 2 EXPERIMENTAL APPARATUS

constant, the specimen is experiencing a bending strain as the surface warps in addition to the uniform contraction. Thus at point B the specimen deformation is sufficient to have reached the elastic limit of the shell material.

It is significant to note, however, that if the external pressure is released at any point prior to B, then no permanent deformation of the shell will result since the action is entirely elastic. Consequently, this procedure represents a nondestructive method for determining the incipient buckling pressure of the shell. Furthermore, it is equally applicable to shells of any geometric configuration, material, or ones having internal ribs, frames, or bulkheads. In these general cases, however, Equations [6] and [8] are not applicable.

Between points B and C, inelastic buckling takes place until point C, which represents the yield point of the material, is reached. Beyond point C the specimen, if the material is ductile, continues to deform inwardly even though the external pressure is maintained nearly constant. This deflection causes a substantial increase in the internal pressure and since the external pressure remains nearly constant, the differential pressure must decrease. If the material is brittle or if the yield point and ultimate strength are nearly the same, then sudden and uncontrolled failure of the specimen will occur in the region of point C.

Experimental Verification

The experimental apparatus necessary to perform a differential pressure test is simply a pressure vessel to contain the shell and two pressure gages to monitor the internal and external pressures. The equipment used at the Naval Ordnance Laboratory for this purpose is shown in Fig. 2. If manual plotting of the data is used, the constancy of the differential pressure is readily detected by observing when the second difference in the external and internal pressures approaches zero. It has been found that personal errors and the labor involved can be reduced substantially by producing a Cartesian plot of the pressure relationships by means of an autographic (X-Y) recorder. One which the author developed from a Baldwin-Lima-Hamilton Corporation electronic stress-strain recorder is shown in Fig. 2. Commercial X-Y or function plotters have recently become available.

In Fig. 3, specimen 3C which was constructed of 28-O aluminum illustrates a typical curve obtained when the differential test is continued until yielding occurs. It will be noted that the differential pressure remained constant for almost a 100-psi increase in external pressure. The curve marked 3C-a is a second trial on the same specimen after it had been removed from the pressure vessel to observe the extent of yielding. It will be noted that buckling continues at a pressure identical with the terminal differential pressure of the first trial. Specimen 21 in Fig. 3 is typical of a differential test carried just to the point of incipient buckling.

Fig. 4 illustrates the differences in specimen deformation that result when differential and external-pressure tests are used. In Table 1 a comparison of results obtained with the differential and external-pressure tests is presented. These data were selected to show results obtained with a wide variety of shell materials and over a wide range of buckling pressures. The 9.3

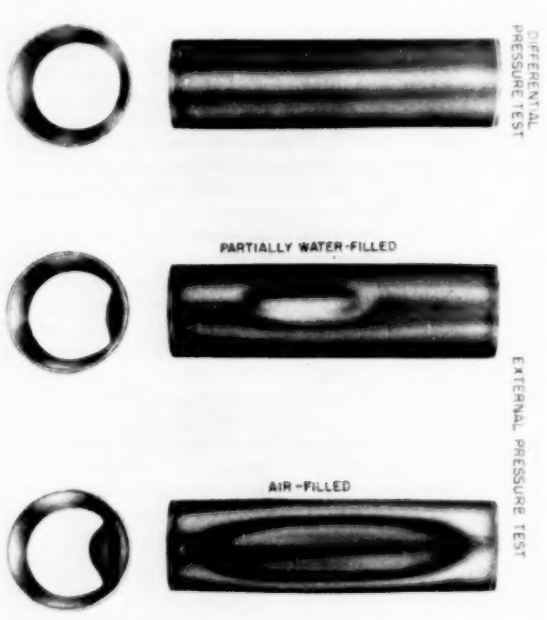

Fig. 4 Pressure Tests of Extruded Aluminum Tubes

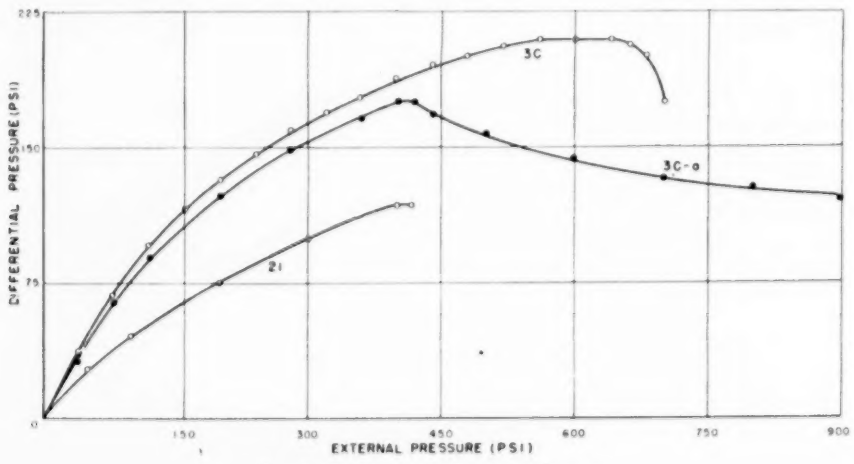

Fig. 3 Differential-Pressure Curves

and 9.1 per cent variations, tabulated for specimens 1 and 2, are attributed to premature discontinuance of the differential-pressure test. It is believed that these percentage variations would have been closer to 5 per cent had the differential test been continued. Nevertheless, it will be noted that the external collapsing pressure is always within 10 per cent of the differential pressure and in most cases is within 5 per cent. These results were obtained on the same specimen; consequently no significant damage could have resulted from the differential-pressure test which preceded the external-pressure test.

TABLE 1 COMPARISON OF DIFFERENTIAL AND EXTERNAL-PRESSURE TESTS

Specimen identification			Buckling pressure, psi		Variation,
No.	Shell material	Geometry	Differential	External	per cent
1	Stainless steel	Cylinder	366	400	+9.3
2	Aluminum	Cylinder	209	228	+9.1
3	Glass cloth-phenolic	Cylinder	600	575	−4.2
4	Mild steel	Cylinder	119	124	+4.2
5	Mild steel	Cylinder	571	554	−3.0
6	Mild steel	Sphere	829	802	−3.3

NOTE: All external tests made on same specimen after differential test.

APPLICATIONS

Buckling Pressures. The differential-pressure test is uniquely applicable for determinations of incipient buckling of thin shells subjected to external pressure. The incipient-buckling pressure is the maximum unit strength of the shell and, moreover, is the maximum external pressure, within the limits of experimental error, which the shell can sustain before total collapse, if the shell is not internally supported by a liquid or solid filling material. Experimental support of this conclusion has been demonstrated by over a hundred tests made at the Naval Ordnance Laboratory on a variety of geometric shapes, materials of construction, and pressure ranges. This test has been adopted as a standard test method by this organization.

Proof Loading. Because of the nondestructive feature of the differential test, proof loading may be conducted to the point of incipient buckling, thereby establishing the safety margin inherent in any given design. Where expensive or "one-of-a-kind" specimens are encountered this test offers an economical and scientific method to evaluate the efficacy of a given structure.

Manufacturing Anomalies. The differential-pressure test readily permits the detection of even the slightest leak by the nonlinear change in the differential-pressure curve during the early stages of the test. Thus a leakage and proof test can be conducted simultaneously with resulting economy. Also, there is some evidence, although inconclusive at this time, that an advantageous "working" of fabricated thin shells to distribute more favorably residual or locked-in stresses can be achieved through repetitive application of the differential test, thereby increasing the mechanical strength of the shell.

Research Problems. The differential-pressure test is a scientific tool which can be exploited in research problems. An illustrative example will be cited to show the versatility of this method.

One of the most serious limitations in any scientific investigation is obtaining sufficient "identical" samples on which to base a statistically significant result. Anomalies in material and fabricating processes are perhaps the greatest deterrents to this end. Since the differential test is nondestructive, its employment will serve to minimize this effect as a single specimen may be used repeatedly. For example, the technical literature shows no universal agreement on the length-diameter parameter in analytical expressions for buckling pressures. To study this condition, one could make up three long cylinders of different diameters. After each successive differential-pressure test, the cylinders could be reduced in length giving a new L/D ratio. Thus by using only three specimens a broad range of L/D ratios could be investigated. By a similar approach, "effective length" and internal rib design and spacing could be investigated.

Effective Modulus Determinations. For an ideal cylindrical shell the elastic portion of the differential pressure curve is a straight line defined by Equations [6] and [8]. By means of either of these equations it is possible to calculate any one of the elastic moduli, provided proper values for the other two are known. The most valuable calculation is that of an "effective compressive modulus" for the shell material. This calculation is particularly applicable for plastic shells which exhibit an effective compressive modulus substantially different from that obtained by routine mechanical tests on standard test specimens. The precision of the result obtained by using this approach is dictated almost entirely by the degree to which the experiment can be idealized. A more comprehensive and detailed examination of this problem is presented in the reference previously cited.[2]

LIMITATIONS

Pressure Vessel. It is inherent in the differential-pressure test that higher pressures be imposed than if only an external pressure test were conducted. This requirement would seem to dictate the use of a pressure vessel having a substantially higher pressure rating. This limitation can be circumvented, when necessary, by a slight alteration in experimental method characterized by a stepwise procedure. This method is understood most readily by following the numerical steps and directed paths shown in Fig. 5. The solid lines indicate an increasing pressure whereas the dashed lines denote a decreasing pressure.

The stepwise procedure consists of building up the external pressure until the maximum rating of the pressure vessel is reached and noting the differential pressure. Next, the external pressure is released to a value slightly greater than the terminal differential pressure. Then the internal pressure is released, practically to zero, leaving a net differential of that first achieved at maximum external pressure. At this point one is ready to start the second step of increasing external pressure. This stepwise action can be repeated as often as necessary to generate the required differential pressure. It is absolutely essential that in releasing the internal pressure the terminal differential pressure of the preceding step not be exceeded. Otherwise the danger exists that the shell will collapse during release of the internal pressure at which time the operator has no control over the action since it occurs suddenly. Experience has been a wise teacher in this detail! That a continuous smooth curve results from this procedure is evident from Fig. 6 which is a replot of the same data as Fig. 5, omitting the overlap areas. Note that a pressure-vessel rating of over twice that used would have been required had the stepwise method not been used.

Experimental Difficulties. The most serious experimental difficulty is eliminating mechanically entrapped air. Its most pronounced effect is to cause the elastic portion of the differential pressure curve to be nonlinear, Fig. 3. If the volume of air is small in comparison to the volume of water used then some entrapped air can be tolerated. Wetting agents, vacuum methods, and Bourdon-gage vent plugs have been most successful in minimizing this problem.

Buckled Areas. Paradoxically, the most serious limitation of the differential-pressure test stems from the fact that it is nondestructive! This feature makes it impossible to determine the region in which elastic buckling takes place unless the test is continued until yielding occurs. This condition, of course, is only a limitation when the test is being used as an experimental design

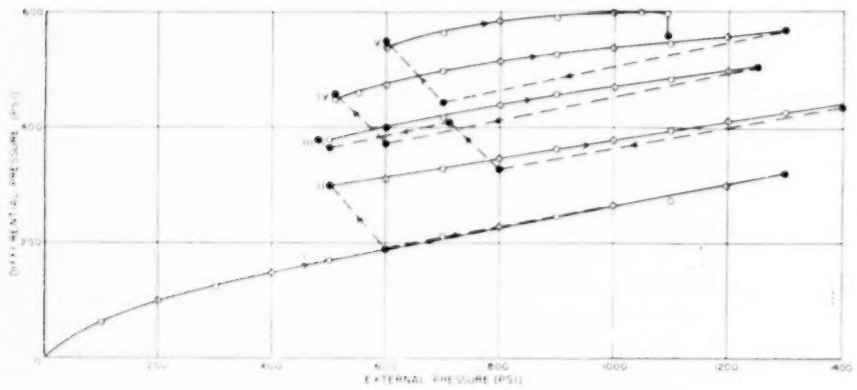

FIG. 5 STEP DIFFERENTIAL-PRESSURE CURVE FOR PLASTIC SHELL

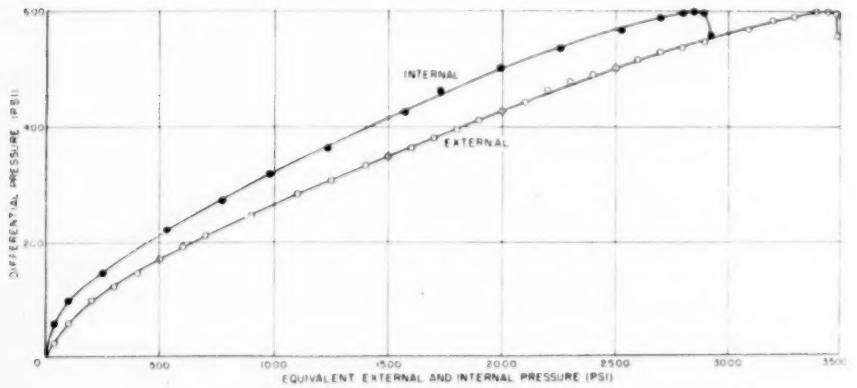

FIG. 6 COMPOSITE PRESSURE CURVE FOR PLASTIC SHELL

tool and it is desired to "beef-up" the weak section. The use of brittle coatings such as hard paints, Portland cement pastes, and Stresscoat lacquers give some promise of buckled-area indicators.

CONCLUSIONS

The differential-pressure test is an experimental method for determining nondestructively the mechanical strength and related properties of thin shells by utilizing the compressibility of an enclosed fluid such as water to control the buckling process. This test yields results within 10 per cent of external pressure tests without destroying the sample. The test method is a scientific tool which can be used in a variety of research and associated problems. Its apparent limitations generally can be circumvented by slight modifications in experimental procedure. Substantial economies can be effected through employment of the differential-pressure test.

ACKNOWLEDGMENT

The opinions expressed in this paper are those of the author and do not necessarily represent those of the Navy Department. Much of the material presented herein was obtained from a Naval report (reference cited), which of necessity has had only a limited distribution.

The author wishes to express his appreciation for the co-operation and assistance he received in releasing this material in its present form.

Numerical Analysis of Forced Vibrations of Beams

By N. O. MYKLESTAD,[1] URBANA, ILL.

In this paper a simple tabular method is developed by which the vibration amplitudes, bending moments, and shear forces of a beam of variable but symmetrical cross section, carrying any number of concentrated masses and acted on by any number of harmonically varying forces, can be found. The driving forces must all have the same frequency but the phase angles may be different. The method is an extension of the one employed by the author to find natural modes of vibration of beams, but in the case of forced vibration only one application of the tabular calculations is necessary, making it essentially a far simpler problem than that of finding the natural modes. Internal damping of the beam material is easily considered and should always be taken into account if there is any danger that the forced frequency is near any one of the natural frequencies.

Introduction

IN the present numerical analysis it is assumed that the beam is subjected to bending in one plane only and that it does not twist during vibration. The mass of the beam must be concentrated at discrete points along the elastic axis and the number of such points will depend on the number of concentrated driving forces as well as on the accuracy desired. The driving forces must all be harmonic and of the same frequency, but need not be in phase. They are conveniently written in the form $\bar{F}\,e^{i\omega t}$, where $\bar{F} = F\,e^{i\alpha}$ is the complex amplitude of a force with real amplitude F and phase angle α with respect to the rotating vector $e^{i\omega t}$. The internal damping is considered by assuming a complex damping factor $2b$ and multiplying each of the elastic coefficients by the quantity $e^{-2bi} = \cos 2b - i \sin 2b$, or $1 - 2bi$ if b is a small quantity and extreme accuracy is not required. All the deflections, slopes, shearing forces, bending moments, and so on, entering the problem will now be harmonic but with complex amplitudes. The term $e^{i\omega t}$ may then be canceled out as usual and only the complex amplitudes used in the calculations.

The beam is divided into sections with concentrated masses at the boundaries, and the elastic coefficients for the nth section are defined as follows: If the left end of the section is clamped and a unit bending moment applied to the right end the slope at this end will be v_{M_n} and the deflection d_{M_n}; while a unit force at the right end would give a slope v_{F_n} and deflection d_{F_n}. For a uniform section of length l and flexural rigidity EI these quantities would be

$$v_M = \frac{l}{EI} \quad [1]$$

$$v_F = d_M = \frac{l^2}{2EI} \quad [2]$$

$$d_F = \frac{l^3}{3EI} \quad [3]$$

Also, $\bar{v}_M = v_M\,e^{-2bi}$, $\bar{v}_F = d_M = v_F\,e^{-2bi}$, $\bar{d}_F = d_F\,e^{-2bi}$, where $2b$ is the complex damping factor. For a nonuniform section more accurate formulas are derived elsewhere.[2]

Beam With Free End

A beam with free end is shown schematically in Fig. 1, where the free end is at the right and the base is at the left end, which may be either free, hinged, or clamped. Fig. 2 shows the nth section of the beam in its extreme position when the free end of

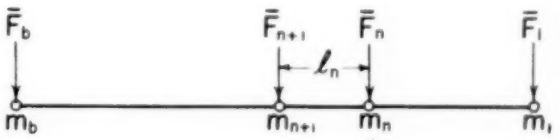

FIG. 1

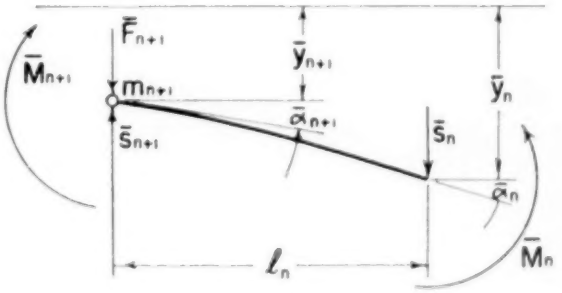

FIG. 2

the beam itself has a deflection $\bar{\delta}$ and a slope $\bar{\varphi}$. The slope and deflection at station n are then $\bar{\alpha}_n$ and $\bar{y}_n$, respectively, while the shearing force immediately to the left of mass m_n is S_n and the bending moment M_n. If these quantities are known at station n they can be found at station $n + 1$ by means of the following equations:

$$S_{n+1} = S_n + m_{n+1}\,\omega^2\,y_{n+1} + F_{n+1} \quad [4]$$

$$M_{n+1} = M_n - l_n S_n \quad [5]$$

$$\bar{\alpha}_{n+1} = \bar{\alpha}_n - v_{F_n} S_n + v_{M_n} M_n \quad [6]$$

[1] Professor of Theoretical and Applied Mechanics, University of Illinois. Mem. ASME.

Contributed by the Applied Mechanics Division and presented at the Fall Meeting, Chicago, Ill., September 8–11, 1952, of THE AMERICAN SOCIETY OF MECHANICAL ENGINEERS.

Discussion of this paper should be addressed to the Secretary, ASME, 29 West 39th Street, New York, N. Y., and will be accepted until April 10, 1953, for publication at a later date. Discussion received after the closing date will be returned.

NOTE: Statements and opinions advanced in papers are to be understood as individual expressions of their authors and not those of the Society. Manuscript received by ASME Applied Mechanics Division, May 19, 1952. Paper No. 52—F-12.

[2] "Vibration Analysis," by N. O. Myklestad, McGraw-Hill Book Company, Inc., New York, N. Y., 1944, p. 201.

$$\bar{y}_{n+1} = \bar{y}_n - l_n \bar{\alpha}_{n+1} - d_{Fn} S_n + d_{Mn} M_n \quad [7]$$

By substituting for $\bar{\alpha}_{n+1}$ from Equation [6] in Equation [7] this becomes

$$\bar{y}_{n+1} = \bar{y}_n - l_n \bar{\alpha}_n + \bar{u}_{Fn} S_n - \bar{u}_{Mn} M_n \quad [7a]$$

where

$$\bar{u}_{Fn} = l_n \bar{v}_{Fn} - d_{Fn} \quad [8]$$

$$\bar{u}_{Mn} = l_n \bar{v}_{Mn} - d_{Mn} \quad [9]$$

For a uniform beam section this gives

$$u_{Fn} = \frac{l_n^3}{6EI} \quad [8a]$$

$$u_{Mn} = \frac{l_n^2}{2EI} \quad [9a]$$

and $\bar{u}_F = u_F e^{-2bi}$, $\bar{u}_M = u_M e^{-2bi}$. Owing to the linear character of these equations each of the foregoing quantities can be written as a linear function of the slope $\bar{\varphi}$ and deflection $\bar{\delta}$ at the free end of the beam. This gives

$$S_n = -\bar{G}_{\varphi n} \bar{\varphi} + \bar{G}_{\delta n} \bar{\delta} + \bar{G}_n \quad [10]$$

$$M_n = \bar{G}'_{\varphi n} \bar{\varphi} - \bar{G}'_{\delta n} \bar{\delta} - \bar{G}_n' \quad [11]$$

$$\bar{\alpha}_n = \bar{f}_{\varphi n} \bar{\varphi} - \bar{f}_{\delta n} \bar{\delta} - \bar{f}_n \quad [12]$$

$$\bar{y}_n = -\bar{g}_{\varphi n} \bar{\varphi} + \bar{g}_{\delta n} \bar{\delta} + \bar{g}_n \quad [13]$$

where the minus signs have been introduced merely to make the coefficients $\bar{G}$, $\bar{G}'$, $\bar{f}$ and $\bar{g}$ positive for most practical problems, which makes the tabular calculations somewhat easier. Substituting Equations [10] to [13] in Equations [4] to [7a], and equating like terms, results in the following system of equations

$$\bar{G}_{\varphi n+1} = \bar{G}_{\varphi n} + m_{n+1} \omega^2 \bar{g}_{\varphi n+1} \quad [14]$$

$$\bar{G}_{\delta n+1} = \bar{G}_{\delta n} + m_{n+1} \omega^2 \bar{g}_{\delta n+1} \quad [15]$$

$$\bar{G}_{n+1} = \bar{G}_n + m_{n+1} \omega^2 \bar{g}_{n+1} + F_n \quad [16]$$

$$\bar{G}_{\varphi n+1}' = \bar{G}'_{\varphi n} + l_n \bar{G}_{\varphi n} \quad [17]$$

$$\bar{G}_{\delta n+1}' = \bar{G}'_{\delta n} + l_n \bar{G}_{\delta n} \quad [18]$$

$$\bar{G}_{n+1}' = \bar{G}_n' + l_n \bar{G}_n \quad [19]$$

$$\bar{f}_{\varphi n+1} = \bar{f}_{\varphi n} + \bar{v}_{Fn} \bar{G}_{\varphi n} + \bar{v}_{Mn} \bar{G}'_{\varphi n} \quad [20]$$

$$\bar{f}_{\delta n+1} = \bar{f}_{\delta n} + \bar{v}_{Fn} \bar{G}_{\delta n} + \bar{v}_{Mn} \bar{G}_{\delta n}' \quad [21]$$

$$\bar{f}_{n+1} = \bar{f}_n + \bar{v}_{Fn} \bar{G}_n + \bar{v}_{Mn} \bar{G}_n' \quad [22]$$

$$\bar{g}_{\varphi n+1} = \bar{g}_{\varphi n} + l_n \bar{f}_{\varphi n} + \bar{u}_{Fn} \bar{G}_{\varphi n} + \bar{u}_{Mn} \bar{G}'_{\varphi n} \quad [23]$$

$$\bar{g}_{\delta n+1} = \bar{g}_{\delta n} + l_n \bar{f}_{\delta n} + \bar{u}_{Fn} \bar{G}_{\delta n} + \bar{u}_{Mn} \bar{G}_{\delta n}' \quad [24]$$

$$\bar{g}_{n+1} = \bar{g}_n + l_n \bar{f}_n + \bar{u}_{Fn} \bar{G}_n + \bar{u}_{Mn} \bar{G}_n' \quad [25]$$

The boundary conditions at the free end now require that $\bar{\alpha}_1 = \bar{\varphi}$, $\bar{y}_1 = \bar{\delta}$, $S_1 = m_1 \omega^2 \bar{\delta} + F_1$, and $M_1 = 0$; which gives

$$\bar{f}_{\varphi 1} = 1 \qquad \bar{f}_{\delta 1} = 0 \qquad \bar{f}_1 = 0 \quad [26]$$

$$\bar{g}_{\varphi 1} = 0 \qquad \bar{g}_{\delta 1} = 1 \qquad \bar{g}_1 = 0 \quad [27]$$

$$\bar{G}_{\varphi 1} = 0 \qquad \bar{G}_{\delta 1} = m_1 \omega^2 \qquad \bar{G}_1 = F_1 \quad [28]$$

$$\bar{G}_{\varphi 1}' = 0 \qquad \bar{G}_{\delta 1}' = 0 \qquad \bar{G}_1' = 0 \quad [29]$$

It is now possible to proceed from the free end of the beam to the base, and by satisfying the boundary conditions at the base, the values of $\bar{\varphi}$ and $\bar{\delta}$ can be obtained. The shearing forces, bending moments, slopes, and deflections may then be obtained from Equations [10] to [13].

Free-Free-Beam

In this case the base of the beam is completely free and the boundary conditions become $S_b = M_b = 0$. Equations [10] and [11] then give

$$\bar{G}_{\varphi b} \bar{\varphi} - \bar{G}_{\delta b} \bar{\delta} = \bar{G}_b \quad [30]$$

$$\bar{G}_{\varphi b}' \bar{\varphi} - \bar{G}_{\delta b}' \bar{\delta} = \bar{G}_b' \quad [31]$$

from which are found

$$\bar{\varphi} = \frac{\bar{G}_b' \bar{G}_{\delta b} - \bar{G}_b \bar{G}_{\delta b}'}{\bar{G}_{\varphi b}' \bar{G}_{\delta b} - \bar{G}_{\varphi b} \bar{G}_{\delta b}'} \quad [32]$$

$$\bar{\delta} = \frac{\bar{G}_{\varphi b} \bar{G}_b' - \bar{G}_{\varphi b}' \bar{G}_b}{\bar{G}_{\varphi b}' \bar{G}_{\delta b} - \bar{G}_{\varphi b} \bar{G}_{\delta b}'} \quad [33]$$

Cantilever Beam

In this case the base of the beam is clamped and the boundary conditions become $\bar{\alpha}_b = \bar{y}_b = 0$. Equations [12] and [13] then give

$$\bar{f}_{\varphi b} \bar{\varphi} - \bar{f}_{\delta b} \bar{\delta} = \bar{f}_b \quad [34]$$

$$\bar{g}_{\varphi b} \bar{\varphi} - \bar{g}_{\delta b} \bar{\delta} = \bar{g}_b \quad [35]$$

from which are found

$$\bar{\varphi} = \frac{\bar{g}_b \bar{f}_{\delta b} - \bar{f}_b \bar{g}_{\delta b}}{\bar{g}_{\varphi b} \bar{f}_{\delta b} - \bar{f}_{\varphi b} \bar{g}_{\delta b}} \quad [36]$$

$$\bar{\delta} = \frac{\bar{f}_{\varphi b} \bar{g}_b - \bar{g}_{\varphi b} \bar{f}_b}{\bar{g}_{\varphi b} \bar{f}_{\delta b} - \bar{f}_{\varphi b} \bar{g}_{\delta b}} \quad [37]$$

Simply Supported Beam

For a simply supported beam it is merely necessary to replace Equations [10] to [13] by the following

$$S_n = \bar{G}_{\varphi n} \bar{\varphi} - \bar{G}_{Rn} R_a + \bar{G}_n \quad [38]$$

$$M_n = -\bar{G}_{\varphi n}' \bar{\varphi} + \bar{G}_{Rn}' R_a - \bar{G}_n' \quad [39]$$

$$\bar{\alpha}_n = -\bar{f}_{\varphi n} \bar{\varphi} + \bar{f}_{Rn} R_a - \bar{f}_n \quad [40]$$

$$\bar{y}_n = \bar{g}_{\varphi n} \bar{\varphi} - \bar{g}_{Rn} R_a + \bar{g}_n \quad [41]$$

Substituting these equations in Equations [4] to [7a] and equating like terms gives a system of equations identical with Equations [14] to [25], except that the subscript δ is replaced by the subscript R. The boundary conditions at the right end now become

$$\bar{G}_{\varphi 1} = 0 \qquad \bar{G}_{R1} = 1 \qquad \bar{G}_1 = 0 \quad [42]$$

$$\bar{G}_{\varphi 1}' = 0 \qquad \bar{G}_{R1}' = 0 \qquad \bar{G}_1' = -M_a \quad [43]$$

$$\bar{f}_{\varphi 1} = 1 \qquad \bar{f}_{R1} = 0 \qquad \bar{f}_1 = 0 \quad [44]$$

$$\bar{g}_{\varphi 1} = 0 \qquad \bar{g}_{R1} = 0 \qquad \bar{g}_1 = 0 \quad [45]$$

in which it has been assumed that $S_1 = -R_a$, $M_1 = M_a$ (where M_a may be due to an overhang but is usually zero), $\bar{\alpha}_1 = -\bar{\varphi}$, and $\bar{y}_1 = 0$

At the left end of the beam, which is now the base, the boundary conditions are $\bar{y}_b = M_b = 0$, and Equations [41] and [39] then give

$$-\bar{g}_{\varphi b} \bar{\varphi} + \bar{g}_{Rb} R_a = \bar{g}_b \quad [46]$$

$$-\bar{G}_{\varphi b}'\,\bar{\varphi} + \bar{G}_{Rb}'\,R_a = \bar{G}_b' \qquad [47]$$

From these two simultaneous equations in $\bar{\varphi}$ and R_a are obtained

$$\bar{\varphi} = \frac{\bar{g}_b\,\bar{G}_{Rb}' - \bar{G}_b'\,\bar{g}_{Rb}}{\bar{G}_{\varphi b}'\,\bar{g}_{Rb} - \bar{g}_{\varphi b}\,\bar{G}_{Rb}'} \qquad [48]$$

$$R_a = \frac{\bar{G}_{\varphi b}'\,\bar{g}_b - \bar{g}_{\varphi b}\,\bar{G}_b'}{\bar{G}_{\varphi b}'\,\bar{g}_{Rb} - \bar{g}_{\varphi b}\,\bar{G}_{Rb}'} \qquad [49]$$

Examples

1 As an example of a free-free beam consider a three-cylinder reciprocating engine resting on flexible supports. The mass is all concentrated at the centers of the cylinders and the crank angle is 120 deg, so that the primary reciprocating inertia force at cylinder 2 is 120 deg behind cylinder 1 and cylinder 3 is 240 deg behind cylinder 1. The amplitude of the exciting force is $F_1 = 1000$ lb at $\omega = 100$ radians per sec which gives $F_2 = 1000\,e^{-2\pi i/3} = 1000\,(\cos 120 - i \sin 120) = -500 - 866i$, and $F_3 = 1000\,(\cos 240 - i \sin 240) = -500 + 866\,i$. The three concentrated masses are calculated to be $m_1 = 2$ lb-sec^2/in., $m_2 = 1.5$ lb-sec^2/in., and $m_3 = 3$ lb-sec^2/in., and the cast-iron frame of the engine may be considered equivalent to a uniform beam of $I = 10$ in.^{4} and $E = 15 \times 10^6$ psi. With a cylinder spacing of $l = 10$ in. this gives $v_M = (10/150) \times 10^{-6} = 0.00667 \times 10^{-6}$ lb^{-1} in.$^{-1}$, $v_F = v_M = (100/300) \times 10^{-6} = 0.3333 \times 10^{-6}$ lb^{-1}, and $u_F = (1000/900) \times 10^{-6} = 1.111 \times 10^{-6}$ in./lb. The damping in the structure is equivalent to a complex damping factor of $2b = 0.30$, giving $\cos 2b = 0.955$ and $\sin 2b = 0.2956$. The complex elastic coefficients become

$$\bar{u}_F \times 10^6 = \begin{cases} 1.011 \\ -0.3284 \end{cases} \qquad \bar{u}_M \times 10^6 = \begin{cases} 0.3183 \\ -0.09852 \end{cases}$$

$$\bar{v}_F \times 10^6 = \begin{cases} 0.3183 \\ -0.09852 \end{cases} \qquad \bar{v}_M \times 10^6 = \begin{cases} 0.06367 \\ -0.01971 \end{cases}$$

With these values for the fundamental quantities columns 1 to 14 of Table 1 are completed. Equations [32] and [33] then give

$$\bar{\varphi} = \begin{cases} -0.00295740 \\ 0.00189416 \end{cases} \qquad \bar{\delta} = \begin{cases} -0.0354599 \\ 0.0208169 \end{cases}$$

This means that at the front end of the engine the maximum deflection is $\delta = |\bar{\delta}| = 0.0411$ in. and the maximum slope is $\varphi = |\bar{\varphi}| = 0.00351$ radians $= 0.201$ deg. In column 15 the bending moments are worked out, and the fact that it is zero at station b is a check on the values for $\bar{\varphi}$ and $\bar{\delta}$. The maximum bending moment is $M_2 = |M_2| = 5070$ in-lb. If the engine is bolted to a rigid foundation the vibrating motion of the engine and foundation together, considered as a free body, can easily be found by merely equating the elastic coefficients to zero and adding the mass of the foundation to that of the engine.

2 A 2-in-diam steel shaft carries four disks as shown in Fig. 3.

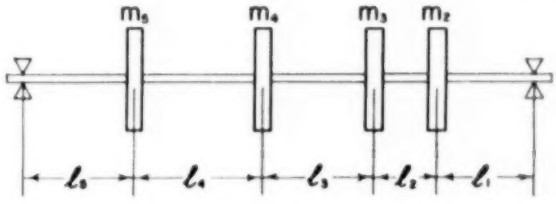

Fig. 3

The disks have slight eccentricities that all lie in the same plane but not necessarily to the same side of the axis of the shaft. The shaft rotates with an angular velocity $\omega = 316.228$ radians per sec, giving $\omega^2 = 100{,}000$, and all the fundamental data for the system are given in Table 2. The exciting forces are the inertia forces $m\omega^2\rho \cos \omega t$, where ρ is the eccentricity which may be either positive or negative, and it is desired to find the deflection curve for the shaft during rotation.

Solution: Since the deflections during rotation are identical to the amplitude of lateral vibration with exciting forces given by $m\omega^2\rho \cos \omega t$, where ω is the angular velocity of rotation, the method of this section may be used. In Table 3 the amplitudes coefficients are worked out, and Equations [48] and [49] then give

$$\varphi = 0.00134303 \text{ and } R_a = 145.760 \text{ lb}$$

TABLE 1

	1	2	3	4	5
	$m\omega^2$	$\bar{g}_\varphi = (2) + I\,(3)$	$\bar{f}_\varphi = (3) + v_M\,(4)$	$\bar{G}_\varphi' \times 10^{-6} = (4)$	$\bar{G}_\varphi \times 10^{-6} = (5)_{n-1}$
n	10^6	$+ \bar{u}_M\,(4) + \bar{u}_F(5)$	$+ v_F\,(5)$	$+ I\,(5)$	$+ (1)\,(2)$
		for $n = 1$	for $n = 1$	for $n = 1$	
1	0.02	0	1	0	0
	0	0	0	0	0
2	0.015	10	1	0	0.15
	0	0	0	0	0
3	0.03	20.1592	1.04775	1.5	0.754776
	0	−0.04927	−0.01478	0	−0.001478

	15	6	7	8	9
	$M \times 10^{-6}$	$\bar{g}_\delta = (6) + I\,(7)$	$\bar{f}_\delta = (7) + v_M(8)$	$\bar{G}_\delta' \times 10^{-6} = (8)$	$\bar{G}_\delta \times 10^{-6} = (9)_{n-1}$
n	$= \varphi\,(4)$	$+ \bar{u}_M(8) + u_F\,(9)$	$+ v_F\,(9)$	$+I\,(9)$	$+ (1)\,(6)$
	$- \delta\,(8)$	for $n = 1$	for $n = 1$	for $n = 1$	
	$-(13)$				
1	0	1	0	0	0.02
	0	0	0	0	0
2	−0.00290802	1.02122	0.006366	0.2	0.0353183
	−0.00416338	−0.006568	−0.001970	0	0.00009852
3	0	1.18000	0.030352	0.553183	0.0708983
	0	−0.057681	−0.009424	−0.0009852	−0.0018295

	10	11	12	13	14
	E	$g = (11) + I\,(12)$	$f = (12)$	$G' \times 10^{-6} = (13)$	$G \times 10^{-6} = (14)_{n-1}$
n	10^6	$+ u_M\,(13) + u_F\,(14)$	$+ v_M\,(13)$	$+ I\,(14)$	$+ (10)\cdot(n-1)\,(11)$
			$+ v_F\,(14)$		
		for $n = 1$	for $n = 1$	for $n = 1$	
1	0.001	0	0	0	0.001
	0	0	0	0	0
2	−0.0005	0.00106111	0.0003183	0.01	0.00051592
	−0.000866	−0.0003284	−0.00009852	0	0.000870926
3	−0.0005	0.00768916	0.0010334	0.0151592	0.0024659
	0.000866	−0.0033925	−0.0006236	0.0087926	0.00010670

TABLE 2

n	m	l	$u_M \times 10^4$	$u_F \times 10^4$	$v_M \times 10^4$	$v_F \times 10^4$	$F \times 10^{-4}$
1	0	25	0.2720	1.105	0.01062	0.1330	0
2	0.25	15	0.04775	0.238	0.00637	0.0478	0.01
3	0.4	20	0.08480	0.589	0.00850	0.0852	−0.05
4	0.35	10	0.0212	0.0711	0.00425	0.0213	0.03
5	0.3	30	0.19130	1.9060	0.01275	0.1912	0.02
6	0						0

TABLE 3

	1	2	3	4	5
	$m\omega^2 \times 10^{-4}$	$g_\varphi = (2) + l\,(3) + u_M\,(4) + u_F\,(5)$ for $n-1$	$f_\varphi = (3) + v_M\,(4) + v_F\,(5)$ for $n-1$	$G_\varphi' \times 10^{-4} = (4) + l\,(5)$ for $n-1$	$G_\varphi \times 10^{-4} = (5)_{n-1} + (1)\,(2)$
n					
1	0	0	1	0	0
2	2.5	25	1	0	62.5
3	4.0	54.875	3.9875	937.5	282.0
4	3.5	374.582	35.9826	6577.5	1593.04
5	3	987.116	97.8687	22507.9	4554.39
6	0	16909.5	1255.64	159139.6	4554.39

	15	6	7	8	9
	$y = \varphi\,(2) - Ra \times 10^{-4}\,(6) + (11)$	$g_R = (6) + l\,(7) + u_M\,(8) + u_F\,(9)$ for $n-1$	$f_R = (7) + v_M\,(8) + v_F\,(9)$ for $n-1$	$G_R' \times 10^{-4} = (8) + l\,(9)$ for $n-1$	$G_R \times 10^{-4} = (9)_{n-1} + (1)\,(6)$
n					
1	0	0	0	0	1
2	0.01747	1.1050	0.1330	25	3.7625
3	0.00044	5.1892	0.4721	81.4375	24.5194
4	−0.00689	35.4886	3.2534	571.8255	148.73
5	−0.00568	90.7200	8.8516	2059.13	420.890
6	0	1552.38	115.579	14685.8	420.890

	10	11	12	13	14
	$F \times 10^{-4}$	$\eta = (11) + l\,(12) + u_M\,(13) + u_F\,(14)$ for $n-1$	$f = (12) + v_M\,(13) + v_F\,(14)$ for $n-1$	$G' \times 10^{-4} = (13) + l\,(14)$ for $n-1$	$G \times 10^{-4} = (14)_{n-1} + (10) + (1)\,(11)$
n					
1	0	0	0	0	0
2	0.01	0	0	0	0.01
3	−0.05	0.00283	0.000478	0.15	0.03048
4	0.03	0.0073168	−0.000843896	−0.4596	0.0251288
5	0.02	−0.00907910	−0.00226196	−0.208312	0.0178915
6	0	−0.0826867	−0.00149708	0.328433	0.0178915

With these values the deflections are worked out in column 15 of Table 3 and there appears to be a node very close to station 3.

It is interesting to compare the deflections y with the corresponding values of the eccentricity ρ, which values are easily found to be $\rho_2 = 0.004$ in., $\rho_3 = -0.0125$ in., $\rho_4 = 0.00857$ in., and $\rho_5 = 0.00667$ in. The centers of gravity of the disks then move in circles with radii $\rho_2 + y_2 = 0.02147$ in., $\rho_3 + y_3 = -0.01206$ in., $\rho_4 + y_4 = 0.00168$ in., and $\rho_5 + y_5 = 0.00099$ in., where a negative radius merely means a phase shift of 180 deg. If the stationary shaft were loaded with the static forces $m\omega^2(\rho + y)$ the deflection curve should be identical to that obtained in column 15 of Table 3, which fact may be used as a check on the calculations.

In the present example all the exciting forces were in phase and damping was neglected. If the eccentricities of the disks had been in different directions it would be necessary to use complex amplitudes and the deflections would then be out of phase with each other, just as in Example 1.

On Asymmetric Flow in an Axial-Flow Compressor Stage

By W. R. SEARS,[1] ITHACA, N. Y.

It is suggested that flow patterns without axial symmetry may occur when an axial-compressor stage operates in a steady, uniform stream, provided that the blade airfoil characteristics exhibit certain peculiarities. For example, blades acting close to the stall may show nonlinearity, hysteresis, and/or time lags, and these may cause asymmetric flow patterns. Conditions necessary for existence of such phenomena are analyzed by consideration of an annulus of infinitely many blades and very large radius. It is shown that rotational-flow effects due to vortex shedding by the blades must be considered. The induced velocities resulting from asymmetrical loadings are calculated. The final step of the calculation is to show that these induced effects may actually support the circulation distribution that produces them. This step is only partly taken in the present paper. It is shown that time lag in the development of lift of a blade may produce such "eigen-solutions." Detailed study of the results of nonlinearity in the blade characteristics is left for another investigation.

Nomenclature

The following nomenclature is used in the paper:

B = number of blades in rotor
c = blade chord
$c_l(\varphi)$ = lift coefficient as function of φ
D = a dimension defined in Fig. 3
g = amplitude of sinusoidal circulation: $\gamma(y) = gU \cos \lambda y$
g_n = Fourier coefficient of circulation distribution
k = $\omega \bar{r}/U$
K = constant in Equation [49], et seq.
m = constant lift-curve slope $dc_l/d\varphi$
n = index of summation
p = static pressure
$p_{-\infty}, p_{+\infty}$ = values of p at $x = -\infty$ and $x = +\infty$, respectively
P = principal value (of improper integral)
$\bar{r}$ = mean radius of blade row
t = time
u = perturbation velocity component in x-direction, $u(x, y)$
$u_0(y)$ = $u(0, y)$
U = free-stream velocity in x-direction
v = perturbation velocity component in y-direction, $v(x, y)$
$v_-(y), v_+(y)$ = $v(-0, y), v(+0, y)$
v_∞ = $v(+\infty, y)$ (a constant)
$\bar{v}(y)$ = $[v_-(y) + v_+(y)]/2$
x = co-ordinate in axial direction
y = co-ordinate in tangential direction
α = angle of inclination of stream to axis at $x = -\infty$ (Fig. 1)
β = blade angle, measured from axis (Fig. 5)
$\gamma(y)$ = circulation distribution (+ clockwise)
γ_1 = constant part of circulation distribution
Γ = circulation about a blade
Δ = phase-lag angle in case of airfoil with lagging circulation
δt = time interval (Fig. 4)
δy = increment of y (Fig. 4)
ϵ = shed circulation strength (per unit length of wake) (+ clockwise)
η = variable of integration
λ = constant defining wave length of sinusoidal circulation distribution
ν = frequency of oscillation of wing (Equation [51])
ρ = air density
φ = angle of incidence
φ_{const} = constant part of φ, corresponding to γ_1
ψ = stream function
ω = rate of rotation of rotor relative to co-ordinate system
Ω = vorticity (+ counterclockwise)

Superscripts:

(1) = irrotational part of flow
(2) = rotational part of flow

Introduction

There is experimental evidence that axial-flow compressor stages may produce asymmetrical flow patterns when they are operated near the stall. For example, stalled "areas" are said to occur, which cover only part of the rotor circumference and which rotate about the axis in either the direction of rotation or opposite to it at rates much slower than the rate of rotor rotation. This suggests a study of the possibilities of asymmetric-flow situations in a symmetrical rotor placed in a duct carrying a flow that is uniform far ahead.

There is some parallel to this study in the realm of wing theory. In a previous paper[2] the author pointed out the existence of eigen-solutions of the Prandtl wing equations in the case of reversed lift-curve slope, and these included a family of antisymmetrical lift distributions on symmetrical wings at no incidence. Following a related suggestion by Prof. von Kármán, R. S. Schairer[3] investigated the possibilities of asymmetrical lift loadings on symmetrical wings with nonlinear (partly stalled) airfoil

[1] Director, Graduate School of Aeronautical Engineering, Cornell University.

Contributed by the Applied Mechanics Division and presented at the Fall Meeting, Chicago, Ill., September 8–11, 1952, of The American Society of Mechanical Engineers.

Discussion of this paper should be addressed to the Secretary, ASME, 29 West 39th Street, New York, N. Y., and will be accepted until April 10, 1953, for publication at a later date. Discussion received after the closing date will be returned.

Note: Statements and opinions advanced in papers are to be understood as individual expressions of their authors and not those of the Society. Manuscript received by ASME Applied Mechanics Division, March 20, 1952. Paper No. 52—F-15.

[2] "A New Treatment of the Lifting-Line Wing Theory, With Applications to Rigid and Elastic Wings," by W. R. Sears *Quarterly of Applied Mathematics*, vol. 6, 1948, pp. 240–255.

[3] "Unsymmetrical Lift Distributions on a Stalled Monoplane Wing," by R. S. Schairer, thesis California Institute of Technology, Pasadena, Calif., 1939.

characteristics. He found that such solutions do occur. In both of these cases the asymmetrical lift distribution is supported by the induced velocities produced by this lift distribution; the peculiarities of the section characteristics make this possible.

The first step in the present investigation is the determination of the induced-velocity field due to an arbitrary, asymmetric circulation distribution. To simplify this analysis, the annulus of blades will be replaced here by an annulus of infinitely many blades of very small chord, i.e., an "actuator annulus," and also the annulus radii will be assumed to be infinite, i.e., the plane-flow problem of an "actuator strip" will be treated instead of the annulus. For annuli of many blades and large radii, the results should be directly applicable; in other cases they will have only qualitative value. This limitation should not be disturbing, since the main purpose of the study is qualitative, being an exploration of the possibilities of asymmetrical solutions rather than an accurate study of their properties. Compressibility of the air is neglected throughout.

Analysis of Problem

The Idealized Actuator Disk. The plane-flow problem is sketched in Fig. 1. Here $\gamma(y)$ denotes the circulation distribution in the rotor disk. To relate this idealized setup to a real annulus of B blades, Fig. 2, whose circulation is $\Gamma(y)$, one would write

$$\gamma(y) = \frac{B\Gamma(y)}{2\pi r}$$

where r denotes the mean radius of the annulus.

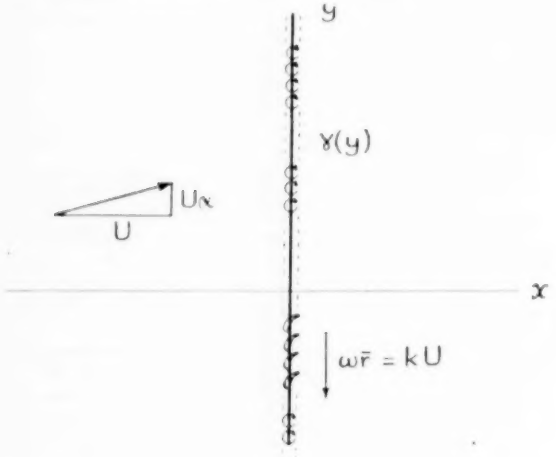

Fig. 1

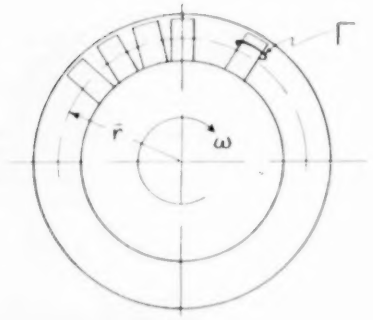

Fig. 2

The assumption that $\gamma = \gamma(y)$ does not imply that the flow pattern is actually steady with respect to fixed co-ordinates, but only that it is steady with respect to some rotating co-ordinate system. It is presumed, moreover, that this co-ordinate system rotates at a rate different from the rotor speed; in fact, it will be assumed that the speed of rotation of the co-ordinate system is small, and that the incidence of the stream vector is small,[4] namely, $\alpha << 1$. Let the angular velocity of the rotor relative to the co-ordinates be ω. Then, in Fig. 1, the blade row is moving downward with speed ωr, which is equal to kU, say. It is not assumed that k is small.

The blade row, which has now been replaced by a vortex sheet along the y-axis, produces flow perturbations u and v, upon which the following boundary conditions may be imposed

$$\text{At } x = -\infty: \quad u = 0, v = U\alpha \qquad [1]$$

$$\text{At } x = 0: \quad v(-0, y) - v(+0, y) = \gamma(y) \qquad [2]$$

$$u(-0, y) = u(+0, y) = u_0(y), \text{ say} \qquad [3]$$

Conditions far downstream will be considered farther below; at present it is only required that the pressure be uniform there

$$\text{At } x = +\infty: \quad p = \text{const} = p_{+\infty} \qquad [4]$$

Vortex Shedding. The individual blades of the rotor, since they move relative to the fixed circulation distribution, are in the condition of unsteady flow. Thus, in accordance with the theory of airfoils in such flows, they shed wakes of vortexes at their trailing edges. Furthermore, according to the approximations of "lightly loaded airfoil" theory, which assumes that all induced velocities are small compared to the stream speed U, these wake vortexes move with the free-stream vector velocity, or approximately at speed U in the x-direction.

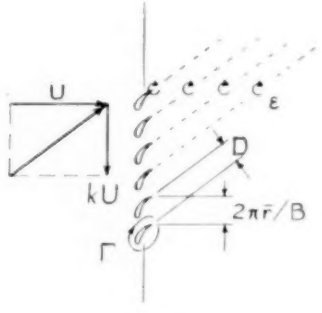

Fig. 3

Let us study this situation with the aid of Fig. 3. Returning, for a moment, to a finite number of discrete blades, we note that for one of them

$$\frac{d\Gamma}{dt} = -kU\frac{d\Gamma}{dy}$$

so that the wake-vortex strength ϵ shed by such a blade is given by[5]

[4] The consequences of large α have been investigated; it has been concluded that this refinement does not change the qualitative results of the present investigation.

[5] "Airfoil Theory for Non-Uniform Motion," by Theodore von Kármán and W. R. Sears, *Journal of Aeronautical Sciences*, vol. 5, 1938, pp. 379–390.

$$\epsilon = \frac{-1}{U\sqrt{1+k^2}}\frac{d\Gamma}{dt} = \frac{-k}{\sqrt{1+k^2}}\frac{d_4}{dy}$$

Moreover, ϵ is dependent upon y only.

Now let us pass over to an infinite number of blades. The result is that the space downstream of the disk is densely filled with infinitesimal vortexes (vorticity) whose distribution is given (see Fig. 3).

$$\Omega = \Omega(y) = -\frac{\epsilon}{D} = -\frac{\epsilon B}{2\pi r}\sqrt{1+k^2}$$

$$= k\frac{B}{2\pi r}\frac{d\Gamma}{dy} = -k\gamma'(y) \qquad [5]$$

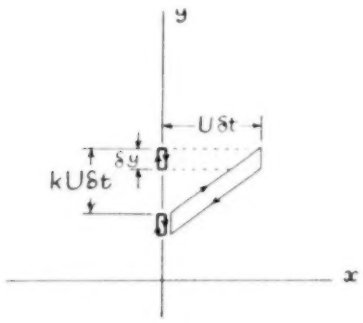

FIG. 4

(This result could have been derived by considering the conservation of total circulation for an element of the disk, Fig. 4, together with its wake, viz.

$$\gamma\,\delta y = (\gamma + kU\,\delta t\,\gamma')\delta y - \Omega\,\delta y\,U\,\delta t$$

which immediately gives Equation [5].)

The conclusion of this paragraph is that the small-perturbation flow problem stated previously is a rotational one behind the disk, whereas it is clearly an irrotational one upstream. The vorticity distribution is, fortunately, a simple one, and is related to the circulation distribution $\gamma(y)$.

Boundary-Value Problem. The mathematical problem to be solved in order to calculate the induced velocities is, therefore, the following, in terms of the plane stream function $\psi(x, y)$

For $x < 0$

$$\nabla^2\psi = 0 \qquad [6]$$

$$\left.\begin{aligned} u &= \psi_y = 0 \\ v &= -\psi_x = U\alpha \end{aligned}\right\} \text{ at } x = -\infty \qquad [7]$$

For $x > 0$

$$\nabla^2\psi = -\Omega(y) = k\gamma'(y). \qquad [8]$$

At $x = 0$

$$v(-0, y) - v(+0, y) = \gamma(y) \qquad [9]$$

$$u(-0, y) = u(+0, y) = u_0(y). \qquad [10]$$

The boundary condition at $x = +\infty$ can now be established. Bernoulli's equation holds upstream of the disk, while in the rotational flow region downstream it applies only along streamlines, which are approximately lines of constant y. The increase of Bernoulli constant at the disk is equal to the pressure jump across the disk, which is in turn equal to the load on the disk, viz., $\rho kU\gamma(y)$.

To be more exact, the load on the disk might be calculated on the basis of unsteady lift theory, in which it is found to be given by a somewhat more complicated expression (see, for example, reference 5). The additional terms, however, are proportional to the blade chord, and are therefore neglected here in consequence of the actuator-disk approximation. This means that the blade chords are small compared to the wave lengths over which $\gamma(y)$ varies, so that the blades themselves can be considered as in quasi-steady motion, even though their wake vortexes have to be considered in the theory. The approximation $\rho kU\gamma(y)$ will therefore be adopted for the pressure rise.

Thus, writing p for the static pressure, and in particular $p_{-\infty}$ for its value far upstream, one has, in the small perturbation approximation.

For $x < 0$

$$p_{-\infty} = p + \rho Uu = \text{const.} \qquad [11]$$

For $x > 0$

$$p + \rho Uu = p_{-\infty} + \rho kU\gamma(y)$$

and at $x = +\infty$, where $p = p_{+\infty} = \text{const}$

$$p_{+\infty} + \rho Uu(\infty, y) = p_{-\infty} + \rho kU\gamma(y)$$

or

$$u(\infty, y) = \frac{p_{-\infty} - p_{+\infty}}{\rho U} + k\gamma(y). \qquad [12]$$

Equation [12] implies that $\partial u/\partial x = 0$ at $x = +\infty$. Hence, from continuity

$$\frac{\partial v}{\partial y} = 0 \text{ at } x = +\infty$$

or

$$v(\infty, y) = \text{const} = v_\infty, \text{ say} \qquad [13]$$

Uniform-Turning Solution. Note that certain constants in the boundary-value problem of the preceding section represent simply a uniform turning angle through the disk

$$\left.\begin{aligned} v &= -\psi_x = U\alpha \text{ for all } x < 0 \\ &= v_\infty \text{ for all } x > 0 \\ \gamma &= U\alpha - v_\infty = \gamma_0, \text{ say} \\ \frac{p_{+\infty} - p_{-\infty}}{\rho U} &= k\gamma_0; \text{ thus, from Equation [12]} \\ u(\infty, y) &= 0; \text{ in fact, } u = \psi_y = 0 \text{ everywhere} \end{aligned}\right\} \qquad [14]$$

Consequently, our work may be simplified by considering only the variable part of $\gamma(y)$, i.e., the part whose average value is zero. For this variable part the correct boundary conditions are simply:

At $x = -\infty$

$$\psi_x = \psi_y = 0 \qquad [15]$$

At $x = +\infty$

$$\left.\begin{aligned} u &= \psi_y = k\gamma(y) \\ v &= -\psi_x = 0 \end{aligned}\right\} \qquad [16]$$

The uniform solution given by Equations [14] can be superimposed after the calculation has been made.

Rotational and Irrotational Parts. This mathematical problem is now attacked by the familiar device of dividing $\psi(x, y)$ into an irrotational part $\psi^{(1)}$ and a rotational part $\psi^{(2)}$. Thus $\psi^{(1)}$ is identical with ψ for $x < 0$, while for $x > 0$, from Equation [8]

$$\nabla^2\psi^{(2)} = k\,\gamma'(y) \quad [17]$$

The most convenient solution of Equation [17] is the particular integral

$$\psi^{(2)} = k \int\int \gamma'(y)\,dy\,dy = k \int \gamma(y)\,dy \quad [18]$$

This is our choice for $\psi^{(2)}$ for $x > 0$. The corresponding velocity components are

$$u^{(2)} = \psi_y{}^{(2)} = k\,\gamma(y) \text{ for } x > 0 \quad [19]$$

$$v^{(2)} = -\psi_x{}^{(2)} = 0 \quad [20]$$

This leaves a relatively simple potential problem for $\psi^{(1)}$, viz., from Equations [15] and [16]

$$\left.\begin{aligned} \nabla^2\psi^{(1)} &= 0 \\ u^{(1)} = v^{(1)} &= 0 \text{ at } x = \pm\infty \end{aligned}\right\} \quad [21]$$

while, from Equation [10]

$$\left.\begin{aligned} u^{(1)}(-0, y) &= u_0(y) \\ u^{(1)}(+0, y) &= u_0(y) - k\gamma(y) \end{aligned}\right\} \quad [22]$$

and

$$v^{(1)}(-0, y) - v^{(1)}(+0, y) = \gamma(y) \quad [23]$$

Solution of Boundary-Value Problem. The relationships between $u^{(1)}(-0, y)$ and $v^{(1)}(-0, y)$, and similarly between $u^{(1)}(+0, y)$ and $v^{(1)}(+0, y)$, can be written down immediately. To shorten the writing, let $v_-(y)$ and $v_+(y)$ denote $v^{(1)}(-0, y)$ and $v^{(1)}(+0, y)$. Also note that $u^{(1)}(-0, y)$ is equal to $u_0(y)$. First, the problem for $x < 0$ may be solved by distributing vortexes of strength $2\,v_-(y)$ along the y-axis; the resulting velocity $u_0(y)$ is given by

$$u_0(y) = \frac{1}{\pi} P \int_{-\infty}^{\infty} \frac{v_-(\eta)\,d\eta}{y - \eta} \quad [24]$$

Alternatively, the same problem might have been solved by a distribution of sinks $2u_0(y)$ along the axis; the vertical component would then be

$$v_-(y) = -\frac{1}{\pi} P \int_{-\infty}^{\infty} \frac{u_0(\eta)\,d\eta}{y - \eta} \quad [25]$$

In either case, of course, the flow in the half-plane $x > 0$ would be ignored.

To solve the actual problem for $x > 0$, one considers a distribution of sources of strength $2u^{(1)}(+0, y)$ along the y-axis, noting that, according to Equations [22] and [23], this strength is equal to $2u_0(y) - 2k[v_-(y) - v_+(y)]$. Thus

$$v_+(y) = \frac{1}{\pi} P \int_{-\infty}^{\infty} \frac{u_0(\eta)\,d\eta}{y - \eta} - \frac{k}{\pi} P \int_{-\infty}^{\infty} \frac{v_-(\eta)\,d\eta}{y - \eta} + \frac{k}{\pi} P \int_{-\infty}^{\infty} \frac{v_+(\eta)\,d\eta}{y - \eta} \quad [26]$$

$$= -v_-(y) - ku_0(y) + \frac{k}{\pi} P \int_{-\infty}^{\infty} \frac{v_+(\eta)\,d\eta}{y - \eta} \quad [27]$$

But Equation [27] can be inverted, just as Equation [24] was inverted in Equation [25]

$$kv_+(y) = -\frac{1}{\pi} P \int_{-\infty}^{\infty} \frac{v_+(\eta) + v_-(\eta) + ku_0(\eta)}{y - \eta}\,d\eta \quad [28]$$

$$= -\frac{1}{\pi} P \int_{-\infty}^{\infty} \frac{v_+(\eta)\,d\eta}{y - \eta} - u_0(y) + kv_-(y) \quad [29]$$

Eliminating

$$\frac{1}{\pi} P \int_{-\infty}^{\infty} \frac{v_+(\eta)\,d\eta}{y - \eta}$$

between Equations [27] and [29], one has

$$(1 + k^2)v_+(y) + (1 - k^2)v_-(y) = -2\,ku_0(y) \quad [30]$$

Therefore the circulation distribution is

$$\gamma(y) = v_-(y) - v_+(y)$$

$$= v_-(y) - \frac{-2ku_0(y) - (1 - k^2)\,v_-(y)}{1 + k^2}$$

$$= 2\,\frac{v_-(y) + ku_0(y)}{1 + k^2} \quad [31]$$

$$= \frac{2}{1 + k^2}\left\{ku_0(y) - \frac{1}{\pi} P \int_{-\infty}^{\infty} \frac{u_0(\eta)\,d\eta}{y - \eta}\right\} \quad [32]$$

Equation [32] relates the circulation distribution to the induced inflow component $u_0(y)$. All of the induced velocities at the disk are now known in terms of $u_0(y)$.

It may be more convenient, however, to treat $\gamma(y)$ as known and to calculate the other induced quantities in terms of it. Equation [29] leads to such a relation, for it can be written

$$kv_+(y) = -\frac{1}{\pi} P \int_{-\infty}^{\infty} \frac{v_-(\eta) - \gamma(\eta)}{y - \eta}\,d\eta - u_0(y) + kv_-(y) \quad [33]$$

By means of Equation [24], this becomes

$$kv_+(y) = -2u_0(y) + \frac{1}{\pi} P \int_{-\infty}^{\infty} \frac{\gamma(\eta)\,d\eta}{y - \eta} + kv_-(y)$$

or

$$2u_0(y) = k\gamma(y) + \frac{1}{\pi} P \int_{-\infty}^{\infty} \frac{\gamma(\eta)\,d\eta}{y - \eta} \quad [34]$$

$v_-(y)$ can also be expressed in terms of $\gamma(y)$, for $u_0(y)$ can be eliminated from Equation [34] by means of Equation [31]. The result is

$$\left.\begin{aligned} 2v_-(y) &= \gamma(y) - \frac{k}{\pi} P \int_{-\infty}^{\infty} \frac{\gamma(\eta)\,d\eta}{y - \eta} \\ \text{or} \\ v_-(y) + v_+(y) &= -\frac{k}{\pi} P \int_{-\infty}^{\infty} \frac{\gamma(\eta)\,d\eta}{y - \eta} \end{aligned}\right\} \quad [35]$$

Blade-Characteristic Relation. The desired relationships between the circulation distribution $\gamma(y)$ and the induced velocities at the disk have now been calculated successfully. To complete the problem, the auxiliary relation must be introduced which gives $\gamma(y)$ as a function of the angle of incidence of the blade; this relation involves the airfoil characteristics. Its form is, for a single blade

$$\Gamma = \frac{1}{2}\sqrt{1 + k^2}\,Vcc_l(\varphi) \quad [36]$$

where c is the blade chord and $c_l(\varphi)$ denotes the blade characteristic, i.e., the lift coefficient as function of the effective angle of attack φ.

Thus the distributed circulation $\gamma(y)$ for a cascade of many blades is

$$\gamma(y) = \frac{\Gamma}{2\pi r/B} = \frac{\sqrt{1+k^2}}{4\pi}\frac{Bc}{r} U\, c_l(\varphi) \quad [37]$$

The determination of φ in terms of the induced velocities is a matter of geometry, Fig. 5

$$\varphi = \tan^{-1}\left(\frac{kU + \alpha U + \bar{v}}{U + u_0}\right) - \beta \quad [38]$$

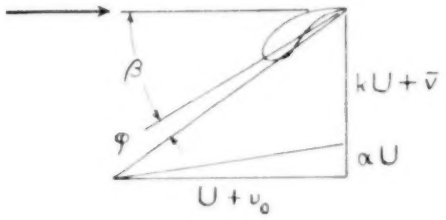

FIG. 5

This can be simplified by taking into account that u_0, $\bar{v}$, and αU are small compared to U; the result is

$$\varphi \approx \tan^{-1} k + \frac{1}{1+k^2}\left(\alpha + \frac{\bar{v} - ku_0}{U}\right) - \beta \quad [39]$$

Here $\bar{v}$ is the mean value of v_- and v_+, as is well known from cascade theory. Also, it is clear that part of φ in Equation [39] corresponds to the uniform flow components of Equations [14]; this part is

$$\varphi_{const} = \tan^{-1} k + \frac{\alpha}{1+k^2} - \beta \quad [40]$$

Hence

$$\gamma_1 = \frac{\sqrt{1+k^2}}{4\pi}\frac{Bc}{r} U\, c_l(\varphi_{const}) \quad [41]$$

The variable part of the flow field, which has been calculated in preceding sections, is therefore related to the induced velocities as follows

$$\gamma(y) = \frac{\sqrt{1+k^2}}{4\pi}\frac{Bc}{r} U\, c_l\left(\frac{v_- + v_+ - 2ku_0}{2U(1+k^2)}\right) \quad [42]$$

Combination of Equations [34], [35] and [42] would yield a homogeneous integral equation giving $\gamma(y)$ as a function of known quantities only; this is, in fact, the equation which must give a nontrivial solution if we are to find any asymmetrical flow patterns of the variety considered here. The equation involves the unspecified blade characteristic $c_l(\varphi)$, however, and there seems to be no particular value in writing it out here. Instead, we shall proceed to show how it may be simplified by assuming $\gamma(y)$ to be sinusoidal.

Example: Sinusoidal Circulation Distribution. Suppose $\gamma(y) = gU \cos \lambda y$. Then, according to Equations [35]

$$v_-(y) + v_+(y) = -\frac{k}{\pi} P \int_{-\infty}^{\infty} \frac{\gamma(\eta)\,d\eta}{y - \eta} = -kgU \sin \lambda y \quad [43]$$

and from Equations [34]

$$u_0(y) = \frac{1}{2} gU(k \cos \lambda y + \sin \lambda y) \quad [44]$$

The induced angle of incidence φ therefore becomes (refer to Equation [42])

$$\left.\begin{aligned}\varphi &= \frac{-gk\,(k \cos \lambda y + 2 \sin \lambda y)}{2\,(1+k^2)} \\ &= -\frac{gk\sqrt{4+k^2}}{2\,(1+k^2)} \cos\left[\lambda y - \tan^{-1}\left(\frac{2}{k}\right)\right]\end{aligned}\right\} \quad [45]$$

It is interesting to note that the induced effects do not depend on λ, except, of course, in their period. In other words, the induced velocities for any sinusoidal circulation distribution $gU \cos \lambda y$ are sinusoidal with the same period; their amplitude and phase depend on k, but their amplitude is independent of λ.

It might be valuable to consider the consequences of this in the case of an arbitrary $\gamma(y)$, which could be expanded in a Fourier series. Let

$$\gamma(y) = U \sum_1^{\infty} g_n \cos ny \quad [46]$$

Then

$$\varphi(y) = -\frac{k\sqrt{4+k^2}}{2\,(1+k^2)} \sum_1^{\infty} g_n \cos\left[ny - \tan^{-1}\left(\frac{2}{k}\right)\right] \quad [47]$$

It should be noted that, according to Equations [46] and [47], $\varphi(y)$ is not a function similar to $\gamma(y)$, shifted by the amount of a phase angle, as might seem the case at first glance.

Solutions for Special Blade Characteristics. Some simple assumptions regarding the blade characteristic $c_l(\varphi)$ will now be considered.

(*a*) *Linear, unstalled:* Suppose $c_l(\varphi) = m\varphi$, $(m > 0)$, as for a blade operating well away from the stall and in quasi-steady conditions. Equation [42] reads, for this case and for sinusoidal circulation

$$gU \cos \lambda y = \frac{\sqrt{1+k^2}}{4\pi}\frac{Bc}{r} Um \frac{-gk}{2(1+k^2)} (k \cos \lambda y + 2 \sin \lambda y) \quad [48]$$

or

$$\cos \lambda y = -K \cos\left[\lambda y - \tan^{-1}\left(\frac{2}{k}\right)\right] \quad [49]$$

where

$$K = \frac{m}{8\pi}\frac{Bc}{r}\sqrt{1+k^2}\, k$$

Equation [49] has no solution in the range of our interest. Thus the sinusoidal solutions do not occur in this case.

Moreover, the same conclusion is reached in the case of an arbitrary distribution $\gamma(y)$ as expressed in a Fourier series in Equation [46]. This is most easily seen if the complex-variable notation for sinusoidal functions is used, i.e., the circulation equation, Equation [42], takes on the following form (where real parts are implied)

$$\sum_1^{\infty} g_n e^{iny} = -K \sum_1^{\infty} g_n e^{iny - i(\tan^{-1} 2/k)} \quad [50]$$

Since the g_n are real, as well as the constant, Equation [50] does

not admit a nontrivial solution. Thus the asymmetric eigen-solutions contemplated here apparently do not occur in rotors with this simple type of linear blade characteristic.

(*b*) *Linear, stalled:* A change of sign of m in the case just considered makes $K < 0$, but does not produce solutions. This is in contrast to the Prandtl-wing problem,[2] where negative m results immediately in eigen-solutions. The difference lies in the presence of the phase shift in Equation [49].

(*c*) *Linear, with lag:* Actually, since the blades are in unsteady flow conditions, their circulation lags behind the angle of incidence by an amount depending on the ratio of the chord to the wave length of the pattern $\gamma(y)$; however, as has already been mentioned, the assumption of small chords leads consistently to neglect of such unsteady potential flow effects. On the other hand, it has been found that for airfoils operating near or above the stall, a good approximation to the lift, when $\varphi \sim e^{i\nu t}$, is obtained by introducing an empirically determined phase lag Δ, i.e.

$$\text{Lift} = (\text{potential-flow-lift}) \times e^{i\Delta} \sim e^{i(\nu t - \Delta)} \quad \ldots\ldots\ldots\ldots [51]$$

Mendelson[6] has determined the phase lag Δ from experiments on various airfoils, and has concluded that it depends on the lift coefficient and not, in the first approximation at least, on the frequency ν. The values of Δ reported reach the order of magnitude of 1 radian near the stall.

Therefore it may be permissible to postulate the same sort of lag in the development of circulation.

Instead of Equation [50], then, one has

$$\sum_1^\infty g_n e^{in\psi} = -K \sum_1^\infty g_n e^{in\psi - i\tan^{-1}(2/k) + i\Delta} \quad \ldots\ldots [52]$$

The possible solutions to Equation [52] are

$$K = -1, \qquad \Delta = \tan^{-1}\left(\frac{2}{k}\right) \quad \ldots\ldots\ldots\ldots [53]$$

and

$$K = +1, \ \Delta = \pi + \tan^{-1}\left(\frac{2}{k}\right) \quad \ldots\ldots\ldots [54]$$

where the arctan is always in the first quadrant.

We may conclude from Equations [53] and [54] that there are possibilities of asymmetrical sinusoidal solutions due to lift lag near the stall, with either positive or negative lift-curve slope m. However, the time-lag angle Δ required for such solutions seems improbably great for $m > 0$ (Equations [54]). Since k is likely to be $O(1)$, we might assume $\tan^{-1}(2/k) \approx 1$ radian; this means that Equations [54], where $m > 0$, requires Δ to be of the order of 4 radians. Equations [53], on the other hand, which applies to a stalled airfoil ($m < 0$), requires much smaller lag, namely, about 1 radian. As has already been mentioned, Mendelson found lift lags of this magnitude.

(*d*) *Nonlinear:* Surely the most interesting possibilities of these asymmetrical solutions lie in the realm of nonlinear blade characteristics. The author's colleagues are therefore proceeding, at the Graduate School of Aeronautical Engineering, to look for solutions of this type. In Fig. 6 are sketched some of the nonlinearities that are being studied. In each case the possibilities of lag and hysteresis must be considered with these characteristics; hysteresis is indicated by arrow heads in some of the curves of Fig. 6.

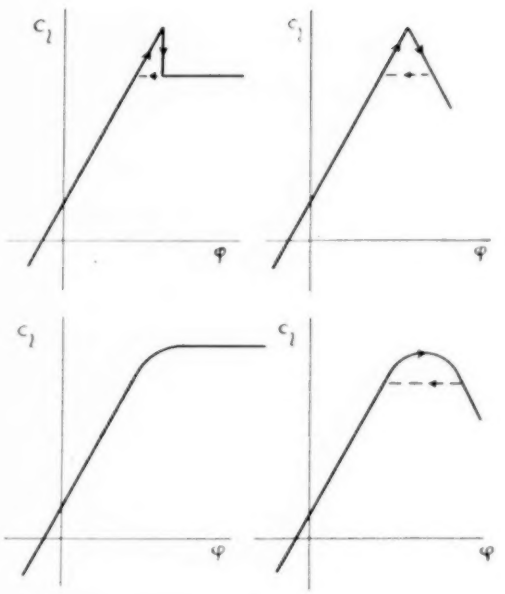

FIG. 6 SKETCHES OF TYPICAL BLADE CHARACTERISTICS

The results of this additional study must await a subsequent publication.

It also might be of interest to carry out certain refinements of the present theory. It already has been mentioned that the inclusion of large α—which may be interpreted either as large swirl in the incoming stream or large rate of rotation of the circulation pattern relative to fixed axes—does not seem to affect the results in an important way. Another refinement that might alter appreciably the quantitative conclusions is the consideration of potential-flow time lags, both in the determination of the pressure rise through the disk and in the relation between circulation and incidence. Since the lag required in case (*c*), to permit eigen-solutions, is much larger than potential-flow values,[4] it seems unlikely that this would change our conclusions profoundly; however, several authors have pointed out that this potential-flow lag does increase rapidly with increasing "reduced frequency" near zero, so that quasisteady theory is sometimes misleading in just this respect.

CONCLUSIONS

Asymmetrical flow patterns, either stationary or rotating at a rate different from the rotor speed, involve rotational flow downstream of the rotor disk.

A simplified analysis of this type of flow leads to relatively simple relations between the circumferential circulation distribution and the induced velocities at the disk. These have been evaluated in particular for sinusoidal distributions.

Brief consideration of the possibilities of asymmetrical eigen-solutions leads to the conclusion that they might be caused by time lag in the blade characteristic function $c_l(\varphi)$, especially beyond the stall.

The most interesting cases to be studied are those involving nonlinear $c_l(\varphi)$; these are under study at the present time, but no results are yet available.

[6] "Effect of Aerodynamic Hysteresis on Critical Flutter Speed at Stall," by Alexander Mendelson, NACA Research Memo. No. ESRO4, Washington, D. C., June 18, 1948.

Symmetric Turbulent Mixing of Two Parallel Streams[1]

By T. P. Torda,[2] W. O. Ackermann,[3] and H. R. Burnett,[4] Urbana, Ill.

The analysis of turbulent, incompressible, symmetric mixing of two parallel streams is presented. The influence of the upstream boundary layers on the mixing process is taken into account. The von Kármán integral concept is applied to a momentum and energy equation. These equations are used to evaluate the thickness of the mixing region and the velocity distribution in it. The results are presented in nondimensional form. A numerical illustrative example is given. Comparison with Tollmien's analytical results and with experimental data of Liepmann and Laufer is made.

Introduction

An analysis of the plane turbulent jet issuing into a medium at rest was presented by W. Tollmien in 1926 (1).[5] In 1935, A. M. Kuethe (2) extended Tollmien's calculations to the turbulent mixing of two parallel streams of different velocities but of the same densities and temperatures. Both of these analyses, and all subsequent ones, assume uniform velocity distribution in the streams before mixing. Both Tollmien and Kuethe used the transformation from the x, y-plane into an η-plane, where η is proportional to y/x, with a consequent loss of generality. The boundaries of the mixing region correspond to constant values of η and the lines of constant η are straight lines owing to the transformation used. This restrictive transformation is necessary because the velocity distribution as well as the width of the mixing region have to be determined from one equation, i.e., the momentum equation. Although the continuity equation is also used, the introduction of a stream function automatically satisfies this equation, and it cannot be used for the determination of a second unknown.

The two discussed analyses employ the mixing-length theory of Prandtl. In this theory an assumed characteristic length is used. This length is taken as constant across each section of the mixing region and as being a linear function of the distance from the start of mixing. Although in some cases it gives relatively good approximations, the Prandtl mixing-length theory is not applicable for the calculation of mixing of parallel streams, since the mechanism of turbulent exchange of momentum varies across the cross section of the mixing zone. There is no theory of turbulence available at present which would allow the accurate evaluation of the mixing of two streams. However, according to recent experimental results, the assumption of a constant exchange coefficient across each cross section seems to yield better results than the assumption of a constant mixing length. This was pointed out by Dr. Theodore von Kármán in a recent discussion with the senior author.

H. Görtler (3) evaluated some turbulent mixing phenomena with the exchange coefficient suggested by Prandtl (4). However, Görtler's results lack general validity, since he used the assumption that the width of the mixing region is a linear function of the distance from the start of mixing, and he did not take into account the developed boundary layers of the streams.

In the present analysis the turbulent mixing of two parallel streams is presented for the case of identical velocity distributions in both streams. The velocity distribution in the mixing zone, and its width are calculated from the integrals of the momentum and the energy equations. The use of both the momentum and the energy equations allows the evaluation of the width of the mixing zone as a function of the distance from the start of mixing, and it is not necessary to assume a linear variation as was done by previous investigators. The history of the streams before mixing is taken into account in the analysis, which means that the effect on the mixing of the boundary layers along the dividing plane is considered. A quartic polynomial, satisfying all boundary conditions, is assumed as an approximation of the velocity profile in the mixing zone. It is assumed that the turbulent shear is proportional to an exchange coefficient, and that the exchange coefficient is constant over each cross section of the mixing zone. In the present paper the exchange coefficient as recommended by Prandtl and used by Görtler is employed. However, it is planned that in subsequent analyses different exchange coefficients will be used and the results of these will be compared with those of the present analysis. Already the present analysis shows that good qualitative agreement can be obtained with the careful experiments of H. W. Liepmann and J. Laufer (5), although these experiments were made for a two-dimensional stream mixing with a fluid at rest. No such agreement can be obtained between the analyses of Tollmien and Kuethe and the experiments of Liepmann and Laufer.

Analysis

The two-dimensional, viscous, turbulent, incompressible mixing of two parallel streams separated by an infinitely thin flat plate is investigated. In this symmetric case both streams have the same mean velocity distribution, Fig. 1. All velocities used in this analysis are averages. The development of the boundary layer along the flat plate upstream of the mixing is taken into account. The von Kármán integral concept is followed, that is, the determination of the mixing region and the velocity distribution in it is accomplished by use of the momentum and energy equations in an integrated form.

The boundary layer momentum equation is

---

[1] The work was carried out under Air Force Contract: "Theoretical Studies of the Mixing Process of a Jet Impinging Into a Stream of Large Mass," Contract No. AF 33-038-21251.

[2] Professor of Aeronautical Engineering, University of Illinois.

[3] Research Assistant, Department of Aeronautical Engineering, University of Illinois.

[4] Research Assistant, Department of Aeronautical Engineering, University of Illinois.

[5] Numbers in parentheses refer to the Bibliography at the end of the paper.

Contributed by the Applied Mechanics Division and presented at the Fall Meeting, Chicago, Ill., September 8–11, 1952, of The American Society of Mechanical Engineers.

Discussion of this paper should be addressed to the Secretary, ASME, 29 West 39th Street, New York, N. Y., and will be accepted until April 10, 1953, for publication at a later date. Discussion received after the closing date will be returned.

Note: Statements and opinions advanced in papers are to be understood as individual expressions of their authors and not those of the Society. Manuscript received by ASME Applied Mechanics Division, February 29, 1952. Paper No. 52—F-14.

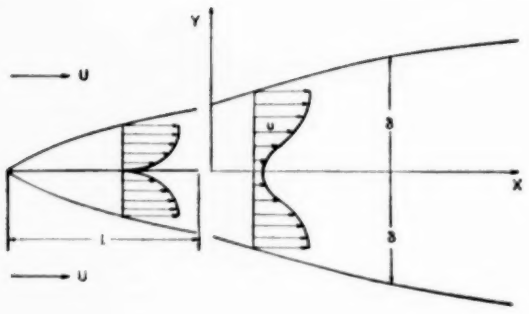

FIG. 1 DIAGRAM OF TURBULENT SYMMETRIC MIXING

$$\rho u \frac{\partial u}{\partial x} + \rho v \frac{\partial u}{\partial y} = \frac{\partial \tau}{\partial y} \quad \ldots\ldots [1]$$

The appropriate energy equation is

$$\rho u^2 \frac{\partial u}{\partial x} + \rho u v \frac{\partial u}{\partial y} = u \frac{\partial \tau}{\partial y} \quad \ldots\ldots [2]$$

The continuity equation is

$$\frac{\partial \rho u}{\partial x} + \frac{\partial \rho v}{\partial y} = 0 \quad \ldots\ldots [3]$$

where

x, y = Cartesian co-ordinates indicated in Fig. 1
u, v = average velocities in mixing region in x, y-directions, respectively
ρ = density of fluid
τ = shear stress

The boundary conditions are for

$$\left.\begin{aligned} y = \pm\delta : u = U;\ \frac{\partial u}{\partial y} = 0 \\ y = 0 : \frac{\partial u}{\partial y} = 0 \end{aligned}\right\} \quad \ldots\ldots [4]$$

where

δ = half width of mixing region
U = velocity of potential flow

It should be observed that instead of using the mixing-length theory for expressing the shear stress, a newer concept of an exchange coefficient, as suggested by von Kármán, is used. The particular exchange coefficient used is due to Prandtl and is

$$\left.\begin{aligned} \tau = \rho\, \epsilon \frac{\partial u}{\partial y} \\ \epsilon = \kappa\, b(x)\, (u_{\max} - u_{\min}) \end{aligned}\right\} \quad \ldots\ldots [5]$$

where

κ = const
$b(x)$ = thickness of mixing region ($= 2\delta$ for this case)
$u_{\max} = U$
$u_{\min} = Ua$ where a is nondimensional velocity along x-axis

The velocity distribution in the mixing region is approximated in the same manner as was done in the analysis of the laminar case (6), i.e., by a quartic polynomial which satisfies all five boundary conditions. Since it is necessary for $\partial u/\partial y$ to be zero at the boundaries of the mixing region and at $y = 0$, the following expression may be used for the nondimensional velocity

$$\frac{\partial}{\partial y}\left[\frac{u}{U}\right] = \frac{A(x)}{\delta}\,[\eta\,(\eta - 1)\,(\eta + 1)] \quad \ldots\ldots [6]$$

or

$$\left[\frac{u}{U}\right] = \frac{A(x)}{4}\,\eta^2\,(\eta^2 - 2) + a\,(x) \quad \ldots\ldots [7]$$

where

$$\eta = \frac{y}{\delta}$$

$A(x)$ = function of x to be determined from remaining boundary conditions
$a(x)$ = arbitrary function of integration

At the boundaries [4], i.e.

$$\eta = \pm 1\ (y = \pm\delta) : \left[\frac{u}{U}\right] = 1$$

From Equation [7]

$$A = -4(1 - a)$$

and the expression for $[u/U]$ becomes

$$\left[\frac{u}{U}\right] = a\,(\eta^2 - 1)^2 - \eta^2\,(\eta^2 - 2) \quad \ldots\ldots [8]$$

It is sufficient to treat only one half of the flow in the symmetric case. For incompressible flow, the following is obtained from the integration of Equations [1] and [2] when the boundary conditions have been used

$$\frac{d}{dx}\int_0^\delta u^2 dy - U\frac{d}{dx}\int_0^\delta u\,dy = 0 \quad \ldots\ldots [9]$$

$$\frac{1}{2}\frac{d}{dx}\int_0^\delta u^3 dy - \frac{U^2}{2}\frac{d}{dx}\int_0^\delta u\,dy + \kappa\, b(x)\, U\,(1 - a)\int_0^\delta \left(\frac{\partial u}{\partial y}\right)^2 dy = 0 \quad \ldots [10]$$

Note that the integration of Equations [1] and [2] are carried out in detail in the Appendix.

Using Equation [8], the evaluation of Equations [9] and [10] yields two simultaneous differential equations for δ and $a(x)$ (see Appendix). (In the following, prime denotes d/dx.)

[From Equation [9]

$$\delta' F(a) + \delta\, F'(a) = 0 \quad \ldots\ldots [11]$$

where

$$F(a) = 16\,a^2 - 11\,a - 5 \quad \ldots\ldots [12]$$

From Equation [10]

$$\delta'\, G(a) + \delta\, G'(a) - \frac{\kappa\, b(x)}{\delta} H(a) = 0 \quad \ldots\ldots [13]$$

where

$$G(a) = 320\,a^3 + 184\,a^2 - 327\,a - 177 \quad [14]$$

and

$$H(a) = 2288\,(a-1)^2. \quad [15]$$

Solving Equation [11] one obtains

$$\delta = \frac{c_1}{F(a)} \quad [16]$$

where c_1 is an arbitrary constant arising from the integration. Making use of this expression for δ and replacing $b(x)$ by $2\,\delta$ (see Equation [5]), the evaluation of Equation [13] yields

$$\frac{c_1}{\kappa}\int K(a)\,da = x + c_2 \quad [17]$$

where c_2 is the constant of integration and

$$K(a) = \frac{640\,a^4 - 880\,a^3 - 199\,a^2 + 478\,a - 39}{572\,(a-1)^3\,(16\,a^2 - 11\,a - 5)^2} \quad [18]$$

The integration of Equation [17] is carried out graphically as indicated in Figs. 2, 3, 4, and 5, where $K = K(a)$ is shown. The result of this integration is given in Fig. 6 where $a = a(\xi)$ is drawn. Here

$$\xi = \frac{\kappa}{c_1}(x + c_2) \quad [19]$$

In order to eliminate double valued solutions which are indicated in Fig. 6, c_2 was determined so as to shift the $a = a(\xi)$-curve tangential to the a-axis. The shifted curve $a = a(\zeta)$ is shown in Fig. 7. Here

$$\zeta = \frac{\kappa x}{c_1} \quad [20]$$

Only those values of a are used which are larger than $a_{\min} = 0.086$. This value corresponds to the point where the a-axis is tangential to the curve $a = a(\zeta)$. This means that the approximation is valid only from the corresponding point on along the x-axis ($x = 0$). The reason for this short "gap" from the end of the plate to the point where this analysis is valid is due to the degree of approximation used in specifying the velocity distribution in the mixing region. Thus, if a higher order of polynomial were used, a smaller $a_{\min}$-value would result and the "gap" could be made as small as desired.

A nondimensional mixing region width curve $\Delta = \Delta(\zeta)$ is shown in Fig. 8. Here

$$\Delta = \frac{\delta}{c_1}$$

The data used in evaluating the various figures are listed in Table 1. Velocity profiles in the mixing region are shown in Fig. 9 for several values of ζ.

Numerical Example

For any particular problem, the velocity of the potential flow U, the kinematic viscosity ν, and the plate length l, are known. The following values will be used in the present example:

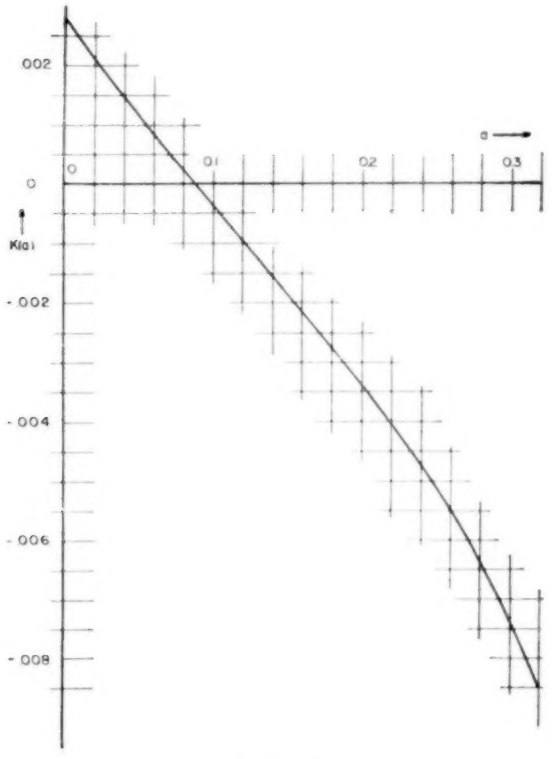

Fig. 2 $K = K(a)$

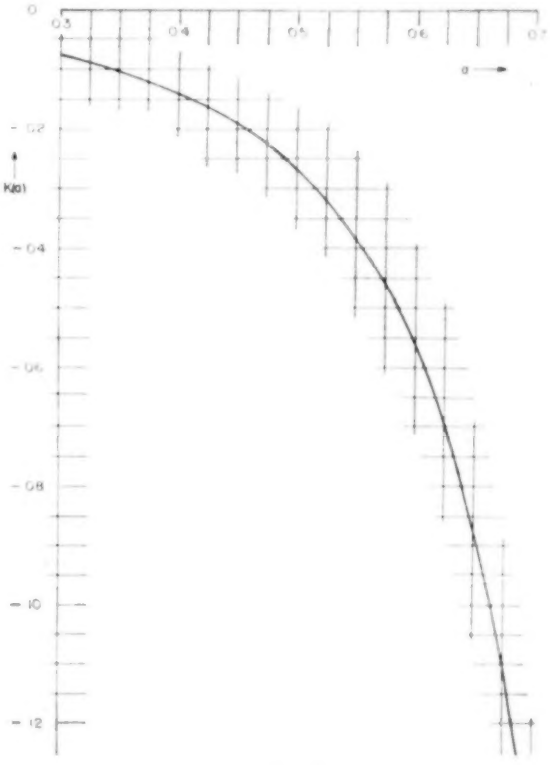

Fig. 3 $K = K(a)$

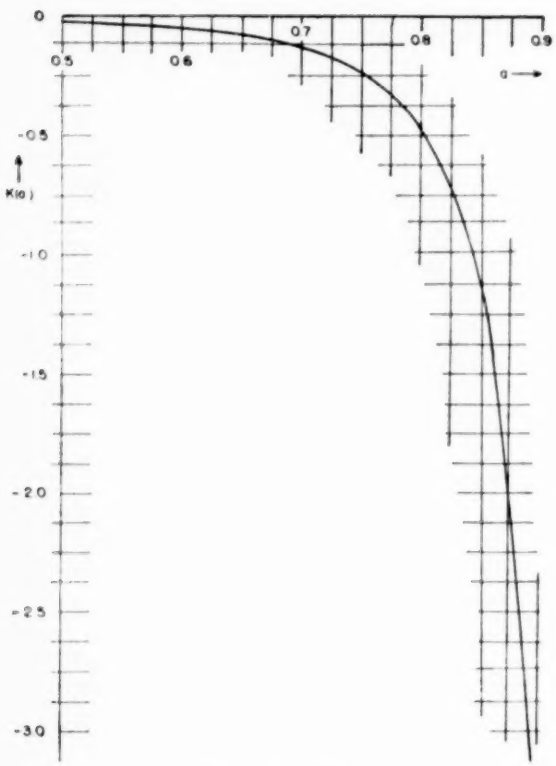

Fig. 4 $K = K(a)$

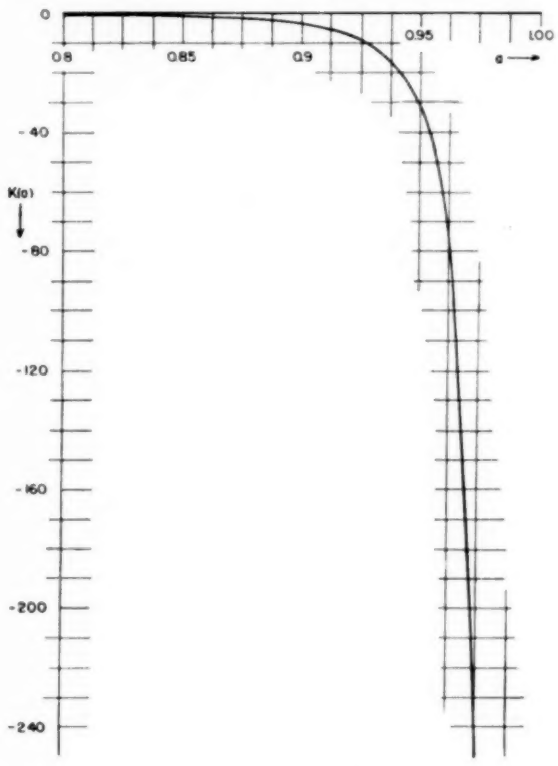

Fig. 5 $K = K(a)$

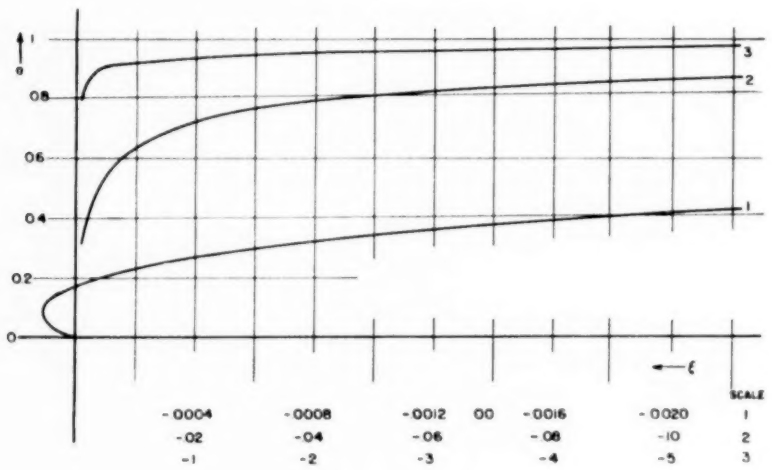

Fig. 6 $\xi = \xi(a)$

TABLE 1 DATA FOR EVALUATING FIGURES

a	$K(a)$	a	$\int_0^a K(a)\,da$	$\zeta = \frac{\kappa x}{c_1}$	$\Delta = -\frac{\delta}{c_1}$
0	+ 0.002727	0	0	0	0.1716
0.001	0.002690	0.020	0.00004713	−0.0002	0.1522
0.010	0.002365	0.086	0.0001136	−0.0006	0.1464
0.100	− 0.0004075	0.120	0.00009704	−0.0010	0.1452
0.200	− 0.003383	0.200	−0.0000789	−0.0015	0.1455
0.300	− 0.007356	0.300	−0.0005996	−0.0025	0.1483
0.400	− 0.01391	0.400	−0.001639	−0.0050	0.1604
0.500	− 0.02656	0.500	−0.003593	−0.0100	0.1816
0.600	− 0.05526	0.600	−0.007404	−0.0200	0.2181
0.700	− 0.1368	0.700	−0.01656	−0.0400	0.2753
0.800	− 0.4764	0.800	−0.04245	−0.0800	0.3628
0.850	− 1.1428	0.850	−0.07875	−0.2000	0.5269
0.875	− 1.9860	0.900	−0.1843	−0.7500	0.7305
0.900	− 3.8987	0.925	−0.5958	−2.0000	1.0953
0.925	− 9.2877	0.950	−1.516	−4.0000	1.5244
0.950	− 31.4822	0.975	−6.562	−6.5600	1.9646
0.975	−253.10				

$$U = 100 \text{ fps}$$
$$l = 10 \text{ ft}$$
$$\nu = 0.1566 \text{ ft}^2/\text{sec}$$

No reliable value has been determined for the constant κ. It is hoped that it might have a universal value, but it is possible that its value will vary for various problems; κ can be evaluated by comparing the results of analysis with experimental data. In this problem a comparison with experimental results given by Liepmann and Laufer (5) indicates that κ is of the order of 0.1. This value was used in this problem. The boundary-layer thickness at the end of the plate, δ^*, is (7)

$$\delta^* = 0.377\, l\, (\text{Re})^{-1/5}$$

where the Reynolds number is

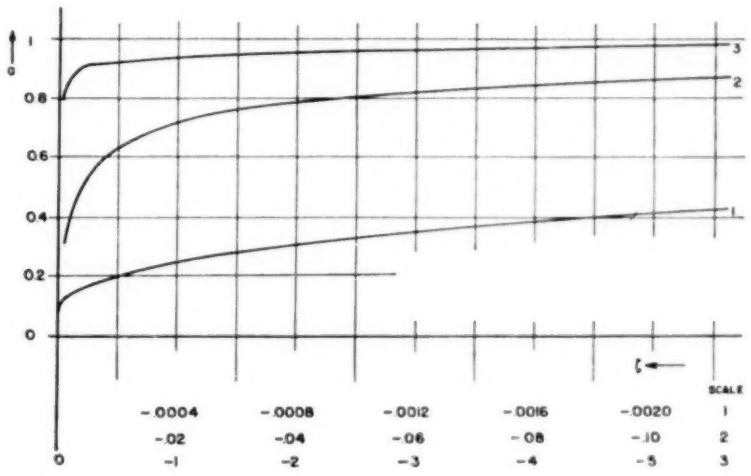

FIG. 7 $\zeta = \zeta(a)$

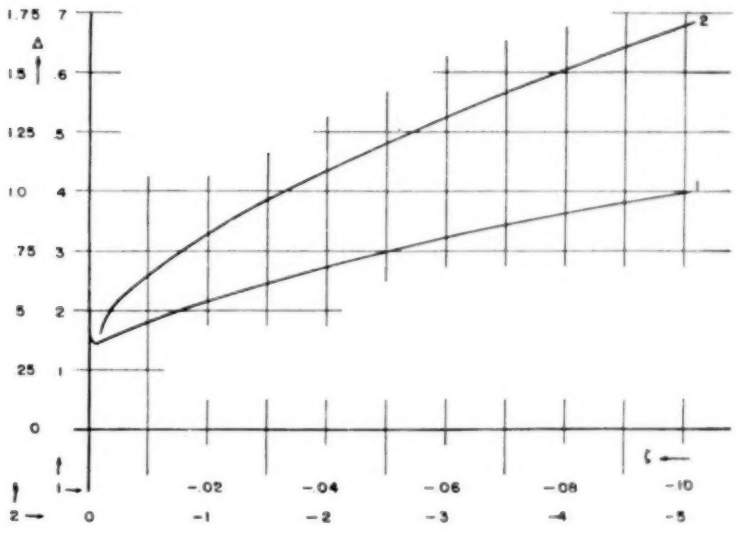

FIG. 8 $\Delta = \Delta(\zeta)$

$$\text{Re} = \frac{Ul}{\nu} = 6{,}386{,}000$$

Then

$$\delta^* = 0.1641 \text{ ft}$$

Since the continuation of the boundary-layer thickness is the boundary of the mixing region, $\delta = \delta^*$ at $x = 0$, if the small effect of the gap is neglected.
From Equation [16]

$$c_1 = -0.9563 \text{ ft}$$

The curve $\delta = \delta(x)$ for this example is given in Figs. 10 and 11.

Kuethe has extended Tollmien's analysis of turbulent mixing of a uniform stream with a fluid at rest and included turbulent mixing of two parallel uniform streams of different velocities. Since the boundary layer upstream of the mixing region was not considered, for equal velocities of the two streams, no mixing resulted in his investigations. Thus no comparison of the present work with the results of the Kuethe method can be made. The important difference between the two analyses is that the boundaries of the mixing region are straight lines if the Kuethe method is used, but the present analysis shows a considerable amount of curvature in the region immediately behind the plate. This curve is approximately a straight line, however, for large distances behind the plate. To verify this bending of the boundary, experimental points obtained by Liepmann and Laufer are plotted in Fig. 12, along with the corresponding result of Tollmien for a velocity ratio (ratio of the two potential streams) of zero. The distances behind the plate for the present numerical example corresponding to the values of ζ given in Fig. 9 are also noted on that figure. Table 2 lists the values used in determining the mixing-region thickness for this example.

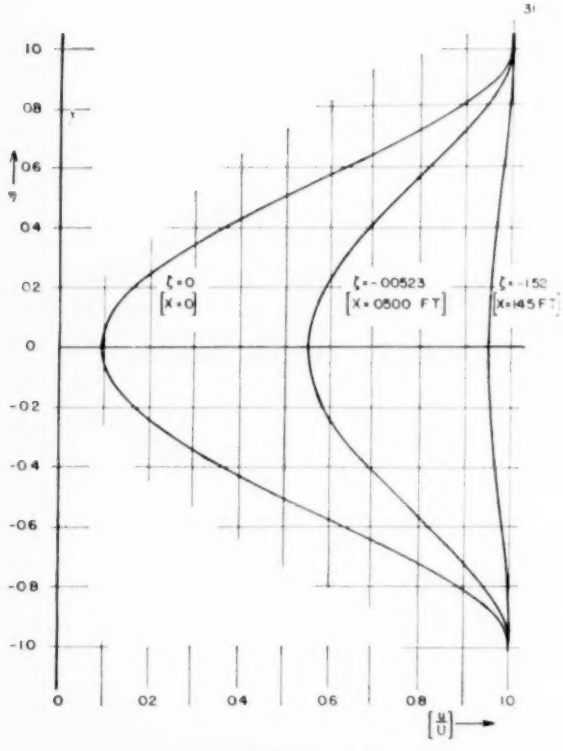

FIG. 9 VELOCITY PROFILES

TABLE 2 VALUES USED IN DETERMINING MIXING-REGION THICKNESS

Data: $l = 10$ ft, $U = 100$ fps, $\nu = 0.1566$ ft²/sec, $\kappa = 0.1$

$\zeta = \frac{\kappa x}{c_1}$	x(ft)	δ(ft)
0	0	0.1641
−0.0004	0.003830	0.1417
−0.0010	0.009563	0.1389
−0.0015	0.01434	0.1391
−0.0020	0.01913	0.1402
−0.0025	0.02391	0.1418
−0.0050	0.04782	0.1534
−0.0100	0.09563	0.1737
−0.0200	0.1913	0.2086
−0.0400	0.3825	0.2633
−0.0600	0.5738	0.3079
−0.0860	0.7650	0.3469
−0.1000	0.9563	0.3858
−0.2000	1.913	0.4925
−0.4000	3.825	0.5824
−0.7500	7.172	0.7077
−1.0000	9.563	0.7842
−2.0000	19.126	1.0474
−4.0000	38.252	1.4578
−6.5600	62.733	1.8787

BIBLIOGRAPHY

1 "Berechnung Turbulenter Ausbreitungsvorgänge," by W. Tollmien, *Zeitschrift für angewandte Mathematik und Mechanik*, vol. 6, 1926, pp. 468–478.

2 "Investigations of the Turbulent Mixing Regions Formed by Jets," by A. M. Kuethe, JOURNAL OF APPLIED MECHANICS, Trans. ASME, vol. 57, 1935, pp. A-87–95.

3 "Berechnung von Aufgaben der freien Turbulenz auf Grund eines neuen Näherungsansatzes," by H. Görtler, *Zeitschrift für angewandte Mathematik und Mechanik*, vol. 22, 1942, pp. 244–254.

4 "Bemerkungen zur Theorie der freien Turbulenz," by L. Prandtl, *Zeitschrift für angewandte Mathematik und Mechanik*, vol. 22, 1942, pp. 241–243.

5 "Investigations of Free Turbulent Mixing," by H. W. Liepmann and J. Laufer, National Advisory Committee for Aeronautics, Technical Note No. 1257, 1947.

6 "Symmetric Laminar Mixing of Two Parallel Streams," by T. P. Torda, Air Force Technical Report M-T-1, University of Illinois, October, 1951, Contract No. AF 33-038-21251.

7 "Über laminare und turbulente Reibung," by Th. von Kármán, *Zeitschrift für angewandte Mathematik und Mechanik*, vol. 1, 1921, pp. 233–252; see National Advisory Committee for Aeronautics, Technical Memorandum No. 1092, 1946.

APPENDIX
INTEGRATION OF MOMENTUM AND ENERGY EQUATIONS

The boundary-layer momentum equation is

$$\rho u \frac{\partial u}{\partial x} + \rho v \frac{\partial u}{\partial y} = \frac{\partial \tau}{\partial y} \qquad [1]$$

The integration of Equation [1] from the axis of symmetry, $y = 0$, to the edge of the mixing zone, $y = \delta$, yields

$$\int_0^\delta \rho u \frac{\partial u}{\partial x} dy + \int_0^\delta \rho v \frac{\partial u}{\partial y} dy - \int_0^\delta \frac{\partial \tau}{\partial y} dy = 0 \qquad [21]$$

Integrating the second term by parts gives

$$\int_0^\delta \rho v \frac{\partial u}{\partial y} dy = \left[\rho v u\right]_0^\delta - \int_0^\delta u \frac{\partial(\rho v)}{\partial y} dy$$

From the continuity equation, Equation [3]

$$\frac{\partial(\rho v)}{\partial y} = -\frac{\partial(\rho u)}{\partial x}$$

and therefore

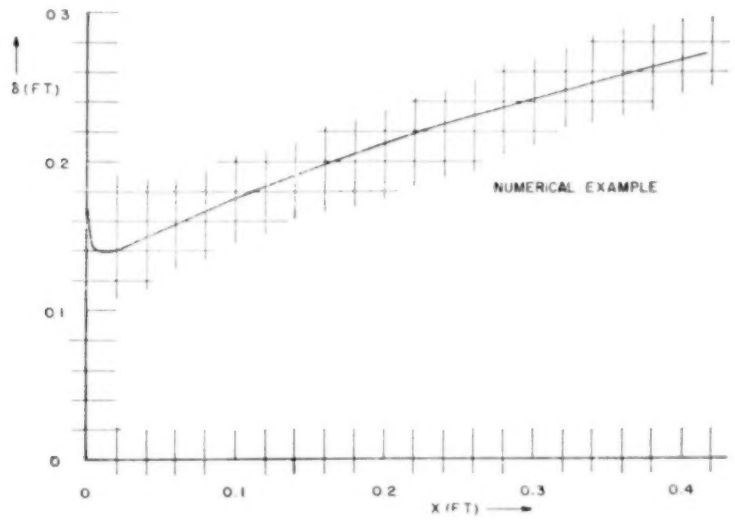

FIG. 10 $\delta = \delta(x)$

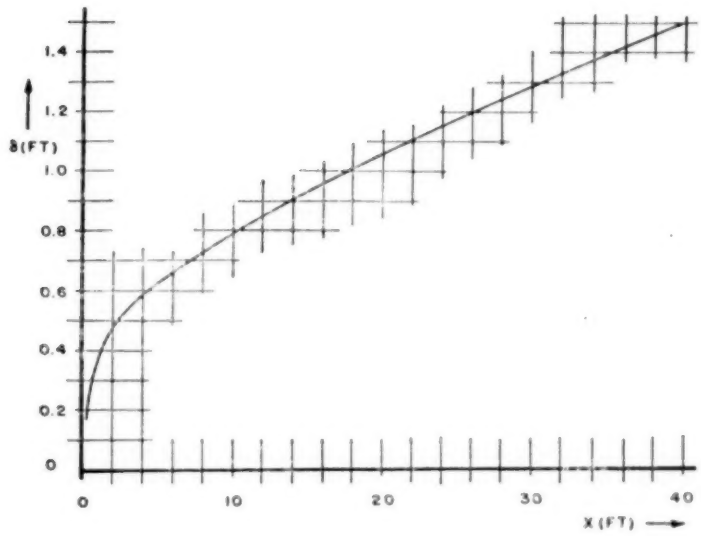

FIG. 11 $\delta = \delta(x)$

$$\int_0^\delta \rho v \frac{\partial u}{\partial y}\, dy = \left[\rho v u\right]_0^\delta + \int_0^\delta u \frac{\partial(\rho u)}{\partial x}\, dy$$

Also

$$\int_0^\delta \frac{\partial \tau}{\partial y}\, dy = \left[\tau\right]_0^\delta = \left[\rho_K b(x)(U - Ua) \frac{\partial u}{\partial y}\right]_0^\delta$$

(see Equation [5])

From

$$\int_0^\delta \frac{\partial}{\partial x}\left(\rho \frac{u^2}{2}\right) dy = \int_0^\delta \rho u \frac{\partial u}{\partial x}\, dy + \int_0^\delta u \frac{\partial \rho u}{\partial x}\, dy$$

substitute for the first term of Equation [21] and obtain

$$\int_0^\delta \frac{\partial}{\partial x}\left(\rho \frac{u^2}{2}\right) dy + \left[\rho v u\right]_0^\delta - \left[\tau\right]_0^\delta = 0$$

where

$$\int_0^\delta \frac{\partial}{\partial x}\left(\rho \frac{u^2}{2}\right) dy = \frac{d}{dx}\int_0^\delta \rho u^2\, dy - [\rho u^2]_\delta \frac{d\delta}{dx}$$

Applying the boundary conditions, Equation [4], the fact that $v_0 = 0$ due to symmetry, and considering incompressible flow Equation [21] becomes

$$\frac{d}{dx}\int_0^\delta u^2\, dy - U^2 \frac{d\delta}{dx} + U v_\delta = 0$$

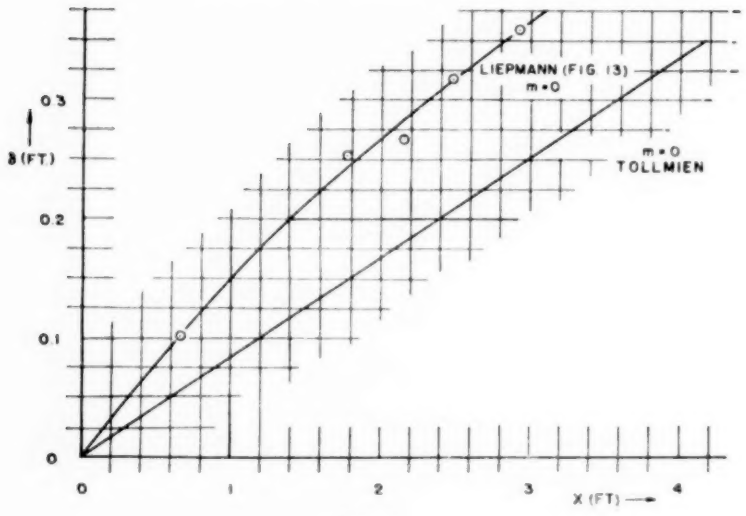

FIG. 12

Integration of the incompressible continuity equation gives

$$v_\delta = v_0 - \int_0^\delta \frac{\partial u}{\partial x}\,dy = -\frac{d}{dx}\int_0^\delta u\,dy + U\frac{d\delta}{dx}$$

The final result of the integration of the momentum equation is then

$$\frac{d}{dx}\int_0^\delta u^2\,dy - U\frac{d}{dx}\int_0^\delta u\,dy = 0 \quad \ldots\ldots [9]$$

The energy equation is

$$\rho\,u^2\frac{\partial u}{\partial x} + \rho\,u\,v\frac{\partial u}{\partial y} = u\frac{\partial \tau}{\partial y} \quad \ldots\ldots [2]$$

The integration of this equation from the axis of symmetry to the edge of the mixing region yields

$$\int_0^\delta \rho\,u^2\frac{\partial u}{\partial x}\,dy + \int_0^\delta \rho\,u\,v\frac{\partial u}{\partial y}\,dy - \int_0^\delta u\frac{\partial \tau}{\partial y}\,dy = 0 \ldots [22]$$

A procedure similar to that used in the integration of the momentum equation is followed

$$\int_0^\delta \rho\,u\,v\frac{\partial u}{\partial y}\,dy = \frac{1}{2}\int_0^\delta \rho\,v\frac{\partial u^2}{\partial y}\,dy = \frac{1}{2}\left[\rho\,v\,u^2\right]_0^\delta$$

$$-\frac{1}{2}\int_0^\delta u^2\frac{\partial(\rho v)}{\partial y}\,dy = \frac{1}{2}\left[\rho\,v\,u^2\right]_0^\delta + \frac{1}{2}\int_0^\delta u^2\frac{\partial(\rho u)}{\partial x}\,dy$$

$$\int_0^\delta u\frac{\partial \tau}{\partial y}\,dy = \left[u\,\tau\right]_0^\delta - \int_0^\delta \tau\frac{\partial u}{\partial y}\,dy$$

$$\int_0^\delta \frac{\partial}{\partial x}\left(\rho\frac{u^3}{2}\right)dy = \int_0^\delta \frac{\rho u}{2}\frac{\partial u^2}{\partial x}\,dy + \int_0^\delta \frac{u^2}{2}\frac{\partial(\rho u)}{\partial x}\,dy$$

Substituting the foregoing values into Equation [22] gives

$$\int_0^\delta \frac{\partial}{\partial x}\left(\rho\frac{u^3}{2}\right)dy + \frac{1}{2}\left[\rho\,v\,u^2\right]_0^\delta - \left[u\,\tau\right]_0^\delta + \int_0^\delta \tau\frac{\partial u}{\partial y}\,dy = 0$$

or

$$\frac{d}{dx}\int_0^\delta \frac{\rho u^3}{2}\,dy - \left[\frac{\rho u^3}{2}\right]_\delta \frac{d\delta}{dx} + \frac{1}{2}\left[\rho\,v_\delta u^2\right]_0^\delta - \left[u\,\tau\right]_0^\delta + \int_0^\delta \tau\frac{\partial u}{\partial y}\,dy = 0$$

Applying the boundary conditions and considering incompressible flow, the foregoing equation becomes

$$\frac{1}{2}\frac{d}{dx}\int_0^\delta u^3 dy - \frac{1}{2}U^3\frac{d\delta}{dx} + \frac{1}{2}U^2 v_\delta + \int_0^\delta \tau\frac{\partial u}{\partial y}\,dy = 0$$

or substituting for v_δ and τ, the final result is

$$\frac{1}{2}\frac{d}{dx}\int_0^\delta u^3\,dy - \frac{U^2}{2}\frac{d}{dx}\int_0^\delta u\,dy + \kappa\,b(x)\,U(1-a)\int_0^\delta \left(\frac{\partial u}{\partial y}\right)^2 dy = 0 \quad [10]$$

DERIVATION OF DIFFERENTIAL EQUATIONS FOR $\delta = \delta(x)$ AND $a = a(x)$

The velocity distribution in the mixing zone is

$$\left[\frac{u}{U}\right] = a(x)\,(\eta^2 - 1)^2 - \eta^2(\eta^2 - 2) \quad \ldots\ldots [8]$$

The integrated momentum equation is

$$\frac{d}{dx}\int_0^\delta u^2\,dy - U\frac{d}{dx}\int_0^\delta u\,dy = 0 \quad \ldots\ldots [9]$$

The energy equation in the integrated form is

$$\frac{1}{2}\frac{d}{dx}\int_0^\delta u^3\,dy - \frac{U^2}{2}\frac{d}{dx}\int_0^\delta u\,dy + \kappa\,b(x)\,U(1-a)\int_0^\delta \left(\frac{\partial u}{\partial y}\right)^2 dy = 0 \ldots [10]$$

Using Equation [8] to evaluate Equations [9] and [10], the following is obtained

$$\int_0^\delta u^2\,dy = U^2\delta\left[a^2\left(\frac{1}{9}-\frac{4}{7}+\frac{6}{5}-\frac{4}{3}+1\right)\right.$$
$$\left.-a\left(\frac{2}{9}-\frac{8}{7}+\frac{10}{5}-\frac{4}{3}\right)+\left(\frac{1}{9}-\frac{4}{7}+\frac{4}{5}\right)\right]$$
$$=\frac{U^2\delta}{315}(128\,a^2+80\,a+107)$$
$$\int_0^\delta u\,dy = U\delta\left[a\left(\frac{1}{5}-\frac{2}{3}+1\right)-\left(\frac{1}{5}-\frac{2}{3}\right)\right]$$
$$=\frac{U\delta}{15}(8\,a+7)$$

Therefore

$$\frac{d}{dx}\left[(U^2\delta/315)(128\,a^2+80\,a+107)\right.$$
$$\left.-(U^2\delta/15)(8\,a+7)\right]=0$$
$$\frac{d}{dx}\left[\delta\,(16\,a^2-11\,a-5)\right]=0$$
$$\delta'(16\,a^2-11\,a-5)+\delta\,a'(32\,a-11)=0$$

where prime denotes differentiation with respect to x.
Let

$$F(a)=16\,a^2-11\,a-5 \quad\ldots\ldots[12]$$

then

$$\delta'F(a)+\delta F'(a)=0 \quad\ldots\ldots[11]$$

This is the differential equation used to determine the width of the mixing region.

$$\int_0^\delta u^2\,dy = U^2\delta\left[a^2\left(\frac{1}{13}-\frac{6}{11}+\frac{15}{9}-\frac{20}{7}+\frac{15}{5}-\frac{6}{3}+1\right)\right.$$
$$+a^2\left(-\frac{3}{13}+\frac{18}{11}-\frac{42}{9}+\frac{48}{7}-\frac{27}{5}+\frac{6}{3}\right)$$
$$+a\left(\frac{3}{13}-\frac{18}{11}+\frac{39}{9}-\frac{36}{7}+\frac{12}{5}\right)$$
$$\left.+\left(-\frac{1}{13}+\frac{6}{11}-\frac{12}{9}+\frac{8}{7}\right)\right]$$
$$\int_0^\delta\left(\frac{\partial u}{\partial y}\right)^2 dy=\frac{16U^2}{\delta}\left[(a^2-2\,a+1)\left(\frac{1}{7}-\frac{2}{5}+\frac{1}{3}\right)\right]$$

Therefore

$$\frac{d}{dx}\left[\delta\,(320\,a^2+184\,a^2-327\,a-177)\right]$$
$$-\frac{\kappa\,b(x)}{\delta}2288\,(a-1)^3=0$$

Let

$$G(a)=320\,a^3+184\,a^2-327\,a-177 \quad\ldots\ldots[14]$$
$$H(a)=2288\,(a-1)^3 \quad\ldots\ldots[15]$$

then

$$\delta'G(a)+\delta G'(a)-\frac{\kappa\,b(x)}{\delta}H(a)=0 \quad\ldots\ldots[13]$$

Some Problems of Orthotropic Plane Stress

By H. D. CONWAY,[1] ITHACA, N. Y.

Many plane-stress problems in isotropic elasticity are solved conveniently by considering the Airy stress functions in the form of Fourier series (periodic loading) or Fourier integrals (nonperiodic loading) of harmonic and biharmonic functions. The object of this paper is to show how many of these solutions can be extended to the case where the material is orthotropic. For illustrative purposes, the following seven problems are solved: (*a*) Half plane subjected to normal loading; (*b*) wedge subjected to axial loading; (*c*) half plane subjected to a normal force applied through a rigid punch; (*d*) half plane subjected to tangential loading; (*e*) wedge subjected to transverse loading; (*f*) force applied at a point in an infinite plane; and (*g*) analysis of deep beams.

Introduction

FOR the solution of plane-stress problems in which the loading is periodic, the use of stress functions in the form of Fourier series is very valuable. Similarly, when the loading is nonperiodic, stress functions in the form of Fourier integrals may be used to advantage. Many interesting examples of the foregoing are given in a book by Girkmann (1).[2] In a paper, Girkmann (2) also has made valuable use of Fourier integrals to solve problems of infinite strips subjected to concentrated loads.

It will be shown in this paper how many of the corresponding problems of orthotropic elasticity may be solved, and several illustrative problems will be given.

Development of Basic Equations

The following development of the basic equations for the stress analysis of problems in orthotropic plane stress follows closely that given by Wolf (3). Defining the strains in the X- and Y-directions as ϵ_x and ϵ_y, respectively, we write the corresponding stress-strain equations

$$\epsilon_x = \frac{\sigma_x}{E_x} - \nu_x \frac{\sigma_y}{E_y}; \quad \epsilon_y = \frac{\sigma_y}{E_y} - \nu_y \frac{\sigma_x}{E_x} \qquad [1]$$

where the symbols used are self-explanatory. The principal axes of orthotropy are X, Y.

The strain-energy density U, is given by

$$U = A\epsilon_x^2 + B\epsilon_y^2 + 2C\epsilon_x\epsilon_y + D\gamma_{xy}^2 \qquad [2]$$

where A, B, C, and D are constants, and it follows that

$$\left.\begin{aligned} \sigma_x &= \frac{\partial U}{\partial \epsilon_x} = 2A\epsilon_x + 2C\epsilon_y \\ \sigma_y &= \frac{\partial U}{\partial \epsilon_y} = 2B\epsilon_y + 2C\epsilon_x \\ \tau_{xy} &= \frac{\partial U}{\partial \gamma_{xy}} = 2D\gamma_{xy} \end{aligned}\right\} \qquad [3]$$

Obtaining expressions for the stresses σ_x and σ_y from Equations [1] and observing, from Equations [3], that the coefficient of ϵ_y in σ_x equals that of ϵ_x in σ_y, we obtain

$$\nu_x E_x = \nu_y E_y \qquad [4]$$

The relationship between the elastic constants yields

$$\frac{\tau_{xy}}{\gamma_{xy}} = G = \frac{E_x E_y}{E_x + E_y(1 + 2\nu_y)} \qquad [5]$$

As in isotropy, the stresses are written in terms of a function $\phi(x, y)$ by means of the equations

$$\sigma_x = \frac{\partial^2 \phi}{\partial y^2}; \quad \sigma_y = \frac{\partial^2 \phi}{\partial x^2}; \quad \tau_{xy} = -\frac{\partial^2 \phi}{\partial x \partial y} \qquad [6]$$

and, since the relationship between the direct and shearing strains is

$$\frac{\partial^2 \epsilon_x}{\partial y^2} + \frac{\partial^2 \epsilon_y}{\partial x^2} = \frac{\partial^2 \gamma_{xy}}{\partial x \partial y} \qquad [7]$$

it follows that the differential equation for ϕ is

$$\left(\frac{\partial^2}{\partial x^2} + k^2 \frac{\partial^2}{\partial y^2}\right)\left(\frac{\partial^2}{\partial x^2} + \frac{\partial^2}{\partial y^2}\right)\phi = 0 \qquad [8]$$

where $k^2 = E_y/E_x$. Problems in orthotropic plane stress thus resolve themselves into the solution of Equation [8] subject to the boundary conditions implicit in Equations [6].

As illustrations of the method to be used, several typical problems of orthotropic plane stress will be solved.

Orthotropic Plane-Stress Problems

(*a*) *Half Plane Subjected to a Normal Concentrated Load.* To solve the problem of the isotropic half plane subjected to a normal concentrated load P, Fig. 1, the stress function ϕ used by Girkmann (4) is the Fourier integral form

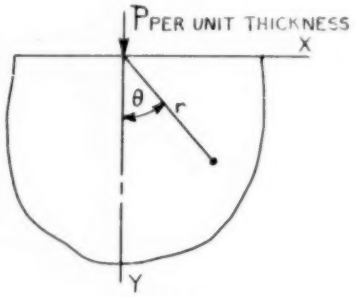

Fig. 1

[1] Professor of Mechanics, Cornell University. Jun. ASME.

[2] Numbers in parentheses refer to the Bibliography at the end of the paper.

Contributed by the Applied Mechanics Division and presented at the Annual Meeting, New York, N. Y., November 30–December 5, 1952, of The American Society of Mechanical Engineers.

Discussion of this paper should be addressed to the Secretary, ASME, 29 West 39th Street, New York, N. Y., and will be accepted until April 10, 1953, for publication at a later date. Discussion received after the closing date will be returned.

Note: Statements and opinions advanced in papers are to be understood as individual expressions of their authors and not those of the Society. Manuscript received by ASME Applied Mechanics Division, November 23, 1951. Paper No. 52—A-4.

$$\phi = \int_0^\infty \frac{1}{\alpha^2}(A + \alpha y B)e^{-\alpha y}\cos \alpha x \, d\alpha \quad \ldots\ldots [9]$$

It will be observed that the function $e^{-\alpha y}\cos \alpha x$ is harmonic (and therefore biharmonic) while the function $ye^{-\alpha y}\cos \alpha x$ is biharmonic. The first function is therefore a solution to Equation [8], while the second is not.

To solve the corresponding problem of the orthotropic half plane—the modulus E_x corresponding to the direction of the plane boundary—we use, for $k \neq 1$, a stress function of the form

$$\phi = \int_0^\infty \frac{1}{\alpha^2}\left(Ae^{-\alpha y} + Be^{-\frac{\alpha y}{k}}\right)\cos \alpha x \, d\alpha \quad \ldots [10]$$

where A and B are certain constants depending on k. This function yields the stresses

$$\sigma_x = \int_0^\infty \left(Ae^{-\alpha y} + \frac{B}{k^2}e^{-\frac{\alpha y}{k}}\right)\cos \alpha x \, d\alpha$$

$$\sigma_y = -\int_0^\infty \left(Ae^{-\alpha y} + Be^{-\frac{\alpha y}{k}}\right)\cos \alpha x \, d\alpha$$

$$\tau_{xy} = -\int_0^\infty \left(Ae^{-\alpha y} + \frac{B}{k}e^{-\frac{\alpha y}{k}}\right)\sin \alpha x \, d\alpha$$

The normal loading on the boundary is represented in the form

$$\underset{c \to 0}{\text{Limit}} \frac{P}{\pi}\int_0^\infty \frac{\sin \alpha c}{\alpha c}\cos \alpha x \, d\alpha$$

and hence the boundary conditions are

$$(\sigma_y)_{y=0} = -\int_0^\infty (A + B)\cos \alpha x \, d\alpha = \underset{c \to 0}{\text{Limit}} \frac{P}{\pi}\int_0^\infty \frac{\sin \alpha c}{\alpha c}\cos \alpha x \, d\alpha$$

$$(\tau_{xy})_{y=0} = \int_0^\infty \left(A + \frac{B}{k}\right)\sin \alpha x \, d\alpha = 0$$

The constants A and B are therefore given by

$$A = -\frac{B}{k} = -\frac{P}{\pi(1-k)}$$

Considering, for example, the σ_x-stress

$$\sigma_x = \frac{-P}{\pi(1-k)}\left(\int_0^\infty e^{-\alpha y}\cos \alpha x \, d\alpha - \frac{1}{k}\int_0^\infty e^{-\frac{\alpha y}{k}}\cos \alpha x \, d\alpha\right)$$

$$= \frac{-P}{\pi(1-k)}\left(\frac{y}{x^2+y^2} - \frac{1}{k}\frac{ky}{k^2x^2+y^2}\right)$$

$$= \frac{P(1+k)x^2y}{\pi(x^2+y^2)(k^2x^2+y^2)} \quad \ldots\ldots [11]$$

Similarly

$$\left.\begin{aligned}\sigma_y &= \frac{P(1+k)y^3}{\pi(x^2+y^2)(k^2x^2+y^2)} \\ \tau_{xy} &= \frac{P(1+k)xy^2}{\pi(x^2+y^2)(k^2x^2+y^2)}\end{aligned}\right\} \quad \ldots\ldots [12]$$

By placing $k = 1$ in the foregoing expressions, we obtain the well-known results for the isotropic half plane. The problem just cited of the orthotropic half plane has been treated by Wolf (5); his answers are incorrect.

For use in a later problem, the displacements v will now be computed. The strain ϵ_y is given by

$$\epsilon_y = \frac{\partial v}{\partial y} = \frac{\sigma_y}{E_y} - \nu_y\frac{\sigma_x}{E_x} = \frac{\sigma_y}{E_y} - \nu_x\frac{\sigma_x}{E_y}$$

from Equation [4]; hence

$$E_y v = \int (\sigma_y - \nu_x\sigma_x)dy + f(x) = \frac{P(1+k)}{\pi}\left[\int \frac{y^3 dy}{(x^2+y^2)(k^2x^2+y^2)} - \nu_x\int \frac{x^2 y\,dy}{(x^2+y^2)(k^2x^2+y^2)}\right] + f(x)$$

The function $f(x)$ may be shown to be a constant C and, after performing the foregoing integrations by means of partial fractions, we obtain

$$E_y v = \frac{P}{2\pi(k-1)}[(k^2+\nu_x)\log(k^2x^2+y^2) - (1+\nu_x)\log(x^2+y^2)] + C$$

To evaluate C, it is usual to assume that v is zero at a point on the boundary $x = \pm a, y = 0$. It follows that

$$E_y v = \frac{P}{2\pi(k-1)}\left[(k^2+\nu_x)\log\frac{k^2x^2+y^2}{k^2a^2} - (1+\nu_x)\log\frac{x^2+y^2}{a^2}\right] \quad [13]$$

If k is placed equal to unity, an indeterminate form results. Evaluating this by means of L'Hospital's rule

$$Ev = \frac{P}{\pi}\left[\log\frac{x^2+y^2}{a^2} - (1+\nu)\frac{y^2}{x^2+y^2}\right] \quad \ldots\ldots [14]$$

which is the well-known result.

Putting the stress equations for the orthotropic case in polar form

$$\sigma_r = \frac{P(1+k)}{\pi r}\frac{\cos\theta}{k^2\sin^2\theta + \cos^2\theta}; \quad \sigma_\theta = \tau_{r\theta} = 0 \quad \ldots [15]$$

(b) Wedge Subjected to Axial Concentrated Load. Observing, from Equations [15], that σ_θ and $\tau_{r\theta}$ are zero, we may extend the results to the case of an orthotropic wedge loaded as shown in Fig. 2. Taking the stress distribution in the form

$$\sigma_r = \frac{A}{r}\frac{\cos\theta}{k^2\sin^2\theta + \cos^2\theta}; \quad \sigma_\theta = \tau_{r\theta} = 0$$

the constant A is found from the equation of vertical equilibrium

$$2\int_0^\beta \frac{A}{r}\frac{\cos\theta}{k^2\sin^2\theta + \cos^2\theta}r\cos\theta\, d\theta = P$$

from which it is found that

$$\sigma_r = \frac{P(1-k^2)}{2r}\frac{\cos\theta}{(k^2\sin^2\theta + \cos^2\theta)(\beta - k\tan^{-1}[k\tan\beta])} \quad \ldots [16]$$

For $k = 1$, Equation [16] is evaluated by L'Hospital's rule to give

$$\sigma_r = \frac{P \cos\theta}{r\left(\beta + \frac{1}{2}\sin 2\beta\right)} \quad \ldots\ldots [17]$$

which result is due to Michell (6).

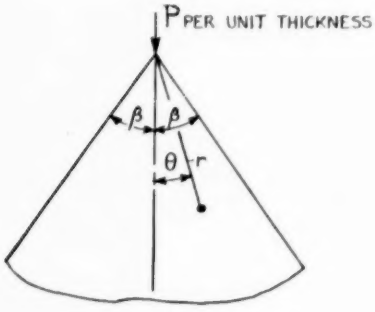

Fig. 2

It is relevant to mention here that the case of a cylindrically aeolotropic wedge loaded in this manner has been discussed by Carrier (7). Carrier finds that the stress distribution is the same as in the isotropic case, when the axis of aeolotropy corresponds to the vertex of the wedge.

(c) *Half Plane Subjected to Normal Force Applied Through a Rigid Punch.* The isotropic version of this problem was first investigated by Sadowsky (8), and it is interesting to consider the corresponding orthotropic case. The problem is shown diagrammatically in Fig. 3, it being assumed that the punch is rigid and that, for the plane

$$(v)_{y=0} = \text{const for } -c \leqslant x \leqslant c$$

From Equation [13], the displacement dv due to the loading element $p(\xi)d\xi$ at distance ξ from the origin is

$$dv = \frac{p(\xi)d\xi}{2\pi E_y(k-1)}\left[(k^2 + \nu_x)\log\frac{k^2(x-\xi)^2 + y^2}{k^2a^2} - (1+\nu_x)\log\frac{(x-\xi)^2 + y^2}{a^2}\right]$$

Hence

$$(dv)_{y=0} = \frac{p(\xi)d\xi}{2\pi E_y(k-1)}\left[(k^2+\nu_x)\log\left(\frac{x-\xi}{a}\right)^2 - (1+\nu_x)\log\left(\frac{x-\xi}{a}\right)^2\right]$$

$$= \frac{(k+1)\,p(\xi)}{\pi E_y}\,d\xi\log\left(\frac{x-\xi}{a}\right)$$

It follows that

$$(v)_{y=0} = \frac{k+1}{\pi E_y}\int_{\xi=-c}^{\xi=c} p(\xi)\log\left(\frac{x-\xi}{a}\right)d\xi$$

Since the foregoing expression is constant over the loaded region of the half plane

$$\int_{\xi=-c}^{\xi=c} p(\xi)\log\left(\frac{x-\xi}{a}\right)d\xi = \text{const}$$

This is the same equation as obtained by Girkmann (9) for the isotropic case, and the pressure p at a distance x from the origin is

$$p = \frac{1}{\sqrt{c^2-x^2}}\int_{-c}^{c} p(\xi)d\xi = \frac{P}{\sqrt{c^2-x^2}} \quad \ldots\ldots [18]$$

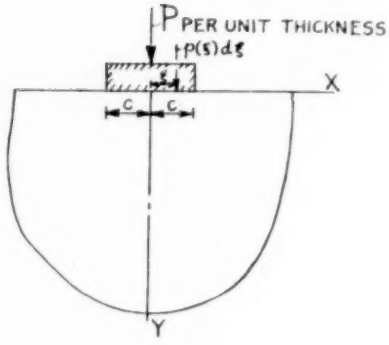

Fig. 3

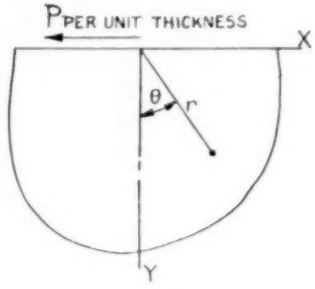

Fig. 4

as in the isotropic case. This result is far from obvious.

(d) *Half Plane Subjected to a Tangential Concentrated Load.* This problem, Fig. 4, is solved by the stress function

$$\phi = \int_0^\infty \frac{1}{\alpha^2}\left(Ae^{-\alpha y} + Be^{-\frac{\alpha y}{k}}\right)\sin\alpha x\,d\alpha \quad \ldots\ldots [19]$$

in precisely the same way as the half plane subjected to a normal load. The stresses obtained in the present case are

$$\sigma_x = \frac{-Pk(1+k)x^3}{\pi(x^2+y^2)(k^2x^2+y^2)};\quad \sigma_y = \frac{Pk(1+k)xy^2}{\pi(x^2+y^2)(k^2x^2+y^2)}$$

$$\tau_{xy} = \frac{-Pk(1+k)x^2y}{\pi(x^2+y^2)(k^2x^2+y^2)}$$

In polar form, these stresses may be rewritten as

$$\sigma_r = \frac{-Pk(1+k)\sin\theta}{\pi r(k^2\sin^2\theta + \cos^2\theta)};\quad \sigma_\theta = \tau_{r\theta} = 0 \quad \ldots\ldots [20]$$

(e) *Wedge Subjected to a Transverse Concentrated Load.* Observing from Equations [20], that the circumferential and shearing stresses are zero, the foregoing results may be applied to the case of the wedge loaded as shown in Fig. 5. Proceeding as in case (b), we obtain

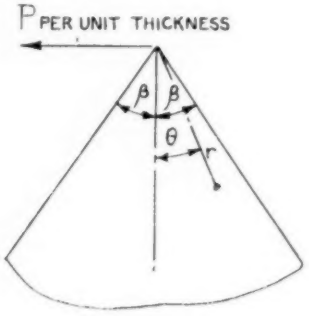

Fig. 5

$$\sigma_r = \frac{Pk(1-k^2)}{r} \frac{\sin\theta}{(k^2\sin^2\theta + \cos^2\theta)\left(\pi - 2k\beta - 2\tan^{-1}\left[\frac{\cot\beta}{k}\right]\right)} \quad \ldots [21]$$

For $k = 1$, the indeterminate form is again evaluated by L'Hospital's rule to give

$$\sigma_r = \frac{P\sin\theta}{r\left(\beta - \frac{1}{2}\sin 2\beta\right)} \quad \ldots [22]$$

The cylindrically aeolotropic form of this problem is also treated by Carrier (7) who again finds that the stress distribution is the same as in the isotropic case.

(*f*) *Force Applied at a Point in an Infinite Plane.* The stress function necessary for the solution of the problem shown diagrammatically in Fig. 6 is that given in Equation [19]. Considering

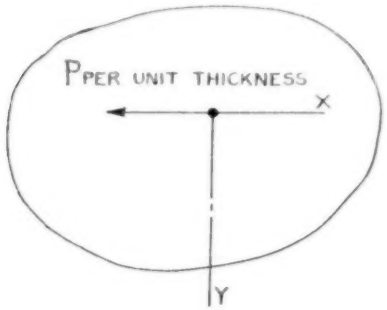

Fig. 6

the plane as divided in two along the X-axis, the shearing force applied to each side of the division is $P/2\pi$. The shearing stress on the straight boundary of each half plane is then

$$\text{Limit}_{c\to 0} \frac{P}{2\pi}\int_0^\infty \frac{\sin\alpha c}{\alpha c}\cos\alpha x\, d\alpha$$

and, equating this to the shearing stress along $y = 0$ obtained from the stress function, a relationship between the constants A and B is determined. The other equation necessary for finding A and B is obtained from the condition of zero displacement v along $y = 0$.

Carrying out this procedure, the following stresses are obtained

$$\left.\begin{aligned}
\sigma_x &= \frac{-Px}{2\pi(1-k^2)}\left[\frac{k^2+\nu_x}{x^2+y^2} - \frac{k(1+\nu_x)}{k^2x^2+y^2}\right] \\
\sigma_y &= \frac{Px}{2\pi(1-k^2)}\left[\frac{k^2+\nu_x}{x^2+y^2} - \frac{k^3(1+\nu_x)}{k^2x^2+y^2}\right] \\
\tau_{xy} &= \frac{-Py}{2\pi(1-k^2)}\left[\frac{k^2+\nu_x}{x^2+y^2} - \frac{k(1+\nu_x)}{k^2x^2+y^2}\right]
\end{aligned}\right\} \quad \ldots [23]$$

Carrier (7) has solved the cylindrically aeolotropic version of this problem, assuming that the load is applied at the axis of symmetry of the material. Okubo (10) has obtained the foregoing results by means of complex stress functions.

(*g*) *Analysis of Deep Beams* One of the more difficult problems of plane stress is encountered in the analysis of beams having length and breadth of comparable magnitude. Such beams are commonly called "deep beams." Methods similar to one

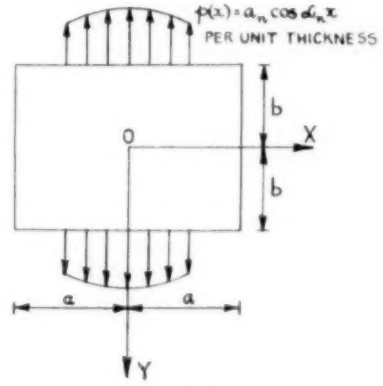

Fig. 7

another for the solution of isotropic deep beams have been given independently by Pickett (11) and Girkmann (12). Okubo (10) also has discussed the solution of orthotropic deep beams using complex stress functions.

As an example of the present analysis of orthotropic deep beams, the problem, shown diagrammatically in Fig. 7, will be solved; the corresponding isotropic problem has been solved by Girkmann by means of the stress function

$$\phi = \sum_{n=1,3,5,}^{\infty} \frac{1}{\alpha_n^2}(A_n\cosh\alpha_n y + \alpha_n y B_n\sinh\alpha_n y)\cos\alpha_n x$$

$$+ \sum_{m=1,3,5,}^{\infty} \frac{1}{\beta_m^2}(C_m\cosh\beta_m x + \beta_m x D_m\sinh\beta_m x)\cos\beta_m y \quad \ldots [24]$$

where

$$\alpha_n = \frac{n\pi}{2a} \text{ and } \beta_m = \frac{m\pi}{2b}$$

For the orthotropic problem, we write the stress function in the form

$$\phi = \sum_{n=1,3,5,}^{\infty} \frac{1}{\alpha_n^2}\left(A_n\cosh\alpha_n y + B_n\cosh\frac{\alpha_n y}{k}\right)\cos\alpha_n x$$

$$+ \sum_{m=1,3,5,}^{\infty} \frac{1}{\beta_m^2}(C_m\cosh\beta_m x + D_m\cosh k\beta_m x)\cos\beta_m y \quad \ldots [25]$$

which yields the stresses

$$\left.\begin{aligned}
\sigma_x &= \sum_{n=1,3,5,}^{\infty}\left(A_n\cosh\alpha_n y + \frac{B_n}{k^2}\cosh\frac{\alpha_n y}{k}\right)\cos\alpha_n x \\
&\quad - \sum_{m=1,3,5,}^{\infty}(C_m\cosh\beta_m x + D_m\cosh k\beta_m x)\cos\beta_m y \\
\sigma_y &= -\sum_{n=1,3,5,}^{\infty}\left(A_n\cosh\alpha_n y + B_n\cosh\frac{\alpha_n y}{k}\right)\cos\alpha_n x
\end{aligned}\right\} \quad \ldots [26]$$

$$+ \sum_{m=1,3,5,}^{\infty} (C_m \cosh \beta_m x + D_m k^2 \cosh k\beta_m x) \cos \beta_m y$$

$$\tau_{xy} = \sum_{n=1,3,5,}^{\infty} \left(A_n \sinh \alpha_n y + \frac{B_n}{k} \sinh \frac{\alpha_n y}{k} \right) \sin \alpha_n x \quad \ldots [26] \ (cont.)$$

$$+ \sum_{m=1,3,5,}^{\infty} (C_m \sinh \beta_m x + D_m k \sinh k\beta_m x) \sin \beta_m y$$

The boundary conditions

$$\sigma_x = 0 \text{ for } x = \pm a; \ \sigma_y = p(x) = a_n \cos \alpha_n x \text{ for } y = \pm b$$

yield the following equations

$$C_m \cosh \beta_m a + D_m \cosh k\beta_m a = 0 \quad \ldots [27]$$

$$- \left(A_n \cosh \alpha_n b + B_n \cosh \frac{\alpha_n b}{k} \right) = a_n \quad \ldots [28]$$

The remaining boundary conditions

$$\tau_{xy} = 0 \text{ for } x = \pm a; \ \tau_{xy} = 0 \text{ for } y = \pm b$$

yield

$$\sum_{n=1,3,5,}^{\infty} \left(A_n \sinh \alpha_n y + \frac{B_n}{k} \sinh \frac{\alpha_n y}{k} \right) (-1)^{\frac{n-1}{2}}$$

$$+ \sum_{m=1,3,5,}^{\infty} (C_m \sinh \beta_m a + D_m k \sinh k\beta_m a) \sin \beta_m y = 0 \quad [29]$$

and

$$\sum_{n=1,3,5,}^{\infty} \left(A_n \sinh \alpha_n b + \frac{B_n}{k} \sinh \frac{\alpha_n b}{k} \right) \sin \alpha_n x$$

$$+ \sum_{m=1,3,5,}^{\infty} (C_m \sinh \beta_m x + D_m k \sinh k\beta_m x) (-1)^{\frac{m-1}{2}} = 0. \quad [30]$$

Substituting Equations [27] and [28] in Equations [29] and [30], we obtain two equations in two unknowns. In the first of these equations it is necessary to expand sinh $\alpha_n y$ and sinh $\alpha_n y/k$ in a Fourier series of sin $\beta_m y$ whereas, in the second, sinh $\beta_m x$ and sinh $k\beta_m x$ are expanded in Fourier series of sin $\alpha_n x$. A doubly infinite system of equations then results which are solved by considering only a finite number of terms. Iteration may be used, and the final solution of the set of equations is similar to that used by Timoshenko (13) in his solution to the problem of the bending of the uniformly loaded and clamped rectangular plate.

BIBLIOGRAPHY

1 "Flächentragwerke," by K. Girkmann, Julius Springer-Verlag, Vienna, 1946.

2 "Angriff von Einzellasten in der Streifenförmigen Scheibe," by K. Girkmann, *Ingenieur-Archiv.*, vol. 13, 1943, p. 273.

3 "Ausbreitung der Kraft in der Halbebene bei anisotropem Material," by K. Wolf, *Zeitschrift für angewandte Mathematik und Mechanik*, vol. 14, 1935, p. 249.

4 Loc. cit. (1), p. 60.

5 Loc. cit. (3), p. 252.

6 "The Inversion of Plane Stress," by J. H. Michell, Proceedings of the London Mathematical Society, vol. 34, 1902, p. 134.

7 "Stress Distributions in Cylindrically Aeolotropic Plates," by G. F. Carrier, JOURNAL OF APPLIED MECHANICS, Trans. ASME, vol. 65, 1943, p. A-117.

8 "Zweidimensionale Probleme der Elastizitätstheorie," *Zeitschrift für angewandte Mathematik und Mechanik*, vol. 8, 1928, p. 107.

9 Loc. cit. (1) p. 70.

10 "Stress Systems in an Aeolotropic Rectangular Plate," by H. Okubo, *Zeitschrift für angewandte Mathematik und Mechanik*, vol. 21, 1941, p. 162.

11 "Application of the Fourier Method to the Solution of Certain Boundary Problems in the Theory of Elasticity," by G. Pickett, JOURNAL OF APPLIED MECHANICS, Trans. ASME, vol. 66, 1944, p. A-176.

12 Loc. cit. (1), p. 84.

13 "Theory of Plates and Shells," by S. Timoshenko, McGraw-Hill Book Company, Inc., New York, N. Y., 1940, p. 222.

The Bending of a Wedge-Shaped Plate

By S. WOINOWSKY-KRIEGER,[1] QUEBEC CITY, CANADA

A general method of solution is given in this paper for the problem of bending of a wedge-shaped thin elastic plate with arbitrary boundary conditions on the radial edges in the case of a single load. The solution is carried out for a plate with clamped edges and a single load on the bisector radius of the plate. Stress distribution along the edges is shown and the behavior of the solution near the corner point is discussed for several opening angles of the plate.

Introduction

THE bending of a sectorial plate clamped along the radial edges has been the subject of several papers recently published. A simple approximate method has been applied by G. F. Carrier and F. S. Shaw (1)[2] to sectorial plates under various conditions, a method credited to Weinstein has been used by H. R. Hassé (2) in considering a semicircular plate under uniform load. Y. S. Uflyand (3, 4) has treated similar problems by means of integral equations. Finally, the bending of a plate carrying a uniform load and bounded by two radial edges and two circular arcs has been considered by G. F. Carrier (5).

In order to obtain a rigorous solution for a sectorial plate with arbitrary homogeneous conditions along the radial edges in the case of a single load an infinite radius of the sector will be assumed in this paper. In eliminating the influence of a third edge and thus in reducing the number of independent parameters to a minimum, such a limitation of the problem proves to be even an advantage in so far as the question of stress distribution near the corner point of the plate is concerned.

Construction of the General Solution

Let us consider a thin elastic plate, Fig. 1, carrying a single load P at $r = r_0$, $\theta = \theta_0$ and limited only by the radial edges $\theta = \pm\alpha$. The conditions along these edges are for the present arbitrary and submitted merely to the exigence of the statical equilibrium of the plate.

The differential equation for the deflection w of the plate

$$\Delta\Delta w = \left(\frac{\partial^2}{\partial r^2} + \frac{1}{r}\frac{\partial}{\partial r} + \frac{1}{r^2}\frac{\partial^2}{\partial\theta^2}\right)^2 w = 0 \quad \ldots\ldots [1]$$

has for the general solution functions of the form $r^k e^{\pm k\theta}$ and $r^k e^{\pm(k-2)i\theta}$ where k is an arbitrary number except for $k = 1$ which gives a special solution. Putting $k = 1 \pm iu$ with a new parameter u and adding a constant factor $e^{\pm iu \log r_0}$ one arrives at a solution of the type

$$w(u) = r \exp\left[\pm(u \pm i)\theta \pm iu \log \frac{r}{r_0}\right] \quad \ldots\ldots [2]$$

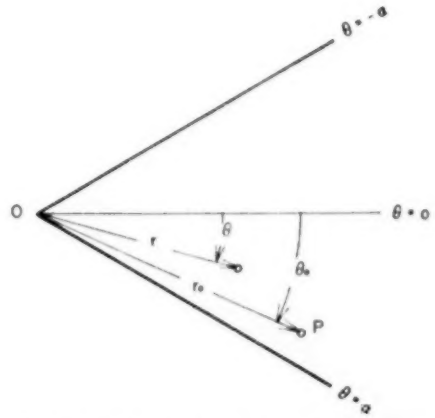

Fig. 1 Wedge-Shaped Plate With Polar Co-Ordinates Used in the General Solution

By taking a linear combination of terms of the form of Equation [2] the solution of Equation [1] can be represented in the following manner:

Range $-\alpha \leq \theta \leq \theta_0$

$$w_1(u) = f_1(\theta,u) r \cos\left(u \log \frac{r}{r_0}\right) + f_2(\theta,u)\, r \sin\left(u \log \frac{r}{r_0}\right) \quad [3]$$

Range $\theta_0 \leq \theta \leq \alpha$

$$w_2(u) = f_3(\theta,u)\, r \cos\left(u \log \frac{r}{r_0}\right) + f_4(\theta,u)\, r \sin\left(u \log \frac{r}{r_0}\right) \quad [4]$$

in which for $i = 1, 2, 3$

$$f_i(\theta,u) = A_i \cosh u\theta \cos\theta + B_i \cosh u\theta \sin\theta + C_i \sinh u\theta \cos\theta + D_i \sinh u\theta \sin\theta \quad \ldots\ldots [5]$$

and A_i, B_i, C_i, D_i are some coefficients depending on u but independent of r and θ.

Boundary Conditions

The twelve coefficients A_i, B_i, C_i, D_i ($i = 1, 2, 3$) contained in Equations [3] and [4] are defined by twelve conditions, from which eight are edge conditions along $\theta = \pm\alpha$ and the remaining four some conditions of continuity and loading along the radius $\theta = \theta_0$.

Let us begin with the consideration of boundary conditions in restricting our attention to the edge $\theta = -\alpha$ and in writing for brevity $f_1, f_1', \ldots$ for $f_1(\theta, u)$, $(\partial/\partial\theta) f_1(\theta, u)$ and so on.

The conditions

$$w_1(u) = 0, \quad \frac{1}{r}\frac{\partial w_1(u)}{\partial\theta} = 0$$

corresponding to a clamped edge lead to the relations

$$f_1 = 0, \; f_1' = 0, \; f_2 = 0, \; f_2' = 0 \text{ at } \theta = -\alpha \quad \ldots\ldots [6]$$

The conditions

[1] Professor of Structural Engineering, Laval University, Quebec, Can.

[2] Numbers in parentheses refer to the Bibliography at the end of the paper.

Contributed by the Applied Mechanics Division and presented at the Annual Meeting, New York, N. Y., November 30–December 5, 1952, of The American Society of Mechanical Engineers.

Discussion of this paper should be addressed to the Secretary, ASME, 29 West 39th Street, New York, N. Y., and will be accepted until April 10, 1953, for publication at a later date. Discussion received after the closing date will be returned.

Note: Statements and opinions advanced in papers are to be understood as individual expressions of their authors and not those of the Society. Manuscript received by ASME Applied Mechanics Division, February 8, 1952. Paper No. 52—A-6.

$$w_i(u) = 0, \ \Delta w_i(u) = 0$$

valid on a simply supported edge are equivalent with

$$f_1 = 0, \ f_1'' = 0, \ f_2 = 0, \ f_2'' = 0 \text{ at } \theta = -\alpha \quad \ldots\ldots [7]$$

The conditions on a free edge are fulfilled if

$$\frac{1}{r}\frac{\partial w_i(u)}{\partial r} + \frac{1}{r^2}\frac{\partial^2 w_i(u)}{\partial \theta^2} + \nu \frac{\partial^2 w_i(u)}{\partial r^2} = 0$$

$$\frac{1}{r}\frac{\partial}{\partial \theta}\Delta w_i(u) + (1-\nu)\frac{\partial^2}{\partial r^2}\left(\frac{1}{r}\frac{\partial w_i(u)}{\partial \theta}\right) = 0$$

ν being the Poisson's ratio of the material of the plate. Substituting Equation [3] in the previous relations one arrives at the system of equations

$$\left.\begin{aligned} &f_1'' + (1-\nu u^2) f_1 + u(1+\nu) f_2 = 0 \\ &f_2'' + (1-\nu u^2) f_2 - u(1+\nu) f_1 = 0 \\ &f_1''' - [(2-\nu)u^2 - 1] f_1' + u(1+\nu) f_2' = 0 \\ &f_2''' - [(2-\nu)u^2 - 1] f_2' - u(1+\nu) f_1' = 0 \end{aligned}\right\} \quad \ldots\ldots [8]$$

valid for $\theta = -\alpha$. To make the boundary conditions complete four further equations analogous to [6], [7] or [8], respectively, must be written for the second edge $\theta = +\alpha$ in accordance with conditions here prescribed.

Conditions of Continuity

Three obvious conditions equating the deflection, the slope, and the curvature of both surfaces $w_1(u)$ and $w_2(u)$ on $\theta = \theta_0$ are

$$w_1(u) - w_2(u) = 0$$

$$\frac{1}{r}\frac{\partial w_1(u)}{\partial \theta} - \frac{1}{r}\frac{\partial w_2(u)}{\partial \theta} = 0$$

$$\frac{1}{r}\frac{\partial w_1(u)}{\partial r} + \frac{1}{r^2}\frac{\partial^2 w_1(u)}{\partial \theta^2} - \frac{1}{r}\frac{\partial w_2(u)}{\partial r} - \frac{1}{r^2}\frac{\partial^2 w_2(u)}{\partial \theta^2} = 0$$

Making use of Equations [3] and [4], and taking into account the first of the previous conditions to simplify the last one, one has for $\theta = \theta_0$

$$\left.\begin{aligned} f_1 - f_2 &= 0 \\ f_1' - f_2' &= 0 \\ f_1'' - f_2'' &= 0 \end{aligned}\right\} \quad \ldots\ldots [9]$$

Conditions for Shearing Forces

In order to introduce into solution the singularity caused by the load P concentrated at the point $r = r_0$, $\theta = \theta_0$ let us determine the difference of shearing forces on both sides of the radius $\theta = \theta_0$, that is, the quantity

$$\delta Q_i(u) = \frac{D}{r}\frac{\partial}{\partial \theta}[\Delta w_2(u) - \Delta w_1(u)] \quad \ldots\ldots [10]$$

where D is the flexural rigidity of the plate.

Equations [3] and [4] when substituted lead to the relation

$$r^2 \delta Q_i(u) = D(f_2''' - f_1''')_{\theta=\theta_0} \cos\left(u \log \frac{r}{r_0}\right) \quad \ldots [11]$$

Let us consider on the other hand the Fourier representation of an arbitrary function

$$\varphi(x) = \frac{1}{\pi}\int_0^\infty du \int_{-\infty}^{+\infty} \varphi(\xi) \cos[u(x-\xi)] d\xi \quad \ldots [12]$$

Putting $x = \log r$, $\xi = \log \rho$ the previous expression becomes

$$\psi(r) = \frac{1}{\pi}\int_0^\infty du \int_{-\infty}^{+\infty} \psi(\rho) \cos\left(u \log \frac{r}{\rho}\right)\frac{d\rho}{\rho} \quad \ldots [13]$$

where $\psi(r)$ is written for $\varphi(\log r)$. Introducing once more δQ_i, i.e., the difference between the shearing forces Q_i on both sides of the radius $\theta = \theta_0$, let $\psi(r) = r^2 \delta Q_i$. The function $\psi(r)$ then must be zero everywhere except in $r = r_0$ on the additional condition that

$$\int_0^\infty \psi(r)\, dr = r_0^2 P \quad \ldots\ldots [14]$$

Hence by Equation [13]

$$\psi(r, r_0) = r^2 \delta Q_i = \frac{P r_0}{\pi}\int_0^\infty \cos\left(u \log \frac{r}{r_0}\right) du \quad \ldots [15]$$

A comparison of Equations [11] and [15] leads to the conclusion that the relation

$$f_2''' - f_1''' = \frac{P r_0}{\pi D} \quad \text{at } \theta = \theta_0 \quad \ldots\ldots [16]$$

must hold and the deflection of the plate is then obtainable in form of the infinite integrals

$$\left.\begin{aligned} w_1 &= \int_0^\infty w_1(u)\, du \quad \text{for} \quad -\alpha \le \theta \le \theta_0 \\ w_2 &= \int_0^\infty w_2(u)\, du \quad \text{for} \quad \theta_0 \le \theta \le \alpha \end{aligned}\right\} \quad \ldots [17]$$

$w_1(u)$ and $w_2(u)$ being functions defined by Equations [3] and [4].

Determination of Coefficients

Four edge conditions of the form of Equations [6], [7], and [8] on $\theta = -\alpha$, four analogous conditions on $\theta = +\alpha$, three conditions of continuity of the form of Equation [9], and the discontinuity condition, Equation [16], are sufficient to determine the twelve unknown coefficients in the most general case. The actual carrying out of the solution is considerably simplified in most cases of practical interest.

If for instance the boundary conditions of the plate represent an arbitrary combination of built-in and simply supported edges, these conditions always can be satisfied by making $f_2(\theta, u)$ zero throughout the plate and by restricting the solution to both functions $f_1(\theta, u)$ and $f_2(\theta, u)$ associated with $r \cos(u \log r/r_0)$. In the case of two clamped edges (or two simply supported edges) a further simplification is possible by decomposition of the given single load in two combinations of loading, namely, a symmetrical and an antisymmetrical one, both with respect to $\theta = 0$. It is readily shown that the number eight of unknown coefficients is then reduced to six for each load combination.

Both edges of the plate being free the same method of decomposition can be used to advantage. A symmetrical function $f_3(\theta, u)$, or an antisymmetrical one, however, must be added in this case, thus increasing the number of unknown coefficients to eight in each part of the solution.

If one edge is simply supported the opening angle of the plate may be doubled and the method of images (6) used with respect to the simply supported edge.

In the case of a single load applied on a nonsupported edge, say, on $\theta = -\alpha$, the third of Equations [8] should be completed by a term on the right in accordance with Equation [16].

By Equation [3] the deflection of the plate is always zero at the corner point of the plate $r = 0$. Consequently, a concentrated reaction should be expected at this point. To make the corner free of forces, a reactive load must be introduced under the con-

dition to give at $r = 0$ a reaction equal in value but opposite in sign to the reaction caused by the given load.

Clamped Plate Under Central Load

Let us apply the general solution given by Equations [3], [5], and [17] to the simplest case of a plate clamped along the edges $\theta = 0$, $\theta = 2\alpha$ and carrying a single load P at $r = r_0$, $\theta = \alpha$. The expression for the deflection is then reduced to

$$w = r \int_0^\infty f_1(\theta,u) \cos\left(u \log \frac{r}{r_0}\right) du \quad (0 \leq \theta \leq \alpha) \ldots [18]$$

the function $f_2(\theta, u)$ being zero because of the assumed conditions on the edges. The boundary conditions for $f_1(\theta, u)$ are now $f_1(\theta, u) = 0$, $(\partial/\partial\theta)f_1(\theta, u) = 0$ on $\theta = 0$ and the conditions on $\theta = \alpha$ are $(\partial/\partial\theta)f_1(\theta, u) = 0$ by symmetry and $(\partial^3/\partial\theta^3)f_1(\theta, u) = -Pr_0/2\pi D$ by Equation [16]. The four coefficients of Equation [5], when determined from these conditions and substituted in the integral, Equation [18], lead finally to the expression

$$w = \frac{Pr r_0}{2\pi D} \int_0^\infty \frac{O_1 U_1 + O_2 U_2}{(1 + u^2)uN} \cos\left(u \log \frac{r}{r_0}\right) du \ldots [19]$$

in which the abbreviations

$$\left.\begin{aligned} O_1 &= \sinh u\theta \cos\theta - u \cosh u\theta \sin\theta \\ O_2 &= \sinh u\theta \sin\theta \\ U_1 &= u \cosh \alpha u \sin\alpha + \sinh \alpha u \cos\alpha \\ U_2 &= (1 + u^2) \sinh \alpha u \sin\alpha \\ N &= \sinh 2\alpha u + u \sin 2\alpha \end{aligned}\right\} \ldots\ldots [20]$$

are used. Expressions O_1, O_2 hold for $0 \leq \theta \leq \alpha$ and θ is to replace by $2\alpha - \theta$ for $\alpha \leq \theta \leq 2\alpha$.

The result, Equation [19], also can be obtained by means of Mellin transform. The form of this method used by C. J. Tranter (7) to treat a two-dimensional problem of the wedge needs only a slight modification to be applied in the present case. Another approach to the problem of the infinite sectorial plate with clamped edges may be found in a paper by I. E. Saharov (8). It should be noted, finally, that the solution, Equation [19], is contained as a limit case in a far more general solution due to A. C. Dixon (9) and concerning the bending of a plate clamped in two circular arcs.

Stress Distribution Along Boundary

The further consideration is reduced to the analysis of the stress distribution along the radial edges of the plate. By differentiation of Equation [19], the following bending moments M_t° and reactive forces V_t on the edge $\theta = 0$ are obtained

$$\left.\begin{aligned} M_t^\circ &= -D\left(\frac{1}{r^2}\frac{\partial^2 w}{\partial\theta^2}\right)_{\theta=0} \\ &= -\frac{Pr_0 \sin\alpha}{\pi r} \int_0^\infty \frac{\sinh \alpha u}{N} \cos\left(u \log \frac{r}{r_0}\right) du \\ V_t &= -D\left(\frac{1}{r}\frac{\partial}{\partial\theta}\Delta w\right)_{\theta=0} \\ &= \frac{Pr_0}{\pi r^2} \int_0^\infty \frac{U_3}{N} \cos\left(u \log \frac{r}{r_0}\right) du \end{aligned}\right\} \ldots [21]$$

where

$$U_3 = u \cosh \alpha u \sin\alpha + \sinh \alpha u \cos\alpha$$

The construction of the preceding expressions is considerably simplified by the fact that the quotients $\partial w/\partial r$ and $\partial^2 w/\partial r^2$ as well as the twisting moments are zero along the edge.

The computation of previous integrals has been carried out by application of Simpson's rule up to a certain limit ($u = 2$ to $u = 4$) while the remainder could be evaluated in a closed form after neglecting in the integrand the terms $e^{-\alpha u}$ arising from the hyperbolic functions. The distribution of the bending moments and reactive forces along the edges obtained in this way for the opening angle of 90 deg is plotted in Fig. 2. The deflection of the plate at the point of application of the load given in the same figure has been computed from Equation [19].

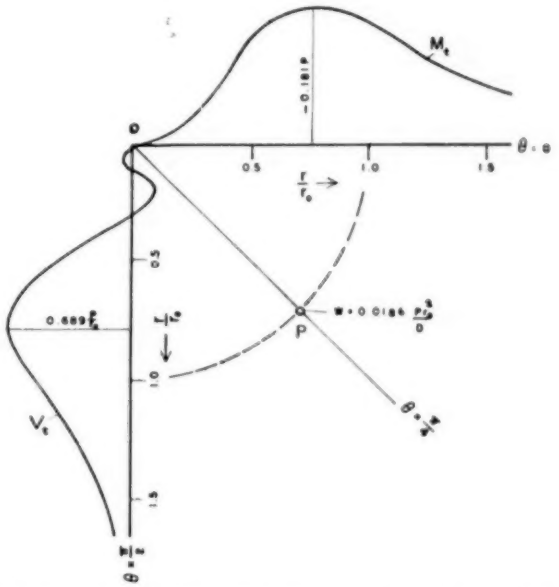

Fig. 2 Bending Moments and Reactions Acting Along the Radial Edges of a Plate Clamped in an Angle With 90 Deg Opening and Subjected to a Single Load ($\alpha = \pi/4$)

For opening angles more than 180 deg the bending moment and reactions can increase to infinity approaching the corner point $r = 0$ of the plate (10). A more detailed investigation of stress distribution near this point will be given in the particular case of an opening angle of 360 deg.

Corner With Opening of 180 Deg

In the particular case of $\alpha = \pi/2$ the denominator of both integrands in Equations [21] is reduced to $N = \sinh \pi u$. The resulting expressions

$$\left.\begin{aligned} M_t^\circ &= -\frac{Pr_0}{2\pi r} \int_0^\infty \frac{\cos\left(u \log \frac{r}{r_0}\right)}{\cosh(\pi u/2)} du = -\frac{Pr_0^2}{\pi(r^2 + r_0^2)} \\ V_t &= \frac{Pr_0}{2\pi r^2} \int_0^\infty \frac{u \cos\left(u \log \frac{r}{r_0}\right)}{\sinh(\pi u/2)} du = \frac{2Pr_0^2}{\pi(r^2 + r_0^2)^2} \end{aligned}\right\} \ldots [22]$$

can also be obtained from the known solution of J. H. Michell for the bending of an infinitely extended cantilever plate under the action of a single load. The corresponding distribution of the edge forces is shown in Fig. 3. It should be noted that the opening angle of 180 deg is the only one giving for M_t° and V_t finite values other than zero at $r = 0$.

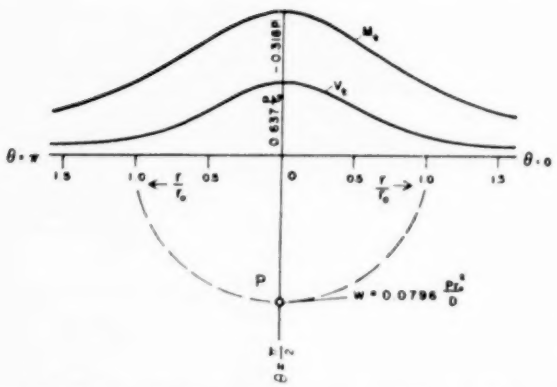

FIG. 3 BENDING MOMENTS AND REACTIONS ALONG THE EDGE OF AN INFINITE CANTILEVER PLATE WITH A SINGLE LOAD ($\alpha = \pi/2$)

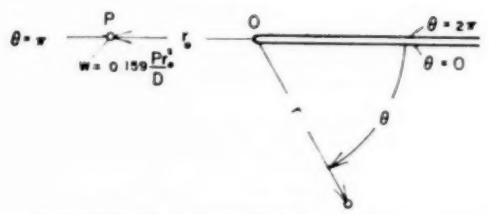

FIG. 4 INFINITE PLATE CLAMPED IN ONE HALF OF A STRAIGHT LINE AND CARRYING A SINGLE LOAD ($\alpha = \pi$)

CORNER WITH OPENING OF 360 DEG

The assumption $\alpha = \pi$ leads to the curious case of an infinite plate rigidly clamped in one half of a straight line, Fig. 4. One has now simply $N = \sinh 2\pi u$ which allows a straightforward representation of the integral contained in Equation [19] as a sum of residues of the integrand in poles which lie in the upper half plane of the complex variable u (reference 11). The position of these poles being given by $u = mi/2$ ($m = 1, 3, 5, \ldots$), the result of evaluation is

$$w = \frac{Prr_0}{\pi D} \sum_{m=1,3,5}^{\infty} \frac{2\cos\theta \sin\frac{m\theta}{2} - m\sin\theta\cos\frac{m\theta}{2}}{m(m^2-4)} (-1)^{\frac{m-1}{2}} \left(\frac{r}{r_0}\right)^{\frac{m}{2}} \quad [23]$$

This expression holds for $0 \leq \theta \leq \pi$, $0 \leq r/r_0 \leq 1$ and r is to interchange with r_0 for $r/r_0 \geq 1$. The value of the deflection at $r = r_0$, $\theta = \pi$ is consequently

$$w_0 = \frac{2Pr_0^2}{\pi D} \sum_{m=1,3,5}^{\infty} \frac{1}{m(4-m^2)} \quad [24]$$

and the result of the summation of this series is given in Fig. 4.

Because of $\sin\alpha = 0$ the moments M_t^0 are zero along the edge which is, however, not the case for bending moments near the corner point itself. In order to obtain the stress distribution for $r \to 0$ let us restrict the sum Equation [23] to its initial term. One has then for the radial and the tangential moments the approximate expressions

$$\left.\begin{aligned} M_r &\sim -\frac{P}{8\pi}\left[\left(3\sin\frac{\theta}{2} - \sin\frac{3\theta}{2}\right) + \nu\left(5\sin\frac{\theta}{2} + \sin\frac{3\theta}{2}\right)\right]\left(\frac{r}{r_0}\right)^{-\frac{1}{2}} \\ M_t &\sim -\frac{P}{8\pi}\left[\left(5\sin\frac{\theta}{2} + \sin\frac{3\theta}{2}\right) + \nu\left(3\sin\frac{\theta}{2} - \sin\frac{3\theta}{2}\right)\right]\left(\frac{r}{r_0}\right)^{-\frac{1}{2}} \end{aligned}\right\} \quad [25]$$

while the remainder is of the order $(r/r_0)^{1/2}$. Therefore, when approaching the corner point $r = 0$, the bending moments increase as $r^{-1/2}$. Their logarithmic increase near the single load can be shown by taking again into consideration the full series Equation [23]. The singular part of bending moments is contained in the quantity

$$M_r + M_t = -D(1+\nu)\Delta w$$

$$= -\frac{P(1+\nu)}{\pi} \sum_{m=1,3,5}^{\infty} \frac{\sin\frac{(m-2)\theta}{2}}{m-2} (-1)^{\frac{m-1}{2}} \left(\frac{r}{r_0}\right)^{\frac{m-2}{2}} \quad [26]$$

The summation of this series, easy to perform, gives for $\theta = \pi$

$$M_r + M_t = \frac{P(1+\nu)}{\pi}\left(\frac{1}{2}\log\frac{r_0+r}{r_0-r} - 1\right) \quad [27]$$

which is the desired result. Equation [26] can be used as well to obtain the distribution of reactions along the edge and the result

$$V_t = -D\left(\frac{1}{r}\frac{\partial}{\partial\theta}\Delta w\right)_{\theta=0} = -\frac{P}{2\pi(r+r_0)}\left(\frac{r_0}{r}\right)^{\frac{3}{2}} \quad [28]$$

is valid for $0 < r < \infty$.

Let us consider next the behavior of the shearing forces near $r = 0$. Taking into consideration but the initial term of the series Equation [26], one arrives at the approximate expressions

$$\left.\begin{aligned} Q_r &= -D\frac{\partial}{\partial r}\Delta w \sim \frac{P}{2\pi} r_0^{\frac{1}{2}} r^{-\frac{3}{2}} \sin\frac{\theta}{2} \\ Q_t &= -\frac{D}{r}\frac{\partial}{\partial\theta}\Delta w \sim -\frac{P}{2\pi} r_0^{\frac{1}{2}} r^{-\frac{3}{2}} \cos\frac{\theta}{2} \end{aligned}\right\} \quad [29]$$

showing that the forces Q increase to infinity with $r \to 0$.

Let us determine, finally, the resultant shearing force

$$R_r = 2\int_0^{\pi} Q_r r d\theta \sim \frac{2P}{\pi}\left(\frac{r_0}{r}\right)^{\frac{1}{2}} \quad [30]$$

as well as the total reaction transmitted to the plate by the edges $\theta = 0$ and $\theta = 2\pi$ together. Making use of Equation [28] and leaving for the present the lower limit of the integration free one concludes that

$$R_t = 2\int_r^{\infty} V_t dr \sim P - \frac{2P}{\pi}\left(\frac{r_0}{r}\right)^{\frac{1}{2}} - \frac{2P}{\pi}\arctan\sqrt{\frac{r}{r_0}} \quad [31]$$

The result

$$\lim_{r \to 0}(R_r + R_t) = P \quad [32]$$

readily obtainable from Equations [30] and [31] asserts the simple fact that both reactive forces R_r and R_t, although unbounded

near $r = 0$, compensate each other with a positive excess equal to the value of the single load P applied to the plate.

Application of Solution to a Sectorial Plate

A certain analogy existing between the solution of the form of Equation [5] and the general solution obtainable by Lévy's method for the rectangular plate with two opposite edges simply supported becomes more evident by consideration of a plate bounded by two radial edges and two circular arcs, say $r = b > 0$ and $r = a > b$.

At first let us expand a given function $\psi(r)$ in a series of the form

$$\psi(r) = \sum_{n=1}^{\infty} a_n \sin\left(n\pi \frac{\log \frac{ar}{b^2}}{\log \frac{a}{b}}\right) \quad \ldots\ldots [33]$$

for $b \leq r \leq a$. Multiplying both sides of this equation by

$$\sin\left(n'\pi \frac{\log \frac{ar}{b^2}}{\log \frac{a}{b}}\right) \frac{dr}{r}$$

where n' is an integer and integrating the result between $r = a$ and $r = b$, one arrives at the expression

$$a_n = \frac{2}{\log \frac{a}{b}} \int_b^a \sin\left(n\pi \frac{\log \frac{ar}{b^2}}{\log \frac{a}{b}}\right) \frac{\psi(r)dr}{r} \quad \ldots\ldots [34]$$

If, in particular, $\psi(r) = r^2 P$ at $r = r_0$ and $\psi(r) = 0$ for $r \neq r_0$, then

$$\psi(r, r_0) = \frac{2Pr_0}{\log \frac{a}{b}} \sum_{n=1}^{\infty} \sin\left(n\pi \frac{\log \frac{ar_0}{b^2}}{\log \frac{a}{b}}\right) \sin\left(n\pi \frac{\log \frac{ar}{b^2}}{\log \frac{a}{b}}\right) [35]$$

Comparing this result with Equation [15] and observing the solution in Equation [19] one concludes that the deflection of a plate clamped for instance along the radial edges $\theta = 0$, 2α and subjected to a single load P at $r = r_0$, $\theta = \alpha$ is given by

$$w = \frac{Pr r_0}{D \log \frac{a}{b}} \sum_{n=1}^{\infty} \frac{O_1 U_1 + O_2 U_2}{(1 + u_n^2) u_n N} \sin\left(u_n \log \frac{ar_0}{b^2}\right) \times \sin\left(u_n \log \frac{ar}{b^2}\right) \quad [36]$$

in which $u_n = n\pi/\log a/b$ and besides that the notation, Equations [20], holds with u_n instead of u. The deflection clearly vanishes on $r = a$, $r = b$, but such is the case neither with the slope $\partial w/\partial r$ nor with the radial bending moments acting along the curved edges of the plate.

BIBLIOGRAPHY

1 "Some Problems in the Bending of Thin Plates," by G. F. Carrier and F. S. Shaw, Proceedings of Symposia in Applied Mathematics, vol. 3, 1950, p. 125.

2 "The Bending of Uniformly Loaded Clamped Plate in the Form of a Circular Sector," by H. R. Hassé, *The Quarterly Journal of Mechanics and Applied Mathematics*, Oxford, England, vol. 3, 1950, p. 271.

3 "The Integral Equation of Bending of a Sectorial Plate With Fixed Radial Edges," by Y. S. Uflyand, Doklady Akademii Nauk SSSR, vol. 72, 1950, p. 251.

4 "The Bending of Sectorial Plates With Fixed Boundary," by Y. S. Uflyand, Akademia Nauk SSSR, Prikladnaya Matematika y Mehanika, vol. 15, 1951, p. 515.

5 "The Bending of the Clamped Sectorial Plate," by G. F. Carrier, Journal of Applied Mechanics, Trans. ASME, vol. 66, 1944, p. A-134.

6 "Theory of Plates and Shells," by S. Timoshenko, McGraw-Hill Book Company, Inc., New York, N. Y., first edition, 1940, p. 174.

7 "The Use of the Mellin Transform in Finding the Stress Distribution in an Infinite Wedge," by C. J. Tranter, *The Quarterly Journal of Mechanics and Applied Mathematics*, Oxford, England, vol. 1, 1948, p. 125.

8 "The Bending of a Wedge-Shaped Clamped Plate Under Action of an Arbitrary Load," by I. E. Saharov, Doklady Akademii Nauk SSSR, vol. 70, 1948, p. 407.

9 "The Theory of a Thin Elastic Plate, Bounded by Two Circular Arcs and Clamped," by A. C. Dixon, Proceedings of the Mathematical Society of London, England, vol. 19, 1920, p. 373.

10 "Surface Strain Singularities Resulting From Various Boundary Conditions in Angular Corner of Plates Under Bending," by M. L. Williams, Jr., First U. S. National Congress of Applied Mechanics.

11 "A Course of Modern Analysis," by E. T. Whittaker and G. N. Watson, University Press, Cambridge, England, fourth edition, 1927, p. 115.

The Stress Distributions Induced by Concentrated Loads Acting in Isotropic and Orthotropic Half Planes

By H. D. CONWAY,[1] ITHACA, N. Y.

Using a Fourier integral method, the solution is obtained to an isotropic half plane subjected to a concentrated load acting at some distance from the straight edge. This problem was discussed previously by Melan,[2] using a complex variable method of solution. The Fourier integral method is then extended to solve the corresponding problems of the orthotropic half plane.

Introduction

THE use of stress functions in the form of Fourier integrals is valuable in the solution of plane-stress problems, many isotropic problems having been treated by Girkmann.[3] In a recent paper,[4] it was shown that the method may be extended easily to problems in orthotropic plane stress.

The object of the present discussion is to use the Fourier integral method to solve the problem of the half plane subjected to a concentrated load acting at some finite distance from the straight edge. For illustrative purposes, the isotropic half plane problem is first solved, the results obtained being the same as those previously given by Melan.[2] The results are then extended to include the more general problem of the orthotropic half plane. In that which follows, the principal axes of orthotropy are x, y.

Analysis

(*a*) *Isotropic Half Plane Load Line Normal to Straight Edge.* The problem to be solved is shown diagrammatically in Fig. 1, the distance a being finite. To solve this problem, we first consider the isotropic plane loaded as shown in Fig. 2. The stresses induced for this case may be written down immediately by superposition from the solution to the plane subjected to a single concentrated load.[5] They are

$$\left.\begin{aligned}
\sigma_y &= -\frac{P(1+\nu)}{4\pi}\left\{1-\nu\left[\frac{y+a}{x^2+(y+a)^2}-\frac{y-a}{x^2+(y-a)^2}\right]-2x^2\left[\frac{y+a}{[x^2+(y+a)^2]^2}-\frac{y-a}{[x^2+(y-a)^2]^2}\right]\right\}\\
\sigma_x &= \frac{P(1+\nu)}{4\pi}\left\{3+\nu\left[\frac{y+a}{x^2+(y+a)^2}-\frac{y-a}{x^2+(y-a)^2}\right]-2x^2\left[\frac{y+a}{[x^2+(y+a)^2]^2}-\frac{y-a}{[x^2+(y-a)^2]^2}\right]\right\}\\
\tau_{xy} &= \frac{Px(1+\nu)}{4\pi}\left\{1-\nu\left[\frac{1}{x^2+(y+a)^2}-\frac{1}{x^2+(y-a)^2}\right]+2\left[\frac{(y+a)^2}{[x^2+(y+a)^2]^2}-\frac{(y-a)^2}{[x^2+(y-a)^2]^2}\right]\right\}
\end{aligned}\right\} \quad \ldots [1]$$

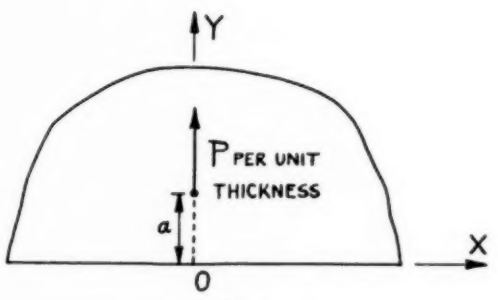

Fig. 1

The shearing stress is zero on $y = 0$ and

$$\left.\begin{aligned}
(\sigma_y)_{y=0} &= \frac{P(1+\nu)}{2\pi}\left\{\frac{3+\nu}{1+\nu}\frac{a}{x^2+a^2}-\frac{2ax^2}{(x^2+a^2)^2}\right\}\\
&= \frac{P(1+\nu)}{2\pi}\left\{\frac{2}{1+\nu}\frac{a}{x^2+a^2}+\frac{a(a^2-x^2)}{(x^2+a^2)^2}\right\}
\end{aligned}\right\} \quad \ldots [2]$$

Noting that $\displaystyle\int_0^\infty e^{-\alpha a}\cos\alpha x\, d\alpha = \frac{a}{x^2+a^2}$;

we write $\displaystyle\int_0^\infty \alpha e^{-\alpha a}\cos\alpha x\, d\alpha = \frac{a^2-x^2}{(x^2+a^2)^2}$

$$(\sigma_y)_{y=0} = \frac{P(1+\nu)}{2\pi}\int_0^\infty\left(\frac{2}{1+\nu}+\alpha a\right)e^{-\alpha a}\cos\alpha x\, d\alpha \quad [3]$$

---

[1] Professor of Mechanics, Cornell University. Jun. ASME.

[2] "Der Spannungszustand der durch eine Einzelkraft im Innern beanspruchten Halbscheibe," by E. Melan, *Zeitschrift für angewandte Mathematik und Mechanik*, vol. 12, 1932, p. 343.

[3] "Flächentragwerke," by K. Girkmann, Julius Springer-Verlag, Vienna, Austria, 1946.

[4] "Some Problems of Orthotropic Plane Stress," by H. D. Conway, contributed by Applied Mechanics Division and presented at the Annual Meeting, New York, N. Y., Nov. 30–Dec. 5, 1952, of, The American Society of Mechanical Engineers. Paper No. 52—A-4.

[5] "Theory of Elasticity," by S. Timoshenko and J. N. Goodier, McGraw-Hill Book Company, Inc., New York, N. Y., and London, England, second edition, 1951, p. 114.

Contributed by the Applied Mechanics Division and presented at the Annual Meeting, New York, N. Y., November 30–December 5, 1952, of The American Society of Mechanical Engineers.

Discussion of this paper should be addressed to the Secretary, ASME, 29 West 39th Street, New York, N. Y., and will be accepted until April 10, 1953, for publication at a later date. Discussion received after the closing date will be returned.

Note: Statements and opinions advanced in papers are to be understood as individual expressions of their authors and not those of the Society.

Manuscript received by ASME Applied Mechanics Division, June 9, 1952. Paper No. 52—A-14.

The next step is to solve the problem of the isotropic half plane subjected on its straight boundary to the loading given by Equation [3]. To do this, we write the Airy stress function in the form

$$\phi = \int_0^\infty \frac{1}{\alpha^2}(A + \alpha y B)e^{-\alpha y}\cos \alpha x \, d\alpha; \quad y \geqslant 0$$

which gives

$$\left.\begin{aligned}
\sigma_x &= \frac{\partial^2\phi}{\partial y^2} = \int_0^\infty [(A - 2B) + \alpha y B]e^{-\alpha y}\cos \alpha x \, d\alpha \\
\sigma_y &= \frac{\partial^2\phi}{\partial x^2} = -\int_0^\infty (A + \alpha y B)e^{-\alpha y}\cos \alpha x \, d\alpha \\
\tau_{xy} &= -\frac{\partial^2\phi}{\partial x \, \partial y} = -\int_0^\infty [(A - B) + \alpha y B]e^{-\alpha y}\sin \alpha x \, d\alpha
\end{aligned}\right\} \quad \ldots\ldots [4]$$

Using the boundary condition given by Equation [3] and remembering that the shearing stress is zero on $y = 0$, we obtain

$$A = B = \frac{-P(1+\nu)}{2\pi}\left(\frac{2}{1+\nu} + \alpha a\right)e^{-\alpha a}$$

and hence, from Equations [4]

$$\sigma_x = \frac{P(1+\nu)}{2\pi}\int_0^\infty \left(\frac{2}{1+\nu} + \alpha a\right)(1 - \alpha y)e^{-\alpha(y+a)}\cos \alpha x \, d\alpha$$

$$\sigma_y = \frac{P(1+\nu)}{2\pi}\int_0^\infty \left(\frac{2}{1+\nu} + \alpha a\right)(1 + \alpha y)e^{-\alpha(y+a)}\cos \alpha x \, d\alpha$$

$$\tau_{xy} = \frac{P(1+\nu)}{2\pi}\int_0^\infty \left(\frac{2}{1+\nu} + \alpha a\right)\alpha y e^{-\alpha(y+a)}\sin \alpha x \, d\alpha$$

The integrations are easily performed and

$$\left.\begin{aligned}
\sigma_x &= \frac{P(1+\nu)}{2\pi}\left\{\frac{2}{1+\nu}\frac{y+a}{x^2+(y+a)^2} - \frac{2y}{1+\nu}\frac{[(y+a)^2 - x^2]}{[x^2+(y+a)^2]^2} + \frac{a[(y+a)^2 - x^2]}{[x^2+(y+a)^2]^2} + \frac{2ay(y+a)[3x^2 - (y+a)^2]}{[x^2+(y+a)^2]^3}\right\} \\
\sigma_y &= \frac{P(1+\nu)}{2\pi}\left\{\frac{2}{1+\nu}\frac{y+a}{x^2+(y+a)^2} + \frac{2y}{1+\nu}\frac{(y+a)^2 - x^2}{[x^2+(y+a)^2]^2} + \frac{a[(y+a)^2 - x^2]}{[x^2+(y+a)^2]^2} - \frac{2ay(y+a)[3x^2 - (y+a)^2]}{[x^2+(y+a)^2]^3}\right\} \\
\tau_{xy} &= \frac{Px(1+\nu)}{2\pi}\left\{\frac{2y}{1+\nu}\frac{2(y+a)}{[x^2+(y+a)^2]^2} + \frac{2ay[3(y+a)^2 - x^2]}{[x^2+(y+a)^2]^3}\right\}
\end{aligned}\right\} \quad .[5]$$

Subtracting Equations [5] from Equations [1], the problem, shown in Fig. 1, is solved and we obtain, after rearranging

$$\left.\begin{aligned}
\sigma_x &= \frac{-P(1+\nu)}{4\pi}\left\{2\left[\frac{x^2(y-a)}{[x^2+(y-a)^2]^2} + \frac{(y+a)(x^2+2a^2) - 2ax^2}{[x^2+(y+a)^2]^2} + \frac{8ay(a+y)x^2}{[x^2+(y+a)^2]^3}\right]\right. \\
&\quad \left. + \frac{1-\nu}{1+\nu}\left[-\frac{(y-a)}{x^2+(y-a)^2} + \frac{y+3a}{x^2+(y+a)^2} + \frac{4x^2y}{[x^2+(y+a)^2]^2}\right]\right\} \\
\sigma_y &= \frac{-P(1+\nu)}{4\pi}\left\{2\left[\frac{(y-a)^3}{[x^2+(y-a)^2]^2} + \frac{(y+a)[(y+a)^2 + 2ay]}{[x^2+(y+a)^2]^2} - \frac{8ay(a+y)x^2}{[x^2+(y+a)^2]^3}\right]\right. \\
&\quad \left. + \frac{1-\nu}{1+\nu}\left[\frac{y-a}{x^2+(y-a)^2} + \frac{3y+a}{x^2+(y+a)^2} - \frac{4x^2y}{[x^2+(y+a)^2]^2}\right]\right\} \\
\tau_{xy} &= \frac{-Px(1+\nu)}{4\pi}\left\{2\left[\frac{(y-a)^2}{[x^2+(y-a)^2]^2} + \frac{y^2 - 2ay - a^2}{[x^2+(y+a)^2]^2} + \frac{8ay(a+y)^2}{[x^2+(y+a)^2]^3}\right]\right. \\
&\quad \left. + \frac{1-\nu}{1+\nu}\left[\frac{1}{x^2+(y-a)^2} - \frac{1}{x^2+(y+a)^2} + \frac{4y(a+y)}{[x^2+(y+a)^2]^2}\right]\right\}
\end{aligned}\right\} \quad \ldots [6]$$

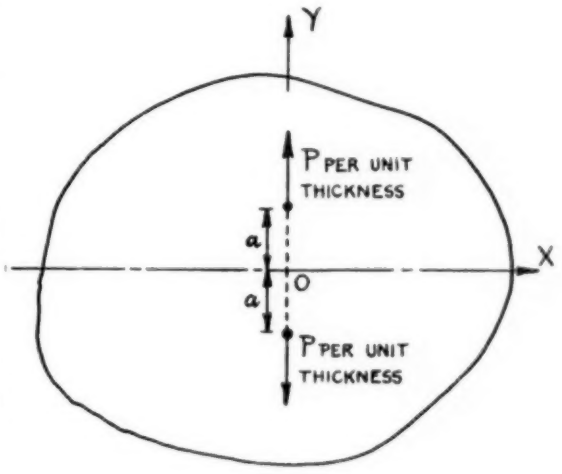

FIG. 2

These are Melan's results.[3]

(*b*) *Orthotropic Half Plane—Load Line Normal to Straight Edge.* The problem, shown in Fig. 1, will now be solved for the orthotropic half plane. As has been shown in a previous paper,[4] problems in orthotropic plane stress resolve themselves into the solution of the equation

$$\left(\frac{\partial^2}{\partial x^2} + k^2\frac{\partial^2}{\partial y^2}\right)\left(\frac{\partial^2\phi}{\partial x^2} + \frac{\partial^2\phi}{\partial y^2}\right) = 0$$

subject to the boundary conditions, where $k^2 = E_y/E_x$ is the ratio of the moduli of elasticity in the X and Y-directions. As in isotropic plane stress, the stresses are given by

$$\sigma_x = \frac{\partial^2\phi}{\partial y^2}; \quad \sigma_y = \frac{\partial^2\phi}{\partial x^2}; \quad \tau_{xy} = -\frac{\partial^2\phi}{\partial x \, \partial y}$$

The principal axes of orthotropy are x, y.

Using the results obtained in a previous paper[4] for the orthotropic plane subjected to a concentrated load, the problem shown in Fig. 2 yields the stresses

$$\left.\begin{aligned}
\sigma_x &= \frac{-P}{2\pi(1-k^2)}\left\{(1+k^2\nu)\left[\frac{y+a}{x^2+(y+a)^2}-\frac{y-a}{x^2+(y-a)^2}\right]\right.\\
&\qquad\left.-k(1+\nu)\left[\frac{y+a}{k^2x^2+(y+a)^2}-\frac{y-a}{k^2x^2+(y-a)^2}\right]\right\}\\
\sigma_y &= \frac{P}{2\pi(1-k^2)}\left\{(1+k^2\nu)\left[\frac{y+a}{x^2+(y+a)^2}-\frac{y-a}{x^2+(y-a)^2}\right]\right.\\
&\qquad\left.-k^2(1+\nu)\left[\frac{y+a}{k^2x^2+(y+a)^2}-\frac{y-a}{k^2x^2+(y-a)^2}\right]\right\}\\
\tau_{xy} &= \frac{Px}{2\pi(1-k^2)}\left\{(1+k^2\nu)\left[\frac{1}{x^2+(y+a)^2}-\frac{1}{x^2+(y-a)^2}\right]\right.\\
&\qquad\left.-k^2(1+\nu)\left[\frac{1}{k^2x^2+(y+a)^2}-\frac{1}{k^2x^2+(y-a)^2}\right]\right\}
\end{aligned}\right\}\quad\ldots\ldots[7]$$

where ν is defined by the equation

$$\epsilon_y = \frac{\sigma_y}{E_y} - \nu\frac{\sigma_x}{E_x}$$

The shearing stress is zero on $y = 0$ and

$$(\sigma_y)_{y=0} = \frac{Pk^2a}{\pi(k^2-1)}\left[\frac{k(1+\nu)}{k^2x^2+a^2}-\frac{1+k^2\nu}{k^2(x^2+a^2)}\right]\quad\ldots[8]$$

Since

$$\int_0^\infty e^{-\alpha a}\cos\alpha x\,d\alpha = \frac{a}{x^2+a^2}$$

$$\int_0^\infty e^{-\alpha a/k}\cos\alpha x\,d\alpha = \frac{ka}{k^2x^2+a^2}$$

we write

$$(\sigma_y)_{y=0} =$$

$$\frac{P}{\pi(k^2-1)}\left\{\begin{aligned}&k^2(1+\nu)\int_0^\infty e^{-\alpha a/k}\cos\alpha x\,d\alpha\\&-(1+k^2\nu)\int_0^\infty e^{-\alpha a}\cos\alpha x\,d\alpha\end{aligned}\right\}\quad[9]$$

To solve the problem of the orthotropic half plane subjected to this loading on its straight edge, we write the stress function in the form

$$\phi = \int_0^\infty \frac{1}{\alpha^2}(Ae^{-\alpha y}+Be^{-\alpha y/k})\cos\alpha x\,d\alpha;\quad y\geq 0$$

which gives

$$\left.\begin{aligned}
\sigma_x &= \frac{\partial^2\phi}{\partial y^2} = \int_0^\infty\left(Ae^{-\alpha y}+\frac{B}{k^2}e^{-\alpha y/k}\right)\cos\alpha x\,d\alpha\\
\sigma_y &= \frac{\partial^2\phi}{\partial x^2} = -\int_0^\infty(Ae^{-\alpha y}+Be^{-\alpha y/k})\cos\alpha x\,d\alpha\\
\tau_{xy} &= -\frac{\partial^2\phi}{\partial x\,\partial y} = \int_0^\infty\left(Ae^{-\alpha y}+\frac{B}{k}e^{-\alpha y/k}\right)\sin\alpha x\,d\alpha
\end{aligned}\right\}\quad\ldots[10]$$

From Equation [9] and from the fact that the shearing stress is zero on $y = 0$

$$A = -\frac{B}{k} = \frac{P}{\pi(1-k)(1-k^2)}[k^2(1+\nu)e^{-\alpha a/k}-(1+k^2\nu)e^{-\alpha a}]$$

Thus, from Equations [10], we obtain, after integrating

$$\left.\begin{aligned}
\sigma_x &= \frac{-P}{\pi(1-k)(1-k^2)}\left\{(1+k^2\nu)\left[\frac{y+a}{x^2+(y+a)^2}-\frac{y+ka}{k^2x^2+(y+ka)^2}\right]\right.\\
&\qquad\left.-k^2(1+\nu)\left[\frac{k(y+a)}{k^2x^2+(ky+a)^2}-\frac{y+a}{k^2x^2+(y+a)^2}\right]\right\}\\
\sigma_y &= \frac{P}{\pi(1-k)(1-k^2)}\left\{(1+k^2\nu)\left[\frac{y+a}{x^2+(y+a)^2}-\frac{k^2(y+ka)}{k^2x^2+(y+ka)^2}\right]\right.\\
&\qquad\left.-k^2(1+\nu)\left[\frac{ky+a}{k^2x^2+(ky+a)^2}-\frac{k(y+a)}{k^2x^2+(y+a)^2}\right]\right\}\\
\tau_{xy} &= \frac{Px}{\pi(1-k)(1-k^2)}\left\{(1+k^2\nu)\left[\frac{1}{x^2+(y+a)^2}-\frac{k^2}{k^2x^2+(y+ka)^2}\right]\right.\\
&\qquad\left.k^2(1+\nu)\left[\frac{1}{k^2x^2+(ky+a)^2}-\frac{1}{k^2x^2+(y+a)^2}\right]\right\}
\end{aligned}\right\}\quad\ldots[11]$$

Subtracting Equations [11] from Equations [7], the orthotropic version of the problem shown in Fig. 1 yields the stresses

$$\left.\begin{aligned}
\sigma_x &= \frac{-P}{2\pi(1-k^2)}\left\{(1+k^2\nu)\left[\frac{y+a}{x^2+(y+a)^2}-\frac{y-a}{x^2+(y-a)^2}\right]-k(1+\nu)\left[\frac{y+a}{k^2x^2+(y+a)^2}-\frac{y-a}{k^2x^2+(y-a)^2}\right]\right\}\\
&\quad+\frac{P}{\pi(1-k)(1-k^2)}\left\{(1+k^2\nu)\left[\frac{y+a}{x^2+(y+a)^2}-\frac{y+ka}{k^2x^2+(y+ka)^2}\right]\right.\\
&\quad\left.-k^2(1+\nu)\left[\frac{k(ky+a)}{k^2x^2+(ky+a)^2}-\frac{y+a}{k^2x^2+(y+a)^2}\right]\right\}\\
\sigma_y &= \frac{P}{2\pi(1-k^2)}\left\{(1+k^2\nu)\left[\frac{y+a}{x^2+(y+a)^2}-\frac{y-a}{x^2+(y-a)^2}\right]-k^2(1+\nu)\left[\frac{y+a}{k^2x^2+(y+a)^2}-\frac{y-a}{k^2x^2+(y-a)^2}\right]\right\}\\
&\quad-\frac{P}{\pi(1-k)(1-k^2)}\left\{(1+k^2\nu)\left[\frac{y+a}{x^2+(y+a)^2}-\frac{k^2(y+ka)}{k^2x^2+(y+ka)^2}\right]\right.\\
&\quad\left.-k^2(1+\nu)\left[\frac{ky+a}{k^2x^2+(ky+a)^2}-\frac{k(y+a)}{k^2x^2+(y+a)^2}\right]\right\}\\
\tau_{xy} &= \frac{Px}{2\pi(1-k^2)}\left\{(1+k^2\nu)\left[\frac{1}{x^2+(y+a)^2}-\frac{1}{x^2+(y-a)^2}\right]-k^2(1+\nu)\left[\frac{1}{k^2x^2+(y+a)^2}-\frac{1}{k^2x^2+(y-a)^2}\right]\right\}\\
&\quad-\frac{Px}{\pi(1-k)(1-k^2)}\left\{(1+k^2\nu)\left[\frac{1}{x^2+(y+a)^2}-\frac{k^2}{k^2x^2+(y+ka)^2}\right]\right.\\
&\quad\left.-k^4(1+\nu)\left[\frac{1}{k^2x^2+(ky+a)^2}-\frac{1}{k^2x^2+(y+a)^2}\right]\right\}
\end{aligned}\right\}\quad\ldots[12]$$

It will be observed that for isotropy and $k = 1$, the indeterminate form of the foregoing stresses may be evaluated by L'Hospital's rule to give Equations [6].

(c) Orthotropic Half Plane—Load Line Parallel to Straight Edge. The problem shown diagrammatically in Fig. 3 will now be solved for the case of an orthotropic material. The stresses for the orthotropic plane loaded as shown in Fig. 4 are first written down by superposition from the solution for a single concentrated load given in a previous paper.[4] The stresses are

$$\left.\begin{aligned}
\sigma_x &= \frac{-Px}{2\pi(1-k^2)}\left\{(k^2+\nu)\left[\frac{1}{x^2+(y+a)^2}-\frac{1}{x^2+(y-a)^2}\right]-k(1+\nu)\left[\frac{1}{k^2x^2+(y+a)^2}-\frac{1}{k^2x^2+(y-a)^2}\right]\right\}\\
\sigma_y &= \frac{Px}{2\pi(1-k^2)}\left\{(k^2+\nu)\left[\frac{1}{x^2+(y+a)^2}-\frac{1}{x^2+(y-a)^2}\right]-k^2(1+\nu)\left[\frac{1}{k^2x^2+(y+a)^2}-\frac{1}{k^2x^2+(y-a)^2}\right]\right\}\\
\tau_{xy} &= \frac{-P}{2\pi(1-k^2)}\left\{(k^2+\nu)\left[\frac{y+a}{x^2+(y+a)^2}-\frac{y-a}{x^2+(y-a)^2}\right]-k(1+\nu)\left[\frac{y+a}{k^2x^2+(y+a)^2}-\frac{y-a}{k^2x^2+(y-a)^2}\right]\right\}
\end{aligned}\right\}\quad\ldots[13]$$

where ν is defined by the equation

$$\epsilon_x = \frac{\sigma_x}{E_x} - \nu\frac{\sigma_y}{E_y}$$

As before, the principal axes of orthotropy are x, y.

The stress σ_y is zero on $y = 0$ and

$$\left.\begin{aligned}
(\tau_{xy})_{y=0} &= \frac{-Pa}{\pi(1-k^2)}\left\{\frac{k^2+\nu}{x^2+a^2}-\frac{k(1+\nu)}{k^2x^2+a^2}\right\}\\
&= \frac{-P}{\pi(1-k^2)}\left\{(k^2+\nu)\int_0^\infty e^{-\alpha a}\cos\alpha x\,d\alpha\right.\\
&\quad\left.-(1+\nu)\int_0^\infty e^{-\alpha a/k}\cos\alpha x\,d\alpha\right\}
\end{aligned}\right\}\quad\ldots[14]$$

To solve the problem of the half plane subjected to the loading given by Equation [14], we write the stress function in the form

$$\phi = \int_0^\infty \frac{1}{\alpha^2}(Ae^{-\alpha y}+Be^{-\alpha y/k})\sin\alpha x\,d\alpha;\quad y \geqslant 0$$

from which the stresses are

$$\left.\begin{aligned}
\sigma_x &= \int_0^\infty\left(Ae^{-\alpha y}+\frac{B}{k}e^{-\alpha y/k}\right)\sin\alpha x\,d\alpha\\
\sigma_y &= -\int_0^\infty(Ae^{-\alpha y}+Be^{-\alpha y/k})\sin\alpha x\,d\alpha\\
\tau_{xy} &= \int_0^\infty\left(Ae^{-\alpha y}+\frac{B}{k}e^{-\alpha y/k}\right)\cos\alpha x\,d\alpha
\end{aligned}\right\}\quad\ldots[15]$$

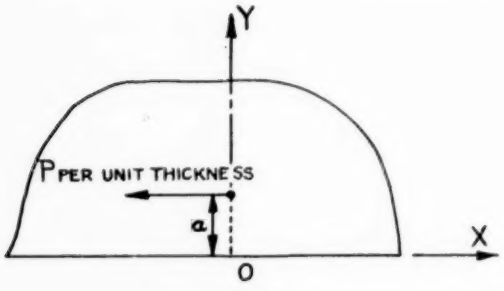

FIG. 3

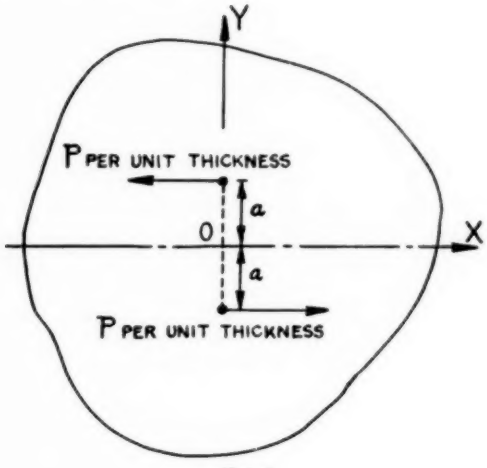

FIG. 4

It follows that

$$A = -B = \frac{Pk}{\pi(1-k)(1-k^2)}\left[(k^2+\nu)e^{-\alpha a} - (1+\nu)e^{-\alpha a/k}\right]$$

From Equations [15] we obtain, after integrating

$$\left.\begin{aligned}
\sigma_x &= \frac{Pkx}{\pi(1-k)(1-k^2)}\left\{(k^2+\nu)\left[\frac{1}{x^2+(y+a)^2} - \frac{1}{k^2x^2+(y+ka)^2}\right]\right. \\
&\qquad \left. -(1+\nu)\left[\frac{k^2}{k^2x^2+(ky+a)^2} - \frac{1}{k^2x^2+(y+a)^2}\right]\right\} \\
\sigma_y &= \frac{-Pkx}{\pi(1-k)(1-k^2)}\left\{(k^2+\nu)\left[\frac{1}{x^2+(y+a)^2} - \frac{1}{k^2x^2+(y+ka)^2}\right]\right. \\
&\qquad \left. -k^2(1+\nu)\left[\frac{1}{k^2x^2+(ky+a)^2} - \frac{1}{k^2x^2+(y+a)^2}\right]\right\} \\
\tau_{xy} &= \frac{Pk}{\pi(1-k)(1-k^2)}\left\{(k^2+\nu)\left[\frac{y+a}{x^2+(y+a)^2} - \frac{y+ka}{k^2x^2+(y+ka)^2}\right]\right. \\
&\qquad \left. -(1+\nu)\left[\frac{k(ky+a)}{k^2x^2+(ky+a)^2} - \frac{y+a}{k^2x^2+(y+a)^2}\right]\right\}
\end{aligned}\right\} \quad \ldots [16]$$

Subtracting Equations [16] from Equations [13], the problem of the orthotropic half plane shown in Fig. 3 is solved and yields the stresses

$$\left.\begin{aligned}
\sigma_x &= \frac{-Px}{2\pi(1-k^2)}\left\{(k^2+\nu)\left[\frac{1}{x^2+(y+a)^2} - \frac{1}{x^2+(y-a)^2}\right] - k(1+\nu)\left[\frac{1}{k^2x^2+(y+a)^2} - \frac{1}{k^2x^2+(y-a)^2}\right]\right\} \\
&\quad \frac{-Pkx}{\pi(1-k)(1-k^2)}\left\{(k^2+\nu)\left[\frac{1}{x^2+(y+a)^2} - \frac{1}{k^2x^2+(y+ka)^2}\right] - (1+\nu)\left[\frac{k^2}{k^2x^2+(ky+a)^2} - \frac{1}{k^2x^2+(y+a)^2}\right]\right\} \\
\sigma_y &= \frac{Px}{2\pi(1-k^2)}\left\{(k^2+\nu)\left[\frac{1}{x^2+(y+a)^2} - \frac{1}{x^2+(y-a)^2}\right] - k^2(1+\nu)\left[\frac{1}{k^2x^2+(y+a)^2} - \frac{1}{k^2x^2+(y-a)^2}\right]\right\} \\
&\quad \frac{+Pkx}{\pi(1-k)(1-k^2)}\left\{(k^2+\nu)\left[\frac{1}{x^2+(y+a)^2} - \frac{1}{k^2x^2+(y+ka)^2}\right] - k^2(1+\nu)\left[\frac{1}{k^2x^2+(ky+a)^2} - \frac{1}{k^2x^2+(y+a)^2}\right]\right\} \\
\tau_{xy} &= \frac{-P}{2\pi(1-k^2)}\left\{(k^2+\nu)\left[\frac{y+a}{x^2+(y+a)^2} - \frac{y-a}{x^2+(y-a)^2}\right] - k(1+\nu)\left[\frac{y+a}{k^2x^2+(y+a)^2} - \frac{y-a}{k^2x^2+(y-a)^2}\right]\right\} \\
&\quad \frac{-Pk}{\pi(1-k)(1-k^2)}\left\{(k^2+\nu)\left[\frac{y+a}{x^2+(y+a)^2} - \frac{y+ka}{k^2x^2+(y+ka)^2}\right] - (1+\nu)\left[\frac{k(ky+a)}{k^2x^2+(ky+a)^2} - \frac{y+a}{k^2x^2+(y+a)^2}\right]\right\}
\end{aligned}\right\} \quad \ldots [17]$$

As before, for the isotropic case when $k = 1$, the indeterminate form of the foregoing equations may be evaluated by L'Hospital's rule.

The End Problem of Rectangular Strips

By G. HORVAY,[1] SCHENECTADY, N. Y.

J. Fadle was first to derive a solution for the stresses in a rectangular strip subject on one of its narrow edges to a self-equilibrating system of stresses; i.e., stresses which have zero resultant force and zero resultant moment. Fadle's solution is rather unwieldy because of the use of complex (biharmonic) eigenfunctions. These eigenfunctions are associated with the roots of the equation $\sin 2\gamma \pm 2\gamma = 0$. The first (nonvanishing) root, as determined to seven decimals by Mittelman and Hillman, is $\gamma_2 = 2.1061961 + 1.1253643i$. In this paper we derive a variational solution of the same problem in the form $\varphi(x, y) = \Sigma c_n \varphi_n$ where, in first approximation, $\varphi_n = f_n(y) g_n(x)$. The series $\Sigma c_n f_n(y)$ is obtained by expansion of the boundary values $\varphi(0, y)$ of the Airy function φ into a complete set of self-equilibrating orthogonal polynomials $f_n(y)$; the functions $g_n(x)$ are then determined from the Euler-Lagrange equations of the associated variational problem. This procedure has the advantage of staying entirely in the real domain. The first approximation corresponds to the physical concept that the longitudinal fibers of the strip are beams on elastic foundation (the adjacent fibers furnish the elastic foundation) subject to end thrusts and lateral loads. Incidental to this idea there are provided quantitative formulas which relate depth of penetration of an applied traction to its shape (number of its wiggles). The eigenvalues γ_n, the real parts of which furnish the extinction coefficients, are obtained from a quadratic equation in γ^2. One finds that the lowest (nonvanishing) eigenvalue is $\gamma_2 = 2.075 + 1.145i$. In higher approximations coupling effects between derivatives of the orthogonal modes $f_n g_n$ are also taken into account. The jth approximation to a mode φ_n is obtained by evaluating a $2j - 1$-rowed determinantal equation involving the functions $f_{n-j+1}\ g_{n-j+1}$ to $f_{n+j-1}\ g_{n+j-1}$. High modes are calculated with the same facility and accuracy as is the fundamental except that the fundamental mode φ_2 not being preceded by other modes, requires, in jth approximation, only a j-rowed determinantal equation. One thus finds that in third approximation γ_2 is the root of a 6th degree equation in γ^2, and has the value $\gamma_2 = 2.1061964 + 1.1253644i$.

Introduction

S. Timoshenko was the first to make systematic use of the variational method in problems of stress analysis. The method, introduced shortly after the turn of the century, found immediate favor, and early textbooks, like Föppl's "Drang und Zwang" leaned heavily on this approach. As the method increased in popularity its shortcomings also became more evident. The method was primarily suited for determining average properties; regions of rapid stress variations, or stress-concentration factors, could not be adequately handled. It was suspected that the class of functions utilized in the variational approach was not the proper one. But the trouble was never really identified or remedied, and as other more exact (and lengthier, differential-equation type) methods were developed the variational approach gradually lost favor.

Timoshenko's first English publications on the variational treatment of plane stress problems appeared in 1923, ten years after the publication of his Russian language book, giving the theory of the method. Independently C. E. Inglis, also treated some plane stress problems in 1923 by the strain energy approach. The method was developed further by J. N. Goodier in 1931, who applied it, in his doctor's dissertation, to several problems of interest (1*a*).[2] Among these is the problem of determining the stresses in the rectangle, Fig. 1 (arrows in lower half of Figure should point outward), due to the applied edge tractions[3]

$$\bar{\sigma}_x = Sy^2 \qquad [1]$$

Assuming a stress function in the form

$$\varphi = \varphi' + (x^2 - a^2)^2 (y^2 - 1)^2 [n_1 y + n_3 x^2 y + n_5 y^3 + n_4 x^2 y^2 + \dots] \qquad [2a]$$

$$\varphi' = Sy^5/20 \qquad [2b]$$

Goodier determined the coefficients $n_1, \dots, n_4$ from the requirement that the strain energy

$$U = \frac{1}{2E} \int_{x=-a}^{+a} dx \int_{y=-1}^{+1} (\varphi_{xx}^2 + 2\varphi_{xy}^2 + \varphi_{yy}^2)\, dy \qquad [3]$$

be a minimum. Other, more involved edge tractions have recently been considered, along the lines of Equation [2], by Conway, Chow, and Morgan (2).

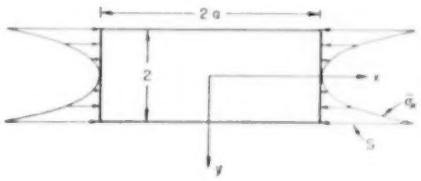

Fig. 1

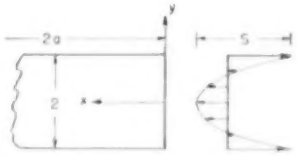

Fig. 2

A similar, but less tractable, problem is that of a semi-infinite strip, free along the edges, loaded by self-equilibrating tractions along the narrow side, as illustrated in Fig. 2. This is a funda-

[1] General Electric Company, Knolls Atomic Power Laboratory. The Knolls Atomic Power Laboratory is operated by the General Electric Company for the Atomic Energy Commission. The work reported here was carried out under contract No. W-31-109 Eng-52.

Contributed by the Applied Mechanics Division and presented at the Annual Meeting, New York, N. Y., November 30–December 5, 1952, of The American Society of Mechanical Engineers.

Discussion of this paper should be addressed to the Secretary, ASME, 29 West 39th Street, New York, N. Y., and will be accepted until April 10, 1953, for publication at a later date. Discussion received after the closing date will be returned.

Note: Statements and opinions advanced in papers are to be understood as individual expressions of their authors, and not those of the Society. Manuscript received by ASME Applied Mechanics Division, April 10, 1952. Paper No. 52—A-2.

[2] Numbers in parentheses refer to the Bibliography at the end of paper.

[3] Bars denote edge tractions. We shall always consider all loads as given per inch thickness of the strip.

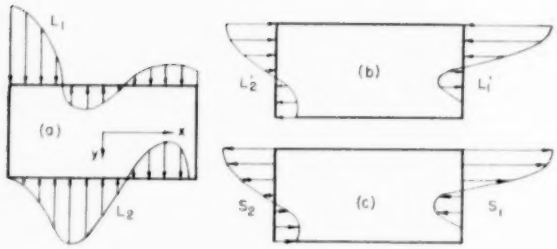

FIG. 3

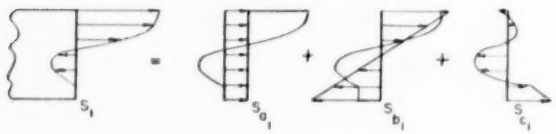

FIG. 4

mental problem of plane elasticity. It usually arises when one considers the general problem of a rectangle, as in Fig. 3(a), under arbitrary edge loading L_1, L_2 on the long sides, s_1, s_2 on the short sides. For simplicity we assume that the combined tractions L_1, L_2 are mutually self-equilibrating, and that so are s_1, s_2. (In Fig. 3(a) we represent the special case when $s_1 = s_2 = 0$.) The most satisfactory analysis of a problem like that of Fig. 3(a) proceeds as follows:

By use of a Fourier series or Fourier integral expansion of the Airy function

$$\varphi_{\text{even}} = \sum_{\alpha} \text{ or } \int_{\alpha} [\{A_0(\alpha) + B_0(\alpha)\alpha y\}e^{-\alpha y} + \{A_2(\alpha) + B_2(\alpha)\alpha y\}e^{\alpha y}]\cos \alpha x d\alpha \quad [4]$$

$$\varphi_{\text{odd}} = \sum_{\alpha} \text{ or } \int_{\alpha} [\{A_1(\alpha) + B_1(\alpha)\alpha y\}e^{-\alpha y} + \{A_2(\alpha) + B_2(\alpha)\alpha y\}e^{\alpha y}]\sin \alpha x d\alpha \quad [5]$$

one can determine the stresses that result from the loading—system L_1, L_2—applied on the long sides. This method is discussed at length in Timoshenko-Goodier (1b) and Girkmann (3). The solutions, Equations [4] and [5], usually create some stresses—we call them L_1', L_2'—on the short sides of the strip, as indicated in Fig. 3(b).

The next task is to evaluate the effect of the resultant S_1 of $-L_1'$ and s_1, and the resultant S_2 of $-L_2'$ and s_2, as indicated in Fig. 3(c). (Remember that, in the figure, we have chosen $s_1 = s_2 = 0$.) This task is carried out in three steps: We decompose the S_1, S_2 stresses, as indicated in Fig. 4 for S_1, into stress systems $S_{a1} = S_{a2}$ causing simple tension, into stress systems $S_{b1} = S_{b2}$ causing simple bending, and into the residual systems S_{c1}, S_{c2} for the two ends which generally differ from each other but each of which is self-equilibrating. Solution for the effects of S_a, S_b is elementary, solution for the effects of S_{c1}, S_{c2} resolves to solution of the problem of the semi-infinite strip.* This presupposes that the rectangle is long enough to permit disregard of interaction between the two end conditions. However it will be shown that when $a \geqslant 1$ then the requirement is satisfied. Thus all rectangles can be treated as semi-infinite strips with respect to loads applied at their narrow sides.

The problem of the semi-infinite strip differs significantly from the problem in Fig. 1. No factors, like $(x^2 - a^2)^2$ of Equation [2], can now be applied to make φ vanish at some convenient place. Nor is one now concerned with average behavior—the averages cancel out, force and moment averages were eliminated purposely before start of the analysis—stress distribution in the immediate neighborhood of the applied tractions is the main concern. This problem therefore requires a more rigorous approach.

A variational treatment of the problem has not been attempted heretofore. However, J. Fadle has obtained a solution by expanding the given boundary tractions into biharmonic eigenfunctions (4). The eigenfunctions Φ_n are of the form

$$\Phi_{\text{even}} = e^{-\gamma x}(\kappa \cos \gamma y + \gamma y \sin \gamma y) \quad [6]$$

$$\Phi_{\text{odd}} = e^{-\gamma x}(\kappa \sin \gamma y + \gamma y \cos \gamma y) \quad [7]$$

The values of the parameters κ_n, γ_n are determined from the requirement that the horizontal edges be free of stresses

$$\sigma_y(x) = \Phi_{xx}(x, \pm 1) = 0, \quad \tau(x) = -\Phi_{xy}(x, \pm 1) = 0 \quad [8]$$

There result the consistency criteria

$$\left.\begin{aligned} \sin 2\gamma + 2\gamma &= 0 \text{ (even case)} \\ \sin 2\gamma - 2\gamma &= 0 \text{ (odd case)} \end{aligned}\right\} \quad [9]$$

the eigenvalues

$$\left.\begin{aligned} \gamma_0 &= 0 & \gamma_1 &= 0 \\ \gamma_2 &= 2.1061 + 1.1254i & \gamma_3 &= 3.7488 + 1.3843i \\ \gamma_4 &= 5.3563 + 1.5516i & \gamma_5 &= 6.9500 + 1.6761i \\ \gamma_6 &= 8.5367 + 1.7755i & &\cdots \end{aligned}\right\} \quad [10]$$

and the amplitude ratios

$$\left.\begin{aligned} \kappa_n &= -\gamma_n \tan \gamma_n \quad \text{(even case)} \\ \kappa_n &= -\gamma_n \cot \gamma_n \quad \text{(odd case)} \end{aligned}\right\} \quad [11]$$

Fadle has listed roots γ_2 to γ_{11} to 5 decimal places, and the foregoing values are taken from his paper. Odd roots γ_3 to γ_{21} to six decimal places are given by A. P. Hillman and H. E. Salzer (5), and even roots γ_2 to γ_8 to seven decimal places are given by B. S. Mittelman and A. P. Hillman (6).

We note that if γ is a root, then so are $-\gamma$ and γ^*, $-\gamma^*$.† Hence

$$\varphi_{\text{even}} = \sum_k (A_{2k}\Re + B_{2k}\Im)\Phi_{2k} \quad [12]$$

$$\varphi_{\text{odd}} = \sum_k (A_{2k+1}\Re + B_{2k+1}\Im)\Phi_{2k+1} \quad [13]$$

are proper expansions of the Airy function into biharmonic eigenfunctions. The coefficients A_n, B_n, must be determined from the prescribed boundary conditions

$$\varphi_{yy}(0, y) = \sigma_x, \quad -\varphi_{xy}(0, y) = \tau \quad [14]$$

While Fadle's functions Φ_n satisfy the stress equations exactly, their linear combinations, Equations [12], [13] are likely to adhere to the boundary conditions [14] rather poorly, because determination of the expansion coefficients A_n, B_n for these unwieldy complex functions is a laborious job; in a practical problem the series, Equations [12] and [13], are likely to be terminated after just a few terms.

The method to be followed attacks the problem from the opposite end. We shall satisfy the boundary conditions exactly, but the stress equations only approximately. This approach will prove preferable because it enables us to stay entirely in the real domain and work with simple, fast converging, and at the same time, physically significant functions.

* In the present example, where L_1 and L_2 are mutually equilibrating, $S_a = S_b = 0$.

† Conjugate is noted by a star. $\Re$ and $\Im$ stand for real part and imaginary part, respectively.

The Variational Method

We write the stress function, i.e., the solution of the equation

$$\nabla^4\varphi = 0 \quad \ldots\ldots [15]$$

in the form

$$\varphi(x, y) = \Sigma\, c_k\varphi_k = \Sigma\, c_k f_k(y) g_k(x) \quad \ldots\ldots [16]$$

where for f_k we shall use the complete set of orthonormal polynomials that are appropriate for the prescribed homogeneous boundary conditions (at $y = \pm 1$); the g_k-factors will be determined from the Euler-Lagrange equations that result from minimization of the strain energy. We owe inspiration for this approach to E. Reissner's numerous papers (7). Other authors have also applied the variational method to expansions in product functions, notably Kantorovitch (8), Poritsky (9), as well as Goodier and his students (10). Poritsky, in particular, has considered general expansions of the form $\varphi(x, y) = \Sigma\, c_k f_k(x, y)\, g_k(x)$, and has established Equations [21].

We first treat the case when

$$\varphi(x, y) = \frac{S}{12}(1 - y^2)^2 g(x);\ g(0) = 1,\ g'(0) = g(\infty) = g'(\infty) = 0 \quad \ldots\ldots [17]$$

(We use the abbreviations $f' = df(y)/dy$, $g' = dg(x)/dx$.) One obtains

$$\left.\begin{aligned} &\varphi_{yy}(0, y) = \sigma_x(y) = S(y^2 - 1/3),\ -\varphi_{xy}(0, y) = \tau(y) = 0 \\ &\varphi_{xx}(x, \pm 1) = \sigma_y(x) = 0,\ -\varphi_{xy}(x, \pm 1) = \tau(x) = 0 \end{aligned}\right\} \quad \ldots\ldots [18]$$

i.e., the foregoing φ represents the stresses that result from a parabolically distributed self-equilibrating traction $\sigma_x = S(y^2 - 1/3)$ applied at the edge, $x = 0$, as illustrated in Fig. 2. Variation of the strain energy

$$U = \frac{1}{2E}\int_0^\infty dx \int_{-1}^{+1} (\varphi_{xx}^2 + 2\varphi_{xy}^2 + \varphi_{yy}^2)\, dy \quad [19a]$$

$$= \frac{S^2}{E}\int_0^\infty dx \int_0^1 \left[\frac{(1 - y^2)^4}{144} g''^2 + \frac{2}{9} y^2(1 - y^2)^2 g'^2 + \left(\frac{1}{3} - y^2\right)^2 y^2\right] dy$$

$$= \frac{8/3}{9!!}\frac{S^2}{E}\int_0^\infty \left[y^{iv} + 6g'^2 + \frac{63}{2} g^2\right] dx \quad \ldots\ldots [19b]$$

yields the Euler-Lagrange Equation

$$g^{iv} - 6g'' + \frac{63}{2} g = 0 \quad \ldots\ldots [20]$$

The solution of this equation that conforms to the boundary conditions, Equations [17], is

$$g(x) = e^{-\alpha x}\left(\cos \beta x + \frac{\alpha}{\beta}\sin \beta x\right) \quad \ldots\ldots [21a]$$

where

$$\gamma = \alpha + \beta i = (3 + 1.5i\sqrt{10})^{1/4} = 2.075 + 1.143i \quad [21b]$$

is root of the biquadratic equation

$$\gamma^4 - 6\gamma^2 + 63/2 = 0 \quad \ldots\ldots [21c]$$

One recognizes (11) that Equation [21a] gives the deflection of a 1-in-thick infinite beam on elastic foundation, subject to axial tension N, and to a lateral load P applied at the center, $x = 0$. The stiffness of an h wide filament of the beam is

$$D = Eh^3/12(1 - \mu^2),\ \text{lb in}^2/\text{in.} \quad \ldots\ldots [22a]$$

the foundation spring constant is

$$k = \frac{63}{2}\frac{D}{h^4},\ (\text{lb/in.})/\text{sq in.} \quad \ldots\ldots [22b]$$

the applied axial tension is

$$N = 6D/h^2,\ \text{lb/in.} \quad \ldots\ldots [22c]$$

and the lateral load is

$$P = 6\alpha\sqrt{14\, D/h^2}\ \text{lb/in.} \quad \ldots\ldots [22d]$$

From the stress function, Equations [17], [21], we derive the stresses

$$\left.\begin{aligned} \sigma_x &= \varphi_{yy} = S(y^2 - 1/3)e^{-\alpha x}\left(\cos \beta x + \frac{\alpha}{\beta}\sin \beta x\right) \\ \sigma_y &= \varphi_{xx} = \frac{\alpha^2 + \beta^2}{12} S(1 - y^2)^2 e^{-\alpha x}\left(-\cos \beta x + \frac{\alpha}{\beta}\sin \beta x\right) \\ -\tau &= \varphi_{xy} = \frac{\alpha^2 + \beta^2}{3\beta} Sy(1 - y^2)e^{-\alpha x}\sin \beta x \end{aligned}\right\} \quad \ldots\ldots [23]$$

We refer to α as the attenuation constant, to

$$l = 1/\alpha = 0.48 \quad \ldots\ldots [24]$$

as the penetration distance or "attenuation length" of the parabolic distribution. It gives the distance (in multiples of the half-width of the strip) in which the amplitude of the stresses decrease to about $1/e$ of their edge value.

Two questions now arise: (a) How to improve the approximation, [17], [21], which, clearly, does not satisfy the biharmonic equation; (b) how to treat other, more complicated end tractions; for instance, the self-equilibrating quartic parabola distribution of normal stresses

$$\sigma_x = S(y^4 - 1/5) \quad \ldots\ldots [25]$$

We first consider question (b), as this will also show the way to solution of the first problem.

For the distribution [25] one would be inclined to assume the stress function

$$\varphi = \frac{S}{30}(2 - 3y^2 + y^6)\, g(x);\ g(0) = 1,\ g'(0) = 0 \quad [26]$$

for this yields

$$\left.\begin{aligned} &\sigma_x(y) = \varphi_{yy}(0, y) = S(y^4 - 1/5),\ \tau(y) = -\varphi_{xy}(0, y) = 0 \\ &\sigma_y(x) = \varphi_{xx}(x, \pm 1) = 0,\ \tau(x) = -\varphi_{xy}(x, \pm 1) = 0 \end{aligned}\right\} \quad \ldots\ldots [27]$$

hence is in accordance with the prescribed boundary conditions. The variational equation for Equation [26] becomes

$$g^{iv} - \frac{1170}{209} g'' + \frac{1365}{38} g = 0 \quad \ldots\ldots [28a]$$

and has the solution

$$\left.\begin{aligned} g(x) &= e^{-\alpha x}\left(\cos \beta x + \frac{\alpha}{\beta}\sin \beta x\right) \\ \gamma &= \alpha + i\beta = 2.097 + 1.264i \end{aligned}\right\} \quad \ldots\ldots [28b]$$

This solution is badly in error. The reason for this is that the curve $y^4 - 1/5$ looks very much like the curve $y^2 - 1/3$, and the properties of the latter obscure the behavior of the truly quartic

part of the $y^4 - 1/5$ curve. Before we can apply the variational method properly, we must write σ_x in the form

$$\sigma_x/S = \left[y^4 - \frac{138}{165}y^2 + \frac{13}{165}\right] + \frac{138}{165}[y^2 - 1/3] \ldots [29]$$

i.e., we must decompose the associated φ into its orthogonal quartic and quadratic constituents

$$\varphi/S = \frac{1}{330}\chi_4(y)g_4(x) + \frac{23}{330}\chi_2(y)g_2(x) \ldots\ldots [30a]$$

where

$$g_2(0) = g_4(0) = 1, \quad g_2'(0) = g_4'(0) = 0 \ldots\ldots [30b]$$

and χ_2, χ_4 are unnormalized, f_2, f_4 are normalized orthogonal self-equilibrating polynomials

$$\left.\begin{aligned} f_2 = N_2\chi_2 &= \frac{3}{16}\sqrt{5\cdot 7}\,(1 - 2y^2 + y^4), \\ & \qquad f_2(\pm 1) = f_2'(\pm 1) = 0 \\ f_4 = N_4\chi_4 &= \frac{3}{32}\sqrt{7\cdot 13}\,(-1 + 13y^2 - 23y^4 + 11y^6), \\ & \qquad f_4(\pm 1) = f_4'(\pm 1) = 0 \end{aligned}\right\} \ldots [31a]$$

$$< 2, 2 > = < 4, 4 > = 1, \qquad < 2, 4 > = 0. \ldots [31b]$$

Here and in what follows we shall consistently abbreviate

$$< FG > \equiv \int_{-1}^{+1} F(y)G(y)dy \ldots\ldots [32]$$

In particular, when F, G are members f_n, f_m of the orthonormal set, we shall write briefly

$$\left.\begin{aligned} < n, m > \equiv \int_{-1}^{+1} f_n f_m\, dy, \quad < n', m' > \equiv \int_{-1}^{+1} f_n' f_m'\, dy \\ < n'', m'' > \equiv \int_{-1}^{+1} f_n'' f_m''\, dy \end{aligned}\right\} \ldots [33]$$

From the variation of the f_4g_4 term of φ/S

$$E\delta U = \frac{1}{2}\delta\int_0^\infty dx \int_{-1}^{+1} dy\,[f_4^2 g_4''^2 + 2f_4'^2 g_4'^2 + f_4''^2 g_4^2]$$

$$= \frac{1}{2}\delta\int_0^\infty dx\,[g_4''^2 + 2 < 4', 4' > g_4'^2 + < 4'', 4'' > g_4^2]$$

$$= \int_0^\infty dx\,[g_4^{IV} - 2 < 4', 4' > g_4'' + < 4'', 4'' > g_4]\,\delta g_4 = 0 \ldots [34]$$

there results the frequency equation

$$\gamma^4 - 46.8\,\gamma^2 + 1017.9 = 0 \ldots\ldots [35a]$$

and hence the complex frequency

$$\gamma_4 = \alpha_4 + \beta_4 i \doteq 5.259 + 2.062i \ldots\ldots [35b]$$

The $\chi_4 g_4$ solution therefore is

$$\chi_4 g_4 = (-1 + 13y^2 - 23y^4 + 11y^6)e^{-5.26x} \times (\cos 2.062x + 2.55 \sin 2.062x) \ldots\ldots [36a]$$

The $\chi_2 g_2$ solution, determined earlier in a similar manner, gave

$$\chi_2 g_2 = (1 - 2y^2 + y^4)e^{-2.03x}(\cos 1.143x + 1.82 \sin 1.143x) \ldots\ldots [36b]$$

Because the modes $\chi_2 g_2$ and $\chi_4 g_4$ are precisely orthogonal, their derivatives can be considered as weakly coupled. Hence, in first approximation we can neglect the interaction of these terms that would result were we to place the entire φ expression into the strain-energy formula. Thus in first approximation

$$\varphi/S = \frac{1}{330}\chi_4 g_4 + \frac{23}{330}\chi_2 g_2 \ldots\ldots [37]$$

is the Airy function, associated with the quartic parabola input $\sigma_x/S = y^4 - 1/5$, and the stresses are given by

$$\left.\begin{aligned} \sigma_x/S = \frac{1}{330}\chi_4''g_4 + \frac{23}{330}\chi_2''g_2, \quad \sigma_y/S = \frac{1}{330}\chi_4 g_4'' \\ + \frac{23}{330}\chi_2 g_2'' \\ \tau/S = -\frac{1}{330}\chi_4' g_4' - \frac{23}{330}\chi_2' g_2' \end{aligned}\right\} \ldots [38]$$

It is now seen that at distances $> l_4 \sim 0.2$ from the edge the high-frequency, γ_4, component of the input is fairly obliterated and only the low-frequency component, γ_2, persists. This also gets extinguished at distances $> l_2 \sim 0.5$. In particular, if we deal with a square, only $\exp(-2/0.5) \sim 3$ per cent of the fundamental mode and $\exp(-2/0.2) \sim 0.8$ per cent of the second symmetric mode reaches the opposite face. (This then justifies us in neglecting e^{+ax} type terms in the solution whenever $a \geq 1$.) We shall refer to the gradual elimination of high-frequency components of given inputs with depth of penetration as "frequency degradation."

Self-Equilibrating Orthonormal Polynomials

It is clear that the general procedure must be as follows: We decompose the boundary values of the Airy function of an applied end traction, $\bar{\sigma}_x(y)$ or $\bar{\tau}(y)$ into its self-equilibrating orthonormal components

$$\int_A^y d\eta \int_B^\eta \bar{\sigma}_x(\eta_1)\,d\eta_1 = \bar{\varphi}(y) = < \bar{\varphi}, f_2 > f_2 + < \bar{\varphi}, f_3 > f_3 + \ldots [39a]$$

or

$$-\int_A^y \bar{\tau}(\eta)d\eta = \bar{\varphi}_x(y) = < \bar{\varphi}_x, f_2 > f_3 + < \bar{\varphi}_x, f_3 > f_3 + \ldots\ldots [39b]$$

(for $\bar{\sigma}_x$ even, $\bar{\tau}$ odd take $B = 0$, $A = -1$; for $\bar{\sigma}_x$ odd, $\bar{\tau}$ even take $B = -1$, $A = 0$)
then write, in first approximation

$$\left.\begin{aligned} \varphi(x, y) = \sum c_k\varphi_k, \quad c_k = < \varphi, f_k > \quad \text{or} \quad < \bar{\varphi}_x, f_k > \\ \varphi_k(x, y) = f_k(y)\,g_k(x), \quad \text{or} \quad \varphi_k(x, y) = f_k(y)h_k(x) \end{aligned}\right\} \ldots [40]$$

where the choice

$$g_k = e^{-\alpha_k x}\left(\cos\beta_k x + \frac{\alpha_k}{\beta_k}\sin\beta_k x\right) \ldots\ldots [41a]$$

or

$$h_k = e^{-\alpha_k x}\frac{\sin\beta_k x}{\beta_k} \ldots\ldots [41b]$$

(the first is used when $\bar{\sigma}_x$ is given, $\bar{\tau} = 0$; the second when $\bar{\tau}$ is given, $\bar{\sigma}_x = 0$) insures that

$$\left.\begin{aligned} g_k(0) = 1, \quad g_k'(0) = 0 \\ h_k(0) = 0, \quad h_k'(0) = 1 \end{aligned}\right\} \ldots\ldots [41c]$$

The complex frequency $\gamma_k = \alpha_k + i\beta_k$ is determined from the eigenvalue equation

$$F_k(\gamma) \equiv \gamma^4 - 2 < k', k' > \gamma^2 + < k'', k'' > = 0 \quad [41d]$$

Finally we obtain σ_x, σ_y, τ as the derivatives

$$\left.\begin{aligned} \sigma_x(x, y) &= \varphi_{yy} = \Sigma\, c_k f_k'' g_k \\ \sigma_y(x, y) &= \varphi_{xx} = \Sigma\, c_k f_k\, g_k'' \\ \tau(x, y) &= -\varphi_{xy} = -\Sigma\, c_k f_k' g_k' \end{aligned}\right\} \quad [42]$$

of φ when δ_x is given. Similar expressions hold—in h_k—when $\bar{\tau}$ is given. (To avoid saying the same thing twice we shall, in what follows, frequently make statements concerning the series $\Sigma\, c_k f_k g_k$ only, without adding that corresponding statements hold also for the series $\Sigma\, c_k f_k h_k$.) We record that

$$\left.\begin{aligned} -(\alpha^2 + \beta^2)h &= g' = -\frac{\alpha^2 + \beta^2}{\beta} e^{-\alpha x} \sin \beta x \\ g^* &= (\alpha^2 + \beta^2) e^{-\alpha x}\left(-\cos \beta x + \frac{\alpha}{\beta} \sin \beta x\right) \\ \bar{g} &= -\frac{2\alpha}{\alpha^2 + \beta^2} e^{-\alpha x}\left(\cos \beta x + \frac{\alpha^2 - \beta^2}{2\alpha\beta} \sin \beta x\right) \end{aligned}\right\} \quad [43]$$

We used the notation

$$\bar{g} = \int_\infty^x g(x)\, dx \quad [44]$$

for the integral of g; $\bar{h}$ is defined similarly. We shall make use of these functions when calculating displacements.

We shall now survey some properties of the polynomials f_n. The even functions are characterized by absence of tractions on the horizontal edges,

$$\sigma_x(x, \pm 1) = 0; \text{ i.e., } f(\pm 1) = 0 \quad [45a]$$

$$\tau(x, \pm 1) = 0; \text{ i.e., } f'(\pm 1) = 0 \quad [45b]$$

and by zero stress resultant along the vertical edge

$$\int_{-1}^{+1} \delta_x dy = g(0) \int_{-1}^{+1} f''(y) dy = g(0)[f'(1) - f'(-1)] = 0 \quad [46a]$$

or, alternately

$$-\int_{-1}^{+1} \bar{\tau} dy = h'(0) \int_{-1}^{+1} f'(y) dy = h'(0)[f(1) - f(-1)] = 0 \quad [46b]$$

according to whether δ_x is given, and $\bar{\tau}$ is zero, or vice-versa. Clearly, the third condition, Equations [46], is implied by the first two, Equations [45a] and [45b]. The condition of zero resultant δ_x moment is automatically taken care of by the choice of f as even function.

The odd polynomials are characterized by the absence of tractions on the horizontal edges, Equations [45a, b], and zero moment or shear resultant along the vertical edge

$$\int_{-1}^{+1} \delta_x y dy = g(0) \int_{-1}^{+1} y f'' dy = g(0)\left[y f'\right]_{-1}^{+1} - g(0) \int_{-1}^{+1} f' dy = 0 \quad [47a]$$

or, alternately

$$-\int_{-1}^{+1} \bar{\tau} dy = h'(0) \int_{-1}^{+1} f' dy = h'(0)[f(1) - f(-1)] = 0 \quad [47b]$$

according to whether δ_x is given, and $\bar{\tau}$ is zero, or vice-versa.

Clearly, the third condition, Equations [47], is again implied by the first two, Equations [45a], [45b]. Furthermore the condition of zero resultant δ_x force is taken care of automatically by the choice of f as odd function. General end tractions are obtained by superposition of even and odd, and of σ_x and $\bar{\tau}$ effects.

The question now arises how to construct the functions f_n. Obviously, an even function is automatically orthogonal to an odd function. The construction of an even function, like f_6 thus requires orthogonalization only with respect to its even predecessors f_0, f_4. One writes

$$f_6 = a + by^2 + cy^4 + dy^6 + ey^8 \quad [48a]$$

and determines the coefficients $a, \ldots, e$ from the five conditions

$$f_6(1) = 0,\ f_6'(1) = 0,\ < 6, 2 > = 0,\ < 6, 4 > = 0,\ < 6, 6 > = 1 \quad [48b]$$

This procedure while correct, involves ever-increasing labor in determining successive polynomials. One readily recognizes that a function defined by

$$\left.\begin{aligned} f_{n+1} &= a_{n+1}(y f_n + b_{n+1} f_{n-1}) \\ b_{n+1} &= -< f_n y f_{n-1} >,\ a_{n+1}^2 = [-b_{n+1}^2 + < y^2 f_n^2 >]^{-1} \end{aligned}\right\} \quad [49]$$

is orthogonal to f_{n-1} by definition of b_{n+1}, and is normalized, by definition of a_{n+1}. If $f_1, f_2, \ldots, f_n$ are the first n functions of an orthonormal set, i.e., if $< k, m > = \delta_{km}$ for $k, m \leq n$, then f_{n+1}, constructed in the foregoing manner, is the $(n+1)$st such function: $< k, m > = \delta_{km}$ also for $k, m \leq n+1$. To prove this, we must demonstrate the orthogonality of f_{n+1} to all its predecessors. It suffices to consider only $< n+1, n-3 >$. One finds

$$\begin{aligned} \frac{1}{a_{n+1}} < n+1, n-3 > &= < y f_n, f_{n-2} > + b_{n+1} < f_{n-1}, f_{n-3} > \\ &= < f_n, y f_{n-2} > + 0 = < f_n, \frac{f_{n-2}}{a_{n-2}} - b_{n-2} f_{n-4} > \\ &= \frac{1}{a_{n-2}} < n, n-2 > - b_{n-2} < n, n-4 > = 0 \end{aligned} \quad [50]$$

Formula [49] thus provides a recursive determination of the polynomials f_n. In Table 1 we list the first nine such functions in the form

$$f_n = N_n \chi_n \quad [51]$$

where χ_n is the y-dependent part, N_n the normalization factor.

TABLE 1 SELF-EQUILIBRATING ORTHONORMAL POLYNOMIALS $f_n = N_n \chi_n$

n	N_n	χ_n
2	$\frac{3}{16}\sqrt{5 \cdot 7}$	$1 - 2y^2 + y^4$
3	$\frac{3}{16}\sqrt{5 \cdot 7 \cdot 11}$	$y - 2y^3 + y^5$
4	$\frac{3}{32}\sqrt{7 \cdot 13}$	$-1 + 13y^2 - 23y^4 + 11y^6$
5	$\frac{3}{32}\sqrt{5 \cdot 7 \cdot 11}$	$-3y + 19y^3 - 29y^5 + 13y^7$
6	$\frac{3}{128}\sqrt{7 \cdot 11 \cdot 17}$	$1 - 28y^2 + 118y^4 - 156y^6 + 65y^8$
7	$\frac{3}{128}\sqrt{5 \cdot 7 \cdot 11 \cdot 13 \cdot 19}$	$y - 12y^3 + 38y^5 - 44y^7 + 17y^9$
8	$\frac{3}{256}\sqrt{5 \cdot 7 \cdot 11 \cdot 13}$	$-1 + 47y^2 - 346y^4 + 878y^6 - 901y^8 + 323y^{10}$
9	$\frac{3}{256}\sqrt{7 \cdot 11 \cdot 13 \cdot 23}$	$-5y + 95y^3 - 498y^5 + 1054y^7 - 969y^9 + 323y^{11}$

They are associated with the frequency equation [41d], and yield the complex frequencies

$$\gamma_n = \alpha_n + i\beta_n = [< n', n' > + i\{< n'', n'' > - < n', n' >^2\}^{1/2}]^{1/2} \quad \ldots\ldots [52]$$

as follows in Table 2.

TABLE 2 COMPLEX NATURAL FREQUENCIES

$\gamma_3 = 2.075 + 1.143i$	$\gamma_5 = 3.656 + 1.538i$
$\gamma_4 = 5.259 + 2.062i$	$\gamma_6 = 6.942 + 2.682i$
$\gamma_8 = 8.729 + 3.405i$	....

In the foregoing we made use of the numerical values $< n', m' >$, $< n'', m'' >$ for equal n and m. In Table 3 we list these, for later purposes, also for unequal n and m up to $n, m = 6$, and those for equal n and m up to 9.

TABLE 3 SCALAR PRODUCTS

n, m	$< n', m' >$	$< n'', m'' >$
2,2	3	$9 \cdot 7/2$
2,4	$-(3/2)\sqrt{13/5}$	$9\sqrt{13/5}$
2,6	$-4\sqrt{17/(5 \cdot 11)}$	$(3/2)\sqrt{11 \cdot 17/5}$
4,4	$9 \cdot 13/5$	$27 \cdot 13 \cdot 29/10$
4,6	$-(7/10)\sqrt{13 \cdot 17/11}$	$(3 \cdot 4 \cdot 7/5)\sqrt{11 \cdot 13 \cdot 17}$
6,6	$17 \cdot 19/5$	$3 \cdot 17 \cdot 1511/10$
8,8	$7 \cdot 19$	$3 \cdot 23203/2$
3,3	11	$11 \cdot 45/2$
3,5	$-7/2$	$33 \cdot 5$
5,5	41	$3 \cdot 5 \cdot 409/2$
7,7	95	$3 \cdot 19 \cdot 601/2$
9,9	$3 \cdot 13 \cdot 23/5$	$9 \cdot 23 \cdot 3187/10$

In terms of the stresses, Equations [42], we determine the x and y-displacements u, v (using $(\infty, 0)$ as fixed point, the x-axis as fixed axis)

$$Eu = \int_\infty^x (\sigma_x - \mu\sigma_y)dx = \Sigma\, c_k(f_k''\tilde{y}_k - \mu f_k g_k') \quad [53a]$$

$$Ev = \int_0^y (\sigma_y - \mu\sigma_x)dy = \Sigma\, c_k[\tilde{f}_k g_k'' - \mu f_k' g_k]_0^y \quad [53b]$$

where the $\tilde{y}$, g, g', g'' expressions were given earlier, in Equations [43], the f expressions were listed in Table 1, and the f', f'' and

$$\tilde{f} = \int_0^y f dy \quad \ldots\ldots [54]$$

expressions are given in Table 4, for the first six f_n-polynomials.

are not in agreement. However, an average of the two expressions probably gives a fair estimate as to what the shear strain really is. We also note that the self-equilibrating polynomials satisfy the differential equation

$$(1 - y^2)^2 f^{iv} - 10y(1 - y^2)f''' + [(n + 2)(n + 3) - 24](1 - y^2)f'' + [12 - 4(n + 2)(n + 3)]yf' - 2(n + 2)(n + 3)f = 0 \quad \ldots\ldots [56][5]$$

Higher Approximations

In the preceding section we used the expansion $\varphi = \Sigma\, c_k f_k g_k$ for the Airy function where the f_k were orthonormal polynomials, and the g_k were defined by Equations [41]. We formed the strain-energy expression[6]

$$U = \frac{1}{2E}\int_0^\infty dx \int_{-1}^{+1} [\varphi_{xx}^2 + 2\varphi_{xy}^2 + \varphi_{yy}^2]\, dy = U_{even} + U_{odd}$$

$$U_{even} = \frac{1}{2E}\int_0^\infty dx[\{c_2^2 G_2''^2 + c_4^2 G_4''^2 + \ldots\} + 2\{c_2^2 < 2', 2' > G_2'^2 + 2c_2c_4 < 2', 4' > G_2'G_4' + c_4^2 < 4', 4' > G_4'^2 + \ldots\} + \{c_2^2 < 2'', 2'' > G_2^2 + 2c_2c_4 < 2'', 4'' > G_2G_4 + c_4^2 < 4'', 4'' > G_4^2 + \ldots\}] \quad \ldots\ldots [57]$$

U_{odd} = similar in $G_3, G_5, \ldots$

In the foregoing we utilized the relation $< k, l > = \delta_{kl}$. Next we assumed that $< k', l' >$, $< k'', l'' >$ are negligible for $k \neq l$. This permitted us to write U, in first approximation, in the form

$$U = \Sigma\, U_k \sim \frac{1}{2E}\Sigma\, c_k^2 \int_0^\infty [g_k''^2 + 2 < k', k' > g_k'^2 + < k'', k'' > g_k^2]dx \quad \ldots\ldots [58]$$

involving only "diagonal" terms.

It is now our aim to determine functions G_k which eliminate, upon y and x-integration, cross terms of type $G_i'G_k'$ from Equations [57], hence which lead to accurate diagonalization of U

$$U = \Sigma U_k = \frac{1}{2E}\Sigma\, c_k^2 \int_0^\infty [G_k''^2 + 2 < k', k' > G_k'^2 + < k'', k'' > G_k^2]dx \quad \ldots\ldots [59]$$

TABLE 4 DERIVATIVES AND INTEGRALS OF f_n

n	f'/N	f''/N	$\tilde{f}/N$
2	$4(-y + y^3)$	$4(-1 + 3y^2)$	$y - \frac{2}{3}y^3 + \frac{1}{5}y^5$
3	$1 - 6y^2 + 5y^4$	$4(-3y + 5y^3)$	$\frac{1}{2}y^2 - \frac{1}{2}y^4 + \frac{1}{6}y^6$
4	$2(13y - 46y^3 + 33y^5)$	$2(13 - 138y^2 + 165y^4)$	$-y + \frac{13}{3}y^3 - \frac{23}{5}y^5 + \frac{11}{7}y^7$
5	$-3 + 57y^2 - 145y^4 + 91y^6$	$2(57y - 290y^3 + 273y^5)$	$-\frac{3}{2}y^2 + \frac{19}{4}y^4 - \frac{29}{6}y^6 + \frac{13}{8}y^8$
6	$8(-7y + 59y^3 - 117y^5 + 65y^7)$	$8(-7 + 177y^2 - 585y^4 + 455y^6)$	$y - \frac{28}{3}y^3 + \frac{118}{5}y^5 - \frac{156}{7}y^7 + \frac{65}{9}y^9$

By the foregoing we have provided a complete solution of the problem of determining the first-order effects of prescribed applied self-equilibrating end tractions or their prescribed displacements. We again point out the fact that the functions $f_n g_n$, $f_n h_n$ do not satisfy the biharmonic equation. Therefore, the shear-strain expressions, calculated by

$$\gamma_{xy} = u_y + v_x \quad \ldots\ldots [55a]$$

or by

$$\gamma_{xy} = \tau/G \quad \ldots\ldots [55b]$$

[5] The author succeeded in establishing this equation only after he completed the remainder of the paper. Once the equation is available the investigation of the properties of f_n can be carried out faster, and more systematically.

[6] We shall write henceforth G_k for the x-dependent factor of φ_k, retaining the symbols g_k, h_k, for the specific functions, Equations [41a, b].

Clearly, such functions G_k cannot be solutions of 4th order differential equations (the best that is available in this nature are the functions g_k, h_k), but will be solutions of higher order, in fact of infinite order, equations, which can be approximated in a progressive manner.

In order not to get wrapped up in a maze of symbols we shall assume that there is applied to the strip an end traction

$$\vartheta_x(y) = f_4'' \quad \ldots\ldots\ldots\ldots\ldots\ldots [60]$$

and we consider the problem of finding the second approximation to the corresponding Airy function φ_4. (The first approximation was $f_4\, g_4$.) We write

$$\varphi_4(x, y) = f_2(y)\, G_2(x) + f_4(y)\, G_4(x) + f_6(y)\, G_6(x) \quad [61a]$$

$$\begin{aligned} &G_4(0) = 1 \\ &G_4(\infty) = 0 \end{aligned} \qquad G_2\binom{0}{\infty} = G_6\binom{0}{\infty} = G_2'\binom{0}{\infty} = G_4'\binom{0}{\infty} = G_6'\binom{0}{\infty} = \mathbf{0} \quad [61b]$$

i.e., in addition to the distribution f_4 excited by the applied traction, we expect a feeble appearance also of the two neighboring distributions, f_2 and f_6. But not at $x = 0$; here only f_4 can exist.

Then we can immediately utilize Equations [57] and, abbreviating

$$F_k\{G_k\} = \left[\frac{d^4}{dx^4} - 2 < k', k' > \frac{d^2}{dx^2} + < k'', k'' >\right] G_k,$$

$$F_{ik}\{G_i\} = \left[-2 < k', l' > \frac{d^2}{dx^2} + < k'', l'' >\right] G_i \quad [62a]$$

we find the Euler-Lagrange equations

$$\left.\begin{aligned} F_2\ \{G_2\} + F_{24}\ \{G_4\} + F_{26}\ \{G_6\} &= 0 \\ F_{42}\{G_2\} + F_4\ \{G_4\} + F_{46}\{G_6\} &= 0 \\ F_{26}\{G_2\} + F_{46}\{G_4\} + F_6\ \{G_6\} &= 0 \end{aligned}\right\} \quad \ldots\ldots\ldots [63]$$

Denoting furthermore

$$F_k(\gamma) = \gamma^4 - 2 < k', k' > \gamma^2 + < k'', k'' >,$$

$$F_{ik}(\gamma) = -2 < k', l' > \gamma^2 + < k'', l'' > \quad \ldots\ldots\ldots\ldots [62b]$$

there results the frequency equation

$$\Delta \equiv \begin{vmatrix} F_2 & F_{24} & F_{26} \\ F_{42} & F_4 & F_{46} \\ F_{62} & F_{64} & F_6 \end{vmatrix} = F_2F_4F_6 - F_2F_{46}^2 - F_4F_{62}^2 - F_6F_{24}^2 + 2\,F_{24}F_{46}F_{62} \quad \ldots\ldots\ldots\ldots [64a]$$

$$= \gamma^{12} - 182\,\gamma^{10} + 15775.5\,\gamma^8 - 592488\,\gamma^6 + 10{,}195185\,\gamma^4 - 59{,}729670\,\gamma^2 + 223{,}986262.5 \quad \ldots\ldots\ldots\ldots [64b]$$

$$= (\gamma^4 - 6.339236227\,\gamma^2 + 32.51859826)$$
$$(\gamma^4 - 51.87829987\,\gamma^2 + 948.8053555)$$
$$(\gamma^4 - 123.7824639\,\gamma^2 + 7258.907188) = 0 \quad \ldots\ldots [64c]$$

All coefficients in Equation [64b] are integers or half-integers. We factored this equation into products

$$\Delta = (\gamma^4 + p_2\gamma^2 + q_2)\,(\gamma^4 + p_4\gamma^2 + q_4)\,(\gamma^4 + p_6\gamma^2 + q_6) \quad [65]$$

as given by Equation [64c], by following the procedure outlined in reference (12). When γ is a root

$$\gamma_n = \left[-(p_n/2) + i\sqrt{q_n - (p_n/2)^2}\right]^{1/2} = (\rho_n + i\sigma_n)^{1/2} = \alpha_n + i\beta_n \quad \ldots\ldots\ldots [66]$$

of Equation [65], to-wit

$$\left.\begin{aligned} \gamma_2 &= (3.16961811 + 4.74047669i)^{1/2} \\ &= 2.10619636 + 1.12536438i \\ \gamma_4 &= (25.9391499 + 16.6149287i)^{1/2} \\ &= 5.32650426 + 1.55964662i \\ \gamma_6 &= (61.8912320 + 58.5523919i)^{1/2} \\ &= 8.57585135 + 3.41379471i \end{aligned}\right\} \quad \ldots\ldots\ldots [67]$$

then the Equation System [63] is consistent.[7] In order to determine the "eigenmode" u_n, v_n, w_n associated with the "eigenvalue" γ_n we place

$$G_2 = u_n e^{-\gamma_n x},\ G_4 = v_n e^{-\gamma_n x},\ G_6 = w_n e^{-\gamma_n x} \quad \ldots\ldots\ldots\ldots [68]$$

into Equations [63] and obtain

$$\left.\begin{aligned} \gamma_2\text{:}\quad & u_2 : v_2 : w_2 = 1 : (-0.02690773 - 0.03389137i) : \\ & \qquad (-0.00029084 + 0.00113864i) \\ \gamma_4\text{:}\quad & u_4 : v_4 : w_4 = (-0.11805559 + 0.11844268i) : \\ & \qquad 1 : (-0.18392725 - 0.07294037i) \\ \gamma_6\text{:}\quad & u_6 : v_6 : w_6 = (-0.050222166 + 0.030256531i) : \\ & \qquad (0.00558379 + 0.26270133i) : 1 \end{aligned}\right\} \quad \ldots\ldots [69]$$

For the conjugate roots $\gamma_n{}^*$ one obtains the conjugate modes, $u_n{}^*, v_n{}^*, w_n{}^*$. In general G_2, G_4, G_6 are combinations of the six modes

$$\left.\begin{aligned} G_2 &= u_2 e^{-\gamma_2 x} + u_4 e^{-\gamma_4 x} + u_6 e^{-\gamma_6 x} + \text{conjugate} \\ G_4 &= v_2 e^{-\gamma_2 x} + v_4 e^{-\gamma_4 x} + v_6 e^{-\gamma_6 x} + \text{conjugate} \\ G_6 &= w_2 e^{-\gamma_2 x} + w_4 e^{-\gamma_4 x} + w_6 e^{-\gamma_6 x} + \text{conjugate} \end{aligned}\right\} \quad \ldots [70]$$

By Equations [61b] they are subject to the six boundary conditions

$$\left.\begin{aligned} G_2(0) &= 2\Re\{u_2 + u_4 + u_6\} = 0 \\ G_4(0) &= 2\Re\{v_2 + v_4 + v_6\} = 1 \\ G_6(0) &= 2\Re\{w_2 + w_4 + w_6\} = 0 \end{aligned}\right\} \quad \ldots\ldots [71]$$

$$\left.\begin{aligned} G_2'(0) &= -2\Re\{\gamma_2 u_2 + \gamma_4 u_4 + \gamma_6 u_6\} = 0 \\ G_4'(0) &= -2\Re\{\gamma_2 v_2 + \gamma_4 v_4 + \gamma_6 v_6\} = 0 \\ G_6'(0) &= -2\Re\{\gamma_2 w_2 + \gamma_4 w_4 + \gamma_6 w_6\} = 0 \end{aligned}\right\} \quad \ldots [72]$$

Writing

$$u_2 = u + iU,\ v_4 = v + iV,\ w_6 = w + iW \quad \ldots\ldots [73]$$

for real and imaginary parts of u_2, v_4, w_6, Equations [69], [71], [72] permit determination of $u, \ldots, W$. One finds

$$\left.\begin{aligned} u &= 0.2700820 & v &= 0.5638912 & w &= -0.0201872 \\ U &= -0.5748462 & V &= 1.6907801 & W &= 0.1409543 \end{aligned}\right\} \quad [74a]$$

and hence, by Equations [69], also

$$\left.\begin{aligned} u_4 &= -0.2668310 - 0.1328172i & u_6 &= -0.0032540 - 0.0076898i \\ v_2 &= -0.0267496 + 0.0063144i & v_6 &= -0.0371416 - 0.0045161i \\ w_2 &= 0.0005760 + 0.0004747i & w_4 &= 0.0196112 - 0.3521109i \end{aligned}\right\} \quad [74b]$$

[7] The formulas $\cos\left(\frac{1}{2}\arctan u\right) = \left[\frac{1}{2} + \frac{1}{2}(1+u^2)^{-1/2}\right]^{1/2}$, $\sin\left(\frac{1}{2}\arctan u\right) = \left[\frac{1}{2} - \frac{1}{2}(1+u^2)^{-1/2}\right]^{1/2}$ come handy in evaluating the roots without the use of trigonometric tables. The root γ_8 in the foregoing is a "third" approximation, because it was determined in terms of f_2 and two right neighbors f_4, f_6, two left neighbors $f_0 = f_{-2} \equiv 0$. Similarly γ_4, determined in terms of f_4 and f_2, f_6, is a "second" approximation, and γ_6 determined in terms of f_6 and f_4, f_2 is a slightly improved "first" approximation. All our numerical results are uncertain in the last digit shown. (Except, of course Equation [64b], which is precise.)

One can write the solution, Equations [70], more conveniently in the form

$$\left.\begin{aligned} G_2 &= a_2 g_2 + A_2 h_2 + a_4 g_4 + A_4 h_4 + a_6 g_6 + A_6 h_6 \\ G_4 &= b_2 g_2 + B_2 h_2 + b_4 g_4 + B_4 h_4 + b_6 g_6 + B_6 h_6 \\ G_6 &= c_2 g_2 + C_2 h_2 + c_4 g_4 + C_4 h_4 + c_6 g_6 + C_6 h_6 \end{aligned}\right\} \quad [75a]$$

where

$$g_n = e^{-\alpha_n x}\left(\cos\beta_n x + \frac{\alpha_n}{\beta_n}\sin\beta_n x\right),\ h_n = e^{-\alpha_n x}\frac{\sin\beta_n x}{\beta_n} \quad [75b]$$

and

$$\left.\begin{aligned} a_n &= 2\Re\{u_n\} \quad A_n = 2\beta_n\Im\{u_n\} - 2\alpha_n\Re\{u_n\} \\ b_n &= 2\Re\{v_n\} \quad B_n = 2\beta_n\Im\{v_n\} - 2\alpha_n\Re\{v_n\} \\ c_n &= 2\Re\{w_n\} \quad C_n = 2\beta_n\Im\{w_n\} - 2\alpha_n\Re\{w_n\} \end{aligned}\right\} \quad [76]$$

One obtains the numerical values

$$\left.\begin{aligned} a_2 &= 0.540160 & a_4 &= -0.533662 & a_6 &= -0.006502 \\ A_2 &= -2.431514 & A_4 &= 2.428257 & A_6 &= 0.003257 \\ b_2 &= -0.053499 & b_4 &= 1.127782 & b_6 &= -0.074283 \\ B_2 &= 0.126892 & B_4 &= -0.733099 & B_6 &= 0.606208 \\ c_2 &= 0.001152 & c_4 &= 0.039222 & c_6 &= -0.040374 \\ C_2 &= -0.001358 & C_4 &= -1.307255 & C_6 &= 1.308623 \end{aligned}\right\} \quad [77]$$

hence, by Table 1 and Equation [61*a*] determination of the second approximation to φ_4 is completed.

It must be remembered that φ_4 of Equation [61*a*] is the second approximation for the Airy function of the applied traction f_4. However f_4 is not the boundary value of the true second eigenfunction, Φ_{4y}. Therefore the function φ_4 is a mixture of Φ_{4y}, Φ_{2y}, Φ_{2h}, Φ_{6y}, Φ_{6h}. (Subscripts g, h refer to g-type and h-type behavior, as in Equations [41*c*].) In particular, one has, in second approximation,

$$(1/N)\,\Phi_{4y}(x, y) = g_4(a_4 f_4 + b_4 f_4 + c_4 f_6) + h_4(A_4 f_2 + B_4 f_4 + C_4 f_6) \quad [78]$$

(N is the normalization factor.) We note that the coefficient of g_4 gives the second approximation to the true shape of the boundary value, $\Phi_{4y}(0, y)$, of the second symmetric mode.

Extension of the foregoing procedures to other modes and higher approximations, or to cases $a < 1$ when $e^{+\alpha x}$ terms must also be taken into account are obvious and need not be discussed.

Applications

The method described appears to be most useful for solution of multidimensional vibration and eigenvalue problems. A survey of some simple applications is given in a separate paper (13). In the narrower field of stress analysis the method permits one to write down the solution for many, formerly regarded as difficult, problems, so to speak, by inspection. Several of these, dealing with thermal stresses, will be discussed in a subsequent publication (14). In a later study the problem of the circular cylinder subject to self-equilibrating end tractions will be treated. The method also can be adapted to contact stress problems, but here further development is necessary.

Acknowledgment

The idea of regarding the fibers of a strip as beams on elastic foundation was first suggested to the author by his colleague, D. R. Miller, two years ago. The author wishes to express his appreciation to Mr. Miller for stimulating discussions, and to Miss Sarah Carter and Miss Olga Podmajersky for performing the numerical work.

BIBLIOGRAPHY

1 "Theory of Elasticity," by S. Timoshenko and J. N. Goodier, McGraw-Hill Book Company, Inc., New York, N. Y., 1951, (a), p. 171; (b) p. 47.

2 "Analysis of Deep Beams," by H. D. Conway, L. Chow, and G. W. Morgan, Trans. ASME, vol. 73, 1951, p. 163. See also discussion of the paper by M. Z. Krzywoblocki, ibid., 1951, p. 421, who questions the convergence of Conway's approach.

3 "Flächentragwerke," by K. Girkmann, Julius Springer, 1948, p. 77.

4 "Die Selbstspannungs-Eigenwertfunktionen der Quadratischen Scheibe," by J. Fadle, *Ingenieur-Archiv*, vol. 11, 1941, p. 125.

5 "Roots of Sin $z = z$," by A. P. Hillman and H. E. Salzer, *Philosophical Magazine*, vol. 34, 1943, p. 575.

6 "Zeros of $z + \sin z$," by B. S. Mittelman and A. P. Hillman, MTAG, vol. 2, 1946, p. 60.

7(*a*) "Analysis of Shear Lag in Box Beams, by the Principle of Minimum Potential Energy," by E. Reissner, *Quarterly of Applied Mathematics*, vol. 4, 1946, p. 268.

(*b*) "Bending of Elastic Plates," by E. Reissner, *Quarterly of Applied Mathematics*, vol. 5, 1947, p. 55.

(*c*) "Torsion and Transverse Bending of Cantilever Plates," by E. Reissner and M. Stein, NACA Technical Note 2369, 1951.

8 "Mathematical Theory of Elasticity," by I. S. Sokolnikoff, McGraw-Hill Book Company, Inc., New York, N.Y., 1946, p. 315.

9 "Reduction of the Solution of Certain Partial Differential Equations to Ordinary Differential Equations," by H. Poritsky, Proceedings of the 5th International Congress of Applied Mechanics, 1938.

10 "Thermal Stresses in a Rectangular Plate Clamped Along an Edge," by B. J. Aleck, Trans. ASME, vol. 71, 1949, p. A-118.

11 "Beams on Elastic Foundation," by M. Hetenyi, University of Michigan Press, Ann Arbor, Mich., 1946, p. 129.

12 "Numerical Calculus," by W. E. Milne, Princeton University Press, Princeton, N. J., 1949, p. 54.

13 "The Use of Orthogonal Boundary Polynomials in the Solution of Eigenvalue Problems," by G. Horvay and F. N. Spiess, to be published elsewhere.

14 "Thermal Stresses in Rectangular Strips," by G. Horvay and others, in preparation.

Nonlinear Distribution of Bending Stresses Due to Distortion of the Cross Section[1]

By H. H. BLEICH,[2] NEW YORK, N. Y.

A theory is presented to explain the nonlinear distribution of bending stresses found in recent tests on a passenger ship with long superstructure and in model tests. The hull and the superstructure are considered as separate beams which are forced to act together by shearing forces and by vertical forces resisting relative displacements of the two beams. The case of constant cross section of the beams is treated, and solutions in qualitative agreement with the tests are obtained for two types of loading.

1 Introduction

As part of a series of recent structural tests on a passenger ship reported by Vasta[3] the strains due to bending of the ship acting as a beam were measured. It was found that at midship the distribution of bending strains was not linear over the effective section consisting of the hull and deckhouse. Fig. 1 shows the strain distribution found, indicating a pronounced break on the level of the promenade deck, where the cross section is offset horizontally (the side plating of the hull ends on this level). Navier's hypothesis, that plane sections remain plane after bending, and the conventional theory of bending of beams appear not applicable.

Similar tests on small models were reported by Holt[4] showing a definite, but less pronounced break on a model with horizontally offset superstructure, Fig. 2. It is significant that in the case of another model where the superstructure is not horizontally offset, Fig. 3, the strain distribution was found to be linear. The model tests offered a clue for the cause of the deviations from the conventional linear strain distribution.[5] It was observed that the deflections of hull and superstructure, measured at points *A* and *B* in Fig. 2, differed by about 10 per cent,[6] indicating that the cross sections of the beam consisting of hull and superstructure distort under loading.

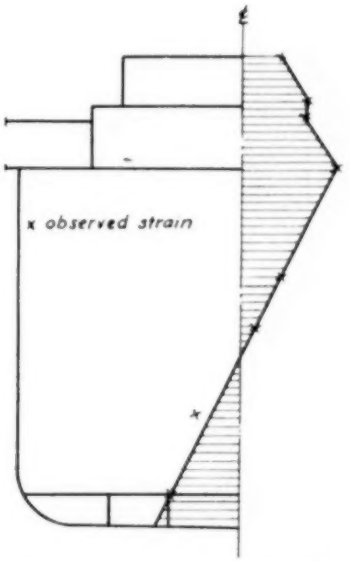

Fig. 1 Nonlinear Distribution of Strains Observed in Tests on a Passenger Vessel

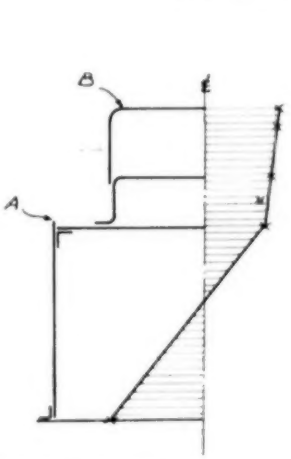

Fig. 2 Nonlinear Distribution of Strains Observed in Model Tests

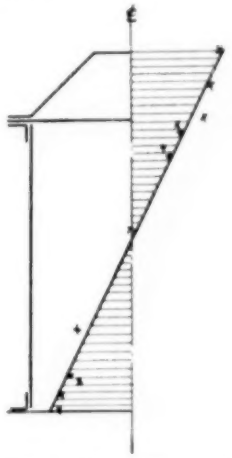

Fig. 3 Linear Distribution of Strains Observed in Model Tests

It is a known fact that Navier's hypothesis for a structure acting as a beam is applicable only if the cross sections of the beam do not distort. An example for nonlinear stress distribution due to distortion of the cross section is the case of a thin cylindrical shell acting as a beam.[7] In order to explain the nonlinearity

[1] This paper presents parts of a "Study on the Structural Action of Superstructures on Ships," undertaken for the Ship Structure Committee under Bureau of Ships Contract NObs—50538 (Index No. NS—731—034).

[2] Professor of Civil Engineering, Columbia University.

[3] "Structural Tests on the Passenger Ship S.S. President Wilson—Interaction between Superstructure and Main Hull Girder," by J. Vasta, Trans. of the Society of Naval Architects and Marine Engineers, vol. 57, 1949, p. 253.

[4] "Structural Tests of Models Representing a Steel Ship Hull With Aluminum Alloy and Steel Superstructures," by M. Holt, paper presented at the March, 1949, Meeting, New England Section of The Society of Naval Architects and Marine Engineers. Copies are obtainable from Mr. E. H. Robinson, editor, Bethlehem Steel Company, Quincy 69, Mass.

[5] See discussions of Ref. 3 by Holt, Crawford, Ramsey, and author.

[6] Reference 3, fig. 47.

[7] "Design of Cylindrical Concrete Shell Roofs," American Society of Civil Engineers, Manuals of Engineering Practice, No. 31, 1952, fig. 23.

Contributed by the Applied Mechanics Division and presented at the Annual Meeting, New York, N. Y., November 30–December 5, 1952, of The American Society of Mechanical Engineers.

Discussion of this paper should be addressed to the Secretary, ASME, 29 West 39th Street, New York, N. Y., and will be accepted until April 10, 1953, for publication at a later date. Discussion received after the closing date will be returned.

Note: Statements and opinions advanced in papers are to be understood as individual expressions of their authors and not those of the Society. Manuscript received by ASME Applied Mechanics Division, May 13, 1952. Paper No. 52—A-7.

found in the tests, this paper studies the effect of this distortion on a bar the cross section of which consists of two cells, Fig. 4(*a*). Because of the application intended it is, however, not necessary to consider the most general case of distortion, which would require a shell analysis, but it is assumed that the symmetrical cross section consists of two nondistorting portions which can move relative to each other, Fig. 4(*b*). The justification for this assumption lies in the tests which show that Navier's hypothesis is applicable for the hull and superstructure each by itself.

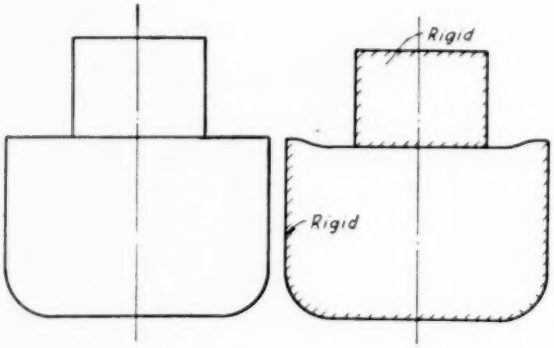

FIG. 4(*a*) FIG. 4(*b*)

Starting from this assumption, the paper will consider the problem of two separate beams forced to act together by horizontal shear forces and by vertical forces acting at the junction of hull and superstructure. The vertical forces are due to elastic resistance of the deck framing or bulkheads against the motion of the superstructure with respect to the hull. The system consists therefore essentially of a beam elastically supported by another beam, with a shear connection to enforce equal strains at deck level. The case of constant section will be treated for two loading cases. It will be seen that the theoretical stress distributions found are of the type observed in the experiments.

Before analyzing the full problem we will consider in section 2 a simplified structure in which the action of vertical forces between hull and deckhouse is neglected. This simplified structure does not describe the actual conditions but because of its relative simplicity it is easier to study the play of forces; the understanding gained is of value in treating the full problem in section 3. The simplified approach in section 2 may be considered a generalization of Hovgaard's theory of a beam attached to a deck plate subjected to tension or compression due to the bending of the hull.[8]

It might be of interest to note that the solution obtained can be applied also to other structures, not only ships. The stresses in a girder having a cross section, as shown in Fig. 5, under vertical loads are similarly affected by distortion of the cross section and the equations found in this paper are applicable to this case.

2 Analysis of a Simplified Two-Cell Structure

Consider the structure shown in Fig. 6(*a*), a hollow box beam with two cells. The lower box, the hull, is of length L, while the upper box, the deckhouse, is shorter, and of length l; both boxes are assumed to be of constant cross section. The cross-sectional area and the moment of inertia of the upper section, Fig. 6(*c*), and

[8] "A New Theory of the Distribution of Shearing Stresses in Riveted and Welded Connections and Its Application to Discontinuities in the Structure of a Ship," by W. Hovgaard, Trans. of the Institution of Naval Architects, vol. 73, 1931, pp. 108–126.

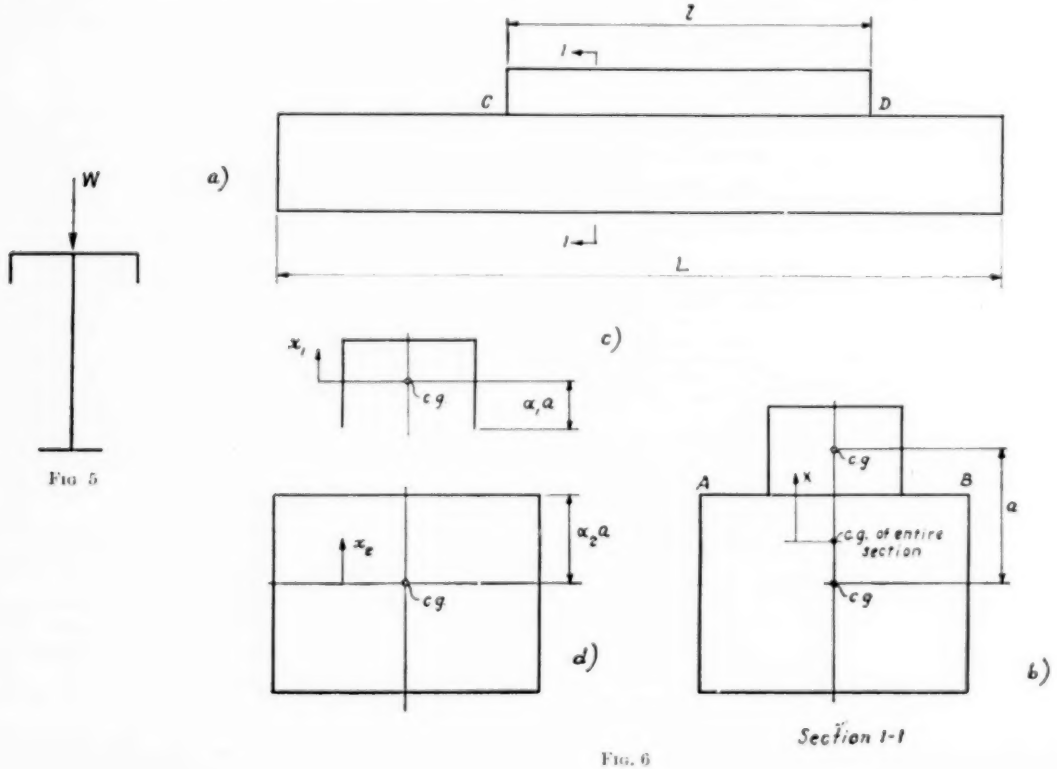

FIG. 5

FIG. 6

of the lower section, Fig. 6(*d*), are A_1, I_1, and A_2, I_2, respectively; the distances of the respective centers of gravity from each other and from the deck are a, $\alpha_1 a$ and $\alpha_2 a$, respectively, Figs. 6(*b*, *c*, *d*).

In this section the important simplifying assumption is made that the deck *A-B*, Fig. 6(*b*), and its supports have no stiffness, and will not resist any relative vertical movements between hull and deckhouse. This assumption is of course not justified in any real ship and will be abandoned in the next section. The structure is subjected to vertical loads and buoyancy forces acting on the hull only, producing bending moments M in the vessel. No external loads are assumed to act on the deckhouse.

Take a section at the distance z from the center of the deckhouse, and consider the free-body diagrams for the deckhouse and hull, Fig. 7(*a*). The moment and direct forces in the deckhouse and hull are M_1, N_1, and M_2, N_2, respectively. Moments M_1 and M_2 are positive if they produce compression on top of deckhouse or hull, and direct forces N_1 and N_2 are positive if they create tension. The external loads and buoyancy acting on the hull to the left of the section have a moment M; further, a shear force T of unknown magnitude will act on the under side of the deckhouse, and a similar force T will act in the opposite direction on the hull. The shear force T is counted positive if it acts as shown in Fig. 7(*a*). Equilibrium of the portions of deckhouse and hull in Fig. 7(*a*), requires the relations

$$N_1 = -T, \quad M_1 = -a\alpha_1 T \ldots [1a]$$

$$N_2 = T, \quad M_2 = M - a\alpha_2 T \ldots [1b]$$

Owing to the assumption that Navier's hypothesis is valid for the deckhouse and hull separately, the stresses can be determined at points at a distance x_1 or x_2 from the respective center of gravity. Counting tension stresses σ as positive, the stress is, in the deckhouse

$$\sigma_1 = \frac{N_1}{A_1} - \frac{M_1}{I_1} x_1 \ldots [2a]$$

in the hull

$$\sigma_2 = \frac{N_2}{A_2} - \frac{M_2}{I_2} x_2 \ldots [2b]$$

The stresses σ_1 and σ_2 at the junction of house and hull must be alike, and Equations [1] and [2] furnish, with $x_1 = -a\alpha_1$, $x_2 = a\alpha_2$

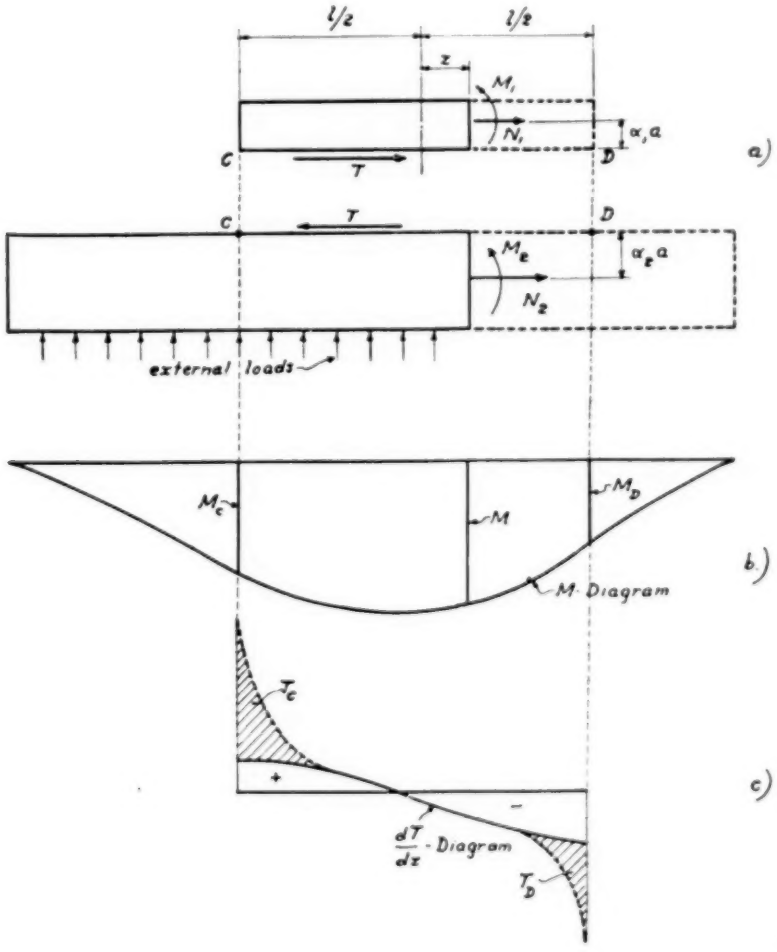

Fig. 7

$$T = \frac{a\alpha_2 I_1}{\frac{I_1 I_2}{A_1} + \frac{I_1 I_2}{A_2} + a^2(\alpha_2^2 I_1 + \alpha_1^2 I_2)} M \quad [3]$$

Introducing this value of T into Equations [1] and [2] one can determine moments and stresses at any point.

T was defined as the total horizontal shear force acting between the left end of the deckhouse and the section at z. According to Equation [3], T is proportional to the moment M, and the unit horizontal shear $(dT)/(dz)$ which will be transferred by rivets or welds from the hull to the deckhouse, will be

$$\frac{dT}{dz} = \frac{a\alpha_2 I_1}{\frac{I_1 I_2}{A_1} + \frac{I_1 I_2}{A_2} + a^2(\alpha_2^2 I_1 + \alpha_1^2 I_2)} V \quad [4]$$

where $V = (dM)/(dz)$ is the total shear force in the structure. However, it will be noticed that at the end C of the deckhouse the shear T is not zero, but equal to

$$T_C = \frac{a\alpha_2 I_1}{\frac{I_1 I_2}{A_1} + \frac{I_1 I_2}{A_2} + a^2(\alpha_2^2 I_1 + \alpha_1^2 I_2)} M_C \quad [5]$$

At a point slightly to the left of point C in Fig. 7(a) there is no deckhouse and therefore $T = 0$; this means that in addition to the distributed shear $(dT)/(dz)$, according to Equation [4], there must be a concentrated horizontal shear force T_C according to Equation [5] at point C, and a similar concentrated shear force T_D, at the other end D of the deckhouse. The typical distribution of the forces $(dT)/(dz)$ is indicated in Fig. 7(c).

It is obvious that the concentrated shear forces T_C and T_D cannot exist in any actual structure; their occurrence results from the fact that shear-lag effects were neglected when we assumed Navier's hypothesis to be correct for the full length of the deckhouse. In reality the forces T_C and T_D will distribute themselves over a finite distance, presumably of the magnitude of the depth of the deckhouse. This distribution is indicated by the broken line in Fig. 7(c), the shaded areas representing T_C and T_D. This means that the stresses in the vicinity of the end of the house found from Equations [2] are incorrect; but, according to Saint Venant's theorem, the effect of the simplification will not affect the stresses in the center portions of the structure.

The expressions for the moments M_1, M_2 and direct forces N_1 and N_2 obtained in the following become somewhat simpler if the notations

$$I_A = a^2 \frac{A_1 A_2}{A_1 + A_2} \quad [6a]$$

$$\mu = \frac{I_1 + \alpha_1 I_A}{I_2 + \alpha_2 I_A} \quad [6b]$$

are used. Term μ will be called the size factor; it is a measure of the size of the deckhouse in relation to the hull. The moment of inertia I of the total section consisting of hull and deckhouse can be expressed by the moments of inertia I_1, I_2 and by the constant I_A

$$I = I_1 + I_2 + I_A \quad [7]$$

Making use of the notation in Equations [6], the following expressions were derived

$$N_2 = -N_1 = T = \frac{MI_A}{aI} - \frac{MI_A}{a} \frac{\mu(\alpha_1 - \mu\alpha_2)}{(1+\mu)(\alpha_2 I_1 + \mu\alpha_1 I_2)} \quad [8a]$$

$$M_1 = M\frac{I_1}{I} - MI_1 \frac{\mu}{(1+\mu)(\alpha_2 I_1 + \mu\alpha_1 I_2)} \quad [8b]$$

$$M_2 = M\frac{I_2}{I} + MI_2 \frac{\mu^2}{(1+\mu)(\alpha_2 I_1 + \mu\alpha_1 I_2)} \quad [8c]$$

These expressions could be used to determine the stresses σ_1 and σ_2 in the deckhouse and hull. However, each of the three expressions consists of two terms, the first one being the value of the respective N or M if the conventional bending theory were applicable to the entire section. Therefore the actual stresses σ can be expressed as the sum of the stresses σ_N according to Navier's hypothesis, and a correction $\Delta\sigma$

$$\sigma = \sigma_N + \Delta\sigma \quad [9]$$

Navier's stresses σ_N can be found from the conventional equation

$$\sigma_N = -\frac{M}{I} x \quad [10]$$

where x is counted from the centroid of the entire section, Fig. 6(b). The corrective stresses $\Delta\sigma_1$ and $\Delta\sigma_2$ in the deckhouse and hull, respectively, are

$$\Delta\sigma_1 = \frac{\Delta N_1}{A_1} - \frac{\Delta M_1}{I_1} x_1, \quad \Delta\sigma_2 = \frac{\Delta N_2}{A_2} - \frac{\Delta M_2}{I_2} x_2 \quad [11]$$

where ΔN and ΔM are corrections of N and M given by the second terms of Equations [8]

$$\Delta N_1 = -\Delta N_2 = \frac{MI_A}{a} \frac{\mu(\alpha_1 - \mu\alpha_2)}{(1+\mu)(\alpha_2 I_1 + \mu\alpha_1 I_2)} \quad [12a]$$

$$\Delta M_1 = -MI_1 \frac{\mu}{(1+\mu)(\alpha_2 I_1 + \mu\alpha_1 I_2)} \quad [12b]$$

$$\Delta M_2 = MI_2 \frac{\mu^2}{(1+\mu)(\alpha_2 I_1 + \mu\alpha_1 I_2)} \quad [12c]$$

Fig. 8 shows typical stress distributions σ_N, $\Delta\sigma$, and $\sigma = \sigma_N + \Delta\sigma$ computed for Holt's model, Fig. 2. Owing to the fact that the structure analyzed in this section was simplified by omitting vertical forces acting between hull and deckhouse, the results are of limited significance; the typical break in the stress distribution at deck level is, however, already there. The value of the foregoing analysis lies in the fact that the more accurate analysis presented in the next section shows that the actual stresses can be expressed in the form $\sigma = \sigma_N + \Phi\Delta\sigma$, where Φ is a numerical factor depending on the various dimensions of hull and deckhouse and on the stiffness of the bulkheads.

It might be added at this point that the reasoning presented would be fully applicable also if hull and deckhouse would not be of constant section. All formulas derived in this section remain unchanged, except Equation [4] for the unit shear $(dT)/(dz)$; when deriving this equation from Equation [3] the fraction on the right-hand side would no longer be a constant, resulting in an added term in Equation [4]. The important result, that the stress at the midship section can be expressed as the sum of the stress σ_N, according to Navier's theory, and the correction $\Delta\sigma$ remains valid.

3 General Analysis of Two-Cell Structure

Consider again the structure indicated in Fig. 6; differing from the treatment in the preceding section the assumption is made that any relative displacement of the deckhouse with respect to the hull will be resisted by the internal vertical forces required to deflect bulkheads and transverse beams supporting the deckhouse. The deckhouse is, in effect, considered as a beam elastically supported on the hull, and is further attached to the hull at deck level so as to enforce equal strains.

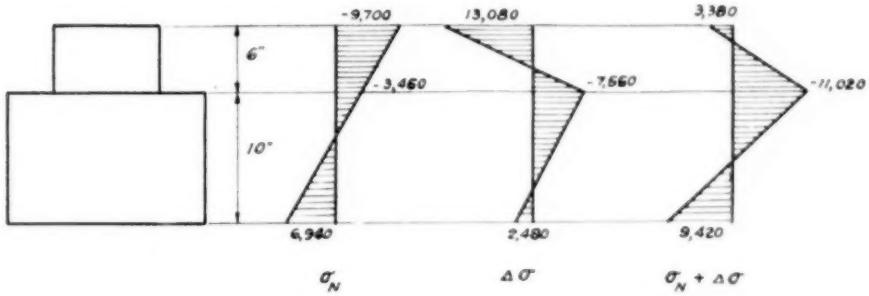

FIG. 8 TYPICAL STRESS DISTRIBUTION σ_N, $\Delta\sigma$, $\sigma_N + \Delta\sigma$ COMPUTED FOR MODEL REFERRED TO IN FIG. 2

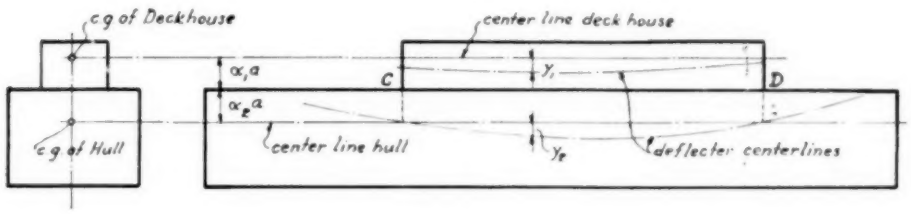

FIG. 9

Under the action of external vertical loads and buoyancy the structure indicated in Fig. 9 will deflect and we can describe the deformations by the deflections y_1 and y_2 of the center lines of the deckhouse and hull, respectively. In order to exclude motions of the entire vessel as a rigid body, y_1 and y_2 are defined not as the absolute displacements, but as the relative displacements measured from a straight line *C-D* rigidly connected to the hull. As a result of this definition the displacement y_2 of the centroid of the hull at points *C* and *D* must always be zero.

It is further assumed that the stiffness of bulkheads or deck beams resisting relative vertical displacements of the deckhouse is constant for the full length of the deckhouse, the magnitude of the stiffness being given by a spring constant K. This spring constant K is defined as the force per unit length of deckhouse required to produce a relative deflection equal to one unit of length, Fig. 10. Therefore the vertical reaction between hull and deckhouse will be $K(y_1 - y_2)$ per unit of length.

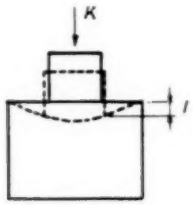

FIG. 10

The structure analyzed here consists therefore of two beams having areas A_1, A_2 and moments of inertia I_1 and I_2; the two beams are connected along *C-D* in such a way that both horizontal shear forces and vertical reactions can be transferred. Fig. 11 indicates a general type of loading for the vessel, including the shear and moment diagrams. We assume Navier's hypothesis to be valid for the hull and for the deckhouse separately, and there is no problem concerning the determination of stresses fore and aft of the deckhouse; we can, therefore, restrict the analysis to the center portion *C-D* of the structure. This center portion, indicated in Fig. 12, will be under the action of vertical loads p_1 on the deckhouse, p_2 on the hull (which includes buoyancy), shear forces S_C, S_D, and moments M_C and M_D.

The differential equation for the two deflections y_1 and y_2 describing the deformation of the structure can be obtained conveniently from the "theorem of stationary potential energy" stating that the deformations of any structure are such that the total potential energy U of the system is a minimum. In the present case the potential energy U consists of the internal strain energy V, and the potential U_w of the external forces p_1, p_2, S_C, S_D, M_C, and M_D. The total potential energy $U = V + U_w$ is[9]

$$U = \frac{1}{2}\int_{-l/2}^{l/2} [EI_1 y_1''^2 + EI_2 y_2''^2 + EI_A(\alpha_1 y_1'' + \alpha_2 y_2'')^2 + K(y_1 - y_2)^2 - 2p_1 y_1 - 2p_2 y_2]dz + [My_2']_{-l/2}^{l/2} - [Sy_2]_{-l/2}^{l/2} \quad [13]$$

U will be a minimum if the variation

$$\delta U = 0 \quad [14]$$

Using the rules of the calculus of variations[10] one can derive the set of two simultaneous differential equations

$$E(I_1 + \alpha_1^2 I_A)y_1^{IV} + Ky_1 + \alpha_1\alpha_2 EI_A y_2^{IV} - Ky_2 = p_1 \quad [15a]$$

$$\alpha_1\alpha_2 EI_A y_1^{IV} - Ky_1 + E(I_2 + \alpha_2^2 I_A)y_2^{IV} + Ky_2 = p_2 \quad [15b]$$

The process of variation also furnishes the boundary conditions required to determine the eight arbitrary constants which will appear in the general solutions of the differential Equations [15]. For $z = +l/2$ and $z = -l/2$

$$y_2 = 0 \quad [16a]$$

$$E(I_1 + \alpha_1^2 I_A)y_1'' + \alpha_1\alpha_2 EI_A y_2'' = 0 \quad [16b]$$

$$\alpha_1\alpha_2 EI_A y_1'' + E(I_2 + \alpha_2^2 I_A)y_2'' = -M \quad [16c]$$

[9] See Appendix, Equations [37] and [40].

[10] "Buckling Strength of Metal Structures," by F. Bleich, McGraw-Hill Book Company, Inc., New York, N. Y., 1952, pp. 91–102.

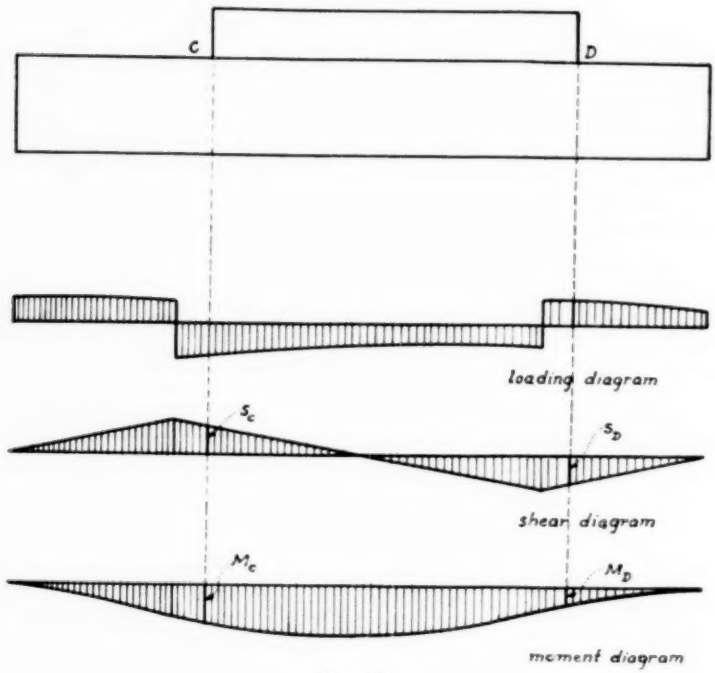

FIG. 11

$$E(I_1 + \alpha_1^2 I_A) y_1''' + \alpha_1 \alpha_2 E I_A y_2''' = 0 \quad \ldots\ldots [16d]$$

The meaning of the first of these boundary conditions is obvious, but the other three require physical interpretation. The moments M_1 and M_2 of the longitudinal stresses in the deckhouse and hull can be expressed by the usual relationships $M_1 = -EI_1 y_1''$ and $M_2 = -EI_2 y_2''$; Equations [16*b*, *c*] can therefore be rearranged

$$M_1 = \alpha_1 E I_A (\alpha_1 y_1'' + \alpha_2 y_2'') \quad \ldots\ldots [17a]$$

$$M_2 = M + \alpha_2 E I_A (\alpha_1 y_1'' + \alpha_2 y_2'') \quad \ldots\ldots [17b]$$

These equations indicate that the moments M_1 and M_2 at the end of the deckhouse are not equal to zero, and M, respectively, as might have been expected. Using the expression Equation [42] for the horizontal shear T derived in the Appendix, Equations [17] become

$$M_1 = -a\alpha_1 T \quad \ldots\ldots [18a]$$

$$M_2 = M - a\alpha_2 T \quad \ldots\ldots [18b]$$

and these equations are identical with Equations [1] for the simplified structure considered in section 2. It must be remembered that Equations [18] apply only at the end points of the deckhouse; but at these points the moments and stresses as determined in section 2 occur, and the conclusion that concentrated horizontal shear forces must be presumed to act at these points remains valid. The magnitude of these forces is given by Equation [5].

The fourth boundary condition, Equation [16*d*] expresses the fact that the shear force at the end of the deckhouse must vanish; this can be seen by comparison with the expression for the shear force, Equation [44], derived in the Appendix.

4 Solution of Differential Equation for Constant Moment M

Consider first the simple case that the loads p_1, p_2 and the shears S_C and S_D are zero, the only loads being $M_C = M_D = M$. Equations [15] are then homogeneous, and the general solution of these equations contains eight arbitrary constants to satisfy the eight boundary conditions, Equations [16]. The problem considered is symmetrical with respect to the origin of the co-ordinate z, and using only symmetrical functions, the general symmetrical solution will contain only four arbitrary constants. This general solution is

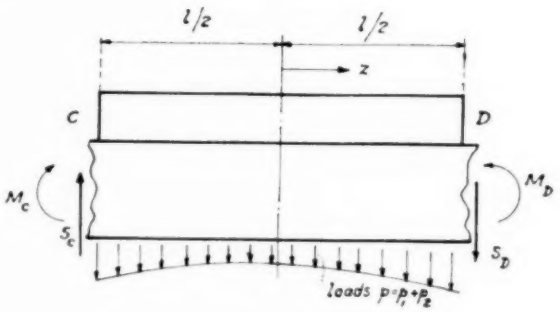

FIG. 12

$$y_1 = C_1 + C_2 z^2 + C_3 \sin \gamma z \sinh \gamma z + C_4 \cos \gamma z \cosh \gamma z. \quad [19a]$$

$$y_2 = C_1 + C_2 z^2 - \mu C_3 \sin \gamma z \sinh \gamma z - \mu C_4 \cos \gamma z \cosh \gamma z \ldots [19b]$$

where

$$\gamma = \sqrt[4]{\frac{K}{4E} \frac{1 + \mu}{\alpha_2 I_1 + \mu \alpha_1 I_2}} \quad \ldots\ldots [20]$$

and μ is defined by Equation [6*b*].

Introduction of Equations [19] into the boundary conditions, Equations [16], leads to the values of the constants

$$C_2 = -\frac{M}{2EI} \quad [21a]$$

$$C_3 = \frac{1}{2\gamma^2} \frac{\mu \Phi_1 M}{(1+\mu)E(\alpha_2 I_1 + \mu \alpha_1 I_2)} \quad [21b]$$

$$C_4 = \frac{1}{2\gamma^2} \frac{\mu \Psi_1 M}{(1+\mu)E(\alpha_2 I_1 + \mu \alpha_1 I_2)} \quad [21c]$$

The value of C_1 is not given as it describes only a rigid-body motion of the structure not required for the purposes of this paper. Φ_1 and Ψ_1 are

$$\Phi_1 = \frac{\sin u \cosh u + \cos u \sinh u}{\sin u \cos u + \sinh u \cosh u} \quad [22a]$$

$$\Psi_1 = \frac{\cos u \sinh u - \sin u \cosh u}{\sin u \cos u + \sinh u \cosh u} \quad [22b]$$

where

$$u = \frac{\gamma l}{2} = \frac{l}{2} \sqrt[4]{\frac{K}{4E} \frac{1+\mu}{\alpha_2 I_1 + \mu \alpha_1 I_2}} \quad [23]$$

The stresses can be computed from the expressions for the moments M_1, M_2 and direct forces N_1, N_2

$$M_1 = -E I_1 y_1'', \quad M_2 = -E I_2 y_2'' \quad [24a]$$

$$N_1 = -N_2 = \frac{EI_A}{a}(\alpha_1 Y_1'' + \alpha_2 y_2'') \quad [24b]$$

(for derivation of Equation [24b] see Appendix, Equation [41]).

For the midship section, $z = 0$, the following values were found

$$N_2 = -N_1 = M \frac{I_A}{aI} - \Phi_1 M \frac{I_A}{a} \frac{\mu(\alpha_1 - \mu\alpha_2)}{(1+\mu)(\alpha_2 I_1 + \mu \alpha_1 I_2)} \quad [25a]$$

$$M_1 = M \frac{I_1}{I} - \Phi_1 M I_1 \frac{\mu}{(1+\mu)(\alpha_2 I_1 + \mu \alpha_1 I_2)} \quad [25b]$$

$$M_2 = M \frac{I_2}{I} + \Phi_1 M I_2 \frac{\mu^2}{(1+\mu)(\alpha_2 I_1 + \mu \alpha_1 I_2)} \quad [25c]$$

Comparing Equations [25] and Equations [8] obtained in section 2, we see as only difference the factor Φ_1, appearing in the second term of each of Equations [25]. In section 2 we had found that the first term of each Equations [8] represented the result of Navier's theory, while the second term was a correction. The refined theory in this section furnished a similar result, but the "correction" found in section 2 is to be multiplied by a factor Φ_1. To compute the stresses according to the refined theory we can use the relationship

$$\sigma = \sigma_N + \Phi_1 \Delta\sigma \quad [26]$$

where Navier's stresses σ_N, the corrective stresses $\Delta\sigma_1$, $\Delta\sigma_2$, and the corrective forces ΔN_1, ΔN_2 and moments ΔM_1, ΔM_2 are to be computed from Equations [10], [11], and [12] in section 2. Numerical values of the deviation factor Φ_1 are given in Table 1.

This result, Equation [26], is surprisingly simple; it indicates that the deviation of the stress distribution from Navier's calculations is indicated by the value of the nondimensional factor Φ_1 which will be called "Deviation Factor." Fig. 13 shows Φ_1 as function of the parameter u defined by Equation [23]. Term u is a function of the dimensions of hull and deckhouse and of the stiffness factor K of the bulkheads, and is proportional to the length of the deckhouse, and increases with rising value of K. According to Fig. 13, $\Phi_1 = 1$ for $u = 0$ and decreases for rising values of u; for $u > 2$ the factor Φ_1 is a small positive or even negative number, indicating that for such values Navier's stress distribution at the midship section is approximately correct.

Equation [26] was derived for the midship section, $z = 0$. The solution of the differential equations found in the foregoing permits the computation of the stresses at any other section too, and a similar relationship

$$\sigma = \sigma_N + \Phi_1(z) \Delta\sigma \quad [27]$$

exists all along the deckhouse; however, the value of the deviation factor is not the same as at the midship section $z = 0$; $\Phi_1(z)$ is a function of u and of the ratio z/l, defining the location of the cross section. Fig. 14 shows $\Phi_1(z)$ as a function of the ratio z/l for several values of u. The value of the deviation factor at the end of the deckhouse $z/l = 0.5$ is 1 for all values of u; for large values of u, $\Phi_1(z)$ is very small everywhere, except near the end of the deckhouse, indicating the validity of Navier's theory in the center portions of the deckhouse.

TABLE 1 VALUES OF DEVIATION FACTORS Φ_1 AND Φ_2

u	Φ_1	Φ_2	u	Φ_1	Φ_2
0	1.000	1.000	2.0	0.144	0.249
0.2	1.000	1.000	2.2	0.054	0.165
0.4	0.996	0.997	2.4	−0.009	0.103
0.6	0.979	0.982	2.6	−0.050	0.059
0.8	0.935	0.944	2.8	−0.074	0.029
1.0	0.852	0.872	3.0	−0.084	0.009
1.2	0.728	0.764	3.5	−0.078	−0.012
1.4	0.573	0.629	4.0	−0.052	−0.014
1.6	0.411	0.487	4.5	−0.026	−0.010
1.8	0.264	0.357	5.0	−0.009	−0.004

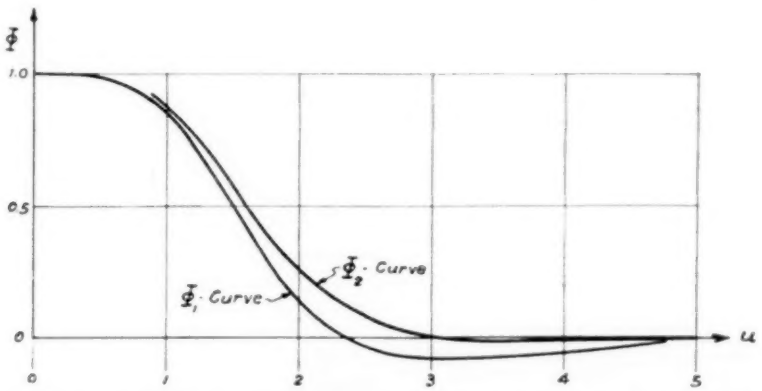

FIG. 13 DEVIATION FACTORS Φ_1 AND Φ_2 AT CENTER OF VESSEL ($z = 0$) AS FUNCTION OF NONDIMENSIONAL PARAMETER u

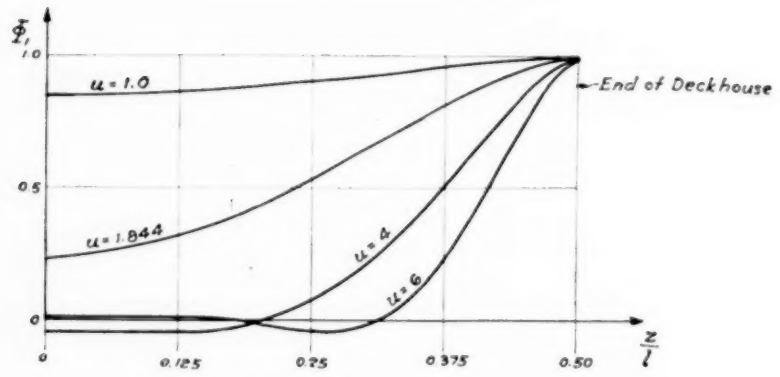

FIG. 14 LONGITUDINAL VARIATION OF DEVIATION FACTOR Φ_1

5 SOLUTION OF DIFFERENTIAL EQUATION FOR EQUALLY DISTRIBUTED LOADS

In this section the case is considered of equally distributed loads p_1 and p_2, acting on deckhouse and hull, respectively, while the moments at the end of the deckhouse are $M_C = M_D = 0$. Equilibrium requires external shear forces

$$S_C = -S_D = \frac{l}{2}(p_1 + p_2)$$

at the ends C and D. The moment in the midship section due to the loads p_1 and p_2 is

$$M_p = \frac{p_1 + p_2}{8} l^2 \quad \ldots\ldots [28]$$

The loading being symmetrical, the general symmetrical solutions of Equation [5] are

$$y_1 = C_1 + C_2 z^2 + C_3 \sin \gamma z \sinh \gamma z + C_4 \cos \gamma z \cosh \gamma z + \frac{p_1 + p_2}{24\,EI} z^4 + \frac{p_1}{(1+\mu)K} \quad \ldots\ldots [29a]$$

$$y_2 = C_1 + C_2 z^2 - \mu C_3 \sin \gamma z \sinh \gamma z - \mu C_4 \cos \gamma z \cosh \gamma z + \frac{p_1 + p_2}{24\,EI} z^4 + \frac{\mu p_2}{(1+\mu)K} \quad \ldots\ldots [29b]$$

where γ is defined by Equation [20].

The boundary conditions, Equations [16], furnish the values of the arbitrary constants

$$C_2 = -\frac{M_p}{2EI} \quad \ldots\ldots [30a]$$

$$C_3 = \frac{1}{2\gamma^2} \frac{\mu \Phi_2 M_p}{(1+\mu)E(\alpha_2 I_1 + \mu \alpha_1 I_2)} \quad \ldots\ldots [30b]$$

$$C_4 = \frac{1}{2\gamma^2} \frac{\mu \Psi_2 M_p}{(1+\mu)E(\alpha_2 I_1 + \mu \alpha_1 I_2)} \quad \ldots\ldots [30c]$$

where M_p is the moment at mid-span given by Equation [28], and

$$\Phi_2 = \frac{2}{u} \frac{\sin u \sinh u}{\sin u \cos u + \sinh u \cosh u} \quad \ldots\ldots [31a]$$

$$\Psi_2 = \frac{2}{u} \frac{\cos u \cosh u}{\sin u \cos u + \sinh u \cosh u} \quad \ldots\ldots [31b]$$

$u = \gamma l/2$ is defined by Equation [23].

Equations [30] are quite similar to Equations [21] and the further computation follows the pattern of the preceding section, the only difference being that instead of the deviation factor Φ_1 a factor Φ_2 appears. The stresses at the midship section, $z = 0$, are

$$\sigma = \sigma_N + \Phi_2 \Delta\sigma \quad \ldots\ldots [32]$$

Equations [10], [11], and [12] are to be used to compute σ. Numerical values of the deviation factor Φ_2 are given in Table 1.

Fig. 13 shows Φ_1 and Φ_2 as functions of the parameter u. In the important range $u < 3$, Φ_2 is larger than Φ_1, indicating that equally distributed load produces larger deviations from Navier's stresses than a constant moment. There is only a quantitative difference between the two loading cases considered in this and the preceding section; the spanwise variation of the deviation factor for distributed load will be similar to the one shown in Fig. 14 for constant moment.

6 EXAMPLE AND DISCUSSION OF RESULTS

Consider the model of a ship's structure shown in Fig. 15, loaded by equal end moments corresponding to the case treated in section 4. The section properties are as follows:[11]

Deckhouse: $A_1 = 2.95$ sq in., $I_1 = 11.4$ in.^{4}, $\alpha_1 = 0.372$, $l = 70$ in.

Hull: $A_2 = 7.85$ sq in., $I_2 = 160.9$ in.^{4}, $\alpha_2 = 0.628$, $K = 20{,}000$ psi

General: $E = 29 \times 10^6$ psi, $a = 9.36$ in., $M = 375{,}000$ in.-lb

The stresses σ_N and $\Delta\sigma$, determined from Equations [10], [11], and [12] are shown in Fig. 8. The actual stress distribution is according to Equation [26]

$$\sigma = \sigma_N + \Phi_1 \Delta\sigma$$

where Φ_1 is a function of the parameter u, Equation [23]. One finds $u = 1.92$ and by interpolation from Table 1, $\Phi_1 = 0.192$. The final stress distribution is shown in Fig. 16. For comparison purposes Fig. 16(a) also shows the conventional linear stress distribution. The distribution is similar to the one found by Holt, Fig. 2; a numerical comparison is not possible as the test loading differs from those treated in the paper.

Equation [26] shows that the deviation from the linear stress distribution depends on the factor Φ which, according to Table 1, has its largest value $\Phi = 1$ for $u = 0$, and is quite small when the parameter $u > 0$. The value of this parameter, Equation [22]

[11] The properties of the section agree with those of the center portion of the model used by Holt, except for the value of K which could not be ascertained. The moment M selected is equal to the maximum value at the center in Holt's test.

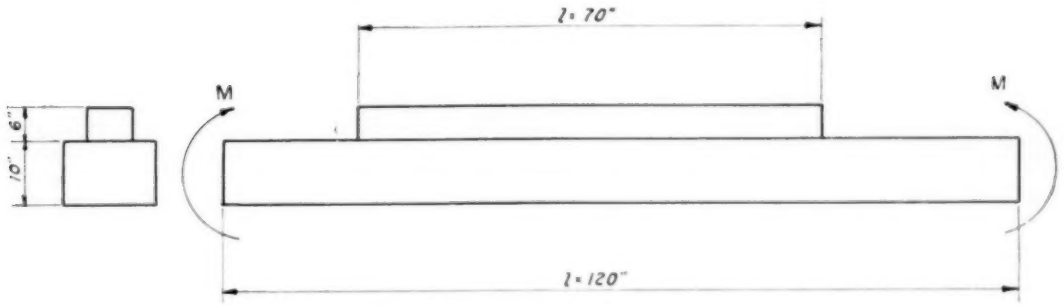

Fig. 15

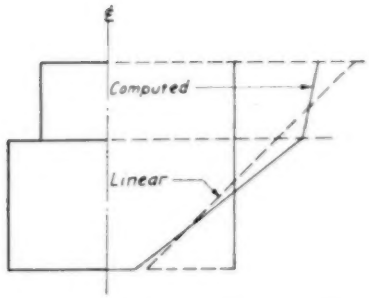

Fig. 16 Comparison of Computed and Linear Stress Distributions

depends on all the section properties; u increases when the length l of the deckhouse is increased; it is also sensitive to changes in the spring constant K describing the resistance of the section to distortion. If either l or K is sufficiently large to make $u > 3$ the stress distribution at the center will be close to linear. However, even for large values of u, the deviation factor Φ will be close to unity near the end of the superstructure, Fig. 14, and the stress distribution in this region will not be linear. (It must be noted that in this region the stress distribution will be further affected by shear effects not considered in this paper.)

The dependency of the parameter u on K furnishes the explanation why the tests on the model shown in Fig. 3 indicated good agreement with the conventional linear theory. Because of the continuity of the side plating the resistance to relative displacements of superstructure and hull is very large, and K is very large. In this case, u is also large, making the deviation factor very small, which agrees with the test result.

A point worth discussing is the rather surprising result, expressed by Equations [26] and [27], that the stress distribution can always be considered a linear combination of the distributions σ_N and $\Delta\sigma$. The stresses σ_N and $\Delta\sigma$ are determined from considerations of equilibrium alone, and the factor Φ expresses the only effect of the compatibility conditions represented by the differential Equations [15]. The cause lies in the assumption on which this paper is based that each of the two beams of which the structure consists have linear stress distribution. Due to this assumption the bending stresses in any cross section can be described by three parameters, two of which are defined by equilibrium conditions (the horizontal resultant of all stresses vanishes, and their moment equals the external moment). This leaves only one parameter free, for which Φ can be selected. It appears, therefore, that a relation $\sigma = \sigma_N + \Phi\Delta\sigma$ will exist not only for the two cases analyzed in this paper, but also for any other loading condition and for structures with variable cross sections and spring constants. In any such structure the state of stress can be described fully by a deviation function $\Phi(z)$, which conclusion should be of considerable value in interpreting results of tests.

Appendix

Derivation of Strain Energy of Structure

Denoting by ϵ_1 and ϵ_2 the average longitudinal strain in the deckhouse and hull, respectively, the strain energy of the longitudinal stresses will be as follows:

Deckhouse:

$$\frac{E}{2}\int_{-l/2}^{l/2}(A_1\epsilon_1^2 + I_1 y_1''^2)dz$$

Hull:

$$\frac{E}{2}\int_{-l/2}^{l/2}(A_2\epsilon_2^2 + I_2 y_2''^2)dz$$

The strains ϵ are counted positive if they represent elongation.

In addition to the strain energy of the longitudinal stresses, there will be energy stored in the bulkheads or deck beams which resist the relative vertical displacements of deckhouse and hull; this part of the strain energy can be expressed by the spring constant K in the form

$$\frac{1}{2}\int_{-l/2}^{l/2}K(y_1 - y_2)^2\,dz$$

The strain energy of the shear stresses will be neglected; it is small because we consider the case of long deckhouses only. The total strain energy V is

$$V = \frac{E}{2}\int_{-l/2}^{l/2}\left[A_1\epsilon_1^2 + I_1 y_1''^2 + A_2\epsilon_2^2 + I_2 y_2''^2 + \frac{K}{E}(y_1 - y_2)^2\right]dz \quad \ldots\ldots [33]$$

The stresses in the deckhouse and hull can be expressed by the average strains ϵ_1 and ϵ_2, and by the second derivatives of the deflections y_1'' and y_2''

Deckhouse: $\sigma = E\epsilon_1 + E\,y_1''\,x_1$

Hull: $\sigma = E\epsilon_2 + E\,y_2''\,x_2$

where x_1 and x_2 are defined in Fig. 6. Because hull and deckhouse are connected by rivets or welds, the stresses on the main deck level must be alike and we have for $x_1 = -a\alpha_1$, $x_2 = a\alpha_2$

$$E\epsilon_1 - E\,a\alpha_1\,y_1'' = E\epsilon_2 + E\,a\alpha_2 y_2'' \quad \ldots\ldots [34]$$

Further, the longitudinal resultant of all stresses in the deckhouse N_1, must be equal to $EA_1\epsilon_1$ and, similarly, $N_2 = EA_2\epsilon_2$. The resultant of all longitudinal forces, $N_1 + N_2$, must vanish

$$N_1 + N_2 = E(\epsilon_1 A_1 + \epsilon_2 A_2) = 0 \quad \ldots\ldots [35]$$

By means of Equations [34] and [35], ϵ_1 and ϵ_2 can be expressed by the curvatures y_1'' and y_2''

$$\epsilon_1 = \frac{aA_2}{A_1 + A_2}(\alpha_1 y_1'' + \alpha_2 y_2'')$$

$$\epsilon_2 = -\frac{aA_1}{A_1 + A_2}(\alpha_1 y_1'' + \alpha_2 y_2'') \quad \ldots\ldots [36]$$

Substituting these values into Equation [33]

$$V = \frac{E}{2}\int_{l/2}^{l/2}\left[I_1 y_1''^2 + I_2 y_2''^2 + I_A(\alpha_1 y_1'' + \alpha_2 y_2'')^2 + \frac{K}{E}(y_1 - y_2)^2\right] dz \quad \ldots\ldots [37]$$

Potential Energy U_w of External Forces

Counting p_1 and p_2 positive if acting downward, their potential energy is

$$-\int_{-l/2}^{l/2}(p_1 y_1 + p_2 y_2)\, dz \quad \ldots\ldots [38]$$

The shear forces S_C and S_D and the moments M_C and M_D act immediately outside points C and D, and their potential energy will depend on the vertical displacements y_{2C} and y_{2D} and on the rotations of the end surfaces of the hull, y_{2C}' and y_{2D}'. Taking into account the direction of the shears and moments shown in Fig. 12, the potential energy will be

$$-S_D y_{2D} + S_C y_{2C} + M_D y_{2D}' - M_C y_{2C}' = -[S_{y_2}]_{-l/2}^{l/2} + [M_{y_2}']_{-l/2}^{l/2} \quad \ldots\ldots [39]$$

and the total potential energy U_w of the external loads is

$$U_w = [M_{y_2}']_{-l/2}^{l/2} - [S_{y_2}]_{-l/2}^{l/2} - \int_{-l/2}^{l/2}(p_1 y_1 + p_2 y_2)\, dz \quad \ldots [40]$$

Expressions for Longitudinal Forces and Horizontal and Vertical Shears

The resultants N_1 and N_2 of the longitudinal stresses in the deckhouse and hull are $N_1 = EA_1\epsilon_1$ and $N_2 = EA_2\epsilon_2$, or with reference to Equations [36] and [6a]

$$\left.\begin{aligned} N_1 &= \frac{EI_A}{a}(\alpha_1 y_1'' + \alpha_2 y_2'') \\ N_2 &= -\frac{EI_A}{a}(\alpha_1 y_1'' + \alpha_2 y_2'') \end{aligned}\right\} \quad \ldots\ldots [41]$$

T being the total shear force from the left end of the deckhouse to a point having the co-ordinate z, equilibrium requires

$$T = -N_1 = -\frac{EI_A}{a}(\alpha_1 y_1'' + \alpha_2 y_2'') \quad \ldots\ldots [42]$$

and the unit horizontal shear will be

$$\frac{dT}{dz} = -\frac{EI_A}{a}(\alpha_1 y_1''' + \alpha_2 y_2''') \quad \ldots\ldots [43]$$

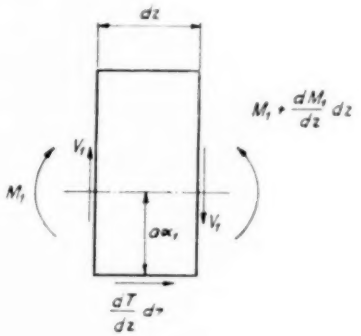

Fig. 17

To obtain the expression for the vertical shear V_1 in the deckhouse, consider an element of the deckhouse of length dz, Fig. 17. Equilibrium of moments with respect to the centroid requires

$$V_1 - a\alpha_1\frac{dT}{dz} = \frac{dM_1}{dz}$$

Substituting $M_1 = -EI_1 y_1''$ and Equation [43]

$$V_1 = -E(I_1 + \alpha_1^2 I_A)y_1''' - \alpha_1\alpha_2 EI_A y_2''' \quad \ldots\ldots [44]$$

The vertical shear in the hull is similarly

$$V_2 = -\alpha_1\alpha_2 EI_A y_1''' - E(I_2 + \alpha_2^2 I_A)y_2''' \quad \ldots\ldots [45]$$

The Necking and the Rupture of Rods Subjected to Constant Tensile Loads

By N. J. HOFF,[1] BROOKLYN, N. Y.

A one-dimensional theory of the behavior of a nonlinear viscoelastic bar subjected to a constant tensile load is developed with the aid of a creep law considering secondary creep alone. The theoretical value of the time at which the bar ruptures and the shape calculated for the necked portion of the bar are in satisfactory agreement with the results of experiments.

Introduction

THEORETICAL and experimental investigations of the necking and the rupture of bars subjected to the ordinary tensile test are discussed in detail in Nadai's treatise "Theory of Flow and Fracture of Solids," (1).[2] Most of the research men mentioned in this book predicted necking from the stress-strain curve or obtained the stress distribution in the necked portion of the bar experimentally. Ilyushin (2)[3] was the first investigator to introduce viscous effects into his analysis. By means of a two-dimensional viscoplastic theory he studied the stability of the flow in a thin strip of material subjected to tension. The relationship between strain rate and stress was assumed to be linear in agreement with the results of his tests carried out at very high speeds of straining.

In the present note a simple one-dimensional analysis is carried out on the assumption that the material is perfectly viscoelastic. The connection between strain rate and stress underlying the calculations is a nonlinear one derived from creep-test data obtained with metals. The load is assumed to be constant as it usually is in creep tests. The rupture time and the shape of the necked portion of the bar obtained from the theory are in satisfactory agreement with the results of experiments carried out by Dorn and Tietz (3) and with the photographs in Nadai's book (1).

Behavior of a Perfect Cylindrical Bar

When uniformly distributed tensile stresses are applied to the ends of a perfectly cylindrical bar of uniform material properties, the state of stress is one dimensional and the bar distorts uniformly. It is assumed that the deformations consist of two parts, one elastic and the other of the creep type. Tests carried out with rods subjected to constant tensile loads have shown that at first the rod elongates rather rapidly, but soon it settles down to a uniform rate of elongation designated as the steady creep rate. In the present note the first stage of deformation is disregarded and it is assumed that the creep deformations at any particular temperature are defined with sufficient accuracy by the creep law

$$\dot{\epsilon} = (d\epsilon/dt) = f(\sigma) \quad [1]$$

This implies that the time rate of the tensile strain $\dot{\epsilon}$ is constant for any given stress at a given temperature. The dependence of the creep rate $\dot{\epsilon}$ on the stress must be determined by experiment.

It is known (4) that the steady rate of creep changes over to a monotonically increasing one as soon as the decrease in cross-sectional area accompanying the stretching of the bar causes the stress to increase substantially. It is reasonable, therefore, to modify the empirical creep law of Equation [1] by replacing the stress and strain in it by their instantaneous values at any given time. The new creep law is then applicable to an extended test in which the bar elongates materially and its cross-sectional area decreases correspondingly. If the volume is assumed to be constant, the instantaneous value of the stress is

$$\sigma = \sigma_n(1 + \epsilon) \quad [2]$$

and is known as the true stress. The load divided by the original area is the nominal stress σ_n. The instantaneous value of the strain is called the natural strain, or the true strain, and is defined as

$$\epsilon_n = \lg(1 + \epsilon) \quad [3]$$

where lg designates the natural logarithm. If the notation is introduced

$$R = (1 + \epsilon) \quad [4]$$

the creep law of Equation [1] in its generalized form is

$$(d/dt) \lg R = (\dot{R}/R) = f(\sigma_n R) \quad [5]$$

The elastic strain ϵ_e is defined as

$$\epsilon_e = \sigma/E \quad [6]$$

and thus upon substitution of the true stress and the natural strain in place of the conventional values, the law governing the total deformations becomes

$$(\dot{R}/R) = (\sigma_n/E)\dot{R} + f(\sigma_n R) \quad [7]$$

The variables can be separated in this differential equation and the solution can be given in the form

$$t = \int [1/f(\sigma_n R)]\,[(1/R) - (\sigma_n/E)]dR + C \quad [8]$$

where C is a constant of integration. It must be determined from the initial conditions

---

[1] Head, Department of Aeronautical Engineering and Applied Mechanics, Polytechnic Institute of Brooklyn. Mem. ASME.

[2] Numbers in parentheses refer to the Bibliography at the end of the paper.

[3] After this article was accepted for publication, Prof. E. H. Lee of Brown University brought to the attention of the author a paper entitled, "High-Speed Tension Tests at Elevated Temperatures — Parts II and III," by A. Nadai and M. J. Manjoine, JOURNAL OF APPLIED MECHANICS, Trans. ASME, vol. 63, 1941, pp. A-77–A-91. In this paper the tension test was investigated with the aid of linear, power function, and hyperbolic-sine type laws of viscosity, and the shape of the necked portion was presented in diagrams calculated for linearly viscous and linearly viscoplastic materials. The author regrets that he had overlooked this important paper in which the concept of viscosity was used to explain the necking process long before Ilyushin's publication.

Contributed by the Applied Mechanics Division and presented at the Annual Meeting, New York, N. Y., November 30–December 5, 1952, of THE AMERICAN SOCIETY OF MECHANICAL ENGINEERS.

Discussion of this paper should be addressed to the Secretary, ASME, 29 West 39th Street, New York, N. Y., and will be accepted until April 10, 1953, for publication at a later date. Discussion received after the closing date will be returned.

NOTE: Statements and opinions advanced in papers are to be understood as individual expressions of their authors and not those of the Society. Manuscript received by ASME Applied Mechanics Division, May 6, 1952. Paper No. 52—A-12.

$$\epsilon = (\sigma_o/E) = \epsilon_o, \quad R = 1 + \epsilon_o = R_o, \quad \text{when } t = 0 \ldots [8a]$$

The results of creep tests are usually presented as the logarithm of the stress plotted against the logarithm of the steady creep rate. The curves obtained are often straight lines. When such is the case the creep function in Equation [1] can be represented as (5)

$$f(\sigma) = (\sigma/\lambda)^n \ldots [9]$$

that is

$$f(\sigma_o R) = (\sigma_o R/\lambda)^n \ldots [10]$$

Substitution of this function in Equation [8] and consideration of the initial conditions yield

$$t = (\lambda/\sigma_o)^n \left[\frac{R_o^{-n} - R^{-n}}{n} - \frac{\sigma_o}{E} \frac{R_o^{-(n-1)} - R^{-(n-1)}}{n-1} \right] \ldots [11]$$

provided

$$n > 1 \ldots [11a]$$

If the elastic deformations are disregarded this equation becomes

$$t = (\lambda/\sigma_o)^n (1/n) (R_o^{-n} - R^{-n}) \ldots [12]$$

But in the absence of elastic deformations $R_o = 1$ and at $t = 0$, Equations [1], [2], [3], and [9] yield

$$\dot{\epsilon}_{no} = \dot{\epsilon}_o/(1 + \epsilon_o) = \dot{\epsilon}_o = f(\sigma_o) = (\sigma_o/\lambda)^n \ldots [13]$$

Hence Equation [12] also can be written as

$$t = (1/n\dot{\epsilon}_o) (1 - R^{-n}) \ldots [14]$$

When the nominal strain approaches infinity, R also approaches infinity and the cross-sectional area tends to zero. The time at which this happens is designated as the critical time t_{cr}. From Equation [14]

$$t_{cr} = (1/n\dot{\epsilon}_o) = (1/n) (\lambda/\sigma_o)^n \ldots [15]$$

and the equation governing the deformations of the bar can be written in the final form

$$t = t_{cr}(1 - R^{-n}) \ldots [16]$$

In the curve marked $^9/_{18}$ in Fig. 1 the change Δr in the radius r of a cylindrical bar of circular cross section is plotted as $\Delta r/r$ against the time ratio t/t_{cr} in accordance with Equation [16]. The material constants were determined from experimental data presented by Dorn and Tietz (3) for 248-T3 aluminum alloy at 400 F. The creep law derived from the data is

$$\dot{\epsilon} = (\sigma/74{,}000)^{8.5} \ldots [17]$$

where $\dot{\epsilon}$ is the strain rate per hour and σ is the stress in pounds per square inch. It follows from the assumption of the constancy of the volume during the deformations that

$$\Delta r/r = 1 - (1/\sqrt{R}) \ldots [18]$$

Necking

An actual bar does not remain cylindrical throughout the tensile test but is known to neck down in some section which is weaker than the others because of unavoidable inaccuracies in the geometry of the bar and random variations in the properties of its material. The progress of necking was calculated from Equation [16] for the aluminum-alloy bar characterized by Equation [17]. It was assumed that the material properties were constant but the cross-sectional area of the bar was 1 per cent greater at the two ends of the bar than in the middle and the area varied along the bar according to a sine law. An increase of 1 per cent in the area corresponds to 1 per cent decrease in stress and to 18.44 per cent increase in the critical time of a bar for which Equation [17] holds. Therefore the radius-time relationship for the end sections was obtained from the curve marked $^9/_{18}$ in Fig. 1 by keeping the ordinates unchanged and multiplying the abscissas by 1.1844. The result is the curve marked $x/L = 0$. The other curves shown correspond to intermediate sections. For the actual computation of the shape of the necked portion of the bar more curves were used than the ones shown and the range of the diagram was extended to larger values of $\Delta r/r$.

The points of intersection of any straight line t = const with the curves define the shape of the bar at that time if the assumption of a one-dimensional state of stress can be maintained. Obviously this is a good approximation as long as the shape of the deformed bar does not differ much from a cylinder but it becomes progressively worse as the contour of the bar deviates more and more from the straight line.

The progress of necking is illustrated in Fig. 2. The shape at

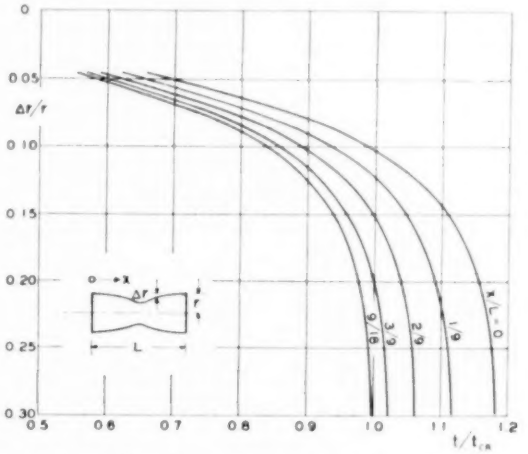

Fig. 1 Radius-Time Relationship for an Imperfect Tension Bar of Circular Cross Section

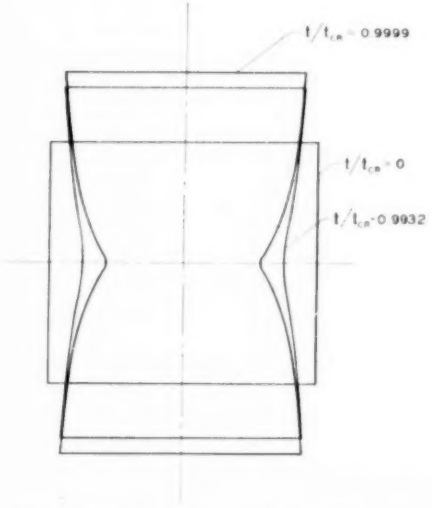

Fig. 2 Successive Shapes of Bar in Tension

$t = 0$ is not cylindrical but the $\frac{1}{2}$ per cent increase in the radius of the end sections (corresponding to the 1 per cent increase in cross-sectional area) as compared to the radius of the middle section is not visible in the drawing. At $t = 0.9932t_{cr}$ the necking becomes noticeable and progresses very rapidly since at $t = 0.9999t_{cr}$ the bar assumes the grooved shape shown by the third curve, and at $t = t_{cr}$ the necking penetrates to the axis of the bar.

The necking is accompanied by elongations in the axial direction which vary along the bar. When the curves in Fig. 2 were drawn, the average nominal strain between two consecutive reference sections was computed and the corresponding value of $R = 1 + \epsilon$ was multiplied by the initial distance between the sections. This increased distance was used in locating the final relative positions of the sections in the drawing.

As the shape of the necked portion shown in Fig. 2 resembles the photographs of test specimens in Nadai's book (1), the deviations from the one-dimensional state of stress may not have a significant influence upon necking in the stages of deformation shown.

Rupture Time

According to Equation [15], the time t_{cr} necessary for the cross-sectional area of the rod to be reduced to zero is inversely proportional to the steady creep rate $\dot{\epsilon}_o$ at the initial stress caused by the load and to the exponent n of the creep function in Equation [9].

An actual bar subjected to a constant load will naturally fail in a shorter time, namely, when the cross-sectional area becomes so small that the tensile stress in it causes rupture. The condition of failure also is influenced by the radial and tangential stresses prevailing in the necked sections. However, the time values indicated in Fig. 2 show the necking to take place so rapidly that the value of t_{cr} should be very close to the time when the rod fails except when the initial stress differs little from the stress at rupture. This latter case is of little significance in creep testing. For these reasons t_{cr} will be assumed to be the time at which the rod ruptures. As both the creep rate and the time-to-rupture values usually are presented on double logarithmic paper, the experimental creep law and the critical time formula are rewritten here in a logarithmic form

$$\log \dot{\epsilon}_o = -n \log \lambda + n \log \sigma_o \quad \ldots\ldots\ldots [19]$$

$$\log t_{cr} = -\log n - \log \dot{\epsilon}_o \quad \ldots\ldots\ldots [20]$$

where log is the logarithm to base 10.

It follows from these equations that the double-logarithmic plot of the stress against the rupture time is a straight line if the double-logarithmic plot of the stress-strain rate relationship is linear. The two straight lines are mirrored images of each other with the mirroring taking place about the line

$$\log \dot{\epsilon}_o = -(\tfrac{1}{2}) \log n \quad \ldots\ldots\ldots [21]$$

These statements are illustrated in Fig. 3. The value of n is the ratio A/B provided the proper linear scales are used in measuring these quantities. For instance, in the figure the length of a unit on the σ_o scale is 4.75 times the length of a unit on the $\dot{\epsilon}_o$ scale. Hence $n = 2 \times 4.75 = 9.5$. As $\log 9.5 = 0.9777$, the line $\sigma_o = f_1(\dot{\epsilon}_o)$ must be mirrored about the line $\log \dot{\epsilon}_o = -0.48885$. In the usual creep diagram the scales of $\dot{\epsilon}_o$ and t_{cr} are shifted relative to each other.

The results of the tests carried out by Dorn and Tietz on six materials at four different temperatures were compared with the predictions of the theory just developed. Theoretical values of t_{cr} were calculated from the initial creep rates and plotted in the diagrams showing the experimental values. Fig. 4, presenting data on 38-H18 aluminum alloy, may serve as an example for the

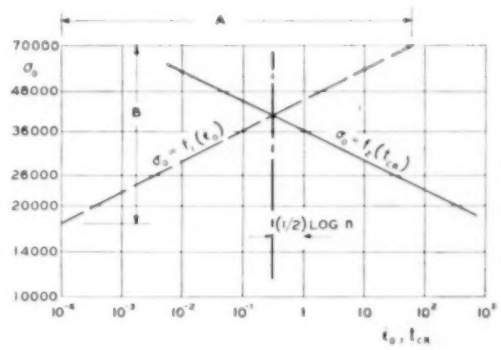

Fig. 3 Graphic Determination of t_{cr} From the $\dot{\epsilon}$-Values

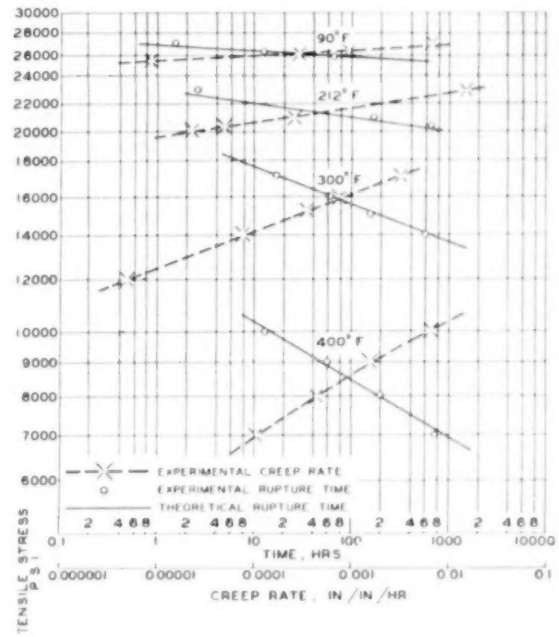

Fig. 4 Comparison of Theory and Experiment; 38-H18 Aluminum Alloy Tested by Dorn and Tietz

satisfactory agreement obtained. The crosses are the experimental $\dot{\epsilon}_o$-values, the dotted lines their connecting lines, the circles the experimental rupture times, and the full lines the theoretical curves obtained from Equation [15].

The agreement was similarly good with the other materials (38-H12, 528-H32, 528-H38, 618-T6, and 248-T3 aluminum alloys) except in the case of three test series. These were made on 618-T6 specimens at 400 F and on 248-T3 specimens at 300 F and 400 F. As these two materials were precipitation-hardened, it is reasonable to assume that their metallographic and mechanical properties may have changed during tests carried out at such high temperatures. The specimens softened and failed at times amounting only to $\frac{1}{3}$ to $\frac{1}{10}$ the theoretical values. The comparison was somewhat inconclusive in the case of tests at 90 F because the small slope could not be determined with sufficient accuracy. At such temperatures, however, aluminum alloys can hardly be expected to behave as perfectly viscoelastic materials.

It should be mentioned that the tests cited were carried out with thin sheet specimens. It is possible that the effect of the three-dimensional state of stress is more pronounced with circular cylindrical specimens and thus there may be a greater difference between the rupture times of the latter and the critical time values predicted by the theory than between the rupture times of the sheet specimens of Dorn and Tietz and the theoretical values.

Acknowledgment

The author acknowledges his indebtedness to S. Patel for his help with the computations and to Matthew G. Forte and Thomas J. Toomey for tracing the diagrams.

Bibliography

1 "Theory of Flow and Fracture of Solids," by A. Nadai, second edition, McGraw-Hill Book Company, Inc., New York, N. Y., vol. 1, 1950, p. 70.

2 Ibid., p. 85; also "The Deformation of a Visco-Plastic Solid," by A. A. Ilyushin, Uchenye Zapiski Moskovskogo Gosudarstvennogo Universiteta, Mekhanika, vol. 39, 1940, p. 1; translated by the Graduate Division of Applied Mathematics, Brown University, Providence, R. I., 1947.

3 "Creep and Stress-Rupture Investigations on Some Aluminum Alloy Sheet Metals," by J. E. Dorn and T. E. Tietz, Proceedings of the American Society for Testing Materials, vol. 49, 1949, p. 815.

4 General information on creep can be found in Nadai's book (1); also in "Engineering Materials," by Joseph Marin, Prentice-Hall, Inc., New York, N. Y., 1952, p. 250, and in "The Creep of Metals," by E. Orowan, *Journal of the West of Scotland Iron and Steel Institute*, Session 1946–1947, p. 46.

5 See p. 417 of reference (1), and p. 265 of Marin's book (reference 4).

6 Reference (1), p. 77.

On Turbulent Flow Between Parallel Plates

By S. I. Pai,[1] College Park, Md.

The Reynolds equations of motion of turbulent flow of incompressible fluid have been studied for turbulent flow between parallel plates. The number of these equations is finally reduced to two. One of these consists of mean velocity and correlation between transverse and longitudinal turbulent-velocity fluctuations $u_1'u_2'$ only. The other consists of the mean pressure and transverse turbulent-velocity intensity. Some conclusions about the mean pressure distribution and turbulent fluctuations are drawn. These equations are applied to two special cases: One is Poiseuille flow in which both plates are at rest and the other is Couette flow in which one plate is at rest and the other is moving with constant velocity. The mean velocity distribution and the correlation $\overline{u_1'u_2'}$ can be expressed in a form of polynomial of the co-ordinate in the direction perpendicular to the plates, with the ratio of shearing stress on the plate to that of the corresponding laminar flow of the same maximum velocity as a parameter. These expressions hold true all the way across the plates, i.e., both the turbulent region and viscous layer including the laminar sublayer. These expressions for Poiseuille flow have been checked with experimental data of Laufer fairly well. It also shows that the logarithmic mean velocity distribution is not a rigorous solution of Reynolds equations.

Nomenclature

The following nomenclature is used in the paper:

a = half width between parallel plates
a_1 = coefficient in mean velocity distribution of Couette flow, Equation [65]
a_2 = coefficient in mean velocity distribution of Poiseuille flow Equation [45]
a_{2n} = coefficient in mean velocity distribution of Poiseuille flow, Equation [45]
a_{2n+1} = coefficient in mean velocity distribution of Couette flow, Equation [65]
A = constant
B = constant
C = constant
C_f = coefficient of friction defined by Equation [22]
f = any quantity of the mean flow, Equation [2]
n = exponential factor
p = pressure
p_o = a reference pressure
P = a component of pressure defined by Equation [35]
r = nondimensional correlation coefficient defined by Equation [25]
$\mathbf{R}^*$ = U^*a/ν, Reynolds number
$\mathbf{R}_o$ = $U_o\,a/\nu$, Reynolds number
$\mathbf{R}_m$ = $U_m\,a/\nu$, Reynolds number
s = τ_o/τ_l
t = time
u_i = ith component of velocity
U = velocity of moving plate in Couette flow
U^* = $\sqrt{\tau_o/\rho}$; reference velocity
U_o = average mean velocity defined by Equation [20]
U_m = maximum velocity in Poiseuille flow
V = u_1/U^*; nondimensional velocity
V_m = u_1/U_m; nondimensional velocity
x_i = ith co-ordinate
y = nondimensional co-ordinate similar to η
α = constant
δ = distance from plate
η = x_2/a nondimensional co-ordinate of x_2
ν = coefficient of kinematic viscosity
ξ = x_1/a nondimensional co-ordinate of x_1
ρ = density of fluid
σ = nondimensional transverse turbulent intensity defined by Equation [26]
τ_l = laminar shearing stress on wall
τ_o = shearing stress on the wall
ϕ = certain function
ω = nondimensional pressure defined by Equation [24]
— (bar) means mean values
′ (prime)—fluctuating values
Without bar or prime; instantaneous values
Sub i (or j, or k); means 1, 2, or 3
1—in direction of mean flow
2—in direction perpendicular to plates
3—in direction perpendicular to 1 and 2

Introduction

The essential characteristic of turbulent motion is that the turbulent fluctuations are random in nature. Hence the final and logical solution of the turbulence problem requires the application of methods of statistical mechanics. Osborne Reynolds first introduced elementary statistical notions into the consideration of the turbulence problem. He assumed that the instantaneous velocity components u_i of the fluid satisfy the Navier-Stokes equations and that these instantaneous velocity components may be decomposed into two parts, the mean velocity components u_i and the turbulent fluctuating-velocity components u_i' which are zero in the mean, i.e.

$$u_i = \bar{u}_i + u_i' \qquad [1]$$

If we substitute u_i from Equation [1] into the Navier-Stokes equations of motion for an incompressible fluid, and use the rules that we may derive for taking means, a new set of equations, known as Reynolds equations, is obtained. This differs from Navier-Stokes equations only in the presence of additional terms, Reynolds stresses or eddy stresses, added to the mean values of the stresses due to viscosity.

The solutions of Reynolds equations will represent properly the turbulent flow. However, there are only four equations of Reynolds for ten unknowns, namely, the mean pressure, three mean velocity components and six Reynolds stresses. In general, the

[1] Associate Research Professor, Institute for Fluid Dynamics and Applied Mathematics, University of Maryland.

Contributed by the Applied Mechanics Division and presented at the Annual Meeting, New York, N. Y., November 30–December 5, 1952, of The American Society of Mechanical Engineers.

Discussion of this paper should be addressed to the Secretary, ASME, 29 West 39th Street, New York, N. Y., and will be accepted until April 10, 1953, for publication at a later date. Discussion received after the closing date will be returned.

Note: Statements and opinions advanced in papers are to be understood as individual expressions of their authors and not those of the Society. Manuscript received by ASME Applied Mechanics Division, May 13, 1952. Paper No. 52—A-5.

Reynolds equations are not sufficient to determine these unknowns.

In so far as the mean velocity distribution is concerned, some semiempirical theories, sometimes known as phenomenological theories, of fully developed turbulent flow have been developed. The application of these theories to some engineering problems has been quite successful. The best known theory among these is Prandtl's mixing-length theory.[2] The famous von Kármán's logarithmic velocity distribution is derived from the mixing-length theory. Even though Prandtl's mixing-length theory had predicted successfully the mean velocity distribution in turbulent flow, it is now generally believed to have serious limitations and inconsistencies. The mixing length deduced from measurements of the mean velocity is of the same order of magnitude of the dimension of the mean flow, but in the theory it should be very small. The assumption on the distribution of mixing length is not true in general as revealed from hot-wire anemometer measurements of these quantities. The boundary condition at the wall is not satisfied. Usually one can only say that the result of the mixing-length theory does not hold true for a laminar sublayer and a viscous layer which are near the wall. Furthermore, it definitely fails in prediction of turbulent fluctuations.

In order to understand more thoroughly the mechanism of turbulent flow, it is better to study the Reynolds equations themselves without introducing the concept of mixing length. Professor Kampe de Feriet[3] recently studied the Reynolds equations for turbulent flow of incompressible fluid between two fixed parallel walls, i.e., so-called Poiseuille flow. Some interesting results have been obtained. This paper, in addition to some of Professor Kampe de Feriet's results which are not quite well known in this country, extends his results in two respects: (*a*) A solution of Reynolds equations for mean velocity distribution between parallel fixed walls is obtained, which holds true not only in the turbulent-flow region but also in the laminar sublayer and the viscous layer, i.e., it holds true across the whole channel. Such a solution has been checked very well with experimental data of Laufer[4] for turbulent flow in a channel. The correlation of turbulent fluctuations, i.e., Reynolds stresses, obtained from the mean velocity distribution, also agrees with the experimental data. (*b*) The whole analysis is extended to the case of Couette flow, i.e., one wall is fixed and the other is moving with a constant velocity. Since there is no known experimental data for this case, it has not been checked with experimental data.

Statement of Problem

Consider the turbulent flow of incompressible fluid between two infinite parallel plates; one is at rest and the other may be at rest or in uniform motion. The distance between the plates is $2a$. The co-ordinate axes are Ox_1-x_2-x_3 shown in Fig. 1, where $x_1 = 0$ is arbitrarily chosen. The plates are located at $x_2 = \pm a$ and they are extended to

$$-\infty < x_1 < +\infty, \quad -\infty < x_3 < +\infty$$

The velocity of the upper plate is $u_1 = U'$, which is equal to or greater than zero.

Furthermore, we assume that the mean flow is steady and two-dimensional, i.e.

$$\frac{\partial \bar{f}}{\partial t} = 0, \quad \frac{\partial \bar{f}}{\partial x_3} = 0, \quad \therefore \bar{f} = \bar{f}(x_1, x_2) \ldots\ldots [2]$$

where $\bar{f}$ may represent any quantity of the mean flow such as mean velocity $\bar{u}_1$ or mean pressure $\bar{p}$, and so on.

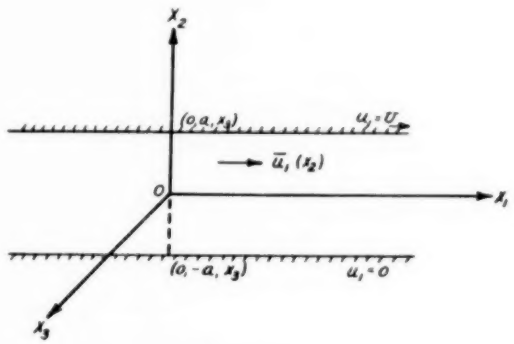

Fig. 1 Flow Between Parallel Walls

The instantaneous velocity components of the flow are u_1, u_2, and u_3 along the x_1, x_2, and x_3 axes, respectively. We assume that the mean flow has velocity components along x_1-axis only, i.e.

$$\bar{u}_1 = \bar{u}_1(x_1, x_2); \quad \bar{u}_2 = \bar{u}_3 = 0 \ldots\ldots [3]$$

The turbulent-velocity components along the x_1, x_2, and x_3 axes, respectively, are

$$u_1' = u_1 - \bar{u}_1, \; u_2' = u_2, \; u_3' = u_3 \ldots\ldots [4]$$

In the equations of motion of turbulent flow, Reynolds equations, (Equation [9]), we have the following mean values of turbulent fluctuations

$$\overline{u_1'^2}(x_2), \; \overline{u_2'^2}(x_2), \; \overline{u_3'^2}(x_2), \; \overline{u_1'u_2'}(x_2), \; \overline{u_2'u_3'}(x_2), \; \overline{u_3'u_1'}(x_2) \ldots [5]$$

Here we assume that these mean values of turbulent fluctuations are functions of x_2 only. This is due to the fact that we consider a problem which has the same statistical properties at all planes $x_1 = \text{const}$.

Fundamental Equations

We assume that the instantaneous velocity components of the flow satisfy the Navier-Stokes equations

$$\frac{du_i}{dt} = -\frac{1}{\rho}\frac{\partial p}{\partial x_i} + \nu \frac{\partial^2 u_i}{\partial x_k \, \partial x_k} \ldots\ldots [6]$$

where

$$\frac{d}{dt} = \frac{\partial}{\partial t} + u_i \frac{\partial}{\partial x_i}, \quad \frac{\partial^2}{\partial x_k \partial x_k} = \frac{\partial^2}{\partial x_1^2} + \frac{\partial^2}{\partial x_2^2} + \frac{\partial^2}{\partial x_3^2}$$

ρ = density and ν = coefficient of kinematic viscosity, $k, i = 1, 2,$ or 3 and the summation convention is used.

The equation of continuity is

$$\frac{\partial u_i}{\partial x_i} = 0 \ldots\ldots [7]$$

Substituting

$$p = \bar{p} + p', \; u_i = \bar{u}_i + u_i' \ldots\ldots [8]$$

into Equations [6] and [7] and averaging, we have

[2] "Modern Developments in Fluid Dynamics," by S. Goldstein, Oxford University Press, London, England, vols. 1 and 2, 1938.

[3] "Sur l'Écoulement d'un fluide visqueux incompressible entre deux plaques parallèles indefinies," by J. Kampe de Feriet, La Houille Blanche, Grande-Rue, Grenoble, France, vol. 23, November-December, 1948, pp. 1–9.

[4] "Some Recent Measurements in a Two-Dimensional Turbulent Channel," by J. Laufer, *Journal of the Aeronautical Sciences*, vol. 17, 1950, pp. 277–287.

$$\frac{\delta \overline{u_i}}{\delta t} = -\frac{1}{\rho}\frac{\partial \bar{p}}{\partial x_i} - \frac{\partial \overline{u_i' u_j'}}{\partial x_j} + \nu \frac{\partial^2 \overline{u_i}}{\partial x_k \partial x_k} \quad [9]$$

where

$$\frac{\delta}{\delta t} = \frac{\partial}{\partial t} + \overline{u_i}\frac{\partial}{\partial x_i}$$

$j = 1, 2, \text{ or } 3$

$$\frac{\partial \overline{u_i}}{\partial x_i} = 0 \quad [10]$$

Equations [9] and [10] are known as Reynolds equations, which are the fundamental equations for turbulent flow of incompressible fluid. There are ten unknowns: $\bar{p}$ (1), $\overline{u_i}$ (3) and $\overline{u_i' u_j'}$ (6). The four Reynolds equations are not sufficient in general to find the ten unknowns. However, in our present problem, because of the simplicity of the configuration of the problem, it is possible to get some information from these fundamental equations.

Turbulent Flow Between Parallel Walls

If we substitute Equation [3] into Equation [10], we have

$$\left.\begin{aligned} \frac{\partial \overline{u_1}}{\partial x_1} &= 0 \\ \text{or} \qquad \overline{u_1} &= \overline{u_1}(x_2) \end{aligned}\right\} \quad [11]$$

We see that the mean velocity u_1 is a function of x_2 only.

Consider the case $x_1 = x_2$ in Equation [9] with the help of Equations [2], [3], and [5], we have

$$\frac{\partial}{\partial x_2}(\overline{u_2' u_3'}) = 0 \quad [12]$$

Since on the wall

$$\overline{u_2' u_3'} = 0$$

we conclude that

$$u_2' u_3' = 0 \quad [13]$$

for the whole velocity field. In this type of flow, the correlation between u_2' and u_3' is zero in the entire flow field.

The other two equations of Equation [9] become

$$\frac{1}{\rho}\frac{\partial \bar{p}}{\partial x_1} - \nu \frac{d^2 \overline{u_1}}{dx_2^2} + \frac{d}{dx_2}(\overline{u_1' u_2'}) = 0 \quad [14]$$

$$\frac{1}{\rho}\frac{\partial \bar{p}}{\partial x_2} + \frac{d}{dx_2}(\overline{u_2'^2}) = 0 \quad [15]$$

Now we have four unknowns: $\overline{u_1}(x_2)$, $\bar{p}(x_1, x_2)$, $\overline{u_1' u_2'}(x_2)$ and $\overline{u_2'^2}(x_2)$ but only two Equations [14] and [15]. We cannot solve this problem completely, i.e., we cannot find these four unknowns from two relations. However, it is possible to obtain some relations between these four unknown quantities.

Before discussing these relations we will first transform the equations into nondimensional form.

We define the nondimensional co-ordinates as follows

$$\xi = \frac{x_1}{a}, \quad \eta = \frac{x_2}{a} \quad [16]$$

The plates are now located at $\eta = \pm 1$.

Let τ_o be the shearing stress on the lower plates, i.e., at $\eta = -1$; τ_o is a constant in the present problem. We define a reference velocity

$$U^* = \sqrt{\tau_o/\rho} \quad [17]$$

and the corresponding Reynolds number $\mathbf{R}^*$

$$\mathbf{R}^* = U^* a/\nu \quad [18]$$

The nondimensional mean velocity is defined as

$$V = \overline{u_1}/U^* = V(\eta, \mathbf{R}^*) \quad [19]$$

The average of the mean velocity over any section $x_1 = \text{const}$ is U_o, i.e.

$$U_o = \frac{1}{2a}\int_{-a}^{a} \overline{u_1} dx_2; \quad \frac{U_o}{U^*} = \frac{1}{2}\int_{-1}^{1} V d\eta \quad [20]$$

The corresponding Reynolds number is

$$\mathbf{R}_o = \frac{U_o a}{\nu} \quad [21]$$

The coefficient of friction on the plate is defined as

$$C_f = \frac{\tau_o}{\rho U_o^2/2} \quad [22]$$

Hence

$$\frac{\mathbf{R}^*}{\mathbf{R}_o} = \frac{U^*}{U_o} = \sqrt{\frac{C_f}{2}} \quad [23]$$

The nondimensional pressure is defined as

$$\bar{\omega} = \frac{\bar{p} - \bar{p}_o}{\rho U^{*2}} = \bar{\omega}(\xi, \eta, \mathbf{R}^*) \quad [24]$$

where $\bar{p}_o$ is a reference pressure which may be taken, for example, as the mean pressure at the point $x_1 = 0$, $x_2 = -a$ or ($\xi = 0$, $\eta = -1$)

The nondimensional forms of turbulent fluctuations are

$$r(\eta, \mathbf{R}^*) = \frac{\overline{u_1' u_2'}}{U^{*2}} \quad [25]$$

and

$$\sigma(\eta, \mathbf{R}^*) = \frac{\overline{u_2'^2}}{U^{*2}} \quad [26]$$

In nondimensional form, Equations [14] and [15] become

$$\frac{\partial \bar{\omega}}{\partial \xi} - \frac{1}{\mathbf{R}^*}\frac{d^2 V}{d\eta^2} + \frac{dr}{d\eta} = 0 \quad [27]$$

$$\frac{\partial \bar{\omega}}{\partial \eta} + \frac{d\sigma}{d\eta} = 0 \quad [28]$$

The boundary conditions are

$$\left.\begin{aligned} &(a) \quad V(-1, \mathbf{R}^*) = 0; \quad V(+1, \mathbf{R}^*) = 0 \\ &\text{for Poiseuille flow.} \\ &V(-1, \mathbf{R}^*) = 0; \quad V(+1, \mathbf{R}^*) = \frac{U}{U^*} \end{aligned}\right\} \quad [29]$$

for Couette flow.

$$(b) \quad r(-1, \mathbf{R}^*) = r(+1, \mathbf{R}^*) = 0 \quad [30]$$

$$(c) \quad \sigma(-1, \mathbf{R}^*) = \sigma(+1, \mathbf{R}^*) = 0 \quad [31]$$

$$(d) \quad \tilde{\omega}(0, -1, \mathbf{R}^*) = 0 \qquad [32]$$

Equation [32] is obtained because of the choice of p_o in Equation [24].

Integration of Equations [27] and [28] gives

$$\tilde{\omega}(\xi, \eta, \mathbf{R}^*) + \sigma(\eta, \mathbf{R}^*) = A\xi + C \qquad [33]$$

$$\frac{1}{\mathbf{R}^*}\frac{d}{d\eta} V(\eta, \mathbf{R}^*) - r(\eta, \mathbf{R}^*) = A\eta + B \qquad [34]$$

where A, B, and C are constants. From Equations [31] and [32], we have that $C = 0$. Hence the mean pressure $\tilde{\omega}$ becomes

$$\tilde{\omega}(\xi, \eta, \mathbf{R}^*) = A\xi + P(\eta, \mathbf{R}^*) \qquad [35]$$

where $P(\eta, \mathbf{R}^*)$ is a function of η and $\mathbf{R}^*$ but independent of ξ.

Poiseuille Flow—Flow in Channel

In this case both plates are at rest and the flow is symmetrical with respect to $\eta = 0$. The shearing stresses on the walls in non-dimensional form are

$$\left.\begin{aligned} \mathbf{R}^* &= \frac{dV}{d\eta} \quad \text{at } \eta = -1 \\ \mathbf{R}^* &= -\frac{dV}{d\eta} \quad \text{at } \eta = +1 \end{aligned}\right\} \qquad [36]$$

Substituting Equations [30] and [36] into Equation [34], we have

$$A = -1, \quad B = 0 \qquad [37]$$

Hence Equations [33] and [34] become

$$\tilde{\omega} + \sigma = -\xi \qquad [38]$$

$$-\frac{1}{\mathbf{R}^*}\frac{dV}{d\eta} + r = \eta \qquad [39]$$

It is interesting to note that the four unknown quantities are divided into two groups, V and r in one group, and $\tilde{\omega}$ and σ in another. The correlation $\overline{u_1' u_2'}$ influences only the mean velocity profile, while the transverse turbulent velocity intensity $\overline{u_2'^2}$ affects only the mean pressure distribution.

From Equation [40] two conclusions of practical interest may be drawn for the mean pressure

(*a*) Since $\sigma(\eta)$ is independent of ξ, the mean pressure $\tilde{\omega}$ decreases linearly with increase of ξ in the same manner as in laminar flow.

(*b*) For a given section of $x_1 = \text{const}$, since $\sigma(\eta) \geq 0$, the mean pressure in the fluid is less than or equal to the mean pressure on the wall.

Because of symmetry with respect to $\eta = 0$, we have

$$\left.\begin{aligned} V(\eta, \mathbf{R}^*) &= V(-\eta, \mathbf{R}^*) \\ \tilde{\omega}(\xi, \eta, \mathbf{R}^*) &= \tilde{\omega}(\xi, -\eta, \mathbf{R}^*) \end{aligned}\right\} \qquad [40]$$

From Equations [39] and [40], we see that $r(\eta, \mathbf{R}^*)$ must be an odd function of η, i.e.

$$r(-\eta, \mathbf{R}^*) = -r(\eta, \mathbf{R}^*) \qquad [41]$$

and in particular

$$r(0, \mathbf{R}^*) = 0 \qquad [42]$$

Integration of Equation [39] gives

$$V(\eta, \mathbf{R}^*) = \frac{\mathbf{R}^*}{2}(1 - \eta^2) + \mathbf{R}^* \int_{-1}^{\eta} r(y, R^*)\, dy \qquad [43]$$

If $r(\eta, \mathbf{R}^*) \equiv 0$, Equation [43] reduces to the velocity profile of laminar Poiseuille flow.

By symmetry conditions of Equations [40], we have

$$\frac{U_m}{U^*} = \frac{\overline{u_1}_{\max}}{U^*} = V(0, \mathbf{R}^*) = \frac{\mathbf{R}^*}{2} + \mathbf{R}^* \int_{-1}^{0} r(y, \mathbf{R}^*) dy \qquad [44]$$

where $u_{\max} = U_m$ is the maximum x_1-wise velocity component of the mean flow which occurs on the axis of symmetry.

If we express $V(\eta, \mathbf{R}^*)$ as a power series of η, we find that in order to satisfy Equation [43] and the boundary conditions, Equations [29] and [30], the power series can contain only three terms of even power of η. In order to comply with the results of laminar flow, we have to write the expression of $V(\eta, \mathbf{R}^*)$ as follows

$$V = \frac{U_m}{U^*}(1 + a_2\eta^2 + a_{2n}\eta^{2n}) \qquad [45]$$

where n is an integer larger than or equal to 2 but otherwise arbitrary. Substituting Equation [45] into [43] and using the boundary conditions, Equations [29] and [30], we have

$$a_2 = \frac{s - n}{n - 1}, \quad a_{2n} = \frac{1 - s}{n - 1} \qquad [46]$$

where

$$s = \frac{\mathbf{R}^* U^*}{2U_m} = \frac{\tau_w}{\frac{\mu}{a}\frac{2U_m}{a}} = \frac{\tau_w}{\tau_l} \qquad [47]$$

i.e., s is the ratio of the shearing stress τ_w on the wall in turbulent flow to the corresponding shearing stress on the wall for laminar flow τ_l with the same maximum velocity U_m.

Hence the mean velocity profile is

$$V(\eta, \mathbf{R}^*) = \frac{U_m}{U^*}\left(1 + \frac{s - n}{n - 1}\eta^2 + \frac{1 - s}{n - 1}\eta^{2n}\right) \qquad [48]$$

and the correlation r is

$$r(\eta, \mathbf{R}^*) = \eta\,[1 - \eta^{2n-2}]\,\frac{n(s-1)}{s(n-1)} \qquad [49]$$

If $s = 1$, Equation [48] reduces automatically to the case of laminar flow, and Equation [49] is identical to zero. In turbulent flow s is larger than 1. The value of n has to be determined from experimental data. From Laufer's measurements[4] of turbulent flow in channel, we find roughly from the average of three curves that

$$n \doteqdot 1.40\, s \qquad [50]$$

We may choose n as the nearest integer given by Equation [50]. For instance, in Laufer's measurements, for Reynolds number $\mathbf{R}_m = aU_m/\nu = 12{,}300$, we have $s = 11.06$, and $n \doteqdot 16$, hence

$$V_m(\eta, \mathbf{R}^*) = 1 - 0.3293\eta^2 - 0.6707\,\eta^{32} \qquad [51]$$

where $V_m = \overline{u_1}/U_m$ and the correlation r is

$$r(\eta, \mathbf{R}^*) = 0.9702\eta[1 - \eta^{30}] \qquad [52]$$

Equations [51] and [52] are plotted in Fig. 2, where Laufer's experimental data are also indicated. Fig. 2(*a*) is the same as Fig. 2, except that the scale is changed so that we see more clearly the values near the wall. It shows that the theoretical curves check with experimental data fairly well, not only in the turbulent region in the usual sense, but also in the laminar sublayer and the viscous layer as well.

The coefficient of friction C_f is given by the following formula from Equations [20], [23], and [43]

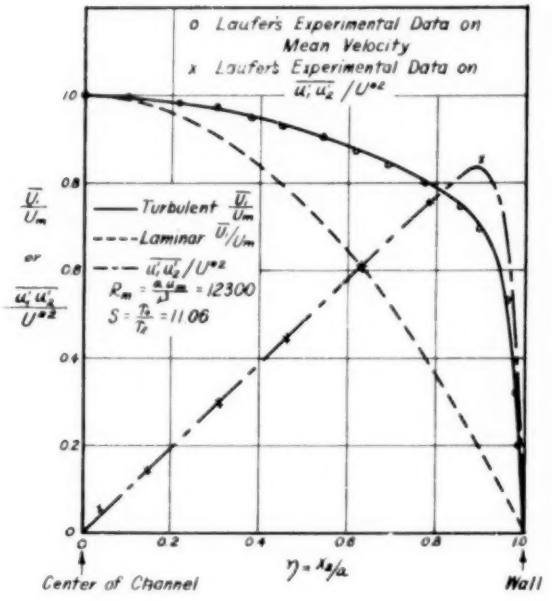

FIG. 2 TURBULENT FLOW IN CHANNEL

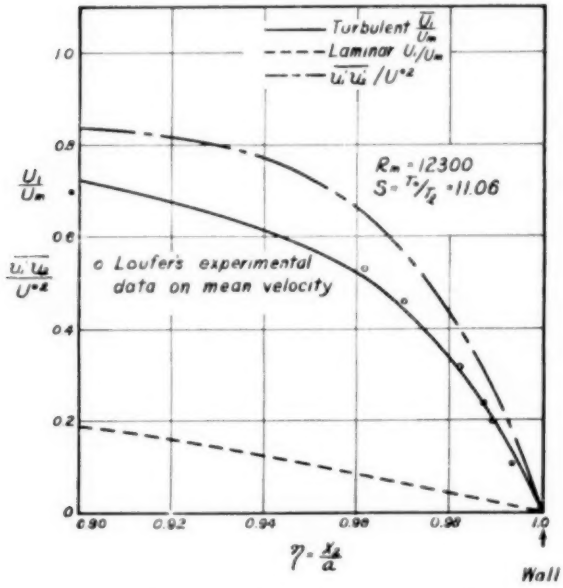

FIG. 2(a) TURBULENT FLOW IN CHANNEL NEAR WALL

$$\sqrt{\frac{2}{C_f}} = \frac{\mathbf{R}^*}{3} - \mathbf{R}^* \int_0^1 \eta\, r(\eta, \mathbf{R}^*) d\eta \quad \ldots\ldots [53]$$

Substituting the value of r of Equation [52] into [53], we have

$$\sqrt{\frac{2}{C_f}} = \frac{\mathbf{R}^*}{3}\left[1 - \frac{2n(s-1)}{s(2n+1)}\right] = \frac{R^*}{3}\left[1 - \frac{2.8(s-1)}{2.8\,s+1}\right] \quad [54]$$

According to Professor Kampe de Feriet,[2] the necessary and sufficient conditions for the existence of logarithmic velocity distribution of von Kármán are as follows:

1 A universal profile (due to Prandtl and Nikuradse) with abscissa $\delta U^*/\nu$ where δ is the distance from the plate and ordinance u_1/U^* exists. In the present notation

$$\left.\begin{aligned} V(\eta, \mathbf{R}^*) &= \phi[(1-\eta)\mathbf{R}^*] \quad 0 \le \eta \le 1 \\ V(\eta, \mathbf{R}^*) &= \phi[(1+\eta)\mathbf{R}^*] \quad -1 \le \eta \le 0 \end{aligned}\right\} \quad \ldots\ldots [55]$$

2 The following Stanton's law holds

$$\frac{U_m - U_0}{U^*} = \alpha = \text{const}$$

that is

$$V(0, \mathbf{R}^*) = \int^1 V(\eta, \mathbf{R}^*) d\eta = \alpha \quad \ldots\ldots [56]$$

Substituting Equations [55] into Equation [56], we have

$$\phi(\mathbf{R}^*) - \int_0^1 \phi[(1-\eta)\mathbf{R}^*]\, d\eta = \alpha \quad \ldots\ldots [57]$$

Changing the variable η to $q = (1-\eta)\mathbf{R}^*$, Equation [57] becomes

$$\phi(\mathbf{R}^*) - \frac{1}{\mathbf{R}^*} \int_0^{R^*} \phi(q)\, dq = \alpha \quad \ldots\ldots [58]$$

Differentiating Equation [58] with respect to $\mathbf{R}^*$, we have

$$\phi(q) = \alpha \log q + \beta \quad \ldots\ldots [59]$$

where β is an arbitrary constant.

From Equations [55] and [59], we have the logarithmic velocity distribution as follows

$$V(\eta, \mathbf{R}^*) = \alpha \log [(1-\eta)\mathbf{R}^*] + \beta, 0 \le \eta \le 1 \quad \ldots\ldots [60]$$

However at $\eta = 1$, $V(1, \mathbf{R}^*)$ becomes infinite. Hence, usually it is said that Equation [60] holds true only in the region $0 \le \eta \le 1 - \epsilon$, where ϵ is the thickness of the laminar sublayer. Since the logarithmic velocity distribution does not satisfy the boundary condition at the wall, it is not a rigorous solution of Reynolds equations.

COUETTE FLOW

In this case one plate is at rest and the other is moving at a constant velocity U, Fig. 1. Now the total shearing stress is constant across the flow. The shearing stresses on the walls in nondimensional form are

$$\mathbf{R}^* = \frac{dV}{d\eta} \quad \text{at } \eta = \pm 1 \quad \ldots\ldots [61]$$

Substituting Equations [30] and [57] into Equation [34], we have

$$A = 0, \quad B = 1$$

Hence Equations [33] and [34] become

$$\tilde{\omega} + \sigma = 0 \quad \ldots\ldots [62]$$

$$\frac{1}{\mathbf{R}^*}\frac{dV}{d\eta} - r = 1 \quad \ldots\ldots [63]$$

From Equation [62] we see that the mean pressure is independent of ξ but varies with η. The mean pressure in the fluid is also less than or equal to that on the wall.

Integration of Equation [60] gives

$$V(\eta, \mathbf{R}^*) = \mathbf{R}^*(1+\eta) + \mathbf{R}^* \int_{-1}^{\eta} r(y, \mathbf{R}^*) dy \quad [64]$$

If $r(\eta, \mathbf{R}^*) = 0$, Equation [61] reduces to the velocity profile of laminar Couette flow.

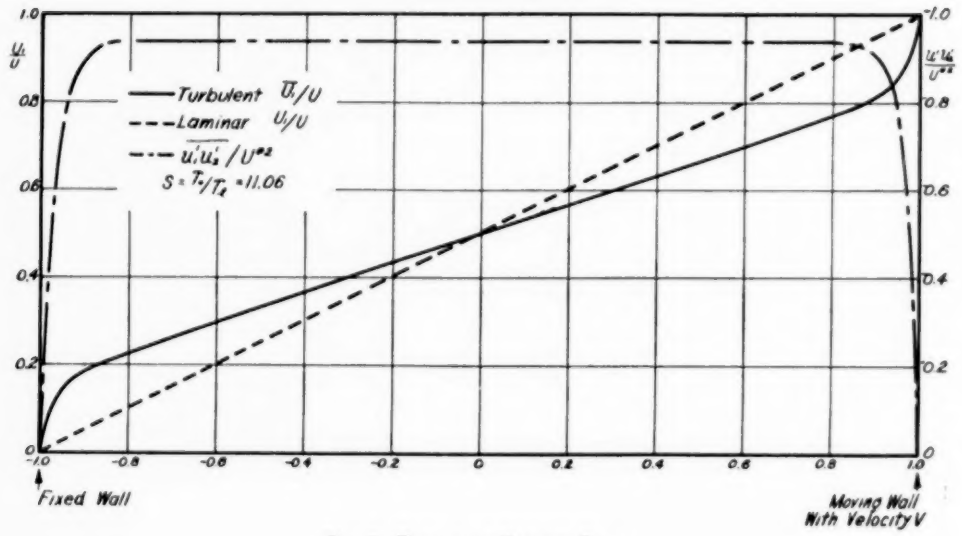

FIG. 3 TURBULENT COUETTE FLOW

Again, if we express the solution of $V(\eta, \mathbf{R}^*)$ in power series of η and if it satisfies Equation [64] and the boundary conditions, Equations [29] and [30], $V(\eta, \mathbf{R}^*)$ can contain only three terms with a constant and two odd powers of η. In order to comply with the results of laminar flow, we have to write the expression of $V(\eta, \mathbf{R}^*)$ as follows

$$V(\eta, \mathbf{R}^*) = \frac{U}{2U^*}\left[1 + a_1\eta + a_{2n+1}\eta^{2n+1}\right] \quad [65]$$

where n is an arbitrary integer. Substituting Equation [65] into Equation [64] and using the boundary conditions, Equations [29] and [30], we have

$$a_1 = \frac{2n + 1 - s}{2n}, \quad a_{2n+1} = \frac{s - 1}{2n} \quad [66]$$

where $s = \tau_2/\tau_1$, and $\tau_1 = \mu U/2a$ which is the shearing stress for the laminar Couette flow. Since $U/2U^* = \mathbf{R}^*/s$, we have finally

$$V(\eta, \mathbf{R}^*) = \frac{\mathbf{R}^*}{s}\left[1 + \frac{2n + 1 - s}{2n}\eta + \frac{s - 1}{2n}\eta^{2n+1}\right] \quad [67]$$

If $s = 1$, Equation [67] reduces automatically to the case of laminar flow.

There is no experimental data available for the turbulent-plane Couette flow yet. Just to show the characteristics of the solution of Equation [67], we use that value of Equation [50] for n and plot the mean velocity distribution for the turbulent Couette flow as shown in Fig. 3 for $s = 11.06$.

The correlation coefficient $r(\eta, \mathbf{R}^*)$ is

$$r = \frac{(2n + 1)(1 - s)}{2ns}\left[1 - \eta^{2n}\right] \quad [68]$$

The value of r for $s = 11.06$ is also shown in Fig. 3, with the assumption of Equation [50].

The coefficient of friction C_f is given by the following formula from Equations [20], [23], and [63]

$$\sqrt{\frac{2}{C_f}} = \mathbf{R}^*\left[1 + \frac{1}{2}\int_{-1}^{1}(1 - y)\, r(y, \mathbf{R}^*)\, dy\right] \quad [69]$$

Substituting the value of r of Equation [68] into [69], we have simply

$$\sqrt{\frac{2}{C_f}} = \frac{\mathbf{R}^*}{s} = \frac{U}{2U^*}$$

By similar hypotheses as those of Equations [55] and [56], one can easily show that in the Couette flow, the logarithmic velocity distribution[5] can be obtained. However, the boundary conditions on the walls are not satisfied. Hence this logarithmic velocity profile is not a rigorous solution of Reynolds equations.

CONCLUSIONS

The Reynolds equations have been studied for the turbulent flows between parallel plates and the following conclusions may be drawn:

1 The correlation of the two turbulent-velocity fluctuations not in the direction of mean flow, i.e., $\overline{u_2'u_3'}$, is zero for the whole velocity field.

2 The mean pressure distribution may be divided into two parts; one varies in a similar manner as that in laminar flow, i.e., it decreases linearly with x_1-wise distance in Poiseuille case and it is independent of x_1 in Couette case. The other part is influenced by the transverse turbulent intensity $u_2'^2$ which is a function of co-ordinates perpendicular to the plates. The mean pressure in the fluid is less than or equal to the mean pressure on the plates.

3 The mean velocity distribution and the correlation of $u_1'u_2'$ may be expressed by a polynomial of the distance perpendicular to the plates, with the ratio of the shearing stress on the wall to that of the corresponding laminar shear stress of the same maximum mean velocity as a parameter and an empirical constant. These expressions hold true all the way across the plate, i.e., both the turbulent region and viscous layer including laminar sublayer. These expressions for Poiseuille flow have been checked with the experimental data of Laufer fairly well.

4 The logarithmic mean velocity distribution is not a rigorous solution of Reynolds equations.

[5] "The Fundamentals of the Statistical Theory of Turbulence," by Th. von Kármán, *Journal of the Aeronautical Sciences*, vol. 4, 1937, pp. 134–138.

Water-Channel Analog to High-Velocity Combustion

By A. K. OPPENHEIM,[1] BERKELEY, CALIF.

This paper is a sequel to one presented in 1951, by the author (1).[2] It was shown that during the development of detonation, the combustion zone which appears first in a unidimensional flow field as a single discontinuity, is later transformed into an unsteady, double discontinuity system, and it was demonstrated that such a transformation is necessary because of the restrictions imposed on the system by the dynamic boundary conditions. In the water channel the combustion-front discontinuity is simulated by a unidimensional source formed by admitting water from the bottom. By a proper selection of state parameters analogous relationships are derived to those between pressure and specific volume in a gaseous combustion system. Thus the consequences of restrictions imposed by dynamic boundary conditions on the propagation of combustion are illustrated in an analogous system which, being simpler in nature, is easier to understand. Moreover, the water-channel analog is utilized as an illustrative model of a system where controlled, stationary detonation could be achieved.

Nomenclature

The following nomenclature is used in the paper:

a = local velocity of sound $(a = \sqrt{kRT})$
c = small amplitude water-wave velocity $(c = \sqrt{gh})$
c_v = specific-heat capacity at constant volume
f = stream force function per unit area $(f = p + mV)$
g = acceleration of gravity
h = water depth
k = specific heat ratio
m = mass flow rate per unit area
$\mathbf{M}$ = Mach number
p = pressure
q = flow rate per unit width $(q = V.h)$
$\mathbf{q}$ = thermal energy addition per unit mass
q_a = unit flow rate in front of source
q_b = unit flow rate behind source
q_s = unit flow rate from source
R = gas constant
s = entropy
T = temperature
v = specific volume
V = flow velocity
x = analog to specific volume $\left(x = \frac{\lambda^2}{h}\right)$
y = analog to pressure $\left(y = \frac{1}{2} gh^2\right)$
α = slope angle of Rayleigh line
ϵ = characteristic process parameter $(\epsilon = q_a/\sqrt{gh_1^3}$ for analog and $\epsilon = \mathbf{q}/RT_1$ for gas system)
λ = flow rate ratio $\left(\lambda = \frac{q_b}{q_a}\right)$
ν = nondimensional specific volume ($\nu = x/x_1$ for analog and $\nu = v/v_1$ for gas system)
π = nondimensional pressure ($\pi = y/y_1$ for analog and $\pi = p/p_1$ for gas system)
ϕ = slope angle of isentrope
ψ = slope angle of Hugoniot curve

Introduction

In the previous paper (1) the gas dynamic aspects of the development of gaseous detonation were analyzed. The salient features of this study are as follows:

1 The combustion system is restricted by its dynamic boundary conditions which imply that, if the combustion front is treated as a discontinuity in the flow field, the process across it can be idealized as one at constant stream-force function per unit area, $f = p + mV = \text{const}$. This process is represented on a state diagram as the Rayleigh line (R-line) which in the p-v coordinates is a straight line.

2 In order to explain adequately the development of detonation, the process must be considered to be taking place, during the predetonation period, in an unsteady double discontinuity system consisting of a shock front preceding the combustion front, as illustrated in Fig. 1.

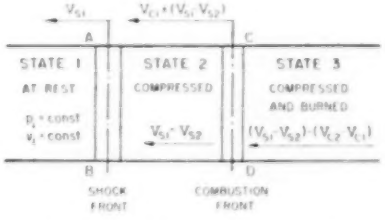

Fig. 1 Unsteady, Double Discontinuity Combustion System

3 The analysis indicates that the locus of states of the burned gases (state ③ in Fig. 1), is given by the Q-curve, represented in Fig. 2, which is referred to a constant state ① and determined by the following conditions:

(*a*) Change of state ①–② across the shock is specified by an adiabatic R_s-line

(*b*) Change of state ②–③ across the combustion front is speci-

[1] Assistant Professor of Mechanical Engineering, University of California. Mem. ASME.

[2] Numbers in parentheses refer to the Bibliography at the end of the paper.

Contributed by the Applied Mechanics Division and presented at the Annual Meeting, New York, N. Y., November 30–December 5, 1952, of The American Society of Mechanical Engineers.

Discussion of this paper should be addressed to the Secretary, ASME, 29 West 39th Street, New York, N. Y., and will be accepted until April 10, 1953, for publication at a later date. Discussion received after the closing date will be returned.

Note: Statements and opinions advanced in papers are to be understood as individual expressions of their authors and not those of the Society. Manuscript received by ASME Applied Mechanics Division, April 7, 1952. Paper No. 52—A-3.

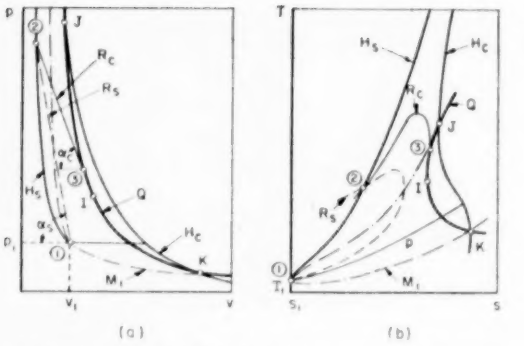

FIG. 2 LOCI OF STATES DURING DEVELOPMENT OF DETONATION

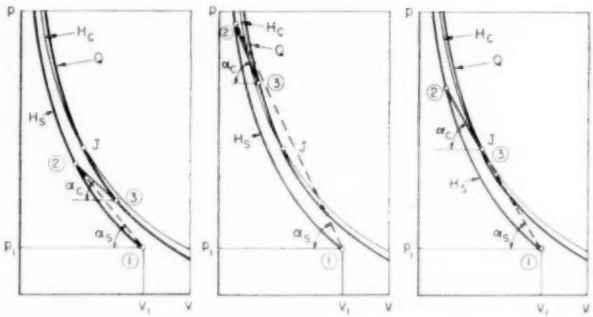

FIG. 3 CHARACTERISTIC PROCESSES DURING DEVELOPMENT OF DETONATION

fied by an R_c-line for which the thermal-energy addition to the system per unit mass of substance is constant.

(c) The Mach number of state ② is unity; i.e., the combustion zone moves at a local velocity of sound with respect to burned gases.

4 As a result of the analysis it is shown that in the initial stages of the development of detonation the shock front runs away from the combustion front, and the detonation wave can be formed only if sufficiently high pressure is attained in the intermediate zone (state ② in Fig. 1), so that the velocity of the combustion front could exceed that of the shock and the two fronts coalesce. This is demonstrated in Fig. 3 where the velocities of the shock, V_{s2}, and of the combustion front V_{c1}, relative to the intermediate state ②, are proportional to the square roots of slopes tan α_s and tan α_c, respectively.

5 The analysis leads to the conclusion that it should be possible to achieve detonation without the ignition of the shock front (as, indeed, demonstrated experimentally by Schmidt and co-workers, reference 2) and that it should be possible to attain stationary detonation if provision is made for the expanding system of the unsteady shock-combustion front zone.

Since the combustion system is quite complex and, at the same time, the processes are restricted primarily by the dynamic boundary conditions, it is thought that the understanding of the phenomenon can be enhanced by an illustration obtained from a hydraulic system with analogous boundary conditions. The analog can serve also as an illustrative model of a combustion system where controlled, stationary detonation could be achieved.

PRINCIPLE OF THE ANALOGY

The restriction imposed by the dynamic boundary condition on a shock or a combustion-front discontinuity implies that, at each instant, the stream-force function referred to the state immediately behind must be equal to that referred to the state immediately in front of the discontinuity. The locus of states behind such a discontinuity, with respect to a constant state in front, is obtained in form of the Hugoniot curve (Rankine-Hugoniot curve for the shock) by imposing an additional restriction on the system, which, for a gaseous discontinuity, is derived from the energy equation. The analogous hydraulic system is formed by an open channel represented schematically in Fig. 4, where a similar dynamic boundary condition is satisfied by the configuration of the flow system, and where the possibility of introducing an additional restriction is provided by the control of the water rate admitted from the bottom. Only the one-dimensional case is considered so that the channel width is constant and the hydraulic system represents essentially a unidimensional source-uniform flow combination.

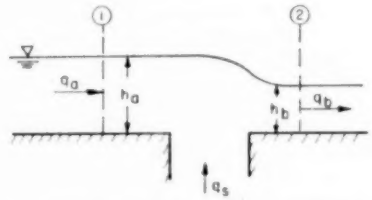

FIG. 4 SYSTEM DIAGRAM OF WATER-CHANNEL ANALOG

The energy equation cannot be utilized in the hydraulic system since undetectably small variations in internal energy correspond to extremely large variations in water depth, and the system cannot be considered to be adiabatic as in the gasdynamic case. The restriction specified by the energy equation for the combustion system is thus substituted by the restriction specified by the continuity equation for the water channel. Since the continuity equation is essential in determining the change of state for the gasdynamic process, the analogous hydraulic process must be made determinable without resorting to this equation.

This is achieved by a proper selection of characteristic state parameters, namely (see Fig. 4)

$$y = \frac{1}{2} g h^2 \text{ analogous to pressure} \quad [1]$$

and

$$x = \frac{\lambda^2}{h} \text{ analogous to specific volume} \quad [2]$$

where

$$\lambda = \frac{q_b}{q_a} = 1 + \frac{q_s}{q_a} \quad [3]$$

In the foregoing $q = V.h$ is the flow rate per unit channel width, q_a denotes the flow rate immediately in front of the source, q_b that immediately behind the source and q_s the flow rate admitted from the source, all flow rates being expressed per unit width of the channel.

The dynamic equation applied to the system in Fig. 4 can be written as

$$\frac{1}{2} g h_1^2 + q_1^2 \frac{1}{h_1} = \frac{1}{2} g h_2^2 + q_2^2 \frac{1}{h_2} = \frac{1}{2} g h_2^2 + q_1^2 \frac{\lambda^2}{h_2} = \text{const}^*$$

* Subscripts 1 and 2 are substituted here for subscripts a and b shown in Fig. 4 and used for the general definition of λ expressed by Equation [3].

whence, treating state ② as variable and, consequently, dropping subscript 2

$$\frac{y - y_1}{x_1 - x} = q_1^2 = \left(\frac{q}{\lambda}\right)^2 \quad \ldots\ldots\ldots\ldots\ldots\ldots [4]$$

Equation [4] represents the Rayleigh line (or, shortly the *R*-line) for the hydraulic system: the analogous equation for the gaseous system is

$$\frac{p - p_1}{v_1 - v} = m^2$$

Similarly, as in the gasdynamic case the square root of the *R*-line slope is, at a given state i, proportional to flow velocity since

$$\sqrt{\tan \alpha} = \sqrt{\frac{y - y_1}{x_1 - x}} = q_i = h_i V_i$$

where, at a given state, h_i is constant.

The Mach number is expressed by

$$\mathbf{M} = \frac{V}{c} = \frac{(q/h)}{\sqrt{gh}} = \frac{q}{\lambda}\sqrt{\frac{x}{2y}} \quad \ldots\ldots\ldots\ldots [5]$$

which is analogous to the expression

$$\mathbf{M} = m\sqrt{\frac{v}{kp}}$$

for the gasdynamic case. The characteristic feature of the conventional water-channel analogy (3), namely that it corresponds to a hypothetical case of a gas with $k = 2$, is thus maintained here also.

The equation of the line of constant λ in the $y - x$ co-ordinates is analogous to that of an isentrope, since, from Equations [1] and [2]

$$yx^2 = \frac{g}{2}\lambda^4 \quad \ldots\ldots\ldots\ldots\ldots\ldots [6]$$

which is analogous to $\quad pv^k = e^{\Delta s/c_v}$

The analogous Hugoniot curve (or, shortly, *H*-curve) is given by the locus of states ② for a constant state ① (i.e., $x_1 = \text{const}$ and $y_1 = \text{const}$) and constant value of q_s, and its equation is

$$yx^2 = \frac{g}{2}\left(1 + q_s\sqrt{\frac{x_1 - x}{y - y_1}}\right)^4 \quad \ldots\ldots [7]$$

While this equation does not have the same form as that of the gasdynamic Hugoniot curve, which for a perfect gas with constant specific heats, is

$$\frac{pv - p_1v_1}{k - 1} = \frac{p + p_1}{2}(v_1 - v)$$

it has the analogous property concerned with the deflagration and the detonation states. As demonstrated in the Appendix, at the point where the *H*-curve is tangent to the *R*-line passing through state ①, it is also tangent to the isentrope, and the Mach number is unity. This means that, similarly as in the gaseous system, for the fully developed deflagration or detonation, the relative flow velocity behind the discontinuity and with respect to it is equal to the local critical velocity. Unlike the gasdynamic Hugoniot curve its analog is discontinuous and passes through state ①, Figs. 6 and 7; however, this is inconsequential since, in the gasdynamic case, points lying in the quadrant $\pi > 1$ and $\nu > 1$ have no physical meaning.

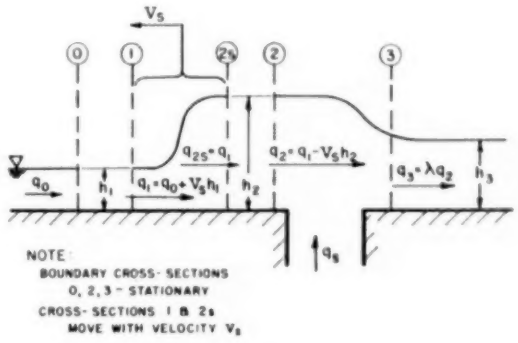

FIG. 5 ANALOGY TO UNSTEADY, DOUBLE DISCONTINUITY COMBUSTION SYSTEM

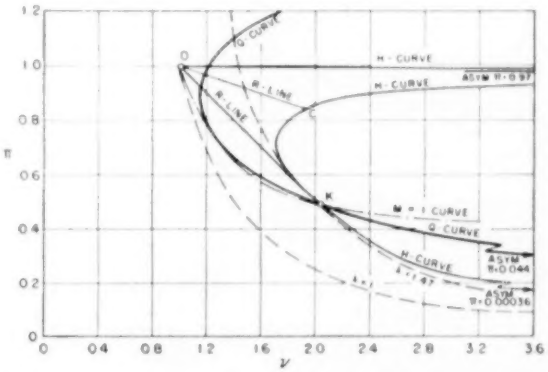

FIG. 6 ANALOGOUS PRESSURE-SPECIFIC VOLUME ($\pi - \nu$) DIAGRAM OF THE ANALOGY; DEFLAGRATION REGIME ($\epsilon = 0.1$)

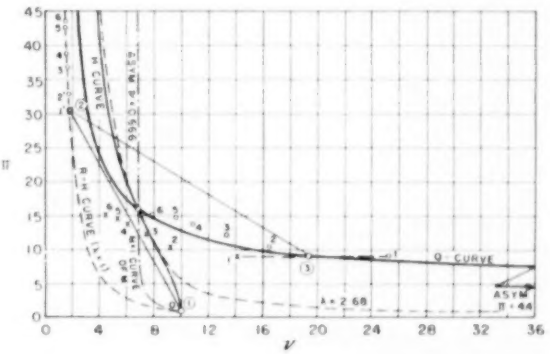

FIG. 7 ANALOGOUS PRESSURE-SPECIFIC VOLUME ($\pi - \nu$) DIAGRAM OF THE ANALOGY; DETONATION REGIME ($\epsilon = 3$)

For the case of $q_s = 0$ the *H*-curve represents the locus of states behind a hydraulic jump and becomes analogous to the Rankine-Hugoniot curve representing the locus of states behind a shock front. However, here this case corresponds also to $\lambda = 1$ and the equation of the *H*-curve, Equation [7], reduces to that of the isentrope, Equation [6]. Thus, in the analogy, the Rankine-Hugoniot curve degenerates into an isentrope. Because of the specific meaning of Equation [6] this does not mean, of course, that the corresponding process is isentropic.

The analogous *Q*-curve is obtained by considering a double

discontinuity system defined in Fig. 5. Besides the dynamic boundary conditions the process is restricted by the requirements

$$q_s = \text{const, and } \mathbf{M}_3 = 1$$

The change of state ①-② across the hydraulic jump is restricted by the condition

$$y_2 x_2^2 = y_1 x_1^2 \quad \ldots\ldots [8]$$

representing the analogous Rankine-Hugoniot equation. The change of state ②-③ must obey the analogous Hugoniot Equation [7] referred to this process, namely

$$y_3 x_3^2 = \frac{g}{2}\left(1 + q_s\sqrt{\frac{x_2 - x_3}{y_3 - y_2}}\right)^4 \quad \ldots\ldots [9]$$

and the condition of $\mathbf{M}_3 = 1$ is, by eliminating (q/λ) from Equations [4] and [5]

$$\frac{x_2 - x_3}{y_3 - y_2} = \frac{x_3}{2y_3} \quad \ldots\ldots [10]$$

In the foregoing equations the value of the characteristic parameter λ used in defining x is for x_2 as well as for x_1, $\lambda = 1$, while for x_3, according to Equation [3], $\lambda = q_3/q_2$.

From the last two equations,

$$y_3 x_3^2 = \frac{g}{2}\left(1 + q_s\sqrt{\frac{x_3}{2y_3}}\right)^4 \quad \ldots\ldots [11]$$

representing explicitly the locus of states ③, i.e., the equation of the Q-curve. Thus, for the analogous system, the parameters of state ② can be eliminated directly from Equations [9] and [10] without the use of Equation [8]. In the gasdynamic case all three equations are needed for this purpose, and the elimination of state ② parameters is so involved that it is simpler to represent the equation of the Q-curve in parametric form (see Equations [8], [9], [10] of reference 1, which are, respectively, analogous to similarly numbered equations in this paper). The fact that the Q-curve in the $y - x$ co-ordinates is independent of state ① is inconsequential since in the analysis it is referred to this state by the use of the nondimensional co-ordinates.

The analogy in terms of the nondimensional parameters is summarized in Table 1. The equation numbers in the hydraulic-analogy column denote the reference equation on which the nondimensional expression is based; the equations of the gasdynamic system refer to the idealized case of a perfect gas with constant specific heats and the equations numbers are those of reference (1).

The functions listed in the table are shown, plotted to scale, in Figs. 6 and 7, the former referring to the deflagration regime and $\epsilon = 0.1$ and the latter to the detonation regime and $\epsilon = 3$.

Analogous Model of Combustion System

The water-channel analog is illustrated in Figs. 8 and 9, showing the side and top views of the apparatus. The water is flowing in a closed circuit through a centrifugal pump and tank situated on the bottom platform, Fig. 8, and admitted to the channel from the pressure box at the left and from the bottom well at the middle-right. Both flow rates are controlled by gate valves and measured by means of orifices and U-tube manometers, and the channel is provided with three depth gages as shown in Fig. 8. Furthermore, the main flow is controlled by the sluice at the outlet from the pressure box and the back pressure can be adjusted by means of the sluice situated behind the source and by the weir at the end of the channel. These two controls can be seen better in the top view, Fig. 9, which demonstrates also that the channel is made up of two concentric ducts, the middle one forming the main test section and furnished with the source extending over its full width. The source is made up of a rectangular well covered with a fine mesh perforated brass plate which provides a smooth bottom and prevents any contribution from the source to the horizontal component of momentum. The plan size of the outer duct is 12 in. × 115 in., that of the middle duct 6 in. × 90 in., and the source cross section is 6 in. × 10 in.; the rear edge of the source is 12 in. in front of the middle duct end sluice gate.

The double duct design is necessary in order to accommodate the intermediate zone at state ②, Fig. 5, which is expanding initially because of the fact that the hydraulic jump, similarly as the shock front in the gaseous system, Fig. 3(*a*), runs away from the source. By virtue of this design feature the hydraulic jump is stabilized in front of the middle duct where it forms a bow wave, Fig. 10.

TABLE 1 NONDIMENSIONAL ANALOGOUS FUNCTIONS

No.	Specification	Hydraulic analogy	Gasdynamic system
1	State parameters	$\pi = y/y_1 \ldots\ldots [1]$	$\pi = p/p_1$
2		$\nu = x/x_1 \ldots\ldots [2]$	$\nu = v/v_1$
3	R-line	$\frac{\pi - \pi_1}{\nu_1 - \nu} = 2\frac{\pi_1}{\nu_1}\mathbf{M}_1^2 = 2\frac{\pi}{\nu}\mathbf{M}^2 \ldots [4]$ and [5]	$\frac{\pi - \pi_1}{\nu_1 - \nu} = k\frac{\pi_1}{\nu_1}\mathbf{M}_1^2 = k\frac{\pi}{\nu}\mathbf{M}^2$ [32]
4	Isentrope	$\pi\nu^2 = \lambda^4$	$\pi\nu^k = e^{(k-1)s}$
5	H-curve	$\pi\nu^2 = \left(1 + \epsilon\sqrt{2\frac{1 - \nu}{\pi - 1}}\right)^4 \ldots [7]$	$\frac{k+1}{k-1}\pi\nu - \pi + \nu - \left(2\epsilon + \frac{k+1}{k-1}\right) = 0$ [3]
		where	where
		$\epsilon = \frac{q_s}{\sqrt{gh_1^3}} = \frac{q_s}{\sqrt{2y_1/x_1}} = \text{const}$	$\epsilon = \frac{\mathbf{q}}{RT_1} = \frac{\mathbf{q}}{p_1v_1} = \text{const}$
6	Q-curve	$\pi\nu^2 = \left(1 + \epsilon\sqrt{\frac{\nu}{\pi}}\right)^4 \ldots\ldots [11]$	$\begin{cases} \frac{k+1}{k-1}\pi_2\nu_2 - \pi_2 + \nu_2 - \frac{k+1}{k-1} = 0 \ldots\ldots [11] \\ \frac{k+1}{k-1}\pi\nu - \pi\nu_2 + \pi_2\nu - \frac{k+1}{k-1}\pi_2\nu_2 - 2\epsilon = 0 \\ \qquad \ldots\ldots [12] \\ (k-1)\pi\nu - k\pi\nu_2 - \pi_2\nu = 0 \ldots\ldots [13] \end{cases}$
		where	where
		$\epsilon = \frac{q_s}{\sqrt{gh_1^3}} = \frac{q_s}{\sqrt{2y_1/x_1}} = \text{const}$	$\epsilon = \frac{\mathbf{q}}{RT_1} = \frac{\mathbf{q}}{p_1v_1} = \text{const}$

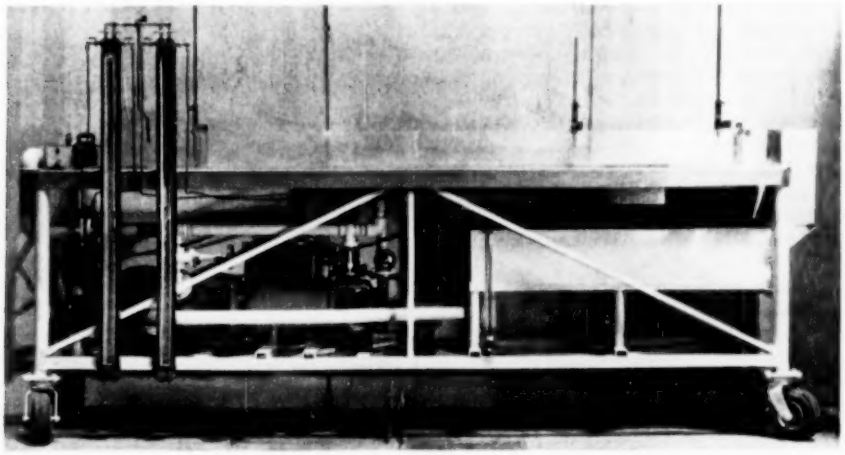

FIG. 8 WATER-CHANNEL ANALOG; SIDE VIEW

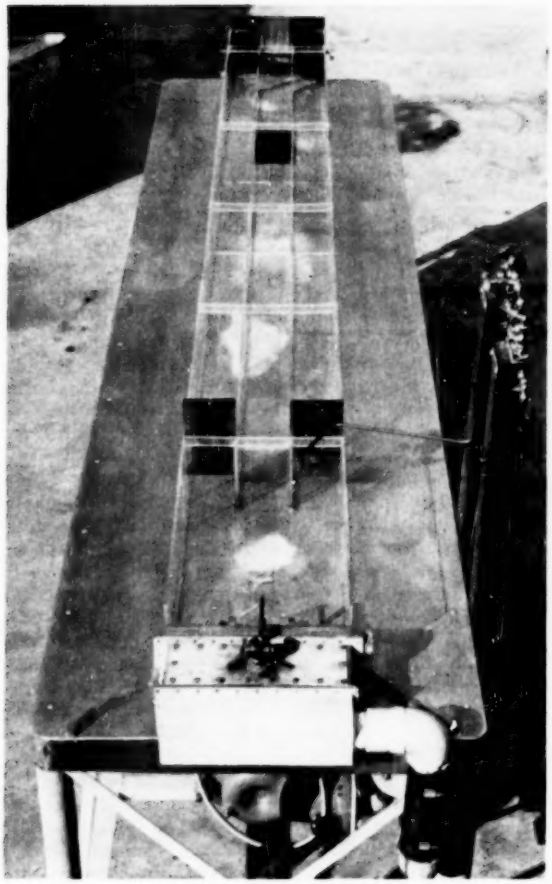

FIG. 9 WATER-CHANNEL ANALOG; TOP VIEW

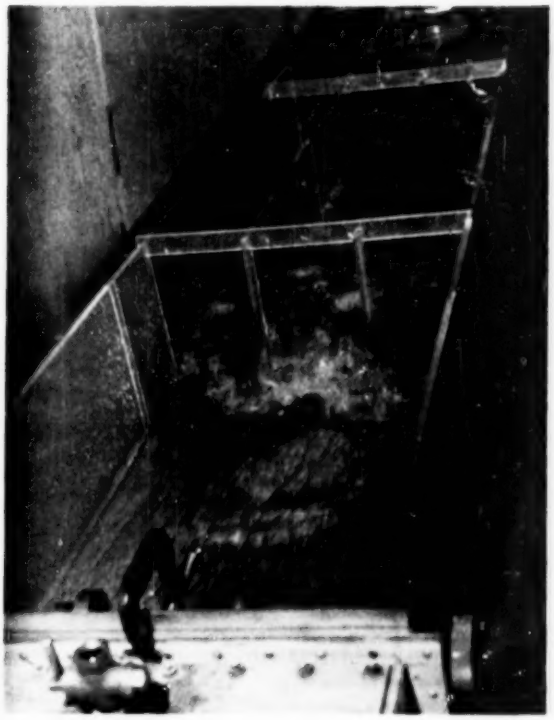

FIG. 10 HYDRAULIC JUMP OF UNSTEADY SYSTEM FORMING A BOW WAVE

It should be noted that the hydraulic as well as the gaseous system is unsteady because of the storage of mass at state ③ between the two discontinuities. However, both systems represent examples of a steady-state flow system since, at each in-

stant, energy is stored by the increase of mass and not by the change of state. Systems of this kind can be made steady by providing them with means for accommodating the increasing mass of state ② as done in the channel by the spill around the walls of the middle duct in the wake of the bow wave as illustrated in Fig. 10. Since the source simulating the combustion front has a fixed position in the channel, the hydraulic system satisfies the same requirement as a combustion system with a fixed position of the combustion front. Hence the water channel with all its controls may be considered as representing an analogous model of a combustion system where stationary detonation could be achieved.

The sequence of processes leading to the attainment of stationary detonation is illustrated in Fig. 11.

The initiation of the process of "combustion" (by letting in water from the bottom to the horizontal stream) is performed at low subsonic velocity through the "combustion chamber" achieved by restricting the flow by means of the sluice situated at the end of the middle duct. Under these circumstances the pressure must decrease across the "combustion front" as demonstrated in Fig. 11(a), where, it should be remembered, the water depth is proportional to the square root of pressure. This corresponds to the well-known effect of the flame on the pressure gradient across it (4, 5). The corresponding process is represented by a line O–C in Fig. 6.

By removing this restriction, a fully developed deflagration is obtained, Fig. 11(b), where the flow behind the combustion front is critical ($\mathbf{M}_b = 1$) and the corresponding state is represented by point K in Fig. 6.

Further development of the process is performed by increasing the velocity of the incoming flow from the upper reservoir while the flow rate from the source should be kept constant. Since in the next stage supercritical (-supersonic) flow should be attained, there should be a minimum of restrictions in the flow field and, consequently, in preparation for this condition, the gates at the entrance to side ducts are removed, Fig. 11(c). Although this changes the value of the characteristic process parameter, $\epsilon = \mathbf{M}_1 q_e/q_1$, which corresponds to shifting to another Hugoniot curve, it is necessary in order to attain later the high velocities of state ① required for the achievement of "detonation." Thus the flow pattern, represented by Fig. 11(c), corresponds to a fully developed deflagration similar to that in Fig. 11(b), but referred to a higher value of the process parameter ϵ. It is of interest to note here that, as demonstrated in the Appendix, the value of ϵ for the deflagrative flow pattern is limited to $\epsilon < 1$, while for the analogy to the detonative mode of combustion ϵ is unlimited. There is no restriction of this kind on the value of corresponding

$$\epsilon = \mathbf{M}_1 \frac{kq}{V_1 a_1}$$

in the combustion system.

The supercritical flow of state ① is then attained by increasing the pressure in the upper reservoir, Fig. 11(d). This is associated with a substantial decrease of water depth of state ① and a corresponding change of this state. The process parameter ϵ is again increased, quite substantially this time, from a value of an order of 0.1, for the process in Figs. 11(a-c), to the value of approximately 3; but, again, this is necessary in order to achieve detonation with the comparatively limited flow rate obtainable in the apparatus. Thus the required high Mach numbers are obtained by decreasing the pressure at state ① instead of the much more expensive increase of the capacity and hence power requirement of the pump (or compressor in the analogous combustion system). The flow pattern in Fig. 11(d) is the same as

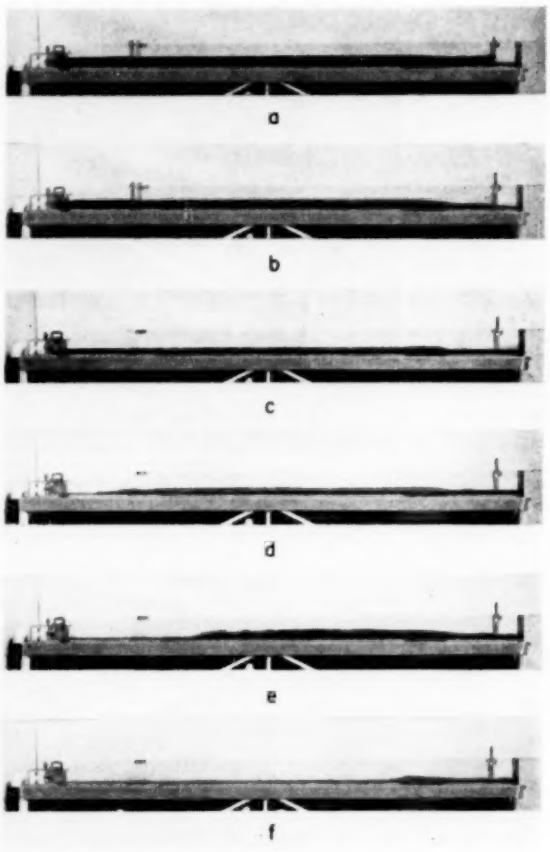

FIG. 11 ANALOGY TO DEVELOPMENT OF DETONATION

that in Fig. 10 which shows the top view of the hydraulic jump forming the bow wave at this stage of the process. The corresponding processes are represented by lines ①-② across the jump, and ②-③ across the source, on the $\pi - \nu$ diagram, Fig. 7.

From this stage on state ① remains unaltered and hence the process parameter ϵ is constant. The subsequent stages are attained by increasing the pressure in the upper reservoir, and the corresponding processes are represented by 0-2′-2, 0-3′-3, 0-4′-4, and 0-5′-5 in the state diagram in Fig. 7. The points indicated there represent typical experimental results while the Q-curve is plotted for the corresponding value of $\epsilon = 3$. A detailed description of experiments and their analysis is recorded in reference (6). With the instrumentation used in the experiment, the value of λ could not have been evaluated accurately and the extent of uncertainty involved by this is indicated by the "corrected" cross points with respect to the "uncorrected" circle points. Although the inaccuracy is quite substantial, the theoretical Q-curve is bracketed by the experimental points, demonstrating thus that it represents the locus of states of the "burned gases" during the development of the process.

When the flow velocity of state ① is increased further the jump is swallowed into the duct as shown in Fig. 11(e). The corresponding process is represented in Fig. 7 by 0-6′-6 irrespective of where the jump is situated, provided it is inside the duct. In the hydraulic system the jump can be stabilized at any position within the duct by virtue of the wall friction but in a gaseous

system the effect of wall friction is comparatively much smaller and the shock would rapidly coalesce with the combustion front as illustrated in Fig. 11(*f*). Thus fully developed detonation is achieved. The situation, represented by Fig. 11(*f*), limits the development of gaseous detonation. In the water channel the hydraulic jump can be forced to pass the source, while in the combustion system the shock is necessary for compression in order to provide a sufficiently high-temperature condition for the correspondingly high combustion rate, and, since it is also much thinner than the combustion front, it will remain in front. The experimental proof of this fact is the well known—remarkable stability of the detonation wave.

Conclusion

The hydraulic analogy to a unidimensional combustion system has been derived and applied to the problem of the development of detonation. For this purpose the water channel was treated as an illustrative model of a combustion system where stationary detonation could be achieved. The flow configurations in the intermediate stages of the development of detonation have been indicated together with the necessary controls for the stabilization of the intermediate processes. The water channel can be considered to provide a satisfactory analogy to the combustion process in so far as the consequences of the dynamic restrictions are concerned.

Acknowledgment

The author wishes to extend his sincere appreciation to Mr. J. O. Tearnen for his valuable help in the design of the apparatus, experiments, and computations.

BIBLIOGRAPHY

1 "A Contribution to the Theory of the Development and Stability of Detonation in Gases," by A. K. Oppenheim, Journal of Applied Mechanics, Trans. ASME, vol. 74, 1952, pp. 63–71.

2 "Flame and Schlieren Photographs of the Combustion of Gas Mixtures in Tubes," by E. Schmidt, H. Steinicke, and U. Neubert, VDI Forschungsheft 431, *Forschung auf dem Gebiete des Ingenieurwesens*, edition B, vol. 17, 1951.

3 "Application of the Methods of Gas Dynamics to Water Flows With Free Surface," by E. Preiserk, Mitteilungen aus dem Institute für Aerodynamik, E. T. H., Zurich, Switzerland, 1938; translation: NACA TM No. 934 and 935, 1940.

4 "Explosion and Combustion Processes in Gases," by W. Jost, Julius Springer, Berlin, Germany, 1939; translated by H. O. Croft, McGraw-Hill Book Company, Inc., New York, N. Y., 1946, p. 80.

5 "Combustion, Flames and Explosions of Gases," by B. Lewis and G. von Elbe, Academic Press, Inc., New York, N. Y., 1951, pp. 240, 260, and 524.

6 "A Water Channel Analogy to a Problem in Gaseous Combustion," by J. O. Tearnen, MS thesis, University of California, Berkeley, Calif., 1951.

Appendix

Properties of Analogous Hugoniot Curve

The salient feature of the Hugoniot curve, representing the locus of states behind a combustion front, is the fact that the point of tangency of this curve to the isentrope is also the point of tangency of the Rayleigh line passing through state 1 to these curves and corresponds to a state at which the flow velocity is sonic ($\mathbf{M} = 1$). The same property will be demonstrated here for the analogous Hugoniot curve.

The slope of the *H*-curve

$$\tan \psi = -(\partial \pi / \partial \nu)_{\epsilon}$$

is given by the following equation obtained by differentiating Equation [5] of Table 1

$$\nu \tan \psi - 2\pi + 4\pi^{3/2}\nu^{1/2} \frac{1 - \dfrac{1-\nu}{\pi - 1} \tan \psi}{\sqrt{2(1-\nu)(\pi - 1)}} = 0$$

The slope of the isentrope is

$$\tan \phi = -\left(\frac{\partial \pi}{\partial \nu}\right)_{\lambda} = 2\frac{\pi}{\nu}$$

as obtained from Equation No. 4 of Table 1.

The locus of points of tangency of these two families of curves is obtained by eliminating $\tan \phi = \tan \psi$ from the foregoing equations. This yields the condition

$$\frac{\pi - 1}{1 - \nu} = 2\frac{\pi}{\nu}$$

which describes also the locus of those states of Rayleigh lines passing through state ① ($\pi_1 = 1$; $\nu_1 = 1$) at which $\mathbf{M} = 1$ as immediately evident from Equation No. 3 of Table 1. This proves the salient property of the analogous Hugoniot curve.

Unlike the gasdynamic Hugoniot curve, in the analogous hydraulic case, the curve can correspond to a deflagrative process only for limited values of the characteristic parameter ϵ, namely, for $\epsilon < 1$. This stems from the following argument:

The condition for deflagration is $\mathbf{M}_2 = 1$, obtained through a single discontinuity from state ① at which the flow is subsonic (subcritical). From the equation of the Rayleigh line passing through state ①

$$\frac{\pi - 1}{1 - \nu} = 2\,\mathbf{M}_1^2 = 2\frac{\pi}{\nu}\,\mathbf{M}^2$$

it follows that for $\mathbf{M} = 1$ and $\mathbf{M}_1 < 1$: $\pi < \nu$ which is satisfied only by the lower branch of the Hugoniot curve or for $h_2 < h_1$.

From the continuity equation, for fully developed deflagration ($\mathbf{M}_2 = 1$)

$$q_1 + q_a = q_2 = \sqrt{g h_2^3}$$

or, dividing by $\sqrt{g h_1^3}$

$$\mathbf{M}_1 + \epsilon = (h_2/h_1)^{3/2}$$

which yields the condition that for $\mathbf{M}_1 < 1$ and $\dfrac{h_2}{h_1} < 1$

$$\epsilon < 1$$

Elastic Waves Created During Tensile Fracture[1]

The Phenomenon of a Second Fracture

By JULIUS MIKLOWITZ,[2] PASADENA, CALIF.

In some tensile tests with brittle materials, it was noted that fractures were produced at two different cross sections of the specimen when the rupture load was reached. The phenomenon of the second fracture prompted the present investigation. It is believed that the second fracture is caused by the destructive action of the elastic strain waves created during the first of the two fractures. The analytical and experimental work carried out was focused on describing the character of these waves. Consideration of the mechanics involved reduces the problem to that of a vibrating cantilever beam with time-dependent boundary conditions. Two types of waves are shown to exist. The first is a longitudinal unloading wave (compression). The other is a group of flexural strain waves caused by the moment that develops at the initial fracture section. The methods of operational mathematics and the electric-analog computer have been employed in the analytical study.

Nomenclature

The following nomenclature is used in the paper:

In the nomenclature, the subscript 0 is used to define quantities at time $t = 0$. Subscripts x and t indicate partial differentiation. A lower-case letter is used to define the transform of a function originally written with a capital letter; i.e., $u(x, s)$ is the transform of $U(x, t)$.

$A(t)$, A_0 = area of intact material in initial fracture section

$F(t)$, F_0 = force acting on $A(t)$

$M(t)$ = moment developed at initial fracture section

$\frac{M_m}{\pi}$ = maximum $M(t)$

$P(t)$, P_0 = stress defined by $\frac{F(t)}{A_0}$

$R(t)$ = eccentricity of $F(t)$

$U(x, t)$, U_0 = longitudinal displacement of beam element

$U_x(x, t)$ = longitudinal strain in beam

$[U_x(x, t)]_r$ = longitudinal strain at beam outer fiber due to bending

$V(x, t)$ = lateral deflection of beam element

$a = \sqrt{\frac{EIg}{A_0\gamma}}$

where E = modulus of elasticity; I = moment of inertia of beam cross section with respect to neutral axis of bending; g = acceleration due to gravity; γ = specific weight of beam material

c = velocity of propagation of elastic extensional deformation, defined by $\sqrt{\frac{Eg}{\gamma}}$

k = crack propagation time, equal to the rise time of the unloading wave

l = cantilever length

q = variable dependent on transformation parameter s

q_n = roots of frequency equation $\Gamma(q)$

r = radius of cantilever, equal to maximum $R(t)$

s = transformation parameter

t = time

x = co-ordinate along cantilever

y = co-ordinate perpendicular to x

Introduction

In some ordinary tension tests with brittle materials, it was observed that fractures occurred at two different cross sections of the specimen, seemingly simultaneously. The specimens shown in Fig. 1, demonstrate this type of fracturing. Since it is highly improbable that the two ruptures actually happened simultaneously, the creation of elastic strain waves during the first fracture, and the subsequent destructive action of these waves in causing a second fracture, suggests itself as a possible explanation.

The purpose of the work described in this paper was to study the nature of these elastic waves.

According to the analysis presented later, two types of waves emanate from the initial rupture section. One is a longitudinal compression wave, actually an unloading wave associated with the decrease in load in the fracture process. The other is a group of flexural strain waves produced by the moment that develops as the crack propagates across the bar from its origin at a surface discontinuity. The second fracture usually occurs at a gage cross section adjacent to the specimen head farthest from the initial fracture surface. The analysis shows that this second failure is due to the superposition of the longitudinal strain (from the unloading wave, which through reflections becomes tension) and the resultant flexural strain, which together total more than the original static tensile fracture strain.

The analysis has been developed by considering the action of one part of the specimen on the other, the initial fracture interface dividing the specimen. The longer part of the specimen was taken as the "free body" which is essentially a cantilever beam, the head and heavy grip creating the fixed end. The manner in which the crack propagates determines the free-end conditions. Since the crack propagates across the bar, the resultant force, dependent upon the area of intact material, must

[1] The work reported here was supported by the Bureau of Ordnance, U. S. N., through Task Assignment Re6a-268-11, which is concerned in general with Dynamic Loading of Aircraft Torpedo Structures.

[2] Research Engineer, Naval Ordnance Test Station.

Contributed by the Applied Mechanics Division and presented at the Annual Meeting, New York, N. Y., November 30–December 5, 1952, of The American Society of Mechanical Engineers.

Discussion of this paper should be addressed to the Secretary, ASME, 29 West 39th Street, New York, N. Y., and will be accepted until April 10, 1953, for publication at a later date. Discussion received after the closing date will be returned.

Note: Statements and opinions advanced in papers are to be understood as individual expressions of their authors and not those of the Society. Manuscript received by ASME Applied Mechanics Division, January 28, 1952. Paper 52—A-10.

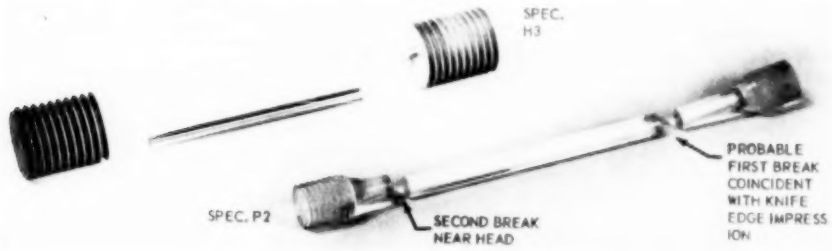

FIG. 1 PHENOMENON OF A SECOND FRACTURE

decrease continuously from the fracture load to zero. Furthermore, the line of action of this force moves from the bar center to the surface, and, therefore, the force can be replaced by an equivalent force acting axially and a couple. (It should be pointed out that when the crack originates within the specimen, the moment, and hence the flexural strain waves that develop are not as great as in the present case, which is the most severe.) Essentially then, the problem reduces itself to that of a vibrating cantilever beam with time-dependent boundary conditions.

The wave equation governs the solution for the case of the axial force. The couple is treated by electric-analog-computer methods, shear force and rotary inertia having been considered. The analog solution lends itself nicely to a discussion of waves. As a check on the order of magnitude of the strains exhibited by the analog results, a solution for the couple case was derived from the elementary bending equation.[3]

A discussion of the experimental work follows the section on analysis.

ANALYSIS

This work in no way attempts to present new facts on the actual mechanism of the brittle-type fracture, this being a very broad and important subject in itself. The purpose here was to study the waves produced during this type of fracture. Toward this end, a rupture mechanism has been assumed in a first approximation. This is backed partially by the experimental results of this work, and information available in the literature. The theory developed here is based on the assumed rupture mechanism and other necessary assumptions. Future work will be directed toward getting more experimental verification of this theory.

Fig. 2 shows a typical fracture surface of the many Plexiglas specimens tested in this work. This surface was usually normal to the tensile axis of the specimen. A radial mode of crack propagation toward the left from a surface discontinuity on the right is emphatically indicated. In the general vicinity of this discontinuity a uniform region of intense lighting, containing parabola-like markings, may be observed. Within this region, in the immediate vicinity of the crack origin, a pronounced semicircle is seen to mark the onset of the parabola-like markings and the straight lines emanating from their focal points. Other photographs showed these parabola-like markings more definitely in the later regions of fracture also. These markings are typical of those discussed by Kies, Sullivan, and Irwin in their work with lucite (3).[4] They point out that the parabola outlines the area

FIG. 2 PLEXIGLAS FRACTURE SURFACE

included in an individually initiated subsidiary fracture, which begins at the focus of the parabola. These subsidiary initiations are known to occur ahead of the main crack front, but it is pointed out that in high-speed fractures the initiations occur close to this front. Hence it would appear that in the present work the existence of a main crack front of regular shape could be assumed.

Poncelet (4) discusses the work of Smekal (5, 6), as experimental evidence of Poncelet's postulations concerning forking, which is defined as the formation of cracks deviating from the original crack. Smekal worked with glass rods and noted a mirrored surface in the vicinity of the crack origin, which was the trace of the smooth original crack before forking set in. The semicircular boundary in Fig. 2, encloses a similar unmarked high glossy surface. It would appear then, that this boundary marks the initiation of forking. Outside of this boundary, indications are that there is a gradual build-up toward an intense level of forking, which is reached when the crack front has traversed only a small amount of area. Poncelet points out that associated with forking is a critical crack velocity, which is a constant for the material.

On the basis of the preceding discussion a main crack front of circular shape, the radius of which increases at a constant rate with time, has been assumed. The intact area $A(t)$ at the initial fracture section is plotted in Fig. 3; the dashed curve according to this assumption. This assumption does not consider the ve-

[3] Because of its nonwave character, and its reputation for yielding inaccurate transient solutions, the elementary equation yields a product which is of secondary interest here. Uflyand (1), for instance, discusses these shortcomings of the simple bending equation. He points out the wave character of the more exact Timoshenko equation (2) (including shear force and rotary inertia terms), and cautions that this is the equation to be used for transient solutions.

[4] Numbers in parentheses refer to the Bibliography at the end of the paper.

locity variation before intense forking sets in. It is suggested by Poncelet (4) that velocities in this region are less than the constant critical crack velocity. Neglecting this factor does not affect the assumed curve seriously. For later mathematical simplicity the function

$$\left.\begin{aligned} A(t) &= \frac{A_0}{2}\left(\cos\frac{\pi}{2k}t + \cos^2\frac{\pi}{2k}t\right), \quad 0 \leqq t < k \\ &= 0 \qquad\qquad\qquad\qquad\quad t \geqq k \end{aligned}\right\} \quad \ldots [1]$$

has been chosen to represent the intact area. This curve, shown by a solid line in Fig. 3, resembles very closely the constant crack velocity curve, deviating only a little near $t = k$.

The works of Poncelet (4) and Smekal (5, 6) support a constant tensile force acting on the intact area until forking begins, and a constant tensile fracture stress acting over the intact area during

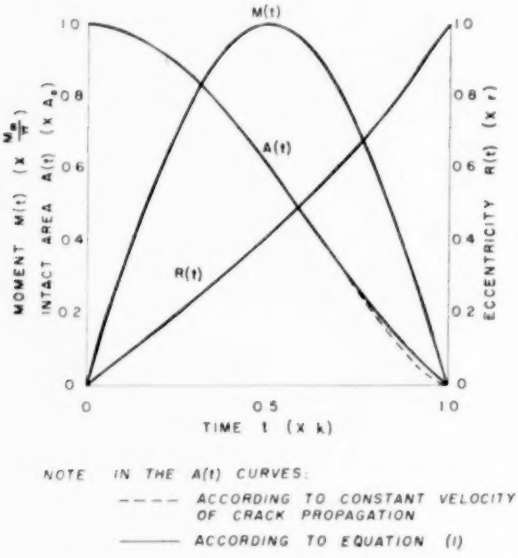

FIG. 3 FUNCTIONS REPRESENTING INTACT AREA, MOMENT, AND ECCENTRICITY DURING CRACK PROPAGATION

intense forking. Since forking seems to begin very early in the specimens of the present work, close agreement with the quoted works is obtained if the tensile force $F(t)$, acting on the intact area $A(t)$, is written as

$$F(t) = P_0 A(t) \quad \ldots [2]$$

The initial fracture process with reference to the idealized specimen and machine grips is shown in Fig. 4. Fig. 4(a) shows the conditions when the fracture load has been reached. At this point ($t = 0$), the crack initiates, probably under the influence of a small stress concentration, at a surface point of a random section C-C, and begins its propagation across the bar. The fracture load F_0 (equal to $P_0 A_0$) on section C-C acts axially at this instant. In Fig. 4(b), ($0 < t < k$), the crack has traveled part of the way across the bar. Now the force $F(t)$ has decreased according to Equation [2], and acts under an eccentricity of $R(t)$, which is governed by the location of the centroid of the intact area. This centroid lies at all times on the diametral path traversed by the crack front center. In Fig. 4(c), ($t = k$), the initial fracture process is complete. The force $F(t)$ is reduced to zero,

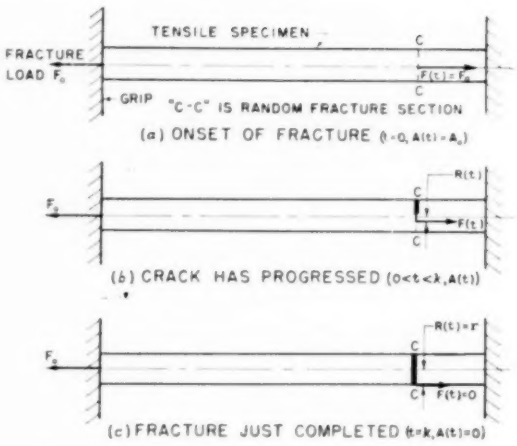

FIG. 4 STAGES IN DEVELOPMENT OF INITIAL FRACTURE

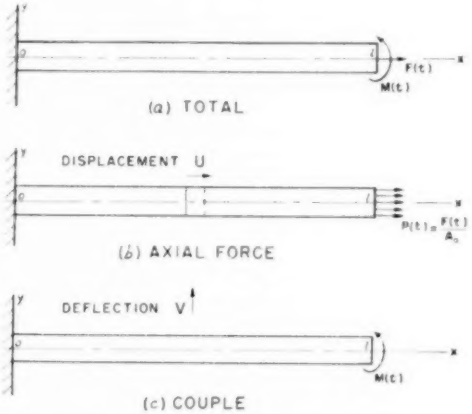

FIG. 5 IDEALIZED PROBLEM AND COMPONENTS

and the eccentricity $R(t)$ reaches its maximum value r at this stage.

Considering the part of the specimen to the left of C-C as a free body, acted upon by the part on the right, the idealized problem and its components, shown in Fig. 5, are formulated. To obtain this idealization the eccentrically acting force $F(t)$ has been replaced by an axial force $F(t)$ and a couple $M(t)$, the latter being given by

$$M(t) = F(t)\,R(t) \quad \ldots [3]$$

This moment must be such that it is 0 at $t = 0$, passes through a maximum, and is again 0 at $t = k$. The sine function

$$\left.\begin{aligned} M(t) &= \frac{M_m}{\pi}\sin\frac{\pi}{k}t, \quad 0 \leqq t < k \\ &= 0 \qquad\qquad\quad t \geqq k \end{aligned}\right\} \quad \ldots [4]$$

has been assumed. This function is plotted in Fig. 3. Equations [2], [3], and [4] then, require that

$$R(t) = \frac{M(t)}{F(t)} = \frac{2M_m \sin\frac{\pi}{k}t}{\pi F_0\left(\cos\frac{\pi}{2k}t + \cos^2\frac{\pi}{2k}t\right)} \quad \ldots [5]$$

If $M_m = (\pi/4)F_0 r$, Equation [5] satisfies both end conditions required of $R(t)$, namely, that

$$\lim_{t \to 0} R(t) = 0, \text{ and } \lim_{t \to k} R(t) = r$$

A plot of Equation [5] is shown in Fig. 3.

The nature of the waves involved has been obtained by solving separately the component boundary-value problems, i.e., the axial-force case shown in Fig. 5(*b*), and the couple case shown in Fig. 5(*c*). In solving these problems the small amount of plastic flow, at and adjacent to the fracture section, if present at all, has been neglected. The two materials used in this work, Plexiglas and high-speed steel, were extremely brittle. No macroscopic plastic flow was detected in the tests. The transparency and high polish of the Plexiglas specimens before testing returned immediately after testing. In no case, even at the fracture sections, was there a diameter change great enough to be attributed to flow (measurements made with micrometers). The high-speed-steel specimens kept what seemed to be their original grind finish too. No diameter changes were detectable. Hardness readings were made on one of the double fractured specimens. Eight readings on the four fracture surfaces gave an average of 63 RC. Four readings on the heads and mid-gage point gave an average of 60.7 RC. This suggests possibly a small amount of microscopic flow at the fracture surface.

Damping and the radial mode of vibration also have been neglected. Since the interesting phenomena in this work occur in a very short time (as pointed out later, the second fracture in Plexiglas is believed to happen at about $t = 250\ \mu$ sec), the damping influence is probably small. Some experimental data exist which suggest that the rise time of the unloading wave (known to be equal to the crack-propagation time) was large enough to make considerations of the radial mode of vibration unnecessary. Two methods were used to measure the crack-propagation time in Plexiglas. The first employed two brittle gold paint strips, one over a fine notch on the specimen, and the other diametrically opposite the first. The paint strips completed two independent electric circuits and the time difference in the breaking of the two circuits was noted on an oscilloscope. The second method employed the Plexiglas specimen itself as an optic system. Light was played longitudinally through a painted specimen onto a photocell. The crack-propagation time was associated with a difference in light levels before and after fracture, due to the production of a fracture surface with some opaqueness, Fig. 2. The light levels were noted on an oscilloscope. An average value from the total of 15 tests, using both methods, gave the crack-propagation time as 37 μ sec. The length equivalent of this time is 3.33 in. (calculated on the basis of $c = 7500$ fps), which is large compared to the Plexiglas specimen diameter of $^3/_8$ in.

With the impulsive functions shown in Fig. 5, acting equally as well on the shorter portion of the specimen, wave reflections from the closer fixed end pass through the intact area of section *C-C*, Fig. 4. Based on the fracture positions of Specimen P2, Fig. 1, the solid $A(t)$-curve in Fig. 3, and Donnell's work (7), rough calculations showed the amount of longitudinal strain transmitted across section *C-C* to be very small. The compressive nature of the transmitted wave would probably retard the initial fracture process a little. The slower-traveling bending strain probably would have even less influence. The same remarks apply to the high-speed-steel specimens even though they exhibited initial fractures closer to the specimen head. This shorter distance is balanced by a much shorter crack-propagation time (but a larger c-value) and a radial dissipation of wave energy into the large head. Hence, transmission of strain through the intact area has been neglected.

On the basis of the foregoing discussion the axial-force problem may be stated as follows

$$\left.\begin{aligned} &U_{tt}(x,t) = c^2 U_{xx}(x,t) \qquad (0 < x < l,\ t > 0) \\ &U(x,0) = \frac{U_0}{l}x,\ U_t(x,0) = 0 \\ &U(0,t) = 0,\ EU_x(l,t) = P(t) \\ &\text{where} \\ &P(t) = \frac{F(t)}{A_0} = \frac{P_0}{2}\left(\cos\frac{\pi}{2k}t + \cos^2\frac{\pi}{2k}t\right), \quad 0 \le t < k \\ &\qquad = 0 \qquad\qquad t \ge k \end{aligned}\right\} \ldots [6]$$

The methods of operational mathematics (8) produce the following wave solution for the strain

$$\left.\begin{aligned} U_x(x,t) = \frac{U_0}{4l}\sum_{n=0}^{\infty}(-1)^n \Bigg\{ &\left[1 + \cos\frac{\pi}{k}(t-b)\right] + \left[1 + \cos\frac{\pi}{k}(t-d)\right] \\ &- \left[1 - \cos\frac{\pi}{k}(t-k-b)\right] - \left[1 - \cos\frac{\pi}{k}(t-k-d)\right] \\ &+ 2\left[\cos\frac{\pi}{2k}(t-b) + \cos\frac{\pi}{2k}(t-d) + \sin\frac{\pi}{2k}(t-k-b)\right. \\ &\left. + \sin\frac{\pi}{2k}(t-k-d)\right] - 4c\frac{\partial}{\partial x}\left[(t-b) - (t-d)\right]\Bigg\} + \frac{U_0}{l}, \text{ for } t \ge 0 \end{aligned}\right\} \ldots [7]$$

where

$$b = \frac{(2n+1)l - x}{c} \quad \text{and} \quad d = \frac{(2n+1)l + x}{c}$$

and where it is understood that the bracketed quantities such as $[1 + \cos \pi/k\,(t-b)]$ and $(t-b)$, and the trigonometric functions such as $\cos \pi/2k\,(t-b)$ are to be replaced by zero when $t < b$. Hence this is a finite series for any fixed t value.

Fig. 6, derived from Equation [7], shows the character of the unloading wave and its propagation.[5] The time k was taken as $(9/16)\,(l/c)$, which is about 37 μ sec. The front, of course, reflects the assumed relation of Equation [2]. The various stages shown bring out the nature of the reflections of the wave. The stages have been chosen so that the basic cause of the strain changes with time, at section $x = l/8$ (approximate location of second fracture), also could be shown. The horizontal portions of the curves in each of the stages are actually coincident at the maximum ordinate U_0/l. They have been spread out, in Fig. 6, to enable the reader to follow the wave as it goes through its reflections. In all stages, the upper dashed line is the initial fracture strain. Note that the theoretical wave has no back. The strain-time curve for section $x = l/8$, appearing in Fig. 7, is easily constructed with the aid of Fig. 6.

At stage 7 in Fig. 6, the full value of the unloading wave, the front portion of which is now tension because of reflections, has arrived at section $x = l/8$. It is believed that, with the aid of additional strain created by the flexural waves, the unloading wave action causes the second fracture just after stage 7. The

[5] Poncelet (4) discusses the existence of similarly formed compression waves in his work with glass squares.

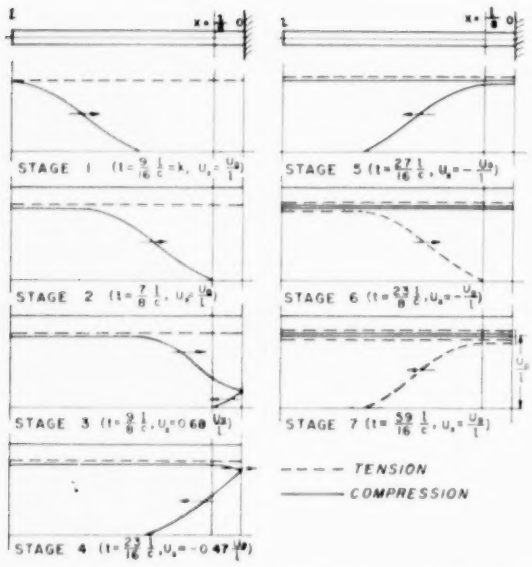

FIG. 6 STAGES IN PROPAGATION OF LONGITUDINAL UNLOADING WAVE INDICATED BY STRAIN DISTRIBUTIONS

In this method the beam was represented by 18 cells. The effects of shear force and rotary inertia were included. Details of the method can be found in the literature (10, 11).

Fig. 8 shows the resultant moment-time diagrams, at each of the mass stations of the cantilever beam, when the moment given by Equation [4] is applied at Station 17.5. The station positions are shown in a sketch inserted in Fig. 9. The maximum applied moment M_m/π corresponds to an axial strain of (U_0/l) at the outer fiber of the beam. The diagrams at the other stations have the same scales as that of the applied moment. The time and moment origins are designated for Station 0.5. Similar locations apply to the other diagrams in Fig. 8.

The propagation of the applied moment (hence strain) down the bar is clear from Fig. 8. Note that the time necessary for action to occur at a particular station increases uniformly with the station's distance from 17.5. Fig. 8 also points out the dispersion of the moment as it propagates down the beam. This is brought out by a comparison of the initial disturbances at any two adjacent stations. These disturbances reflect the applied moment's shape as it travels down the beam for the first time. Observe the change in shape, for instance, as the moment propagates from Station 17.5 to 12.5. Note the broadening out, and the building of negative ends, at the expense of the initial amplitude.[6] Interesting too, is the fact that no disturbances are greater than the initial amplitude. Note also that the diagram for Station 0.5 contains evidence of the reflection of the moment at the fixed end. This is indicated by the fact that the initial negative dip and positive peak show a greater increase in magnitude, when the Station 0.5 and 1.5 diagrams are compared, than

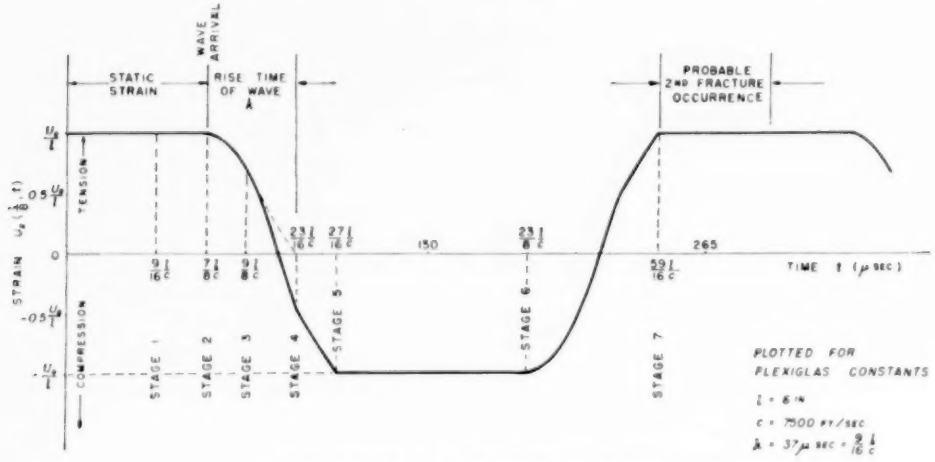

FIG. 7 UNLOADING WAVE STRAIN VERSUS TIME
(At $x = l/8$, position of second fracture.)

additional flexural strain is probably needed because of several factors. One factor is related to the speed-sensitivity of certain materials, of which Plexiglas is one (9). In materials of this type, under the faster rates of straining (due to the unloading wave), strains greater than the static fracture value U_0/l could be resisted without failure. The other factors are related to the neglected quantities, plastic flow, damping, and radial mode of vibration, which would probably extract a small amount of energy from the unloading wave.

The flexural strain waves have been studied with the aid of a solution for the couple case, Fig. 5(*c*) and Equations [4], which was obtained through the use of the CIT electric analog computer. they do for any other two adjacent diagrams. The Station 1.5 diagram also shows some reflection effects. The times involved here are such that the initial positive peak has superposed upon it the reflection of the forerunning negative dip. Note that the magnitude of the positive peak is no greater than it was in Station 2.5. In the lower right corner of Fig. 8, a diagram of the action at Station 3.5, up to about 1.1 ms, is shown. More severe strains, at the later times, are not indicated.

Curve 1 in Fig. 9 is an enlarged plot of the diagram at Station

[6] The initial positive peak at Station 14.5 does not fit in with the general deterioration exhibited by the other diagrams. In later curves, Station 14.5 points have been excluded.

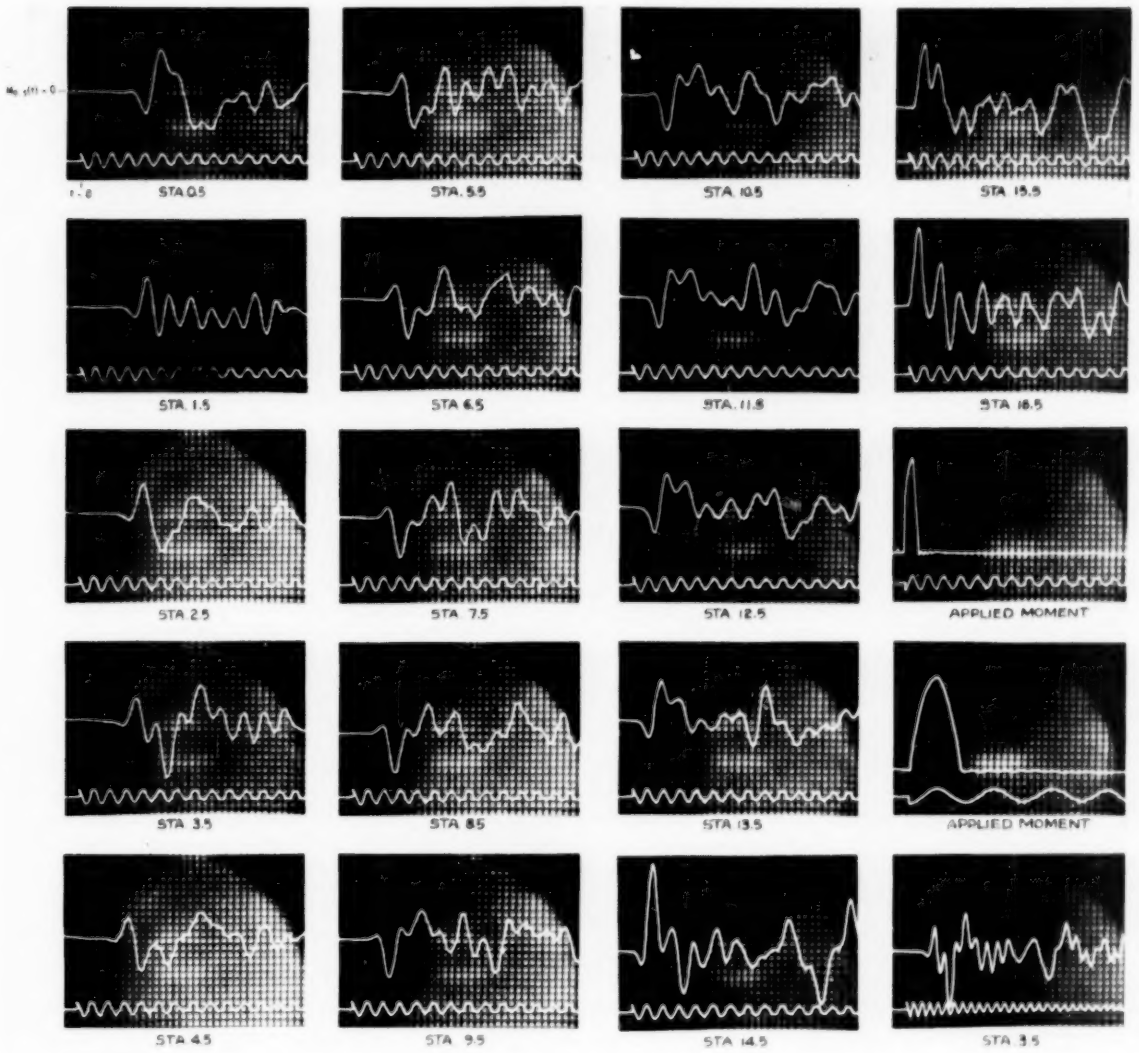

FIG. 8 ELECTRIC ANALOG COMPUTER MOMENT-TIME DIAGRAMS
(All diagrams to same scale as applied moment. Timing scale: 1 cycle = 40 μ sec.)

2.5.[7] The first noticeable strain occurs at approximately 67 μ sec. According to the more exact theory (1) the fastest flexural wave travels with the speed c. This would indicate the first appearance of strain at about 55 μ sec at Station 2.5 (point A in Fig. 9). Other stations show a similar lagging.[8] Hence, the analog solution seems to indicate that the fastest flexural wave travels with a speed less than c. The plot shows a maximum outer fiber strain of about four tenths the magnitude of the unloading wave. This maximum strain occurs at 200 μ sec. Reference to Fig. 7 will show that at this time the longitudinal unloading wave is producing compression near the beam base. It is believed that the second failure occurs later with the aid of one of the bending strains within the region indicated in Fig. 9. This is just after Stage 7 in Fig. 7.

A concept of the strain waves and their propagation in the early times t can be obtained from Fig. 10. The figure, derived from the analog results, contains plots of the outer fiber strain versus position for the times 40 and 65 μ sec, both of which are greater than k. The time necessary for the fastest flexural wave to arrive at the beam base is 65 μ sec. Hence, these plots are free of reflections and represent the first leg of wave travel down the beam. The progress of the strain waves toward the base of the beam is obvious from the shift of the peaks, with time. This shift is indicated by the arrows in the figure. Lagging of the waves is indicated since the 65 μ sec curve should show evidence of strain very close to $x = 0$, and the 40 μ sec curve should show its first disturbances at 0.37 l.[8]

As a basic check on the order of magnitude of the strains produced by the analog solution, an expression for the strain accord-

[7] Fig. 9 contains a curve derived from the elementary theory which will be discussed later.

[8] These statements are based on measurements taken from an enlargement of Fig. 8. To verify what is indicated, the vertical scale of the diagrams would have to be expanded in the earlier time regions.

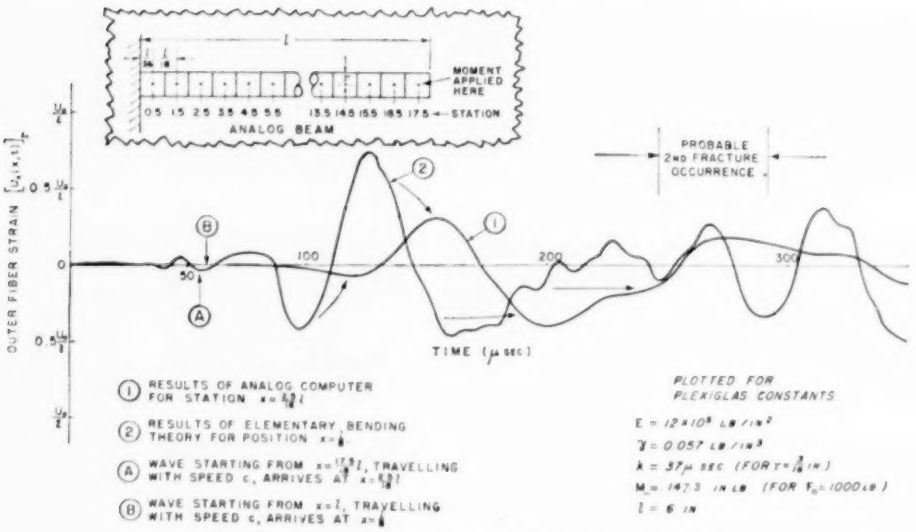
MOMENT APPLIED HERE
0.5 1.5 2.5 3.5 4.5 5.5 13.5 14.5 15.5 16.5 17.5 → STATION
ANALOG BEAM
PROBABLE 2ND FRACTURE OCCURRENCE
OUTER FIBER STRAIN
TIME (μ sec)
(1) RESULTS OF ANALOG COMPUTER FOR STATION
(2) RESULTS OF ELEMENTARY BENDING THEORY FOR POSITION
(A) WAVE STARTING FROM TRAVELLING WITH SPEED c, ARRIVES AT
(B) WAVE STARTING FROM TRAVELLING WITH SPEED c, ARRIVES AT
PLOTTED FOR PLEXIGLAS CONSTANTS
E = 1.2 × 10⁶ LB/IN²
γ = 0.057 LB/IN³
k = 37μ SEC (FOR
M = 147.3 IN LB (FOR
l = 6 IN

FIG. 9 OUTER FIBER STRAIN VERSUS TIME—NEAR BEAM BASE

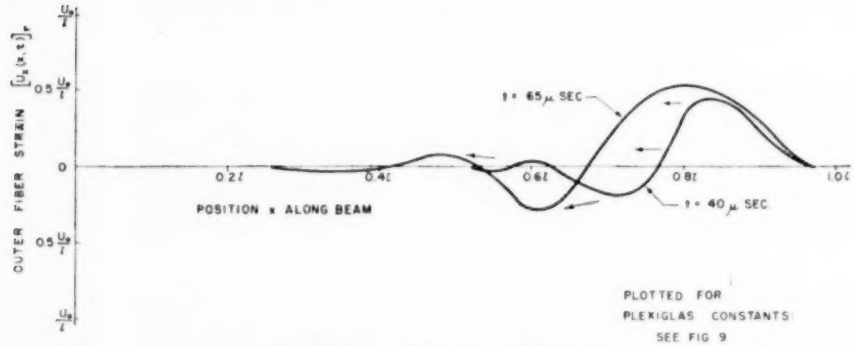

FIG. 10 OUTER FIBER STRAIN VERSUS POSITION

ing to the elementary bending theory has been derived. The outer fiber strain was obtained from the beam deflection, derived in the Appendix, by making use of the relation

$$[U_x(x, t)]_r = rV_{xx}(x, t)$$

which yields

$$[U_x(x, t)]_r = \frac{U_0}{l}\left[-\frac{2\pi a}{kl}\sum_{n=1}^{\infty}\frac{\psi_{xx}(q_n, x)}{q_n\left[\frac{\pi^2}{k^2} - a^2q_n^4\right]\phi(q_n)}\sin aq_n^2 t + \frac{ka}{2\pi}\frac{\psi_{xx}\left(\sqrt{\frac{\pi}{ak}}, x\right)}{\Gamma\left(\sqrt{\frac{\pi}{ak}}\right)}\sin\frac{\pi}{k}t\right], 0 \leq t < k \quad [8a]$$

$$= -\frac{U_0}{l}\left[\frac{2\pi a}{kl}\sum_{n=1}^{\infty}\frac{\psi_{xx}(q_n, x)}{q_n\left[\frac{\pi^2}{k^2} - a^2q_n^4\right]\phi(q_n)}[\sin aq_n^2 t + \sin aq_n^2(t-k)]\right], t \geq k \quad [8b]$$

Curve 2 in Fig. 9 is a plot of Equations [8] for the position $x = l/8$. Twenty terms, $q_1, q_2, \ldots\ldots q_{20}$, have been used in the summation.

In the later times t (>150 μ sec) the strain ordinates of curve 2 offer a favorable magnitude check on those of curve 1. In the earlier times t (<150 μ sec) curve 2 differs considerably from curve 1; the well-known criticism that the elementary theory strains occur too early and that they are too severe stands out in Fig. 9. Point B marks the first occurrence of strain according to the more exact theory (1); hence strains to the left of point B are fictitious. The arrows in Fig. 9 indicate the displacements that would bring closer agreement between the two curves.

EXPERIMENTAL WORK

The Plexiglas used in this work was of the type IA in 1¼-in. plate form. The steel had the following composition: C-0.73, Mn-0.31, P-0.014, S-0.018, Si-0.33, Cr-4.00, V-1.07, W-18.43 per cent. Its form was 1¼-in-diam bar stock. The steel was given a treatment which consisted of a heating to 2300 F, a quench in salt, and a 2-hr temper at 1050 F. This imposed maximum brittleness on the steel.

The occurrence of a second break was first noted in the Plexi-

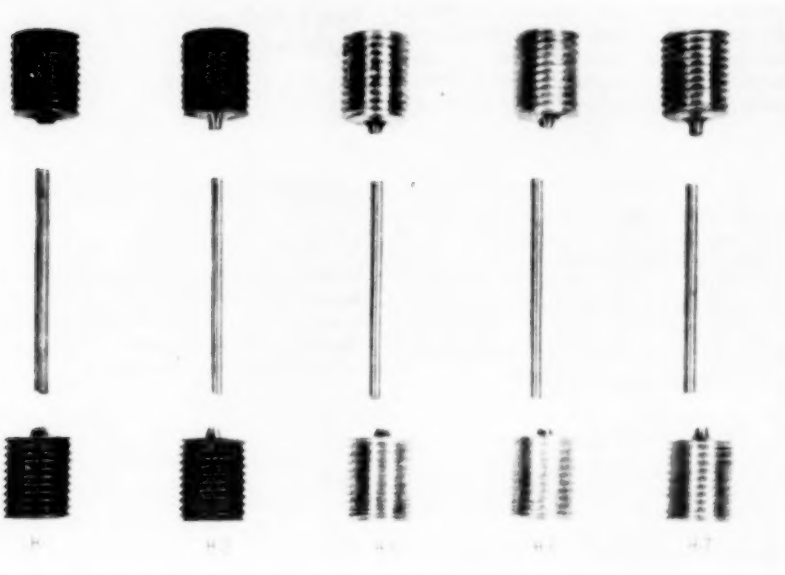

FIG. 11 HIGH-SPEED-STEEL SPECIMENS EXHIBITING TWO FRACTURES

glas. The specimens had a gage length of 6 in., a gage diameter of $^3/_8$ in., and a $^7/_8$-in. head radius. The gage surfaces might be described as highly polished. The specimens were pulled in a 60,000-lb Baldwin-Southwark universal testing machine with the aid of $^3/_4$-in. standard grips and spherical seats. A loading rate of 300 lb per min was used.

Specimen P2, Fig. 1, exhibited the cleanest fractures (some other specimens exhibited second fractures in the threads). The first break, in all probability, coincided with an impression on the specimen produced by the knife-edge of a mounted extensometer. The second break occurred near the head; i.e., the first gage region to be subjected to the tension of the reflected unloading wave.

Most of the experiments with Plexiglas proved to be inconsistent in producing the double fracture, probably because of the speed-sensitivity of this material. The consistency of the high-speed steel in producing two fractures shifted attention to this material.

Fig. 11 shows five specimens exhibiting the second fracture. Heavy 6-in-diam steel heads were used in these tests to approximate the conditions of fixed ends. The specimens had a gage length of 4 in., a gage diameter of $^1/_4$ in., a $^1/_4$-in. head radius, and a $1^1/_4$-in-diam head. They were ground to finished size. When the two fractures occurred they were usually at or near the fillets, as shown in the photographs. A loading rate of 2000 lb per min was used here.

Table 1 presents some interesting fracture data. Specimens H8, 9, and 10, with their low fracture stresses and resultant single rupture, reflect the smaller magnitude of the unloading waves involved. The notches, employed for instrumentation purposes, are responsible of course. The fact that the stubbier beams resisted the second fracture is shown by a comparison of the data of specimens H1 and 2, or that of H3 and 4 (in both of these pairs the fracture stresses were approximately equal). Note too that specimens H5, 6, and 7, which exhibited two breaks, had large beam ratios (17:1).

Specimens H3 and 4 seem to indicate that the stress concentration at the fillet is of the order of one due to an ordinary non-homogeneity in the material, i.e., with approximately equal stresses, specimen H3 broke at the fillet, and H4 at mid-gage.

TABLE 1 FRACTURE DATA ON HIGH-SPEED-STEEL SPECIMENS

Specimen	Initial fracture stress ($\times 10^3$ psi)	Cantilever length-to-diameter ratio	No. of breaks	1st break at
H1[a]	245	17 to 1	2	Fillet
H2[a]	221	10 1/2 to 1	1	Near gage mid-point
H3	306	17 to 1	2	Fillet
H4[b]	302	9 to 1	1	Gage mid-point
H5	244	17 to 1	2	Fillet
H6	239	17 to 1	2	Fillet
H7	236	17 to 1	2	Fillet
H8[c]	102	21 to 1	1	Notch
H9[c]	104	21 to 1	1	Notch
H10	143	17 to 1	1	Notch

[a] Machine finish.
[b] Specimens H4 to H10 had a shallow notch near one fillet; in no case was it more than 0.025 in. deep.
[c] 5-in. gage length.

Specimens H5, 6, and 7 show lower stresses, indicating a somewhat larger stress concentration. The mean of these cases gives the factor of stress concentration involved in these tests as only 1.1.

FUTURE WORK AND APPLICATIONS

The work described in this paper suggests the use of the rupture process in brittle materials as a means of studying, experimentally, the uniaxial elastic compression wave and the flexural strain waves created by a couple. Plans are to continue work along these lines. The work will have two phases. One will be directed toward obtaining more exact information on the fracture process. Support for, or possibly modification of, the impulsive functions and hence waves could result. High-speed photographs of the fracture surface during rupture are planned using the longitudinal optic system of the Plexiglas specimen. The second phase will be directed toward actual strain-wave measurements by means of bonded-wire resistance gages. Artificial fracture initiation by a slight notch at mid-gage will eliminate any possibility of wave transmission across the intact area during fracture. This method of studying the compression wave should be valuable since in it a wave of large magnitude is produced and this magnitude is known, i.e., the fracture load is measured. The latter gives a basic check on the results obtained from the dynamic measuring technique employed.

The future experimental work should produce data on the validity of the basic assumptions made in the present work. Some electronic strain-time records already have been obtained and some agreement is indicated with the theoretical curve in Fig. 7. More quantity is needed, however, before definite conclusions are justified.

Acknowledgment

Acknowledgment is due Drs. G. D. McCann and R. H. MacNeal for deriving the moment-time diagrams shown in Fig. 8. The author also appreciates the work done by Mr. H. J. Martin in evaluating numerically the solutions involved. Thanks are extended to Mr. A. G. Loveberg, Jr., for his electronic instrumentation and general help in the testing program. Acknowledgment is due the U. S. Naval Ordnance Test Station for permission to publish the results of this investigation.

Bibliography

1 "The Propagation of Waves in the Transverse Vibration of Bars and Plates," by Ya. S. Uflyand, *Prikladnaia Matematika i Mekhanika*, vol. 12, May–June, 1948, pp. 287–300 (in Russian). See Rev. 33, AMR 3.

2 "Vibration Problems in Engineering," by S. Timoshenko, D. Van Nostrand Company, Inc., New York, N. Y., 1937, p. 338.

3 "Interpretation of Fracture Markings," by J. A. Kies, A. M. Sullivan, and G. R. Irwin, *Journal of Applied Physics*, vol. 21, July, 1950, pp. 716–720.

4 "Fracture and Comminution of Brittle Solids," by E. F. Poncelet, Metals Technology, AIME, Technical Publication No. 1684 April, 1944.

5 "Über den Zerreisvorgang der Gläser," by A. Smekal, Glastechn, Berlin, vol. 13, 1935, p. 141.

6 "Die Festigkeitseigenschaften spröder Körper," by A. Smekal, *Ergebnisse der exacten Naturwissenschaften*, vol. 15, 1936, pp. 106–186.

7 "Longitudinal Wave Transmission and Impact," by L. H. Donnell, Trans. ASME, vol. 52, 1930, p. A-158.

8 "Modern Operational Mathematics in Engineering," by R. V. Churchill, McGraw-Hill Book Company, Inc., New York, N. Y., 1944.

9 "Strength Properties of Plexiglas—Part II," by W. F. Bartoe, *Aviation*, vol. 42, March, 1943, p. 145.

10 "Beam-Vibration Analysis With Electric-Analog Computer," by G. D. McCann and R. H. MacNeal, Journal of Applied Mechanics, Trans. ASME, vol. 72, 1950, pp. 13–26.

11 "The Solution of Aeroelastic Problems by Means of Electrical Analogies," by R. H. MacNeal, G. D. McCann, and C. H. Wilts, *Journal of the Aeronautical Sciences*, vol. 18, 1951, pp. 777–789.

12 "Vibration of a Cantilever Beam With Prescribed End Motion," by G. A. Nothmann, Journal of Applied Mechanics, Trans. ASME, vol. 70, 1948, pp. 327–334.

Appendix

Based on the elementary theory of beam bending, the boundary-value problem for the couple case shown in Fig. 5(*c*), may be stated as follows

$$\left.\begin{aligned} &V_{tt}(x,t) + a^2 V_{xxxx}(x,t) = 0 \qquad (0 < x < l,\ t > 0)\\ &V(x,0) = V_t(x,0) = 0\\ &V(0,t) = V_x(0,t) = V_{xxx}(l,t) = 0,\ EIV_{xx}(l,t) = M(t) \end{aligned}\right\} \quad [9]$$

where

$$\left.\begin{aligned} M(t) &= \frac{M_m}{\pi}\sin\frac{\pi}{k}t \qquad 0 \leqq t < k\\ &= 0 \qquad t \geqq k \end{aligned}\right\}$$

In these equations, the effects of rotary inertia, shear force, and damping are neglected.[9] The boundary condition $V_{xxx}(l,t) = 0$ is supported physically by the fact that normal sections such as the initial fracture section *C-C*, Fig. 4, are shearless.

The transformed solution is

$$v(x,s) = \frac{M_m}{2EIk}\left[\frac{1}{\left(s^2 + \frac{\pi^2}{k^2}\right)}\right]\left[\frac{\psi(q,x)}{q^2\,\Gamma(q)}\right]\left[1 + e^{-ks}\right]$$

where

$$\psi(q,x) = (\sin ql - \sinh ql)(\sinh qx - \sin qx) + (\cosh ql + \cos ql)(\cosh qx - \cos qx),$$

and

$$\Gamma(q) = 1 + \cos ql \cosh ql$$

The inverse transform $V(x,t)$ is equal to the sum of the residues corresponding to the poles of $v(x,s)$.

For the region $0 \leqq t < k$, the e^{-ks} factor does not contribute to the inverse transform. For this region the beam deflection is given by

$$V(x,t) = \frac{M_m a}{2EIk}\left[-\frac{4}{l}\sum_{n=1}^{\infty}\frac{\psi(q_n,x)}{q_n\left[\frac{\pi^2}{k^2} - a^2q_n^4\right]\phi(q_n)}\sin aq_n^2 t + \frac{k^2}{\pi^2}\frac{\psi\left(\sqrt{\frac{\pi}{ak}},x\right)}{\Gamma\left(\sqrt{\frac{\pi}{ak}}\right)}\sin\frac{\pi}{k}t\right], \text{ where } \phi(q) = \frac{1}{l}\frac{d\Gamma(q)}{dq} \quad [10a]$$

For the region $t \geqq k$, we add the translation function due to e^{-ks}, which yields

$$V(x,t) = -\frac{2M_m a}{EIkl}\sum_{n=1}^{\infty}\frac{\psi(q_n,x)}{q_n\left[\frac{\pi^2}{k^2} - a^2q_n^4\right]\phi(q_n)}\left[\sin aq_n^2 t + \sin aq_n^2(t-k)\right] \quad [10b]$$

Equations [10] have been verified as the solution of the problem given by Equations [9].

[9] More of the details in the solution that follows may be found in a NOTS Report (NAVORD No. 1961) by the author. Similar problems are treated in the works of Churchill (8) and Nothmann (12).

Influence Coefficients of Tapered Cantilever Beams Computed on SEAC

By SAMUEL LEVY,[1] WASHINGTON, D. C.

A description is given of a method for computing the influence coefficients in bending of a nonuniform cantilever beam using a basic code devised for the National Bureau of Standards electronic automatic computer SEAC. The given data for a particular problem are n, the number of stations at which influence coefficients are desired; EI_0, EI_1, . . . EI_n, the bending stiffnesses at the root and at successive stations; and l_1, l_2, . . . l_n, the distances between these stations. The basic code can be used in any case where the number of stations n is fewer than 23. In an example for a beam having 9 stations, the computing time was 3 min.

Introduction

IN the design of machines and structures, an important factor in the choice of methods of analysis is the time available. Limited time results in the use of estimates and approximate formulas where more accurate though cumbersome formulas are available, and in the study of only a few design variables where a more thorough search might yield a more efficient design. Any means of reducing analysis time, particularly if it does not result in an increase in cost, is therefore of prime importance in determining what design methods will be used. The advent of high-speed digital computing machines shows promise of reducing analysis time.

The results given in this paper were obtained on the National Bureau of Standards Eastern Automatic Computer, SEAC.[2] The high speed with which this machine performs all of the simple arithmetical operations makes it possible to obtain much more accurate approximate solutions to important engineering problems than could be obtained in a reasonable period of time by conventional computing methods. Addition or subtraction of 13-digit numbers is completed in about a millisec; multiplication or division in about 3 millisec. The machine will carry out basic orders of the following types: addition, subtraction, multiplication, division, comparison, logical transfer, and input and output control. Coded instructions and numerical data are supplied to the machine by means of magnetic wire or tape. Once the code has been written for a given problem it is a simple matter to solve all similar problems, since only the numerical data need be changed. The application of SEAC to the computation of influence coefficients, a tedious problem in the dynamic analysis of aircraft, is given in this report.

The influence coefficients of an elastic structure are defined as the deflections of selected points on the structure when a unit force is applied to any one of these points. The array, or matrix, of influence coefficients describes the flexibility of a structure in a form suitable for the computation of the normal modes of vibration.[3,4] They are also of value in determining the deformation of a structure due to static loads.

The computation of influence coefficients for uniform cantilever beams in bending is customarily carried out by methods similar to those given by Timoshenko.[5] In those cases where the beam is of nonuniform section, equation [121],[6] is applicable. If the variation of bending rigidity with position along the beam can be expressed in analytical form, this equation can be used directly. In some built-up structures, where the variation of bending rigidity cannot be expressed analytically, it is convenient to assume that either the bending rigidity or its reciprocal varies linearly from station to station along the beam.[7]

The methods of computing deflections of nonuniform beams, though clear and straightforward to apply, are time-consuming, particularly since the number of individual deflections needed increases as the square of the number of stations along the beam. Thus, in the case of a beam with 10 stations, 100 deflections are needed. The basic computational procedure is the same for each of these deflections. This procedure has been coded to be applicable without modification to beams with any number of stations between 1 and 23 in order to avoid the necessity for writing a new code for each new beam to be analyzed.

The present paper gives the development for the equations based on beam theory, used in coding SEAC; the essential computational procedures carried out automatically by SEAC; and the results of the computations by SEAC for a beam having 9 stations.

This work was conducted at the National Bureau of Standards under the sponsorship and with the financial assistance of the Bureau of Aeronautics, Department of the Navy.

Development of Equations Based on Beam Theory

It has been shown by Timoshenko[8] that the bending of beams is governed by the equation (taking positive moment in the sense as causing positive curvature)

$$d^2y/dx^2 = M/EI \quad \ldots\ldots\ldots\ldots\ldots\ldots [1]$$

where

[1] Chief of Aircraft Structures Group, National Bureau of Standards. Mem. ASME.

[2] Anon: SEAC, Tech. News Bulletin, National Bureau of Standards, vol. 34, 1950, pp. 121–129.

Contributed by the Applied Mechanics Division and presented at the Annual Meeting, New York, N. Y., November 30–December 5, 1952, of The American Society of Mechanical Engineers.

Discussion of this paper should be addressed to the Secretary, ASME, 29 West 39th Street, New York, N. Y., and will be accepted until April 10, 1953, for publication at a later date. Discussion received after the closing date will be returned.

Note: Statements and opinions advanced in papers are to be understood as individual expressions of their authors and not those of the Society. Manuscript received by ASME Applied Mechanics Division, June 30, 1952. Paper No. 52—A-25.

[3] "Solution of Oscillation Problems by Matrices," by W. J. Duncan and A. R. Collar, *Philosophical Magazine*, S., vol. 17, 1934, pp. 866–909.

[4] "Dynamic Loads on Aircraft Structures During Landing," by M. A. Biot and R. L. Bisplinghoff, NACA ARR No. 4H10, October, 1944.

[5] "Strength of Materials, Part 1," by S. Timoshenko, D. Van Nostrand Company, New York, N. Y., second edition, 1940, pp. 140–142.

[6] Ibid., p. 210.

[7] "A Simple Tabular Method of Calculating Deflections and Influence Coefficients of Beams," by N. O. Myklestad, *Journal of the Aeronautical Sciences*, vol. 13, 1946, pp. 23–28.

[8] Reference 5, p. 135.

x = distance along axis of beam
y = lateral deflection of beam
M = bending moment in beam
$(1/EI)$ = flexibility of beam

The beam for which it is desired to compute influence coefficients is shown in Fig. 1. The stations, 0 to n, are shown in the

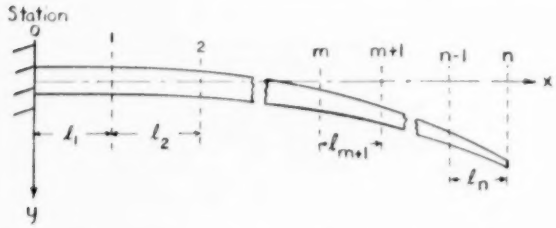

FIG. 1 BEAM FOR WHICH INFLUENCE COEFFICIENTS ARE DESIRED

figure. The flexibility at stations 0, 1, 2. . .n is denoted by $1/EI_0$, $1/EI_1$, $1/EI_2$, . . . $1/EI_n$, respectively. The distance from station 0 to station 1 is denoted by l_1, from station 1 to station 2 by l_2, and so on.

The method to be used in the computation will make use of the behavior of the individual segments of beam between successive stations.[7] Consider the piece of beam between stations m and $m + 1$, Fig. 1. If we denote the shearing force in this segment by S_{m+1} and the moment at station $m + 1$ by M_{m+1}, we can write the following equations for the increase in deflection y, and slope θ, in going from station m to station $m + 1$

$$y_{m+1} - y_m = \theta_m l_{m+1} + a_{m+1}S_{m+1} + b_{m+1}M_{m+1} \quad [2]$$

$$\theta_{m+1} - \theta_m = b_{m+1}S_{m+1} + c_{m+1}M_{m+1} \quad [3]$$

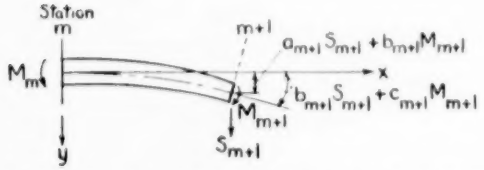

FIG. 2 DEFORMATION AND LOAD FOR ELEMENT OF BEAM BETWEEN STATIONS m AND $m + 1$

where, Fig. 2

a_{m+1} = deflection per unit shear load at station $m + 1$ with station m considered clamped
b_{m+1} = deflection per unit moment at station $m + 1$ (or rotation per unit shear) with station m considered clamped
c_{m+1} = rotation per unit moment at station $m + 1$ with station m considered clamped

The unit constants a_{m+1}, b_{m+1}, and c_{m+1} in Equations [2] and [3] depend on the flexibility at stations m and $m + 1$ and on the distance between them, l_{m+1}. In determining expressions for these constants, it is assumed that the variation in flexibility can be approximated by a linear variation from $1/EI_m$ at station m to $1/EI_{m+1}$ at station $m + 1$. This assumption leads to equations more suitable for machine computation than the assumption of a linear variation in EI used by Myklestad,[7] which leads to the use of logarithms. Referring to Fig. 2

$$1/EI = (1 - x/l_{m+1})(1/EI_m) + (x/l_{m+1})(1/EI_{m+1}) \quad [4]$$

Also, since the moment varies linearly from station $m + 1$ to station m

$$M = M_{m+1} + (l_{m+1} - x)S_{m+1} \quad [5]$$

Substituting Equations [4] and [5] into [1] gives

$$d^2y/dx^2 = [M_{m+1} + l_{m+1}S_{m+1} - xS_{m+1}][1/EI_m + (x/l_{m+1})(1/EI_{m+1} - 1/EI_m)] \quad [6]$$

Multiplying and integrating gives, with $dy/dx = 0$ at $x = 0$

$$dy/dx = x(M_{m+1} + l_{m+1}S_{m+1})(1/EI_m) + x^2[(M_{m+1} + l_{m+1}S_{m+1})(1/EI_{m+1} + 1/EI_m) - l_{m+1}S_{m+1}(1/EI_m)]/(2l_{m+1}) - x^2S_{m+1}(1/EI_{m+1} - 1/EI_m)/(3l_{m+1}) \quad [7]$$

and with $y = 0$ at $x = 0$

$$y = x^2(M_{m+1} + l_{m+1}S_{m+1})(1/EI_m)/2 + x^3[M_{m+1}(1/EI_{m+1} - 1/EI_m) + S_{m+1}l_{m+1}(1/EI_{m+1} - 2/EI_m)]/(6l_{m+1}) - x^4S_{m+1}(1/EI_{m+1} - 1/EI_m)/(12l_{m+1}) \quad [8]$$

Setting $x = l_{m+1}$ gives

$$y_{(x=l_{m+1})} = S_{m+1}l^3_{m+1}(1/4EI_m + 1/12EI_{m+1}) + M_{m+1}l^2_{m+1}(1/3EI_m + 1/6EI_{m+1}) \quad [9]$$

$$(dy/dx)_{(x=l_{m+1})} = S_{m+1}l^2_{m+1}(1/3EI_m + 1/6EI_{m+1}) + M_{m+1}l_{m+1}(1/2EI_m + 1/2EI_{m+1}) \quad [10]$$

Comparing with Equations [2] and [3]

$$\left.\begin{aligned} a_{m+1} &= l^3_{m+1}(1/4EI_m + 1/12EI_{m+1}) \\ b_{m+1} &= l^2_{m+1}(1/3EI_m + 1/6EI_{m+1}) \\ c_{m+1} &= l_{m+1}(1/2EI_m + 1/2EI_{m+1}) \end{aligned}\right\} \quad [11]$$

COMPUTATIONAL PROCEDURE CARRIED OUT BY SEAC

The computational procedure carried out by SEAC is based on the use of Equations [2], [3], and [11] together with the given data of EI_m and l_m for each station and of n, the number of stations. The steps in the procedure followed by SEAC automatically are as follows:

1 Store in the memory of the machine the basic code for the computation of influence coefficients in bending for tapered cantilever beams having no more than 23 stations.

2 Store in the memory of the machine the values of EI_m/r, l_m/k, and r (note, r and k are scale factors. The method of choosing them is explained in step 8).

3 Compute and store in the memory of the machine the values of a_{m+1}, b_{m+1}, and c_{m+1} for each segment of the beam using Equations [11] as the basis for the computation.

4 Compute and temporarily store the values of shear S_{m+1} and moment M_{m+1} at the successive stations with a unit load considered applied at station 1.

5 Compute and temporarily store the values of slope θ_{m+1} at the successive stations using Equation [3] and the previously computed values of S_{m+1} and M_{m+1} (take $\theta_0 = 0$).

6 Compute and print the values of y_{m+1} at the successive stations using Equation [2] and the previously computed values of θ_m, S_{m+1}, and M_{m+1} (take $y_0 = 0$).

7 Repeat steps 4, 5, and 6 successively for a unit load considered applied at station 2, station 3, . . . station n.

8 The operation of SEAC is such that all numbers used by it in computation must be less than 4 in absolute value. The values of EI_m and l_m therefore must be divided by scale factors. The code stored in step 1 has been written on the assumption that the scale factors, r for EI_m, and k for l_m have been determined as follows:

(a) Choose k such that each l_m/k is equal to or less than 1 and $\sum_{m=1}^{n} (l_m/k)$ is less than 4 but greater than 1.

(*b*) Choose r such that the largest value of (EI_m/r) is less than 4 but greater than 1.

(*c*) Choose an additional constant f such that for the smallest value of EI_m the value of (rf/EI_m) is less than 4 but equal to or greater than 0.4 and such that $k^3/rf = 10^p$, p being an integer. The constant f is included in the data given to SEAC for use in the computation.

(*d*) The answers obtained by SEAC must then be multiplied by 10^p, which merely entails shifting of the decimal point.

Due to the great speed of computation in SEAC, the time required to carry out such an influence-coefficient computation is little more than the time required to print the answers.

Typical Results of Computation

As a check of the coding and over-all method, computations were carried out for the influence coefficients of the tapered beam used in landing-impact tests.[9] The flexibility of the beam, $1/EI$, at the root and at 9 successive stations along the beam as well as the distance between stations is given elsewhere.[10] The reciprocal of the flexibility EI, and the distance between stations are given in Table 1 of this paper.

For this case, the values of the scale factors k, r, and f were taken as 50, 10^7, and 0.00125, respectively. Referring to Table 1 and the rules in step 8 for determining these factors, we see that the largest value of l_m/k should be equal to or less than 1. The largest, at station 5, is 10/50 = 0.2. The sum of the l_m/k values should be less than 4 but greater than 1. The sum is 64/50 = 1.28. The largest value of EI_m/r is at station 0 and has a value $10.526 \times 10^6/10^7 = 1.0526$ which is satisfactorily between 4 and 1. The largest value of rf/EI_m is at station 9 and has a value $10^7(0.00125)/(0.005 \times 10^6) = 2.5$ which is between 4 and 0.4 as required. In addition, k^3/rf, the factor by which the SEAC answers must be multiplied to obtain the influence coefficients, is $50^3/(10^7 \times 0.00125) = 10$.

The influence coefficients computed automatically on SEAC in about 3 min are given in Table 2. For comparison, influence coefficients computed and checked by hand in about 2 days on a conventional computing machine are given in Table 3. The lower half of the matrix in Table 3 was not computed since it can be determined from the upper half by symmetry about the principal diagonal. It will be noted that Tables 2 and 3 are in excellent agreement. The number of decimal figures obtained by SEAC is much greater than is customarily required.

[9] "Experimental Verification of Theory of Landing Impact," by Walter Ramberg and Albert E. McPherson, *Journal of Research*, National Bureau of Standards, vol. 41, 1948, pp. 509–520.

[10] Ibid., table 2.

TABLE 1 BENDING STIFFNESS EI, AND DISTANCE l, BETWEEN STATIONS OF TYPICAL BEAM

Station no.	Distance from root, in.	Distance l, from preceding station, in.	Bending stiffness, EI (10^6 lb-in^2)
0	0	...	10.526
1	6.5	6.5	8.621
2	13.5	7.0	6.173
3	21.5	8.0	4.000
4	31.0	9.5	1.848
5	41.0	10.0	1.026
6	49.0	8.0	0.3846
7	53.5	4.5	0.1942
8	59.0	5.5	0.03636
9	64.0	5.0	0.005

Conclusion

It is concluded that the National Bureau of Standards electronic computing machine SEAC can be used with advantage to compute influence coefficients in bending of tapered cantilever beams.

It is recommended that the application of high-speed electronic computing machines to structural analyses such as this, where the analysis is relatively simple but the computations tedious, be pursued further.

Acknowledgment

The author is grateful to Mrs. Ida I. Rhodes of the National Bureau of Standards Machine Development Laboratory and to his colleagues, Miss W. D. Kroll and Mr. I. E. Wilks, for assistance in the preparation of this report. Mrs. Rhodes's help was invaluable in explaining the principles and efficient use of SEAC.

TABLE 2 INFLUENCE COEFFICIENTS OF TYPICAL BEAM AS COMPUTED BY SEAC

Unit load at station	Millionths of an inch deflection at station 1	2	3	4	5	6	7	8	9
1	9.177	24.260	41.498	61.968	83.516	100.754	110.450	122.302	133.075
2	24.260	87.522	168.902	265.541	367.267	448.647	494.424	550.373	601.235
3	41.498	168.902	387.843	668.709	964.357	1200.876	1333.918	1496.524	1644.349
4	61.968	265.541	668.709	1340.253	2106.640	2719.750	3064.625	3486.138	3869.332
5	83.516	367.267	964.357	2106.640	3795.986	5248.514	6065.56	7064.17	7972.00
6	100.754	448.647	1200.876	2719.750	5248.514	7873.918	9436.50	11346.33	13082.53
7	110.450	494.424	1333.918	3064.625	6065.56	9436.50	11683.51	14501.77	17063.83
8	122.302	550.373	1496.524	3486.138	7064.17	11346.33	14501.77	19318.49	24108.88
9	133.075	601.235	1644.349	3869.332	7972.00	13082.53	17063.83	24108.88	35246.36

TABLE 3 INFLUENCE COEFFICIENTS OF TYPICAL BEAM AS COMPUTED BY HAND

Unit load at station	Millionths of an inch deflection at station 1	2	3	4	5	6	7	8	9
1	9.1771522	24.260477	41.498563	61.968790	83.516397	100.75448	110.45091	122.30209	133.07587
2		87.522363	168.90272	265.54189	367.26734	448.64770	494.42415	550.37314	601.2358
3			387.84305	668.70914	964.35767	1200.8765	1333.9183	1496.5250	1644.34939
4				1340.2531	2106.6407	2719.7508	3064.6252	3486.1384	3869.3322
5					3795.9858	5248.5142	6065.5615	7064.1748	7972.0050
6						7873.9187	9436.5030	11346.328	13082.533
7							11683.510	14501.776	17063.836
8								19318.493	24108.879
9									35246.358

Design Data and Methods

It is important that the data contained in technical papers be made readily available to designing engineers. In order to satisfy these needs of industry, this section of the Journal includes a concise presentation of data and information drawn chiefly from papers previously published by the Applied Mechanics Division of The American Society of Mechanical Engineers.

On the Maximum Numerical Value of the Tangential Stress in Thick-Walled Cylinders

By T. RANOV[1] and F. R. PARK[2]

Statements in the literature[3] appear to imply that the numerical value of the circumferential stress in thick-walled cylinders is always a maximum at the inner radius. While this is certainly correct in the case of zero external pressure, the presence of both external and internal pressures creates the possibility of a numerically larger tangential stress occurring at the outer radius. This paper investigates this possibility and establishes a criterion for a check on the location of the numerical tangential stress maximum. A chart is presented for its convenient application.

Nomenclature

The following nomenclature is used in the paper:

- r = radius to any point in thick-walled cylinder
- r_1 = internal radius
- r_2 = external radius
- p_1 = internal pressure
- p_2 = external pressure
- S_r = radial stress at any radius r
- S_t = circumferential (tangential or hoop) stress at any radius r, positive if tensile
- S_{t1} = circumferential stress at inner radius
- S_{t2} = circumferential stress at outer radius
- $R = r_2/r_1$ = ratio of external to internal radius
- $P = p_2/p_1$ = ratio of external pressure to internal pressure
- $\sigma = S_{t1}/S_{t2}$ = ratio of circumferential stress at inner radius to circumferential stress at outer radius

Consider a uniform, homogeneous, circular, hollow cylinder, classified as "thick-walled" by virtue of its relatively large radius ratio. Fig. 1 illustrates the dimensional symbols used and the fact that the cylinder is assumed to be subjected to both internal and external pressures.

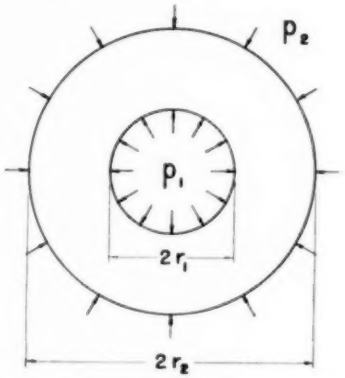

Fig. 1

Lamé Solution for Circumferential Stress

The well-known Lamé solution for the circumferential stress in a thick-walled cylinder subjected to internal and external pressures as described in the foregoing, may be written in the form

$$S_t = \left(\frac{p_1 r_1^2 - p_2 r_2^2}{r_2^2 - r_1^2}\right) + \left(\frac{r_1^2 r_2^2 (p_1 - p_2)}{r_2^2 - r_1^2}\right)\frac{1}{r^2} \quad \ldots\ldots [1]$$

Introducing as characteristic quantities for a given case the stress

$$a = \frac{p_1 r_1^2 - p_2 r_2^2}{r_2^2 - r_1^2}$$

and the force

$$b = \frac{r_1^2 r_2^2 (p_1 - p_2)}{r_2^2 - r_1^2}$$

Equation [1] may be written as

$$S_t = a + \frac{b}{r^2}$$

If the radius-ratio R and the pressure-ratio P, as defined in the nomenclature, are substituted in the foregoing, the characteristic quantities a and b become

$$a = p_1 \frac{1 - PR^2}{R^2 - 1}$$

---

[1] Associate Professor of Engineering, University of Buffalo, Buffalo, N. Y.

[2] Development Engineer, Linde Air Products Company, Tonawanda, N. Y., formerly Assistant Professor of Engineering, University of Buffalo.

[3] "Advanced Mechanics of Materials," by F. B. Seely, John Wiley and Sons, Inc., New York, N. Y., 1948, p. 65.

"Advanced Mechanics of Materials," by G. Murphy, McGraw-Hill Book Company, New York, N. Y., 1946, p. 120.

Discussion of this paper should be addressed to the Secretary, ASME, 29 West 39th Street, New York, N. Y., and will be accepted until April 10, 1953, for publication at a later date. Discussion received after the closing date will be returned.

Note: Statements and opinions advanced in papers are to be understood as individual expressions of their authors and not those of the Society. Manuscript received by the ASME Applied Mechanics Division, June 26, 1952.

and

$$b = p_1 r_2^2 \frac{1 - P}{R^2 - 1}$$

For future reference we also form the ratio of these two expressions

$$\frac{a}{b} = \frac{1 - PR^2}{1 - P} \frac{1}{r_2^2} \quad \ldots\ldots [2]$$

It is convenient to base the search for the location of the numerical maximum of the tangential stress S_t upon the ratio of the stresses at the inner and outer radii, respectively. In other words, the ratio

$$\sigma = \frac{S_{t1}}{S_{t2}}$$

must be examined and the condition found, if it exists, which will make this ratio smaller than unity. Once this is established, it is evident that the existence of a numerically larger stress at the outer radius has been demonstrated. The need for adopting this procedure arises, of course, from the hyperbolic nature of the tangential stress distribution, with no mathematical extremum.

Our attention, therefore, immediately turns to a thorough study of the equation

$$S_t = a + \frac{b}{r^2} = f(r)$$

Depending upon the values and signs of a and b, the general appearance of this function may be either of two families of curves as shown in Fig. 2. The following limiting cases are investigated first and typical curves plotted in Fig. 3:

Case A: $|\sigma| = 1$
Case B: $\sigma = 0$
Case C: $\sigma \to \infty$

Case A. Inspection of Fig. 2 immediately reveals that the stress ratio σ is only equal to -1 when the two tangential stresses are of opposite sign, i.e., when $S_{t1} = -S_{t2}$. On the other hand, $\sigma = +1$ is only possible theoretically for the two limiting cases when the hyperbolas degenerate into the straight lines $S_{t1} = S_{t2} = \pm$ const, respectively. Examining the former of these two conditions, insertion of the appropriate radii into the general expression for S_t and equating with opposite signs yield

$$a + \frac{b}{r_1^2} = -\left(a + \frac{b}{r_2^2}\right)$$

Solving for a/b and substituting the radius ratio R, we find

$$\frac{a}{b} = -\frac{1}{2} \frac{R^2 + 1}{r_2^2} \quad \ldots\ldots [3]$$

Equating [3] to [2] and solving for the pressure ratio give

$$P = \frac{R^2 + 3}{3R^2 + 1} \quad \ldots\ldots [4]$$

It may be verified that this ratio is always less than unity and tends to the limit 1/3 for large R. Physically, this result uniquely determines the pressure ratio for which numerically equal but opposite in sign circumferential stresses at the inner and outer radii may be produced. Examining next the latter of these two conditions, the internal and external stresses are now equated with equal signs. For this purpose it is necessary to first express Equation [1] in terms of the parameters P and R. Then, by substituting the appropriate radii, the stress ratio σ may be written as follows

$$\sigma = \frac{1 + \dfrac{R^2(1 - P)}{1 - R^2 P}}{1 + \dfrac{1 - P}{1 - R^2 P}} \quad \ldots\ldots [5]$$

It is immediately seen that for $P = 1$, $\sigma = 1$, i.e., $S_{t1} = S_{t2}$. It is further seen from Equation [1] that $a = -p_i = -p_2 = -p_e$ and $b = 0$. Therefore

$$S_{t1} = S_{t2} = -p$$

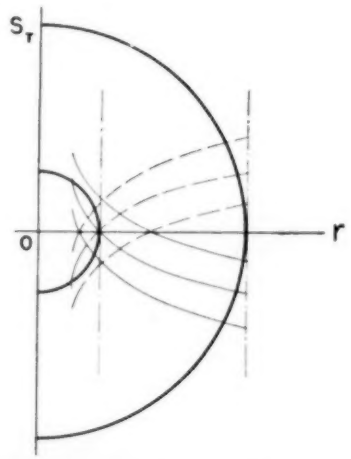

Fig. 2 Family of Curves $S = a + b/r^2$

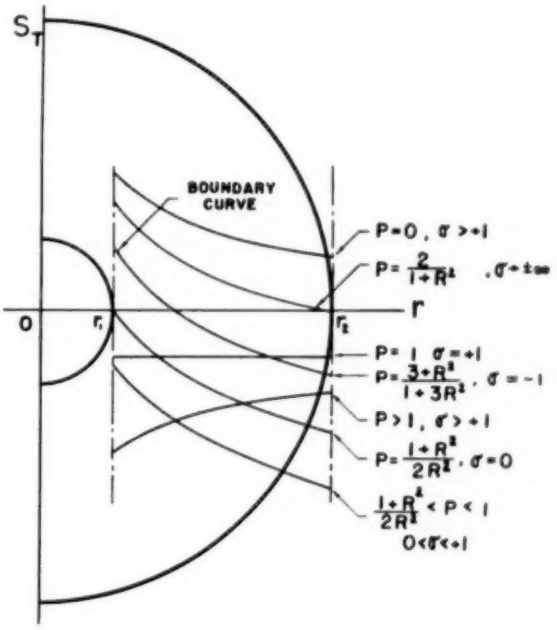

Fig. 3 Typical Hoop-Stress Curves for Different Values of Pressure Ratio P

Consideration of the well-known equation for radial stress will show that for equal pressures, S_r reduces to $-p$ also; hence for these conditions a state of hydrostatic compression exists.

Case B. The case $S_{t1} = 0$ represents all the curves in Fig. 2 which pass through the point $r = r_1$. From the equation of the family of curves we have

$$a + \frac{b}{r_1^2} = 0$$

Solved for r_1, this gives

$$r_1^2 = -\frac{b}{a} \qquad [6]$$

For r_1 to be real, b and a must be of opposite sign. By inspecting Equation [2], this requirement is seen to mean that here also the pressure ratio P must be smaller than unity. To obtain an expression for P in this case, Equation [6] is combined with Equation [2]. Solving for P results in

$$P = \frac{1 + R^2}{2R^2} \qquad [6a]$$

A check of this confirms that zero hoop stress at the inner radius can exist, in general, only if the internal pressure is larger than the external. This ratio tends to the limit 1/2 for large R.

Case C. Analogous to case B, the stipulation of $S_{t2} = 0$ singles out all the curves through $r = r_2$. This gives

$$a + \frac{b}{r_2^2} = 0$$

and

$$r_2^2 = -\frac{b}{a} \qquad [7]$$

Again this only yields real values of the intercept r_2 if a and b are of opposite sign, and the same conclusion for the pressure ratio P is drawn from Equation [2], namely, that P must be less than unity. By combining Equations [2] and [7], we have for this case

$$P = \frac{2}{1 + R^2} \qquad [8]$$

which checks with the requirement that P for this case must be smaller than unity. It is also noted that P tends toward 0 for increasing R.

With the limiting cases investigated and corresponding typical curves sketched in Fig. 3, it appears logical as a next step to proceed with the examination of the cases other than the above special ones, that is, to study the general case of a curve with an intercept anywhere between r_1 and r_2. Consider once again the equation

$$S_t = a + \frac{b}{r^2}$$

The important observation is made here that the quantity a, whether positive or negative, obviously is the asymptotic value of the stress S_t as r approaches infinity.

Writing down the condition for the S_t-curve to cross the r-axis at any point, the resulting intercept

$$r^2 = -\frac{b}{a} \qquad [9]$$

can only be real if a and b are of opposite signs. By definition

$$a = p_i \frac{1 - PR^2}{R^2 - 1}$$

and

$$b = p_i r_2^2 \frac{1 - P}{R^2 - 1}$$

These expressions are now inspected in the following.

Assume Pressure-Ratio $P > 1$ This gives negative values for both a and b and hence a positive ratio b/a. Consequently, by Equation [9], in this case an r-intercept is impossible. Since the asymptotic value a is negative, this also leads to the conclusion that all the S_t-curves for this case must start below the r-axis and approach $-a$ as r increases. More specifically, this means that all the circumferential stress-distribution curves for external pressure greater than internal pressure will lie below the r-axis and never cross it. Compressive stress prevails throughout and is larger at the inner radius.

Assume Pressure-Ratio $P < 1$ By inspection we now have b always positive, but a may be either positive or negative, depending upon the magnitude of the radius-ratio R. The two possibilities are as follows:

(*a*) R is of such magnitude that a is positive. Then, by Equation [9], there can be no intercept; the circumferential stress-distribution curve must start above the r-axis and converge to $+a$.

(*b*) R is of such magnitude that a is negative. Then, by Equation [9], there exists a mathematical intercept and the circumferential stress-distribution curve passes below or above the r-axis at the inner radius, as may be verified from Fig. 3, and approaches the asymptote $-a$ as r increases.

From an inspection of Fig. 3 it is now evident that for certain values of the radius-ratio R and the pressure-ratio P, the stress-ratio σ must have a numerical value less than unity; that is, the fact has been demonstrated that the circumferential stress at the outer radius of the cylinder may be the numerical maximum of hoop stress in the cylinder. It remains to establish the range of stress distributions for which the foregoing situation applies.

One of the limits of this range is known from case A examined earlier. This was the condition given by Equation [4], which stems from $\sigma = -1$, i.e., numerically equal tension and compression at r_1 and r_2, respectively. We are now looking for the other limiting relation between P and R (if any), which should yield the highest value of P for which the stress-ratio σ may be less than unity. By resorting once again to an inspection of Fig. 3, we observe that numerically larger hoop stress at the outer radius exists for all curves below the boundary one characterized by Equation [4] as long as P does not exceed unity. It will be remembered from $P > 1$ as just examined, that these pressure ratios give always numerically larger hoop stresses at the inner wall. A pressure-ratio of unity then obviously represents the sought-for upper limit, which is clearly independent of R.

Conclusions

It has been established, by utilizing the technique of inspecting a family of curves, that for certain values of the pressure ratio, for a given cylinder, the numerically largest circumferential stress in a thick-walled cylinder may occur at the outer radius and will be compressive, while the numerically smallest circumferential stress will be located at the inner radius and will be either tensile or compressive. This fact must be taken into account in solving thick-walled cylinder problems when both internal and external pressures are present.

A graphical representation of the limiting pressure-ratio P against the radius-ratio R is shown in Fig. 4. By use of this "regional" chart, the location and the sense of the maximum

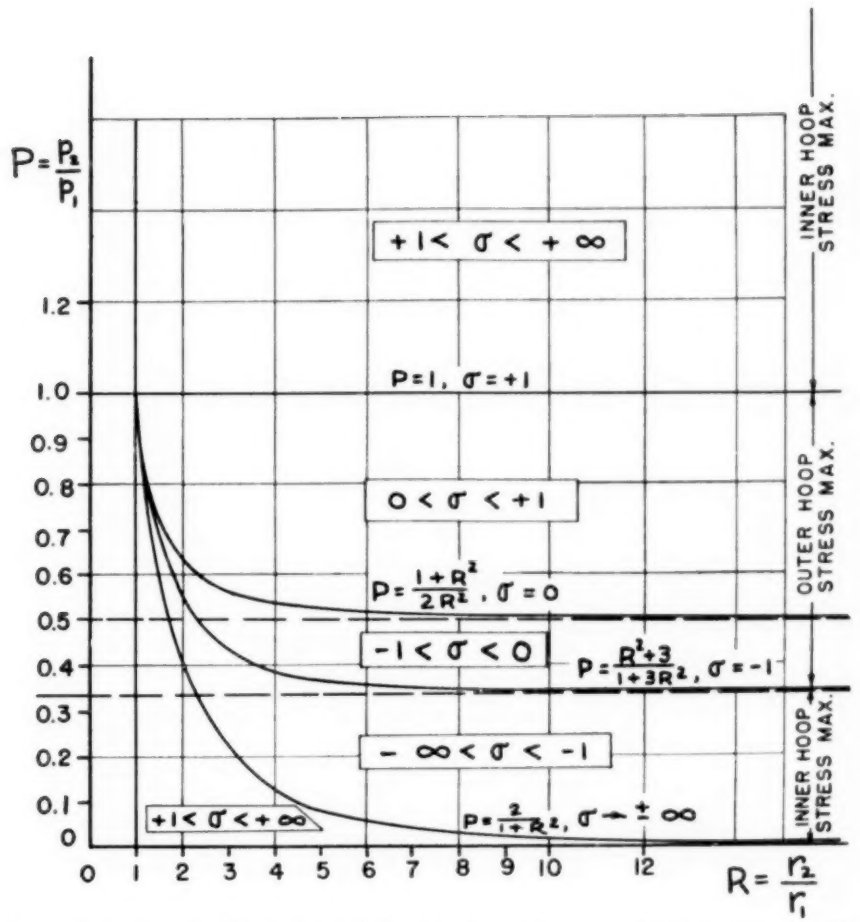

FIG. 4 PRESSURE RATIO P VERSUS RADIUS RATIO R, SHOWING REGIONS OF STRESS RATIO $\sigma = S_{t1}/S_{t2}$

circumferential stress may be noted by inspection for any given combination of dimensions and pressures.

EXAMPLES

The following numerical examples will serve to illustrate the application of the P-R chart, Fig. 4:

Given: Cylinder with $r_1 = 1$ unit and $r_2 = 3$ units. The radius ratio therefore is $R = 3$.

(*a*) Let $P = 0$ (external pressure zero). Locating the point (3, 0) in Fig. 4, shows that this case, being represented by a point on the R-axis, i.e., on the lower border of one of the regions in which $\sigma > 1$, gives, as is to be expected, a larger hoop stress at the inner radius, namely, tension.

(*b*) Let $P = 0.2$ and 0.4. Both the points (3, 0.2) and (3, 0.4) lie within the region bounded by $P = 0$ and $P = (R^2 + 3)/(1 + 3R^2)$ and, therefore, also represent cases of maximum hoop stress at the inner wall. However, their position below and above the curve $P = 2/(1 + R^2)$ indicates that the first point corresponds to tension throughout the cylinder, while the second point means tension at the inner and compression at the outer fibers. The dividing curve involves a discontinuity in the sense that the stress S_{t2} there passes from tension through zero to compression.

(*c*) Let $P = (R^2 + 3)/(1 + 3R^2)$, i.e., $\sigma = -1$. This locates the point (3, $^2/_7$) on the boundary curve and is the case of tension at the inner wall and equal compression at the outer fiber.

(*d*) Let $P = 0.5$. This condition (point 3, 0.5) lies in the region bounded by the curve $P = (R^2 + 3)/(1 + 3R^2)$ and the curve $P = (1 + R^2)/2R^2$ and is representative of the cases in which the compressive stress at the outer fiber numerically exceeds the tensile stress at the inner wall.

(*e*) Let $P = (1 + R^2)/2R^2$, i.e., $\sigma = 0$. This gives in our case the point (3, $^5/_9$) and is a case of zero stress at the outer fiber as discussed earlier in the paper.

(*f*) Let $P = 0.75$. This places the point (3, 0.75) and the value of σ in the region which indicates compression throughout the cylinder, the larger value being at the outer radius.

(*g*) Let $P = 1$. This means equal pressures throughout and causes $\sigma = 1$ for all R-values, which in turn contributes to the hydrostatic case mentioned earlier.

(*h*) Let $P > 1$. This situation is also independent of R and, as stated before, results in compressive stress throughout the wall, the larger value, however, being at the inner radius.

Reviewing these results, we summarize our investigation by stating that for any given thick-walled cylinder, changes of the pressure ratio from zero to values above unity entail a corresponding traversing of a distinct sequence of "zones" representing a variety of circumferential stress conditions, as shown in the P-R graph, Fig. 4. The customarily cited case of maximum tangential stress at the inner radius is contained therein as the two lower zones, as well as the uppermost zone. The intermediate zones comprise the generally overlooked opposite cases of numerical stress maximum at the outer radius. Finally, the commonly occurring condition of internal pressure alone is here a special case represented by the abscissa-axis of the P-R chart.

Stresses in Curved Beams—A Tabular Method of Solution Based on Winkler's Theory

By W. WRIGHT,[1] ABERDEEN, SCOTLAND

The method outlined in this paper is one which is applicable to all shapes of cross section. It is quicker than the orthodox methods and, in the case of irregular or complex sections, not only quicker but also more accurate.

WHEN the initial curvature of a beam is large compared with the depth of the beam, it is well known that the use of the straight-beam theory in such a case results in a very considerable underestimation of the maximum stress.

Apart from the mathematical theory of elasticity there are two theories available in practice which take account of the curvature and its effect on the stress distribution: They are Winkler's theory and the Andrews-Pearson theory. Although the Andrews-Pearson theory makes rather fewer simplifying assumptions, nevertheless, according to Professor Morley,[2] the stresses found by using Winkler's theory are more in accord with experimental values. Another advantage of the Winkler over the Andrews-Pearson formula is its relative simplicity. However, great care is needed in using the Winkler stress formula, since it contains a term $(A' - A)$ where A' is defined as the "modified area" of the section and A its area $(A' - A)$, being small compared with A or A'. Thus a small error in the evaluation of A or A' leads to a large error in the stress.

When A and A' can be found analytically, e.g., in the case of a rectangular or circular section, no difficulty arises since it is necessary to use only a sufficient number of significant figures in the numerical calculation to insure the required accuracy. However, when the section is irregular, or complex as it is, for example, with crane hooks, A and A' are found graphically with the possibility of a large error in the value of $(A' - A)$, and therefore in the stress.

The tabular method of solution outlined in this paper, though based on Winkler's theory, does not suffer from this liability. However, it will not be quite so accurate as the "correct" Winkler solution obtained analytically, since the integration is performed by summation; the error from this cause should not exceed 2 per cent, and for regular sections is very much less.

Tabular Method

Consider a small section of a curved beam of "gravity"[3] axis length ds and radius R_0 subtending an angle θ_0 at the center, Fig. 1. Apply a moment M and a direct compressive load W to the section of such a magnitude as to keep the gravity axis constant in length and let θ_0 change to θ. Then, according to Winkler's theory, the stress at distance y from the gravity axis (y being measured + ive outward from the center of curvature) is

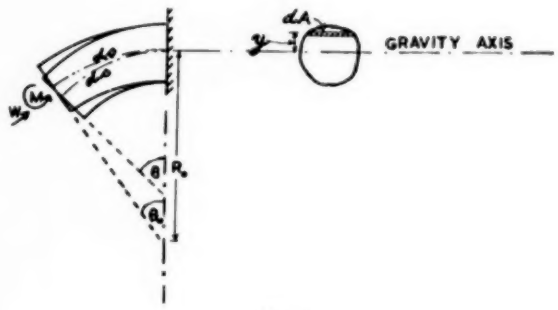

Fig. 1

$$\frac{E(\theta - \theta_0)y}{\theta_0(R_0 + y)} = k\frac{y}{R_0 + y}$$

where k is a constant.

$$\text{Resultant of normal stresses on section} = k\int \frac{y\,dA}{R_0 + y} = -W$$

$$\therefore \text{ Moment of resistance of section} = k\int \frac{y^2 dA}{R_0 + y}$$

This is the moment of resistance due to M alone, since the application of a uniform stress over the section does not change the moment of resistance

$$k\int \frac{y^2 dA}{R_0 + y} = k\int y\,dA - k\int R_0\frac{y\,dA}{R_0 + y} \text{ by division}$$

$$= 0 + WR_0$$

i.e., the moment of resistance due to M alone is WR_0. That is, $M = WR_0$.

Hence, if a curved beam is loaded as shown in Fig. 2, the distribution of stress at section xx is known, being

$$\frac{ky}{R_0 + y} = S_y$$

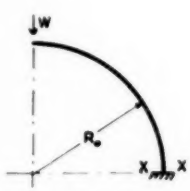

Fig. 2

and if the maximum stress is taken to be some convenient figure (say, 1000 psi) the stress diagram for the section can be drawn. The resultant load W can now be found by computing $\int S_y\,dA$ over the section; this can be done conveniently by dividing the section into laminar strips and summing by Simpson's rule, or some such method.

[1] Lecturer in Engineering, University of Aberdeen.

[2] "Materials and Structures," by E. H. Salmon, vol. 1, Longmans Green and Company, London, England, 1931, p. 178.

[3] The axis about which the first moment of area is zero.

Discussion of this paper should be addressed to the Secretary, ASME, 29 West 39th Street, New York, N. Y., and will be accepted until April 10, 1953, for publication at a later date. Discussion received after the closing date will be returned.

Note: Statements and opinions advanced in papers are to be understood as individual expressions of their authors and not those of the Society. Manuscript received by ASME Applied Mechanics Division, April 8, 1952.

Once W is known, the applied moment $M = WR_0$ can be written down immediately; i.e., the stress (1000 psi) due to both M and W is known. The stress due to M alone can then be computed by deducting the stress due to W, i.e., W/A. Thus the stress set up by the application of a bending moment M acting alone can be computed and therefore, the stress set up by any load system applied to the section in question, easily determined.

To illustrate the method, the case of a rectangular section has been worked out since this can be checked easily against the correct Winkler solution.

Example

A moment of 4 in-tons (ton = 2240 lb) is applied to a curved beam of radius $R_0 = 3$ in., Fig. 3. The section of the beam is rectangular, 1 in. wide and 2 in. deep radially. Find the stress distribution, using 8 strips.

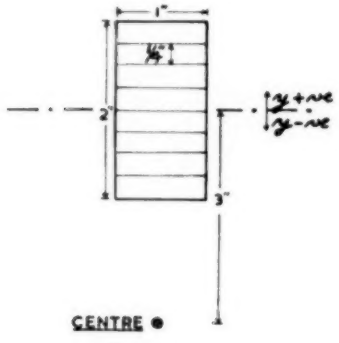

Fig. 3

TABLE 1

1 y, in.	2 $y/R_0 + y$	3 Stress S_y, psi lb/in² (col. 2 × 2000)[a]	4 Stress due to moment of 476.1 in-lb
1	0.25	500	579.3
¾	0.20	400	479.3
½	0.143	286	365.3
¼	0.077	154	233.3
0	0	0	79.3
−¼	−0.091	−182	−102.7
−½	−0.20	−400	−320.7
−¾	−0.333	−666	−586.7
−1	−0.50	−1000	−920.7

[a] The figure 2000 was chosen so as to give a maximum stress of 1000 psi.

$$\text{Load} = \int S_y\,dA = \tfrac{1}{4} \times \tfrac{1}{2}\,(-500 - 1176 - 228) =$$

$$-158.7 \text{ lb} = W$$

$$\text{Stress due to } W = -79.3 \text{ psi}$$

$\therefore$ Stress due to M alone can be written down, see column 4, Table 1

$$M = WR_0 = 3 \times 158.7 = 467.1 \text{ in-lb}$$

i.e., a bending moment of 476.1 in-lb sets up a maximum stress of −920.7 psi.

$\therefore$ A bending moment of 4 in-tons sets up a maximum compressive stress of

$$\frac{4}{476.1} \times 920.7 \times 2240 = -17{,}327 \text{ psi}$$

at the intrados and

$$\frac{4}{476.1} \times 2240 \times 579.3 = 10{,}900 \text{ psi}$$

at the extrados.

The stresses as calculated by the Winkler formula are −17,338 psi and 10,909 psi, respectively, showing a maximum error of 0.07 per cent. In the case of a circular section a similar calculation using 8 strips shows an error of less than 1 per cent.

One advantage of the tabular method over the use of the Winkler formula in the case of sections for which A' can be obtained analytically, as in the previous example, lies in the fact that the tabular solution can be obtained much more quickly though at the cost of a slight loss in accuracy. When the section is irregular, however, the tabular method is not only very much quicker but much more accurate. This is illustrated in the example which follows:

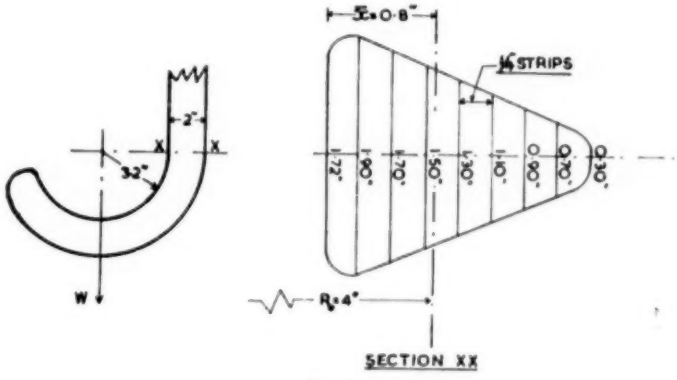

Fig. 4

The maximum permissible tensile stress at section X-X of the crane hook shown in Fig. 4, is 10,000 psi. Find the value of W. $R_0 = 3.2 + \bar{x}$. By taking moments about one end of the section, $\bar{x}$ is found to be 0.8 in. as shown.

$$\therefore R_0 = 4 \text{ in.}$$

TABLE 2

1 y	2 b	3 $\dfrac{y}{R_0 + y}$	4 Stress[a] S_y, psi = col. 3 × 10,000	5 $b \times S_y$, lb/in.
1.2	0.30	0.2308	2308	692.4
0.95	0.70	0.1919	1919	1343.3
0.70	0.90	0.1489	1489	1340.1
0.45	1.10	0.1011	1011	1112.1
0.20	1.30	0.0476	476	618.8
0.05	1.50	−0.0123	−123	−184.5
−0.30	1.70	−0.0818	−818	−1390.6
−0.55	1.90	−0.1504	−1504	−3028.6
−0.80	1.72	−0.2500	−2500	−4300

$\therefore$ Load causing maximum stress of −2500 psi

$$= \int S_y\,dA = \tfrac{1}{4} \times \tfrac{1}{2}\,(-3607.6 - 3030.8 + 1136.6)$$

$$= -458.5 \text{ lb}$$

This solution is for the general case where W is a compressive load acting through the center of the curvature. In this example W is a tensile load acting through the center of curvature and, therefore, the maximum tensile stress set up by a load of 458.5 lb will be +2500 psi, and 10,000 psi for a load of 1834 lb, i.e., the required value of W is 1834 lb.

Brief Notes[1]

On the recommendations of the Executive Committee of the ASME Applied Mechanics Division, it has been decided to initiate a section devoted to brief notes on technical matters in mechanics. These notes must not be longer than 750 words (about 2½ double-spaced typewritten pages, including figures) and will be subject to the usual review procedure prior to publication. After approval such notes will be published in the next issue of the Journal. The notes should be submitted to the Secretary of the ASME Applied Mechanics Division.

Movies of Stress Waves in Photoelastic Rubber

By H. C. PERKINS,[2] ITHACA, N. Y.

THE object of the following brief note is to report the successful recording on movie film of stress-wave patterns in gelatin and photoelastic rubber and to advocate the use of rubber for photoelastic studies of impact stress.

The first photoelastic studies of stress waves were described in 1946, by D. A. Senior and A. A. Wells,[3] who stated: "So far as is known, no previous record exists of fringe photographs of stress distribution when a stress wave is traveling through the body.' They showed, by a series of individual photographs, how stress-wave patterns are propagated through celluloid. Their waves traveling 5000 fps required exposures of microsecond duration, timed with great precision.

The motion-picture studies to be described really started in 1939, when W. N. Findley,[4] directed by Prof. T. R. Cuykendall of Cornell University, built a drum camera to photograph impact stress patterns in bakelite and celluloid. Their pictures showed only the relatively steady photoelastic patterns which persist after the initial period of stress-wave propagation, but they observed some interesting phenomena which would merit further study when and if more adequate equipment (in this case a Fastax movie camera) became available.

In 1951 Prof. C. Riparbelli[5] showed 16-mm Fastax movies of photoelastic wave patterns in hanging gelatin specimens struck upward at the bottom. He had trouble with creep and rupture of the suspended specimens. He also reported that when specimens are floated on a liquid, the wave patterns are distorted by the liquid.

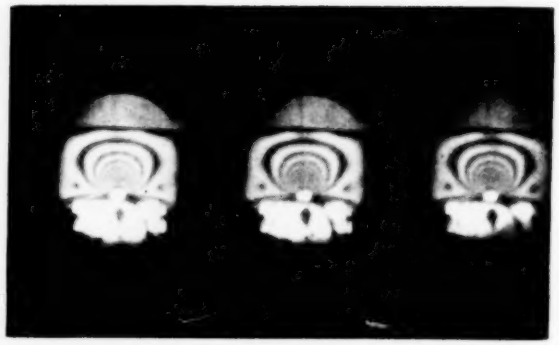

FIG. 1 GELATIN 1 IN. × 2 IN. × 4 IN. WITH 1-IN. EDGES VERTICAL, FREE TO SLIDE HORIZONTALLY

(Struck 2.7 fps, perpendicular to a 1-in. × 4-in. face at its center by a ½-in-diam cylinder on a 2-lb pendulum. Camera speed about 5000 frames per sec.)

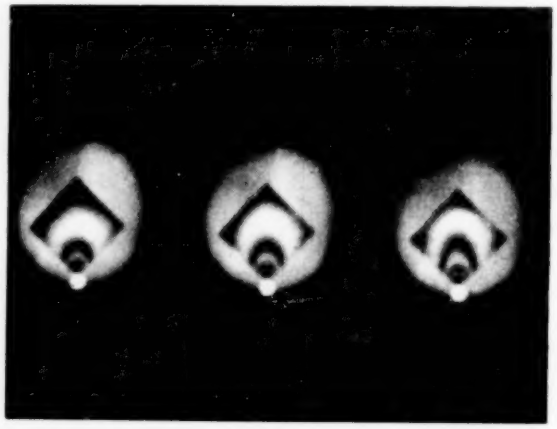

FIG. 2 RUBBER ¼ IN. × 2 IN. × 2 IN. WITH ¼-IN. EDGES VERTICAL, FREE TO SLIDE HORIZONTALLY

(Struck 5.7 fps along a diagonal of a 2-in. × 2-in. face by a ½-in-diam cylinder on 2-lb pendulum. Camera speed about 3500 frames per sec.)

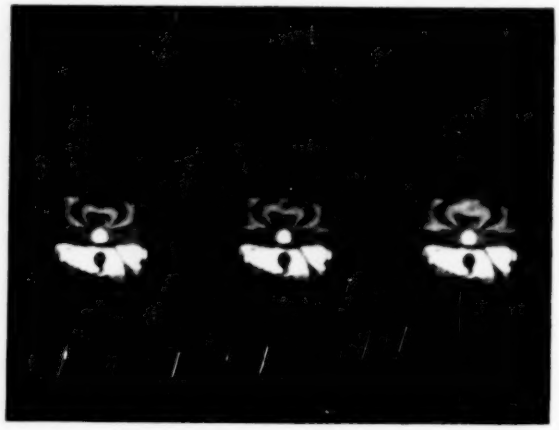

FIG. 3 RUBBER ¼ IN. × 1 IN. × 4 IN. WITH ¼-IN. EDGES VERTICAL, FREE TO SLIDE HORIZONTALLY

(Struck 5.7 fps perpendicular to a ¼-in. × 4-in. face at its center by a ½-in-diam cylinder on a 2-lb pendulum. Camera speed about 3300 frames per sec.)

[1] Discussion of papers in Brief Notes should be addressed to the Secretary, ASME, 29 West 39th Street, New York, N. Y., and will be accepted until one month after final publication of the paper itself in the JOURNAL OF APPLIED MECHANICS.

[2] Associate Professor of Mechanics, Cornell University. Mem. ASME.

[3] "A Photoelastic Study of Stress Waves," by D. A. Senior and A. A. Wells, *Philosophical Magazine*, vol. 7, 1946, pp. 463-469.

[4] "The Fundamentals of Photoelasticity Applied to Dynamic Stresses," by W. N. Findley, Ninth Semi-Annual Eastern Photoelasticity Conference, May 13, 1939, pp. 1-11. Published by the College of Engineering, Cornell University.

[5] "Photoelastic Analysis of Impact Stress Propagation in Two Dimensions," by C. Riparbelli, G. Boehler, and H. Hitch, Fluid Dynamics Division, American Physical Society at Cornell University, September 11, 1951 (unpublished).

NOTE: Statements and opinions advanced in papers are to be understood as individual expressions of their authors and not those of the Society. Manuscript received by ASME Applied Mechanics Division, June 16, 1952.

Fastax movie studies were continued by the Departments of Mechanics and Materials at Cornell University, under the sponsorship of the Applied Physics Laboratory of Johns Hopkins University. In these studies, 31 FP flash bulbs replaced the AH 6 mercury lamp used by Riparbelli, and the specimens were laid flat on a horizontal lucite plate. Gelatin specimens, well lubricated with Nestle wave-set lotion, vibrated freely when struck and showed no apparent frictional effects (see sample frames in Fig. 1). There were no initial fringes and no restrictive boundary conditions.

Best results were obtained with rubber specimens, friction being practically eliminated by polishing the lucite plate with Johnson's car plate. The photoelastic movie specimens were cut from $^1/_8$-in-thick sheet of rubber made by the Goodrich Rubber Company according to the formula recommended and used for static tests by W. E. Thibodeau.[6,7]

Preliminary calculations indicated that a Variac controlled 16-mm Fastax camera might be too slow since, at 5000 frames per sec (top speed) and shutter open one sixth of the time, the $^1/_{30,000}$-sec exposure time permits a 150-fps stress wave to move 0.06 in. Nevertheless, the sample frames in Figs. 2 and 3 show that successful movies of stress waves in rubber have been taken at speeds as low as 3300 frames per sec. It is fascinating to watch the stress-wave patterns develop on the screen, propagate through the specimen, and reflect at boundaries.

For quantitative analysis, the electric-flash technique yields larger, sharper pictures, and, timing being much less critical for rubber than for celluloid, there should be little difficulty in obtaining a set of isoclinics as well as the isochromatic fringe pattern at any desired time after the beginning of impact.

Movies, however, give the best over-all picture of the wave propagation, and rubber, although it has too high a Poisson's ratio to be truly representative of engineering materials, is otherwise an ideal material for photoelastic studies of stress waves.

Bending of Clamped Wedge Plates

By HERBERT REISMANN,[1] FORT WORTH, TEX.

THE objective of this note is to determine the deflection and moments in a uniformly loaded wedge plate of infinite extent, the straight, intersecting boundaries of which are clamped. We shall use the classical, small deflection theory of thin plates and the notation of Timoshenko.[2]

Choosing polar co-ordinates, we must find a function $w = w(r, \theta)$ which satisfies the partial differential equation

$$D\Delta\Delta w = q \qquad [1]$$

and the boundary conditions

$$\left.\begin{aligned} w(r, \pm\alpha) &= 0 \\ \left(\frac{1}{r}\frac{\partial w}{\partial \theta}\right)_{r,\ \pm\alpha} &= 0 \end{aligned}\right\} \qquad [2]$$

Assuming $w = r^4 W(\theta)$ as suggested by E. Reissner,[3] and substituting into Equation [1] results in the ordinary differential equation

$$\frac{d^4W}{d\theta^4} + 20\frac{d^2W}{d\theta^2} + 64\,W = \frac{q}{D} \qquad [3]$$

The solution of Equation [3] is

$$W(\theta) = C_1 \cos 2\theta + C_2 \cos 4\theta + C_3 \sin 2\theta + C_4 \sin 4\theta + \frac{q}{64D} \qquad [4]$$

Satisfaction of the boundary Conditions [2] and the requirements of symmetry, i.e., $w(r, \theta) = w(r, -\theta)$, results in

$$\left.\begin{aligned} C_1 &= -\frac{q\cos 2\alpha}{16\,D\,(2\cos^2 2\alpha + 1)} \\ C_2 &= \frac{q}{64\,D\,(2\cos^2 2\alpha + 1)} \\ C_3 &= C_4 = 0 \end{aligned}\right\} \qquad [5]$$

Thus the deflection may be written

$$\frac{64\,Dw}{qr^4} = 1 + \frac{\cos 4\theta - 4\cos 2\alpha \cos 2\theta}{2\cos^2 2\alpha + 1} \qquad [6]$$

The moments as computed from standard formulas[2] are

$$\left.\begin{aligned} \frac{16\,M_r}{3qr^2} &= \frac{4\cos 2\alpha \cos 2\theta - (1-\nu)\cos 4\theta}{2\cos^2 2\alpha + 1} - \frac{3+\nu}{3} \\ \frac{16\,M_t}{3qr^2} &= \frac{4\nu\cos 2\alpha \cos 2\theta + (1-\nu)\cos 4\theta}{2\cos^2 2\alpha + 1} - \frac{1+3\nu}{3} \\ \frac{8\,M_{rt}}{3(1-\nu)qr^2} &= \frac{(\cos 2\alpha - \cos 2\theta)\sin 2\theta}{2\cos^2 2\alpha + 1} \end{aligned}\right\} \qquad [7]$$

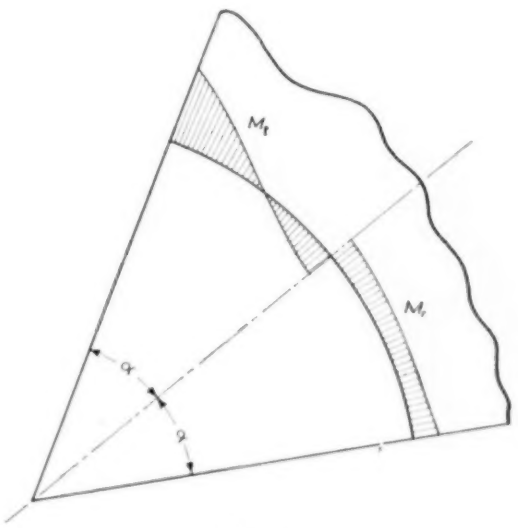

FIG. 1

Radial plots of M_r and M_t are shown in Fig. 1, assuming $\nu = {}^1/_3$ and $\alpha = 30$ deg.

[6] "The Photoelastic Properties of Soft Vulcanized Rubber," by W. E. Thibodeau and A. T. McPherson, *Journal of Research*, National Bureau of Standards, vol. 13, 1934, pp. 887–896.

[7] "Photoelastic Determination of Stress Around a Circular Inclusion in Rubber," by W. E. Thibodeau and L. A. Wood, *Journal of Research*, National Bureau of Standards, vol. 20, 1938, pp. 393–409.

[1] Project Structures Engineer, Consolidated Vultee Aircraft Corporation.

[2] "Theory of Plates and Shells," by S. Timoshenko, McGraw-Hill Book Company, Inc., New York, N. Y., 1940.

[3] "Comments on 'Uniformly Loaded Semiinfinite Wedge-Shaped Plates'" by Eric Reissner, *Journal of the Aeronautical Sciences*, vol. 19, April, 1952, pp. 287–288.

Discussion

Comments on the Free Oscillation of the Centrifugal Pendulum With Wide Angles[1]

R. E. Gorton.[2] The comment has been made that the angle of swing of the pendulum of a vibration absorber as applied to a crankshaft may be increased when the pendulum weight must be reduced to prevent spalling of the supporting pins and holes. The question of possible damage from excessive angle of swing of the pendulum has been raised. It is the writer's belief that in aircraft engines there has been much more difficulty with too little pendulum motion than with too great motion. There is always some sliding of the pins in their holes, rather than pure rolling. This causes wear, and with small pendulum motion this wear is localized to a small area. The tuning of the pendulum is easily affected by a worn area which changes locally the radius of curvature of the surface of the hole on which the pin is riding. It is known that wear hardly sufficient to be visible to the eye, and measurable only with special gages, may change the tuning of the damper sufficiently to reduce its effectiveness. Another factor involved may be that increased pendulum amplitudes aid in preserving an oil film between pins and holes.

Author's Closure

Mr. Gorton has kindly presented several practical reasons advocating the use of wider angles of motion in design. His support for my analysis is appreciated. The reduction in the weight of the pendulum, however, cannot go too far, for the maximum exciting torque amplitude that a pendulum can counteract depends (for a given harmonic order) upon $e^2 \sin \varphi_0$ which is proportional to the pendulum mass.

Torsion of a Circular Shaft With Diametrically Opposite Flat Sides[1]

W. O. Richmond.[2] This paper presents results obtained by the relaxation or the numerical integration method for the stresses and rigidity in torsion of a shaft cross section of common occurrence in machine design. It indicates, as have previous papers, the value of this method of solution for practical problems which cannot be solved by exact methods.

The writer would like to take this opportunity of presenting the results obtained by this method for a similar shaft cross section during the course of a master's degree thesis research[3] carried out by F. J. Shumas, at the University of British Columbia under his direction. The cross section treated was that of a segment of a circle with one flat side and one of constant curvature, as shown in Fig. 1 of this discussion. The values for the maximum shear stresses along the sides and the rigidity of the cross section are given in Table 1 of this discussion, using the notation of the authors.

TABLE 1 VALUES OF MAXIMUM SHEAR STRESS AND TORSIONAL STIFFNESS.

	Maximum shear stress		Torsional stiffness
w/r	Flat side	Curved side	
0	$0.865G\theta r$	$0.725G\theta r$	$0.298G\theta r^4$
0.2	0.765	0.640	0.158
0.3	0.640	0.545	0.099
0.4	0.540	0.505	0.059
0.5	0.480	0.460	0.035

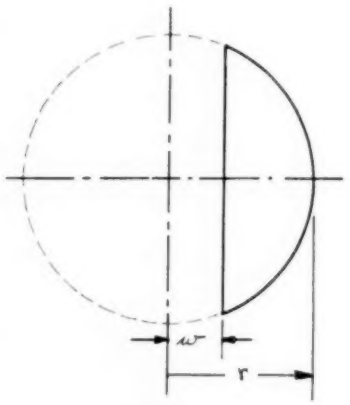

Fig. 1

The results for the semicircular cross section ($w/r = 0$) agreed within 2 per cent with those obtained by Saint Venant[4] for a section of a circle with sectorial angle equal to π.

These results were used in an investigation of the bending and shear stresses in a slotted shaft subjected to torsion.

Minimum Weight of Tapered Round Thin-Walled Columns[1]

Edward Adams Richardson.[2] This interesting and comprehensive paper proceeds to determine the shapes of tapered struts of various forms so as to secure the minimum weight where principal buckling by column action and local buckling by sheet crippling occur. This minimum weight makes no attempt to consider space limitations.

At an earlier time, when long struts were used in airplanes, exposed to the air stream and subject to considerable drag, the optimum condition required that the engine power to lift the strut and overcome drag should be made a minimum. Under such conditions, local crippling need not be a governing feature.

[1] By F. R. E. Crossley, published in the September, 1952, issue of the Journal of Applied Mechanics, Trans. ASME, vol. 74, pp. 315–319.

[2] Development Engineer, Pratt & Whitney Aircraft, East Hartford, Conn.

[1] By W. J. Carter and J. B. Oliphint, published in the September, 1952, issue of the Journal of Applied Mechanics, Trans. ASME, vol. 74, pp. 249–251.

[2] Head, Department of Mechanical Engineering, University of British Columbia, Vancouver, Canada. Mem. ASME.

[3] "The Effect of a Slot on the Stresses and Rigidity of a Shaft Subject to Torque" by F. J. Shumas, University of British Columbia, master's thesis, 1949.

[4] "Theory of Elasticity," by S. Timoshenko, McGraw-Hill Book Company, Inc., New York, N. Y., 1934.

[1] By Morris Feigen, published in the September, 1952, issue of the Journal of Applied Mechanics, Trans. ASME, vol. 74, pp. 375–380.

[2] Partner of Edward, (Nellie), and George Richardson; also Engineer in Publications Department, Bethlehem Steel Company, Bethlehem, Pa. Mem. ASME.

A preliminary treatment of this case was made in the year 1923.[3]

It was assumed that an acceptable straight strut had been designed. It was further assumed that wall buckling would not set a limit. It was recognized that the differential equation could be made integrable quite easily by letting

$$\frac{d^2y}{dx^2} = \frac{P(a - y)}{EI} = \text{const}$$

In other words, the deflection curve of the column would be a circular arc and the stiffness of the column cross section would be proportional to the deflection of the given column cross section as failure occurred by buckling. Nothing was said about local stress in compression, since for long columns the direct stress is low and ample area would be available at all sections excepting the very end of a strut tapered to zero moment of inertia. Small additions of material at the end, as suggested in the paper, were contemplated.

In a later paper,[4] the suggestion was made that the second derivative of the deflection y of the strut could be some function of the longitudinal distance x. Since columns could be solid, or made of material of uniform thickness, or made of sheet material of constant cross section longitudinally (as by expanding with fluid pressure into a mold), or cast with walls of thickness varying with x, a variety of shapes were obtainable. Where fluid drag and weight were to be the conditions for optimum shape, very important savings could be made, as shown in the earlier paper.[3]

Obviously, the buckling load could be calculated through integration of the differential equation

$$\frac{d^2y}{dx^2} = F(x)$$

and the fitting of the boundary conditions.

The purpose of this discussion is to point out that simple mathematical solutions of the column equation were obtained early and that reasonable forms of tapered column were obtained therefrom suited to a variety of modes of construction. It has seemed well to emphasize the fact that the optimum used in this paper, though of considerable interest, is merely one of the possible compromises that may be forced upon the engineer or designer, not "the" compromise.

Author's Closure

The author wishes to thank Mr. Richardson for his comments and interest in the problem. However, before replying specifically to any of the comments the author wishes to restate a few points which are implied in the original paper and because of their absence may be misleading.

For a given material, column load, column length, and cross-sectional shape there is only *one* column, whose dimensions are then determined, that will have the minimum weight and still support the load. Any dimensional deviation (in the cross section) will result in a heavier column provided the changed column can still support the load.

It is not at all implied that this minimum-weight column should be used in design but that it serves only as a basis for estimating the efficiency of other columns. In general, the minimum weight of a structure is also important in establishing rational methods of weight estimations, as shown by F. R. Shanley[5] in his recent book.

Mr. Richardson is quite correct that space limitation was not considered. Since weight only was being optimized, the spatial dimensions then become fixed. Any considerations of space limitations will result in a heavier column.

Any lack of consideration for local buckling in designing early airplane struts merely indicates that the strut used was heavier than the theoretical optimum. The author realizes that considerations other than minimum weight undoubtedly governed the design.

With respect to Mr. Richardson's last sentence, the author wishes to clarify a point. The minimum-weight column presented in the paper has an optimum shape for minimum weight and is not an all-inclusive "optimum" column. The author fully agrees that due to other design considerations the final column configuration may be different from that considered in the paper; however, it will also be heavier.

[3] "The Strength and Air Resistance of Tapered Struts," by E. A. Richardson, *Aerial Age*, vol. 16, April, 1923, p. 173.

[4] Letter to the Editor, "Analysis of Long-Tapered Struts," by E. A. Richardson, *Product Engineering*, vol. 14, October, 1943, p. 673.

[5] "Weight-Strength Analysis of Aircraft Structures," by F. R. Shanley, McGraw-Hill Book Company, Inc., N. Y., 1952.

A Mathematical Analysis of the Relaxation Type of Vehicle Suspension[1]

B. S. Cain.[2] This interesting paper compares a relaxation suspension with a more conventional damped suspension. The comparison is based on relative amplitudes of motion due to impulse and to harmonic excitation. In the case of the impulse, the conventional system provides no cushioning whatever, because the damping force approaches infinity and prevents any initial deflection of the spring. Therefore it is important to realize that real systems seldom can be represented by this case. Even a rigid wheel passing over rigid steps does not have an instantaneous vertical displacement. Owing to the fact that the wheel must be large enough to roll over the steps, there will be sudden changes in direction but no impulse displacements. In practice, the displacement itself is not usually the important criterion of a suspension. The velocity, acceleration, or rate of change of acceleration is usually of more value. This makes it still more important to realize that an assumption of impulsive motion on a conventional suspension will result in all these criteria becoming infinite.

The authors refer to the "standard type of suspension consisting of a spring connected in parallel with a dashpot." Real suspensions are seldom of this type; either the damping force has a maximum possible value, as in the case of friction devices, or fluid dampers with relief valves, or else a double suspension is used with two springs in series, one of which is damped and the other practically free. The latter arrangement has one advantage in common with the relaxation type inasmuch as a very rapid motion can take place without forcing the damper to follow this motion. This system is the one used in practically all automobiles, railroad passenger cars, and so on.

These comments do not affect the value of the authors' analysis but merely point out that conclusions based on impulsive response must be used with care when practical comparisons are being made.

The authors use Hurvitz' criterion to establish the stability of motion of the relaxation suspension, but it would appear that the stability is obvious from physical considerations since only positive damping is present.

If only the ratio of the motion of the mass to the harmonic displacement of the road surface is required, as is usually the case in practice, then the equations of motion can be quickly and directly solved for this ratio, avoiding much mathematics.

[1] By Joseph Gallagher and Enrico Volterra, published in the September, 1952, issue of the Journal of Applied Mechanics, Trans. ASME, vol. 74, pp. 389–396.

[2] Locomotive Division, General Electric Company, Erie, Pa. Fellow ASME.

K. KLOTTER.[3] The two systems compared are governed by the following differential equations:

A (standard type)

$$M\ddot{x}_2 + c\dot{x}_2 + k_1x_2 = c\dot{x}_1 + k_1x_1$$

B (new type)

$$cM\dddot{x}_2 + k_2M\ddot{x}_2 + c(k_1 + k_2)\dot{x}_2 + k_1k_2x_2 = c(k_1 + k_2)\dot{x}_1 + k_1k_2x_1$$

The authors investigate the transient responses after applying the discontinuity U' to the co-ordinate x_1 and therefore dU'/dt to $\dot{x}_1$. A discontinuity of this type is a very severe one. Mechanically speaking, it is a kind of "super-super-shock." [In a (regular or simple) shock U' is applied to $\dot{x}$ and dU'/dt to x. A "super-shock" would be one where U' is applied to $\ddot{x}$ and dU'/dt to $\dot{x}$.] Applying such a severe discontinuity to the co-ordinate x_1 makes the difference in the behavior of the two systems very conspicuous. One may doubt, however, whether such a super-super-shock is to be considered if one wants to depict what is happening to vehicles in reality; one may even doubt whether such a super-super-shock can be produced physically at all.

Even so, accepting the super-super-shock as applied to the co-ordinate x_1 (the wheels), the results may be compared on a basis different from the one used by the authors.

The authors compare in the two systems the maximum displacement x_2 produced by the super-super-shock. They find a reduction of approximately 30 per cent in the maximum displacement, as exhibited by comparison of Figs. 4 and 5, or of Figs. 7 and 8 of the paper. No mention is made in the paper, however, of another and—as it seems to the writer—more important difference in the behavior of the two systems, which also is exhibited by the diagrams. All curves in the diagrams pertaining to the new type B (Figs. 4, 6, 7), start out at $t = 0$ from $x_2 = 0$ with a finite slope. This means there is at $t = 0$ a jump in $\dot{x}_2$, or a simple shock. All curves pertaining to the standard type A, however, start out from values $x_2 > 0$. This means there is a jump in x_2, or a super-shock.

In other words, the super-super-shock considered, as applied to the co-ordinate x_1 (the wheels), results in a super-shock to the co-ordinate x_2 (the body of the vehicle) in the standard system, whereas only a simple shock appears in the co-ordinate x_2 of the new-type system.

In order to find this out, there is no need of an elaborate analysis at all. The differential equation itself exhibits this fact (and its generalizations, too) immediately and without any integration or calculation. The differential equations for the two systems have on the left-hand side highest derivatives of order 2 and 3, respectively; on the right-hand side there appear derivatives of both zero and first order in each case. Any discontinuity on the right-hand side results in a discontinuity of the same order in the highest derivative on the left-hand side. The discontinuity in the derivative of highest order on the right-hand side weighs most. Now, apply—as the authors do—a discontinuity U in $\int x_1dt$, equivalent to U' in x_1 and dU'/dt in $\dot{x}_1$ (super-super-shock). It produces a discontinuity of type dU'/dt in $\ddot{x}_2$ for system A (standard type), in $\dddot{x}_2$ for system B (new type); equivalently a jump in $\dot{x}_2$ for A, i.e., a super-shock, and a jump in $\ddot{x}_2$ for B, i.e., a simple shock.

These results may be generalized. Calling D the order of a discontinuity of, say, type U, the order of type U' would be $D + 1$, and so on. Then we may say: If the discontinuity as applied to x_1 is of order D (and, therefore, to $\dot{x}_1$ of order $D + 1$) a discontinuity of order $D + 1$ applies to $\ddot{x}_2$ in system B, to $\dot{x}_2$ in system A. Hence the discontinuity in x_2 is of order $D - 2$ in system B, of order $D - 1$ system A.

The question of dimensions in the equations is dealt with lucidly in Professor Thomson's comment. One may add that, apart from the dimension of an equation as a whole, Equation [39] is inconsistent as to dimensions in itself.

It seems debatable whether the cases of a double root in the differential equation of second order (A) and a triple root in the differential equation of third order (B) are fully equivalent and the proper thing to compare. What is wanted is the limiting case between oscillatory and creeping motion. Therefore it should be sufficient to consider a double root besides a negative real one. Demanding that all three roots should coincide imposes an additional (convenient, but unwarranted) condition on the system.

Finally, the analysis pertaining to the steady-state response seems to be strangely bulky, unusual and, therefore, unconvincing. And quite unnecessarily so, because all that is done between Equations [44] and [54] could be done in two or three lines by a perfectly routine procedure starting out from the differential equation of third order. But as the authors' results ultimately do agree with the ones derived by the usual procedure one may leave it at that—but perhaps leaving some reader somewhat puzzled.

H. O. FUCHS.[4] This paper is most welcome because it draws attention to a system of mass, spring, and dashpot which is widely used in practice, has some very useful properties, lends itself to a reasonably simple analysis, but has been almost completely neglected in the literature. The writer wishes to add to the authors' analysis some interesting, fairly simple results taken from a study of the steady-state response of this and similar systems made some 10 years ago at General Motors. We considered a somewhat more general system of which that shown by the authors' Fig. 1, is a special case and we called it a system with indirect damping.

The steady-state response can be expressed in the following dimensionless formulas

For indirect damping

$$A = \sqrt{\frac{1 + DQ}{(1 - Q)^2 + DQ\,(R - Q)^2}} \qquad \ldots\ldots [1]$$

$$F = \sqrt{\frac{1 + R^2DQ}{1 + DQ}} \qquad \ldots\ldots [2]$$

For ordinary (direct damping)

$$A = \sqrt{\frac{1}{(1 - Q)^2 + CQ}} \qquad \ldots\ldots [1a]$$

$$F = \sqrt{1 + CQ} \qquad \ldots\ldots [2a]$$

For undamped systems

$$A = \frac{1}{1 - Q} \qquad \ldots\ldots [1b]$$

$$F = 1 \qquad \ldots\ldots [2b]$$

where

A = Ratio of amplitude produced by harmonic force on mass to static amplitude produced by same force

[3] Professor of Engineering Mechanics, Stanford University, Stanford, Calif.

[4] Chief Research Engineer, Preco, Incorporated, Los Angeles, Calif. Mem. ASME.

C = square of twice relative damping, calculated from mass and static spring stiffness ($C = c^2$ km in the usual notation)

D = (a damping factor) = CS

F = ratio of maximum force on support produced by harmonic motion of mass to force produced by very slow motion of same amplitude.

Q = square of ratio of forced frequency to natural frequency calculated from mass and static stiffness

R = ratio of stiffness with "frozen" dashpot to static spring stiffness ($R = \infty$ for ordinary damping)

S = square of ratio of static spring stiffness to stiffness of one dashpot terminal relative to other when mass is held fixed ($S = 0$ for ordinary damping)

The formulas define two transmissibilities. The other two interesting transmissibilities, namely, ratio of "amplitude of mass produced by harmonic motion of support" to "amplitude of support" and the ratio of "maximum force on support produced by harmonic force on mass" to "maximum exciting force" are both equal to the product AF. (The curves in Fig. 1 of this discussion show the product QAF plotted over $\sqrt{Q}$.)

An analysis of the transmissibility formulas shows some interesting features, chief among which are the following:

1 With indirect damping the transmissibility F cannot exceed the ratio R. With ordinary damping, F increases indefinitely.

2 With indirect damping the transmissibility curve depends on the damping factor D which is the product of a viscous damping ratio C and a stiffness ratio S; in other words, identical effects can be obtained by various combinations of dashpots and springs.

3 The response curve depends much more on the stiffness ratio R than on the damping factor D.

4 The amplitude-response curves for any factor R all pass through a common point $A = 2/(R-1)$ at $Q = (R+1)/2$.

5 The common point defined under (4) is the peak of the curve when $D = 2/(R+1)$. The peak is not much higher for values of D reasonably near this "optimum" value.

Strictly speaking, all damping used in practice is "indirect" because there are no perfectly rigid connections. Applications in which this effect is particularly important include automobile suspensions. However, the flexible connection of the dashpot to the exciting irregularity is provided by the pneumatic tire and not by a special relaxation spring. In so far as the transmission of shock from the road to the car is concerned, the mass of the wheels is practically negligible so that the connection between the car and the road may be considered "indirectly damped."

Probably the most important application of indirect damping is as an approximation in the analysis of some systems with distributed damping. An engine mounted on rubber is one such system. Attempts to represent the rubber mount as a spring plus a dashpot connected to engine and ground (or frame) lead to the difficulty that the equivalent damping of the rubber is not constant but decreases with increasing frequency. This difficulty can be overcome easily by representing the rubber mount by a spring and indirect damping,[5] as suggested in Fig. 1 of this discussion. The curves in Fig. 1 graphically show one of the main advantages of indirect damping in isolating variable-speed engines.

The problem on such mountings is to cut down the amplitude at resonance without destroying the isolation effect at frequencies above resonance. The figure is drawn on logarithmic scales and the disturbing force is proportional to the square of the engine speed, to correspond with a force produced by unbalance. The reaction on the support is plotted over the frequency ratio (FAQ over $\sqrt{Q}$). It shows how ordinary damping would produce a very harsh mounting at speeds considerably above resonance, and how indirect damping avoids this undesirable effect.

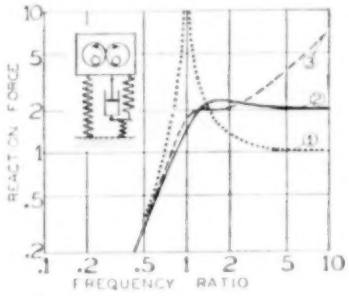

(1) Without damping
(2) With indirect damping ($R = 2$, $D = 2/3$)
(3) With ordinary damping (1/4 critical)

FIG. 1 DAMPING OF ENGINE MOUNTS

(Amplitude of reaction force transmitted to vehicle by unbalance of engine is plotted over ratio of engine speed to resonant speed.)

In the analysis of impulsive response of suspensions, it is essential to keep in mind that the damping used on vehicles is not linear. The characteristics of various dampers used in practice and an analysis of the resulting transient response (obtained by differential analyzer) have been given previously.[6]

AUTHORS' CLOSURE

The authors wish to thank Mr. B. S. Cain, Dr. K. Klotter, and Mr. H. O. Fuchs for their interesting and most welcome comments to their paper. They also greatly appreciated Dr. W. Thomson's contribution at the presentation of the paper and regret that his remarks have not been included in the printed discussion.

Both Mr. Cain and Dr. Klotter criticize the method of analysis used consisting of the application of an impulse to the system. To this remark the authors reply that, given the impulsive response $h(t)$ of a linear system, the response to any arbitrary input $f(t)$ may be found from the use of the convolution integral

$$x_2(t) = \int_0^t f(t-\tau)h(\tau)d\tau$$

i.e., the response to any input depends explicitly on the impulsive response, and this seems a reasonable basis of comparison of the two systems.

The type of suspension consisting of a spring connected in parallel with a dashpot is referred to in the paper as "the standard type" of suspension. Although the authors agree with Mr. Cain that real suspensions of vehicles are seldom of this type, this term seems to be used generally in current technical literature in referring to this type of vehicle suspension, and for this reason also was used in the paper.

Concerning Dr. Klotter's query as to whether the cases of a double root for the standard system and a triple root for the relaxation system are fully equivalent and the proper thing to compare, the authors' answer is that as both cases require the smallest values of the parameters (ζ for the standard type and h and ξ for the relaxation type) for aperiodic motion this seems

[5] "Effectiveness of Shear Stressed Rubber Compounds in Isolating Machinery Vibration," by B. C. Madden, Trans. ASME, vol. 65, 1943, pp. 617–624 (discussion).

[6] "Modern Passenger-Car Ride Characteristics," by R. Schilling and H. O. Fuchs, JOURNAL OF APPLIED MECHANICS, Trans. ASME, vol. 63, 1941, pp. A-59–A-66.

to be a reasonable criterion of comparison. However, this last point raised by Dr. Klotter could be answered more fully by presenting the results for the relaxation system on root-locus diagrams. Therefore the authors are now preparing a brief note in which such root-locus diagrams for the relaxation system will be given.

The authors are grateful to Mr. Fuchs for his interesting discussion at the presentation of the paper and for having pointed out several important applications of relaxation systems.

The authors agree with Dr. Thomson that the results could have been given in a more general form by presenting the transient response in a nondimensional form such as

$$\frac{x_2(t)}{H\omega_{11}} \text{ versus } \omega_{11}t$$

Dr. Thomson also suggested that the system be subjected to an impulse of the form

$$x_1(t) = HU'(t)$$

where H has inch-second as a unit. On this question the authors want to point out that, although not explicitly stated in the paper, H was, in fact, assumed to be equal to unity. This unfortunate omission raised the question on dimensions by Dr. Klotter. The authors reply on this point probably also will answer Dr. Klotter's question about the dimensional consistency of Equation [39] of the paper.

It finally should be noted that although a printing error occurred in the expression for the angle φ in Equation [77] (in the numerator instead of $-2\zeta\xi$ one should read $-2\zeta\eta$) the values given in Fig. 8 of the paper, which are deduced from Equation [77], are correct.

Correlation of Creep Properties by a Diffusion Analogy[1]

R. P. Carreker, Jr.[2] Basically, the author has accepted the empirical equation for the creep curve $\epsilon = Ct^{T/T_m}$ and has defined the quantity C in terms of constants common in rate theory and a parameter, which he terms the "activation energy" Q, that is subject to the same variables as C itself. This parameter then relates the quantities strain and time, or alternatively strain and strain rate, and is a function of stress and temperature. A more conventional approach regards the activation energy as a parameter relating strain rate and temperature which is a function of stress and strain. In either case, one starts with the four variables stress, strain, strain rate or time, and temperature and by calling upon the activation-energy concept reduces the number of variables to three. The salient point is that the author's use of activation energy is quite different from the usual connotation of that term. This difference is apparent in comparing the numerical values of activation energy for the creep of platinum as determined by the author, Fig. 10 of the paper, with the values of activation energy obtained by the writer from the same data by considering the temperature dependence of the strain rate at constant strain and stress (8).[3] Over the range of stress from 1000 to 10,000 psi the author obtains values approximating 160 to 60 K cal/mole while the writer's analysis produces 75 to 25 K cal/mole. The two approaches lead to greatly different answers.

A second point of difference appears in the stress dependence of the activation energy. The author obtained the quantity Q_0 by assuming a linear decrease of his Q with increasing stress. The alternative analysis results in a decidedly nonlinear stress dependence, the activation energy being approximately linear in the logarithm of the stress.

The utility of the author's unconventional approach depends upon the apparent correlation of the temperature dependence of Q_0 with the temperature dependence of the activation energy for self-diffusion, contained in his Fig. 12. In this case the burden of the correlation rests upon the silver self-diffusion data reported by Turnbull and associates. Considering the data represented by crosses in Fig. 12, the writer has attempted to locate the source of each data point. If his conclusions are correct, his confidence in the correlation is considerably shaken. Will the author please check the writer's interpretation of his data sources, which are given in Table 1 of this discussion?

Point 1 represents the volume self-diffusion of silver as measured on both single crystals and polycrystals at high temperatures. This quantity, as measured on single crystals, remains constant at all temperatures down to 500 C (reference 34.)[3] Points 2 and 3 represent the apparent activation energy for self-diffusion in polycrystalline samples measured at temperatures below 700 C, where the short-circuiting effects of grain-boundary diffusion become appreciable. The two points are merely two values reported at different stages of a lengthy experimental program. Points 4 and 5 are values obtained from the same experimental data analyzed so as to separate the effects of grain boundary and volume diffusion, and again represent values reported at two different stages of the experimental program. Point 6 is taken from the Nickerson and Parker measurements of surface diffusion on polycrystalline samples. Others have measured similar numbers at times, but it is unfortunately true that the surface-diffusion process depends very markedly on the nature of the surface so that the significance of these measurements is subject to question.

In brief, the activation energy for self-diffusion in silver is characterized not by a linear dependence on temperature but by two quantities which are independent of temperature, 46 Kcal/mole for volume diffusion and approximately 20 K cal/mole for

[1] By Leon Green, Jr., published in the September, 1952, issue of the Journal of Applied Mechanics, Trans. ASME, vol. 74, pp. 320–326.

[2] Research Associate, General Electric Research Laboratory, Schenectady, N. Y.

[3] Author's Bibliography.

TABLE 1 SOURCES OF DATA

	T_{avg}/T_m	T_{max} deg C	T_{min} deg C	Q, K cal/mole	Source[a]	Remarks
1	0.9	950	800	46.0	Ref (35), Turnbull Ref (34), Hoffman and Turnbull	Volume diffusion, single and polycrystals
2	0.7	700	500	26.4	Ref (34), Hoffman and Turnbull	Grain boundary, apparent D
3	0.65	600	500	26.1	Ref (35), Turnbull	Grain boundary, apparent D
4	0.56	475	370	23.8	Ref (33), Hollomon and Turnbull	Grain boundary, Fisher analysis, preliminary results, line by eye
5	0.57	475	350	20.2	Ref (34), Hoffman and Turnbull	Grain boundary, Fisher analysis, final results, line by least squares
6	0.45	350	225	10.3	Ref (31), Nickerson and Parker	Surface of polycrystalline sample

[a] Numbers in parentheses refer to the author's bibliography.

grain-boundary diffusion, together with a third poorly defined surface-diffusion effect. In the light of such interpretation, the observed correlation of the temperature dependence of self-diffusion activation energies with the temperature dependence of creep-activation energies seems more fortuitous than fundamental.

It may be worth mentioning that the results of some unpublished work on the creep of silver show that α of the equation $\epsilon = Ct^{\alpha}$, is not always equal to T/Tm but in some cases is much less.

The writer would be truly interested in the author's remarks concerning these points, and i. grateful to him for the stimulation his analysis has provided.

Author's Closure

Mr. Carreker's valuable comments raise several points which deserve amplification. The first concerns the definition of activation energy. In his study of the creep of platinum wires, Carreker employs the conventional definition in terms of instantaneous strain rate

$$\frac{d\epsilon}{dt} = k\epsilon^{-\frac{Q}{RT}}$$

This approach was deliberately avoided by the author, since in a constant-stress experiment the strain rate $d\epsilon/dt$ decreases continuously with time, thus requiring the activation energy Q to increase accordingly. Reference to the platinum-wire experiments (see Fig. 22 of the author's reference 8) shows that at a stress of 1000 psi, for instance, Q (as defined by the foregoing conventional expression) increased from about 60 Kcal/mole at $\epsilon = 0.005$ to about 74 Kcal/mole at $\epsilon = 0.030$. The existence of such a strain (or time) dependence of the activation energy would appear physically questionable. Rather than postulate such a dubious dependence (which, moreover, complicates the empirical representation to a degree precluding easy engineering application of creep data) the author chose to express the creep strain as $\epsilon = (t/\tau)^{\alpha}$, where, by invoking an analogy with the case of self-diffusion, the time parameter τ was expressed as a function of an activation energy. It has been pointed out in the foregoing discussion that the two alternative definitions of the activation energy for creep yield numerical values of different magnitudes. It also was noted that the conventional definition yielded values of Q which vary with stress in a decidedly nonlinear fashion, whereas the author's definition yields values which appear to show a linear stress dependence. This linear dependence was not assumed a priori; it was selected on the basis of the data for copper and tin presented in the author's Figs. 9 and 11, the only data which permitted a reliable fit. The author originally noted the need for further experimental work upon the stress-dependence problem, and wishes to emphasize this point again. While awaiting additional data, the author believes that his proposed definition of Q is recommended by the feature that (in contrast to the activation energy defined by the conventional expression given in the foregoing) it is independent of strain and appears to vary linearly with stress.

Mr. Carreker's principal reservation concerns the temperature dependence of the apparent activation energy for creep, as defined by the author. The utility of the proposed approach, however, does not depend (as he states) upon the agreement between the temperature dependence of Q_0 and that of the apparent activation energy for self-diffusion. The practical value of the method lies in the fact that the apparent activation energies for creep of several dissimilar metals have been unified in the author's Fig. 12 by presentation in the group $Q_c/(RT_m)$ as a function of reduced temperature. The self-diffusion data are presented only for purpose of a comparison which indicates that the "*apparent*" activation energies for self-diffusion, presented in the group $Q/(RT_m)$, show a qualitatively similar temperature dependence.

The author regrets that the significance of the word apparent (which he was careful to insert in his Fig. 12) was not given more emphasis. In his concise enumeration of the mechanisms of self-diffusion in silver and in his detailed tabulation of the diffusion data for silver presented in the author's Fig. 12, Mr. Carreker correctly points out that the activation energies for volume, grain boundary, and possibly surface diffusion are not functions of temperature. The author certainly did not intend to imply otherwise. Nevertheless, the relative degree in which these different mechanisms contribute to the total amount of diffusion (or creep) observed in a polycrystalline metal is necessarily a function of temperature as well as grain size. The author's Fig. 12 merely suggests that this temperature dependence of the apparent observed activation energy may be represented by a linear approximation. The author noted that this approximation was less satisfactory in the case of the diffusion data than for the creep data; certainly he is not laboring under the delusion that either approximation is "fundamental." Since all creep correlations (if not all knowledge) are necessarily empirical in nature, the author is inclined to feel that Mr. Carreker's confidence in the one presently proposed has been shaken without due cause.

The fact that the exponent α in the expression $\epsilon = Ct^{\alpha}$ is not necessarily equal to T/T_m is indeed worth mentioning. The author noted that the approximation was not generally valid, and suggested that deviations might possibly be attributable to the presence of impurities and (in the case of small wire specimens) to nonrandom grain orientations. Metals which strongly absorb gases at high temperature, for instance, would not be expected to obey this rough rule. Engineeringwise, the important point is that the large deviations from this approximation are downward, i.e., $\alpha \leq T/T_m$. For this reason the approximation is conservative; the creep strain predicted by the author's Equation [11] will be larger than that actually observed.

In conclusion, the author would again like to emphasize the fact that his proposed correlation of creep data in dimensionless groups is frankly empirical and is advanced primarily as a possible method of predicting strain-time relationships for engineering purposes. On the basis of the unified presentations of creep data in Figs. 12 and 13, together with the approximate Equation [11], a rough estimate of the creep behavior of a pure metal may be ventured from knowledge of its melting point, atomic volume, and the prevailing conditions of stress and temperature. Despite the crudeness of his tentative stress-dependence correlation (Fig. 13), the author has found the "horseback estimates" made on this basis to be of value for purposes of preliminary design.

Temperature Development in a Heated Contact With Application to Sliding Contacts[1]

G. M. Dusinberre.[2] An engineering paper should be of use to other engineers, and the author recognizes this by presenting a worked-out example. This is a typical engineering problem in that it offers to start with data, presumably easily obtainable, and, by calculation, to predict the outcome of an experiment which would be inconvenient to perform.

[1] By R. Holm, published in the September, 1952, issue of the Journal of Applied Mechanics, Trans. ASME, vol. 74, pp. 369–374.

[2] Department of Mechanical Engineering, The Pennsylvania State College, State College, Pa. Mem. ASME.

As a minor point, the curves as printed can be read to perhaps 2 per cent of the range, or two significant figures at most. Perhaps the original curves were drawn to a larger scale, for the final solution of the problem is expressed to three significant figures.

A more serious point concerns the data, presumably easily obtainable. The whole solution hinges on two factors, μ and ξ, each expressed to one significant figure, or 10 per cent at the best. Perhaps this is not the author's intention. Probably he knows those factors within 2 per cent or he would not have bothered to calculate even 2 per cent curves to make use of them.

But let us put ourselves in the place of an engineer who wants to use the author's work. Not being experts on friction, we look in a handbook for some values of μ. In many cases they are expressed to two significant figures, it is true, but it is easy to find a spread of 10 per cent or more in reported values. Perhaps we feel that we had better try an experiment, which at least will be simpler than the one we are trying to predict.

With ξ, the case is even worse. This factor is the proportion of the heat generated at the contact surface, which flows into the semi-infinite plate. The part flowing into the slider would be $1 - \xi$.

It would seem to the writer that this is a factor not even as simple as μ. It would seem that this fraction must depend not only on the materials, the force between them, the velocity, and other known quantities but upon the design of the slides in respect to conduction, convection, and radiation. Also, for the transient cases which the author does not treat, the heat capacities of the sliding parts must be specified.

If the writer is correct in this contention, then any practical study of these phenomena must take account of the whole system, stationary and moving. For this purpose, step numerical methods or analog methods would seem to be in order. With these, actual systems can be represented closely and we are not limited to semi-infinite surfaces. Of the two methods suggested, the former would be less expensive.

If the writer is wrong in this contention, then the author is urged to publish a simple, easy, and reliable method for estimating ξ with a precision consistent with that of his curves.

Author's Closure

The author welcomes the opportunity to answer the question of Mr. G. M. Dusinberre, which may be shared by many other readers.

The readings for Table 1 were made on the author's own large-scale diagram. Readings on the small-scale printed diagrams would not have shown any positive differences between the values to be compared.

Concerning the friction coefficient mentioned in the example: A dependable friction coefficient should be based on an experiment. The values given in handbooks are averages and often based on quite obsolete measurements.

Concerning the factor ξ in the example: There are cases in which a sufficient determination of ξ is easy. For instance, when a poorly cooled slider runs on a large (stationary) contact member the fraction of the heat which is transferred to the slider is small and a rough computation of it will be sufficient, giving ξ between 0.8 and 1. No simple rules can be given for the calculation of ξ is more complicated cases.

Most often the large contact member will be well represented by a semi-infinite body.

In practice even the order of magnitude of z for a given $B(z)$ may be of interest. Figs. 1 and 2 of the paper are well suited for the accuracy that can be based on practically defined conditions.

Measurement of Recovery Factors and Friction Coefficients for Supersonic Flow of Air in a Tube

Part I—Apparatus Data and Results Based on a Simple One-Dimensional Flow Model[1]

W. B. Brown.[2] The wealth of data contained in this paper should be a boon to investigators in the field. The care used to eliminate errors and to obtain accurate data is to be commended.

The difference in the f-values between the two flow models used shows the importance of having one that is correct and should stimulate the theoretical workers in this field. In the two-dimensional model presented, the values found for f depend appreciably on the assumed ratio of V_b to V_c. In the numerical example given, a change in this ratio from 0.5 to 0.6 changes the resulting value of f about 20 per cent.

A momentum thickness that takes into account simultaneously the effects of curvature of the wall, high Mach number, variable fluid properties, and pressure gradient would be suitable. Since the separate effects have been analyzed in three recent papers, curvature by Seban and Bond,[3] high Mach number, and variable properties by Klunker and McLean,[4] pressure gradient and variable fluid properties by Brown and Donoughe,[5] perhaps the combined effects can be calculated before long. The tables of carefully measured and tabulated data offer an attractive inducement to try. Remember Kepler!

Carl Gazley, Jr.[6] It is gratifying to note that the authors' results, when evaluated with the "two-dimensional flow model"[7] agree approximately with recent data obtained on flat plates. However, the precision of the authors' data appears to be considerably less than that obtained in boundary layers on flat plates and bodies of revolution. It is not sufficiently precise, for example, to enable evaluation of the effect of Mach number on skin friction. This lack of precision is probably due to (*a*) the extensive and approximate methods necessary to evaluate the skin-friction coefficient and recovery factor from the measured data, (*b*) the sensitivity of the compressible boundary layer to its "history" (i.e., upstream conditions) as well as to local conditions, and (*c*) the complicating effects of wall curvature which probably necessitate a "three-dimensional flow model" for accurate evaluation of the data. In connection with point (*b*), it may be

[1] By J. Kaye, J. H. Keenan, K. K. Klingenstuith, G. M. Ketchum, and T. Y. Toong, published in the March, 1952, issue of the Journal of Applied Mechanics, Trans. ASME, vol. 74, pp. 77–86.

[2] Aeronautical Research Scientist, National Advisory Committee for Aeronautics, Lewis Flight Propulsion Laboratory, Cleveland Airport, Cleveland, Ohio.

[3] "Skin-Friction and Heat Transfer Characteristics of a Laminar Boundary Layer in a Cylinder in Axial Incompressible Flow," by R. A. Seban and R. Bond, *Journal of the Aeronautical Sciences*, vol. 18, October, 1951, p. 671.

[4] "Laminar Friction and Heat Transfer at Mach Numbers From 1 to 10," by E. B. Klunker and F. E. McLean, NACA Technical Note 2499, October, 1951.

[5] "Tables of Exact Laminar Boundary Layer Solutions When the Wall Is Porous and Fluid Properties Are Variable," by W. B. Brown and P. S. Donoughe, NACA Technical Note 2479, September, 1951.

[6] General Engineering Laboratory, General Electric Company, Schenectady, N. Y. Present address, Rand Corporation, Santa Monica, Calif.

[7] "Part 2—Results Based on a Two-Dimensional Flow Model for Entrance Region," by J. Kaye, T. Y. Toong, and R. H. Shoulberg, published in the June, 1952, issue of the Journal of Applied Mechanics, Trans. ASME, vol. 74, pp. 185–194.

noted that a laminar compressible boundary layer on flat plate (zero pressure gradient) is affected appreciably by small changes in leading-edge radius or waviness.[8] Furthermore, a laminar compressible boundary layer in a pressure gradient is affected not only by the local pressure gradient at a given point but also by the pressure gradients existing everywhere upstream of that point.[9]

This brings us to the question as to why the authors chose to study supersonic boundary layers in a tube rather than on a flat plate or body of revolution. The writer can think of no practical application of supersonic flow in a tube of constant cross section. If the purpose of the study was academic or basic research, it would appear that it might better have started with a simpler flow configuration with subsequent introduction of such complexities as pressure gradient and wall curvature.

RICHARD SCHERRER.[10] The authors have conducted an exceedingly careful and accurate experimental investigation and have proved conclusively that the results obtained are practically unaffected by the design of the test equipment or instrumentation accuracy. It is interesting that for the case of laminar boundary layers at the higher Reynolds numbers, but not near the end of the tube, that the theoretical and experimental values of recovery factor and friction coefficient are in good agreement. This is where the boundary layer is thinnest and therefore is where the best agreement could be expected. The fact that the location of transition is in good agreement with that measured on a flat plate tends to indicate a relatively shock-free flow in the major part of the tube with laminar boundary layers. The one-dimensional flow model appears to be adequate for laminar boundary layers at high Reynolds numbers and the two-dimensional model[2] seems adequately to represent the low-Reynolds-number laminar-flow condition.

In the case of turbulent boundary layers, (*a*) the inclusion of lines on the figures for $Pr^{1/2}$ would have been helpful, and (*b*) it is apparent that there is something unusual about the skin-friction data. In addition, the values of recovery factor are rather low relative to values measured on flat plates. It is the writer's opinion that the cause for the results shown is that with turbulent boundary layers the flow is no longer shock-free. The inseparability of weak shock waves and turbulent boundary layers can be observed in any clear schlieren or shadow photograph of such a boundary layer, especially on bodies of revolution. In a tube of large length-to-diameter ratio the effect of many weak shocks could be expected to compound rapidly and it is possible that strong shocks could exist in the flow toward the end of the tube. The pressure changes from shock and possibly expansion waves in the tube with a turbulent boundary layer are possible causes for the unusual character of the friction-coefficient data. Whether or not the longitudinal pressure drop can be used to obtain the friction coefficient depends upon the relative magnitudes of the pressure loss due to friction and that due to shock waves.

The local values of recovery factor are likely to be too low when the boundary layer is thick because the calculated free-stream Mach number based on the assumed one-dimensional flow model would be low. This is obviously what led to the two-dimensional flow model[2] of the second half of this investigation. It appears that the most important factor in obtaining more accurate values of turbulent boundary-layer recovery factor in future experiments would be to measure the radial velocity distribution and if possible the radial temperature distributions at several stations in the tube. This could be accomplished by making measurements at the exit of separate tubes of various lengths as a separate set of test runs. With this information accurate flow models for the various flow regimes could be selected directly and the friction coefficient possibly could be determined with better accuracy.

Whether or not the need exists for more accurate friction and recovery-factor measurements in tubes depends entirely on the use for which the data are intended.

AUTHORS' CLOSURE

The points raised in the discussions deal mainly with the interpretation of the experimental data. The authors have long recognized the difficulties of interpretation of these data and have attempted to get a better understanding of the phenomena of supersonic flow in a round tube by use of the two flow models discussed in the papers and also by a still more "exact" method. This exact method consists essentially of the integration of the partial differential equations of motion, continuity, and energy for a compressible laminar boundary layer in the entrance region of a round tube, with the boundary conditions corresponding to the experimental ones. Although the results of this integration, using the differential analyzer, are not complete at present, the preliminary results indicate excellent agreement between interpretations based on our crude two-dimensional flow model and those based on this exact method, where it appears that a laminar boundary layer exists in the tube. However, this exact method is not applicable to those data where a turbulent boundary layer exists in the tube.

In regard to Mr. Brown's discussion, we would be pleased to see his results of combining the effects of wall curvature, high Mach number, variable fluid properties, and pressure gradient with respect to the data.

Mr. Scherrer's summary of the results where, it appears, a laminar boundary layer exists in the tube agrees with our own. His statement, "that for the turbulent boundary layer, the flow is no longer shock-free" is probably correct. We plan to make measurements, similar to those he suggests, for radial velocity and temperature profiles in the boundary layer near or upstream of the exit plane of the tube, in order to study the phenomena occurring in the downstream portion of the tube. We do not agree with Mr. Scherrer's statement that the values of the turbulent recovery factors for the tube flow are rather low relative to values measured on flat plates; a survey of such recovery factors on flat plates and other shapes indicates that our tube-recovery factors agree within 2 per cent with most data.

Mr. Gazley's contention that the precision of the tube data is considerably less than that obtained in boundary layers on flat plates and bodies of revolution is incorrect. For example, one experimental study of skin friction in supersonic flow over flat plates by interferometric means yielded results which scattered considerably and were from 7 to 40 per cent larger than the theoretical values. Similarly in another study, skin-friction coefficients based on impact-pressure surveys of the boundary layer in supersonic flow were from 37 to 94 per cent larger than the theoretical values and scattered appreciably. In contrast the tube-recovery factors for a laminar boundary layer agreed within 2 per cent with experimental values based on flat plates and on cones.

Mr. Gazley raises the question of why the authors chose to study supersonic boundary layers in a tube rather than on a flat plate or on a body of revolution. The cost of experimentation

[8] "Interferometer Corrections and Measurements of Laminar Boundary Layers in Supersonic Stream," by R. E. Blue, NACA Technical Note 2110, 1950.

[9] "Effects of Pressure Gradient on Stability and Skin Friction in Laminar Boundary Layers in Compressible Flow," by H. Weil, *Journal of the Aeronautical Sciences*, vol. 18, 1951, pp. 311–318.

[10] Ames Aeronautical Laboratory, Moffett Field, Calif. Jun. ASME.

with supersonic flow in a tube is very much less than the cost of experiments on a flat plate of similar dimensions. In addition, the entrance portion for supersonic flow in a tube should give essentially the same result as the upstream portion of supersonic flow over a flat plate. This hypothesis has been verified recently. The supersonic flow over a flat plate is disturbed by the type of leading edge as well as by the radius of curvature of the leading edge. Comparable effects are absent in a well-designed tube experiment.

Experiments made with a flat plate of finite width have edge effects which contaminate the flow. These effects can be pushed further downstream at the longitudinal center line of the plate by increasing the width, which means a larger and more expensive wind tunnel. Similar limitations exist in supersonic flow in a tube because the boundary layer encroaches on the core of the fluid and affects its pressure. These effects can be pushed further downstream by enlarging the tube diameter with a relatively small increase in cost. Thus the experiments with a tube yield precise results at low cost on recovery factors, friction coefficients, and heat-transfer coefficients which are applicable to tube flow or plate flow for low-length Reynolds numbers up to and through transition to turbulent flow. It is recognized that the data obtained for the downstream portion of the tube require considerable interpretation.

It is not a foregone conclusion that heat transfer for supersonic flow in tubes or ducts is of no engineering consequence. The design of supersonic wind tunnels for high stagnation temperatures is one example of a problem where data obtained in experiments of the sort under discussion would prove to be important.

On the Stresses in a Rotating Disk of Variable Thickness[1]

I. Malkin.[2] From the point of view of practical application to design problems the general solutions of the strength problem of rotating disks represent the basis for selection of special solutions, characterized by a minimum number of constant parameters, favorable stress distribution, and simplicity of the computations involved. Two convenient special solutions of the latter kind have been developed by the writer without use of general solutions.[3] The author's contention that the writer's solutions are expressed in infinite series is not quite correct; the second solution appears in closed form for profile as well as for the two stress components. General solutions are the subject of a considerable number of publications not mentioned by the author and apparently not known to him.[4] His profile curve [3], affected by two parametric constants (generalized exponential profile) and leading to a solution by confluent hypergeometric series, already has been treated extensively in the two papers of R. G. Olsson.[4] The second of his two publications also contains numerical tables. Therefore it might be advisable for the author to compare his tables with those of Olsson and to see whether and in how far his own paper offers new material, which might be a valuable addition to Professor Olsson's work.

Author's Closure

The author acknowledges with appreciation the discussion of Dr. Malkin, particularly the comment on the general solutions from the practical point of view. The present work was, in fact, carried out in an attempt for improving the design of the turbine disk of a certain engine; the disk was formerly designed in a uniformly tapered form.

The author wishes to thank Dr. Malkin for his mentioning some additional German publications dealing with the same subject, but unfortunately such publications are not available here. He will gladly make such comparison as suggested by Dr. Malkin when they become accessible.

Besides, the author wishes to correct a loose statement in the introduction of his paper. The sentence referring to Dr. Malkin's previous solutions should be read as follows: "In 1934, Malkin developed two analytic solutions for disks of two particular exponential profiles, one expressed in infinite series and the other in closed form by a clever choice of Poisson's ratio."

An Airy Integral Analysis of Beam Columns With Distributed Axial Loading Having a Fixed Line of Action[1]

R. K. Koegler.[2] The application to beam columns of the recently developed methods of solving the equation $y'' - yx = f(x)$, using Airy integral functions is very interesting and very well done and the authors are to be congratulated. It represents a worth-while advance toward the development of closed solutions for some of the more complicated column cases which are so often met in practice.

The authors point out that the case solved is that in which the distributed axial loads are along the undeflected beam axis. They also mention that for beam curvature all of one sign, this solution is conservative for the cases (1) where these loads move with the beam but remain parallel to their initial direction, and (2) where the distributed axial loads act tangentially to the deflected beam axis. Since these latter two types of conditions are more frequently met in practice, it is hoped that the investigation will progress further to cover either a closed solution for these latter cases, or an investigation by tests or theory of the degree of conservatism incurred by analyzing typical cases by the method given in this paper. With this information at hand, designers may well find the method and other data given in this paper very useful in many cases.

Authors' Closure

The authors appreciate Mr. Koegler's kind remarks and agree that the two cases not treated are of more practical interest, especially in aircraft design. The analysis presented provides an upper bound for these other cases. A lower bound can be obtained readily by considering that the axial loading acts at

[1] By Ti-Chiang Lee, published in the September, 1952, issue of the Journal of Applied Mechanics, Trans. ASME, vol. 74, pp. 263–266.

[2] Standards and Design Engineer, Foster-Wheeler Corporation, New York, N. Y.

[3] "Festigkeitsberechnung rotierender Scheiben," by I. Malkin, Julius Springer, Berlin, 1935; see also the author's reference (5).

[4] "Beitrag zur genauen Berechnung der Dampfturbinenscheibenräder mit veränderlicher Dicke," by A. Fischer, *Zeitschrift des Oesterreichischen Ingenieur und Architekten-Vereines*, vol. 74, 1922, pp. 46–49.

"Neue Lösungen des Problems der rotierenden Schiebe," by R. Grammel, *Ingenieur-Archiv*, vol. 7, 1936, pp. 137–139.

"Über einige Lösungen des Problems der rotierenden Scheibe," by R. Gran Olsson, *Ingenieur Archiv*, vol. 8, 1937, pp. 270–275 and 373–380.

"Lösungen des Problems der rotierenden Scheibe zu vorgegebenen Spannungsverteilungen," by A. Held, *Ingenieur Archiv*, vol. 10, 1939, pp. 339–370.

[1] By C. M. Tyler, Jr., and J. G. Christiano, published in the September, 1952, issue of the Journal of Applied Mechanics, Trans. ASME, vol. 74, pp. 275–283.

[2] Cornell Aeronautical Laboratory, Inc., Buffalo, N. Y.

the calculated deflection curve and then finding the reduction in bending moment by simple statics. This lower bound will provide an estimate of the degree of conservatism involved.

W. T. Rouleau, graduate student in mechanical engineering, Carnegie Institute of Technology, and the senior author have developed a closed-form solution for case 1, where the axial loads move with the beam but remain parallel to their initial direction. To date, publication sponsorship has not been obtained for this work including a tabulation of integrals of Airy integrals necessary for numerical calculations.

Large Plastic Deformations of Beams Under Transverse Impact[1]

T. H. H. Pian.[2] The writer has recently made an extension to this problem.[3] The authors' method is adopted to determine the plastic strains in a simply supported uniform beam subjected to a concentrated impulsive load at the center of the beam.

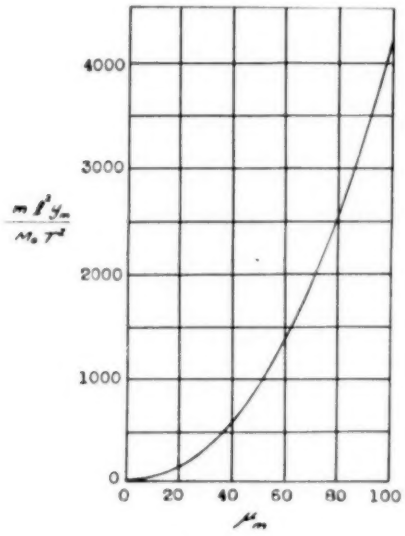

Fig. 1

Based on "plastic-rigid" theory, it is shown again that under moderate loads a plastic hinge is formed at the mid-span of the beam, while at very high loads, two additional plastic hinges are formed, one on each side of the mid-span. The hinge point on either side has been shown to travel along the beam as the load varies. The calculation of this phase of the motion involves the solution of a nonlinear differential equation. The writer has shown that when the impulsive load has a square shape, this equation can be solved in closed form, and the time histories of the acceleration, the velocity, and the dis,placement of the beam can be evaluated easily.

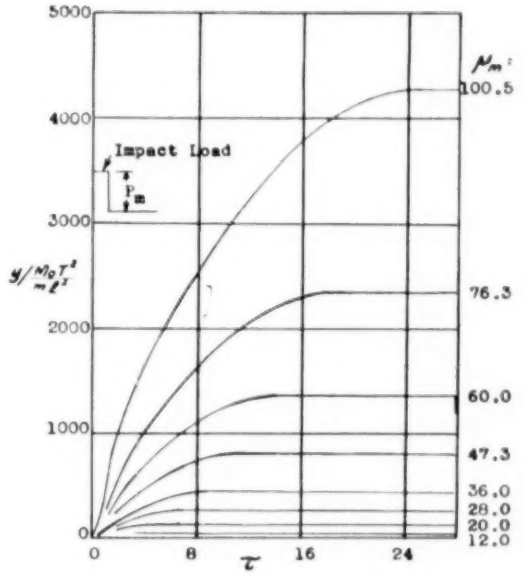

Fig. 2

Fig. 1 of this discussion shows the variation of the final permanent deformation at the center of the beam as a function of the magnitude of the impact force. Fig. 2, herewith, shows the variation of the mid-span displacement with respect to time. In these figures, the following nomenclature is used:

M_0 = fully plastic moment
T = duration of impact
l = length of beam
m = mass of beam per unit length
y_m = permanent mid-span deformation
P_m = amplitude of impact
$\mu_m = P_m l/4M_0$
$\tau = t/T$

Irwin Vigness.[4] The employment of plastic hinges to facilitate the determination of collapse loads of structures has generally neglected changes in the shape of the structures and of inertial effects which would be present under dynamic conditions. The present paper applies the plastic-hinge concept to a problem where the effects of changes in shape are not as important as in more complicated multiple-connected structures and where the dynamic aspects are no longer neglected but are principal considerations of the problem. The present approach provides a powerful and relatively simple method for determining the plastic deformations of a beam when subjected to a transversely applied force.

However, a solution giving the plastic deformation under transverse impacts of simple bars and plates having finite boundary conditions cannot be obtained practically without rather drastic assumptions. The degree to which the assumptions affect the accuracy of the results can best be determined experimentally. In the present case experimentalists normally would design tests first using materials that most closely fulfilled the assumed physi-

[1] By E. H. Lee and P. S. Symonds, published in the September, 1952, issue of the Journal of Applied Mechanics, Trans. ASME, vol. 74, pp. 308–314.

[2] Assistant Professor of Aeronautical Engineering, Massachusetts Institute of Technology, Cambridge, Mass.

[3] "A Note on Large Plastic Deformations of Beams Under Transverse Impact" M.I.T. Aero-Elastic and Structures Research Lab. Report for ONR (Contract N5ori-07833) May, 1952. (Paper presented at the Eighth International Congress of Theoretical and Applied Mechanics, Istanbul, Turkey, Aug. 20–28, 1952.)

[4] Mechanical Division, Naval Research Laboratory, Washington, D. C.

cal properties and second, employing others that had more practical interest. They would attempt to apply a suitable force to the beam so that they could plot experimental points corresponding to the theoretical curves shown by the authors' Figs. 8 and 9. However, because of the change of acceleration response of the beam to a given force, as one goes from one "phase" of motion to another, they would find great experimental difficulties in applying many mathematically simple types of force functions, in particular, the triangular-shaped one used in the authors' present illustration. If it can be done with reasonable effort it is suggested that the authors indicate how these techniques are applied when the method of excitation, instead of being a triangularly shaped force function, is one of the following:

(*a*) A sudden attainment of a constant velocity in the manner as assumed by Duwez, et al [5]

(*b*) A square wave-force function, which could be obtained by a greatly extended spring acting between closely spaced stops.

It would of course be appreciated if the authors would suggest other methods of excitation that would be suitable from both a theoretical and experimental viewpoint.

Authors' Closure

The authors thank Messrs. Pian and Vigness for their pertinent comments. They are interested in the finite-beam application with pin-jointed ends.

The simplification introduced by the assumption of a rectangular force pulse had been observed already by the authors, but since the application in which we were particularly interested involves a pulse which is approximately triangular in form, the influence of the different form must be investigated before the simpler analysis can be utilized in this connection. Such a study has been carried out,[6] and it is found that if a triangular force pulse is replaced by a rectangular one, having the same total impulse and maximum force, the final deformation will be overestimated by about 20 to 30 per cent. A simple empirical formula is suggested[6] by which the plastic deformation can be estimated from a knowledge of the impulse and the peak-force value. It would be valuable to have this result subjected to tests to define its limits of practical usefulness.

Dr. Vigness' suggestion (*b*) is discussed fully in the reference cited.[6] Suggestion (*a*) of using an impact comprising a suddenly applied constant velocity involves some difficulty of interpretation, since the impact commences with an impulsive force which leads to a singularity in the solution; initially, three hinges are produced locally at the point of impact. One remains there, the other two move out and eventually disappear. This situation for an infinitely long beam has been discussed by Conroy.[7] In view of the case of realizing this type of impact experimentally, this solution perhaps should be evaluated, but some difficulty is to be expected adjacent to the point of impact owing to the effect of the impulsive force and the high local strains produced. Thus it seems that the most convenient case for experimental check is the rectangular force pulse. Such a check would provide a valuable adjunct to the theoretical analysis, as a means of assessing the idealizations involved.

[5] "Behavior of Long Beams Under Impact Loading," by P. E. Duwez, D. S. Clark, D. S. Wood, Journal of Applied Mechanics, Trans. ASME, vol. 72, 1950, pp. 27–34.

[6] "The Influence of Load Characteristics on Plastic Deformations of Beams Under Concentrated Dynamic Loading," by P. S. Symonds, Report No. 9 of Brown University to Office of Naval Research under Contract N7onr-35810 (to be published).

[7] "Plastic-Rigid Analysis of Long Beams Under Transverse Impact Loading," by M. F. Conroy, Journal of Applied Mechanics, Trans. ASME, vol. 74, 1952, pp. 465–470.

Plastic Flow in a V-Notched Bar Pulled in Tension[1]

G. Sachs[2] and D. Hoffman.[3] The author has presented a very interesting analysis of the spreading of the plastic region in a notched tensile test bar under conditions of plane strain. This method of analysis has been initiated by Prandtl (1)[4] and applied to the indentation of a narrow punch. Hill's (2) and Lee's work on notched bars deals essentially with the same problem and arrives at the same final answer for full plasticity, namely, that the stress should then be $(1 + \pi/2) = 2.57$ times that required for homogeneous plastic flow.

Unfortunately, however, the author does not present any experimentation which supports his analysis. It is also rather regrettable that he has paid no attention to the limitations of the theory and its relation to available experimental evidence. Apparently he is not aware of the fact that the results of Prandtl's analysis were shown to disagree with the results of experimentation. While some tests by Nadai (3) on steel appeared to yield Lüder's lines in agreement with Prandtl, Sachs (4) has shown that the plastic region, revealed by recrystallization, as well as the actual resistance to indentation are obtained more readily and accurately on the basis of the arbitrary assumption that the onset of plasticity does not change materially the stress distribution in the elastic state. As a result of this work, one of Prandtl's and Nadai's associates, Mesmer (5) reinvestigated this problem completely and arrived essentially at the same results as Sachs.

We are greatly indebted to Hill and Lee for their excellent work on the mathematical theory of plasticity which may be considered as the outstanding development in this field during recent years. However, in his excellent book summarizing all the work on plasticity, Hill (6) is well aware of the limitations of rigorous analysis and, in a rather unusual fashion for a mathematician, he gives full credit to the results of somewhat arbitrary or "elementary" approaches to the problem (7). He expresses his opinion on this book as follows:[5] "There is little point in making extensive calculations of the small error in the elementary theory unless it is done with reasonable accuracy."

In this connection attention also may be called to a recent Harvard University dissertation by G. Hoffman (8) on the extrusion of wax mixtures. In this paper it is shown that under conditions where the extruded mixture is rather brittle the plastic region develops much in agreement with the concepts of Prandtl, Hencky, Hill, and Lee. However, if the mixture is truly plastic, the plastic region is very extended and no limits between plastic and elastic regions are apparent. This observation also explains the fact that Lüder's lines develop in accordance with the mathematical analysis. Their development is generally considered to be more closely related to fracturing than to plasticity.

On the basis of his experimental work on notched tensile test bars, Sachs (9) already has called attention to the fact that the strength of a deeply and sharply notched bar is usually determined by plastic flow and not by fracturing. An experimental analysis of pulled notched tensile test bars also has shown that their hardness pattern corresponds to the elastic stress distribution (10). Unfortunately, no experimental data are available for the condition of plane strain, to date. It may be predicted, however, that

[1] By E. H. Lee, published in the September, 1952, issue of the Journal of Applied Mechanics, Trans. ASME, vol. 74, pp. 331–336.

[2] Research Professor and Director Metallurgical Research, Syracuse University, Syracuse, N. Y. Mem. ASME.

[3] Professor of Civil Engineering, Case Institute of Technology, Cleveland, Ohio.

[4] Numbers in parentheses refer to the Bibliography at the end of this discussion.

[5] Reference (7), p. 72.

the ratio of the limiting strength under such conditions to the regular tensile strength will be close to 2, in agreement with the results of indentation tests, rather than the figure 2.57, postulated by Lee and Hill's analysis.

BIBLIOGRAPHY

1 "Über die Eindringungs-festigkeit (Härte) plastischer Baustoffe und die Festigkeit von Schneiden," by L. Prandtl, *Zeitschrift Angewandte Mathematik und Mechanik*, vol. 1, 1921, pp. 15–20; *Naturwiss.* vol. 15, 1927, p. 265.

2 "Plastic Yielding of Notched Bars Under Tension," by R. Hill, *Quarterly Journal of Mechanics and Applied Mathematics*, vol. 2, 1949, pp. 40–52.

3 "Versuche über die plastischen Formänderungen von keilförmigen Körpern aus Flusseisen," by A. Nadai, *Zeitschrift Angewandte Mathematik und Mechanik*, vol. 1, 1921, pp. 20–28.

4 "Beitrag zum Harteproblem," by G. Sachs, *Zeitschrift für Technische Physik*, vol. 8, 1927, pp. 132–141; *Naturwiss*, vol. 14, 1926, pp. 1219–1223.

5 "Vergleichende spannungsoptische Untersuchungen und Fliessversuche unter konzentriertem Druck," by G. Mesmer, *Technische Mechanik und Thermodynamik*, vol. 1, 1930, pp. 85–100, 106–112.

6 "The Mathematical Theory of Plasticity," by R. Hill, Clarendon Press, Oxford, England, 1950.

7 "Introduction to the Theory of Plasticity for Engineers," by O. Hoffman and G. Sachs, McGraw-Hill Book Company, Inc., New York, N. Y., (in press).

8 "Dissertation," by G. Hoffman, Harvard University, Cambridge, Mass., 1950.

9 "Notched Bar Tensile Test Characteristics of Heat Treated Low Alloy Steels," by G. Sachs, J. D. Lubahn, and L. J. Ebert, Trans. American Society for Metals, vol. 33, 1944, pp. 340–391.

"The Effect of Notches of Varying Depth on the Strength of Heat Treated Low Alloy Steels," by G. Sachs, J. D. Lubahn, and L. J. Ebert, Trans. American Society for Metals, vol. 34, 1945, pp. 517–539.

10 "Notched Bar Tension Tests on Annealed Carbon Steel Specimens of Various Sizes and Contours," by M. L. Fried and G. Sachs, Symposium on Deformation of Metals as Related to Forming and Service, American Society for Testing Materials, 1948, pp. 83–115.

Author's Closure

The author greatly appreciates the detailed discussion of the paper and agrees that the onset of plasticity is associated with the elastic solution, and that plastic effects are observable which are in the main associated with that solution. Such influences are concerned with plastic strains which are of the order of elastic strains, and such is not the concern of the paper under discussion.

Prandtl's solution[6] is what has been termed an initial motion solution; it assumes strains sufficiently small to permit use of the underformed boundaries to prescribe the stress and strain analysis problems, and yet sufficiently large to neglect elastic strains in comparison with plastic strains. In many problems these opposing inequalities can be satisfied because elastic strains for most metals are of the order 10^{-3}, and strains much larger than this, say, 10^{-2}, produce no appreciable change in boundary geometry. The problem under discussion does not suffer from these restrictions, since it offers a stress and velocity field at each stage during the deformation, and takes account of the resulting boundary motion, so that at each stage the stress and velocity fields are based on the instantaneous deformed shape of the boundaries. Thus we have a large strain solution, and the conditions for application are that the strains should be large compared with elastic strains, which is certainly true, and that the material should approximate to the assumed ideally plastic behavior.

The present type of solution thus offers a much better opportunity for comparison with experiment than does the initial motion problem, where the development of plastic flow must be limited to that which does not produce appreciable deformation of the boundaries. Some experimental checks of large strain solutions have appeared in the literature,[7] and good over-all agreement with the theory was exhibited.

Thus in considering comparison with experiment we are concerned with the regions of large plastic flow and the strain distribution in them. The regions of observable plastic flow, in general, will extend far beyond these. This is well illustrated in the work of Mesmer.[8] Presumably the recrystallization work of Sachs[9] pertains also to these regions. The experimental work by G. Hoffman,[10] using wax, showed an appreciable strain-rate influence which would be expected to smooth out the strain discontinuities of the ideal theory, at which point the computed strain rate would approach infinity. This was, in fact, found to occur with the "plastic" wax, but the general form of the strain distribution computed on the basis of ideal plasticity was reproduced experimentally.

In connection with the notch-constraint factor which the discussers state can be expected to be close to 2, rather than the figure 2.57 given by the plane-strain theory, it is interesting to note that the experimental figure given by Orowan, Nye, and Cairns[11] is about 2.6 for annealed mild steel.

The author apologizes to Professor Sachs, and his collaborators, J. D. Lubahn and L. J. Ebert, for overlooking their statement[12] that plastic-flow characteristics determine the strength of sharply notched bars, when he referred to the similar suggestion by Orowan.[13]

[6] Reference (1) of the Bibliography at the end of the discussion.

[7] "The Theory of Wedge Indentation of Ductile Materials," by R. Hill, E. H. Lee, and S. J. Tupper, Proceedings of the Royal Society, series A, vol. 188, 1947, pp. 273–289; and "The Use of Plasticine Models to Simulate the Plastic Flow of Metals," by A. P. Green, *Philosophical Magazine*, vol. 42, 1951, pp. 365–373.

[8] Reference (5) of discussion.

[9] Reference (4) of discussion.

[10] Reference (8) of discussion.

[11] "Theoretical Research Report 16/45," by E. Orowan, J. F. Nye, and W. J. Cairns, Ministry of Supply, Armament Research Department, 1945.

[12] Reference (9) of discussion.

[13] Reference (7) of the paper.

Book Reviews

Dynamics of Systems

MECHANIK, Vol. 3. Dynamik der Systeme. By Hans Ziegler. Verlag Birkhauser, Basel, Switzerland, 1952. Cloth, 6½ × 9½ in., 396 pp., 191 diagrams, 46.80 sw. fr.

REVIEWED BY J. N. GOODIER[1]

THIS is the last of three volumes for engineering students forming a unified presentation of the principles of engineering mechanics. The fundamental equations, theorems, and principles of solid and fluid mechanics, including strength of materials and hydrostatics, are the author's principal concern throughout. They are systematically illuminated by specific systems and their problems, but, in accordance with the author's plan of providing a co-ordinated introduction to the numerous specialized works, these represent limited selections from the extensive resources available.

This volume is in three parts. The first—dynamics of systems of rigid bodies—is in terms of the Lagrange equations ("die heute auch der Ingenieur beherrschen musz") illustrated by a few problems drawn from elementary dynamics. In the second part, they are applied to vibrations. Here the treatment of n degrees of freedom covers the eigenvalues, their reality, the orthogonality of the normal modes, Rayleigh's principle, and, what is not so usual, Courant's maximum-minimum principle. Stability of motion, with the Routh-Hurwitz criteria, appears in a vehicle trailer problem. Sections on longitudinal, torsional, and flexural motions in bars follow in orthodox fashion, and briefly touch on Fourier series and Sturm-Liouville systems. It is in the plan of the book to introduce each subject in all its generality rather than in its barest simplicity, as in the flexural motions, where the bar is at first not uniform, and rotatory inertia is included. However, shear deformation, usually a correction of at least equal importance, is not included.

The third part of the volume is on continua, beginning with an extended general analysis of stress and small strain, although the equations of compatibility are merely mentioned. It is in the main in vector terminology. Hooke's law enters in the general anisotropic form. The simple stress distributions of strength of materials are examined, and the Saint-Venant torsion theory developed and applied to the thin rectangle. The treatment of plane stress is concerned with the variations in the thickness of the plate. The wave equations and velocities of the elastic solid, the equations of the taut elastic diaphragm (in-plane motion included at first), with the vibrating rectangular membrane, close the account of elastic solids. It is followed by a brief section on plastic-flow criteria.

Some 80 pages are devoted to fluid dynamics—the general equations of the frictionless fluid and the Bernoulli and Kelvin theorems preceding the sample problem of steady incompressible flow round a sphere. The Joukowsky airfoil theory is given in detail, followed by the Prandtl finite airfoil theory with evaluation for the elliptic distribution of circulation. The last part on the viscous fluid derives the Navier-Stokes equations, gives Poiseuille flow as a simple solution, and obtains the differential equations of the boundary layer. There is an appendix on tensors (Cartesian), co-ordinating the aspects which have made their appearance at various stages throughout the text.

[1] Professor of Engineering Mechanics, Stanford University, Stanford, Calif. Mem. ASME.

Nonlinear Vibrations

NONLINEAR VIBRATIONS IN MECHANICAL AND ELECTRICAL SYSTEMS. By J. J. Stoker. Interscience Publishers, Inc., New York, N. Y., 1950. Cloth, 6 × 9 in., figs., appendixes, bibliography, index, xix and 273 pp., $6.

REVIEWED BY J. P. DEN HARTOG[2]

THIS book is one of a "series of texts and monographs of Pure and Applied Mathematics" edited by Bohr, Courant, and Stoker of New York University. Although the author is a mathematician, the book is readable for engineers as well and it takes a worthy place among the few books now existing on the subject. In difficulty it is about on a par with the book of Andronof and Chaikin and it is easier than Minorsky. The book starts with an introduction on linear systems and then systematically treats the various nonlinear problems, introducing the "phase plane" (the displacement versus velocity graph) quite early. It gives a particularly good and readable account of Duffing's method for forced vibrations of systems with nonlinear springs. Also remarkable is the last chapter in which the solution to the linear problem of systems with variable coefficients is applied to nonlinear systems. The book ends with six short appendixes on mathematical questions, giving existence and uniqueness proofs that are of great importance to the mathematicians and that are usually accepted by engineers by physical intuition.

In general, the book is warmly recommended to all who want to study the subject of nonlinear vibrations.

Heat and Thermodynamics

HEAT AND THERMODYNAMICS. By Mark W. Zemansky. McGraw-Hill Book Co., Inc., New York, new third edition, 1951. Cloth, 6 × 9 in., xiv and 465 pp., illus., $6.

REVIEWED BY JOSEPH KAYE[3]

THE third edition of this popular textbook in thermodynamics is recommended to engineers as one of the best books available either for use in classroom instruction or for a refresher course of self-instruction in thermodynamics. The material is covered in a logical fashion with a clear style and with interest maintained by constant introduction of appropriate historical material.

The first half of the book, consisting of eleven chapters, covers the concepts of temperature, equilibrium state, work, heat; the zeroth, first and second laws; reversibility, ideal gas, pure substance; and contains a single chapter on the rate of transfer of heat by conduction, convection, and radiation. The material in these eleven chapters could be considered as the foundation for an introductory course in thermodynamics for engineering students. The macroscopic approach to thermodynamics is used throughout, and a few of the pitfalls based on the microscopic approach are discussed. Many problems for classroom use, as well as illustrative problems, are included.

Applications of thermodynamics are discussed in the remaining half of the book. One chapter is devoted to the steam engine

[2] Professor of Mechanical Engineering, Massachusetts Institute of Technology, Cambridge, Mass. Mem. ASME.

[3] Associate Professor of Mechanical Engineering, Massachusetts Institute of Technology, Cambridge, Mass. Mem. ASME.

and the refrigerator; the introduction of the steady-flow energy equation appears to have been added at the end of this chapter as an afterthought. The Maxwell equations are discussed in chapter 13. Special topics are discussed next; these include the porous-plug experiment, black-body radiation, stretched wire, surface film, reversible cell, dielectric, piezoelectric effect, thermoelectric phenomena, and paramagnetic solid. Chapter 15 presents the thermodynamics of phase changes for first-order and second-order transitions. Chapter 16 is a fairly complete summary of modern developments in the physics of low-temperatures and contains also a good discussion of the third law. Chemical thermodynamics, ideal-gas reactions, and heterogeneous systems are discussed in the last three chapters of the book from the viewpoint of the basic contributions of Gibbs.

The treatment of the applications of thermodynamics, given in the second half of the book, is suitable for physicists and chemists but not for undergraduate engineering students. Experience in teaching has demonstrated that engineering students require many and varied applications in order that the fundamental concepts and uses of the first and second laws be mastered in the period of time available for undergraduate instruction.

On page 76 the author states incorrectly that there is no appreciable change in any thermodynamic co-ordinate of a heat reservoir when a finite amount of heat flows in or out; that he really means "per unit mass of the heat reservoir" is seen from the discussion on page 178 wherein he calculates the finite change of entropy of the heat reservoir for a finite heat flow in or out.

Instrument Engineering

INSTRUMENT ENGINEERING. Volume 1. Methods for Describing the Situation of Instrument Engineering. By C. S. Draper, W. McKay, S. Lees. McGraw-Hill Publications in Aeronautical Science, McGraw-Hill Book Company, Inc., New York, N. Y., 1952. Cloth, 8½ × 11 in., xvi and 269 pp., illus., $6.

REVIEWED BY ENRICO VOLTERRA[1]

THIS work, which will consist of three volumes (of which volumes 2 and 3 are expected to be ready in the near future), has been planned with the object of furnishing a textbook of easy reference for everyone, and for the professional engineers in particular, interested in problems of measurement and control of instrument engineering. Fulfilling such an ambitious scheme must certainly not have been an easy task due to the vastness of the material to be described and, particularly, to the aim of exposing in an easy and clear way (without losing the scientific rigor) concepts which often are rather difficult.

One of the principal merits of the first volume of this work, which has just been published, consists in the presentation of principles and methods in such a selected and organized form that it is easily accessible to everyone familiar with college physics and differential equations. It deals with the description of physical devices and variations in physical quantities by graphical and analytical methods. The exposition proceeds clearly and rapidly without being arid and without the authors' losing contact with possible practical applications of the theories developed.

One can be sure that this work will be particularly welcome to students of both graduate and undergraduate levels, as well as to practicing engineers who will be glad to finally see completed a treatise which will fill a gap which existed in the technical literature.

[1] Professor of Mechanics, Rensselaer Polytechnic Institute, Troy, New York. Mem. ASME.

Flames and Furnaces

THE SCIENCE OF FLAMES AND FURNACES. By M. W. Thring. John Wiley & Sons, Inc., New York, N. Y., 1952. Cloth, 5½ × 8½ in., xiv and 416 pp., illus., $6.50.

REVIEWED BY WARREN M. ROHSENOW[2]

THE intent of the author is to bridge the gap between industrial furnace design and such fundamental sciences as physics, chemistry, and physical chemistry; to emphasize the aspect of "diagnosis" of ailments of existing furnaces; and to present the problems of furnace heating in such a way as to be of interest to academic scientists as well as to engineers in charge of design and operation of furnaces. Only flame-heated furnaces are considered and problems associated with the material being heated are considered only in so far as they set furnace-design limitations. The 410 pages of this book contain an excellent and interesting survey of the problems and the current literature associated with furnace design.

Chapter 1 contains a survey of various types of furnaces in different industries.

Chapter 2 discusses the application of thermodynamics laws to furnace heating. The Centigrade Heat Unit (CHU), the amount of heat required to raise 1 lb of water through 1 C, is used in discussing heat balances and the construction of Sankey diagrams for various types of furnaces. In discussing the second law of thermodynamics the author prefers to introduce a quantity which he calls the *virtue* of *energy V*, defined as the amount of an energy quantity Q which could be converted to work in an ideally perfect system. For a quantity of heat Q, transferred from a system at temperature T_A the virtue $V = Q(1 - T_0/T_A)$ which is the work obtainable from a Carnot cycle operating between T_A and the temperature of the atmosphere T_0. A virtue diagram of $(-1/T)$ versus Q is constructed; then the area under the curve representing a particular combustion gas is the change in virtue of energy.

This entire concept of virtue of energy is a limited form of the more generally applicable concept of availability. The virtue of energy concept has only limited usefulness. For most furnace processes its application is valid.

Chapter 3 discusses the combustion processes. After a discussion of combustion chemistry and equilibria there follows an excellent survey of the modern concepts of combustion taking up the subjects of speeds of reaction in gas mixtures, diffusion flames, solid fuels (both pulverized and in beds) and liquid fuels. The various factors influencing these phenomena are discussed and where possible quantitative methods of evaluation are introduced. There is also a brief discussion on combustion control.

Chapter 4 discusses the heat-transfer processes in furnaces. Following a discussion of temperature-measuring methods the empirical heat-transfer relations for conduction, convection, and radiation are presented in forms useful for furnace calculations. These heat-transfer "laws" are then applied to heat-transfer process in the furnace. Here a discussion of radiation from flames is introduced. Both steady state and unsteady state heat-transfer processes are discussed.

Chapter 5 the fluid mechanics of the air and gas flow processes associated with furnaces. Basic principles are discussed including the introduction of an electrical analogy of the flow circuit. Producers of flow such as fans, ejectors, and the mechanism of natural convection or bouyancy are described. After a survey of various flow resistances, the methods of measuring gas flow are presented. There is also an excellent survey of recent litera-

[2] Associate Professor of Mechanical Engineering, Massachusetts Institute of Technology, Cambridge, Mass. Mem. ASME.

ture on gas flow patterns and experimental methods of studying them.

Chapter 6 describes furnace construction—refractory and insulating materials and walls and crown construction.

The final chapter, The Application of Scientific Methods to Furnaces, deals with the consequences of the fact that furnaces are usually not exactly specified, isolated systems and with methods for obtaining benefit from scientific results in spite of it. These methods differ depending on the four objectives which are discussed separately: (1) diagnosis of a single furnace, (2) statistical study of furnace types, (3) design of a modification of an existing type furnace, and (4) invention of new furnace.

Most of the material treated in the book is discussed briefly. To make the material useful, the reader will probably find it necessary to study the references. For example, only one page is devoted to the process of burning pulverized coal. The author's intention, however, was to be brief. This makes the book easily read. The person desiring more detailed information is lead to pertinent reference material.

This book is interesting to read and contains an excellent survey of the up-to-date literature treating the processes associated with furnaces heated by flames.

Technical Reports

Writing the Technical Report. By J. Raleigh Nelson. McGraw-Hill Book Company, Inc., New York, N. Y., third edition, 1952. Cloth, 6 × 9 in., xvi and 356 pp., $4.50.

Reviewed by John M. Lessells[6]

CLOSE association with senior and graduate engineering students clearly shows that the ability of the students to express their thoughts in written form, clearly and distinctly, is greatly lacking in many cases. Because of this the publication of this new edition of this text appears to be timely in stimulating interest in professional writing.

The book consists of five parts devoted to the design and composition of a report with specific directions as to short and long reports. A further section outlines a procedure for the critical examination of a report which is followed by a summary of the fundamentals for ready reference.

One of the important duties of an engineer must be to state clearly and succinctly the nature and evaluation of the salient features of a particular problem. Possibly more student time could be profitably devoted to this particular phase of engineering education. In this respect the publication should prove helpful.

[6] Associate Professor of Mechanical Engineering, Massachusetts Institute of Technology, Cambridge, Mass. Hon. Mem. ASME.

Supersonic Flow and Shock Waves

Supersonic Flow and Shock Waves. By R. Courant and K. O. Friedrichs. Interscience Publishers, Inc., New York, N. Y., 1948. Cloth 6 × 9 in., tables, bibliography symbols and subject indexes. xvi and 464 pp., illus., $7.50.

Reviewed by Ascher H. Shapiro[7]

NORMALLY when a book reaches the hands of the editor four years after publication it would be deemed superfluous to review it. But when, as in this case, the book seems destined to become a classic, it is altogether desirable that a brief review grace the pages of this Journal.

The major contribution of this book is in its unified treatment of nonlinear wave phenomena, covering such varied topics as (1) two-dimensional, steady, supersonic flow, (2) one-dimensional, unsteady motion, (3) wave propagation in elastic-plastic material, and (4) spherical waves. Besides these subjects there are valuable discussions of the mathematical theory of hyperbolic equations, shock waves, detonation, and deflagration waves, and the interaction of various types of waves.

The authors are mathematicians, and so it is natural that the strongest aspect of the presentation is that of mathematical rigor and generality. For the same reasons, however, the audience for the book is restricted to those with considerable mathematical facility. Nevertheless, this work is bound to have an influence on mathematicians, physicists, and engineers alike, for it is a rich source which writers in the field of compressible fluid dynamics will draw on for many years to come.

[7] Professor of Mechanical Engineering, Massachusetts Institute of Technology, Cambridge, Mass. Mem. ASME.

AN ASME PAPER

Its Preparation, Submission and Publication, and Presentation

To a large degree the papers prepared and presented under the ASME sponsorship are evidence by which its professional standing and leadership are judged. It follows, therefore, that to qualify for ASME sponsorship, a paper must not only present suitable subject matter, but it must be well written and conform to recognized standards of good English and literary style.

The pamphlet on "AN ASME PAPER" is designed to aid authors in meeting these requirements and to acquaint them with rules of the Society relating to the preparation and submission of manuscripts and accompanying illustrations. It also includes suggestions for the presentation of papers before Society meetings.

CONTENTS

PREPARATION OF A PAPER—

General Information—Style, Preferred Spelling, Length Limitation, Approvals and Clearances.

Contents of the Paper—Title, Author's Name, Abstract, Body of Paper, Appendixes, Acknowledgments, Bibliographies, Tables, Captions, Photographs, Other Illustrations.

Writing the Paper—Outline Tabulations, Tables, Graphs, Charts for Computation, Drawings, Mathematics, Accuracy, Headings and Numbering, Lantern Slides, Motion Pictures, Typing, Number of Copies.

SUBMISSION AND PUBLICATION OF A PAPER—

Intention to Submit Paper Required in Advance, Meeting Dates, Due Dates for Manuscript, Discussers, Review and Acceptance, Proofs, Advance Copies and Reprints, Discussion and Closure, Publication by Others.

PRESENTATION OF A PAPER—

Time Limit, Addressing Your Audience, Public Address Systems, Use of Slides.

REFERENCES—

References on Writing and Speaking, Engineering Standards.

Price 40¢. No discount allowed. ***A remittance must accompany all orders for $5.00 or less. U. S. Postage Stamps are acceptable.***

THE AMERICAN SOCIETY OF MECHANICAL ENGINEERS

29 West 39th Street, New York 18, N. Y.